Experimental and Theoretical Investigations of Particle Removal from Sand Bed Deposits in Horizontal Wells Using Turbulent Flow of Water and Polymer Fluids

by

Majid Bizhani

A thesis submitted in partial fulfillment of the requirements for the degree of

Doctor of Philosophy

in

Petroleum Engineering

Department of Civil and Environmental Engineering
University of Alberta

Abstract

Turbulent flow of water and polymer fluids over the sand bed deposits in horizontal annuli was studied using a large-scale flow loop equipped with particle image velocimetry (PIV) tool. Tests have been conducted to investigate the effects of near wall turbulence, fluid rheological characteristics and the particle size on the critical flow rate of the bed erosion.

Measurements of the velocity profiles over the sand bed interface were used to quantify the equivalent sand bed roughness. The equivalent roughness was found to be a function of the boundary roughness Reynolds number and could be several times higher than the particles size in the bed. Additionally, bedload transport of particles in the form of a moving layer of particles caused the bed roughness to increase significantly.

The analysis of the flow over stationary sand beds revealed that the addition of polymer significantly delays the transition from smooth to rough flow regime. The delay in transition from the smooth to the rough flow regime further causes the momentum transfer to be slow for polymer fluids comparing to water. Hence, causing the delay in the bed erosion.

The average and interfacial friction factors for the flow of water over the sand beds of varying heights in the eccentric annulus were evaluated. The average friction factor for the flow of water over the sand bed was 45% higher than the flow in the annulus without any sand bed. It was also found that the interfacial friction factor could be significantly different from that of the average friction factor. The onset of the particle movement caused the interfacial friction factor to increase sharply.

The impact of the flow turbulence on particles dislodgment from bed deposits were investigated using the measurement of instantaneous velocity profiles. The results indicated that

the effective fluid velocity felt by the sand particles could be several times higher than the time-averaged velocity. Additionally, the drag force experienced by the particles could be significantly different from the average drag force. Therefore, it is imperative to consider flow turbulence in any solid transport models in horizontal wells.

Critical flow rates for the onset of bed erosion were measured and compared for the flow of water (90 lit/min) and a dilute polymer fluid (0.032% w/w, 200 lit/min). The PIV data revealed that the polymer fluid has a higher local fluid velocity near the stationary cuttings bed interface at the onset of particle movement from bed deposits. Comparison of the Reynolds shear and normal stress profiles showed that the polymer fluid had much higher level of turbulence activity near the cuttings bed interface. Additionally, the bed shear stresses were also evaluated and compared. The minimum bed shear stress for the polymer fluid was much higher than that of water. Analysis of the PIV results together with the bed shear stress data confirmed that the polymer fluid exerted larger drag force on the sand bed than that of water at the onset of the particle movement.

A comparison was also made between fluids with two different polymer concentrations (i.e., 0.032% and 0.064% w/w) at the same flow rate (i.e. 200 lit/min). It was observed that the local fluid velocity near the cuttings bed was not affected significantly by the change in polymer concentration. Analyses of the near wall velocity data combined with the bed shear stress calculations also showed that increasing polymer concentration at the same flow rate led to an increase in the fluid's drag force on the sand bed. However, this increase in the drag force did not lead to a bed erosion either.

To explain this rather, controversial phenomenon, we have looked at the impact of the viscoelastic polymer fluid rheological properties on the bed erosion. It was shown that for viscoelastic polymer fluids, an additional normal force appears that hinders the removal of the particles from sand bed deposits. The normal force arises due to the non-zero first and second normal stress differences in polymer fluids. This additional force causes the sand bed to become more consolidated while imposing an additional resistive force against mobilization of the particles. Estimation of the normal fluid force shows that this force can be considerably higher than the submerged weight of the cuttings.

Preface

The research conducted for this thesis is the original work of Majid Bizhani. The work was carried out under the supervision of Professor Ergun Kuru at the University of Alberta. The collection of data, analyzing results, and compositions of research papers have all been done by Majid Bizhani. Several sections of the current thesis have either been published or pending publication.

The results presented in chapter 6 of the thesis have been published and presented before. This chapter was initially presented at heavy oil conference by SPE in Calgary as Bizhani, M., Corredor, F.E.R, Kuru, E., 2016, "Hole Cleaning Performance of Water vs. Polymer-Based Fluids under Turbulent Flow Conditions", Paper presented at SPE heavy oil conference held in Calgary, Alberta, June 2015. Additionally, it was published as Bizhani, M., Corredor, F.E.R, Kuru, E., 2016, "Quantitative Evaluation of Critical Conditions Required for Effective Hole Cleaning in Coiled Tubing Drilling of Horizontal Wells," SPE Drilling & Completion, SPE-174404-PA, 31(3). The data have been mainly collected by Majid Bizhani for this chapter. Data analysis and composition of the research papers have all been done by Majid Bizhani.

Chapter seven of the thesis is accepted for publication as Bizhani, M., Kuru, E., 2017, "Critical Review of Mechanistic and Empirical (Semi- Mechanistic) Models for Particle Removal from Sand Bed Deposits in Horizontal Annuli by Using Water," SPE Journal, SPE-187948-PA. Data collection, analysis, and writing the research paper have all been done by Majid Bizhani.

Chapter four of the thesis has been submitted for publication as Bizhani, M., Kuru, E., 2017, "Effect of Sand Bed Deposits on the Characteristics of Turbulent Flow of Water in Horizontal Annuli," ASME Fluid Engineering Journal. Data collection, analysis, and writing of the research paper were done by Majid Bizhani.

Chapter eight of the manuscript is accepted for publication as Bizhani, M., Kuru, E., 2017, "Particle Removal from Sand Bed Deposits in Horizontal Annuli Using Viscoelastic Fluids," SPE Journal. I have been responsible for data collection, analysis and writing the research paper.

Chapter eight of the manuscript is accepted for publication as Bizhani, M., Kuru, E., 2017, "Particle Removal from Sand Bed Deposits in Horizontal Annuli Using Viscoelastic Fluids," SPE Journal. I have been responsible for data collection, analysis and writing the research paper.

Chapter nine of the manuscript is submitted for publication as Bizhani, M., Kuru, E., 2017, "Assessemnt of of the Equivalent Sand Bed Roughness and the Interfacial Friction Factor in Hole Cleaning with Water in Horizontal Eccentric Annulus., SPE Journal. I have been responsible for data collection, analysis and writing the research paper.

Chapter twelve of the thesis have been presented as Bizhani, M and E. Kuru, 2015, "Modeling Turbulent Flow of Non-Newtonian Fluids using Generalized Newtonian Models," Proceedings of the ASME 2015 34th International Conference on Ocean, Offshore and Arctic Engineering OMAE2015 May 31-June 5, 2015, St. John's, Newfoundland, Canada. I have been the primary author of data collection, analysis of the results, and writing the paper.

Acknowledgment

I would like to express my gratitude for my supervisor Professor Ergun Kuru. He has given me the support and guidance for accomplishing this research program. I am thankful for his trust and the freedom he has given me throughout this research program. He has always provided me with positive and constructive feedbacks. He values quality data and is always supportive in buying the latest technologies required for the research. I fulfilled my Ph.D. and M.Sc. under his supervision. During the six years of working with him, I have learned a lot from him. He is, without a doubt, the most influential person in my academic life.

I also would like to thank the committe members for serving in my Doctoral defense exam. Dr. Tayfun Babadagli has been on the supervisory committee for my candidacy and defense examination. I sincerely appreciate his positive feedbacks and the time he spent in reviewing my thesis. I also express my appreciation toward Dr. Huazhou (Andy) Li for serving in both my candidacy exam and final P.hD. defence. Dr. Zhehui (Charlie) Jin is also acknowledged for his time spent on reading this manuscript and his feedbacks.

My special thanks go to Dr. Sina Ghaemi who has been in my M.Sc. defense, candidacy exam, and the final Ph.D. defense. He has helped me a lot throughout the past six years. I sincerely acknowledge his help and recommendations especially in the implementation of the PIV technique.

I sincerely thank Professor Rune W. Time for accepting to be in my defense exam. It was an honor for me to have a renowned professor in the field of drilling in my P.hD. defense. I appreciate his comments and feedbacks on this thesis.

The number of people who have helped throughout this study is big. However, one person in the petroleum engineering group at the University of Alberta have provided so much support than the others. Mr. Todd Kinnee has assisted in every aspect of this research program. His knowledge of petroleum engineering and other fields along with his strong work ethics have been helpful in the implantation of new ideas in this research. He has helped in building porotypes in different stages of the current research. I sincerely appreciate his support in this research program.

We thank Natural Sciences and Engineering Research Council of Canada for providing us with the finical support for this research (NSERC RGPIN-2016-04647 KURU and NSERC RGPIN 238623 KURU).

The authors also wish to thank Camara United for providing us the polymer used in this study (Alcomer 110RD).

Table of Contents

List of Tables

List of Figures

1.Introduction

1.1. Overview

The quest to access oil reservoirs in a harsh environment is continually driving the demand for more complex wells. Wellbore trajectories are becoming more and more complex. Use of horizontal, multilateral, and Extended Reach Wells (ERWs) are growing. The higher rate of return and recovery factor is the technical reasons for widespread use directional wells. Horizontal and ERWs are critical in maximizing recovery from many oil fields. In an offshore environment, these technologies are used to drain a large area of a reservoir from a single platform. Consequently, they significantly reduce the cost of expensive infrastructures and platforms. Multilateral wells are essential for recovering from heavy oil reservoirs (Mason 2008, Negrao 2009, Negrao 2014, Ruszka 2014, Aadnøy 2015).

Directional drilling, although more expensive comparing to conventional vertical wells, has many advantages. For example, it exposes a greater portion of the reservoir to production, and hence, enhances production rate. Multilateral wells are a new evolution of horizontal wells where multiple wells are drilled from the main borehole. Uses of multilateral wells are common in heavy oil reservoirs and the offshore environments. Figure 1-1 shows a typical well drilled in Austin Chalk formation (Bosworth et al. 1998). Note how multilateral wells are used to maximize production rate and recovery factor while minimizing drilling costs. ERWs are long horizontal wells drilled to access reservoirs which are remote from the drill site.

Despite offering greater benefits as compared to vertical wells, inclined wells come with greater technical challenges for successful drilling of the well. Among other problems, efficient removal of drilled cuttings is especially challenging in these type of wells (Bybee 2011).

Any drilling operation consists of two major steps. The first step is breaking the rock by the action of the drill bit. The second activity is removing the debris produced by the bit from the well. However, that is easier said than done. A horizontal well has three different sections, namely near-vertical, build section, and finally the horizontal or high-angle section (Figure 1-2).

A different mechanism governs solid transport in each part of the well. The near-horizontal section is the most challenging section for efficient removal of the drilled cuttings.

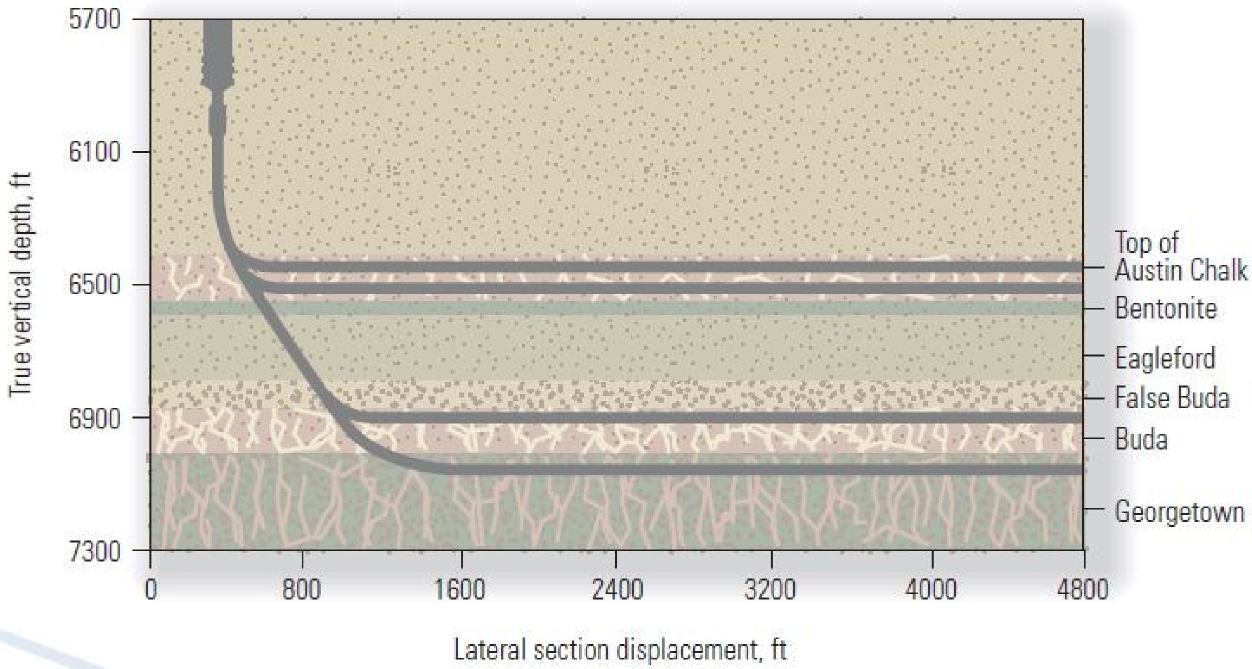

Figure 1-1 Typical Austin Chalk well in South Texas, Stacked drainholes target multiple zones to increase production rate and recovery (Bosworth et al. 1998)

In the near-vertical part of the well, cuttings settle in the opposite direction to that of the fluid velocity. Therefore, hole cleaning can easily be achieved by surpassing the settling velocity of the cuttings (Mitchell et al. 2011). In this section, increasing fluid's viscosity reduces the settling velocity. Hence, the higher viscosity is helpful in transporting the cuttings. Turbulent flow is not desirable in the near vertical sections of the wellbore. Sections of the well with inclination angle less than 10 degrees are characterized as a proximal vertical (Tomren et al. 1986, Pilehvari et al. 1996).

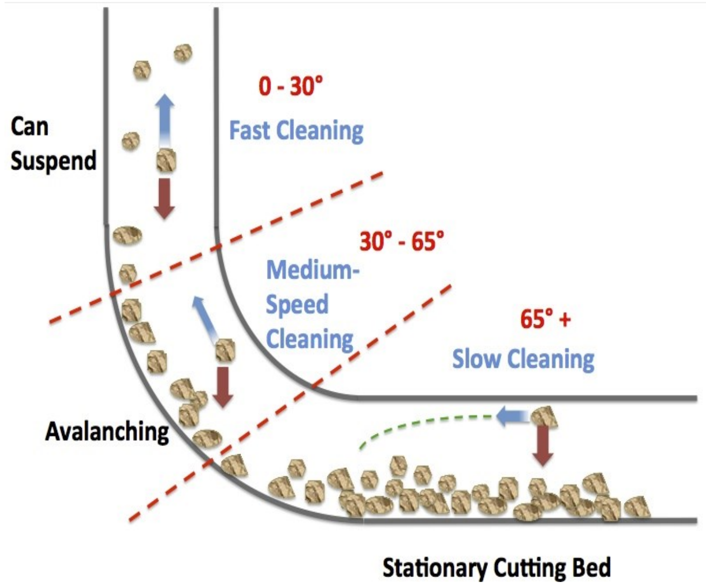

Figure 1-2 Schematic representation of different parts of a directional well[1]

Figure 1-3 shows the interaction of the fluid and solid particles in the vertical sections of a well. The average annular fluid velocity ($\overline{V_a}$) and particles settling velocity ($\overline{V_{sl}}$) is used to determine the net transport velocity of the cuttings ($\overline{V_T}$) (Bourgoyne et al. 1986).

$$\overline{V_T} = \overline{V_a} - \overline{V_{sl}} \qquad \textbf{Eq.(1-1)}$$

If $\overline{V_T}$ has a positive value, then the cuttings move upward toward the surface. Therefore, a fluid velocity higher than the cuttings settling velocity guarantees that cuttings will move upward.

[1] Source: https://agushoe.files.wordpress.com/2013/10/screen-shot-2013-09-27-at-1-41-21-am.jpg

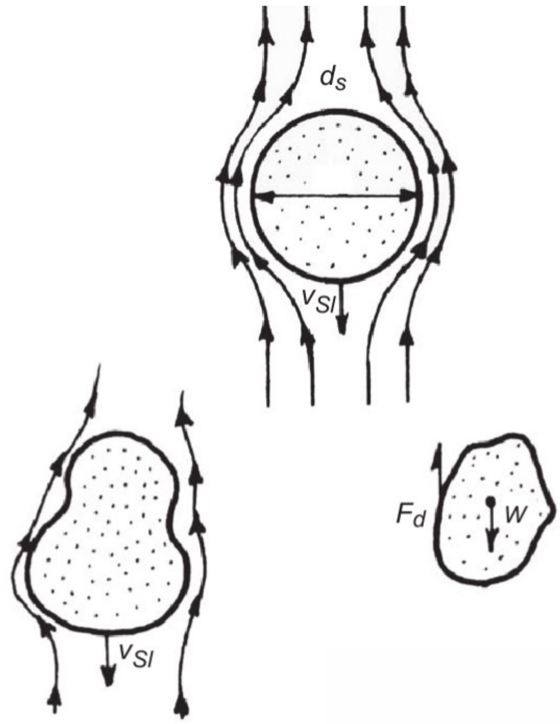

Figure 1-3 Fluid movement around a settling particle (Bourgoyne et al. 1986)

The build section is where the wellbore trajectory starts deviating from the vertical. In the build section, usually, angles between 30 to 60 degrees are experienced. In the build section, the cuttings transport efficiency is significantly reduced compared to the vertical section. Figure 1-4 schematically shows the dominating velocity vectors of cuttings and the drilling fluid in the build section. The main reason for the reduced transport ratio is the reduction in the vertical component of the fluid velocity (Ramadan et al. 2003). Formation of cuttings bed in this range of inclination is dangerous because of the so-called avalanching effect (Mitchell et al. 2011, Li and Luft 2014a). Upon pump shut down or insufficient transport of cuttings, the sand bed, can slide backward and bury the Bottom Hole Assembly (BHA) and the drill bit.

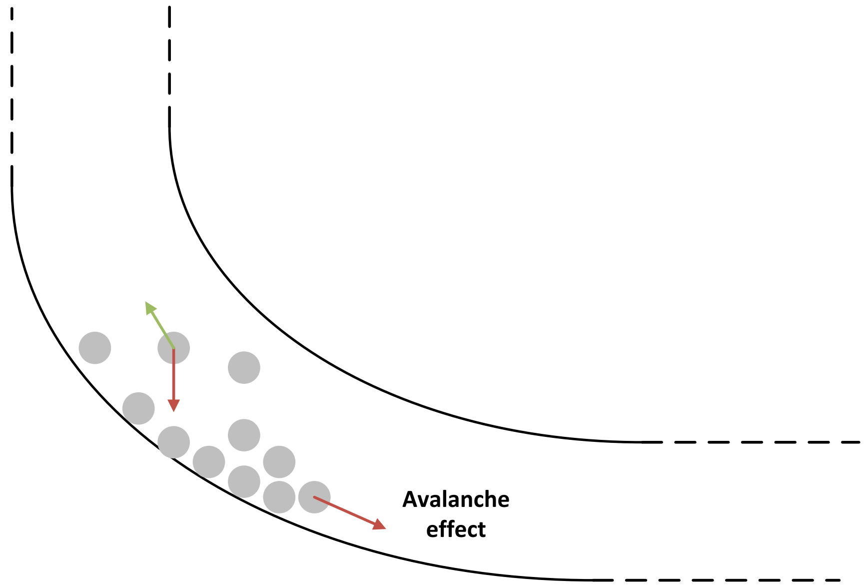

Figure 1-4 Solid transport in the build section of a horizontal well

In the near-horizontal section, cuttings settling velocity is perpendicular to the fluid velocity (see Figure 1-5). Cuttings have thousands of feet to travel before reaching the surface (World record for horizontal drilling as of 2013 is 38415 ft[2]). On the other hand, they have only a few inches to travel before getting trapped in the low-velocity zone near the bottom of the wellbore. Hence, the formation of cuttings bed is inevitable. Once cuttings leave the main flow and reach the low-velocity zone near the bottom, they form a cuttings bed. The avalanche effect does not occur in this range of inclinations. However, other problems arise due to the presence of a stationary sand bed in the annulus. High torque, high friction, difficulty in the running casing, premature bit wear, low ROP and in severe cases pipe sticking can all be experienced due to poor hole cleaning (Nazari et al. 2010, Li and Luft 2014a, Li and Luft 2014b). Figure 1-6 schematically shows a pipe sticking cases due to poor hole cleaning.

[2]Source: http://petrowiki.org/Extended_reach_wells

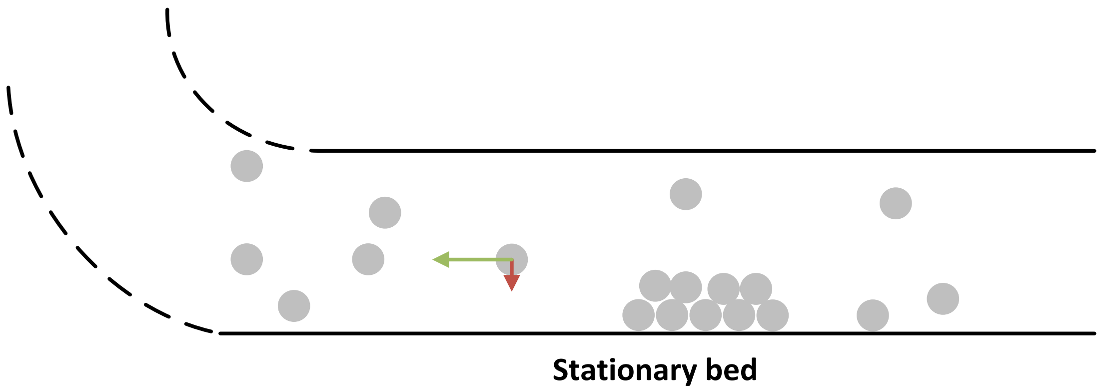

Figure 1-5 Solid transport mechanism in the horizontal part of an inclined well

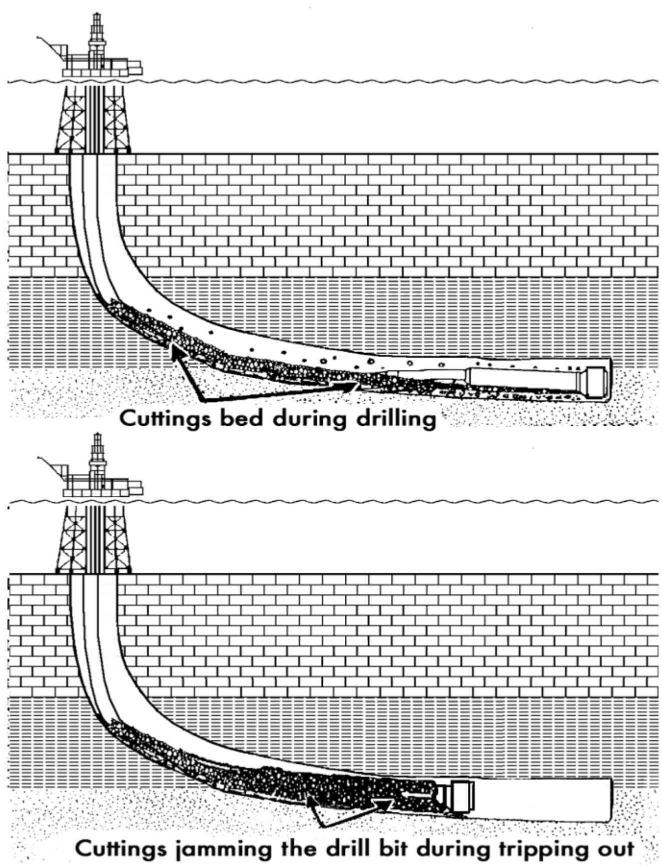

Figure 1-6 Mechanical Pipe sticking due to poor hole cleaning[3]

Despite significant progress made in drilling fluids, tools, and field practices, along with more than 50 years of university and industry research, field experience indicates that hole cleaning is still a major problem on most highly inclined and horizontal wells (Li and Luft

[3] Source: http://petrowiki.org/File%3ADevol2_1102final_Page_436_Image_0001.png#file

2014a, Li and Luft 2014b). Although solids entrainment and deposition mechanisms have been studied extensively over the years, our understanding of fluids-particle interactions near bed interface is still limited. Progress toward such understanding has been relatively slow because of the difficulties inherent in the simultaneous measurement of local solids transport and adjacent near-bed fluid flow.

In the field, once the height of the stationary sand bed reaches a critical value or before running the casing, the stationary sand bed must be removed. This operation is often called hole cleaning. Hole cleaning is done by circulating the drilling fluid down the drill string and up the annulus to sweep the cuttings bed out of the wellbore. Hole cleaning is important from two perspectives. First, from the economic point of view, hole cleaning is a non-productive time in term of drilling. Following equation is the cost per foot equation often used for optimizing drilling operations. In this equation, C_b is the bit cost, C_r is the rig cost per day, t_b is the time that bit is working, t_t is the trip time, t_c is the connection time, and t_{others} is all the other times that the drill bit is not working. F is the footage drilled and C_f is the final cost per foot for the drilling operation (Bourgoyne et al. 1986). The time spent on hole cleaning falls under the t_{others}.

$$C_f = \frac{C_b + C_r(t_b + t_c + t_t + t_{other})}{F} \quad \textbf{Eq.(1-2)}$$

According to this equation, to minimize the drilling cost, the total time of drilling must be kept to a minimum. Therefore, minimizing the hole cleaning time is the key to reducing the drilling costs. According to a new report by Anders Brun et al. (2015), drilling and completion costs between 40 to 50% of the initial investment for exploration, development, and production of oil fields. In offshore drilling, almost 50% of the drilling cost is associated with non-productive times. Therefore, according to this report, the drilling cost can be cut down by nearly 50% in offshore drilling by minimizing the non-productive times.

Another report showed in the Gulf of Mexico NPT index reaches almost 40% of the total drilling time. The cost of NPT is about 60-70 million dollars per rig annually (Negrao 2009). A major part of this NPT is related to hole cleaning. Therefore, the faster this process can be performed; the more time can be spent in drilling, hence, substantially lowering costs.

In addition to the economics of the operation, hole cleaning is a major technical challenge. It must be performed in a safe and timely manner, otherwise, not only it could increase the drilling cost it could result in other problems.

Interaction of drilled cuttings and the drilling fluid governs the efficiency of the cuttings bed removal. The momentum exchange between the phases (cuttings as the particulate phase and drilling fluid as the fluid phase) depends upon many different factors which we will discuss briefly. The critical parameters controlling efficiency of hole cleaning operation could be classified into three main groups. These groups are operational parameters, fluid related factors, and cuttings properties. Figure 1-7 schematically shows different factors that affect cuttings removal and their level of importance and controllability in the field.

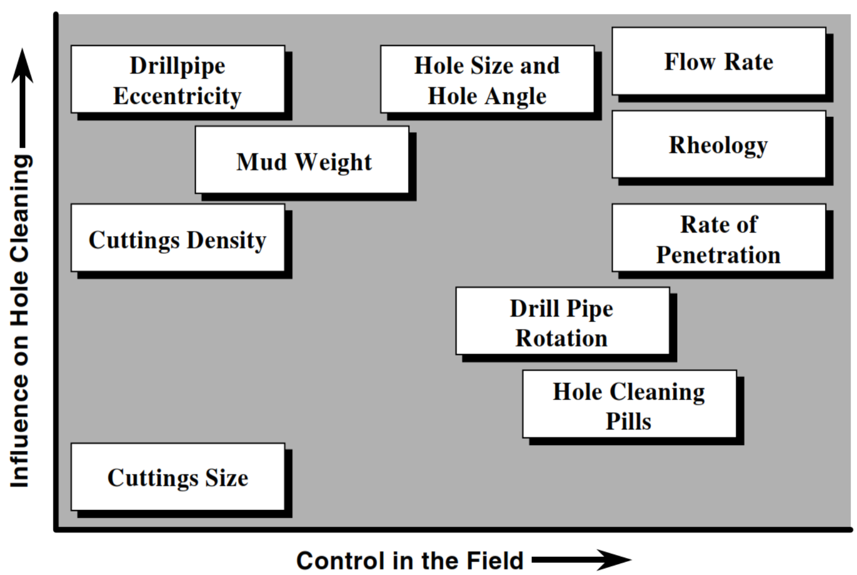

Figure 1-7 Parameters affecting cutting transport in oil wells (Adari et al. 2000)

The operational parameters include inclination angle, inner pipe eccentricity, flow rate, and drill pipe rotation. The flow rate (or annular fluid velocity) has the most profound impact on the bed removal (Mitchell et al. 2011). The higher the flow rate, the better the cuttings removal would be (Azar and Sanchez 1997). However, there are limitations on the use of flow rate as an effective tool for hole cleaning. The first limitation is imposed by the capacity the mud pump. The so-called operating window imposes the second constraint. The operating window is the range of pressure between the pore pressure and formation fracture pressure (Mitchell et al. 2011). In an overbalanced drilling, the mud pressure in the annulus must be greater than pore pressure to prevent formation fluid from in-fluxing into the wellbore. On the other hand, the drilling fluid pressure should not exceed the fracture pressure of the formation, or otherwise, loss circulation would occur. The Equivalent Circulating Density (ECD) is especially a limiting factor in ERWs because these wells are deep and frictional pressure loss is huge in these wells.

The drillstring typically lays against the borehole wall due to the force of gravity (i.e. annulus is eccentric). Eccentricity has been proven to adversely affect hole cleaning (Thomas et al. 1982, Nazari et al. 2010). The main reason has been reported as the reduction of fluid velocity in the narrower gap of the annulus. The narrow gap is usually where the cuttings tend to accumulate.

Inner pipe rotation positively affects the bed removal process through mechanical agitation of the settled sand bed (Mitchell et al. 2011). It is recommended to use the pipe rotation whenever possible. However, pipe rotation is not available when using the downhole motor for rotating the bit (i.e. in coiled tubing drilling) (Leising and Walton 2002, Kelessidis and Bandelis 2004a, Li et al. 2008).

Cuttings related factors that affect hole cleaning are their size, size distribution, and their density. A higher density drilled solid is harder to remove because it settles easier and faster. Drill cuttings can have a broad size distribution, ranging from a couple of hundreds of microns to several centimeters; what controls the size of drill cuttings is the weight on bit (WOB) and the type of the bit (Roller Cone Bits vs. PDC bits) (Leising and Walton 2002). However, in the field, there is little control over these parameters. Comparing to other factors, particles' size has minimal impact on hole cleaning.

The final group of variables that control solid transport in oil wells is the fluid related factors. This category includes fluid density and fluids rheological characteristics. A higher fluid density has a positive impact on bed erosion because it reduces the effective weight of the (buoyed weight) cuttings (Martins and Santana 1992, Mitchell et al. 2011). However, similar limitations to that of pump flow rate apply to fluid density as well (ECD limitation).

Rheological characteristics of the drilling fluid have a profound impact on the solid removal process. They present efficient tools for enhancing hole cleaning because they are easily controllable in the field. Its influence on cuttings removal is rather complicated. The right rheological properties can aid the solid transport and bed removal (Nazari et al. 2010). We will discuss the role of fluid's rheological properties in greater detail in the next section.

In summary, Horizontal and directional wells are imperative in developing offshore fields as well as unconventional resources such as oil sands. Efficient hole cleaning strategies need to be developed to reduce the time associated with hole cleaning. The shorter the hole cleaning time, the more time can be spent on actual drilling and, as a result, a significant reduction in the drilling cost can be attained. Delivering oil wells at lower costs is essential in ensuring accessibility of reserves, which otherwise is not economically sound to exploit. That applies to periods of low oil price.

1.2. Statement of the problem

Since the advent of directional wells, researchers have focused on studying and improving hole cleaning process. The earlier studies were mostly focused on the idea of finding the critical depositional velocity (CDV) (Larsen et al. 1997, Li and Luft 2014a, Li and Luft 2014b). CDV is a velocity which keeps all the cuttings moving toward the surface (i.e. no stationary bed forms). Given the fact that annular fluid velocity is the primary factor in preventing the formation of cuttings bed in the wellbore, many studies have shown even at highest attainable velocities in highly inclined wells it is impossible to avoid the formation of a stationary bed. For conventional drilling, the annular fluid velocity is almost twice as high as that of the coiled tubing drilling (CT) (Li and Luft 2014b). For an average velocity in conventional drilling (less than2 m/s, (Li and Luft 2014b)) or CT operation (less than1.5m/s, (Kelessidis et al. 2002)) formation of a cuttings bed is inevitable. Zhang (2014) experimentally showed that at annular velocities of 1.56 m/s stationary cuttings bed form (for a fully eccentric annulus and a non-zero ROP). Ozbayoglu et al. (2010a), (2010b) study revealed that stable bed forms for annular velocities less than 1.83 m/s. They reported a minimum velocity of 2.44 m/s is required to keep all the cuttings moving (CDV). Li and Luft (2014a) based on previously published data, concluded that at least a minimum velocity of 2.74 m/s is required to establish a no bed condition in an eccentric annulus. Therefore, from previous studies, it becomes clear that formation of a stationary cuttings bed in highly inclined wellbores is inevitable. The problem is more severe for CT intervention because annular fluid velocity is almost half of that encountered in conventional drilling and there is no pipe rotation to help the process.

Once the stationary cuttings bed height reaches a critical value, a level at which the bed height would start to interfere with the drilling operation, hole cleaning must be performed. This cleaning can be carried out in several different ways. Circulating the drilling fluid while the drillstring is stationary (stationary circulation mode), or circulating the fluid while the drill string is rotating (this is only available in conventional drilling and not in CT operation) are two of the possible scenarios. Hole cleaning can be done while the drillstring is pulled out of the hole (back reaming while the drill bit is rotating or wiper trip in CT) (Li and Luft 2014a). In CT operations, the drillstring is stationary, and therefore, only wiper trip mode and stationary circulation mode can be used. Nevertheless, If the minimum hydraulic requirements for bed erosion are not achieved in any of the modes, the fluid circulation can be a waste of time, money, and may even be detrimental to the borehole stability. Hole cleaning is not limited to the drilling operations. In hydraulic fracturing, the stationary sand bed formed by the proponent must be removed after the operation. In this case, only stationary circulation mode can be used (Li and Luft 2014a, Li and Luft 2014b).

The worst-case scenario for hole cleaning is the stationary circulation mode. In this mode, there is no pipe rotation and or wiper trip to aid the removal of the cuttings. Hence, if the efficient hole cleaning could be achieved under these circumstances, they could be sufficiently applied in the other modes of hole cleaning as well. The central scheme of this study is on the hole cleaning under stationary circulation mode. Therefore, from this point on, hole cleaning refers to removal of a settled sand bed in the annulus without pipe rotation unless otherwise is specified.

The complexity of hole cleaning process is several folds. First of all, the flow is usually turbulent, and hence, a theoretical solution to the problem is not reachable. Secondly, the coupling of the phases (solid-fluid) is typically a four-way coupling. The four-way coupling means the fluid phase and the particulate phase both affect each other in term of flow. Additionally, the cuttings also interact with each other. Interaction of phases (momentum exchange) is complex and is not well understood. The complexity increases due to the non-uniform size distribution of irregular shaped solid particles generated by the drill bit. Finally, the fluid is of non-Newtonian nature. All of these reasons have forced the researchers to focus on this problem using experimental studies or simplified mechanistic and semi-mechanistic models.

Despite the existence of a massive body of research in drilling literature on the topic of cuttings transport and hole cleaning (Pilehvari et al. 1996, Nazari et al. 2010, Li and Luft 2014a, Li and Luft 2014b), almost all of these studies investigated the problem in what we can call “an integral” approach. That is these studies usually alter one parameter (e.g. fluid viscosity) and observe its impact on the indicators of proper hole cleaning as the measure of its impact on the process (e.g. total solids concentration in the system).

Currently, mainly empirical or semi-empirical correlations or even some rule of thumbs (e.g. to clean the well, pump 2-3 times the hole volume) are used for performing hole cleaning (Li and Luft 2014a). The performance of these models is often poor. Unjustified and over-simplification of the interaction of the fluid-particle is the main reason for the limiting performance of these models. Researchers and field engineers are often forced to make assumptions and simplifications due to lack of knowledge of fluid related parameters in the wellbore. The empirical models also have a narrow range of applicability. The range (e.g. borehole size, or eccentricity) of applicability is forced by the original data which was used for development of these models. According to Mitchell et al. (2011), there is a need for developing comprehensive cuttings transport models that can be verified by the experimental data.

During any hole cleaning operation, one of the most important factor parameters that the operators have to make sure is satisfied just is that the flow rate in the wellbore, which should be sufficiently high enough to erode the bed. The flow rate at which bed erosion starts taking place is known as the critical flow rate. If the critical flow rate is not achieved, the bed erosion will not take place and the circulation could be a waste of time, money, and may even be detrimental to the wellbore stability.

There have been few experimental studies in which the critical flow rate of the bed erosion has been the main focus of interest (Brown et al. 1989, Ford et al. 1990, Duan et al. 2008, Corredor et al. 2016). The critical flow rate of bed erosion has also been the subject of the mechanistic hole cleaning models. The mechanistic approach typically tries to predict the state of a particle movement (i.e. stationary vs. moving) in the cuttings bed using the force balance (Clark and Bickham 1994, Ramadan et al. 2003, Duan et al. 2007). Figure 1-8 shows a simplified 2-D sketch of the bed interface. In the mechanistic modeling of hole cleaning, the state of the particle of interest is predicted using the net force acting on it. The particle is subjected to forces of two types; resistive and mobilizing forces. The first type includes gravity (buoyed weight of the particle), friction, and van der Walls force (Duan et al. 2007). Resistive forces are trying to keep the particle in its place, and hence, they are called resistive forces. The mobilizing forces are the fluid hydrodynamic forces which seek to remove the cutting.

The easiest path for the particle in Figure 1-8 to move is to roll along the bed interface. The necessary condition for this to happen is that the moment produced by the fluid hydrodynamic force on the particle around the pivoting point surpasses the moment generated by the resistive forces.

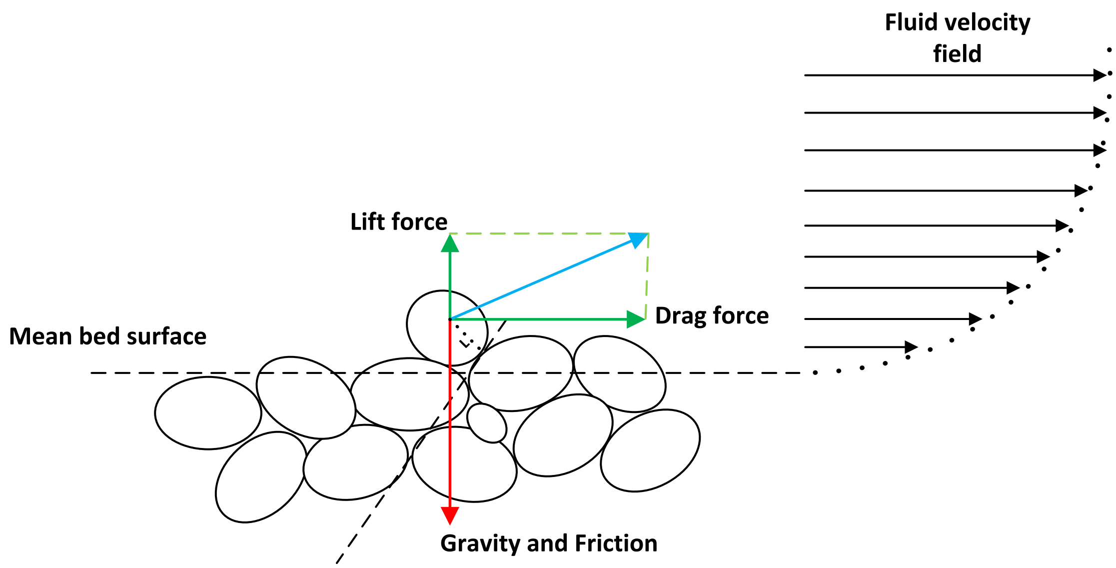

Figure 1-8 Schematic representation of forces acting on a particle in the cuttings bed

For simplicity, we assume that all the forces that are acting on the particle of interest in Figure 1-8 are acting through the center of the mass of that particle. Therefore, the following equation represents the necessary condition for the dislodgement of this sand particle from the sand bed.

$$(F_D + F_L + F_b)L > \left(F_g + F_F + F_{Van}\right)L \qquad \textbf{Eq.(1-3)}$$

In the Eq.(1-3) the left-hand side represents the moment produced by the mobilizing forces around the pivoting point. The right-hand side is the moment generated by the resistive forces. This equation or a similar force balance is the foundation of the mechanistic hole cleaning models.

Although the mechanistic approach in predicting bed erosion has a sound physical background, the outcome of such models is often impaired due to over-simplification of the interaction of phases. To be able to estimate different forces, knowledge of several flow related quantities are necessary. The hydrodynamic fluid force (drag and lift), which is the main force in mobilizing the cuttings, depends on the local fluid velocity near the bed interface. Eq.(1-4) and Eq.(1-5) are the correct equations for calculating the fluid drag and lift force on the particle in the bed. The fluid velocity in these equations is the instantaneous local fluid velocity near the center of gravity of the particle of interest.

$$\hat{F}_D = \frac{1}{2}\rho_f A_p C_D \hat{u}^2 \qquad \textbf{Eq.(1-4)}$$

$$\hat{F}_L = \frac{1}{2}C_L \rho_f A \hat{u}^2 \qquad \textbf{Eq.(1-5)}$$

The local fluid velocity near the interface of the sand bed is not easy to estimate accurately. Often researchers treat the flow near the bed similar to flow near a rough wall (Ramadan et al. 2003, Duan et al. 2007). Such assumption has not been tested using any independent measurement of fluid velocity profiles near the bed interface. Additionally, treating the flow similar to flow near rough walls requires knowledge of the equivalent sand grain roughness height and friction velocity. The roughness height is usually assumed to be equal to the particles size in the bed. However, studies of sediment transport in channels have revealed the equivalent sand bed roughness may vary considerably depending on the interaction of the bed particles and the fluid. Therefore, there is a high level of uncertainty involved in estimation of the local fluid velocity near the interface of the sand bed.

In addition to the difficulties and uncertainties in estimating the local fluid velocity near the bed, many studies have shown fluid force on the particles can significantly vary in turbulent flows (Diplas et al. 2008, Heyman et al. 2013). Diplas et al. (2008) have shown experimentally that fluctuations in velocity are critical in transporting sediment particles. Hence, in the development of mechanistic models turbulence needs to be considered.

As mentioned earlier, almost all of the previous attempts in studying hole cleaning can be labeled as an integral or macroscopic approach. In this method, often one parameter is varied, and its impact on the entire system is monitored. For instance, pipe rotation speed is changed, and its impact on the overall concentration of cuttings or the height of the stationary sand bed in the well is studied. The macroscopic approach does not provide much information on the local, instantaneous interaction of fluid-particle in the system. Hence, studies under this category do not provide any useful information for mechanistic or semi-mechanistic hole cleaning models. The macroscopic approach provides rather general guidelines for the field engineer to perform the hole cleaning in a more timely manner. The results of such studies are often used in the development of empirical models (e.g. the model developed by Larsen et al. (1997)).

The opposite of the integral or macroscopic approach is what we call a “microscopic” approach. In the microscopic approach, the local variables are of interests rather than overall features of the system. Examples of a microscopic variable would be the local fluid velocity over the cuttings bed. The macroscopic counterpart of local velocity is the pump flow rate. Pump flow rate only provides qualitative measures of cuttings bed removal. On the other hand, local fluid velocity gives information on the interaction of the particles and the fluid at small time and length scales.

Examples of macroscopic studies of hole cleaning are numerous (Brown et al. 1989, Larsen et al. 1997, Martins et al. 1997, Corredor et al. 2016). However, the drilling literature is not rich on the microscopic studies of hole cleaning. Few attempts have been made for quantifying hard-to-measure parameters such as local fluid velocity in slurry transport (Rabenjafimanantsoa A. H. et al. 2007, Rabenjafimanantsoa 2007, Zeinali et al. 2012). However, these studies were not conducted in annular geometry.

Overall, one of the fundamental problems in the hole cleaning studies is the lack of microscopic studies which can shed light upon the actual fluid-particle interaction in the wellbore. Such knowledge seems necessary from several perspectives. First, such study would provide the accurate and robust foundation for the development of more realistic mechanistic and semi-mechanistic hole cleaning models. Secondly, it provides valuable data that is much-needed for validating current numerical models. In recent years the number of studies using Computational Fluid Dynamics (CFD) has risen significantly (Bilgesu et al. 2007, Li and Luft 2014b, Akhshik et al. 2015). Thanks to the improvement in computing capabilities as well as improvement in numerical codes, CFD is replacing costly experimental works. However, validation of these models is often problematic due to lack of reliable experimental data.

Part of the reason that there is not that many microscopic investigations of fluid-particles interaction in wells are that conducting such measurements is difficult. It is only recently that such measurements became possible with the advent of non-intrusive measurement techniques such as PIV and PTV. Optical techniques require transparent flow loop facilities along with expensive measurement devices. Something that is not available widely.

In addition to the difficulties and shortcomings mentioned so far, the complex rheological characteristics of the drilling fluid also make the formulation of the hole cleaning process is complicated. The term rheological properties are often inadvertently used interchangeably with the non-Newtonian fluid viscosity in the drilling literature. The non-Newtonian fluid viscosity is only of the viscometric functions that describe the behavior of a complex fluid. Fluid viscoelastic properties along with other material functions are needed for more accurate representation of the non-Newtonian fluids commonly used in oil and gas well drilling. In this context, the number of studies considering the actual role of fluid's rheological properties on the hole cleaning are not many.

Fluid viscoelasticity has been found to have a major influence on cuttings settling characteristics (Gomaa et al. 2015, Khatibi et al. 2016, Arnipally and Kuru 2017). Viscoelasticity reduces the settling velocity and enhances the drag on the particles. Therefore, viscoelasticity could be a desirable property for transporting cuttings in suspension. However, its influence on bed erosion is the opposite. It does delay the bed erosion. Several researchers have attempted to explain the hindering of bed erosion by elastic fluids (Saasen 1998, Saasen and Løklingholm 2002, Ytrehus et al. 2015, Werner et al. 2017). However, to this date, there is no viable explanation for such phenomenon.

In the drilling literature, there are numerous studies in which influence of fluid's viscosity on hole cleaning have been discussed. In the context of the bed erosion, almost all studies point out to the negative impact of fluid's viscosity on the critical flow rate of bed erosion. However, previous studies do not offer any insight into the cause of the increase in the minimum flow rate due to fluid's viscosity. Traditionally this negative side effect of polymer additives is associated with a reduction of flow turbulence (Azar and Sanchez 1997). Nonetheless, such claims have never been tested using reliable measurements of flow turbulence.

Recent studies in cuttings transport have revealed that viscoelastic properties of drilling fluid are more important than its apparent viscosity (Tonmukayakul et al. 2013, Gomaa et al. 2015, Werner et al. 2017). These finding further add to the complexity of the role of fluid rheological properties on hole cleaning. Since viscoelastic properties of drilling fluid are not typically measured, it difficult to associate most of the previous studies of hole cleaning to these properties of the drilling fluid.

A new research result on the influence of settling velocity in viscoelastic fluid suggests that elasticity gives rise to a new fluid force on the particles. This new elastic force is created due to non-zero normal stress differences in this type of fluids. Tonmukayakul et al. (2013) presented a new method for evaluating particle settling velocity in viscoelastic fluids for hydraulic fracturing operations. The authors identified the importance of non-zero normal stress differences in inhibiting particle settling velocity in viscoelastic fluids. They presented the following equation for estimating the settling velocity of particles in viscoelastic fluids:

$$V_s = \frac{2\alpha^2}{9\mu(\dot{\gamma})}\Delta\rho g - \frac{2\alpha}{3}\frac{\alpha|N_1(\dot{\gamma})|}{\mu(\dot{\gamma})} \qquad \textbf{Eq.(1-6)}$$

In Eq.(1-6) α is a parameter related to the strain induced by the weight of the particles. N_1 is the normal stress difference and will be discussed thoroughly in chapter 8. This equation shows that the non-zero normal stress differences in the flow causes a reduction in the settling velocity of the particles. The importance of the presented equation by Tonmukayakul et al. (2013) is that it acknowledges the presence of an additional elastic force on the particles due to non-zero normal stress difference.

The elastic fluid force is well presented in hole cleaning operations when using elastic polymer fluids. However, its role in the delaying the onset of bed erosion and the extent of its impact are not known. Only measurements of local fluid velocity and flow turbulence can reveal the real influence of the elasticity on bed erosion.

To summarize, the biggest problem in the hole cleaning studies is the lack of reliable data on the interaction of fluid-particles in the wellbore at small time and length scales. Such data is the key to the development of realistic solid transport models, including mechanistic and semi-mechanistic models. Additionally, only measurements of local variables such as fluid velocity and flow turbulence can reveal the impact of fluid rheological characteristics on the solid removal process. The improvement in CFD codes also necessitates reliable experimental data for validation of computer models.

1.3. Objectives of the study

The main purpose of this work is to conduct a detailed experimental study of solid transport in horizontal wells under stationary circulation mode. A comprehensive study includes investigating the problem from both macroscopic and microscopic approaches. The ultimate goal of the research is to present a better understanding of the interaction of fluid-particles in the wellbore. Additionally, we are interested in identifying the cause of different interaction between various fluid types (i.e. Newtonian vs. non-Newtonian) and drilled cuttings.

Several questions have been designated as the key issues that need to be investigated in detail to achieve the objectives of this study. These key issues are:

1. How does the presence of a stationary sand bed affect the fluid flow in the wellbore?
2. How does local fluid velocity profiles varies near the interface of a stationary or moving sand bed?
3. How does the turbulence in the primary phase affect the particles in the bed?
4. How does the moving sand particles interact and modify the primary phase flow field?
5. How does changing fluid rheological characteristics affect the interaction of phases in the well?
6. What is the cause of the delayed bed erosion by polymer fluids?
7. How does the critical flow rate of bed erosion vary for a different combination of drilled cuttings size and fluid type?

To answer question six, hole cleaning experiments were carried out in the so-called macroscopic framework. The impact of drilling fluid's viscosity and cuttings size on the minimum flow rate of bed erosion is of interest in this phase. Therefore, the experiments conducted in this phase of the research provide data for the stationary circulation mode of hole cleaning. It also helps in better understanding of the extent of importance of cuttings size and fluid's viscosity on the critical flow rate of bed erosion. Finally, the results of macroscopic experiments are analyzed to identify the dominant factors controlling bed erosion. The parameters that have the greatest impact are then chosen for further examination with the microscopic method.

The objective of the second part of the research is studying hole cleaning in a microscopic framework in both eccentric and concentric annulus. Non-intrusive measurement technique (PIV) is used to explore the interaction of drilling fluid and drill cuttings at the small time and length scales.

The specific aims tasks of the second part of the current research study are i-) to implement the PIV technique to study fluid flow in the annulus that contains a cuttings bed. ; ii) Using PIV measurement to obtain near bed velocity profiles and other turbulence related parameters, which then can be used to investigate the impact of the presence of a cuttings bed on turbulent flow in the wellbore. The analysis can help in better understanding of the coupling of the fluid/solid phases. It also provides insight into local velocity profiles and roughness data that is required in mechanistic hole cleaning models.

The role of fluid's rheological characteristics on particles removal from bed deposits is the focusing point of this research. To achieve this goal, we conduct experiments using polymer fluids. The polymer additive being used is representative of a typical viscosifier agent utilized in the field. Complete characterization of the fluids rheological properties is conducted using a high-resolution rheometer. Further investigation into the influence of fluid rheological properties on cuttings bed erosion is carried out using PIV data as well as other measurements such as frictional pressure loss.

1.4. Contributions of the Research

The main contributions of this research could be summarized in the following points:

1. Developed an understanding of the overall impact of fluid's rheological properties on cuttings bed erosion in horizontal wells
2. Developed an empirical correlation that relates critical Shield's stress to particles Reynolds number in the cuttings bed that could be used for prediction of minimum flow rate required for the onset of bed erosion
3. Implemented and documented the procedure on using PIV technique for hole cleaning studies including designing a unique calibration technique
4. Conducted PIV experiments in both eccentric and concentric annulus with cuttings bed of different heights
5. Quantified the role of flow turbulence on cuttings bed erosion in hole cleaning
6. Identified the role of non-zero normal stress differences in flow of viscoelastic fluids as the main cause of delayed bed erosion by polymer fluids
7. Studied velocity profiles near cuttings bed interface in turbulent flow and quantified the roughness elements height
8. Quantified the impact of presence of the cuttings bed on the flow turbulence
9. Investigated the impact of the bedload transport of cuttings on bed roughness and the flow turbulence which is of importance in developing mechanistic hole cleaning models
10. Evaluate the difference between average friction factor and interfacial friction factor
11. Calculated interfacial friction factor during hole cleaning using PIV data
12. Conducted a thorough experimental study on the critical flow rate and shear stress using different combination of drilling fluid and cuttings size
13. Invalidated the use of available turbulence models for modeling turbulent flow of non-Newtonian fluids which are often used for modeling mud flow
14. Developed an accurate database of fluid flow in concentric and eccentric annulus for future use in validating CFD and other computer models

Among all the achievements of this study, the most notable ones are the identification of the role of fluid's viscoelastic properties on hole cleaning and presenting information about flow related factors such as local fluid velocity profiles , turbulence shear stresses, axial and radial turbulence intensity affecting the cuttings removal from the bed deposits in horizontal wells. The former is important because for the first time in the drilling literature complex nature of stress tensor of viscoelastic fluids is used to explain the delay of the particle removal from the bed deposits that is observed in hole cleaning using viscoelastic fluids.

Documenting related flow parameters such as local velocity profiles, equivalent bed roughness height, and turbulence related factor is important because such data do not exist in the literature for flow in wellbores. These data provide powerful tools for those who intend developing mechanistic hole cleaning models. Additionally, these data provide much-needed experimental evidence for verification of numerical simulation such as CFD models.

1.5. Structure of the thesis

This manuscript is organized in 13 different chapters. The first chapter is the introduction and is intended to give a brief overview of the subject under investigation. In the introduction, the problem of cuttings transport is introduced briefly in the overview section. Following that statement of the problem is made. Objectives of the study are discussed in chapter 1 as well. Finally, a brief list of the notable contributions of the current work is discussed in chapter 1.

Chapter 2 presents a review of the available literature pertinent to the issue of cuttings transport in deviated wellbores. In this chapter, the effort was to summarize as much as possible material that can help in better understanding of analysis that follows in other sections. The literature review chapter is subdivided into different sections to separate different topics. In this chapter, there is a specific section reviewing past works on the impact of viscoelasticity on solid transport and bed erosion. Additionally, a section is devoted to CFD studies in the drilling industry. This section helps those readers who wish to go through chapter 12 of the thesis.

Chapter 3 discusses the methodology and test procedures which have been used in the present work. This chapter summarizes the details about PIV and calibration procedure that have been used. It also discusses rheology measurements and addresses the limitations and inherent errors in these systems.

Chapters 4 to 12 report the findings of the current study. Since experiments have been conducted in both concentric and eccentric annulus in this study, we first present the results obtained in the concentric case. Chapters 4 to 8 are the results collected in the concentric configuration. Following chapters discuss the results of experiments conducted in the eccentric case (chapters 9, 10, and 11). The order of chapters is in such a way that first, we present the results for the flow of water as the baseline scenario. Following that, results obtained using polymer fluids are discussed. Additionally, we first examine the aspects of flow in the annulus from a fluid mechanic point of view. In separate chapters, the results are analyzed with specific reference to solid transport in oil wells.

Chapter 4 of the thesis reports the results of the PIV experiment carried out to investigate the impact of the presence of a stationary cuttings bed on the turbulent flow of water in the annulus. The results and discussions in this chapter present local fluid velocity and turbulence properties of the flow in the concentric annulus that contains erodible sand beds. Properties such as variations of equivalent roughness height of the sand bed and flow turbulence are thoroughly discussed in this chapter.

Chapter 5 summarizes the findings on the turbulent flow of polymer fluids in the concentric annulus in the presence of cuttings bed. The structure of this chapter is similar to chapter 4. However, the data are collected using non-Newtonian fluids. The focus of chapters 4 and 5 are more on the overall impacts of the presence of a stationary sand bed on characteristics of the flow. The results are directly usable by other researchers for validation of computer and CFD models.

Chapter 6 is the product of the macroscopic study of hole cleaning that has been conducted in this work. In this chapter, the results of measurements conducted for quantifying the onset of bed erosion using a combination of different drill cuttings size and fluid viscosity is discussed. The parameters addressed in these chapters are not in term of local variables. Instead, frictional pressure loss and flow rate are measured to quantify the minimum flow rate of bed erosion. The analysis presented in this chapter has resulted in two empirical correlations for estimation of the critical flow rate of bed erosion.

In chapter 7 of the manuscript, we discuss the impact and importance of flow turbulence in solid bed removal. Using the PIV data, the results and discussion in this chapter critically analyze the current assumptions and shortcomings in the mechanistic and semi-mechanistic solid transport models in horizontal wells. The results highlight the areas in which improvements are needed for better modeling the interaction of fluid-particles during solid transports in horizontal wells.

The PIV data for turbulent flow of polymer fluids over sand beds are used in chapter 8 to explore the impact of fluid rheological characteristics on solid's bed removal. In particular, the viscoelastic properties are studied and discussed in detail in this chapter. It is indicated in this chapter that non-zero normal stress differences in the flow of viscoelastic fluids are a major factor in delayed bed erosion by polymer additives.

Chapters 9, 10, and 11 are the results of tests conducted in the eccentric configuration. Essentially, similar experiments to the ones carried out in concentric annulus have been done in the eccentric annulus. As mentioned earlier, the eccentric annulus with no pipe rotation is the worst case scenario for hole cleaning operations. Therefore, to consider the problem comprehensively both configurations of the annulus have been tested.

Chapter 9 summarize the results of the PIV experiments conducted to study the turbulent flow of water in the eccentric annulus over stationary solid beds of different initial heights. The velocity profiles in wall unit are presented and analyzed for assessment of equivalent sand bed roughness height. Additionally, other topics dealt with in this chapter include average and interfacial friction factor which are of importance in the hydraulic design of the drilling operation and solid removal modeling respectively. The interfacial friction factor is evaluated using PIV data.

Chapter 10 is devoted to discussing the PIV results of water flow over sand beds in the eccentric annulus. The data and discussions in this chapter are essentially supplementary to the data presented in chapter 9. The impact of the presence of the sand bed on flow turbulence is analyzed in two cross-sections of the annulus. The impact of bedload transport of particles on flow turbulence is also investigated in this chapter.

In chapter 11, we discuss the results of PIV experiments for turbulent flow of polymer fluid over sand beds in the eccentric annulus. The discussion considers the impact of bed roughness on the universal velocity profiles near the bed interface. Additionally, measurements of turbulence properties such as Reynolds shear and normal stress are presented in this chapter. The results in this chapter can help in the more realistic development of mechanistic solid transport models by non-Newtonian fluids.

In chapter 12 we present the result of a CFD work that was done to study the applicability of available turbulence models in simulating the turbulent flow of non-Newtonian fluids in horizontal wells. The primary motivation of this work was to assess the reliability of the published CFD models of hole cleaning operation in the literature. The results invalidate most of the previous CFD studies in this area.

Finally, chapter 13 summarizes the main conclusions of this work. Some suggestions for future studies of the topic of cuttings transport and hole cleaning are also made in this chapter.

1.6. References

Aadnøy, B. S. (2015). Technology Focus. Journal of Petroleum Technology **67**(5): 114.

Adari, R. B., Miska, S., Kuru, E. et al. (2000). Selecting Drilling Fluid Properties and Flow Rates For Effective Hole Cleaning in High-Angle and Horizontal Wells. SPE Annual Technical Conference and Exhibition. Dallas, Texas, 1–4 October 2000., SPE-63050-MS,DOI: 10.2118/63050-MS.

Akhshik, S., Behzad, M. and Rajabi, M. (2015). CFD–DEM approach to investigate the effect of drill pipe rotation on cuttings transport behavior. Journal of Petroleum Science and Engineering **127**(0): 229-244, DOI: http://dx.doi.org/10.1016/j.petrol.2015.01.017.

Anders Brun, Aerts, G. and Jerkø, M. (2015). "http://webcache.googleusercontent.com/search?q=cache:rYzruPDpEeMJ:www.mckinsey.com/~/media/McKinsey/dotcom/client_service/Oil%2520and%2520gas/PDFs/How%2520to%2520achieve%252050%2520percent%2520reduction%2520in%2520offshore%2520drilling%2520costs.ashx+&cd=1&hl=en&ct=clnk&gl=ca." Retrieved July 19, 2017.

Arnipally, S. K. and Kuru, E. (2017). Effect of Elastic Properties of the Fluids on the Particle Settling Velocity. Proceedings of the ASME 2017 36th International Conference on Ocean, Offshore and Arctic Engineering, OMAE2017-61192, June 25-30, 2017, Trondheim, Norway, Alternative Effect of Elastic Properties of the Fluids on the Particle Settling Velocity.

Azar, J. J. and Sanchez, R. A. (1997). Important Issues in Cuttings Transport for Drilling Directional Wells. Fifth Latin American and Caribbaean Petroleum Engineering Conference and Exibition. held in Rio de Janeiro, Brazil, 30 August -3 Spetember 1997, SPE-39020-MS,DOI: 10.2118/39020-MS.

Bilgesu, H. I., Mishra, N. and Ameri, S. (2007). Understanding the Effect of Drilling Parameters on Hole Cleaning in Horizontal and Deviated Wellbores Using Computational Fluid Dynamics, SPE-111208-MS,DOI: 10.2118/111208-MS.

Bosworth, S., El-Sayed, H. S., Ismail, G. et al. (1998). Key Issues in Multilateral Technology. Oilfiled review

Bourgoyne, A. T., Millheim, K. K., Chenevert, M. E. et al. (1986). Applied Drilling Engineering, Society of Petroleum Engineers.

Brown, N. P., Bern, P. A. and Weaver, A. (1989). Cleaning Deviated Holes: New Experimental and Theoretical Studies. SPE\IADC Drilling Conference New Orleans, Louisiana, February 28-3 March 1989 SPE-18636-MS,DOI: 10.2118/18636-MS.

Bybee, K. (2011). A Review of Cuttings Transport in Directional-Well Drilling. Journal of Petroleum Technology **63**(02), SPE-0211-0052-JPT, DOI: 10.2118/0211-0052-JPT.

Clark, R. K. and Bickham, K. L. (1994). A Mechanistic Model for Cuttings Transport. SPE 69th Annual Tgchniml Conference and Exhlbltion Now ohms, LA, U. S.A., 25-8 .Septemb.ar 1994., SPE-28306-MS,DOI: 10.2118/28306-MS.

Corredor, F. E. R., Bizhani, M. and Kuru, E. (2016). Experimental investigation of cuttings bed erosion in horizontal wells using water and drag reducing fluids. Journal of Petroleum Science and Engineering **147**: 129-142, J Petrol Sci Eng, DOI: 10.1016/j.petrol.2016.05.013.

Diplas, P., Dancey, C. L., Celik, A. O. et al. (2008). The Role of Impulse on the Initiation of Particle Movement Under Turbulent Flow Conditions. Science **322**(5902): 717-720, Science, DOI: 10.1126/science.1158954.

Duan, M., Miska, S. Z., Yu, M. et al. (2007). Critical Conditions for Effective Sand-Sized Solids Transport in Horizontal and High-Angle Wells. SPE Production and Operations Symposium Oklahoma City, Oklahoma, USA, 31 March-3 April 2007., SPE-106707-MS,DOI: 10.2118/106707-MS.

Duan, M., Miska, S. Z., Yu, M. et al. (2008). Transport of Small Cuttings in Extended-Reach Drilling. SPE Drilling & Completion, SPE-104192-PA, DOI: 10.2118/104192-PA.

Ford, J. T., Peden, J. M., Oyeneyin, M. B. et al. (1990). Experimental Investigation of Drilled Cuttings Transport in Inclined Boreholes. SPE Annual Technical Conference and Exhibition, 23-26 September, New Orleans, Louisiana, hSPE-20421-MS,DOI: 10.2118/20421-MS.

Gomaa, A. M., Gupta, D. V. S. V. and Carman, P. S. (2015). Proppant Transport? Viscosity Is Not All It's Cracked Up To Be. SPE Hydraulic Fracturing Technology Conference, 3-5 February, The Woodlands, Texas, USA, SPE-173323-MS,DOI: 10.2118/173323-MS.

Heyman, J., Mettra, F., Ma, H. B. et al. (2013). Statistics of bedload transport over steep slopes: Separation of time scales and collective motion. Geophysical Research Letters **40**(1): 128-133, Geophys Res Lett, DOI: 10.1029/2012gl054280.

Kelessidis, V. C. and Bandelis, G. E. (2004a). Flow Patterns and Minimum Suspension Velocity for Efficient Cuttings Transport in Horizontal and Deviated Wells in Coiled-Tubing Drilling. **SPE** Drilling & Completion **19**(4): 213-227, SPE-81746-PA, DOI: 10.2118/81746-PA.

Kelessidis, V. C., Mpandelis, G., Koutroulis, A. et al. (2002). Significant Parameters Affecting Efficient Cuttings Transport In Horizontal and Deviated Wellbores In Coil Tubing Drilling: A Critical Review. Paper presented at the 1st International Symposium of the Faculty of Mines (ITU) on Earth Sciences and Engineering, 16-18 May 2002, Maslak, Istanbul, Turkey.

Khatibi, M., Time, R. W. and Rabenjafimanantsoa, H. A. (2016). Particles falling through viscoelastic non-Newtonian flows in a horizontal rectangular channel analyzed with PIV and PTV techniques. Journal of Non-Newtonian Fluid Mechanics **235**: 143-153, DOI: http://dx.doi.org/10.1016/j.jnnfm.2016.08.004.

Larsen, T. I., Pilehvari, A. A. and Azar, J. J. (1997). Development of a New Cuttings-Transport Model for High-Angle Wellbores Including Horizontal Wells. **SPE** Drilling & Completion **12**(2): 129-135, SPE-25872-PA, DOI: 10.2118/25872-PA.

Leising, L. J. and Walton, I. C. (2002). Cuttings-Transport Problems and Solutions in Coiled-Tubing Drilling. **SPE** Drilling & Completion **17**(1): 54-66, SPE-77261-PA, DOI: 10.2118/77261-PA.

Li, J. and Luft, B. (2014a). Overview of Solids Transport Studies and Applications in Oil and Gas Industry - Experimental Work. SPE Russian Oil and Gas Exploration & Production

Technical Conference and Exhibition. Moscow, Russia, 14-16 October, SPE-171285-MS,DOI: 10.2118/171285-MS.

Li, J. and Luft, B. (2014b). Overview Solids Transport Study and Application in Oil-Gas Industry-Theoretical Work. International Petroleum Technology Conference. Kuala Lumpur, Malaysia, 10-12 December 2014, IPTC-17832-MS,DOI: 10.2523/IPTC-17832-MS.

Li, J., Misselbrook, J. and Seal, J. W. (2008). Sand Cleanout With Coiled Tubing: Choice of Process, Tools, or Fluids? Europec/EAGE Conference and Exhibition. Rome, Italy, 9-12 June 2008, SPE-113267-MS,DOI: 10.2118/113267-MS.

Martins, A. L., Campos, W., Liporace, F. S. et al. (1997). On the Erosion Velocity of a Cuttings Bed During the Circulation of Horizontal and Highly Inclined Wells, SPE-39021-MS,DOI: 10.2118/39021-MS.

Martins, A. L. and Santana, C. C. (1992). Evaluation of Cuttings Transport in Horizontal and Near Horizontal Wells -A Dimensionless Approach. SPE Latin America Petroleum Engineering Conference. Caracas, Venezuela ,8-11 March, SPE-23643-MS., SPE-23643-MS,DOI: 10.2118/23643-MS.

Mason, C. (2008). Technology Focus. Journal of Petroleum Technology **60**(5): 74.

Mitchell, R. F., Miska, S., Aadnøy, B. S. et al. (2011). Fundamentals of Drilling Engineering, Society of Petroleum Engineers.

Nazari, T., Hareland, G. and Azar, J. J. (2010). Review of Cuttings Transport in Directional Well Drilling: Systematic Approach. SPE Western Regional Meeting Anaheim, Califronia, USA, 27-29 may 2010, SPE-132372-MS,DOI: 10.2118/132372-MS.

Negrao, A. (2009). Technology Focus. Journal of Petroleum Technology **65**(5): 66.

Negrao, A. (2014). Technology Focus. Journal of Petroleum Technology **66**(5): 130.

Ozbayoglu, M. E., Saasen, A., Sorgun, M. et al. (2010a). Critical Fluid Velocities for Removing Cuttings Bed Inside Horizontal and Deviated Wells. Petroleum Science and Technology **28**(6): 594-602, DOI: 10.1080/10916460903070181.

Ozbayoglu, M. E., Sorgun, M., Saasen, A. et al. (2010b). Hole Cleaning Performance of Light-Weight Drilling Fluids During Horizontal Underbalanced Drilling. SPE-136689-PA, DOI: 10.2118/136689-PA.

Pilehvari, A. A., Azar, J. J. and Shirazi, S. A. (1996). State-Of-The-Art Cuttings Transport in Horizontal Wellbores. International Conference on Horizontal Well Technology. Calgary, Alberta, Canada, 18-20 November, SPE-37079-MS,DOI: 10.2118/37079-MS.

Rabenjafimanantsoa, H. A., Time, R.W. and Saasen, A. (2005). Flow regimes over particle beds experimental studies of particle transport in horizontal pipes. Annual Transactions of the Nordic Rheology Society, 13.

Rabenjafimanantsoa, A. H. (2007). Particle transport and dynamics in turbulent Newtonian and non-Newtonian fluids. PhD, University of Stavanger,.

Ramadan, A., Skalle, P. and Johansen, S. T. (2003). A mechanistic model to determine the critical flow velocity required to initiate the movement of spherical bed particles in inclined channels. Chemical Engineering Science **58**(10): 2153-2163, DOI: 10.1016/S0009-2509(03)00061-7.

Ruszka, J. (2014). Technology Focus. Journal of Petroleum Technology **66**(11): 110.

Saasen, A. (1998). Hole Cleaning During Deviated Drilling - The Effects of Pump Rate and Rheology. European Petroleum Conference, 20-22 October, The Hague, Netherlands, SPE-50582-MS,DOI: 10.2118/50582-MS.

Saasen, A. and Løklingholm, G. (2002). The Effect of Drilling Fluid Rheological Properties on Hole Cleaning. IADC/SPE Drilling Conference. Dallas, Texas, 26-28 February, SPE-74558-MS,DOI: 10.2118/74558-MS.

Thomas, R. P., Azar, J. J. and Becker, T. E. (1982). Drillpipe Eccentricity Effect on Drilled Cuttings Behavior in Vertical Wellbores. SPE-9701-PA, DOI: 10.2118/9701-PA.

Tomren, P. H., Iyoho, A. W. and Azar, J. J. (1986). Experimental Study of Cuttings Transport in Directional Wells. SPE Drilling Engineering, SPE-12123-PA, DOI: 10.2118/12123-PA.

Tonmukayakul, N., Morris, J. F. and Prudhomme, R. (2013). Method for estimating proppant transport and suspendability of viscoelastic liquids. Google Patents. United States, US 20110219856 A1.

Werner, B., Myrseth, V. and Saasen, A. (2017). Viscoelastic properties of drilling fluids and their influence on cuttings transport. Journal of Petroleum Science and Engineering **156**: 845-851, DOI: http://dx.doi.org/10.1016/j.petrol.2017.06.063.

Ytrehus, J. D., Taghipour, A., Sayindla, S. et al. (2015). Full Scale Flow Loop Experiments of Hole Cleaning Performances of Drilling Fluids. Proceedings of the Asme 34th International Conference on Ocean, Offshore and Arctic Engineering, 2015, Vol 10.

Zeinali, H., Toma, P. and Kuru, E. (2012). Effect of Near-Wall Turbulence on Selective Removal of Particles From Sand Beds Deposited in Pipelines. Journal of Energy Resources Technology-Transactions of the Asme **134**(2), J Energ Resour-Asme, DOI: Artn 021003 10.1115/1.4006041.

Zhang, F. S. M., M. Yu, E. Ozbayoglu and N. Takach (2014). Pressure Profile in Annulus: Solids Play a Significant Role. Proceedings of the ASME 2014 33rd International Conference on Ocean, Offshore and Arctic Engineering OMAE2014 une 8-13, 2014, San Francisco, California, USA.

2 Literature review and background

2.1 Hole Cleaning in Oil and Gas Well Drilling

During drilling operations, sand debris produced by drill bit must be carried out of the well. One of the functionalities of drilling fluid is to carry these generated cuttings out of the well. Inadequate cuttings transport leads to severe problems, and hence, it is important to optimize the drilling fluid and other conditions for efficient hole cleaning. Cuttings transport in oil wells has been under study by different means for decades. Low annular fluid velocity, lack of inner pipe rotation, and wrong drilling fluid properties are the primary factors in inefficient hole cleaning. Currently, there is no generalized systematic model developed for hole cleaning (Technology 2011).

In the literature, data from 4 different source are available for hole cleaning studies. These sources are experimental studies, CFD simulations, theoretical, empirical and mechanistic models and finally field tests. In the following sections, a brief and complete review of the state of the art knowledge of cuttings transport obtained in previous studies is reported. Results of experimental studies (either lab studies or field tests) are summarized first. Results of studies in other areas pertinent to the hole cleaning operation are also discussed. Mechanistic and empirical correlations are discussed next. In the last part, a review of the applications of CFD simulation in this area is considered.

The early investigations related to cuttings transport started with vertical and near vertical wells (Sifferman et al. 1974, Sample and Bourgoyne 1977, Sample and Bourgoyne 1978, Hussaini and Azar 1983). By early 1980's with the increase in the use of directional wells, the problem of cuttings transport in inclined wellbores became the center of interest. Large-scale flow loop facilities were built around the world to study the fundamental mechanism of cuttings transport in highly inclined wellbores. The impact of many parameters and different operational conditions has been studied ever since.

For vertical and near vertical wellbores the slip velocity was found to be the key in controlling cuttings transport. Slip velocity is the velocity of cuttings settling due the gravity effect attained under equilibrium conditions. If the fluid velocity surpasses slip velocity, cuttings will move upward. Transport ratio is often used to make sure efficient cutting transport is achieved. Tomren et al. (1986) argued that for angles of inclination less than 10 degrees, cuttings transport remains essentially similar to vertical wells. According to Li and Luft (2014a), the cuttings can easily be kept in suspension for angles of inclination up to 40 degrees.

Cutting transport in highly inclined wellbores is governed by a different mechanism than that of vertical wells. The slip velocity is no longer relevant because the fluid velocity is perpendicular to settling velocity. Cuttings only have few inches to establish themselves in the bed as opposed to vertical wells where they must settle far more distance before reaching the bottom of the well. Since 1980 numerous experimental studies have been conducted by researchers to investigate the impact of different parameters on cuttings transport efficiency in inclined wellbores. Comprehensive reviews of the past work could be found in papers written by (Pilehvari et al. 1996, Kelessidis et al. 2002, Li et al. 2010, Nazari et al. 2010, Bybee 2011, Sun Xiaofeng 2013, Wang Kelin 2013, Li and Luft 2014a, Li and Luft 2014b). Parameters affecting cutting transport are classified into three main groups (Bilgesu et al. 2007): Fluid characteristics, cuttings related factors and operational variables. Figure 2-1 graphically shows the most significant factors in controlling solid bed removal in oil wells.

In the following sections, we discuss each group of variables that control hole cleaning and cuttings transport in deviated wells separately.

2.1.1 Operational variables affecting hole cleaning

Operational variables include pump flow rate, hole inclination angle, inner pipe rotation speed, pipe eccentricity and the rate of penetration (ROP).

The pump flow rate or the annular fluid velocity is the most critical factor in controlling cuttings removal (Hemphill and Larsen 1996, Technology 2011). Higher flow rates are always favorable as they promote turbulence (Azar and Sanchez 1997). Many studies have reported a positive impact of higher flow rate on cutting transport and bed erosion (Hussaini and Azar 1983, Tomren et al. 1986, Hemphill and Larsen 1996, Cho et al. 2001, Ozbayoglu et al. 2004, Hemphill and Ravi 2010). According to Adari et al. (2000), high flow rates expedites bed erosion rate. Nevertheless, the flow rate is limited due to pump hydraulics, borehole washout, equivalent circulating density (ECD) considerations and in the case of coiled tubing (CT) drilling by a downhole motor performance (Leising and Walton 2002, Kelessidis and Mpandelis 2003, Nazari et al. 2010, Mitchell et al. 2011).

Given the fact that annular fluid velocity is the primary factor in preventing the formation of cuttings bed in the wellbore, many studies have shown even at highest attainable velocities in highly inclined wells it is impossible to avoid the formation of a stationary bed. For conventional drilling, the annular fluid velocity is almost twice as high as that of CT (Li and Luft 2014a). For an average velocity in conventional drilling (less than 2 m/s, (Li and Luft 2014a)) or CT operation (less than 1.5m/s, (Kelessidis et al. 2002) formation of a cuttings bed is very probable. Zhang (2014) experimentally showed even at annular velocities of 1.56 m/s stationary cuttings bed form (for a fully eccentric annulus and a non-zero ROP). Ozbayoglu et al. (2010a), (2010b) reported that a stable bed formed when annular velocity was less than 1.83 m/s. They reported a minimum velocity of 2.44 m/s is required to keep all the cuttings moving (Critical Deposition Velocity, CDV)). Li and Luft (2014b) based on previously published data, concluded that at least a minimum velocity of 2.74 m/s is required to establish a no bed condition in an eccentric annulus. Therefore, from previous studies, it becomes apparent that formation of a stationary cuttings bed in highly inclined wellbores is very likely. The problem is more severe for CT intervention because annular fluid velocity is almost half of that encountered in conventional drilling.

Pipe eccentricity adversely affects hole cleaning. Eccentricity drives the fluid away from the narrower gap where cuttings tend to go (Thomas et al. 1982, Azar and Sanchez 1997, Li and Luft 2014b). Nazari et al. (2010) mentioned eccentricity to have a significantly negative impact on cutting transport. According to Tomren et al. (1986), concentric configuration gives best transport efficiency. In another study by Yateem et al. (2013) pipe eccentricity was found to increase the hole cleaning time. Walker and Li (2000) showed eccentricity hampers cuttings transport efficiency and this effect increases as the inclination angle increase.

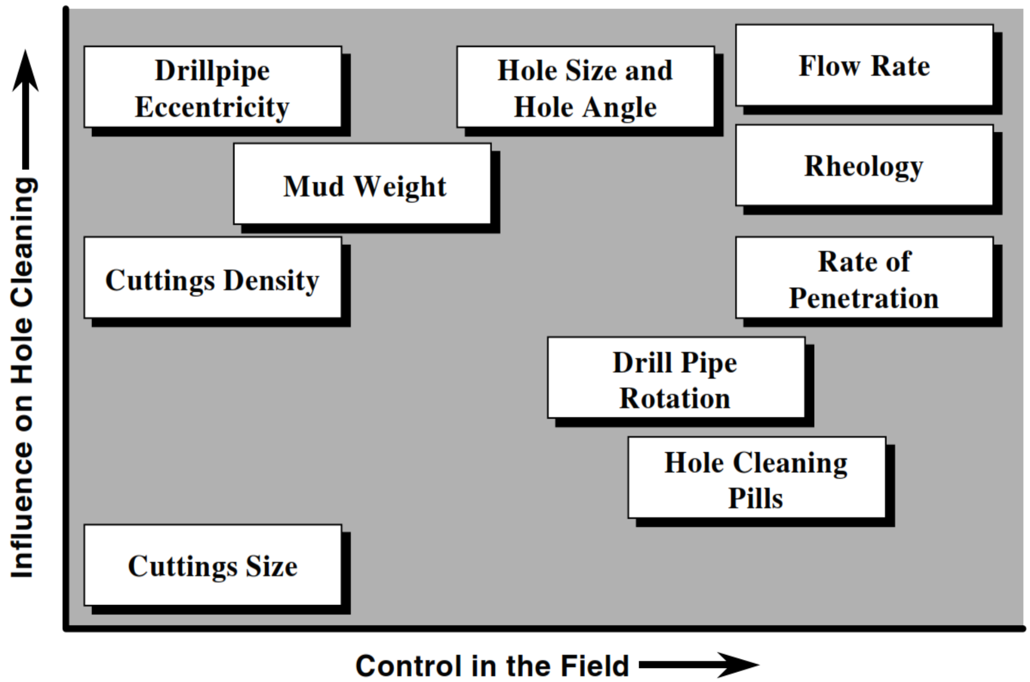

Figure 2-1 Parameters affecting cutting transport (Adari et al. 2000)

Inner pipe rotation enhances cutting transport and bed erosion, as revealed by many studies (Tomren et al. 1986, Peden et al. 1990, Sanchez et al. 1999, Ravi and Hemphill 2006, Technology 2011, Ytrehus et al. 2014, Ytrehus et al. 2015). Pipe rotation enhances cuttings bed removal by mechanically agitating the bed and breaking the gel structure formed by the drilling fluid in the bed (Ravi and Hemphill 2006). Sifferman and Becker (1992) stated that in near-horizontal wellbores, low ROP combined with small cuttings are the most efficient scenario for using pipe rotation effect. Philip et al. (1998) argued pipe rotation enhance lift force on the cuttings. Sanchez et al. (1999) study showed drillstring rotation impact depends on other parameters (such as rheology, cuttings size, flow rate and so on). Duan et al. (2008) showed pipe rotation enhances transport of small cuttings. Despite its positive impact on hole cleaning, pipe rotation is absent in coiled tubing applications (Leising and Walton 2002, Kelessidis and Mpandelis 2003, Li et al. 2008). Results of a field test study by Guild et al. (1995) showed pipe rotation could be significant in hole cleaning. Lockett et al. (1993) in a numerical simulation found pipe rotation causes the production of Taylor vortices. The presence of Taylor vortices produces an additional lift force on cuttings which is big enough that causes them to be lifted off the bottom.

A higher ROP introduces more cuttings into the annulus, and therefore more cuttings must be removed. Higher ROP always causes a higher concentration of cuttings in the annulus (Tomren et al. 1986, Sanchez et al. 1999, Li and Luft 2014a).

Hole inclination angle has a profound influence on cutting transport (Okrajni and Azar 1986, Tomren et al. 1986, Pilehvari et al. 1996, Larsen et al. 1997). For angles of inclination less than 10 degrees, cutting transport remains similar to vertical case (Vieira et al. 2002, Li and Luft 2014a). For larger inclination angles, dramatic reductions occur in the cuttings transportability. The main reason for this is the decline in the vertical component of the fluid velocity (Ramadan et al. 2003). Formation of the bed of cuttings has been observed for angles of inclination beyond 35 (Tomren et al. 1986). At inclination angles between 35 to 65 degrees backsliding of cuttings may occur (Tomren et al. 1986, Peden et al. 1990, Sanchez et al. 1999). This effect is known as the "avalanche" effect. It is recommended to avoid critical angles in wellbore trajectory design (Li and Luft 2014a).

2.1.2 Cuttings related factors

Size, size distribution, shape, and density of drilled cuttings affect their transport efficiency. However, there is little control over these parameters as they are dictated by the type of bit, formation type, Weight on Bit (WOB), ROP, regrinding, and RPM (Mitchell et al. 2011). For angles of inclination from 0 to 60 degrees, smaller cuttings show lower concentration in the annulus. For angles beyond 70 degrees, smaller cuttings have a higher concentration in the annulus (Li and Luft 2014b). Many of the previous studies on cutting transport considered large cuttings, e.g. greater than 2 mm (Brown et al. 1989, Martins and Santana 1992). In certain situations fine cuttings are produced; for example using PDC bits and CT (Leising and Walton 2002). In a typical hydraulic fracturing operation 20/40 mesh size particles are used (600-800 micron) (Li and Luft 2014a, Li and Luft 2014b). Duan et al. (2008) investigated transportation of fine cuttings with water and PAC solution. They found that it is easier to transport fine cuttings with PAC solution than water. In another study, Duan et al. (2007) investigated bed erosion using different fluids. Their results showed smaller cuttings are harder to erode than bigger ones (450 microns and 1.4 mm cuttings were used). Results of an experimental and modeling study by Ozbayoglu et al. (2004) revealed that smaller cuttings are harder to remove if they have developed into bed. Martins and Santana (1992) experimentally showed that smaller cuttings (smallest tested size was 2 mm) were easier to erode than bigger ones. According to Pilehvari et al. (1996) and based on the results of experiments by Larsen et al. (1997), small cuttings (0.1 in) are harder to remove than bigger cuttings. Li and Luft (2014b) mentioned that smaller cuttings have a higher concentration in highly deviated wellbores (70-90 degree).

2.1.3 Fluid-related factors affecting hole cleaning

Fluid properties which affect cutting transport are density and rheology. Higher mud weight improves cutting transport but causes a reduction in ROP (Becker and Azar 1985, Martins et al. 1996, Hemphill 2010). Higher density decreases the effective weight of the cuttings (buoyed weight), and hence, enhances cuttings removal. The primary function of density is to prevent the influx of formation fluid into the wellbore. Therefore, it cannot be used for optimizing cuttings transport process. The upper limit of mud density is dictated by formation fracture pressure (ECD limitation). One of the suggested strategies to improve cuttings transport in highly deviated wellbores is to use pills of high-density mud (Hemphill 2010). Similar to vertical wells, where pills of high-viscosity mud are pumped to sweep the cuttings out of the well, pills of high-density mud is pumped periodically to clean the cuttings out of the wellbore. However, this approach may cause high ECD and lost circulation.

Rheological characteristics of the fluid have a rather more complex impact on the cuttings transport than that of the density. According to Saasen (1998), drilling fluids with identical rheological characteristics based on the API's specifications can perform differently in hole cleaning. Nazari et al. (2010) reported that the rheological characteristic could have either a positive or negative impact on hole cleaning, depending upon other variables. Mitchell et al. (2011) also point out to the controversial role of fluid's rheology in cuttings transport.

The non-Newtonian fluid viscosity is often mistaken in the drilling literature as that of fluid's rheology. However, the shear or apparent viscosity is only one of the functions that are required to describe the behavior of a complex fluid (Bird 1987, Dealy et al. 2013). In most of the work done previously, the impact of fluid's rheological characteristics merely goes beyond the non-Newtonian fluid viscosity to explain the observed results. It is rare to see any papers in the drilling literature where the complex rheological function of the fluid is used to discuss cuttings transport. Viscoelastic properties of drilling fluid are often not measured due to lack of understanding of its impact on different aspects of the drilling operation as well as the lack of equipment that can make such measurements (Lee et al. 2014).

The problem of cutting transport while cuttings are in suspension is different from cleaning a bed of cuttings. In the first case, cuttings are introduced through the inlet of the annulus for a given ROP. In the second scenario, a cuttings bed is placed at the bottom of the annulus. Fluid is pumped to the test section to sweep the bed out of the hole. In the first case, a liquid inducing low particle settling velocity is desirable to keep the cuttings in suspension for the longest possible period. A fluid with high viscosity and polymer additives provides such conditions. On the other hand, for eroding a bed of cuttings, a fluid with entrainment capabilities are desirable. A fluid with excellent suspension characteristic does not necessarily have the desirable particle entrainment attributes.

For the case where cuttings are injected through the inlet, according to Azar and Sanchez (1997), high fluid viscosity reduces the hole cleaning ability in deviated wells. The main functionality of the fluid viscosity is to keep the weighting agents suspended. Therefore, justification must be made in selecting the appropriate amount of viscosifier to be used. Saasen and Løklingholm (2002) pointed out that Xanthan gum must be employed as much as necessary to prevent barite sag. Saasen (1998) and Saasen and Løklingholm (2002) were among the first investigators to discuss the role of fluids rheological properties using some viscoelastic properties of the drilling fluid. According to them, use of polymer solutions causes the cuttings bed to become more consolidated and form a gel-like structure. The reaction of the polymeric mud and the cuttings bed in addition to the compaction posed by the polymer fluid will make hole cleaning more difficult.

Increasing the yield point to plastic viscosity ratio has been reported to have a positive impact on transport efficiency (Hussaini and Azar 1983, Okrajni and Azar 1986). Fluid with a higher consistency index was found to keep the cuttings in suspension for a longer period; likely because a higher viscosity fluid reduces the settling velocity. However, Azar and Sanchez (1997) concluded low viscosity mud perform better hole cleaning at the same flow rate than high viscosity fluid. Okrajni and Azar (1986) showed that under turbulent flow, the impact of fluid rheology diminishes. Results of a three layer bed model proposed by Cho et al. (2000) suggested that decrease in the flow behavior index would lead to an increase in the bed thickness. More recently Duan et al. (2008) found that small cuttings are easier to transport with PAC solution than water, implying a positive effect of higher viscosity for carrying fine particles. Leising and Walton (2002) analyzed three cases of high, medium and low viscosity fluids in CT and recommended low viscosity fluids to be used. Results of experiments by Tomren et al. (1986) showed that higher viscosity fluids result in lower cuttings concentration in the annulus. Larsen et al. (1997) experiments demonstrated that medium rheology drilling fluid is superior to low and high viscosity drilling fluid (Mitchell et al. 2011). Tomren et al. (1986) found that the effect of viscosity should be considered in association with the flow regime. In laminar flow, high viscosity is always better while the difference is less in turbulent flow. Results of a field test by Payne et al. (1994) showed that it is important to select a rheology which ensures either laminar or fully turbulent flow. Transitional flow regime is to be avoided. Becker et al. (1991) investigation also showed mud rheology's importance is related to the flow regime. For near vertical wellbores, a viscous drilling fluid in laminar flow is preferred. For near-horizontal wellbores, however, turbulent flow is desired, and rheology no longer is relevant (Becker et al. 1991). Ford et al. (1990) also found that the effect of fluid rheological properties on the cuttings transport also varies depending on the flow regime. In their experiments water was found to have lower critical velocity for both rolling and suspension mechanism. However, their results showed that the difference between rolling and suspension velocity for a given fluid is less when the medium and high viscosity fluids are used.

Researchers in Norway have been focusing on studying the performance of different drilling fluids during cuttings transport in horizontal wells (Rabenjafimanantsoa et al. 2005, Rabenjafimanantsoa A. H. et al. 2007, Rabenjafimanantsoa 2007, Ytrehus et al. 2013, Ytrehus et al. 2014, Ytrehus et al. 2015, Sayindla et al. 2016, Werner et al. 2016). Ytrehus et al. (2014) have studied the performance of two water-based drilling fluids with similar viscosity profiles according to API's procedure in a horizontal flow loop. Their experiments showed that fluids with similar shear viscosity profile could have different hole cleaning performances. Sayindla et al. (2016) found that yield stress plays a major role in holding the cuttings in suspension at low shear rates. Additionally, they reported a positive impact of pipe rotation on hole cleaning at low string rotation speed.

Studying hole cleaning or cleaning a stationary bed of cuttings (i.e. simulating bed erosion) have been less common than the transport with continuous cuttings feed (i.e. simulating drilling).

According to Li and Luft (2014a), (2014b) the early cuttings transport studies were mostly focused on the idea of finding a critical velocity which would prevent the formation of a stationary bed. However, as mentioned previously in most cases preventing the formation of a stationary bed is impossible. Over the past decade, the focus turned to the prediction of cuttings concentration in the annulus. In the literature a number of experimental works can be found related to bed erosion (Brown et al. 1989, Martins and Santana 1992, Martins et al. 1996, Li and Walker 1999, Adari et al. 2000, Lourenco et al. 2006, Valluri et al. 2006, Rodriguez Corredor et al. 2014). Brown et al. (1989) conducted bed erosion tests using 6.4 mm cuttings. Water under the turbulent condition and HEC polymer solutions under laminar flow condition were used. Water was found to be superior in cleaning the well. Martins and Santana (1992) conducted an experimental study and dimensional analysis of the bed erosion. Cuttings size greater than 2mm was used. The impact of fluid rheological properties was not studied. Adari (1999), (2000) conducted many experiments to determine the hole clean out time for different conditions. Adari (1999) study showed that a higher rheology factor (i.e. higher K/n ratio) has better erosion capability. Duan et al. (2007) studied critical re-suspension velocity in an eccentric annulus. Results revealed that water always initiates bed erosion at lower flow rates than PAC polymer solutions. Less turbulence caused by higher viscosity causes a reduction in erosion capacity of high viscosity fluids, claimed Li et al. (2005). Although previous studies showed that water or less viscous fluids have the better capability in eroding a stationary bed, the thicker more viscous fluid has higher suspension ability. The challenge is to keep the solids in suspension and re-entrain the ones already deposited on the bed. Ozbayoglu et al. (2004) stated that increasing viscosity in CT intervention causes an increase in the thickness of the bed. Walker and Li (2000) have concluded that HEC and Canvas polymer solutions have higher carrying capacity comparing to water. However, they have less capability for eroding a stationary bed.

In addition to shear viscosity, properties such as viscoelasticity and normal stress differences affect cuttings transport. However, the number of studies that focused on the effect of such complex rheological characteristic of the drilling fluid on the cuttings transport is scarce. Viscoelasticity reduces the settling velocity of cuttings (Gomaa et al. 2015, Arnipally and Kuru 2017). Hence, the viscoelasticity is a desirable fluid property when transporting cuttings in the vertical sections of the wellbore. However, its impact on the bed erosion has not been considered widely.

As the review of previous works shows, the major discrepancy still exists about the role of fluid rheological properties on hole cleaning. It is a challenging task for the drilling engineer to decide which rheological properties need to be optimized for better hole cleaning. As pointed out by Mitchell et al. (2011), during transporting drilled cuttings rheological properties must be chosen in such a way that the flow is turbulent in the annulus. However, a problem arises when cuttings develop in the form of a stationary cuttings bed.

2.2 Viscoelastic fluid properties and their importance in hole cleaning

Viscoelasticity is the property of materials that exhibit both viscous and elastic characteristics. A viscous material resists the shear force and strains linearly with shear rate. Examples of viscous materials include honey and water. On the other hand, an elastic material stretches and returns to its original state upon removal of the force. An example of an elastic material is a rubber band. A viscoelastic material shows characteristic of both materials. Polymer melts and polymer solutions are mostly viscoelastic materials.

A complete description of the rheology of viscoelastic fluids requires the knowledge of the shear viscosity (or the apparent viscosity) as well as parameters related to fluid elastic properties (such as first and second normal stress differences). Eq.(2-1) gives the definition of shear viscosity.

$$\mu = \frac{\tau_{xy}}{\dot{\gamma}} \qquad \textbf{Eq.(2-1)}$$

Where τ_{xy} is the shear stress and $\dot{\gamma}$ is the shear rate. For non-Newtonian fluids, the shear viscosity is shear rate dependent.

In addition to shear (apparent) viscosity, elastic and loss moduli of viscoelastic materials are essential features in characterizing rheology of these class of fluids. The latter two properties can be measured using creep test and or oscillatory rheometry measurements. The elastic and viscous moduli of a polymer fluid show which attribute are dominant at a particular timescale of flow (i.e. viscous vs. elastic). The timescale at which elastic and viscous moduli meet is called the longest relaxation time (denoted as λ) which is simply the inverse of the frequency where elastic and viscous modulus cross-over (Figure 2-2)The relaxation time marks the timescale at which the flow passes from the viscosity dominant regime to elasticity dominant regime.

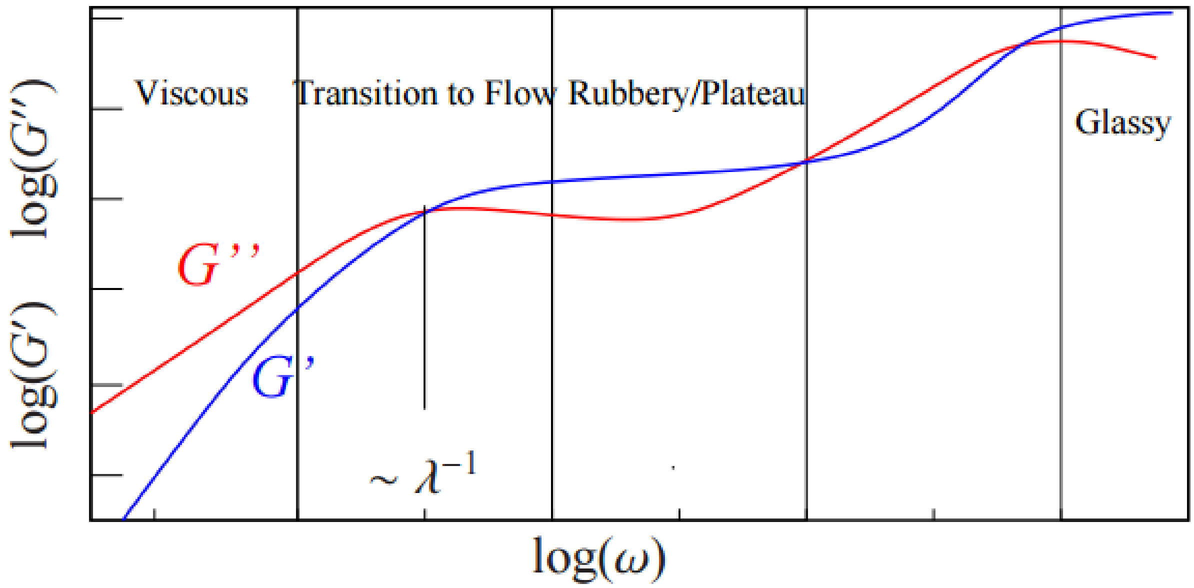

Figure 2-2 Typical regimes in the complex modulus obtained using an oscillatory response of a polymeric liquid (Dealy and Larson 2006)

The ratio of the microscopic timescale to the local strain rate is called the Weissenberg Number (Deshpande 2010).

$$Wi = \lambda \dot{\gamma} \quad \textbf{Eq.(2-2)}$$

For small *Wi* numbers (<1) the elastic effects are negligible. On the other hand, for large Wi numbers, the viscous effects diminish, and elastic effects become important.

In the oscillatory measurements of loss and storage moduli, a sinusoidal shear deformation with radian frequency ω is applied. For viscoelastic materials, the response is sinusoidal, but it is out of phase with the strain (Tropea et al. 2007). Figure 2-3 shows the applied stress and deformation. Following equations describe the relation between the strain (γ) and stress (σ).

$$\gamma(t) = \gamma_0 \sin(\omega t) \quad \textbf{Eq.(2-3)}$$

$$\sigma(t) = \sigma_0 \cos(\,\omega t + \delta) = \gamma_0 (G' \sin(\omega t) + G'' \cos\big((\omega t)\big) \quad \textbf{Eq.(2-4)}$$

δ is the loss angle and it relates to loss and storage moduli in the following manner:

$$G' = \frac{\sigma_0}{\gamma_0}\cos(\delta) \quad \textbf{Eq.(2-5)}$$

$$G'' = \frac{\sigma_0}{\gamma_0}\sin(\delta) \quad \textbf{Eq.(2-6)}$$

Therefore, the storage and viscous moduli are calculated by measuring σ_0, γ_0 and the phase angle (δ).

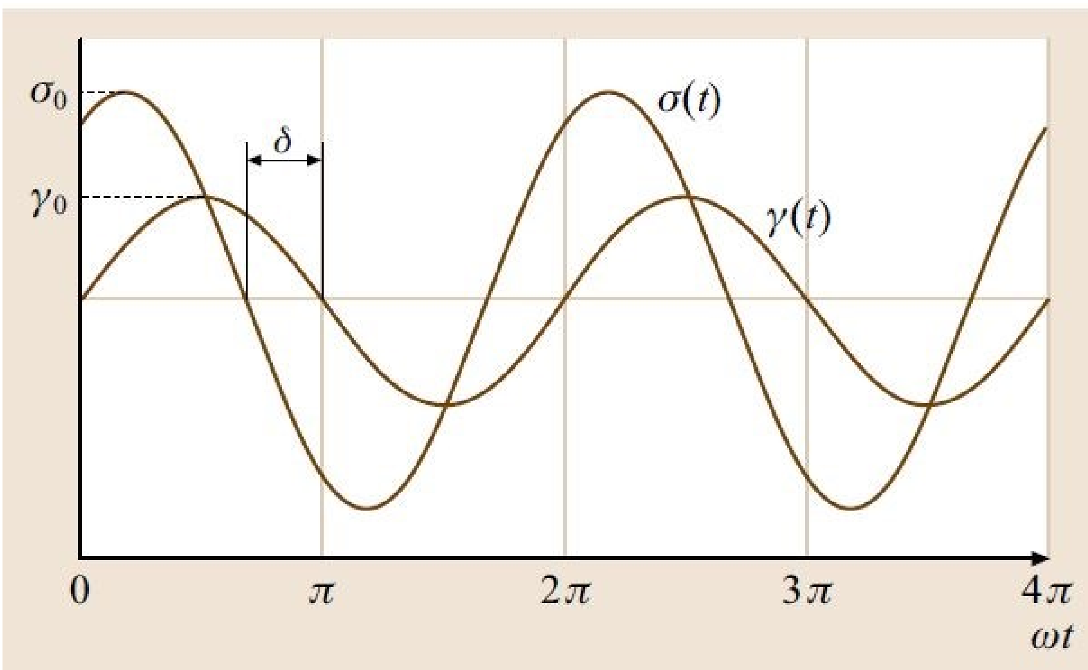

Figure 2-3 sinusoidal stress and deformation δ (rad) out of phase (Tropea et al. 2007)

The knowledge of shear viscosity and loss and storage moduli of viscoelastic materials is not sufficient for fully characterizing their behavior. During the flow of such fluids, anisotropies develop in the flow that gives rise to normal stresses that are not observed in the flow of viscous liquids. A detailed discussion of the state of the stresses acting on the fluid is, therefore, needed. The most general form of the stress tensor (2-D) for an anisotropic material in simple shear flow can be described by the total stress tensor as shown by Eq.(2-7) (Bird 1987).

$$\boldsymbol{\pi} = p\boldsymbol{\delta} + \boldsymbol{\tau} = \begin{bmatrix} p + \tau_{xx} & \tau_{xy} & 0 \\ \tau_{yx} & p + \tau_{yy} & 0 \\ 0 & 0 & p + \tau_{zz} \end{bmatrix}$$ **Eq.(2-7)**

In an anisotropic, incompressible material, there are only three independent stress quantities of rheological significance, namely two differences of normal components and one tangential component: $\tau_{xx} - \tau_{yy}$, $\tau_{yy} - \tau_{zz}$, and τ_{yx}. The third difference $\tau_{xx} - \tau_{zz}$ of normal components is the sum of the first two differences, and the other non-zero tangential (shear) component τ_{xy} is a function of the shear viscosity and equal to τ_{yx} (Lodge 1964). The terms N_1 and N_2 are used to define the first and second normal stress differences as defined by Eq.(2-8) and Eq.(2-9), respectively.

$$N_1 = \tau_{xx} - \tau_{yy}$$ **Eq.(2-8)**

$$N_2 = \tau_{yy} - \tau_{zz}$$ **Eq.(2-9)**

For an inelastic Newtonian fluid, the normal stress differences are zero, that is:

$$\tau_{xx} = \tau_{yy} = \tau_{zz}$$ **Eq.(2-10)**

For viscoelastic fluids, however, the normal stress differences are not zero. Figure 2-4 schematically shows the components of stress tensor in the one-dimensional steady shearing flow of a viscoelastic fluid (Chhabra and Richardson 1999).

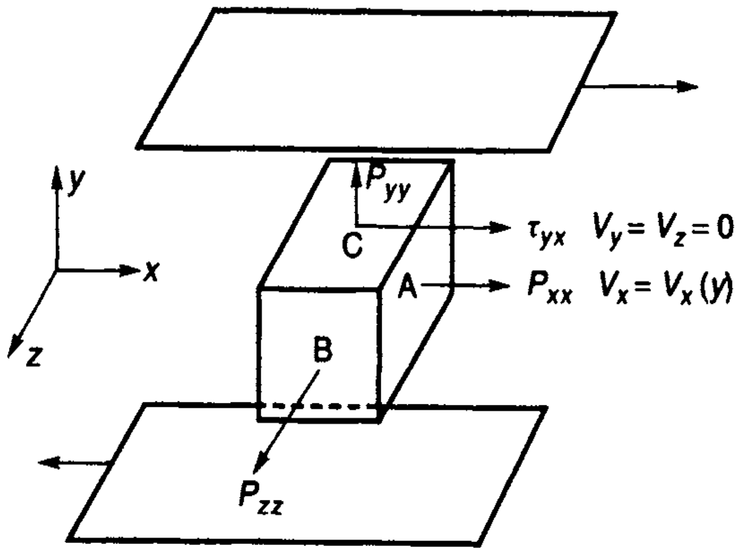

Figure 2-4 2-5 Non-zero elements of stress in the one-dimensional steady shearing motion of a viscoelastic fluid (Chhabra and Richardson 1999)

In polymer based fluids (or more generally viscoelastic fluids) the normal stress differences are not zero due to the anisotropies developed in the polymer molecules. These stress differences are associated with the strain-induced anisotropy in a fluid, and in the case of polymer-based liquids, the anisotropy arises from the departure of molecules from their equilibrium, symmetrical average shape (Dealy et al. 2013). For a Newtonian fluid, the first and second normal stress difference is zero. Hence, a full description of fluid's rheological behavior can be sufficiently obtained from the Newtonian viscosity. On the other hand, for a viscoelastic polymer based fluid, the first and second normal stress difference is not zero. Therefore, a complete description of the rheology of these fluids requires the knowledge of the apparent viscosity and the two normal stress differences.

The anisotropies induced in the microstructures of the polymers caused by the flow are the main reason for the existence of non-zero normal stress difference. In the absence of flow, the coils like structures have a spherical pervaded volume. In the shear flow, the polymer molecules stretch toward the direction of the flow. This results in a pervaded volume that is ellipsoidal and oriented towards the direction of flow. The restoring forces are different in different directions. This results in the anisotropic normal forces (Deshpande 2010).

The non-zero first and second normal stress difference in polymer solutions has interesting consequences. The most related phenomenon to annular flow is the unequal distribution of pressure in each cross sections of the flow. According to Bird (1987) measurements have shown the pressure is higher on the inner wall of annuli than its outer wall. This phenomenon does not happen in the flow of Newtonian fluids.

Another consequence of non-zero normal stress difference is the expansion of fluid when it goes through a diameter change. In this case, due to normal forces and the incompressibility of the fluid, the fluid expands. According to Bird (1987) a negative N_1 and positive N_2 can loosely be thought of as an additional compressive force in the y direction (i.e. perpendicular to the direction of the flow). For flow between two parallel plates, a Newtonian fluid only requires shear stress to maintain the steady flow. However, for a viscoelastic fluid flow, a normal force must be applied to keep the plates in place because of the normal forces in the fluid (Bird 1987).

For incompressible fluids, the normal stress has no significance if the stresses are the same in all directions (i.e. Newtonian fluids). Only non-zero normal stress difference can cause deformation, i.e. stretching and compression. The shear viscosity (μ), the first (N_1) and the second normal (N_2) stress differences are all functions of the shear rate (Bird 1987, Dealy et al. 2013).

$$N_1(\dot{\gamma}) = \Psi_1(\dot{\gamma})\,\dot{\gamma}^2 \qquad \textbf{Eq.(2-11)}$$

$$N_2(\dot{\gamma}) = \Psi_2(\dot{\gamma})\,\dot{\gamma}^2 \qquad \textbf{Eq.(2-12)}$$

Ψ_1 and Ψ_2 are the first and second normal stress difference coefficients (Bird 1987). For any viscometric flow, these three viscometric functions completely describe the rheological behavior of a fluid. For a Newtonian (inelastic) fluid, N_1 and N_2 are zero, therefore, only shear viscosity is required to describe the fluids. For sufficiently low shear rates, viscoelastic fluids show Newtonian behavior (Dealy et al. 2013).

Drilling fluid is a complex mixture of different materials and polymers. Each additive is added for a particular purpose (Mitchell et al. 2011). In most cases, polymers are added for filtration loss control and or preventing sagging of weighting agents. Therefore, most drilling muds exhibit elastic properties. Unfortunately, due to lack of understanding of the impact of such features and lack of necessary equipment, often these properties are not measured. In most of the previously mentioned studies of hole cleaning, viscoelastic properties of the drilling fluids were not measured. Nonetheless, in this section, we try to cite few of previous studies relevant to hole cleaning where viscoelastic properties of drilling fluids have been discussed.

Gomaa et al. (2015) studied the influence of viscoelasticity on proppant transport during hydraulic fracturing operations. In this study, the authors showed that the viscoelasticity significantly reduced the settling velocity of the particles. The difference in flowing characteristic of viscoelastic fluids compared to that of viscoelastic liquids was identified as the cause of this reduction. A viscoelastic fluid, when flowing in the elastic regime, stretches and deforms when subjected to a shear force. On the other hand, a viscous fluid flows as soon as it is subjected to a shear force. The deformation rather than flowing causes the fluid to behave similarly to a semi-solid material that keeps the materials in suspension. The authors tested settling characteristics of few polymers with similar shear viscosity profiles and different elasticities. They found that elasticity significantly affects the particles settling.

Arnipally and Kuru (2017) also performed an experimental study to investigate the influence of fluid's viscoelasticity on particle settling characteristic in viscoelastic fluids. They used state-of-the-art Particle Shadowgraphy technique for their measurements. The results also confirmed that the fluid elasticity reduces the settling velocity.

The previous two studies have exhibited that viscoelasticity has a significant role in reducing particle settling. Hence, it can be a desirable property, especially in vertical sections of the wellbore. However, in horizontal and high angle sections of the wellbore, bed erosion is of greater importance because cuttings eventually form a stationary cuttings bed. The impact of viscoelasticity on bed erosion could be significantly different from its positive impact on cuttings suspension characteristics.

Some researchers recommended the use of viscoelastic fluids that possessing very high low shear rate viscosity (LSRV) values for better hole cleaning (Powell et al. 1991, Zamora et al. 1993, Asadi et al. 2002). The argument in support of the use of high LSRV fluids is that the power law index (n) of these high LSRV fluids is low, typically approximately 0.2 (i.e., highly shear thinning fluid), which leads to high velocity gradient, high shear rate, and as a result, relatively low viscosity near the wall, while it promotes low-velocity gradient, low shear rate and high viscosity in the central region of the flow. Consequently, the high wall shear stirs the cuttings up from the bed and entrains them in the core; once in the core, they are held there by the elevated LSRV. This structure is believed to be conducive to good hole cleaning in highly deviated wells.

Saasen et al. (1998) suggested that the drilling fluid's ability to form gel structures within cuttings bed would be more relevant fluid characteristics for hole cleaning. Field observations, however, indicated that in addition to gel strength, elastic properties of drilling fluids played a significant role in hole cleaning (Saasen and Løklingholm 2002). Saasen and Løklingholm (2002) reported that the smaller the elastic strain that was necessary to break the gel, the easier was to clean the hole. Saasen and Løklingholm (2002) also claimed that polymer fluids cause the bed to become more consolidated, and hence, made the bed harder to erode. Additionally, they argued that polymers usually react in the bed and form a cross-linked structure with the bed material, which then makes the bed erosion more difficult. Rabenjafimanantsoa (2007) also observed the similar effect when using PAC as a viscosifier in the drilling fluid and concluded that an optimum amount of PAC should be used that prevents the formation of gel in the cuttings bed.

Tonmukayakul et al. (2013) presented a new method for evaluating particle settling velocity in viscoelastic fluids for hydraulic fracturing operations. The authors identified the importance of non-zero normal stress differences in inhibiting particle settling velocity in viscoelastic fluids. They presented the following equation for estimating the settling velocity of particles in viscoelastic fluids:

$$V_s = \frac{2\alpha^2}{9\mu(\dot{\gamma})}\Delta\rho g - \frac{2\alpha}{3}\frac{\alpha|N_1(\dot{\gamma})|}{\mu(\dot{\gamma})} \qquad \textbf{Eq.(2-13)}$$

In Eq. (2-13) α is a parameter related to the strain induced by the weight of the particles. This equation shows that the non-zero normal stress differences in the flow causes a reduction in the settling velocity of the particles. This equation also reveals that viscoelastic properties become dominant at higher shear rates where N_1 is significant. The importance of the presented equation by Tonmukayakul et al. (2013) is that it acknowledges the presence of an additional elastic force on the particles due to non-zero normal stress difference.

In a DNS study by Choi et al. (2010) on the migration of sediment particles in the Couette flow of viscoelastic particles, the author found that regardless of the initial position of the particle in the system, the particle always migrates toward the outer cylinder. This finding is relevant to cuttings transport in such a way that rotation of the drill string in the wellbore creates a geometry like Couette flow. The results imply that the use of viscoelastic fluids in conjugation with drill pipe rotation may exacerbate the settling of cuttings in the bed.

Tehrani (1996) experimented the idea of particles migration due to viscoelasticity in pipe flow of slurry flows. The authors claimed that viscoelasticity causes the particles to migrate toward the regions of lower shear rate, notably the center of the tube. However, the migration rate depended upon the rate of shear and the balance between elastic and viscous forces. The results confirmed viscoelasticity is a desirable property for a fracturing fluid to carry the proppant to the formation due to its superior suspension ability.

Goel et al. (2002) experimentally studied the transport of proppants using three different guar gum cross-linked fluids. The authors found that the settling characteristics of proppants correlated with the fluid viscoelasticity and not with their viscosity. Hu et al. (2015) also investigated the role of viscoelasticity in settling characteristic of proppant particles under dynamic condition. They found that elasticity affects particles settling depending on shear rate and relaxation time of the polymer solutions. Gomaa et al. (2014) stated viscoelasticity as a desirable characteristic for a fracturing fluid because of their superior suspension performance. Harris et al. (2008) examined the impact of suspending particles on the rheology of the carrier fluids using three different methods of measurement. They concluded that the suspended particles affect the rheological properties of the fluid. Additionally, they found the shear viscosity holds no relevance for prediction of slurry transport for higher shear rates in a viscoelastic medium.

Acharya (1988) conducted an experimental and theoretical study on proppant transport using different fluids. The authors found that viscoelastic properties of the fluid affect particles transport depending on the flow regime. In the low Reynolds number flows, the viscosity is the dominant factor controlling particles settling. On the other hand, at higher Reynolds numbers settling velocity no longer depends upon viscosity and viscoelasticity controls the settling velocity. They recommended characteristic of an ideal support fluid be one with high elastic and viscous moduli. Van den Brule and Gheissary (1993) also reported similar results to that of Acharya (1988). They showed viscoelasticity becomes a significant factor at higher shear rates.

Jefri and Zahed (1989) studied particles transport and migration in a slit channel flow using three fluids of different viscoelastic behaviors. They found that the fluid with shear thinning characteristic and strong elasticity strongly affects the movement of particles. As opposed to Newtonian fluids, the elastic fluids caused the particle to migrate away from the centerline of the channel causing inhomogeneity in concentration distribution.

Werner et al. (2017) conducted a detailed measure of fluid's rheological properties along with flow loop test to assess the hole cleaning capability of an Oil Based Mud (OBM) and a Wate Based Mud (WBM). The oil based mud appeared to be superior in term of carrying the cuttings out of the wellbore. The author argued the light internal structures at low shear rates and small yield stresses were the main reason for the better hole cleaning performance of the OMB. The viscoelastic measurements showed the WBM had higher elasticity than the OBM. On the other hand; the OBM had a higher shear viscosity than the WBM.

In summary, the available literature regarding the impact of fluid viscoelasticity on the solid transport is mostly limited to settling velocity measurements and transport of fracturing agents in suspension. No such study is available where the effect of fluid elasticity on the bed erosion or hole cleaning has been studied. Nonetheless, the results of previous studies provide some insight into the effect of viscoelasticity on hole cleaning. Almost all of previous studies have shown improving elastic properties of the carrier fluid causes the settling velocity to reduce. Therefore, elasticity is a desirable feature for transporting particles in suspension. Some of the studies have identified the role of non-zero normal stress difference and the elastic fluid force on particles in an elastic medium. This elastic force can be both helpful and detrimental to hole cleaning operations depending on its direction. However, there is no evidence on whether this force is useful for particle removal. At this moment there is no conclusive proof of the role of fluid elasticity on particles removal from a deposited bed of cuttings. Therefore, further research is needed in this area.

2.3 Semi-empirical and mechanistic models of hole cleaning

Mechanistic and semi-mechanistic hole cleaning models study cuttings transport using simplified models. The mechanistic models are drawn up by force balance on cuttings particles in the bed (Clark and Bickham 1994, Ramadan et al. 2001, Ramadan et al. 2003, Duan et al. 2007). Figure 2-6 conceptually illustrates a simplified sketch of the force balance on a cutting lying on the surface of a bed deposit. The idea for the development of all the mechanistic hole cleaning models are similar and revolves around balancing forces and moments to estimate the state of a particle in term of being stationary or otherwise.

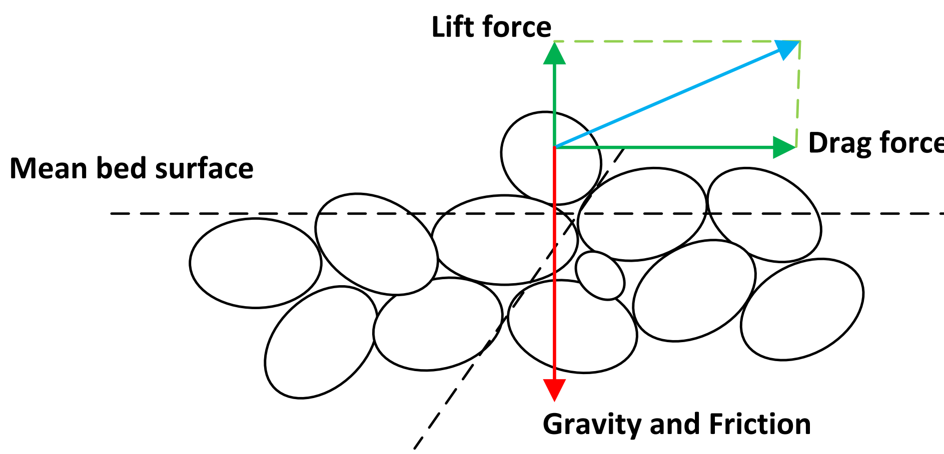

Figure 2-6 Simplified illustration of force balance on a cutting particle in the bed

The forces that act on the particle of interest are two types; holding forces and mobilizing forces. The holding forces include gravity (buoyed weight of the cuttings), friction between particles, and in the case of small size cuttings van Der Walls force. The mobilizing forces are mainly fluid hydrodynamic forces including drag and lifts forces. The necessary condition for the particle of interest to start rolling along the bed surface is that the moment produced by mobilizing forces surpass the moment generated by resistive forces.

One of the biggest problems with mechanistic and layer models are the difficulties in estimating the magnitude of the forces that act on the cuttings. Clark and Bickham (1994) developed a mechanistic model to predict the critical velocity for rolling and suspending cuttings. Similar models have been proposed by other researchers as well (Ramadan et al. 2003, Duan et al. 2007). One of the main issues with the mechanistic models is that they are written in term of local conditions (i.e. velocity and shear stress) over the bed. Therefore, the outcome of the models is often the local fluid velocity that results in dislodgement of the particle. Extending these local conditions to average measurable quantities (such as pump flow rate) is not trivial and accurate. That is because the fluid dynamics of flow in the presence of a bed of cuttings is not very well understood (Li and Luft 2014a, Li and Luft 2014b). Rubiandini R.S (1999) used Moore's slip velocity in vertical wells and modified it to predict the minimum depositional velocity in inclined wellbores. According to the authors, the new model produced results close to Larsen's model for angles of inclination beyond 45 degrees.

To develop a realistic mechanistic model, a good understanding of the nature of the interaction between the drilling fluid and drilled cuttings is necessary. Examples of such interaction are abundant both in nature (e.g. flow over river beds) and in the industrial systems (e.g. tailing ponds). Interaction of phases in these systems is bi-directional; the sediment phase can affect the turbulence in the carrier fluid phase and vice versa (Bagchi and Balachandar 2003). Sediment transport in flumes and channels which are pertinent to flow in rivers have been studied extensively in the past (Wiberg and Rubin 1989, Gore and Crowe 1991, Tsuji et al. 1991, Best et al. 1997, Miyazaki 1999, Carbonneau and Bergeron 2000, Sumer et al. 2003). Most of these bed erosion/sediment transport studies, however, involve water flow (as opposed to the flowing of more complex, non-Newtonian drilling fluids involved in hole cleaning operations in drilling oil and gas wells). Results of these studies have shown the complex nature of interactions of the phases in these systems.

One of the main issues with mechanistic hole cleaning models is that they either require local fluid velocity near the cuttings bed as an input or they predict the local fluid velocity as an output. However, in a turbulent flow, the local fluid velocity is not constant at the time and may deviate significantly from its average value. This approach neglects the presence of the fluctuations in the fluid velocity due to turbulent nature of the flow. Another assumption commonly used in most of the mechanistic models is the roughness of the cuttings bed.

Semi-mechanistic hole cleaning models are referred to the layered modeling of cuttings transport in directional wells. Layer modeling of cuttings transport in highly inclined wellbores was introduced by Gavignet and Sobey (1989) to drilling literature. This work was inspired by the earlier work of Wilson (1976) and Doron and Barnea (1993) on slurry transport in pipes.

Since the work of Gavignet and Sobey (1989) many versions of layer modeling of cuttings transport has been published (Martins et al. , Martins et al. , Iyoho and Takahashi 1993, Nguyen and Rahman 1998, Kamp and Rivero 1999, Cho et al. 2000, Ozbayoglu et al. 2005, Ramadan et al. 2005, Naganawa and Nomura 2006, Espinosa-Paredes et al. 2007, Wang et al. 2009, Guo et al. 2010). Layer models are mostly focused on two and three-layer models. The aim of most of these methods is to predict cuttings concentration in the wellbore. These models are primarily developed based on mass and momentum balance on different defined layers. They often require closure for unknown terms such as diffusivity or interfacial friction factors. These terms are not well understood. Results of these models rarely have been verified with those of experiments (Kelessidis and Mpandelis 2003). Kelessidis and Mpandelis (2004b) reviewed most of the available layer models in drilling literature and pointed out the issues relevant to their validation. Cho et al. (2000) compared predictions of several of these models with those of experiments and showed their inadequacies. In a new approach, Espinosa-Paredes et al. (2007) used volume integration to solve the mass and momentum equation in a two layer approach modeling. Proper coupling of the phases was identified for the condition where two distinct zones (namely stationary bed and suspension layer above it) exist. Numerical solution of the model can yield average pressure loss and velocity in the annulus. The model prediction, however, was not satisfactory for a suspended flow.

In the context of layer modeling, one momentum equation is written for each layer. For the simple case of 2 layer modeling (Figure 2-7), the momentum equations are (Kelessidis and Bandelis 2004a):

$$A_f \frac{dP}{dx} = -\tau_w S_w - \tau_b S_b \qquad \textbf{Eq.(2-14)}$$

$$A_b \frac{dP}{dx} = \tau_b S_b - \tau_{bw} S_{bw} - F_b \qquad \textbf{Eq.(2-15)}$$

In these equations, S_b is the interfacial bed area, S_{bw} is the bed contact area with the wall, S_w is the wetted perimeter of the pipes and A_b is the bed cross sectional area.

Semi-mechanistic and empirical models of hole cleaning all rely on the accurate estimation of the bed shear stress.

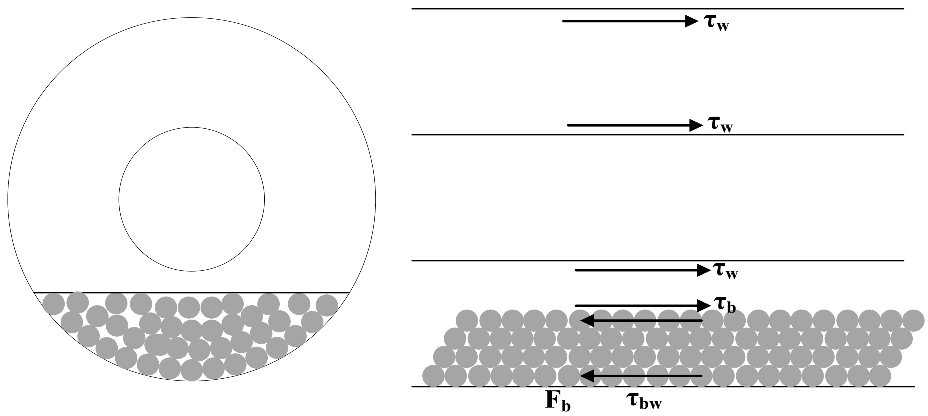

Figure 2-7 Schematic illustration of shear stresses in a two-layer model.

Dimensional analysis is another tool in developing a correlation for predicting cuttings transport efficiency (Luo et al. 1992, Martins and Santana 1992). The dimensional analysis utilizes the Pi theorem to identify the relevant dimensionless groups that govern the system. Different models have been developed for purposes such as predicting stationary bed thickness, cuttings concentration, and frictional pressure loss. Luo et al. (1992) presented a dimensional analysis based on pi-theorem. They identified seven dimensionless groups to be related to cuttings transport and hole cleaning. The model was further developed to predict the minimum flow rate for avoiding the formation of stationary bed. Martins and Santana (1992) also conducted dimensional analysis to study cuttings transport. Ozbayoglu et al. (2010a) did dimensional analysis and found seven independent group related to bed thickness. Li and Luft (2014a) stated that dimensionless analysis based on pi-theorem inherent some deficiencies which make them not suitable for cuttings transport modeling.

Last class of models is empirical correlations (Larsen et al. 1997, Li and Walker 1999, Zou et al. 2000, Sorgun et al. 2011). These correlations are those developed based on the experimental data. Larsen et al. (1997) model are one of the great empirical relationships for predicting critical depositional velocity. Sorgun et al. (2011) also presented an empirical correlation to predict frictional pressure loss in the presence of cuttings bed in an eccentric annulus.

2.4 Sediment transport research in other fields

Transport of solid particles via a fluid is not limited to drilling operations and is observed in many other industries. Examples of such flows include manufacturing, mineral extraction, environmental remediation, river beds, fluidized beds, and particle-laden flows (GarcÁa 2008). The studies conducted in other fields can significantly improve the understanding of the fundamental mechanism of solids transport in deviated wells, even if the results are not directly applicable to hole cleaning. In this section, we try to summarize some of the works conducted in other fields that hold relevance to hole cleaning studies.

2.4.1 The concept of critical shear stress and Shields' parameter

One of the classical problems in sediment transport studies has been that of predicting a flow strength that would result in movement of sediments in incipient motion. The shear stress at which the bed material starts moving is often denoted as the critical shear stress (Grass 1970). Shields (1936) proposed the use of a nondimensional form of shear stress to predict the onset of bed erosion. The nondimensional form of bed shear stress introduced by Shields is often called Shields' stress or parameter and is defined as follows:

$$\tau^* = \frac{\tau_b}{d_p g(\rho_s - \rho_f)} \qquad \textbf{Eq.(2-16)}$$

The Shields' stress represents the fluid force exerted on the sediment particle to that of its submerged weight. Hence, it is a direct measure of the fluids drag force on the bed materials, if multiplied by d_p^2. The concept of the Shields' stress and the existing correlations is to correlate the critical Shields' stress with a boundary Reynolds number. In this manner, Shields' stress at the onset of bed erosion should all fall to the same curve. A quick survey of the literature, especially the earth science and geology field, reveals that there are numerous number of correlations proposed for predicting onset of bed erosion using Shields' criterion (Cheng 1969, Andrews 1983, Carling 1983, Buffington and Montgomery 1998, Beheshti and Ataie-Ashtiani 2008). Figure 2-8 shows an example of shields diagram used in estimating initiation of motion for gravel beds versus boundary Reynolds number. In this graph, D is the particles diameter and u* is the friction velocity.

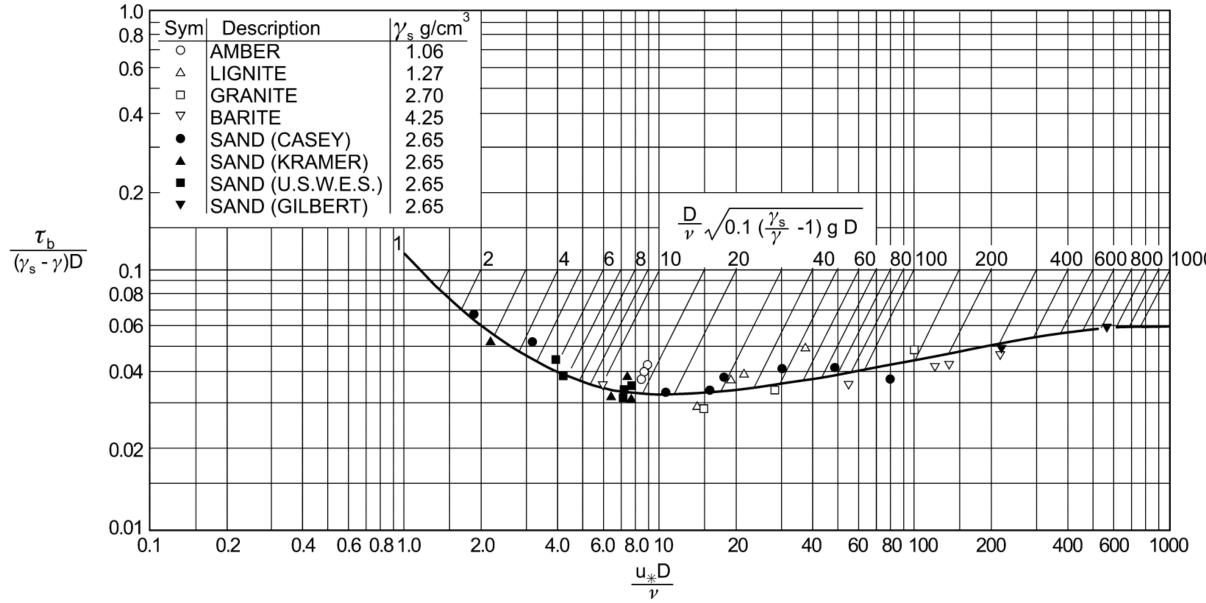

Figure 2-8 Shields diagram for initiation of motion (Vanoni 1975, GarcÁa 2008)

The Shields’ stress approach utilized in the study of the movement of gravel beds have been further extended to pipe flow of slurries. In the literature, there are some papers which report criterion for the onset of bed erosion in pipe flow regarding critical shear stress (Ouriemi et al. 2007, Peysson et al. 2009). The use of Shields parameter is a flattering idea for predicting efficient hole cleaning. If such approach is correct, one should be able to find a correlation that can be employed for predicting the onset of bed erosion.

There have been numerous attempts in sediment transport and cuttings removal studies in highly inclined wellbores to quantify the beginning of bed erosion regarding measurable parameters such as pressure loss and or flow rate (Li and Luft 2014b). However, these models often have limited success. Newly emerging research on sediments transport studies may hold the answer to the limitations of these models.

The traditional approach in estimating onset of particles movement has long been linked to a critical Shields’ number. Numerous correlations in the literature report critical Shields stress (Ouriemi et al. 2007, Peysson et al. 2009). In a recent study, Houssais et al. (2015) looked at the onset of particles moving in a shear flow. The results of their experiment revealed that contrary to the consensus on the existence of a critical shear stress, the beginning of particles movement is a continuous process. They found that bed materials move even at small shear stresses. However, this movement is in the form of the bed creeping flow. Therefore, if a stationary bed is shared at low shear stresses, the particles in the bed creep and rearrange their positions to accommodate for the exerted fluid stress on the cuttings bed. This implies that shearing a cuttings bed at small shear stresses would result in further compaction of the bed. The compaction then makes the bed erosion more difficult.

Houssais et al. (2015) study have shown that particles movement does not stop at a well-defined shear stress. The implication of such observation is that any number reported in the literature as the critical shear stress (or Shields number) becomes subjective to the technique and resolution of the technique used to obtain such number. It would also be affected by the judgment of the researchers who have made the measurements. Another important consequence of the experiments conducted by Houssais et al. (2015) is that the assumption of static friction for the bed does not hold for small shear stresses (or what is called sub-critical shear stress). That is because the bed is continuously rearranging to accommodate the fluid's shear stress on its surface. This assumption is commonly used in the multi-layering approach of cuttings transport in horizontal wells (Kelessidis and Bandelis 2004a).

Creeping of the bed material as a result of fluid shear stress drives the bed toward a more compacted state, and hence it makes the erosion of the bed more difficult. On the other hand, if the shear stress is high enough to erode the bed in bedload form, the bed materials start to dilate. This in turn makes the erosion easier. Therefore, depending on the shearing history of the cuttings bed, the critical shear stress does vary. The consequence of this finding is that the sediment transport is affected by both the fluid hydrodynamic forces as well as the granular flow of the bed material. Capart and Fraccarollo (2011) also found bedload transport of sediments respond to change in flow condition by adjusting granular concentration at the base layer.

Proper modeling of sediment transport requires modeling of both continuum and the granular materials (Ouriemi et al. 2009). The granular material has a viscoplastic behavior (Boyer et al. 2011); that is they exhibit a yield stress before flowing. However, in drilling literature, only the continuum model of the fluid is often used to model the removal of cuttings in the well. There is no mention of the granular materials properties and their flowing characteristics in these models.

Boyer et al. (2011) and Houssais et al. (2015) both pointed out to the fact that hydrodynamic forces do not purely govern sediment transport modeling. Therefore, only considering fluid's shear stress on the cuttings bed does not capture the actual physics of this process; granular flow needs to be considered as well.

Modeling of granular material is a complex topic that requires knowledge of granular viscosity and other properties of the granular material. Recent studies (Boyer et al. 2011) suggest that when a granular material is sheared, there is only one suitable dimensionless number and that is the inertial number.

$$I = \frac{d_p}{\dot{\gamma}} \sqrt{\frac{\rho_s}{P^p}} \qquad \textbf{Eq.(2-17)}$$

In this equation P^p is the confining pressure while $\dot{\gamma}$ is the shear rate at which the granular material is being sheared at. In fact this dimensionless number represents the ratio of rearrangement time ($d_p\sqrt{\frac{\rho_p}{P^p}}$) to that of strain rate ($\frac{1}{\dot{\gamma}}$). For sufficiently small Stokes number ($St = \frac{\rho_p d_p^2 \dot{\gamma}}{\mu}$), the viscous forces are dominant, and hence the system is no longer governed by the inertial number (Eq.(2-17)). In this case the viscous number should be used (Boyer et al. 2011):

$$I = \frac{\mu \dot{\gamma}}{P^p} \qquad \textbf{Eq.(2-18)}$$

Using the inertial number or the viscous number, then the behavior of a granular material can be related to these figures. Houssais et al. (2015) found in their study that the onset of granular flow is associated with a critical viscous number. The importance of viscous number or inertial number is that it includes both fluid related factor as well as granular properties. The inclusion of confining pressure is a major factor that has been missing in the entire drilling literature. The confining pressure can have a significant implication on the importance of viscous or inertial forces.

Overall, the classical sediment transport studies suggest a correlation between bed shear stress (in the form of Shields' stress) and the threshold of particles movement. However, new studies indicate that this view does not sufficiently reflect the actual physics of the process. Using the classical approach may lead to the development of empirical correlations for practical purposes. On the other hand, for fundamental modeling purposes, this method may not produce satisfactory results.

2.4.2 Turbulence and Sediment Transport

In addition to the discussion in the previous section, flow turbulence induces another factor that needs to be addressed in any solid transport study. Flow turbulence is often ignored when critical shear stress approach is used for predicting the onset of bed erosion. However, new studies suggest this assumption may not be valid (Diplas et al. 2008).

Initiation of movement of a sediment particle at the bed interface is directly related to the local fluid velocity near the bed. In turbulent flow, the local flow velocity is time dependent, and hence, the fluid force becomes time dependent. Fluctuations in the effective fluid velocity result in variations in the fluid hydrodynamic force acting on the particles. These changes can create an energy high enough to dislodge the particle. Several studies have shown the importance of flow turbulence in sediment transport (Diplas et al. 2008, Heyman et al. 2013, Schmeeckle 2014).

In an experimental study, Diplas et al. (2008) studied the role of flow turbulence on the initiation of motion of particles. They found out that any instance of particles dislodgment was coincided by a peak in the local velocity. However, not all the positive fluctuations in the velocity resulted in particles movement. Their study showed that a peak in the local velocity was necessary but not sufficient for particles dislodgment. In another word, a peak velocity of sufficient magnitude and duration can initiate movement of the particle. The length of the velocity fluctuation is as important as the scale of the peak. The result of their study showed that critical drag force correlates well with the time of applying the force.

Chan-Braun et al. (2011) numerically studied torque and drag force on a single particle in turbulent flows. The results showed the instantaneous fluctuations are significant. The variations of forces demonstrated a strong non-Gaussian probability density function.

Bagchi and Balachandar (2003) utilized DNS to study the variation of drag and lift force on a single spherical particle in an isotropic turbulent flow. The results revealed that the fluctuations are a function of particle size. For small particles, the variation was small, and the mean drag force was sufficient to predict the fluid force accurately. On the other hand, for larger particles, the instantaneous drag deviated from its average value, showing turbulence becomes significant for larger particles.

Schmeeckle (2014) conducted an LES – DEM study of solids transport in channel flows. The results revealed that particles significantly affect flow turbulence, particularly at the transition point between bedload to suspension load. It was found that particles reduced turbulence in the vertical direction.

In addition to the impact of fluctuation velocities on particles dislodgement, the secondary phase also affects flow turbulence. The method of sediment transport in oil wells is a four-way coupling process (that is a movement of solid particles affects the flow and vice versa, particles affect each other too). In this context, the flow turbulence is also affected by bedload transport of particles or even the mere presence of the sand bed. Studies in channels and river beds have shown turbulence can be either amplified or dampened by the secondary phase (Best et al. 1997, Carbonneau and Bergeron 2000). However, there is no consensus on the impact of particles movement on flow turbulence. Additionally, bedload transport of sand particles can affect equivalent bed roughness height. Movement of sand particles in a bedload layer has been reported to induce an additional source of roughness (Owen 1964, Best et al. 1997, Bigillon et al. 2006). Some researchers even suggest that bedload transport of sediments causes a reduction in von Karman constant (Best et al. 1997, Nikora and Goring 2000, Gaudio et al. 2010).

Overall, the research results from other fields of studies concerning solid transport indicate that flow turbulence is a major factor in the process of solid transport. Similar studies in the drilling literature is scarce. Therefore, further work is needed to be conducted in wellbores to quantify the role of flow turbulence on hole cleaning.

2.5 CFD as a Tool for Multiphase Flow Modeling

Computational Fluid Dynamics (CFD) has great potential to replace expensive and tedious experimental studies. With the enhancement of computer hardware and emerging advanced codes, the use of CFD models is rising significantly. In this context, CFD offers another tool for studying hole cleaning. In this section, we try to summarize some of the efforts that have been made in utilizing state of the art numerical schemes in drilling and other relevant fields. We start by briefly reviewing the basics of CFD and some relevant studies in turbulent flow. After that, a summary of current knowledge of CFD studies in hole cleaning and cuttings transport studies is given.

2.5.1 Numerical approaches to turbulent flow modeling

There are three approaches to fluid flow modeling; namely Direct Numerical Simulation (DNS), Large Eddy Simulation (LES) and Reynolds Average Navier-Stokes (RANS) modeling. In DNS there is no modeling involved as the Navier-Stokes (NS) equations are solved exactly (Orszag 2006). This method requires very fine grids and tiny time steps to capture the smallest scales of turbulence. Computationally this approach is not attractive and applicable in realistic high Reynolds number flows.

In contrast to DNS where all the scales of turbulence are resolved, in LES method only largest eddies are resolved, and smaller eddies are modeled using a sub-grid model. In LES approach, transient NS equations are solved exactly for biggest eddies in the flow. These large eddies contain most of the energy in the system, and therefore, are more critical in sustaining turbulence. Smaller eddies, which are responsible for dissipating energy, contain much less energy. The sub-grid model ensures energy is conserved from largest eddies to the smallest dissipative eddies.

LES is computationally less expensive than DNS. The cut-off size (the size for which smaller eddies are modeled) is determined by the scale of the grid used. Hence, the smaller the grid, the more accurate the model becomes. Even with these advantages of LES over DNS, it is still computationally expensive especially in the wall-bounded flows and has not been used widely in the industry.

Reynolds Average Navier-Stokes (RANS) models apply Reynolds decomposition procedure to NS equation. Each variable has a fluctuating part and a mean value. Navier-Stokes equations are time averaged to get rid of the fluctuating part of the variables. This time averaging results in some unknown quantities (Reynolds stresses) which makes the system of equations an open system (i.e. more unknown than some equations). To solve this system of equations, closure is needed. RANS models try to model the Reynolds stresses with proper closure. Estimating Reynolds stress based on eddy viscosity (or turbulent viscosity) is a common modeling approach in RANS modeling.

Eddy viscosity approach models turbulent stresses (Reynolds stresses) with a scalar eddy viscosity (or equivalently called turbulent viscosity). Turbulence models such as $k-\varepsilon$ and $k-\omega$ and shear stress transport (SST) are all eddy viscosity models. These models estimate the eddy viscosity using additional turbulence entities like turbulent kinetic energy and or dissipation. Each model has its own pros and cons. The computational costs of these models are low.

Reynolds Stress Models (RSM) are also based on RANS formulation. Each term in the Reynolds stress tensor (6 terms since stress is isotropic) have its transport equation. These six additional equations are solved together with mass and momentum equations. The advantage of RSM models over previous eddy viscosity models is that they can model anisotropy in the flow (such as swirling flows). The disadvantage is its computational cost comparing to eddy viscosity models.

There is another class of models which are a blend between LES and RANS models. Detached Eddy Simulation (DES), Scale-Adaptive Simulation (SAS) are two examples. These models blend the different approaches to get the benefit of both models and capture more details of the flow while minimizing the computational expense.

2.5.2 Applications of CFD in turbulence modeling in annulus

CFD has been wieldy used in various disciplines of engineering to solve fluid flow related problems. Turbulent flow modeling of Newtonian fluid flow inside annulus has been done in the past using different methods. Chung et al. (2002) have conducted a DNS study of turbulent flow in the annulus. Their results were in agreement with experimental data. LES also has been performed for turbulent flow of water in annuli with inner body rotation. Results were also in agreement with previous experimental studies (Chung and Sung 2005). Some other studies used RANS formulations to study the turbulent flow of Newtonian fluids inside annular conduits (Naser 1997, Azouz and Shirazi 1998, Neto et al. 2011).

Turbulent flow of Newtonian fluids is not commonly encountered in the drilling industry. Most of the fluids used in the oil field are of non-Newtonian nature. Turbulent flows of non-Newtonian polymeric fluids are different from Newtonian fluids. Certain phenomena occur in the turbulent flow of such fluids which are absent otherwise. Experimentally, turbulent flow of non-Newtonian fluids has been investigated extensively in the past (Fredrickson and Bird 1958, Dodge and Metzner 1959, Virk et al. 1970, Pinho and Whitelaw 1990, Nouri et al. 1993, Escudier et al. 1995, Warholic et al. 1999, Ptasinski et al. 2001, Warholic et al. 2001, Ptasinski et al. 2003, Paschkewitz et al. 2005, Japper-Jaafar et al. 2010, Bizhani et al. 2015, Erge et al. 2015). Some of the key differences of flow of this class of fluids with that of Newtonian fluids are:

- Shift of velocity profiles away from the Newtonian fluids curve in the logarithmic region (Pinho and Whitelaw 1990, Nouri et al. 1993, Escudier et al. 1995, Ptasinski et al. 2001, Japper-Jaafar et al. 2010, Rodriguez-Corredor et al. 2014)
- Thickening of buffer and sublayer (Lumley 1969, Wilson and Thomas 1985)
- Reynolds stress reduction (Pinho and Whitelaw 1990, Nouri et al. 1993, Warholic et al. 2001, Ptasinski et al. 2003, Paschkewitz et al. 2005, Japper-Jaafar et al. 2010, Rodriguez-Corredor et al. 2014),
- Stress deficit (Ptasinski et al. 2001, Ptasinski et al. 2003, Bizhani et al. 2015)
- Vortex inhibition and suppression of radial velocity fluctuations (Pinho and Whitelaw 1990, Nouri et al. 1993, Warholic et al. 2001, Kawaguchi et al. 2002, Japper-Jaafar et al. 2010)

Due to differences in the flow of Newtonian and non-Newtonian fluids, turbulent models developed for modeling Newtonian fluids cannot be directly used for modeling flow of non-Newtonian fluids. If one uses the same transport equations as Newtonian fluids with non-Newtonian viscosity, it will lead to tremendous amount of pressure loss prediction. Naser (1997) tested $k-\varepsilon$ turbulence model for predicting non-Newtonian fluids flow in annulus. The results showed this model cannot be directly applied to model such flow without further modification.

In modeling flow of non-Newtonian fluids, understanding the fundamental underlying physics of flow of such fluids is important. A minute amount of polymer additives can reduce the frictional pressure loss up to 60%. This capability which has great potential in energy saving is referred to as drag reduction. According to Virk's asymptote (Virk et al. 1970), there is a maximum achievable drag reduction for a given flow condition.

Currently, there are two theories on the reduction of frictional pressure loss caused by polymer additives. Lumley (1969) proposed that the stretching of polymers, especially in the buffer layer, increases the effective viscosity of the solution. Therefore, viscous sublayer thickens. The consequence of this phenomena is drag reduction (Wilson and Thomas (1985) reported similar mechanism). Tabor and Degennes (1986) related the elastic behavior of the polymer chains to drag reduction. According to the authors, it is the elastic property of the polymer chains which inhibits the production of turbulent fluctuations at small scales. Elasticity increases the smallest scale of the flow.

At present, there are two main approaches for modeling the turbulent flow of non-Newtonian fluids. The first approach is based on viscoelastic constitutive laws while the second method is based on modified Newtonian turbulent models (also known as Generalized Newtonian Fluid models (GNF)).

Using the kinetic theory, Bird et al. (1980) have derived the governing equations for flow of flexible polymer chains; an approach that is known as Finitely Extensible Non-Linear Elastic (FENE). In FENE, polymer chains are modeled as interconnected beads. The beads are connected using a non-linear spring. Each spring has a maximum extension length and a relaxation time. Since a polymer chain consists of many monomers, and therefore, they have a broad range of length and time scale. For an accurate representation of these chains, the number of interconnected beads to represents them must be enough. For example, if 20 beads are used to represents a polymer chain better results would be obtained than a model which uses two beads. The implication of using a greater number of beads is the higher computational time. That limits the use of a vast number of beads for practical problems (Jin and Collins 2007).

Two main issues are associated with FENE based models or any other viscoelastic model at the present moment. The first is the fact that it applies to very dilute polymer solutions; concentrations at which solution viscosity almost does not change (remains the same as that of solvent). This condition does not exist in real drilling applications. The 2nd difficulty lies in the numerical solution of the conformation tensor (which contains all the information regarding polymer chain length and orientation). The transport equation for conformation tensor is hyperbolic which imposes difficulties in getting convergence and also applying boundary condition at walls.

Despite the challenges in using FENE or other elastic constitutive models (Bird et al. 1977, Bird 1987), they can shed light on important features of turbulent flow of non-Newtonian fluids. These classes of models are mostly used in DNS studies (Sureshkumar et al. 1997, Sibilla and Baron 2002, Min et al. 2003, Min et al. 2003, Ptasinski et al. 2003, Paschkewitz et al. 2005, Jin and Collins 2007). DNS results showed flexible polymer chains absorb the energy which sustains the vortices in the buffer layer by stretching. These stretched chains as they move away from the wall release back some part of the stored energy. They have also illustrated this energy release mainly occur in the streamwise direction which amplifies the streamwise velocity fluctuation and gives rise to strong stress anisotropy (Dubief et al. 2004, Iaccarino et al. 2010). Results of these DNS studies are being used to develop closures for RANS modeling of turbulent flow of non-Newtonian fluids (Pinho et al. 2008, Iaccarino et al. 2010, Resende et al. 2011). Currently, there are numerous numbers of emerging papers with closure equations for modeling turbulent non-Newtonian fluids ((Pinho 2003, Pinho et al. 2008, Iaccarino et al. 2010, Resende et al. 2011)). Almost all of these recent studies use viscoelastic models of polymer solutions. These models have not been yet verified and or coded in commercial CFD packages.

The 2nd approach in modeling turbulent non-Newtonian fluid flow is the so-called Generalized Newtonian Fluid (GNF) approach. In GNF approach, the elastic properties are mostly ignored. However, there are some models, which accounts for elastic properties such as extensional viscosity (e.g. the model proposed by Pinho (2003)). In GNF method, the constitutive equations of Newtonian fluids are modified to produce effects associated with the flow of non-Newtonian fluids. For example, most of these models contain a damping function for eddy viscosity which controls the production of eddy viscosity and produces drag reduction effect. Some of these models are simple zero equation models such as the one proposed by Azouz and Shirazi (1997). Others like turbulence model of Hassid and Poreh (1978) are of 2 equations family models. Several models based on GNF approach have been integrated into CFD package to simulate the flow of polymer solutions in the annulus. Some of these models are capable of reproducing velocity profiles and predicting frictional pressure loss (Hassid and Poreh 1978, Azouz and Shirazi 1997, Pinho 2003, Ro and Ryou 2012).

The discussion on turbulence modeling of non-Newtonian fluid is imperative for understanding the debate in the next section. In the following section, we summarize some of the CFD studies in hole cleaning. The importance of the current discussion becomes clear when we refer to each work and the method they used for modeling turbulence in the wellbore.

2.5.3 CFD as a Tool for Studying Hole Cleaning

Improvement in computer hardware systems and also advanced codes for solving a complex system of equations have opened new horizons for investigating fluid flow related problems. CFD has a great potential to replace expensive laboratory setups. It allows simulating an unlimited number of conditions promptly. Results of CFD can shine lights upon phenomenon where experiments cannot be performed. Use of CFD codes is dramatically increasing. A quick search in the drilling area shows that use of CFD codes has grown drastically recently. There is not much publication before 2007. King et al. (2000) have introduced the concept of using a 3-D numerical solver to improve the cuttings transport process. The idea was to investigate different cases of fluid flow in the annulus to improve the process of cuttings removal.

One of the earlier attempts at using CFD to study cuttings transport was made by Bilgesu et al. (2002). Water and power law fluids were used in the simulations. Cuttings of varying size along with different mud densities were tested. No indication was given on whether the flow is turbulent or laminar. Results confirmed higher flow rates and higher mud densities are favorable in hole cleaning with no further discussion of the details. In another study, Bilgesu et al. (2007) employed the FLUENT Eulerian multiphase model to explore the impact of different variables (such as ROP, inclination angle and so on) on cuttings transport. The authors used $k-\varepsilon$ turbulence model of Newtonian fluids. One of the controversial finding was that transport efficiency was higher for bigger cuttings (8mm versus 3mm). Inner pipe rotation effect was found to be marginal.

Mishra (2007) utilized Eulerian-Eulerian model in FLUENT to investigate the impact of several parameters on cuttings transport. The author used water as drilling fluid. Cuttings size of 3mm and 8mm were used. Increasing ROP resulted in higher concentration. Higher flow rates were reducing the cuttings concentration. Smaller cuttings were found to have a higher concentration than bigger ones under the same operational condition. Pipe rotation marginally enhanced cuttings transport.

Ali (2002) in a study conducted in 2002 used the Lagrangian particle tracking method to study cuttings transport in vertical and horizontal wells. Strangely their results showed for the same drilling fluid; horizontal wells have better hole cleaning than vertical wells which is against experimental and field data. The impact of mud weight, viscosity, cuttings size and hole angle were investigated. Their results confirmed higher viscosity is favorable in hole cleaning. Mud weight enhanced transport efficiency.

Eesa and Barigou (2009) utilized Eulerian-Eulerian approach to investigate the transport of near-neutral coarse particles in laminar pipe flow of power law fluids. Results of simulation were in agreement with particle velocity profile measured experimentally. Pressure loss was also successfully predicted via the model.

Hussain H. Al-Kayiem (2010) used CFD to simulate cuttings transport in a 30 degree inclined well. The flow regime was laminar, and power law viscosity model was used to represent the drilling fluid. According to the author, velocity profiles were found to be flat in the wider range of widths which results in better distribution of drag force, and hence, improved cuttings transport. Smaller cuttings were found to be easier to transport (2.64, 4.45 and 7mm). Lower sphericity was determined to hamper cuttings transport. The author's way of judging convergence is the number of solver iteration, not equations residuals and or other criterions which cast huge doubts on the validity of this work.

In a recent work, Gregory B. Dykes (2014) studied cuttings transport under different conditions using FLUENT. Interest was given to the impact of wellbore geometry (i.e. dimensions) and internal pipe rotation. Results were compared with data of Sanchez et al. (1999) and Tomren et al. (1986). Eulerian-Eulerian multiphase model in conjugation with RSM turbulence model of Newtonian fluids was used to resolve the flow turbulence. Results of validation case (for cuttings concentration in each part of the annulus) were compared with those of experiments. However, a great difference was observed which authors did not discuss further. The second validation case was with non-Newtonian fluids where differences between experimental data and simulation results ranged from 8 up to 74%. The author's stated quantitative comparison between results was not possible. Regardless of the validation cases results, they carried on their simulation to look at the effect of different parameters.

CFD-DEM approach was adopted by Akhshik et al. (2015) for modeling of cuttings transport in the annulus. The primary goal of this study was to investigate the impact of pipe rotation on the dynamic behavior of cuttings transport. Herschel-Bulkley rheology model was used to describe fluid viscosity. The authors did not clarify whether the flow is turbulent or laminar. Simulation results showed the phenomenon of cuttings deposition on the lower side of the wellbore until a constant bed height was reached. Also, the simulation showed distinct regions of cuttings, namely stationary and moving bed plus region above with little cuttings concentration. Results confirmed the fact that pipe rotation causes cuttings distribution to be different from the case of no pipe rotation. Pipe rotation caused an increase in thickness of the moving layer, which results in thinner bed thickness and a greater rate of transport. CFD-DEM showed a dominant mechanism for cuttings transport for high angle wellbores (near horizontal) is rolling while the suspension is observed for low angle wells.

Two fluid multiphase model was used by Hajidavalloo et al. (2013) to study the effect of different parameters such as pipe rotation and eccentricity on cuttings transport by air in vertical wells. Results confirmed the adverse influence of eccentricity. Pipe rotation resulted in a more uniform velocity profile, and hence, improved cuttings transport. Unfortunately, the authors gave no information on whether their simulation is turbulent or laminar. The length of annulus used for the simulation is only five times the hydraulic diameter which makes the results controversial. Results of the simulation showed even in vertical wells, if eccentricity is presented, cuttings tend to accumulate in the narrower gap of the annulus. On the other hand, drill pipe rotation caused the velocity maximum to shift to the smaller gap, hence, improving cuttings transport.

Rooki et al. (2014) utilized CFD two fluid model to study the effect of foam quality, eccentricity, pipe rotation, and hole inclination on cuttings transport. Simulations were performed for laminar flow and ROP of $50\frac{ft}{hr}$ and cuttings size of 3mm. Simulations results confirmed the positive impact of pipe rotation on cuttings transport. Results showed for inclination angles beyond 60 degrees stationary cuttings bed form. For angles between 30 up to 60 moving bed pattern was observed.

Sun et al. (2014) studied the impact of inner pipe rotation on cuttings transport. Inclination angles varied from 45 up to 90. Eulerian approach with realizable $k-\varepsilon$ model and standard wall function were used. Considered fluid has a constant viscosity (i.e. Newtonian fluid). The results showed pipe rotation enhances cuttings transport but its improvement is more at lower flow rates. Pressure loss in the annulus decreased by increasing inner pipe rotation.

Mme and Skalle (2012) used Lagrangian particle tracking in conjugation with $k-\varepsilon$ model and non-Newtonian power law fluids to study cuttings transport. Effect of annular flow behaviour, rheology, hole angle and cuttings properties were considered. Results showed smaller cuttings are easier to transport (3mm). However, the reported results are not compared and validated to other studies. Shape factor was found to have minimal impact on carrying capacity.

Osgouei et al. (2013) simulated fluid-cuttings interactions in the horizontal eccentric annulus (this study only considers water as drilling fluid). Lagrangian particle tracking method was used. Validation was done by comparing pressure loss with those experimentally measured (particle size of 2.06mm). No evidence is given whether the flow is turbulent or not. The finding was rather obvious and qualitative rather than quantitative. For example, the authors showed higher flow rates are better for hole cleaning and or smaller ROP results in less concentration build-up in the wellbore.

Ofei et al. (2014) used the two fluid model approach to predicting pressure loss and cuttings concentration in the horizontal eccentric annulus. The impact of different variables such as fluid velocity, radius ratio, and inner pipe rotation was studied. Turbulent flow of a power law fluid was modeled in four various annuluses. The standard $k-\varepsilon$ turbulence model of Newtonian fluid was used. Their results showed increasing pipe rotation causes an increase in cuttings concentration when water is used as the carrier fluid. The same behaviour was observed for high radius ratios and non-Newtonian fluids. In terms of cuttings carrying capacity, high viscous fluids were found far more effective in transporting the cuttings. Using high viscosity fluids, no bed formed and cuttings traveled the wellbore in suspension.

Yilmaz (2012) utilized Lagrangian particle tracking to study the likelihood of cuttings accumulation on the lower side of an inclined well. One way coupling was assumed (that is only fluid affect particles, but particles do not have any impact on flow or other particles). Turbulence was modeled using SST model for both Newtonian and non-Newtonian fluids. Impact angle and impact velocity of particles interact with the wall were analyzed to assess the probability of particles accumulation on the lower side of the annulus.

Combining the discussion in this section with the previous chapter reveals most of the current CFD works lack credibility in the turbulent modeling of drilling fluid. The drilling fluid is non-Newtonian, and hence, the models adapted and calibrated for simulating the flow of Newtonian fluids cannot be directly used for modeling the flow of these class of fluids. Additionally, almost all of the CFD studies of hole cleaning and cuttings transport suffer from a sound validation. That is partially because there is no data available in the literature that can be directly used for validating CFD models. Overall, although the emerging trend of CFD modeling for hole cleaning is promising, serious concerns and doubts still exist about the results of such models.

2.6 References

Acharya, A. R. (1988). Viscoelasticity of Crosslinked Fracturing Fluids and Proppant Transport. SPE Production Engineering **3**(4), SPE-15937-PA, DOI: 10.2118/15937-PA.

Adari, R. B. (1999). Development of correlations relating bed erosion to flowing time for near horizontal wells. M.Sc. Thesis, University of Tulsa, USA

Adari, R. B., Miska, S., Kuru, E. et al. (2000). Selecting Drilling Fluid Properties and Flow Rates For Effective Hole Cleaning in High-Angle and Horizontal Wells. SPE Annual Technical Conference and Exhibition. Dallas, Texas, 1–4 October 2000., SPE-63050-MS,DOI: 10.2118/63050-MS.

Akhshik, S., Behzad, M. and Rajabi, M. (2015). CFD–DEM approach to investigate the effect of drill pipe rotation on cuttings transport behavior. Journal of Petroleum Science and Engineering **127**(0): 229-244, DOI: http://dx.doi.org/10.1016/j.petrol.2015.01.017.

Ali, M. W. (2002). A Parametric Study of Cutting Transport in Vertical and Horizontal Well Using Computational Fluid Dynamics (CFD). Msc thesis, College of Engineering and Mineral Resources at West Virginia University.

Andrews, E. D. (1983). Entrainment of gravel from naturally sorted riverbed material. Geological Society of America Bulletin **94**(10): 1225-1231, DOI: 10.1130/0016-7606(1983)94<1225:EOGFNS>2.0.CO;2.

Arnipally, S. K. and Kuru, E. (2017). Effect of Elastic Properties of the Fluids on the Particle Settling Velocity. Proceedings of the ASME 2017 36th International Conference on Ocean, Offshore and Arctic Engineering, OMAE2017-61192, June 25-30, 2017, Trondheim, Norway, Alternative Effect of Elastic Properties of the Fluids on the Particle Settling Velocity.

Asadi, M., Conway, M. W. and Barree, R. D. (2002). Zero Shear Viscosity Determination of Fracturing Fluids: An Essential Parameter In Proppant Transport Characterizations. International Symposium and Exhibition on Formation Damage Control, 20-21 February, Lafayette, Louisiana, SPE-73755-MS,DOI: 10.2118/73755-MS.

Azar, J. J. and Sanchez, R. A. (1997). Important Issues in Cuttings Transport for Drilling Directional Wells. Fifth Latin American and Caribbaean Petroleum Engineering Conference and Exibition. held in Rio de Janeiro, Brazil, 30 August -3 Spetember 1997, SPE-39020-MS,DOI: 10.2118/39020-MS.

Azouz, I. and Shirazi, S. A. (1997). Numerical simulation of drag reducing turbulent flow in annular conduits. Journal of Fluids Engineering-Transactions of the Asme **119**(4): 838-846, J Fluid Eng-T Asme, DOI: Doi 10.1115/1.2819506.

Azouz, I. and Shirazi, S. A. (1998). Evaluation of several turbulence models for turbulent flow in concentric and eccentric annuli. Journal of Energy Resources Technology-Transactions of the Asme **120**(4): 268-275, J Energ Resour-Asme, DOI: Doi 10.1115/1.2795047.

Bagchi, P. and Balachandar, S. (2003). Effect of turbulence on the drag and lift of a particle. Physics of Fluids **15**(11): 3496-3513, DOI: doi:http://dx.doi.org/10.1063/1.1616031.

Becker, T. E. and Azar, J. J. (1985). Mud-Weight And Hole-Geometry Effects On Cuttings Transport While Drilling Directionally, SPE-14711-MS.

Becker, T. E., Azar, J. J. and Okrajni, S. S. (1991). Correlations of Mud Rheological Properties With Cuttings-Transport Performance in Directional Drilling. SPE-19535-PA, DOI: 10.2118/19535-PA.

Beheshti, A. A. and Ataie-Ashtiani, B. (2008). Analysis of threshold and incipient conditions for sediment movement. Coastal Engineering **55**(5): 423-430, DOI: https://doi.org/10.1016/j.coastaleng.2008.01.003.

Best, J., Bennett, S., Bridge, J. et al. (1997). Turbulence modulation and particle velocities over flat sand beds at low transport rates. Journal of Hydraulic Engineering-Asce **123**(12): 1118-1129, J Hydraul Eng-Asce, DOI: c 10.1061/(Asce)0733-9429(1997)123:12(1118).

Bigillon, F., Couronne, G., Champagne, J. Y. et al. (2006). Investigation of flow hydrodynamics under equilibrium bedload transport conditions using PIV. River Flow 2006, Vols 1 and 2: 859-865, Proc Monogr Eng Wate, DOI: ://WOS:000241916500090.

Bilgesu, H. I., Ali, M. W., Aminian, K. et al. (2002). Computational Fluid Dynamics (CFD) as a Tool to Study Cutting Transport in Wellbores, SPE-78716-MS,DOI: 10.2118/78716-MS.

Bilgesu, H. I., Mishra, N. and Ameri, S. (2007). Understanding the Effect of Drilling Parameters on Hole Cleaning in Horizontal and Deviated Wellbores Using Computational Fluid Dynamics. SPE Eastern Regional Meeting Lexington, Kentucky, USA, 17-19 October 2007, SPE-111208-MS,DOI: 10.2118/111208-MS.

Bird, R. B., Armstrong, R. C. and Hassager, O. (1987). Dynamics of polymeric liquids. New York,, Wiley.

Bird, R. B., Dotson, P. J. and Johnson, N. L. (1980). Kinetic-Theory and Rheology of a Solution of Macromolecules Modeled as Finitely Extensible Bead-Spring Chains. Journal of Rheology **24**(3): 364-365, J Rheol.

Bizhani, M., Corredor, F. and Kuru, E. (2015). An Experimental Study of Turbulent Non-Newtonian Fluid Flow in Concentric Annuli using Particle Image Velocimetry Technique. Flow, Turbulence and Combustion **94**(3): 527-554, Flow Turbulence Combust, DOI: 10.1007/s10494-014-9589-6.

Boyer, F., Guazzelli, E. and Pouliquen, O. (2011). Unifying Suspension and Granular Rheology. Physical Review Letters **107**(18), Phys Rev Lett, DOI: ARTN 188301 10.1103/PhysRevLett.107.188301.

Brown, N. P., Bern, P. A. and Weaver, A. (1989). Cleaning Deviated Holes: New Experimental and Theoretical Studies. SPE\IADC Drilling Conference New Orleans, Louisiana, February 28-3 March 1989 SPE-18636-MS,DOI: 10.2118/18636-MS.

Buffington, J. M. and Montgomery, D. R. (1998). A systematic analysis of eight decades of incipient motion studies, with special reference to gravel-bedded rivers (vol 33, 1993, 1997).

Water Resources Research **34**(1): 157-157, Water Resour Res, DOI: Doi 10.1029/97wr03138.

Bybee, K. (2011). A Review of Cuttings Transport in Directional-Well Drilling. JPT, SPE-0211-0052-JPT, DOI: 10.2118/0211-0052-JPT.

Capart, H. and Fraccarollo, L. (2011). Transport layer structure in intense bed-load. Geophysical Research Letters **38**, Geophys Res Lett, DOI: hArtn L20402 10.1029/2011gl049408.

Carbonneau, P. E. and Bergeron, N. E. (2000). The effect of bedload transport on mean and turbulent flow properties. Geomorphology **35**(3-4): 267-278, Geomorphology, DOI: g10.1016/S0169-555x(00)00046-5.

Carling, P. A. (1983). Threshold of Coarse Sediment Transport in Broad and Narrow Natural Streams. Earth Surface Processes and Landforms **8**(1): 1-18, Earth Surf Proc Land, DOI: DOI 10.1002/esp.3290080102.

Chan-Braun, C., García-Villalba, M. and Uhlmann, M. (2011). Force and torque acting on particles in a transitionally rough open-channel flow. Journal of Fluid Mechanics **684**: 441-474, DOI: 10.1017/jfm.2011.311.

Cheng, E. D. (1969). Incipient motion of large roughness elements in turbulent open channel flow.

Chhabra, R. P. and Richardson, J. F. (1999). Chapter 1 - Non-Newtonian fluid behaviour. Non-Newtonian Flow in the Process Industries. Oxford, Butterworth-Heinemann**:** 1-36.

Cho, H., Shah, S. N. and Osisanya, S. O. (2000). A Three-Layer Modeling for Cuttings Transport with Coiled Tubing Horizontal Drilling. SPE Annual Technical Conference and Exhibition. Dallas, Texas, 1–4 October 2000., SPE-63269-MS,DOI: 10.2118/63269-MS.

Cho, H., Shah, S. N. and Osisanya, S. O. (2001). Effects of Fluid Flow in a Porous Cuttings-Bed on Cuttings Transport Efficiency and Hydraulics, SPE-71374-MS,DOI: 10.2118/71374-MS.

Choi, Y. J., Hulsen, M. A. and Meijer, H. E. H. (2010). An extended finite element method for the simulation of particulate viscoelastic flows. Journal of Non-Newtonian Fluid Mechanics **165**(11): 607-624, DOI: http://dx.doi.org/10.1016/j.jnnfm.2010.02.021.

Chung, S. Y., Rhee, G. H. and Sung, H. J. (2002). Direct numerical simulation of turbulent concentric annular pipe flow - Part 1: Flow field. International Journal of Heat and Fluid Flow **23**(4): 426-440, Int J Heat Fluid Fl, DOI: 10.1016/S0142-727X(02)00140-6.

Chung, S. Y. and Sung, H. J. (2005). Large-eddy simulation of turbulent flow in a concentric annulus with rotation of an inner cylinder. International Journal of Heat and Fluid Flow **26**(2): 191-203, Int J Heat Fluid Fl, DOI: 10.1016/j.ijheatfluidflow.2004.08.006.

Clark, R. K. and Bickham, K. L. (1994). A Mechanistic Model for Cuttings Transport. SPE 69th Annual Tgchniml Conference and Exhlbltion Now ohms, LA, U. S.A., 25-8 .Septemb.ar 1994., SPE-28306-MS,DOI: 10.2118/28306-MS.

Dealy, J. M. and Larson, R. G. (2006). Structure and Rheology of Molten Polymers: From Structure to Flow Behavior and Back Again, Hanser Publishers.

Dealy, J. M., Wang, J., Dealy, J. M. et al. (2013). Melt rheology and its applications in the plastics industry. Engineering materials and processes,. Dordrecht ; New York: 1 online resource.

Deshpande, A. P. (2010). Rheology of complex fluids. New York: xiii, 257 p.

Diplas, P., Dancey, C. L., Celik, A. O. et al. (2008). The Role of Impulse on the Initiation of Particle Movement Under Turbulent Flow Conditions. Science **322**(5902): 717-720, Science, DOI: 10.1126/science.1158954.

Dodge, D. W. and Metzner, A. B. (1959). Turbulent Flow of Non-Newtonian Systems. Aiche Journal **5**(2): 189-204, Aiche J, DOI: DOI 10.1002/aic.690050214.

Doron, P. and Barnea, D. (1993). A 3-Layer Model for Solid-Liquid Flow in Horizontal Pipes. International Journal of Multiphase Flow **19**(6): 1029-1043, Int J Multiphas Flow, DOI: Doi 10.1016/0301-9322(93)90076-7.

Duan, M., Miska, S. Z., Yu, M. et al. (2007). Critical Conditions for Effective Sand-Sized Solids Transport in Horizontal and High-Angle Wells. SPE Production and Operations Symposium Oklahoma City, Oklahoma, USA, 31 March-3 April 2007., SPE-106707-MS,DOI: 10.2118/106707-MS.

Duan, M., Miska, S. Z., Yu, M. et al. (2008). Transport of Small Cuttings in Extended-Reach Drilling. SPE Drilling & Completion, SPE-104192-PA, DOI: 10.2118/104192-PA.

Dubief, Y., White, C. M., Terrapon, V. E. et al. (2004). On the coherent drag-reducing and turbulence-enhancing behaviour of polymers in wall flows. Journal of Fluid Mechanics **514**: 271-280, J Fluid Mech, DOI: Doi 10.1017/S0022112004000291.

Eesa, M. and Barigou, M. (2009). CFD investigation of the pipe transport of coarse solids in laminar power law fluids. Chemical Engineering Science **64**(2): 322-333, DOI: http://dx.doi.org/10.1016/j.ces.2008.10.004.

Erge, O., Ozbayoglu, E. M., Miska, S. Z. et al. (2015). Laminar to turbulent transition of yield power law fluids in annuli. Journal of Petroleum Science and Engineering **128**: 128-139, DOI: http://dx.doi.org/10.1016/j.petrol.2015.02.007.

Escudier, M. P., Gouldson, I. W. and Jones, D. M. (1995). Flow of Shear-Thinning Fluids in a Concentric Annulus. Experiments in Fluids **18**(4): 225-238, Exp Fluids.

Espinosa-Paredes, G., Salazar-Mendoza, R. and Cazarez-Candia, O. (2007). Averaging model for cuttings transport in horizontal wellbores. Journal of Petroleum Science and Engineering **55**(3-4): 301-316, J Petrol Sci Eng, DOI: f10.1016/j.petrol.2006.03.027.

Ford, J. T., Peden, J. M., Oyeneyin, M. B. et al. (1990). Experimental Investigation of Drilled Cuttings Transport in Inclined Boreholes, SPE-20421-MS,DOI: 10.2118/20421-MS.

Fredrickson, A. G. and Bird, R. B. (1958). Non-Newtonian Flow in Annuli. Industrial and Engineering Chemistry **50**(3): 347-352, Ind Eng Chem, DOI: Doi 10.1021/Ie50579a035.

GarcÁa, M. H. (2008). Sedimentation Engineering: Processes, Measurements, Modeling, and Practice, American Society of Civil Engineers.

Gaudio, R., Miglio, A. and Dey, S. (2010). Non-universality of von Karman's kappa in fluvial streams. Journal of Hydraulic Research **48**(5): 658-663, J Hydraul Res, DOI: http://dx.doi.org/10.1080/00221686.2010.507338.

Gavignet, A. A. and Sobey, I. J. (1989). Model Aids Cuttings Transport Prediction. Journal of Petroleum Technology **41**, SPE-15417-PA, DOI: 10.2118/15417-PA.

Goel, N., Shah, S. N. and Grady, B. P. (2002). Correlating viscoelastic measurements of fracturing fluid to particles suspension and solids transport. Journal of Petroleum Science and Engineering **35**(1): 59-81, DOI: http://dx.doi.org/10.1016/S0920-4105(02)00164-X.

Gomaa, A. M., Gupta, D. V. S. and Carman, P. (2014). Viscoelastic Behavior and Proppant Transport Properties of a New Associative Polymer-Based Fracturing Fluid. SPE International Symposium and Exhibition on Formation Damage Control, 26-28 February, Lafayette, Louisiana, USA, SPE-168113-MS,DOI: 10.2118/168113-MS.

Gomaa, A. M., Gupta, D. V. S. V. and Carman, P. S. (2015). Proppant Transport? Viscosity Is Not All It's Cracked Up To Be. SPE Hydraulic Fracturing Technology Conference, 3-5 February, The Woodlands, Texas, USA, SPE-173323-MS,DOI: 10.2118/173323-MS.

Gore, R. A. and Crowe, C. T. (1991). Modulation of Turbulence by a Dispersed Phase. Journal of Fluids Engineering-Transactions of the Asme **113**(2): 304-307, J Fluid Eng-T Asme, DOI: 10.1115/1.2909497.

Grass, A. J. (1970). Initial Instability of Fine Bed Sand. Journal of the Hydraulics Division **96**(3): 619-632.

Gregory B. Dykes, J. (2014). Cuttings Transport Implications for Drill String Design: A Study with Computational Fluid Dynamics. Msc Thesis, Colorado School of Mines.

Guild, G. J., Wallace, I. M. and Wassenborg, M. J. (1995). Hole Cleaning Program for Extended Reach Wells, SPE-29381-MS,DOI: 10.2118/29381-MS.

Guo, X.-l., Wang, Z.-m. and Long, Z.-h. (2010). Study on three-layer unsteady model of cuttings transport for extended-reach well. Journal of Petroleum Science and Engineering **73**(1–2): 171-180, DOI: http://dx.doi.org/10.1016/j.petrol.2010.05.020.

Hajidavalloo, E., Sadeghi-Behbahani-Zadeh, M. and Shekari, Y. (2013). Simulation of gas-solid two-phase flow in the annulus of drilling well. Chemical Engineering Research & Design **91**(3): 477-484, Chem Eng Res Des, DOI: DOI 10.1016/j.cherd.2012.11.009.

Harris, P. C., Walters, H. G. and Bryant, J. (2008). Prediction of Proppant Transport from Rheological Data. SPE Annual Technical Conference and Exhibition, 21-24 September, Denver, Colorado, USA, SPE-115298-MS,DOI: 10.2118/115298-MS.

Hassid, S. and Poreh, M. (1978). Turbulent Energy-Dissipation Model for Flows with Drag Reduction. Journal of Fluids Engineering-Transactions of the Asme **100**(1): 107-112, J Fluid Eng-T Asme.

Hemphill, T. (2010). A Comparison of High-Viscosity and High-Density Sweeps as Hole-Cleaning Tools: Separating Fiction From Fact. SPE Annual Technical Conference and Exhibition, 19-22 September, Florence, Italy, SPE-134514-MS,DOI: https://doi.org/10.2118/134514-MS.

Hemphill, T. and Larsen, T. I. (1996). Hole-Cleaning Capabilities of Water- and Oil-Based Drilling Fluids: A Comparative Experimental Study. **SPE** Drilling & Completion **11**(4), SPE-26328-PA, DOI: 10.2118/26328-PA.

Hemphill, T. and Ravi, K. (2010). Modeling of Effect of Drill Pipe Rotation Speed on Wellbore Cleanout, SPE-135703-MS,DOI: 10.2118/135703-MS.

Heyman, J., Mettra, F., Ma, H. B. et al. (2013). Statistics of bedload transport over steep slopes: Separation of time scales and collective motion. Geophysical Research Letters **40**(1): 128-133, Geophys Res Lett, DOI: 10.1029/2012gl054280.

Houssais, M., Ortiz, C. P., Durian, D. J. et al. (2015). Onset of sediment transport is a continuous transition driven by fluid shear and granular creep. Nature Communications **6**, Nat Commun, DOI: ARTN 6527 10.1038/ncomms7527.

Hu, Y. T., Chung, H. and Maxey, J. E. (2015). What is More Important for Proppant Transport, Viscosity or Elasticity? SPE Hydraulic Fracturing Technology Conference, 3-5 February, The Woodlands, Texas, USA, SPE-173339-MS,DOI: 10.2118/173339-MS.

Hussain H. Al-Kayiem, N. M. Z., Muhamad Z. Asyraf and Mahir Elya Elfeel (2010). Simulation of the Cuttings Cleaning During the Drilling Operation. American Journal of Applied Sciences **7**(6): 800-806.

Hussaini, S. M. and Azar, J. J. (1983). Experimental Study of Drilled Cuttings Transport Using Common Drilling Muds. SPE-10674-PA, DOI: 10.2118/10674-PA.

Iaccarino, G., Shaqfeh, E. S. G. and Dubief, Y. (2010). Reynolds-averaged modeling of polymer drag reduction in turbulent flows. Journal of Non-Newtonian Fluid Mechanics **165**(7-8): 376-384, J Non-Newton Fluid, DOI: DOI 10.1016/j.jnnfm.2010.01.013.

Iyoho, A. W. and Takahashi, H. (1993). Modeling Unstable Cuttings Transport In Horizontal, Eccentric Wellbores, SPE-27416-MS.

Japper-Jaafar, A., Escudier, M. P. and Poole, R. J. (2010). Laminar, transitional and turbulent annular flow of drag-reducing polymer solutions. Journal of Non-Newtonian Fluid Mechanics **165**(19-20): 1357-1372, J Non-Newton Fluid, DOI: 10.1016/j.jnnfm.2010.07.001.

Jefri, M. A. and Zahed, A. H. (1989). Elastic and Viscous Effects on Particle Migration in Plane-Poiseuille Flow. Journal of Rheology **33**(5): 691-708, DOI: 10.1122/1.550034.

Jin, S. and Collins, L. R. (2007). Dynamics of dissolved polymer chains in isotropic turbulence. New Journal of Physics **9**, New J Phys, DOI: Artn 360 Doi 10.1088/1367-2630/9/10/360.

Kamp, A. M. and Rivero, M. (1999). Layer Modeling for Cuttings Transport in Highly Inclined Wellbores. Latin American and Caribbean Petroleum Engineering Conference, 21-23 April, Caracas, Venezuela, SPE-53942-MS,DOI: 10.2118/53942-MS.

Kawaguchi, Y., Segawa, T., Feng, Z. et al. (2002). Experimental study on drag-reducing channel flow with surfactant additives—spatial structure of turbulence investigated by PIV system. International Journal of Heat and Fluid Flow **23**(5): 700-709, DOI: http://dx.doi.org/10.1016/S0142-727X(02)00166-2.

Kelessidis, V. C. and Bandelis, G. E. (2004a). Flow Patterns and Minimum Suspension Velocity for Efficient Cuttings Transport in Horizontal and Deviated Wells in Coiled-Tubing Drilling. **SPE** Drilling & Completion **19**(4): 213-227, SPE-81746-PA, DOI: 10.2118/81746-PA.

Kelessidis, V. C., Mpandelis, G., Koutroulis, A. et al. (2002). Significant Parameters Affecting Efficient Cuttings Transport In Horizontal and Deviated Wellbores In Coil Tubing Drilling: A Critical Review. Paper presented at the 1st International Symposium of the Faculty of Mines (ITU) on Earth Sciences and Engineering, 16-18 May 2002, Maslak, Istanbul, Turkey.
.

Kelessidis, V. C. and Mpandelis, G. E. (2004b). Hydraulic Parameters Affecting Cuttings Transport for Horizontal Coiled Tubing Drilling. 7th National Congress on Mechanics, Chania, Greece, June, 2004.

King, I., Trenty, L. and Vit, C. (2000). How the 3D Modeling Could Help Hole-Cleaning Optimization, SPE-63276-MS,DOI: 10.2118/63276-MS.

Larsen, T. I., Pilehvari, A. A. and Azar, J. J. (1997). Development of a New Cuttings-Transport Model for High-Angle Wellbores Including Horizontal Wells. **SPE** Drilling & Completion **12**(2): 129-135, SPE-25872-PA, DOI: 10.2118/25872-PA.

Lee, J., Tehrani, A., Young, S. et al. (2014). Viscoelasticity and Drilling Fluid Performance. (45455): V005T011A015, DOI: 10.1115/OMAE2014-23908.

Leising, L. J. and Walton, I. C. (2002). Cuttings-Transport Problems and Solutions in Coiled-Tubing Drilling. **SPE** Drilling & Completion **17**(1): 54-66, SPE-77261-PA, DOI: 10.2118/77261-PA.

Li, J. and Luft, B. (2014a). Overview of Solids Transport Studies and Applications in Oil and Gas Industry - Experimental Work. SPE Russian Oil and Gas Exploration & Production Technical Conference and Exhibition. Moscow, Russia, 14-16 October, SPE-171285-MS,DOI: 10.2118/171285-MS.

Li, J. and Luft, B. (2014b). Overview Solids Transport Study and Application in Oil-Gas Industry-Theoretical Work. International Petroleum Technology Conference. Kuala Lumpur, Malaysia, 10-12 December 2014, IPTC-17832-MS,DOI: 10.2523/IPTC-17832-MS.

Li, J., Misselbrook, J. and Sach, M. (2010). Sand Cleanouts With Coiled Tubing: Choice of Process, Tools and Fluids. Journal of Canadian Petroleum Technology, SPE-113267-PA, DOI: 10.2118/113267-PA.

Li, J., Misselbrook, J. and Seal, J. W. (2008). Sand Cleanout With Coiled Tubing: Choice of Process, Tools, or Fluids? Europec/EAGE Conference and Exhibition. Rome, Italy, 9-12 June 2008, SPE-113267-MS,DOI: 10.2118/113267-MS.

Li, J. and Walker, S. (1999). Sensitivity Analysis of Hole Cleaning Parameters in Directional Wells. SPE/ICoTA Coiled Tubing Roundtable, . Houston, Texas, 25-26 May, SPE-54498-MS,DOI: 10.2118/54498-MS.

Li, J., Wilde, G. and Crabtree, A. R. (2005). Do Complex Super-Gel Liquids Perform Better Than Simple Linear Liquids in Hole Cleaning With Coiled Tubing? SPE/ICoTA Coiled Tubing Conference and Exibition The Woodlands, Texas, USA, 12-13 April 2005, SPE-94185-MS,DOI: 10.2118/94185-MS.

Lockett, T. J., Richardson, S. M. and Worraker, W. J. (1993). The Importance of Rotation Effects for Efficient Cuttings Removal During Drilling, SPE-25768-MS,DOI: 10.2118/25768-MS.

Lodge, A. S. (1964). Elastic liquids; an introductory vector treatment of finite-strain polymer rheology. London, New York;, Academic Press.

Lourenco, A. M. F., Nakagawa, E. Y., Martins, A. L. et al. (2006). Investigating Solids-Carrying Capacity for an Optimized Hydraulics Program in Aerated Polymer-Based-Fluid Drilling. IADC/SPE Drilling Conference Miami, Florida, USA, 21-23 February 2006, SPE-99113-MS,DOI: 10.2118/99113-MS.

Lumley, J. L. (1969). Drag Reduction by Additives. Annual Review of Fluid Mechanics **1**: 367-&, Annu Rev Fluid Mech, DOI: DOI 10.1146/annurev.fl.01.010169.002055.

Luo, Y., Bern, P. A. and Chambers, B. D. (1992). Flow-Rate Predictions for Cleaning Deviated Wells. SPE/IADC Drilling Conference. New Orleans, Louisiana, 18-21 February, SPE-23884-MS., SPE-23884-MS,DOI: 10.2118/23884-MS.

Martins, A. L., Sa, C. H. M., Lourenco, A. M. F. et al. (1996). Optimizing Cuttings Circulation in Horizontal Well Drilling. International Petroleum Conference & Exhibition of Mexico. Villahermosa, Mexico, 5-7 March, 1996., SPE-35341-MS,DOI: 10.2118/35341-MS.

Martins, A. L. and Santana, C. C. (1992). Evaluation of Cuttings Transport in Horizontal and Near Horizontal Wells -A Dimensionless Approach. SPE Latin America Petroleum Engineering Conference. Caracas, Venezuela ,8-11 March, SPE-23643-MS., SPE-23643-MS,DOI: 10.2118/23643-MS.

Martins, A. L., Santana, M. L., Campos, W. et al. Evaluating the Transport of Solids Generated by Shale Instabilities in ERW Drilling. SPE-59729-PA, DOI: 10.2118/59729-PA.

Martins, A. L., Santana, M. L., Gonçalves, C. J. C. et al. Evaluating the Transport of Solids Generated by Shale Instabilities in ERW Drilling - Part II: Case Studies, SPE-56560-MS,DOI: 10.2118/56560-MS.

Min, T., Choi, H. and Yoo, J. Y. (2003). Maximum drag reduction in a turbulent channel flow by polymer additives. Journal of Fluid Mechanics **492**: 91-100, J Fluid Mech, DOI: Doi 10.1017/S0022112003005597.

Min, T., Jung, Y. Y., Choi, H. et al. (2003). Drag reduction by polymer additives in a turbulent channel flow. Journal of Fluid Mechanics **486**: 213-238, J Fluid Mech, DOI: Doi 10.1017/S0022112003004610.

Mishra, N. (2007). Investigation of Hole Cleaning Parameters Using Computational Fluid Dynamics in Horizontal And Deviated Wells. Msc Thesis, Department of Petroleum and Natural Gas Engineering Morgantown, West Virginia.

Mitchell, R. F., Miska, S., Aadnøy, B. S. et al. (2011). Fundamentals of Drilling Engineering, Society of Petroleum Engineers.

Southard, J. (2006). Introduction to Fluid Motions, Sediment Transport, and Current-Generated Sedimentary Structures. Massachusetts Institute of Technology: MIT OpenCourseWare, https://ocw.mit.edu. License: Creative Commons BY-NC-SA.

Miyazaki, K., Chen, G. , Ymamoto, F., Ohta, J., Murai, Y., Horii, K. (1999). PIV measurement of particle motion in spiral gas-solid two-phase flow. Experimental Thermal and Fluid Science **19**(4): 194-203, Exp Therm Fluid Sci, DOI: 10.1016/S0894-1777(99)00020-5.

Mme, U. and Skalle, P. (2012). CFD Calculations of Cuttings Transport through Drilling Annuli at Various Angles. International Journal of Petroleum Science and Technology **6**(2): 129-141.

Naganawa, S. and Nomura, T. (2006). Simulating Transient Behavior of Cuttings Transport over Whole Trajectory of Extended Reach Well. Abu Dhabi International Petroleum Exhibition & Conference, 7-10 November, Abu Dhabi, UAE, SPE-103923-MS,DOI: 10.2118/103923-MS.

Naser, J. A. (1997). Prediction of Newtonian & non-Newtonian Flow Through Concentric Annulus With Centerbody Rotation. Inter Conf on CFD in Mineral & Metal Processing and Power Generation CSIRO 1997.

Nazari, T., Hareland, G. and Azar, J. J. (2010). Review of Cuttings Transport in Directional Well Drilling: Systematic Approach, SPE-132372-MS,DOI: 10.2118/132372-MS.

Neto, J. L. V., Martins, A. L., Neto, A. S. et al. (2011). Cfd Applied to Turbulent Flows in Concentric and Eccentric Annuli with Inner Shaft Rotation. Canadian Journal of Chemical Engineering **89**(4): 636-646, Can J Chem Eng, DOI: Doi 10.1002/Cjce.20522.

Nguyen, D. and Rahman, S. S. (1998). A Three-Layer Hydraulic Program for Effective Cuttings Transport and Hole Cleaning in Highly Deviated and Horizontal Wells. SPE-51186-PA, DOI: 10.2118/51186-PA.

Nikora, V. and Goring, D. (2000). Flow Turbulence over Fixed and Weakly Mobile Gravel Beds. Journal of Hydraulic Engineering **126**(9): 679-690, DOI: doi:10.1061/(ASCE)0733-9429(2000)126:9(679).

Nouri, J. M., Umur, H. and Whitelaw, J. H. (1993). Flow of Newtonian and Non-Newtonian Fluids in Concentric and Eccentric Annuli. Journal of Fluid Mechanics **253**: 617-641, J Fluid Mech, DOI: 10.1017/S0022112093001922.

Ofei, T. N., Irawan, S. and Pao, W. (2014). CFD Method for Predicting Annular Pressure Losses and Cuttings Concentration in Eccentric Horizontal Wells. Journal of Petroleum Engineering **2014**: 16, DOI: 10.1155/2014/486423.

Okrajni, S. and Azar, J. J. (1986). The Effects of Mud Rheology on Annular Hole Cleaning in Directional Wells. SPE-14178-PA, DOI: 10.2118/14178-PA.

Orszag, S. A. (2006). Analytical theories of turbulence. Journal of Fluid Mechanics **41**(2): 363-386, DOI: 10.1017/S0022112070000642.

Osgouei, R. E., Ozbayoglu, M. E. and K., T. (2013). CFD Simulation of Solids Carrying Capacity of a Newtonian Fluid Through Horizontal Eccentric Annulus. Proceedings of the ASME 2013 Fluids Engineering Division Summer Meeting FEDSM2013 July 7-11, 2013, Incline Village, Nevada, USA, DOI: doi:10.1115/FEDSM2013-16204.

Ouriemi, M., Aussillous, P. and Guazzelli, E. (2009). Sediment dynamics. Part 1. Bed-load transport by laminar shearing flows. Journal of Fluid Mechanics **636**: 295-319, J Fluid Mech, DOI: 10.1017/S0022112009007915.

Ouriemi, M., Aussillous, P., Medale, M. et al. (2007). Determination of the critical Shields number for particle erosion in laminar flow. Physics of Fluids **19**(6), Phys Fluids, DOI: Artn 061706 10.1063/1.2747677.

Owen, P. R. (1964). Saltation of uniform grains in air. Journal of Fluid Mechanics **20**(2): 225-242, DOI: 10.1017/S0022112064001173.

Ozbayoglu, M. E., Miska, S. Z., Reed, T. et al. (2004). Analysis of the Effects of Major Drilling Parameters on Cuttings Transport Efficiency for High-Angle Wells in Coiled Tubing Drilling Operations. SPE/ICoTA Coiled Tubing Conference and Exibition. Huston, Texas, USA, 23-24 March 2004, SPE-89334-MS,DOI: 10.2118/89334-MS.

Ozbayoglu, M. E., Miska, S. Z., Reed, T. et al. (2005). Using foam in horizontal well drilling: A cuttings transport modeling approach. Journal of Petroleum Science and Engineering **46**(4): 267-282, DOI: http://dx.doi.org/10.1016/j.petrol.2005.01.006.

Ozbayoglu, M. E., Saasen, A., Sorgun, M. et al. (2010a). Critical Fluid Velocities for Removing Cuttings Bed Inside Horizontal and Deviated Wells. Petroleum Science and Technology **28**(6): 594-602, DOI: 10.1080/10916460903070181.

Ozbayoglu, M. E., Sorgun, M., Saasen, A. et al. (2010b). Hole Cleaning Performance of Light-Weight Drilling Fluids During Horizontal Underbalanced Drilling. SPE-136689-PA, DOI: 10.2118/136689-PA.

Paschkewitz, J. S., Dimitropoulos, C. D., Hou, Y. X. et al. (2005). An experimental and numerical investigation of drag reduction in a turbulent boundary layer using a rigid rodlike polymer. Physics of Fluids **17**(8), Phys Fluids, DOI: Artn 085101 10.1063/1.1993307.

Payne, M. L., Cocking, D. A. and Hatch, A. J. (1994). Critical Technologies for Success in Extended Reach Drilling, SPE-28293-MS,DOI: 10.2118/28293-MS.

Peden, J. M., Ford, J. T. and Oyeneyin, M. B. (1990). Comprehensive Experimental Investigation of Drilled Cuttings Transport in Inclined Wells Including the Effects of Rotation and Eccentricity, SPE-20925-MS,DOI: 10.2118/20925-MS.

Peysson, Y., Ouriemi, M., Medale, M. et al. (2009). Threshold for sediment erosion in pipe flow. International Journal of Multiphase Flow **35**(6): 597-600, Int J Multiphas Flow, DOI: 10.1016/j.ijmultiphaseflow.2009.02.007.

Philip, Z., Sharma, M. M. and Chenevert, M. E. (1998). The Role of Taylor Vortices in the Transport of Drill Cuttings, SPE-39504-MS,DOI: 10.2118/39504-MS.

Pilehvari, A. A., Azar, J. J. and Shirazi, S. A. (1996). State-Of-The-Art Cuttings Transport in Horizontal Wellbores. International Conference on Horizontal Well Technology. Calgary, Alberta, Canada, 18-20 November, SPE-37079-MS,DOI: 10.2118/37079-MS.

Pinho, F. T. (2003). A GNF framework for turbulent flow models of drag reducing fluids and proposal for a k-epsilon type closure. Journal of Non-Newtonian Fluid Mechanics **114**(2-3): 149-184, J Non-Newton Fluid, DOI: Doi 10.1016/S0377-0257(03)00120-4.

Pinho, F. T., Li, C. F., Younis, B. A. et al. (2008). A low Reynolds number turbulence closure for viscoelastic fluids. Journal of Non-Newtonian Fluid Mechanics **154**(2-3): 89-108, J Non-Newton Fluid, DOI: DOI 10.1016/j.jnnfm.2008.02.008.

Pinho, F. T. and Whitelaw, J. H. (1990). Flow of Non-Newtonian Fluids in a Pipe. Journal of Non-Newtonian Fluid Mechanics **34**(2): 129-144, J Non-Newton Fluid, DOI: Doi 10.1016/0377-0257(90)80015-R.

Powell, J. W., Parks, C. F. and Seheult, J. M. (1991). Xanthan and Welan: The Effects Of Critical Polymer Concentration On Rheology and Fluid Performance. International Arctic Technology Conference, 29-31 May, Anchorage, Alaska, SPE-22066-MS,DOI: 10.2118/22066-MS.

Ptasinski, P. K., Boersma, B. J., Nieuwstadt, F. T. M. et al. (2003). Turbulent channel flow near maximum drag reduction: simulations, experiments and mechanisms. Journal of Fluid Mechanics **490**: 251-291, J Fluid Mech, DOI: 10.1017/S0022112003005305.

Ptasinski, P. K., Nieuwstadt, F. T. M., van den Brule, B. H. A. A. et al. (2001). Experiments in turbulent pipe flow with polymer additives at maximum drag reduction. Flow Turbulence and Combustion **66**(2): 159-182, Flow Turbul Combust, DOI: Doi 10.1023/A:1017985826227.

Rabenjafimanantsoa A. H., Rune, W. T. and Saasen, A. (2007). Simultaneous UVP and PIV measurements related to bed dunes dynamics and turbulence structures in circular pipes. 5th International Symposium on Ultrasonic Doppler Methods for Fluid Mechanics and Fluid Engineering.

Rabenjafimanantsoa, A. H. (2007). Particle transport and dynamics in turbulent Newtonian and non-Newtonian fluids. PhD, University of Stavanger,.

Rabenjafimanantsoa, H. A. (2007). Particle transport and dynamics in turbulent Newtonian and non-Newtonian fluids. Other Information: Doctoral theses at UIS; ISSN 1890-1387;

Numerical Data; Thesis or Dissertation; TH: Thesis (PhD); refs, charts, figs, tabs. Norway: 163 pages.

Rabenjafimanantsoa, H. A., Time, R.W. and Saasen, A. (2005). Flow regimes over particle beds experimental studies of particle transport in horizontal pipes. Annual Transactions of the Nordic Rheology Society, 13."

Ramadan, A., Skalle, P. and Johansen, S. T. (2003). A mechanistic model to determine the critical flow velocity required to initiate the movement of spherical bed particles in inclined channels. Chemical Engineering Science **58**(10): 2153-2163, DOI: 10.1016/S0009-2509(03)00061-7.

Ramadan, A., Skalle, P., Johansen, S. T. et al. (2001). Mechanistic model for cuttings removal from solid bed in inclined channels. Journal of Petroleum Science and Engineering **30**(3-4): 129-141, J Petrol Sci Eng, DOI: Doi 10.1016/S0920-4105(01)00108-5.

Ramadan, A., Skalle, P. and Saasen, A. (2005). Application of a three-layer modeling approach for solids transport in horizontal and inclined channels. Chemical Engineering Science **60**(10): 2557-2570, DOI: http://dx.doi.org/10.1016/j.ces.2004.12.011.

Ravi, K. and Hemphill, T. (2006). Pipe Rotation and Hole Cleaning in Eccentric Annulus. IADC/SPE Drilling Conference, 21-23 February, Miami, Florida, USA, SPE-99150-MS,DOI: 10.2118/99150-MS.

Resende, P. R., Kim, K., Younis, B. A. et al. (2011). A FENE-P k-epsilon turbulence model for low and intermediate regimes of polymer-induced drag reduction. Journal of Non-Newtonian Fluid Mechanics **166**(12-13): 639-660, J Non-Newton Fluid, DOI: DOI 10.1016/j.jnnfm.2011.02.012.

Ro, K. and Ryou, H. (2012). Development of the modified k-E > turbulence model of power-law fluid for engineering applications. Science China-Technological Sciences **55**(1): 276-284, Sci China Technol Sc, DOI: DOI 10.1007/s11431-011-4664-x.

Rodriguez-Corredor, F. E., Bizhani, M., Ashrafuzzaman, M. et al. (2014). An Experimental Investigation of Turbulent Water Flow in Concentric Annulus Using Particle Image Velocimetry Technique. Journal of Fluids Engineering-Transactions of the Asme **136**(5), J Fluid Eng-T Asme, DOI: Artn 051203 Doi 10.1115/1.4026136.

Rodriguez Corredor, F. E., Bizhani, M. and Kuru, E. (2014). A Comparative Study of Hole Cleaning Performance — Water Versus Drag Reducing Fluid. (45455): V005T011A018, DOI: 10.1115/OMAE2014-24083.

Rooki, R., Ardejani, F. D., Moradzadeh, A. et al. (2014). Simulation of cuttings transport with foam in deviated wellbores using computational fluid dynamics. Journal of Petroleum Exploration and Production Technology **4**(3): 263-273, J Petrol Explor Prod Technol, DOI: 10.1007/s13202-013-0077-7.

Rubiandini R.S, R. (1999). Equation for Estimating Mud Minimum Rate for Cuttings Transport in an Inclined-Until-Horizontal Well. SPE/IADC Middle East Drilling Technology Conference, 8-10 November, Abu Dhabi, United Arab Emirates, SPE-57541-MS,DOI: 10.2118/57541-MS.

Saasen, A. (1998). Hole Cleaning During Deviated Drilling - The Effects of Pump Rate and Rheology. European Petroleum Conference, 20-22 October, The Hague, Netherlands, SPE-50582-MS,DOI: 10.2118/50582-MS.

Saasen, A., Eriksen, N. H., Han, L. Q. et al. (1998). Is annular friction loss the key parameter? Oil Gas-European Magazine **24**(1): 22-24, Oil Gas-Eur Mag.

Saasen, A. and Løklingholm, G. (2002). The Effect of Drilling Fluid Rheological Properties on Hole Cleaning. IADC/SPE Drilling Conference. Dallas, Texas, 26-28 February, SPE-74558-MS,DOI: 10.2118/74558-MS.

Sample, K. J. and Bourgoyne, A. T. (1977). An Experimental Evaluation Of Correlations Used For Predicting Cutting Slip Velocity, SPE-6645-MS,DOI: 10.2118/6645-MS.

Sample, K. J. and Bourgoyne, A. T., Jr. (1978). Development Of Improved Laboratory And Field Procedures For Determining The Carrying Capacity Of Drilling Fluids, SPE-7497-MS,DOI: 10.2118/7497-MS.

Sanchez, R. A., Azar, J. J., Bassal, A. A. et al. (1999). Effect of Drillpipe Rotation on Hole Cleaning During Directional-Well Drilling. SPE-56406-PA, DOI: 10.2118/56406-PA.

Sayindla, S., Lund, B., Taghipour, A. et al. (2016). Experimental Investigation of Cuttings Transport With Oil Based Drilling Fluids. (49996): V008T011A035, DOI: 10.1115/OMAE2016-54047.

Schmeeckle, M. W. (2014). Numerical simulation of turbulence and sediment transport of medium sand. Journal of Geophysical Research-Earth Surface **119**(6): 1240-1262, J Geophys Res-Earth, DOI: 10.1002/2013jf002911.

Shields, A. (1936). Anwendung der Ähnlichkeitsmechanik und der Turbulenzforschung auf die Geschiebebewegung. Berlin, Eigenverl. der Preußischen Versuchsanst. für Wasserbau und Schiff.

Sibilla, S. and Baron, A. (2002). Polymer stress statistics in the near-wall turbulent flow of a drag-reducing solution. Physics of Fluids **14**(3): 1123-1136, Phys Fluids, DOI: Doi 10.1063/1.1448497.

Sifferman, T. R. and Becker, T. E. (1992). Hole Cleaning in Full-Scale Inclined Wellbores. SPE-20422-PA, DOI: 10.2118/20422-PA.

Sifferman, T. R., Myers, G. M., Haden, E. L. et al. (1974). Drill Cutting Transport in Full Scale Vertical Annuli. SPE-4514-PA, DOI: 10.2118/4514-PA.

Sorgun, M., Aydin, I. and Ozbayoglu, M. E. (2011). Friction factors for hydraulic calculations considering presence of cuttings and pipe rotation in horizontal/highly-inclined wellbores. Journal of Petroleum Science and Engineering **78**(2): 407-414, J Petrol Sci Eng, DOI: DOI 10.1016/j.petrol.2011.06.013.

Sumer, B. M., Chua, L. H. C., Cheng, N.-S. et al. (2003). Influence of Turbulence on Bed Load Sediment Transport. Journal of Hydraulic Engineering **129**(8): 585-596, DOI: 10.1061/(ASCE)0733-9429(2003)129:8(585).

Sun, X., Wang, K., Yan, T. et al. (2014). Effect of drillpipe rotation on cuttings transport using computational fluid dynamics (CFD) in complex structure wells. Journal of Petroleum Exploration and Production Technology **4**(3): 255-261, J Petrol Explor Prod Technol, DOI: 10.1007/s13202-014-0118-x.

Sun Xiaofeng, W. K., Yan Tie, Zhang Yang, Shao Shuai, Luan Shizhu (2013). Review of Hole Cleaning in Complex Structural Wells. The Open Petroleum Engineering Journal **6**: 25-32.

Sureshkumar, R., Beris, A. N. and Handler, R. A. (1997). Direct numerical simulation of the turbulent channel flow of a polymer solution. Physics of Fluids **9**(3): 743-755, Phys Fluids, DOI: Doi 10.1063/1.869229.

Tabor, M. and Degennes, P. G. (1986). A Cascade Theory of Drag Reduction. Europhysics Letters **2**(7): 519-522, Europhys Lett, DOI: Doi 10.1209/0295-5075/2/7/005.

Tehrani, M. A. (1996). An experimental study of particle migration in pipe flow of viscoelastic fluids. Journal of Rheology **40**(6): 1057-1077, DOI: 10.1122/1.550773.

Thomas, R. P., Azar, J. J. and Becker, T. E. (1982). Drillpipe Eccentricity Effect on Drilled Cuttings Behavior in Vertical Wellbores. SPE-9701-PA, DOI: 10.2118/9701-PA.

Tomren, P. H., Iyoho, A. W. and Azar, J. J. (1986). Experimental Study of Cuttings Transport in Directional Wells. SPE Drilling Engineering, SPE-12123-PA, DOI: 10.2118/12123-PA.

Tonmukayakul, N., Morris, J. F. and Prudhomme, R. (2013). Method for estimating proppant transport and suspendability of viscoelastic liquids. Google Patents. United States, US 20110219856 A1.

Tropea, C., Yarin, A. L. and Foss, J. F. (2007). Springer handbook of experimental fluid mechanics. Heidelberg: xxviii, 1557 p.

Tsuji, Y., Kato, N. and Tanaka, T. (1991). Experiments on the unsteady drag and wake of a sphere at high reynolds numbers. International Journal of Multiphase Flow **17**(3): 343-354, DOI: http://dx.doi.org/10.1016/0301-9322(91)90004-M.

Valluri, S. G., Miska, S. Z., Yu, M. et al. (2006). Experimental Study of Effective Hole Cleaning Using "Sweeps" in Horizontal Wellbores. SPE Annual Technical Conference and Exibition. San Antonio, Texas, USA, 24-27 September 2006, SPE-101220-MS,DOI: 10.2118/101220-MS.

Van den Brule, B. H. A. A. and Gheissary, G. (1993). Effects of fluid elasticity on the static and dynamic settling of a spherical particle. Journal of Non-Newtonian Fluid Mechanics **49**(1): 123-132, DOI: http://dx.doi.org/10.1016/0377-0257(93)85026-7.

Vanoni, V. A. (1975). Sedimentation Engineering: Classic Edition, American Society of Civil Engineers.

Vieira, P., Miska, S., Reed, T. et al. (2002). Minimum Air and Water Flow Rates Required for Effective Cuttings Transport in High Angle and Horizontal Wells, SPE-74463-MS,DOI: 10.2118/74463-MS.

Virk, P. S., Mickley, H. S. and Smith, K. A. (1970). Ultimate Asymptote and Mean Flow Structure in Toms Phenomenon. Journal of Applied Mechanics **37**(2): 488-+, J Appl Mech.

Walker, S. and Li, J. (2000). The Effects of Particle Size, Fluid Rheology, and Pipe Eccentricity on Cuttings Transport. g2000 SPE/ICoTA Coiled Tubing Roundtable. Houston, TX, 5–6 April 2000., SPE-60755-MS,DOI: 10.2118/60755-MS.

Wang Kelin, Y. T., Sun Xiaofeng, Shao Shuai, Luan Shizhu (2013). Review and Analysis of Cuttings Transport in Complex Structural Wells. The Open Fuels & Energy Science Journal **6**: 9-17.

Wang, R.-h., Cheng, R.-c., Wang, H.-g. et al. (2009). Numerical simulation of transient cuttings transport with foam fluid in horizontal wellbore. Journal of Hydrodynamics, Ser. B **21**(4): 437-444, DOI: http://dx.doi.org/10.1016/S1001-6058(08)60169-9.

Warholic, M. D., Heist, D. K., Katcher, M. et al. (2001). A study with particle-image velocimetry of the influence of drag-reducing polymers on the structure of turbulence. Experiments in Fluids **31**(5): 474-483, Exp Fluids, DOI: DOI 10.1007/s003480100288.

Warholic, M. D., Massah, H. and Hanratty, T. J. (1999). Influence of drag-reducing polymers on turbulence: effects of Reynolds number, concentration and mixing. Experiments in Fluids **27**(5): 461-472, Exp Fluids, DOI: DOI 10.1007/s003480050371.

Werner, B., Myrseth, V., Lund, B. et al. (2016). Effects of Oil-Based Drilling-Fluid Rheological Properties on Hole-Cleaning Performance. (49996): V008T011A038, DOI: 10.1115/OMAE2016-54050.

Werner, B., Myrseth, V. and Saasen, A. (2017). Viscoelastic properties of drilling fluids and their influence on cuttings transport. Journal of Petroleum Science and Engineering **156**: 845-851, DOI: http://dx.doi.org/10.1016/j.petrol.2017.06.063.

Wiberg, P. L. and Rubin, D. M. (1989). Bed Roughness Produced by Saltating Sediment. Journal of Geophysical Research-Oceans **94**(C4): 5011-5016, J Geophys Res-Oceans, DOI: 10.1029/JC094iC04p05011.

Wilson, K. C. (1976). A unified Physically-based analysis of solid-liquid pipeline flow. Proceeding of the 4th Int. Conf. on the Hydraulic Transport of SOlids in Pipes, Banff, Alberta, Cabnada, Paper A1.

Wilson, K. C. and Thomas, A. D. (1985). A New Analysis of the Turbulent-Flow of Non-Newtonian Fluids. Canadian Journal of Chemical Engineering **63**(4): 539-546.

Yateem, K. S., Qahtani, H. B., Saeed, S. S. et al. (2013). Fill Cleanout Operations in Offshore Saudi Arabian Fields: Case Histories toward Improving Economics and Operational Logistics, IPTC-16677-MS,DOI: 10.2523/IPTC-16677-MS.

Yilmaz, D. (2012). Discrete Phase Simulations of Drilled Cuttings Transport Process in Highly Deviated Wells. Msc thesis, Louisiana State University.

Ytrehus, J. D., Carlsen, I. M., Melchiorsen, J. C. et al. (2013). Experimental Study Of Friction And Cutting Transport In Non Circular Borehole Geometry, SPE-166790-MS,DOI: 10.2118/166790-MS.

Ytrehus, J. D., Taghipour, A., Lund, B. et al. (2014). Experimental Study of Cuttings Transport Efficiency of Water Based Drilling Fluids. (45455): V005T011A017, DOI: 10.1115/OMAE2014-23960.

Ytrehus, J. D., Taghipour, A., Sayindla, S. et al. (2015). Full Scale Flow Loop Experiments of Hole Cleaning Performances of Drilling Fluids. Proceedings of the Asme 34th International Conference on Ocean, Offshore and Arctic Engineering, 2015, Vol 10.

Zamora, M., Jefferson, D. T. and Powell, J. W. (1993). Hole-Cleaning Study of Polymer-Based Drilling Fluids. SPE Annual Technical Conference and Exhibition, 3-6 October, Houston, Texas, SPE-26329-MS,DOI: 10.2118/26329-MS.

Zhang, F. S. M., M. Yu, E. Ozbayoglu and N. Takach (2014). Pressure Profile in Annulus: Solids Play a Significant Role. Proceedings of the ASME 2014 33rd International Conference on Ocean, Offshore and Arctic Engineering OMAE2014 une 8-13, 2014, San Francisco, California, USA.

Zou, L., Patel, M. H. and Han, G. (2000). A New Computer Package for Simulating Cuttings Transport and Predicting Hole Cleaning in Deviated and Horizontal Wells, SPE-64646-MS,DOI: 10.2118/64646-MS.

3 Experimental Setup and Instrumentation

In this chapter, details of the experimental facility and equipment that have been used throughout this study are explained. Proper procedures on how to utilize the instruments along with their limitations are discussed.

3.1 Horizontal Flow Loop

Figure 3-1is a schematic of the flow loop that has been used in this research. Principal components of the flow loop are a 500-liter stainless steel tank, a centrifugal pump, and measurement instruments such as magnetic flow meter and differential pressure transducers. There is an air- driven mixer in the tank for preparing the slurry.

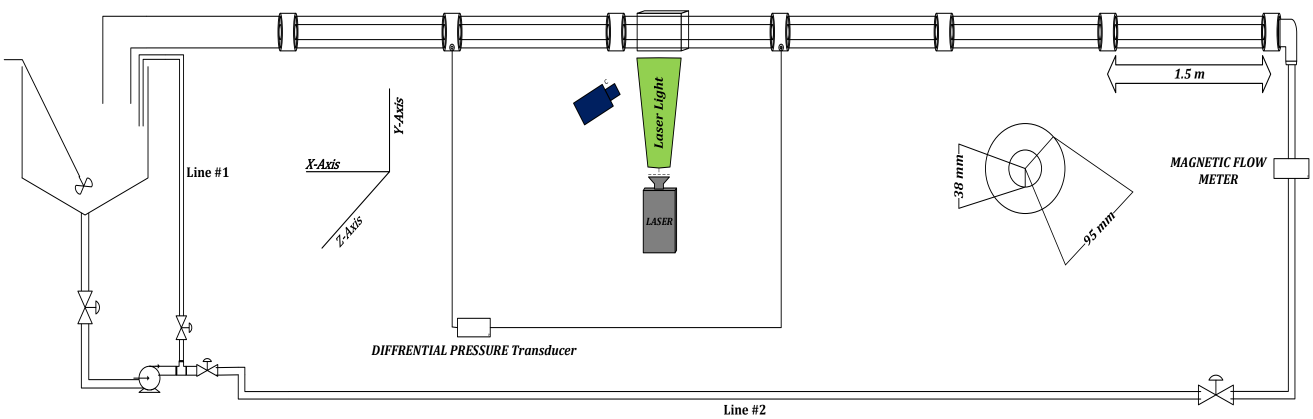

Figure 3-1 Schematic of the Flow Loop

The tank has a capacity of about 500 liters and is made of stainless steel; it can be used for storing the fluid or as mixing pit for preparing solutions (Figure 3-2). The mixer is an air operating mixer with adjustable RPM. The tank is equipped with cooling jackets as well as weight measurement sensors. Temperature sensors are mounted at the bottom of the tank and are used to monitor the temperature variations, if necessary by using cooling jackets, the temperature of the fluid in the tank could be reduced to room temperature for isothermal experiments.

The centrifugal pump equipped with VFD (Variable Frequency Drive) is used for circulating the fluid through the pipelines and the test section (Figure 3-3). Variable Frequency Drive system is used to control the pump flow rate. The operational flow rate range in the current system is 64 lit/min to 420 lit/min.

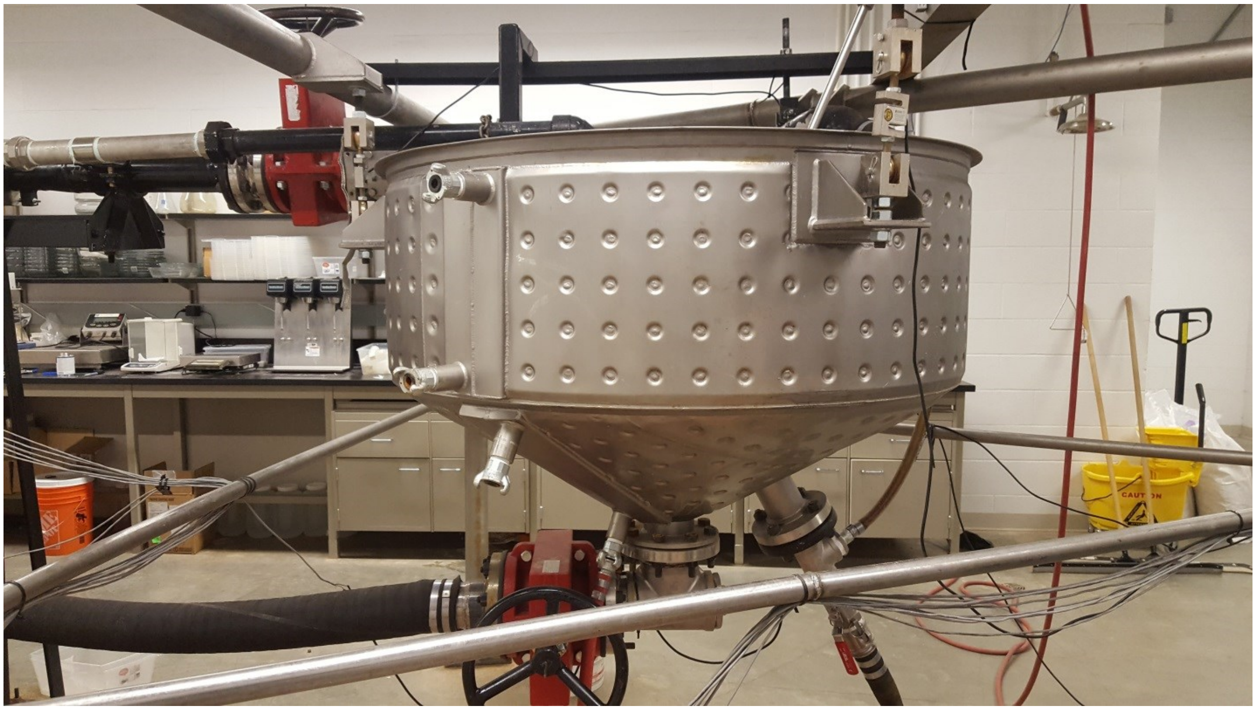

Figure 3-2 The stainless-steel tank in the flow loop

Figure 3-3 The centrifugal pump

The pump discharge line is connected to two lines, one is going back to the tank (Figure 3-1; Line #1) which is a bypass, and the other one is going to the flow meter and the annular section of the flow loop (Figure 3-1, Line#2). For line #2 there are two pipes available to use (1 and 2 inches in diameter); for PIV experiments either line can be used as they do not have any effect on experimental conditions in the annular section. However, it is important to use the line with the smaller diameter in particle transport experiments to make sure that no particle settles down in this part of the system.

A magnetic flow meter installed at the inlet of annular section measures the flow rate (Figure 3-4). The flow meter is an OMEGA FMG607-R with an accuracy of $\pm 0.5\%$.

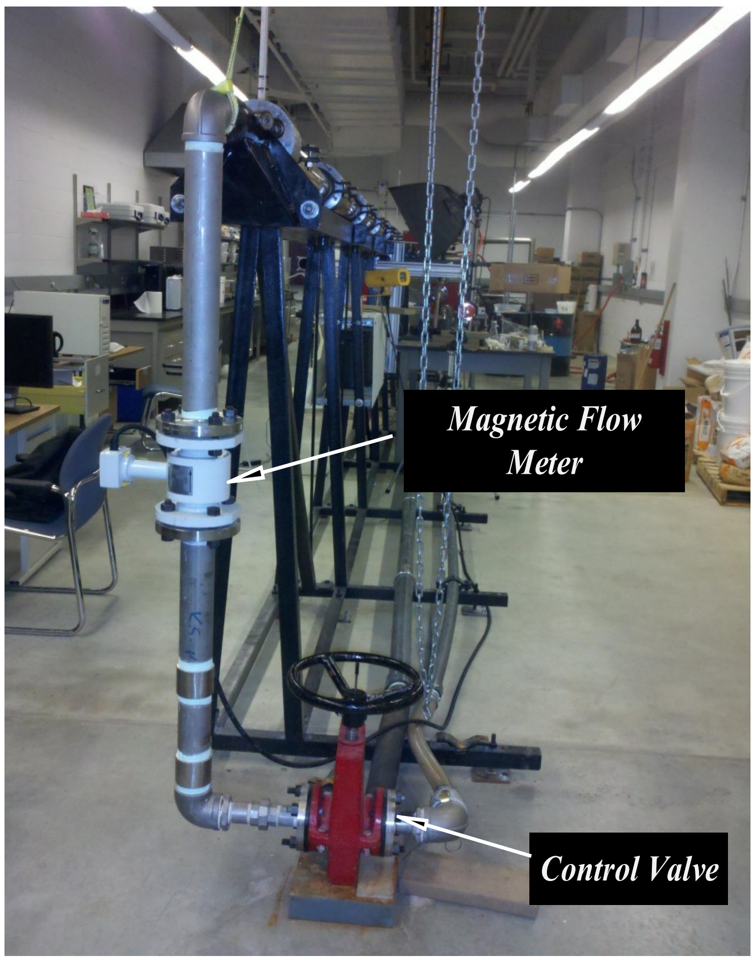

Figure 3-4 Picture of the vertical section of the flow loop including the magnetic flow meter

A high accuracy OMEGA DPG409 differential pressure transducer with an accuracy of $\pm 0.08\%$ was used to record the frictional pressure loss in the annulus. The distance between the two tap lines is 3.08 meter. The first hole is located approximately $\sim 80\mathrm{D_H}$ downstream of the inlet to ensure the flow is fully developed. Calibration of the pressure transducer needs to be done regularly. A digital pressure calibrator is used for calibration of pressure transducers.

The annular section of the flow loop is 9 meters long. It is composed of six 1.5 meters long glass pipe (Figure 3-5). The glass pipes are made of high-quality optical glass with 100% transparency. Glass pipes are Borosilicate glass with a refraction index of 1.47. The pipes are connected using specially designed stainless-steel joints. The joints have an inner diameter identical to the tubes. The inner pipes, which are representative of drillstring, are also made of high-quality optical glass. The thickness of the inner pipes has been chosen properly to reduce sagging and vibration of the inner body during experiments. Inner pipes are 3 meters long each and are kept in the desired position (concentric or eccentric) using thin metal rods at each end.

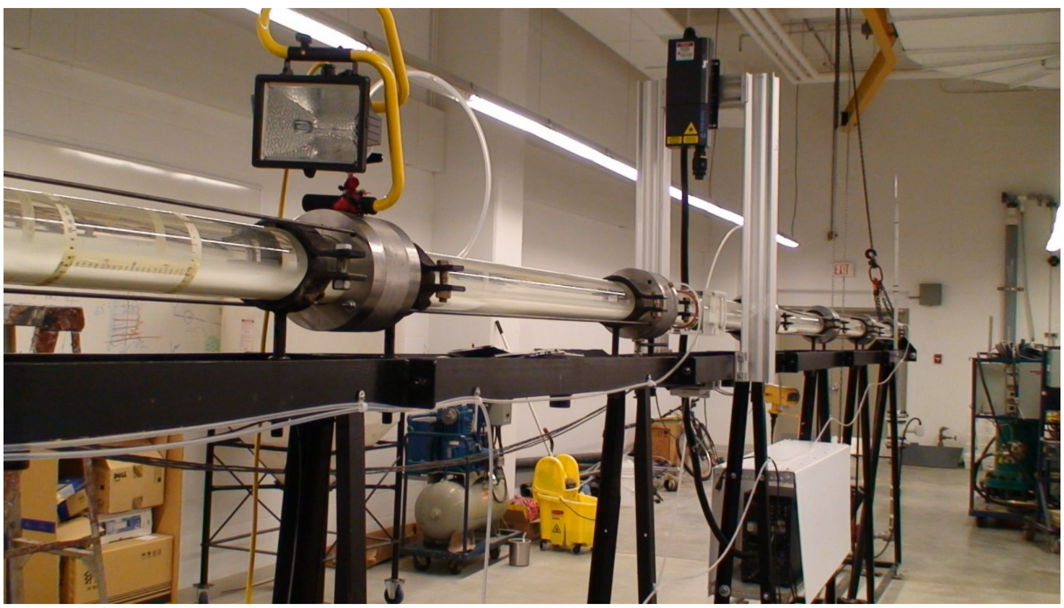

Figure 3-5 Picture of the Glass Pipes and Connections

The outer pipe has an inner diameter of 95 mm and a wall thickness of 5 mm. The inner pipe has an outer diameter equal to 38 mm. The annulus has a hydraulic diameter of $\mathrm{D_H} = 57\ \mathrm{mm}$. The radius ratio is $\alpha = 0.4$. Figure 3-6 graphically shows dimensions of the annulus.

The flow loop has five safety and control valves. The valves could be used to change the passage of the fluid or isolating a section of the system from the rest of the flow loop.

All devices mounted on the flow loop including VFD, flow meter, temperature monitoring devices, and pressure transducers are all connected to data acquisition system which is controlled by LabVIEW software. Figure 3-7 is the user interface of the in-house LabVIEW software. The software is programmed in such a way that allows the user to input the pump RPM which is controlled through VFD system.

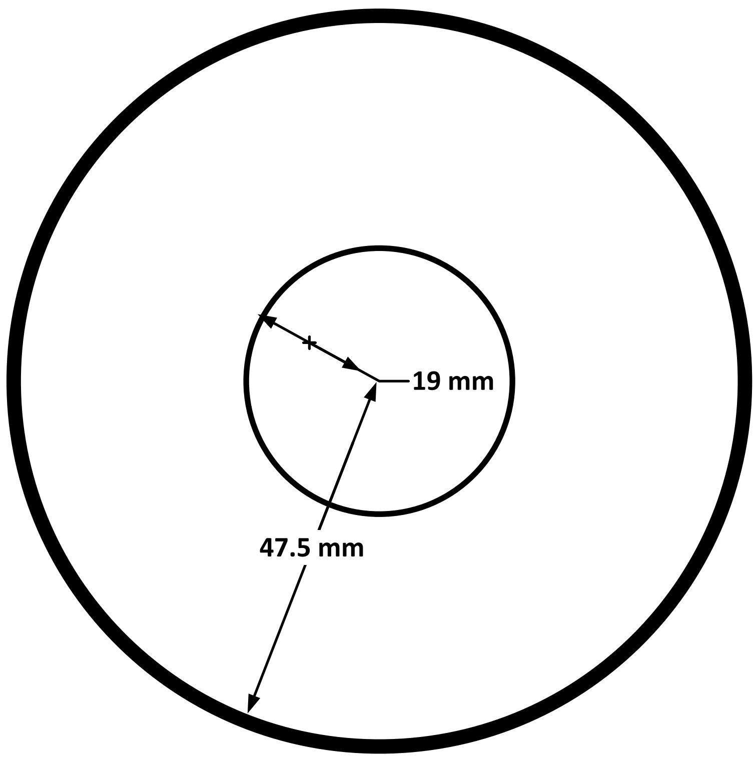

Figure 3-6 Dimensions of the annulus

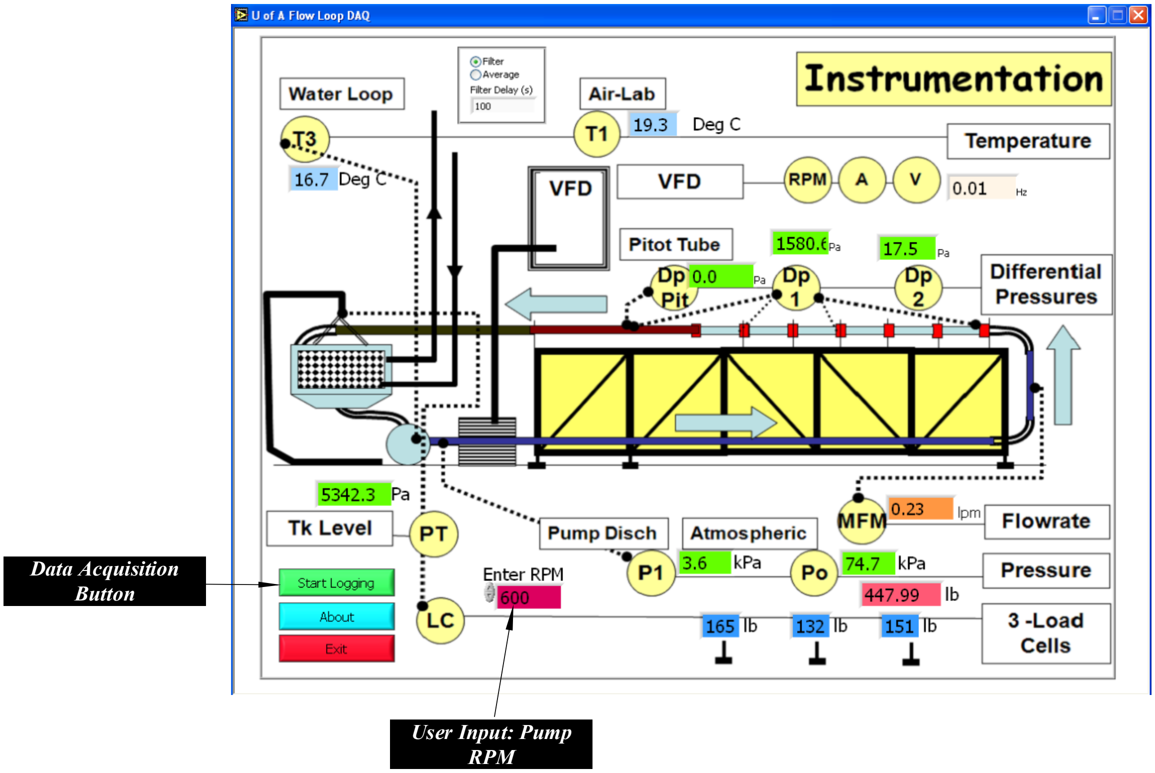

Figure 3-7 Picture of the LABVIEW Software User Interface

The user interface of the in-house LabVIEW program is shown in Figure 3-7. The logging button could be used to record the measurements at different frequencies.

3.1.1 Concentric vs. Eccentric Configuration

The experiments in this study have been conducted in both fully eccentric and concentric configurations. In the concentric configuration, the inner tube is held at the center of the annuli. Figure 3-8 schematically shows the cross-section view of the annulus in an eccentric and concentric position.

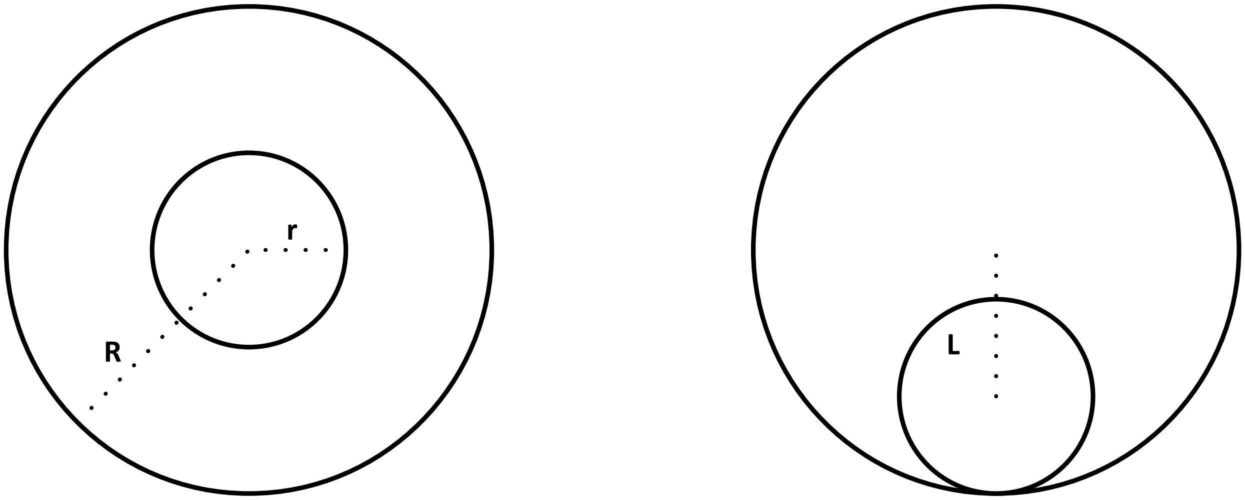

Figure 3-8 Concentric vs. Eccentric configuration

Eccentricity is defined as the ratio of the distance between the centers of the pipes to the difference of radii's.

$$e = \frac{L}{R - r} \qquad \textbf{Eq.(3-1)}$$

In this study eccentricity varied from 0 to 1.

3.2 Macroscopic studies of hole cleaning

The macroscopic approach toward hole cleaning focuses on bulk properties to investigate the impact of each variable on bed erosion. The primary purpose of these experiments is to find the critical velocity required for dislodgement of particles from the surface of a bed of particle deposits.

3.2.1 Establishing a cuttings bed

To establish a stationary cuttings bed in the test section, first, the tank is filled with 500 liters of water. Start circulating water in the flow loop at the highest possible flow rate. Start the air-driven mixer in the tank at its highest rotational speed. In the next step, add the desired amount of sand particles to the fluid in the reservoir gradually. It is important to make sure that sands are added while the pump and the mixer are operating. Otherwise, the sand particles would settle in the pump and will cause the pump to get stuck.

A tip for making sure the flow is not blurred for optical purposes is to wash the sand before adding it to the flow loop. This will cause the sand to be dust free which typically causes the flow to become blur and non-transparent.

Circulate the slurry for at least 10-15 minutes. This will cause a uniform distribution of sand in the entire system. Once the stationary sand bed in the annular section reaches a consistent and constant height, the pump can be shut off. Close valves 4 and 5 to isolate the annular section from the rest of the flow loop (Figure 3-9). Drain the tank and the pump. Wash the tank, the pump, and the transport line to remove any sand particles remained in these sections. The fluid in the annulus need to be allowed to rest for at least 1 hour to let all the particles in suspension to settle down in the bed

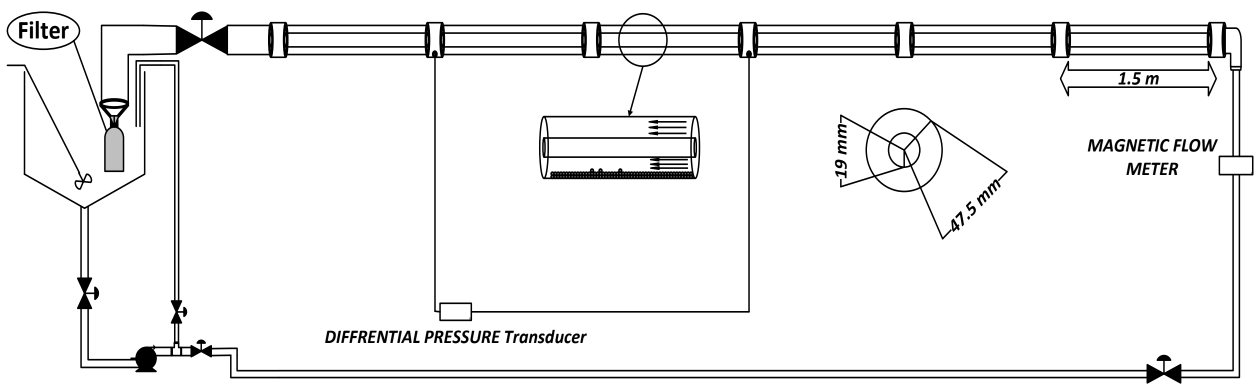

Figure 3-9 Schematic of the Flow Loop

One consideration in establishing a bed is to make sure circulation velocity is high enough in transport lines to avoid particle deposition in this part of the system. One solution to this problem is to use smaller transport lines to make sure that the velocity is high enough to carry the particles out of this pipe. There are two diameter sizes available (1 and 2 inches) for the transport of particles in Figure 3-9, however, for these experiments, the smaller line needs to be used.

The height of the cuttings bed can be controlled through a number of sand particles that are added to the tank. In the current work, mass loading ranging from as low as 3% up to 17% has been used to vary the cuttings bed height. It is not recommended go beyond 20% solid mass loading due to pump limitations.

Two filter bags with openings smaller than the particle size (the opening is 100 micron) were installed at the outlet of the annular section. The purpose of using filter bags are preventing the solids from recirculating in the system and going back to the test section during the experiments. The filter bags would collect any sand particles removed from the test section during the test. Hence, the flow loop was acting like an open-end flow loop in that regard.

3.2.2 Measurement Tools and Techniques

The primary goal of macroscopic experiments is to quantify the minimum flow rate required for the onset of the bed erosion. For this purpose, visualization techniques were adopted. Visualization techniques are often used in sediment transport studies as they provide higher resolution and accuracy than human eyes (GarcÁa 2008). A high-resolution recording camera and a light projector were used to detect particle movement in this study (Figure 3-10).

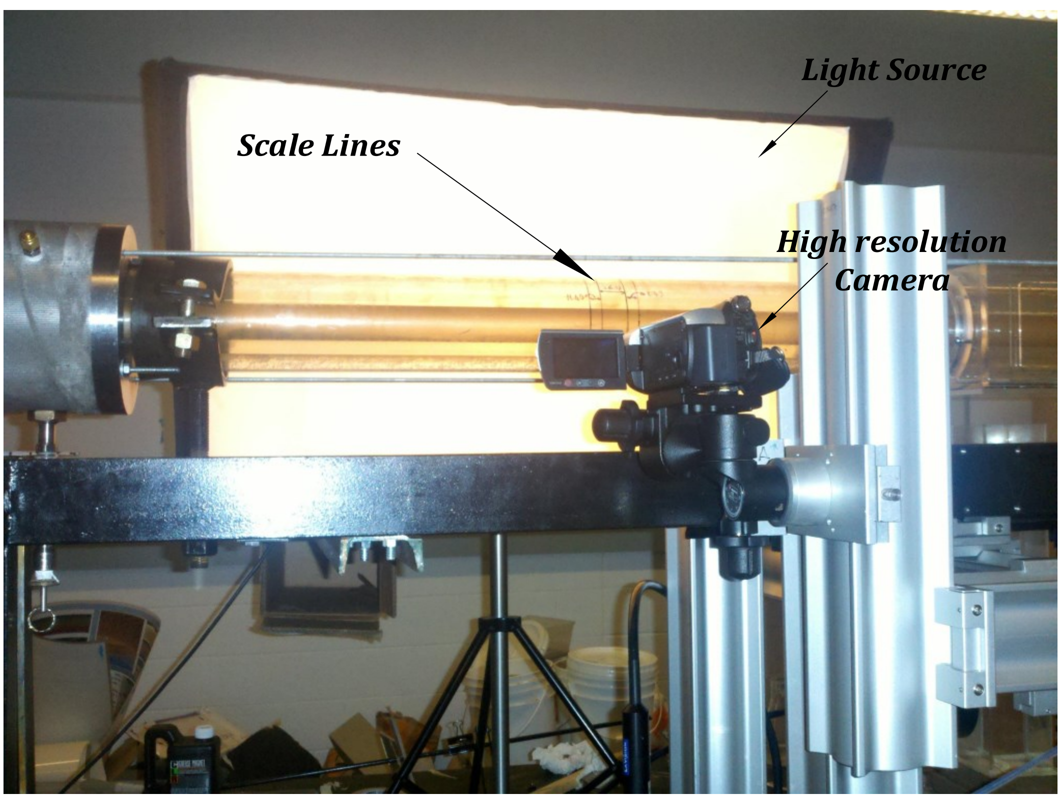

Figure 3-10 Experimental Setup Used for Bed Erosion Experiments (Bizhani 2013)

The experiments always start with the lowest possible flow rate to ensure that the velocity in the annulus is lower than the critical velocity of particle movement (usually at around 0.15 m/s). The velocity is then gradually increased by changing the pump speed until the critical velocity is reached. The critical velocity is judged by the movement of the particles at the bed interface. At the critical flow rate, a moving layer of cuttings exists at the bed interface. Sufficient time must be allowed for each flow rate to establish a fully developed condition in the annulus.

In addition to videotaping the movement of particles in the bed, other variables such as frictional pressure loss are also recorded real time. This is useful in wall shear stress calculation and comparison of the performance of different fluids.

Critical velocity of particle movement in various flow patterns and the wall shear stress required for the movement of particles using various types of fluids and particle diameter are the main output results of these experiments.

3.3 Cuttings size distribution and other physical properties

Sand particles of four different sizes were used in this study. The finest cuttings size was characterized to have a mean sieve diameter of 260 microns, and the biggest cuttings had a diameter of 1240 micron. The other two groups of cuttings had mean sieve diameters of 350 and 600 microns respectively.

Figure 3-11 to Figure 3-14 reports the sieve analysis results of the four sands used in the current research. The ‘y’ axis is the cumulative percentage of the weights that was passed through a certain sieve size. The mean diameter also denoted as d_{50}, is the diameter coinciding to *pf* of 50%. Physically, it means 50% of the cuttings are finer than this diameter.

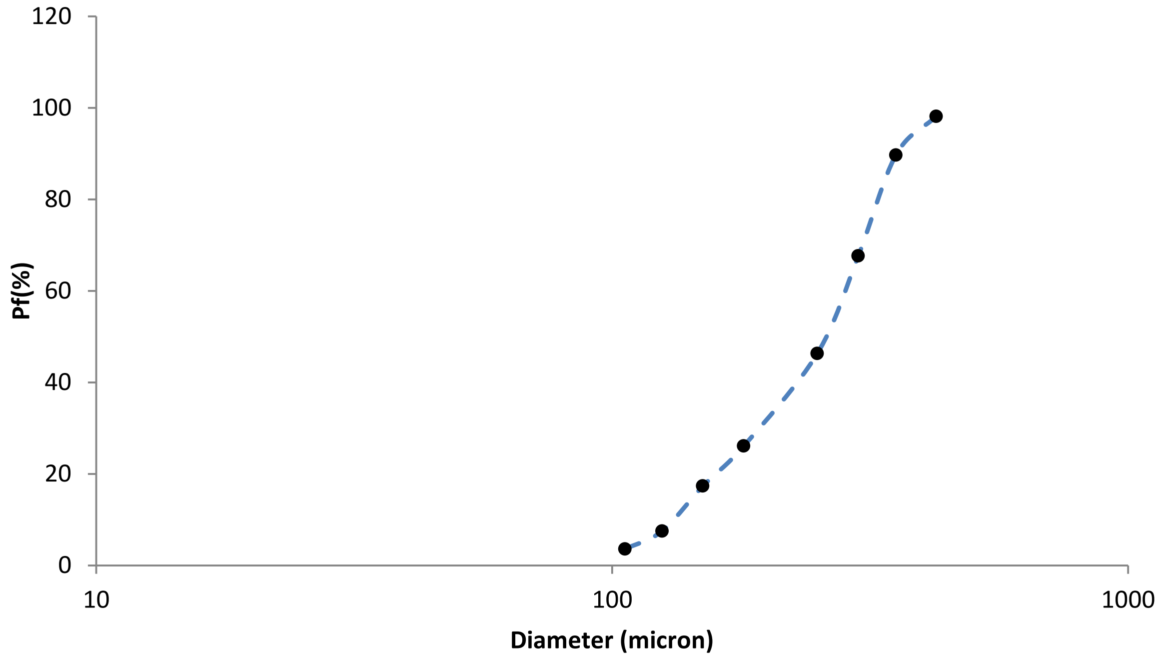

Figure 3-11 Size distribution analysis of sands with mean sieve size of 260 micron

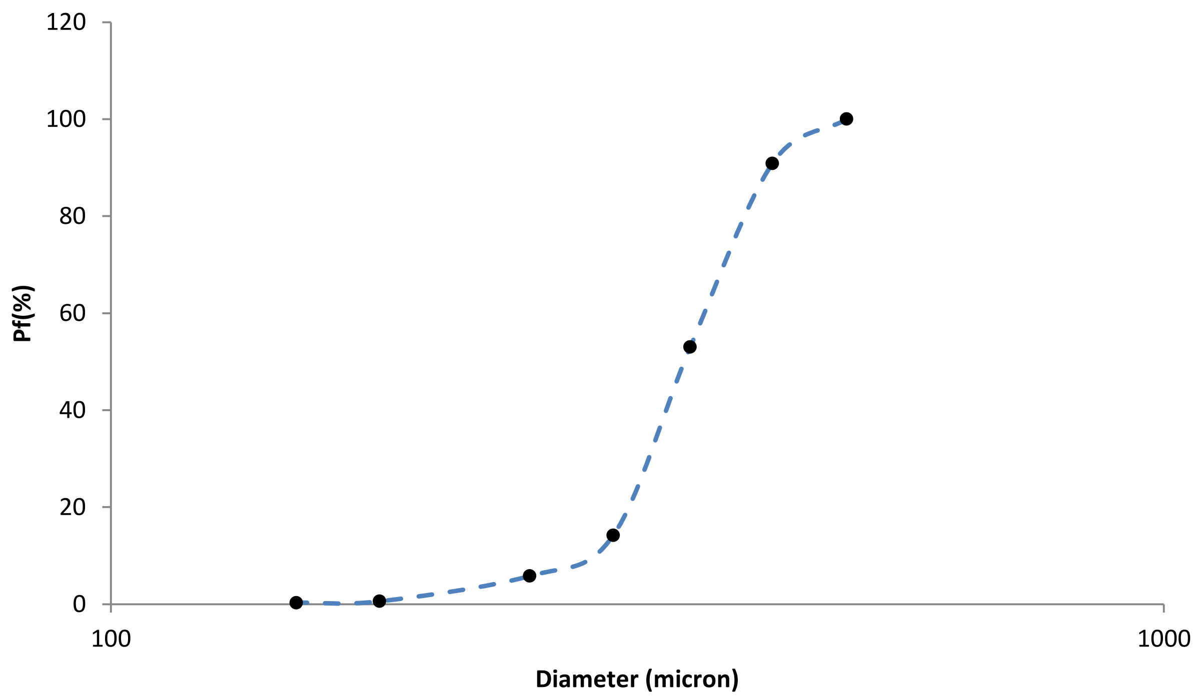

Figure 3-12 Size distribution analysis of sands with mean sieve size of 350 micron

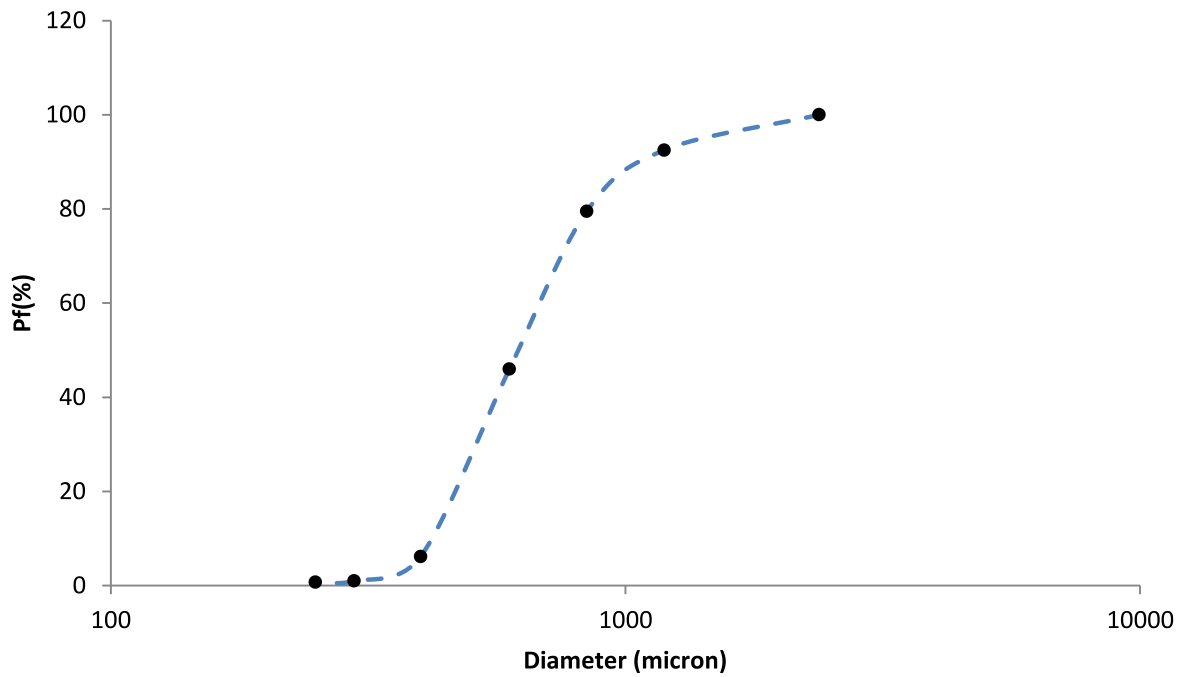

Figure 3-13 Size distribution analysis of sands with mean sieve size of 600 micron

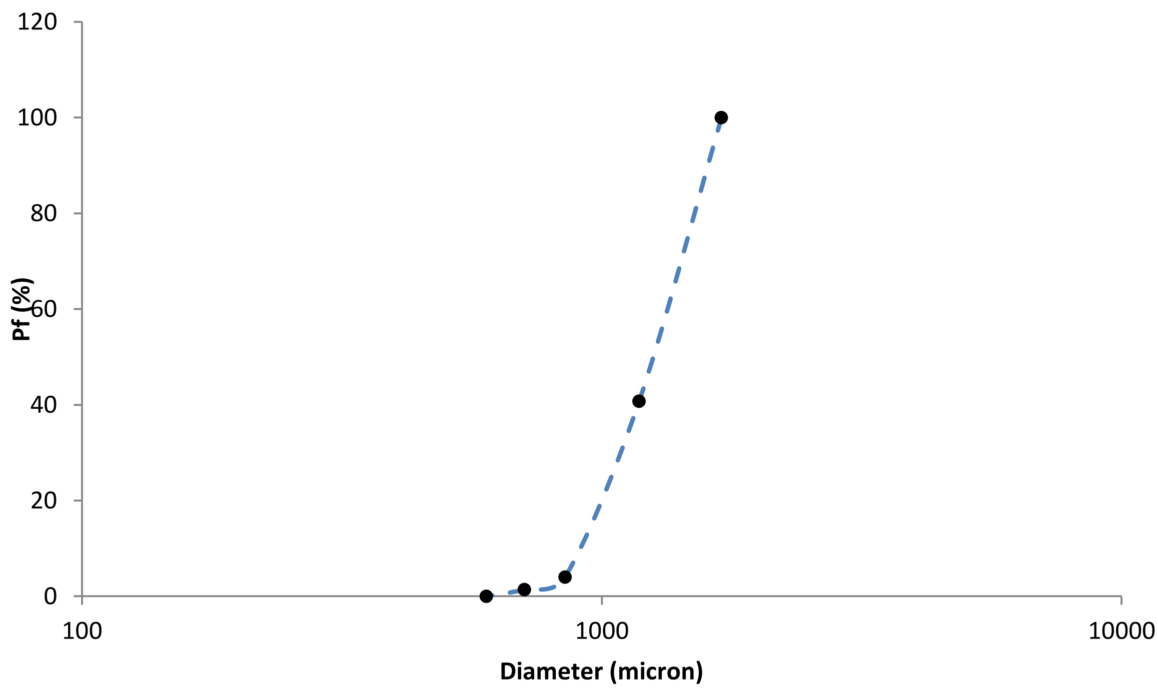

Figure 3-14 Size distribution analysis of sands with mean sieve size of 1240 micron

Table 3-1 reports other properties of the sand particles. All four group of cuttings have a density of 2650 kg/m^3. The cuttings are angular with an irregular shape. Other properties are not of importance to this study.

Table 3-1: Physical Properties of Fine Sand Particles[4]

Property		Test Method	Unit	Typical Values
Mineral		Petrographic	--	Quartz
Shape		Krumbein	--	Sub-Angular
Specific Gravity		ASTM C-128	--	2.65
Bulk Density	aerated	ASTM C-29	Lbs/Ft3	92-95
	Compacted	ASTM C-29	Lbs/Ft3	98-100

3.4 Microscopic Studies of Hole Cleaning

In the second part of this study, hole cleaning has been investigated from a microscopic perspective. The non-intrusive laser-based particle image velocimetry technique (PIV) was the primary measurement technique used for microscopic studies of hole cleaning. In this section, we summarize the details about the measurement technique used. This section also discusses limitations and special considerations that must be taken for the use of PIV technique in hole cleaning studies.

3.4.1 PIV Technique: Concepts and Fundamental

PIV is a nonintrusive laser based imaging technique that can provide high-resolution 2-D instantaneous velocity profiles of the flow field. A planar 2-D PIV consists of a light source and

[4] Data of the Table 3-1 reports other properties of the sand particles. All four group of cuttings have a density of 2650 kg/m^3. The cuttings are angular with an irregular shape. Other properties are not of importance to this study.

Table 3-1 have been taken from Sil Inc. Website
http://sil.ab.ca/

a recording device. The light source is typically a class four green laser. A camera with the double shuttering feature is the other component of a typical PIV system. PIV fundamentally works by detecting tracer particles in the flow. These tracer particles are small glass beads which follow the fluid's motion instantaneously. Upon incident of laser light, these tracers reflect the light towards the camera. The camera takes two images of the tracers in quick succession. Processing these pictures with appropriate algorithm yields the instantaneous velocity field of the flow.

Despite its great accuracy, the PIV technique comes with its limitations and restrictions. The major constraint of the PIV technique is that it requires 100% clear fluid and transparent pipe material. This might not be so desirable with most drilling fluid additives such as bentonite. However, most polymers polymer solutions at low concentration are transparent.

A The 2-D PIV setup requires a light source and a camera or a recording device. A CCD (charge-coupled device) camera with a resolution of 1376×1040 pixels was used for recording the images. The double shuttering feature of the camera allows taking two images with adjustable time intervals in between.

The proper orientation of the camera and laser light sheet is that the camera view is perpendicular to laser light, Figure 3-15. The laser illuminates the flow by pulses of known separation in time and known intensity. The camera is triggered to capture images of the tracers in the flow. Extracting the desired information from these images heavily relies on image processing. Figure 3-16 is a typical PIV picture which shows the boundaries of the system and tracer particles. The tracer particles are the bright white dots.

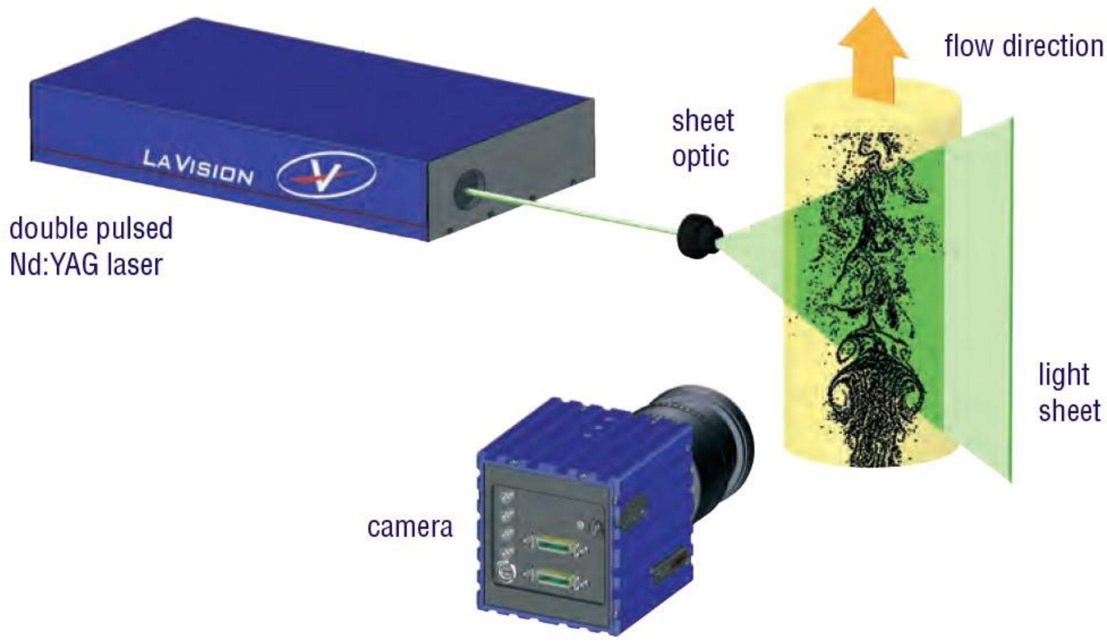

Figure 3-15 Typical 2-D PIV Setup (LAVision)

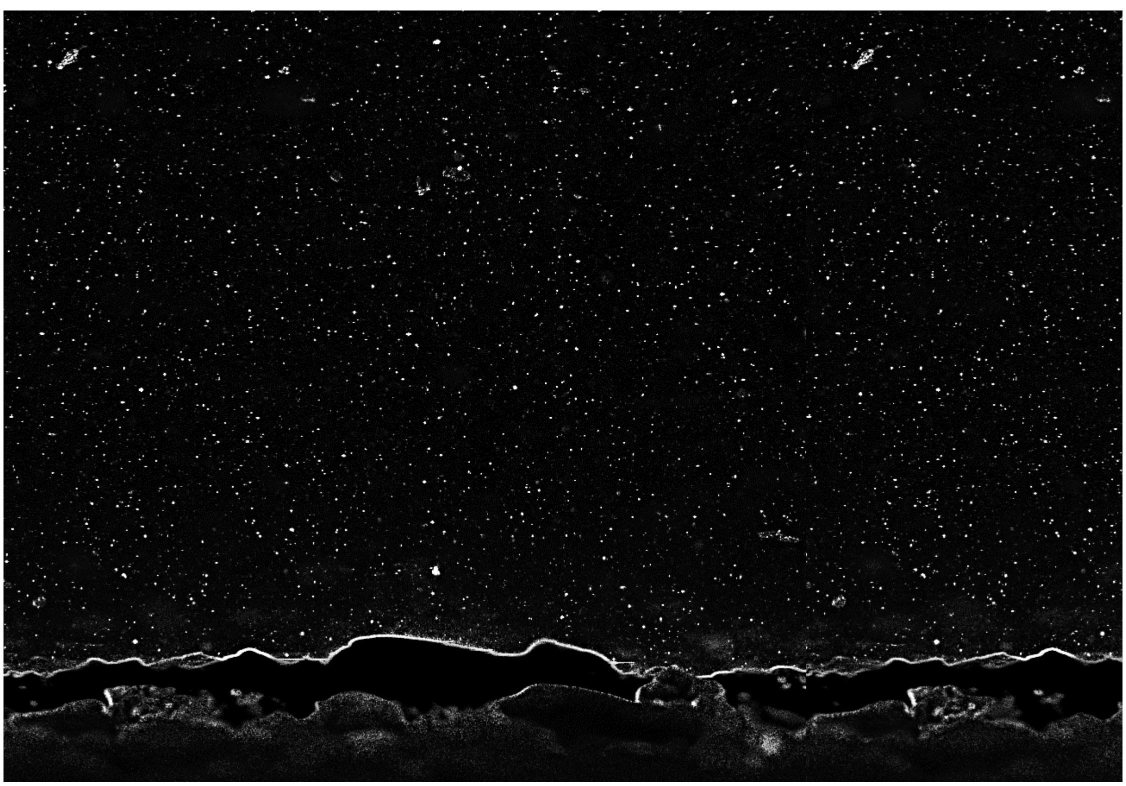

Figure 3-16 A typical PIV picture, note that the bright points are tracer particles in the flow

3.4.2 Image Processing and the Output Results of PIV

In this section, the procedure for obtaining the instantaneous velocity vector field of the flow using PIV images are explained briefly. The procedure includes preprocessing of the pictures, vector field calculations, and post-processing of the vector field. These steps were performed in DAVIS 8.3.0 software.

The preprocessing of the images is a necessary step in reducing the noises and enhancing the signal-to-noise ratio. In this step, the minimum of all the images was first calculated. Following that, the minimum was subtracted from all the raw pictures. Another linear and nonlinear filters may occasionally be applied to eliminate high or low-frequency noise signals. However, the main pre-processing operation in the current research was the subtraction of the minimum from the initial images.

Vector field calculation was performed using the cross-correlation method. In the cross-correlation method, each pair of images is broken down to smaller windows called integration windows. Interrogation windows in the second image are analyzed for probable similarities to that of the first picture (Nezu and Sanjou 2011). Cross-correlation works by cross correlating the local intensity distribution over the interrogation windows. The chosen destiny of each tracer particle is the peak with the highest correlation. After finding the displacement of each tracer particle (Δx and Δy), by using the time interval (Δt) between the images instantaneous velocity can be obtained using following equation:

$$\begin{cases} \widehat{\mathrm{U}} = \dfrac{\Delta \mathrm{x}}{\Delta \mathrm{t}} \\ \widehat{\mathrm{V}} = \dfrac{\Delta \mathrm{y}}{\Delta \mathrm{t}} \end{cases} \qquad \textbf{Eq.(3-2)}$$

Multi-pass cross-correlation method with decreasing of interrogation window size was used for particle displacement calculations. Interrogation window size of 64×64 pixels followed by the window size of 32×32 pixels was utilized in the calculations. Adaptive weighting function with an overlap setting of 50% was used for the vector field calculations. Figure 3-17 schematically summarizes the workflow procedure that PIV follows to calculate the instantaneous vector field. Figure 3-18 is a common vector field results of the instantaneous velocity.

The post-processing step applies linear and nonlinear filters to the calculated vector field to detect and delete outlier vectors. This step is optional. However, it improves the accuracy of the results. Figure 3-17 is a graphical representation of PIV processing procedures (LAVision , Adrian 2005). Figure 3-19 is the vector field of the data presented in Figure 3-18 but after applying the nonlinear vector post-processing filter which removes outlier vectors.

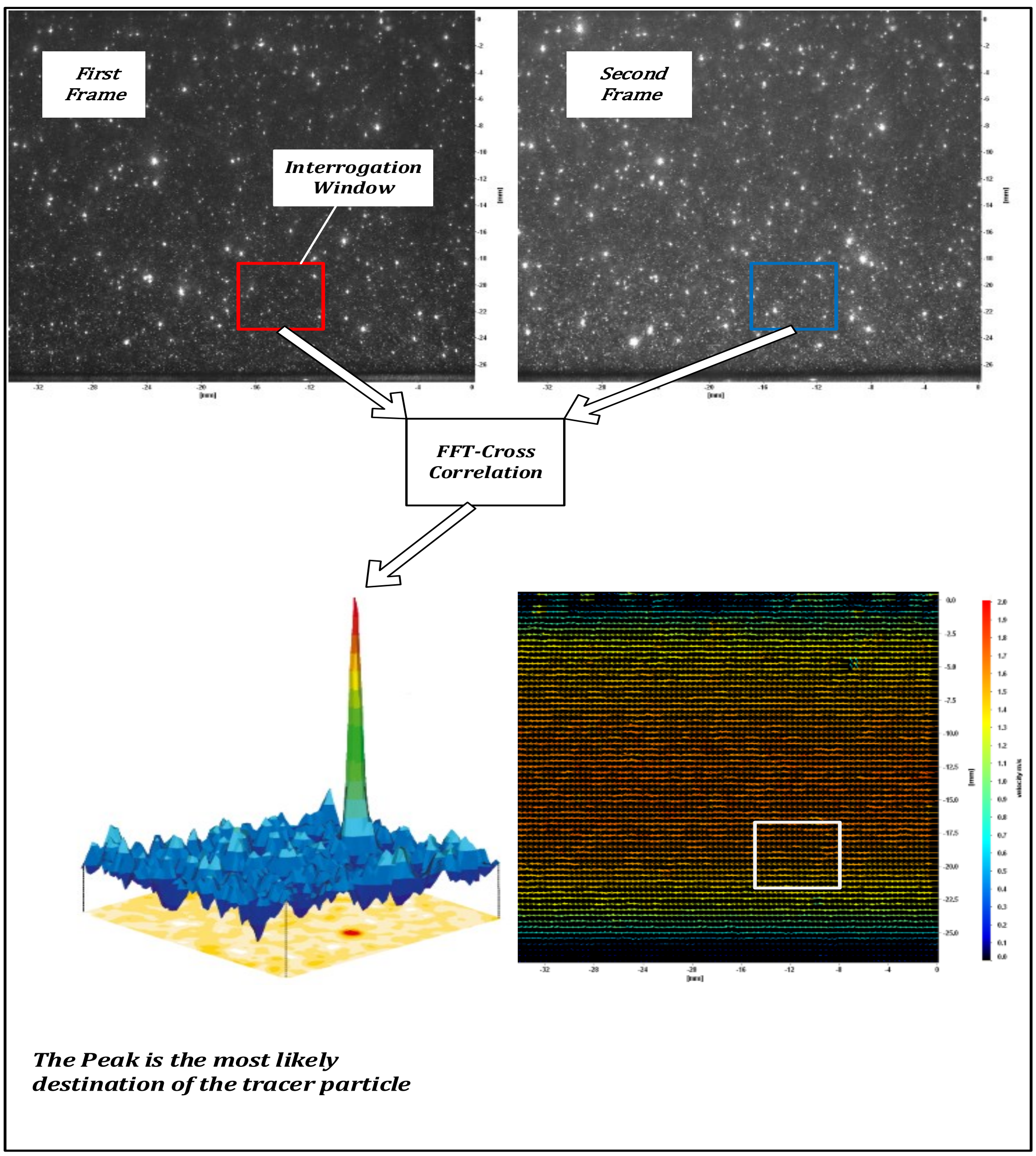

Figure 3-17 PIV post-processing procedure used for obtaining instantaneous velocity field (Bizhani 2013)

After acquiring the instantaneous vector field of the flow, the users depending on their needs can extract different information of the flow. For example, in this particular study, the time average velocity was of keen interest. To obtain the time averaged velocity profiles, the instantaneous velocity vectors were averaged. Different quantities such as Reynolds normal and shear stresses could also be extracted easily.

As a summary of the discussion on the PIV, after taking pictures of a seeded flow, each pair of these pictures are analyzed by applying DCM (Direct Corss-Correlation Method) to find the instantaneous velocity field. Vector post-processing is then applied to remove the outlier vectors. The time average of velocity, RMS of fluctuation velocities, Reynolds stresses, velocity gradients, turbulent kinetic energy, mean kinetic energy, swirling and vorticity all are the parameters, which can be calculated from instantaneous velocity fields using DAVIS software.

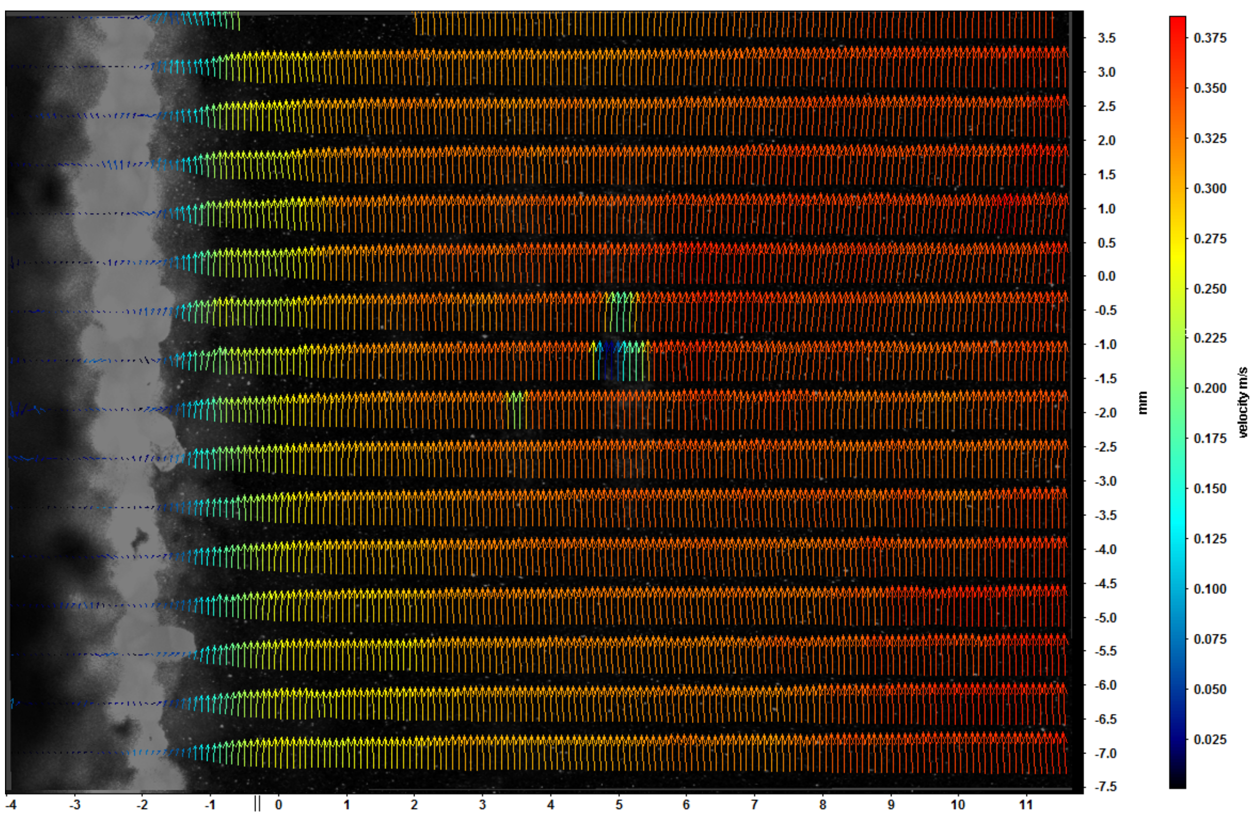

Figure 3-18 Instantaneous velocity field

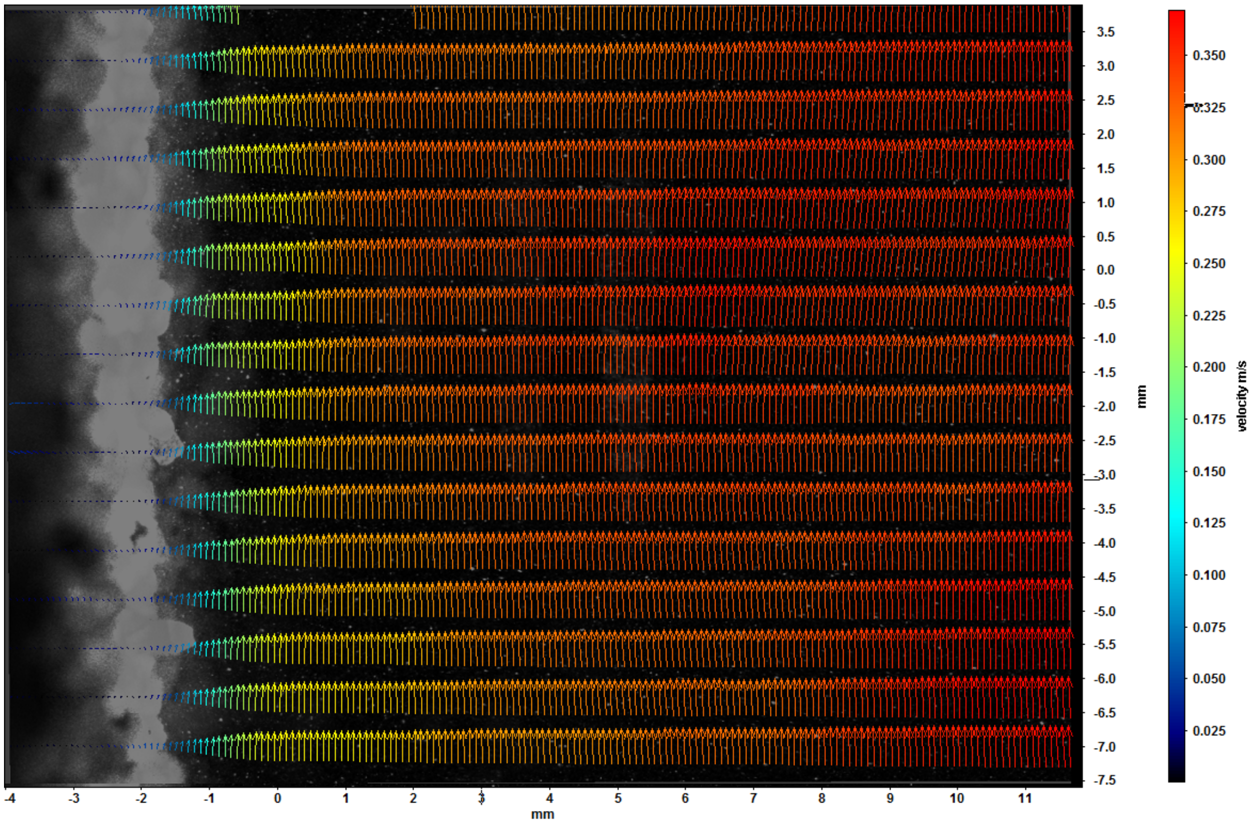

Figure 3-19 Instantaneous velocity field after applying the vector-postprocessing

3.4.3 PIV Components: Descriptions and Details

3.4.3.1 Double Pulsed Laser

The doubled pulsed ND.YAG laser (Figure 3-20) from New Wave Inc. capable of emitting two pulses of light in a short and adjustable period was used as the light source in all PIV measurements.

The wavelength of the light is 532 nm with a frequency of 50 HZ. Each pulse at maximum has an energy of 50mJ per pulse. Laser light is converted to a planar light sheet by a combination of cylindrical and special optical lenses (Solo PIV. Nd:YAG Laser System. Operator's Manual).

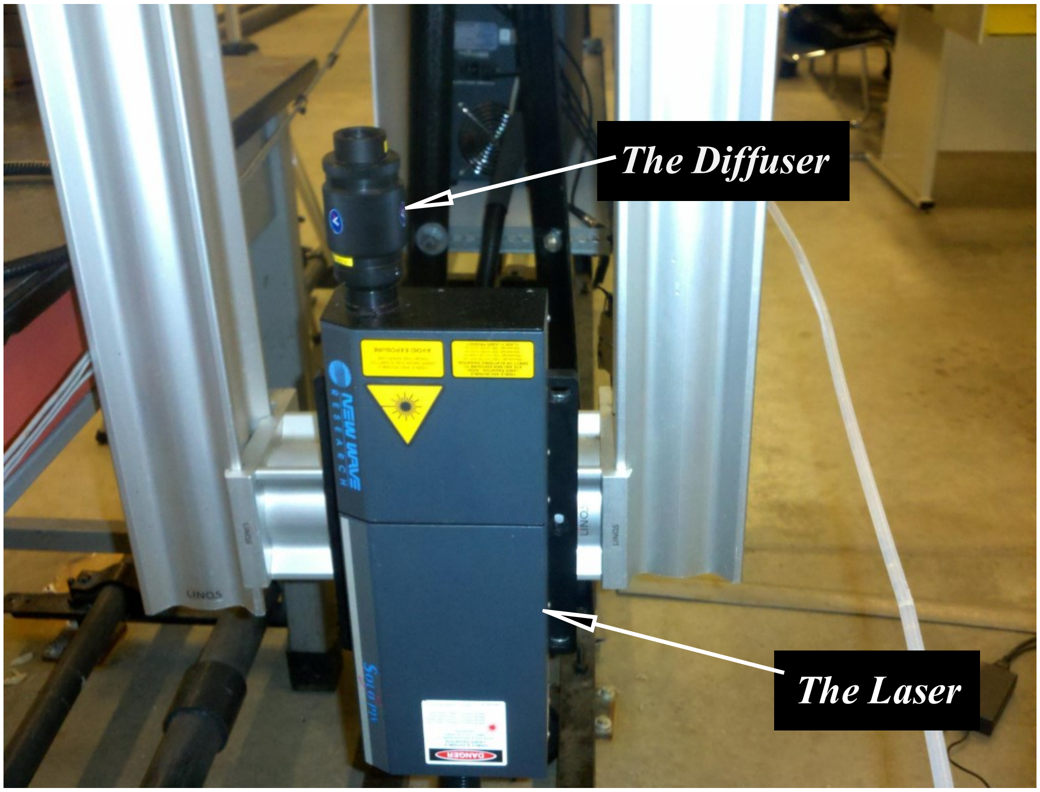

Figure 3-20 Picture of the double pulsed laser and special light diffuser (Bizhani 2013)

The thickness of laser light beams varies from 0.5 mm up to 3.5 mm, however, in this study, it was kept at 0.5 mm for all the experiments. The thick laser light is not favorable and may cause errors in measurements; this is especially important when there is a large gradient of one of the parameters in the direction normal to laser light sheet (Wieneke 2005). In this study, the flow is unidirectional (only axial, no radial or tangential flow) which means there is no significant change in flow parameters along z-axis where laser light thickness may affect the readings.

3.4.3.1 CCD Camera and Lenses

A double frame high resolution (1376×1040 pixels) CCD camera has been used for capturing the pictures of the flow in this research (Figure 3-21). The framing rate of the camera varies and can be as high as five frames per second (each frame is a pair of pictures). The most important feature of the camera is its dual framing capability which allows taking pictures in a short period. The time interval between two pictures of a pair is adjustable and can be as low as 500 ns. This time interval depends upon fluid velocity and field of view of the camera (field of view itself depends upon zooming and the type of lens used) and has to be adjusted before taking any data.

Normally, the time interval should be selected such that allows an individual tracer particle to move about 5 to 8 pixels from the first picture of a pair to the second picture (LaVision. Imager intense).

Depending upon what type of results one is interested in obtaining, different types of lenses may be needed. For example, for obtaining data of near wall characteristic of the flow, lenses with high zooming capabilities need to be utilized. On the other hand, for monitoring the behavior in larger areas smaller lenses are required. A 60 mm Nikon AF Micro Nikkor plus an extension tube of the size of 36 mm has been the primary lens of taking data in wall region where deep zooming is required. To take information in the whole annular gap, a 50 mm Nikon AF Nikkor with a 12-mm long extension tube was used.

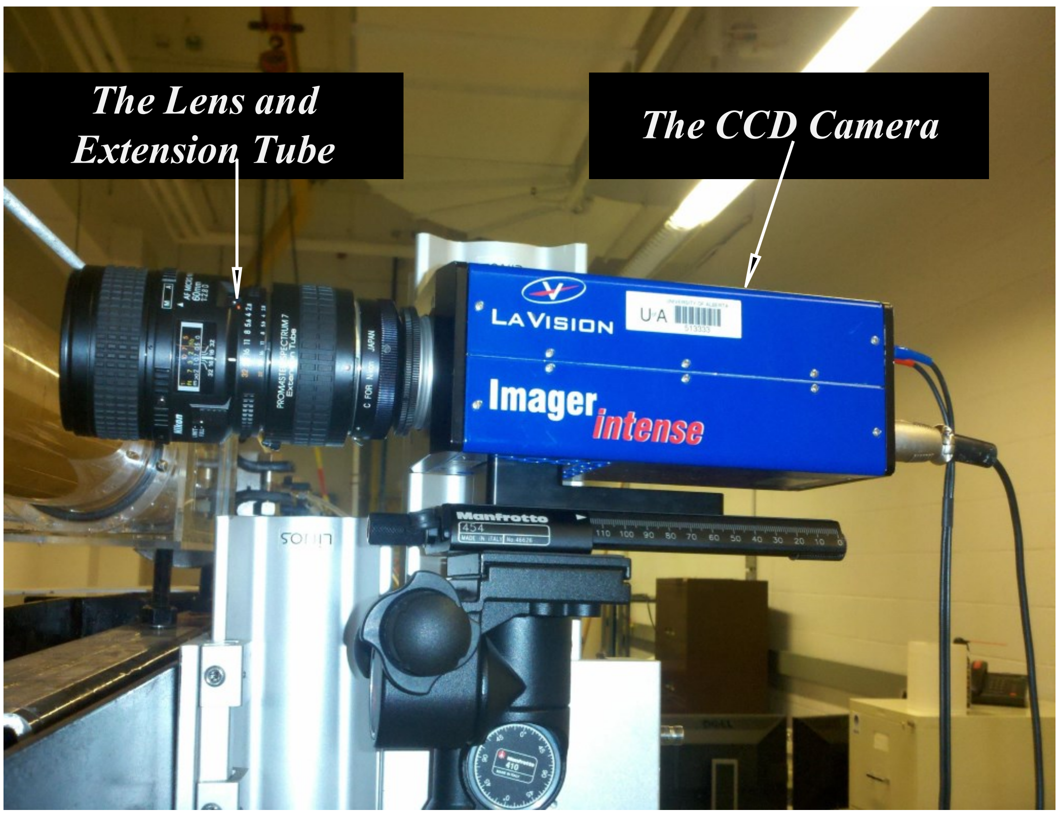

Figure 3-21 Picture of the CCD camera and the lens with extension tube (Bizhani 2013)

3.4.4 The Observation Window

One of the problems associated with the PIV technique is the scattering and refraction of the light. This issue is especially significant in round tubes and may affect the results for near the wall measurements.

Light scattering happens because of the cylindrical shape of the glass pipe. One solution to this problem is to use rectangular channels. However, this is not a representative geometry for a wellbore. One alternative solution to this issue is to design a rectangular box which can surround the glass tubes. This box is rectangular and is made of Plexiglas with 100% transparency. The rectangular shape of the box will prevent and reduce light scattering due to the cylindrical shape of the glass tubes. This box is called the "Observation Window" and is located approximately $\sim 100D_H$ downstream of the inlet, where all the PIV measurement are taken (Figure 3-22).

Refraction of the light happens when light passes through one medium (air) to another (glass) with different refraction indices. The rectangular box was filled up with Glycerol to reduce light refraction due to the difference in refraction indices. Glycerol has a refraction index of 1.47 which is close to the refraction index of the borosilicate glass pipes.

Overall, the observation window is a rectangular box filled up with Glycerol surrounding the glass tubes at a location where PIV measurements are performed. The purpose of installing this box is to reduce the light scattering and refraction of the light in the measurement section of the flow loop.

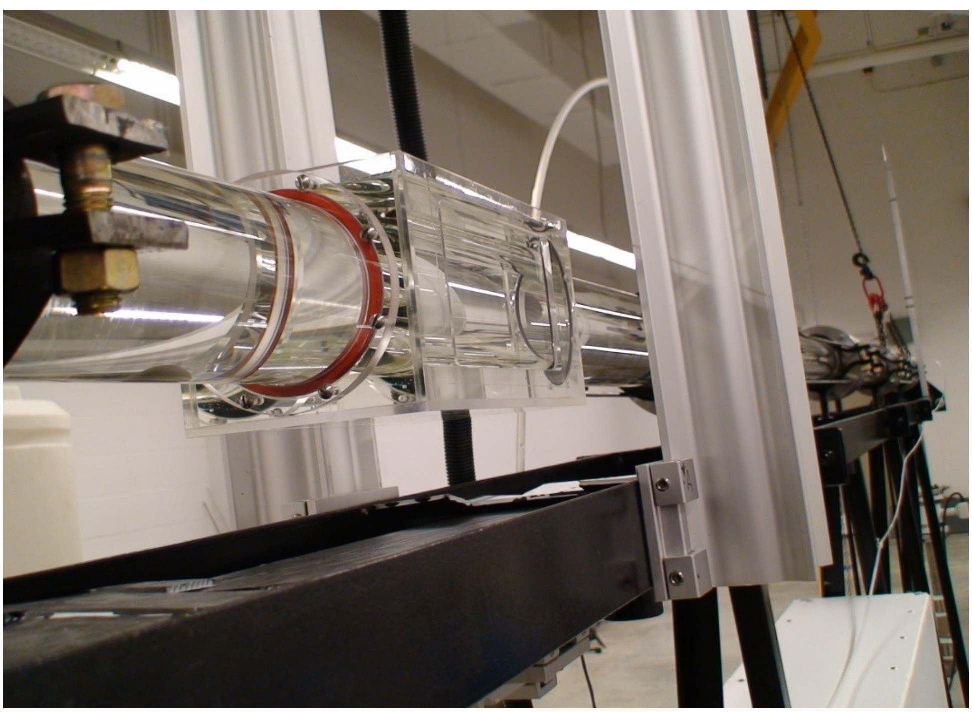

Figure 3-22 Picture of the Observation Window; the Rectangular Box Filled with Glycerol

3.4.5 Camera Calibration

Calibration of the camera is necessary to convert pixels to real world scales. Calculation of tracer's displacement requires knowledge of the actual scales of the images. The scaling of images is done through calibration of the camera. The term calibration and scaling are not the same in the context of the PIV. The former is used when image correction is required due to the light refraction and perspective errors in round pipes. The latter simply implies scaling the distance and no image correction. In this study, because we are dealing with the flow in round tubes, calibration is performed. Although it is only necessary to correct the images for flow near the pipe walls, it was used for all the experiments.

The calibration process is a rather challenging and tricky step in the experiments. It requires a target that is supported by the software. Additionally, the target must be put inside the pipe filled with the fluids that are being tested. Putting the calibration plate inside the tubes in the test section is not possible because of the way the flow loop is designed.

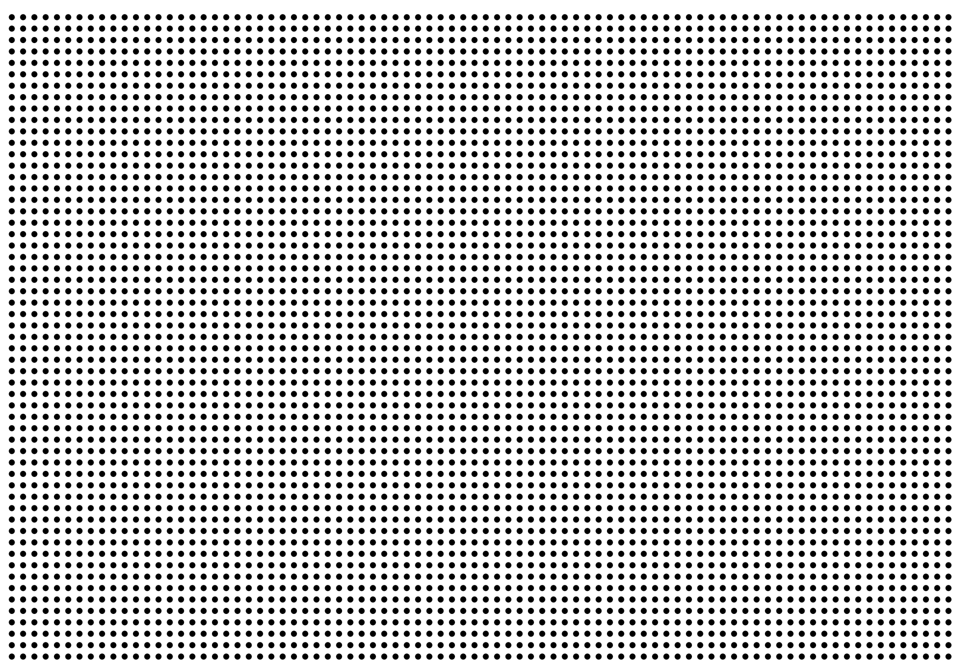

Figure 3-23 Calibration target used for calibrating the camera

The calibration target supported by DAVIS 8.3.0 was designed in Microsoft Visio. The calibration target is black dots on a white background (Figure 3-23). The dots have a diameter of 0.8 mm, and the distance between the center of neighboring dots is 1.5mm.

The calibration target must be inside the test section for proper calibration. However, it is not possible to put the plate inside the annular section while there is a flow in the system. To overcome this challenge, an observation window identical to the observation window of the flow loop was built. The replica of the observation window consists of a glycerol box and a piece of the glass tube used in the flow loop. A calibration target printed on translucent paper is inserted into the pipe. The small tube is filled with water, and both ends are sealed. The calibration tube is immersed in glycerol in a rectangular box. Figure 3-24 and Figure 3-25 show the calibration target inside the pipe and the calibration box respectively.

Figure 3-24 Calibration target inside the pipe filled with water

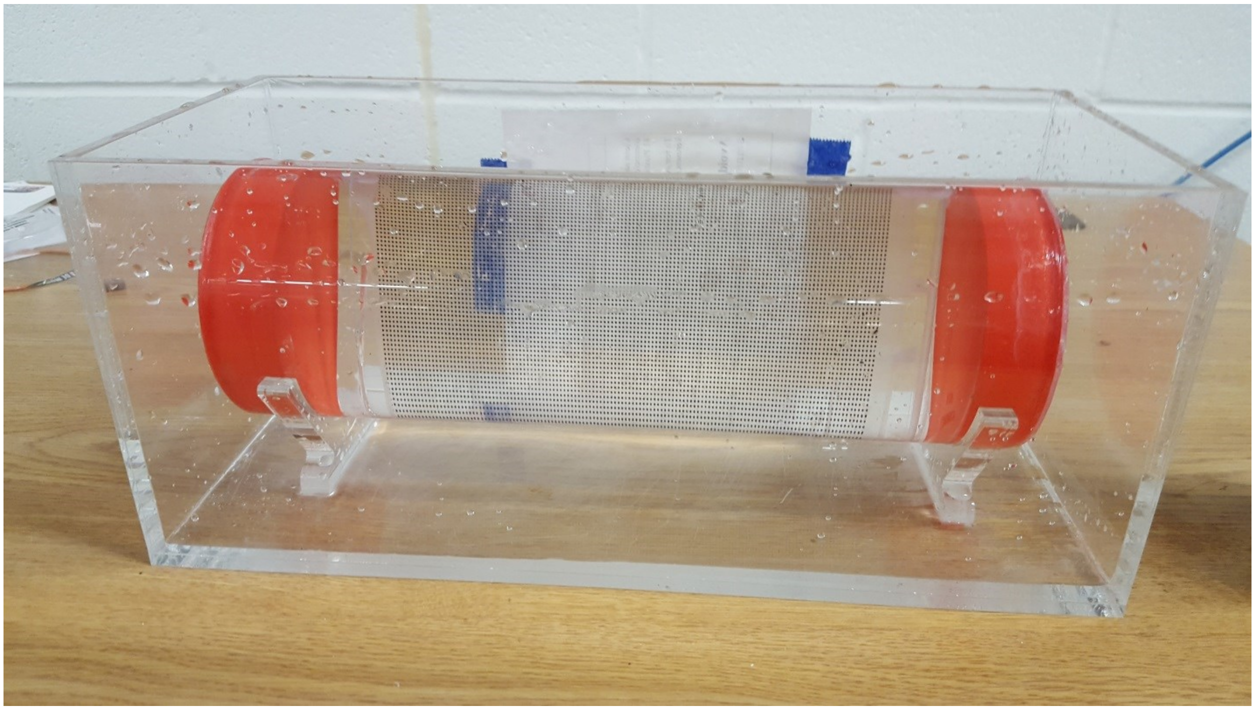

Figure 3-25 The calibration box

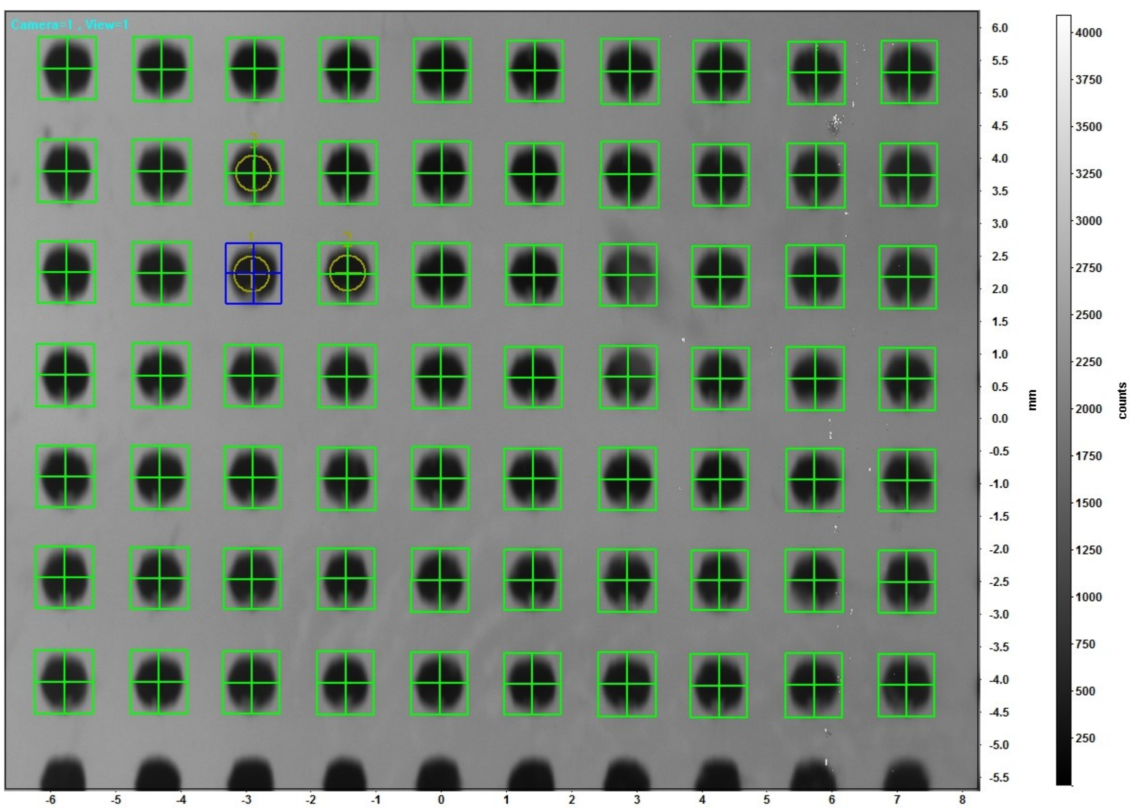

Figure 3-26 Picture of the calibration target captured by the camera

In each experiment, after adjusting the camera and laser light, the calibration box is put over the glycerol box installed in the flow loop. Great care must be taken to align the laser light and the calibration target. In the calibration window of the software, proper choice of the target must then be taken. Finally, an image of the target is taken, and the software performs the calibration. Figure 3-26 is an example of detecting the dots by the software which is then used for calibration.

3.4.6 Tracer Particle Properties

The tracer particles utilized in this study were hollow glass spheres with a mean diameter of 10 microns. Density of the tracers are $1.1 \pm 0.05 \frac{g}{cc}$ which gives near neutrality to them in the working fluids, and hence, keep them suspended in the flow. Addition of the tracer particle is crucial for enhancing spatial resolution of the PIV images which results in more accurate measurements of the velocity profiles (Melling 1997).

3.5 Limitations and uncertainties of the current study

The constraints and uncertainties involved in the present study are from two main sources; from the experimental set-up and the measurement technique. For the first source of error, the configuration of the annulus and imperfections that exist in the flow loop are the main sources of uncertainties. In the concentric annulus, especial care was taken to make sure that the inner pipe is exactly at the center of the annulus. However, in practice, there was always a small offset between the centers of the pipes (less than 0.7 mm according to measurement via PIV technique). The inner pipes are 3 meters long and that caused the pipe to bend slightly during the experiments and that further caused a difference in the annular gaps in the lower and upper annulus.

In the experiments with water in the concentric annulus, the operating flow rates were close to the minimum operating flow rates of the flow loop. Hence, that might have affected the accuracy of the measurements in this case. We ignore the flow through the sand bed in this study, hence, the discussions where velocity profiles are compared in two different sections of the annulus neglect the flow through the bed.

There is also an additional uncertainty involved in the PIV measurements. Part of these errors is inherent errors of the PIV system (Nobach and Bodenschatz 2009). Background noise was tried to be reduced by using proper seeding of the flow and pre-processing of the images. Background noise is insignificant for particle shifts more than 0.4 pixels (the particle shifts in this study was tried to be between 5-10 pixels) (Dabiri).

3.6 References

Adrian, R. J. (2005). Twenty years of particle image velocimetry. Experiments in Fluids **39**(2): 159-169, DOI: 10.1007/s00348-005-0991-7.

Bizhani, M. (2013). Solids transport with turbulent flow of non-Newtonian fluid in the horizontal annuli, University of Alberta.

Dabiri, D. Cross-Correlation Digital Particle Image Velocimetry – A Review. Department of Aeronautics & Astronautics, University of Washington, Seattle, USA

GarcÁa, M. H. (2008). Sedimentation Engineering: Processes, Measurements, Modeling, and Practice, American Society of Civil Engineers.

LAVision, F. M., Product Catalogue, 2006.

LaVision. Imager intense, P. c., 2006.

Melling, A. (1997). Tracer particles and seeding for particle image velocimetry. Measurement Science & Technology **8**(12): 1406-1416, Meas Sci Technol, DOI: 10.1088/0957-0233/8/12/005.

Nezu, I. and Sanjou, M. (2011). PIV and PTV measurements in hydro-sciences with focus on turbulent open-channel flows. Journal of Hydro-Environment Research **5**(4): 215-230, J Hydro-Environ Res, DOI: 10.1016/j.jher.2011.05.004.

Nobach, H. and Bodenschatz, E. (2009). Limitations of Accuracy in PIV Due To Individual Variations of Particle Image Intensities. Experiments in Fluids **47**(1): 27-38, DOI: 10.1007/s00348-009-0627-4.

Solo PIV. Nd:YAG Laser System. Operator’s Manual.

Wieneke, B. (2005). Stereo-PIV using self-calibration on particle images. Experiments in Fluids **39**(2): 267-280, DOI: 10.1007/s00348-005-0962-z.

4. Effect of Sand Bed Deposits on the Characteristics of Turbulent Flow of Water in Horizontal Annuli[5]

In this chapter, the PIV results for flow over sand beds of varying initial heights in the concentric annulus is presented and discussed. Water was used as the test fluid. The primary goal of the data and discussion in this chapter is to analyze the impact of the presence of sand beds on the flow of drilling fluid in horizontal wells.

4.1. Abstract

An experimental program was conducted to investigate the turbulent flow of water over the stationary sand bed deposited in horizontal annuli. A large-scale horizontal flow loop equipped with the state of the art Particle Image Velocimetry (PIV) system has been used for the experiments.

The proposed work was accomplished by conducting experiments to measure the instantaneous local velocity profiles during turbulent flow and examining the impact of the presence of a stationary sand bed deposits on the local velocity profiles, Reynolds shear stresses and turbulence intensities.

Results have shown that the existence of a stationary sand bed causes the volumetric flow to be diverted away from the lower annular gap. Increasing the sand bed height causes further reduction of the volumetric flow rate in the lower annulus. The peak velocity in the lower annulus also decreased with the increasing bed height.

Velocity profiles near the surface of the bed deposits showed a downward shift from the universal law in wall units indicating that the flow is hydraulically rough near the sand bed. The equivalent roughness height varied with flow rates. An equivalent roughness height of $2d_{50}$ was

[5] A version of this chapter has been submitted for publication. Bizhani, M., Kuru, E., 2017, "Effect of Sand Bed Deposits on the Characteristics of Turbulent Flow of Water in Horizontal Annuli," ASME Fluid Engineering Journal, Paper under review

measured at a flow rate less than the critical flow rate of bed erosion. At the critical flow rate of bed erosion, however, the equivalent roughness height was equal to $2.4d_{50}$.

The normalized Reynolds shear stress profiles over the sand bed deposits were measured at a subcritical and critical flow rates of bed erosion and were also compared to the case with the flow in the same annuli and no cuttings bed. At flow rates, less than the critical flow rate, the Reynolds stress profile near the bed interface had slightly higher peak values than that of the case with no sand bed. At the critical flow rate, however, the peak Reynolds stress values for the flow over the sand bed was lower than that of the case with no bed. This behavior is attributed to the bed load transport of sand particles at the critical flow rate.

The Reynolds stress profiles near the sand bed deposits of different heights were nearly the same. However, away from the bed interface, the thicker bed resulted in, the lower Reynolds stress. Nonetheless, the bed shear stress increased with the increasing bed height.

The radial turbulence intensity was also measured. At flow rates less than the critical flow rate, the radial turbulence intensity is almost the same for both cases of flow over the sand bed and no bed. At the critical flow rate, however, the radial turbulence intensity for flow over the cuttings bed was lower than that of the case with no bed.

Keywords: Horizontal well, coiled tubing drilling, Turbulent Flow, Solid transport, Multiphase flow, Hole cleaning, PIV

4.2. Introduction

Turbulent flow of water over a stationary sand bed located in a horizontal annulus is the main subject matter of this study. This situation arises due to poor hole cleaning in horizontal and extended reach wells. Drilled solids (i.e. cuttings) settling on the low side of the wellbore gradually form a stationary cuttings bed. In the hole cleaning operation, the drilling fluid is pumped down the hole to remove the stationary cuttings bed. The presence of a stationary cuttings bed alters the flow in the annulus due to changing of the flow geometry and also through the interaction of cuttings with the flow. Hence these flows behave differently than single-phase fluid flow. Complex nature of interactions of phases coupled with chaotic nature of turbulent flows makes these systems immunes to any analytical treatments.

The single-phase turbulent flow of both Newtonian and non-Newtonian fluids in the horizontal annulus has been the subject of numerous numerical and experimental studies (Rehme 1974, Nouri et al. 1993, Escudier and Gouldson 1995, Chung et al. 2002, Japper-Jaafar et al. 2010, Rodriguez-Corredor 2014). Recently, Rodriguez et al. (2014, 2015) and Bizhani et al. (2015) utilized PIV to study the turbulent flow of water and aqueous polymer solutions in a concentric annulus. Despite the presence of a vast number of studies on the single-phase turbulent flow in annular geometry, there have not been many studies reported in the literature where the interaction of solid-liquid has been investigated in such a geometry. However, sediment transport in rivers and flumes has been investigated extensively (Gore and Crowe 1991, Best et al. 1997, Carbonneau and Bergeron 2000, Sumer et al. 2003, Bigillon et al. 2006) where the impact of the suspended load and the bed load on the turbulence has been investigated (Gore and Crowe 1991, Carbonneau and Bergeron 2000).

Recently several studies have been conducted to investigate fluid-particle interaction using techniques such as PIV or Particle Tracking Velocimetry (PTV) in pipes and channels (Miyazaki 1999, Bigillon et al. 2006, Yan and Rinoshika 2011, Yan and Rinoshika 2012). Zeinali et al. (2012) investigated the impact of near-wall turbulence on the particle removal from bed deposits in a horizontal pipeline. They have measured the near wall velocity distribution using the PIV system. However, Zeinali et al. (2012) did not provide any detailed analyses of turbulence statistics in their study. Effect of particle movements in the bed load on the near wall turbulence has been a point of controversy. Some researchers have suggested that movement of sand particles in the form of the bed load induces an extra roughness height (Best et al. 1997, Bigillon et al. 2006). Other researchers have proposed that bed load may lead to the reduction of the von Karman's constant (Best et al. 1997, Gaudio et al. 2010). To the best of author's knowledge, there has not been any such study conducted for the flow in the horizontal annuli.

In this study, PIV technique was used to investigate the turbulent flow of water over stationary sand beds deposited in the concentric annuli. Instantaneous velocity profiles were measured. For comparison, measurements were also carried out for the flow in the concentric annuli without the presence of a sand bed deposits as well. Natural, irregularly shaped, quartz sand particles with mean sieve diameters (d_{50}) of 600 microns and density of 2650 $\frac{kg}{m^3}$ were used. Measurements were carried out at two flow rates (with resulting superficial velocities of 0.2 m/s and 0.24 m/s). The highest flow rate tested was equal to the critical flow rate for initiating bed erosion (Bizhani et al. 2016) or equivalently there was a bed load transport of particles at this flow rate. Two stationary sand bed heights (6 mm and 16 mm) were tested to assess the impact of the change in the bed height on the turbulence characteristics.

4.3. Experimental set-up and procedure

A schematic view of the large-scale flow loop facility used in this study is shown in Figure 4-1. Principal components of the flow loop are a 500-liter stainless steel tank, a centrifugal pump and measurement instruments such as magnetic flow meter and differential pressure transducers. There is an air-driven mixer in the tank for preparing the slurry. The centrifugal pump equipped with Variable Frequency Drive (VFD) was used to circulate fluid/solids mixture through the flow loop.

The 9 meters long test section consists of high-quality Borosilicate glass pipes. The outer pipe has an inner diameter of 95 mm and a wall thickness of 5 mm. The glass inner pipe has an outer diameter of 38 mm. The inner pipes are 3-meter-long each and are centralized and kept in position using 3 thin metal rods. These metal rods have no impact on the development of the flow as it was shown in the previous studies (Bizhani et al. 2015, Ghaemi 2015). The annulus has a hydraulic diameter of 57 mm and a radius ratio of 0.4. The annulus hydraulic diameter is equal to $D_H = D_o - D_i$ where D_o and D_i are the outer pipe inner diameter and the inner pipe outer diameter, respectively. Near neutral buoyancy condition needs to be met by the inner pipe immersed in the working fluid to minimize sagging and vibration. Inner pipe wall thickness was carefully selected to meet neutral buoyancy condition and, hence, avoid bending of pipes during the experiments (Japper-Jaafar et al. 2010).

The flow rate was measured using a magnetic flow meter installed at the inlet of the test section. The flow meter is an OMEGA FMG607-R with an accuracy of $\pm 0.5\%$. A computerized data acquisition system powered by LabView software was connected to all the measurement devices. The software was used to control the pump flow rate as well as logging all the data (i.e. pressure losses, flow rates and fluid temperature in the flow loop).

Experiments started with establishing a stationary sand bed in the annulus. In this step, water and sand were mixed in the tank while the slurry was circulated through the flow loop at maximum flow rate. The slurry has been distributed for 10 to 15 minutes to achieve a steady state condition. At this moment, the pump was quickly shut down. The closing valves were used to isolate the annular section from the rest of the flow loop (Figure 4-1). Other parts of the flow loop (i.e. the tank, pump, and transport pipelines) were then carefully washed to remove any solids remained in these parts. Two filter bags with openings smaller than the particle size (the opening is 100 micron) were installed at the outlet of the annular section to collect any particle which was removed from the test section and prevent them from going back. To vary the cuttings' bed height different amount of solids were mixed with water in the tank. Different concentration of solids in the flow would result in various stationary cuttings bed height.

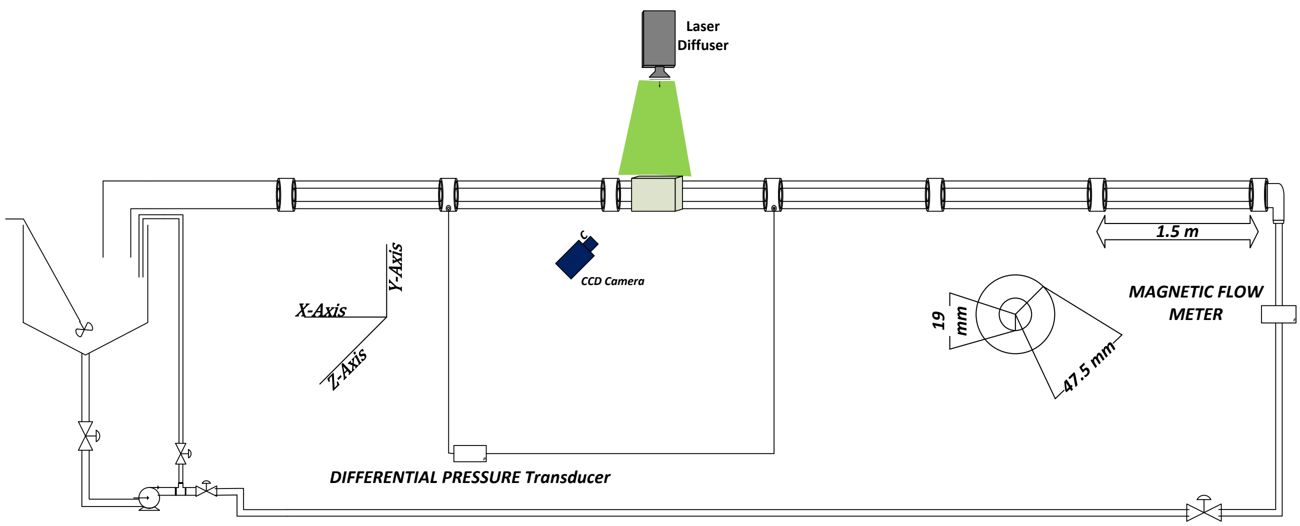

Figure 4-1 The schematic of the flow loop

Experiments in this study were carried out at two superficial liquid velocities of $0.20\,\frac{m}{s}$ and $0.24\,\frac{m}{s}$ over the two cuttings bed heights of approximately 6 and 16 mm. In terms of the percentage of the annular gap, the 6 and 16 mm bed heights occupy 21 and 56% of the total lower annulus, respectively. Superficial velocity, U_s, is calculated as the flow rate, Q, divided by the cross sectional area, A, of the annulus (Eq.(4-1)).

$$U_s = \frac{Q}{A} \qquad \textbf{Eq.(4-1)}$$

The superficial velocity of 0.24 m/s is the critical velocity at which bed erosion starts taking place in rolling type motion. This critical velocity was determined previously in another study (Bizhani et al. 2016).

4.3.1. Velocity Measurement in Turbulent Flow Using PIV Technique

Velocity measurements in turbulent flow were carried out using the PIV technique. Figure 2 shows the plane of velocity measurement along with the location of the stationary sand bed. Measurements have been conducted in both the lower and the upper annular gaps as shown by dashed lines in Figure 4-2. Two sets of experiments have been conducted. In the first set, the overall features of the flow such as the velocity profiles and the turbulence quantities were measured in the entire annulus (i.e. from the outer pipe wall to the inner pipe wall). In the second set of experiments, the measurements were focused only on the flow are very close to the bed interface. The former was aimed at identifying overall changes in the flow caused by the presence of a stationary bed while the latter was to further determine the impact of a stationary bed on the flow near the bed surface.

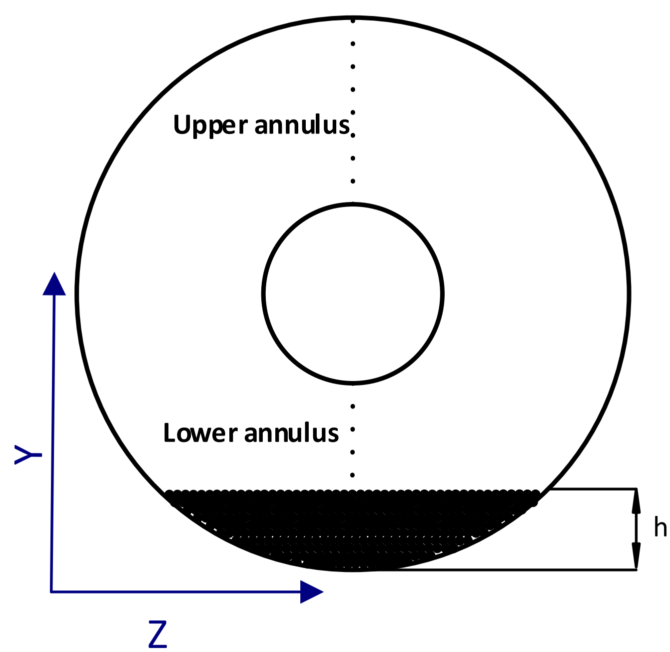

Figure 4-2 Planes of the velocity measurement in the PIV experiments

The measurement window is located at approximately $100D_H$ away from the annuli's inlet. This is necessary to ensure the flow is fully developed; (justification is based on the fact that the laminar flow fully develops over a development length of $88D_H$ (Poole 2010), whereas development length for turbulent flow is much shorter (Japper-Jaafar et al. 2010)). Due to the cylindrical shape of glass pipes, the image distortion is a major issue in the PIV measurements. To remedy this issue, a rectangular box was designed and installed around the outer pipe. Additionally, the box is filled with glycerol (99% Wt/Wt pure glycerol) to reduce the light refraction. Glycerol has a refraction index of 1.47, which is similar to the glass pipe, therefore, helps reducing the refraction of the laser light.

4.3.2. PIV Setup Description and Post-Processing Procedures

A planar 2-D PIV consists of a light source and a recording device. A double pulse laser is used as the light source. The recording device is a camera with the double shuttering feature. Camera view plane should be orthogonal to the laser light (see Figure 4-1). The flow is seeded with tracer particles. Upon incident with the laser light, the tracer particles reflect the light, which is then detected by the camera. The camera captures two successive images. Processing these pictures with an appropriate algorithm will yield the instantaneous velocity field of the flow.

A Nd: YAG double pulsed laser with a wavelength of 532 nm was used in this study. The laser light is converted to a planar light sheet by a combination of the cylindrical and the special optical lenses. The thickness of the laser light sheet could vary from 0.5 to 3 mm. The thick laser light may incur errors in the measurement as a result of the depth of the field thickness. The light thickness was kept at its minimum as 0.5 mm in this study.

A CCD (charge-coupled device) camera with a resolution of 1376×1040 pixels was used for recording the images. The camera has a double shuttering feature, which enables capturing a pair of pictures in a short and controllable time interval. A 50 mm Nikon AF NIKKOR lens with a 12-mm extension tube was used for recording the images.

Figure 4-3 shows the two standard PIV images acquired during the experiments. In these pictures, the sand bed is located at the bottom while the fluid seeded with tracer particles (bright white dots) is flowing over the top. DAVIS 8.3.0 software was used for both the image acquisition and the post-processing of pictures. The software was used for adjusting the appropriate parameters during the experiments (such as the time interval between the two images and the laser power) as well as processing and extracting the data from the pictures. Further details regarding the image processing algorithm are given in the next section. For tracer particles, hollow glass spheres with a mean diameter of 10 microns were used. The tracer particles are nearly neutral in water ($1.1 \pm 0.05 \frac{g}{cc}$) to keep them suspended in the flow. Addition of the trace particles is necessary to enhance the spatial resolution of the PIV images and reduce the bias error towards the sand debris (Melling 1997).

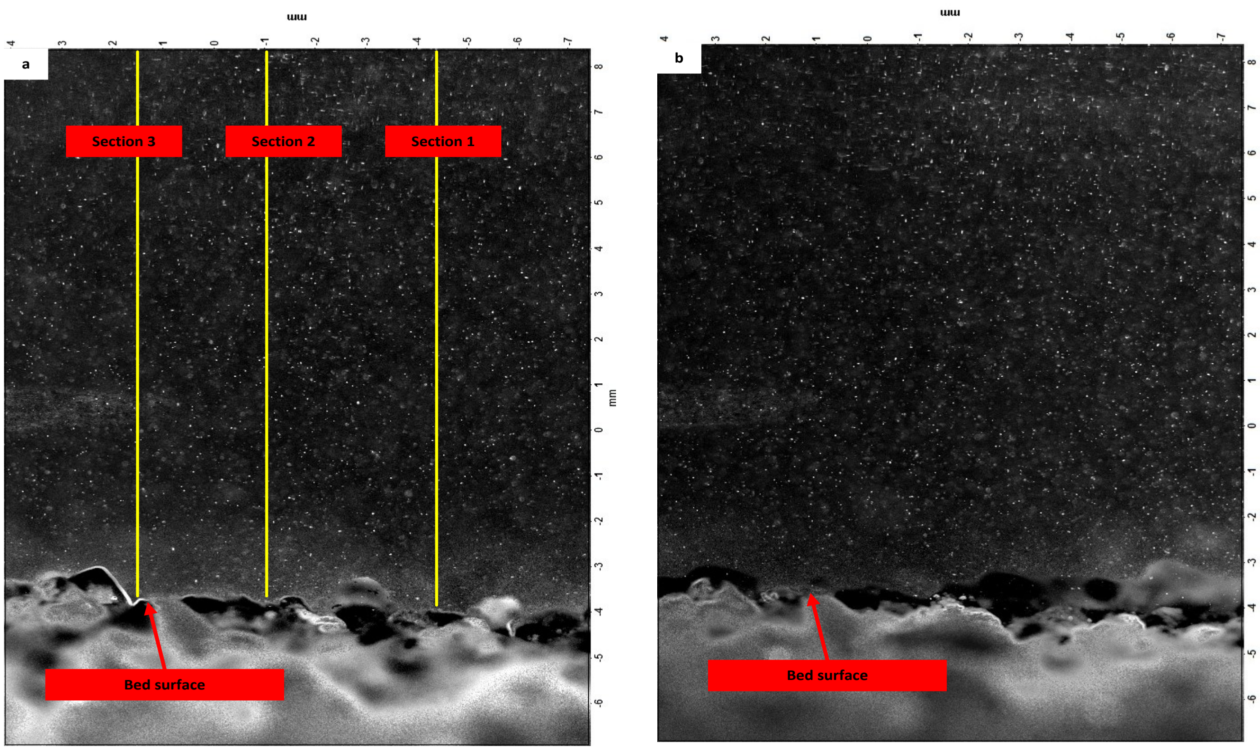

Figure 4-3 The PIV images showing the bed and the tracer particles

4.3.3. PIV Data Post-Processing Procedures

The PIV processing algorithm for velocity calculations follows a cross-correlation based method. After obtaining a pair of images with the tracer particles in the flow, each image is broken down to the smaller windows called the interrogation windows. The interrogation windows are analyzed in the 2nd image for probable similarities to the same interrogation window in the 1st picture (Nezu and Sanjou 2011). To determine the pixel displacement, the cross-correlation method was used. The method works by cross correlating the intensity distribution over a small area (the interrogation window) of the flow. The peaks that show the highest correlation are chosen for the most likely destination of the seed particles. After finding the displacement of a seed particle in the two images (Δx and Δy) and having known the time interval (Δt) between the two images, the velocity of the tracer particle or equivalently the fluid velocity vector is calculated as follows:

$$\begin{cases} \hat{u} = \dfrac{\Delta x}{\Delta t} \\ \hat{v} = \dfrac{\Delta y}{\Delta t} \end{cases} \qquad \textbf{Eq.(4-2)}$$

The multi-pass cross-correlation method with the decreasing of the interrogation window size was used for the particle displacement calculations. An initial interrogation window size of 64×64 pixels followed by the window size of 32×32 pixels was employed in the calculations. The overlap setting was 50%. To enhance the accuracy of the calculated vector fields, the post-processing was also applied on the calculated vectors. The setting for the post processing was set to the universal outlier detections with the appropriate settings to remove the outlier vectors.

4.4. Results and Discussion

4.4.1. Velocity profiles

The velocity profiles were measured in the lower and upper annular gaps of the concentric annuli, which contains a stationary sand bed on the lower side (Figure 4-2). This scenario is similar to the hole cleaning operations conducted in the horizontal wells. The data acquisition started at a flow rate below the critical flow rate of bed erosion (Us= 0.20 m/s). The flow rate was then increased up to the rate where particles in the bed started moving in the rolling type motion (Us = 0.24 m/s). It is important to know that at these flow rates there was no suspended sand particle in the main flow. The flow was fully stratified. However, at the highest flow rate (Us = 0.24 m/s) the sand particles at the bed interface were moving along the bed interface in the rolling and the sliding mode. In the sediment transport literature, such movement of the particles near the bed is called the bed load transport.

For comparison purposes, the velocity profiles in the same annuli were also measured without any sand bed deposits and at the same superficial velocities used for the tests with the stationary sand bed. In all the figures presented, lower annulus refers to the bottom half of the annuli where the cuttings bed is located. The upper annulus relates to the top half of the annuli. The coordinate system is chosen such that "y" increases in the vertical direction (i.e., perpendicular to the direction of the flow). The origin is set at the inner wall of the outer pipe (Figure 4-2); for the lower annulus "y" increases upward from the inner wall of the outer pipe on the low side towards the outer wall of the inner tube. Also note that to make the comparison possible, the vertical distance (y coordinate) in the upper annulus increases downward as the origin was set at the inner wall of the outer pipe. For measurements obtained near the bed interface, y=0 represents the bed interface. The velocity and other parameters used for the characterization of the degree of turbulence were normalized by using the superficial velocity.

4.4.1.1. Impact of Sand Bed Presence on the Annular Velocity Profiles

Figure 4-4 shows the velocity profiles measured in the lower annulus with and without a stationary sand bed at the superficial fluid velocity of 0.20 m/s. The thickness of the bed was approximately 6 mm in this case. Although the volumetric flow rates were the same in both cases, lower velocity values were observed for the flow over the bed than that of the case with no bed. About 11.5 % reduced the peak velocity in the lower annulus due to the presence of 6 mm thick bed deposits. The presence of a stationary sand bed results in diversion of the part of the volumetric flow to the upper annulus and, as a result, causes a shift in velocity profile in the lower annulus.

Another difference in velocity profile was observed in the radial location of the maximum velocity. It appears that presence of the bed causes the radial location of maximum velocity to shift towards the inner pipe wall (i.e., away from the surface of the bed deposits-fluid interface), making the flow more asymmetric.

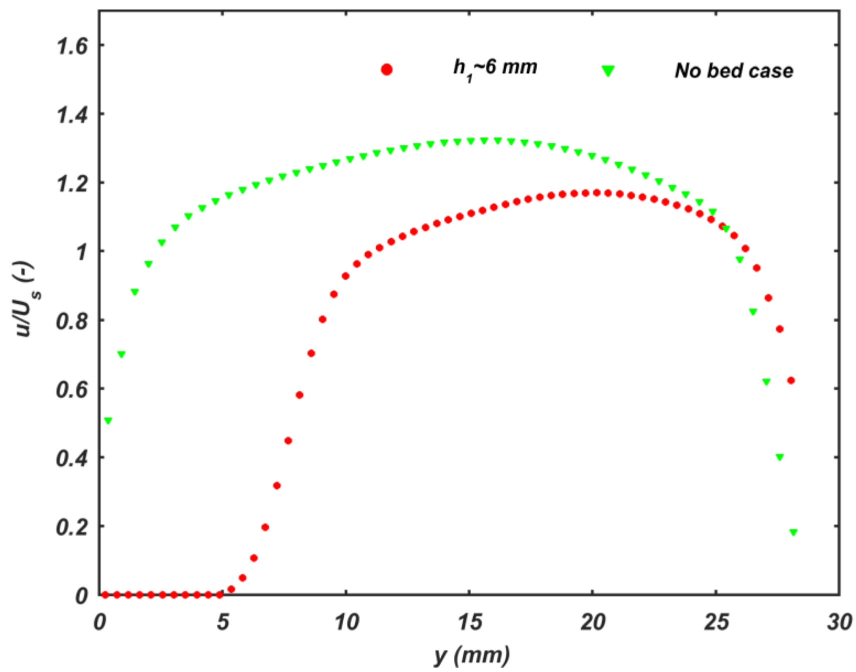

Figure 4-4 Normalized velocity profiles in the lower annulus measured at U_s=0.2 m/s and 6 mm thick solids bed

Figure 4-5 shows the velocity profiles in the lower annulus without any bed deposits and with the presence of 6 mm thick bed deposits at the superficial velocity of 0.24 m/s. The flow rate, in this case, is equal to the critical flow rate for bed erosion. Results are shown in Figure 4-5 also confirm that the presence of a stationary bed causes a reduction in volumetric flow rate and the peak velocity in the lower annulus. However, when the superficial velocity was 0.24 m/s, the percent decrease in the peak velocity due to bed deposits was 10.5%, slightly lower than that of the case where U_s was 0.20 $\frac{m}{s}$ (i.e., 11.5%). The effect of cuttings bed presence on the peak velocity seems to decrease as the volumetric flow rate of the fluid increased. The reason for the slight decrease in the peak velocity change can be attributed to the movement of sand particles at the bed interface. Carbonneau and Bergeron (2000) showed that bed load transport of sediment can contribute to an increase in the fluid velocity near the bed. They explained the reason for this phenomenon by the balance of turbulent kinetic energy and mean kinetic energy. According to Carbonneau and Bergeron (2000), movement of sediment particles at the bed interface may either dampen or enhance production of turbulent kinetic energy; when production of turbulence is suppressed by moving sand particles, the mean kinetic energy increases. This causes fluid velocity near the bed also to increase. It will be shown later that at the critical flow rate both the

Reynolds shear and the normal stresses decrease (i.e., turbulence activity decreases), which is also in line with the explanation given by Carbonneau and Bergeron (2000).

Figure 4-6 and Figure 4-7 shows the velocity profiles measured in the upper annulus with/without the presence of 6 mm thick sand bed at superficial liquid velocities of 0.20 m/s and 0.24 m/s, respectively. Due to the presence of the sand bed, the volumetric flow was diverted away from the lower annulus to the upper annulus and, as a result, the volumetric flow rate in the upper annulus increased. The increased flow rate in the upper annulus resulted in higher peak velocities as shown in these figures

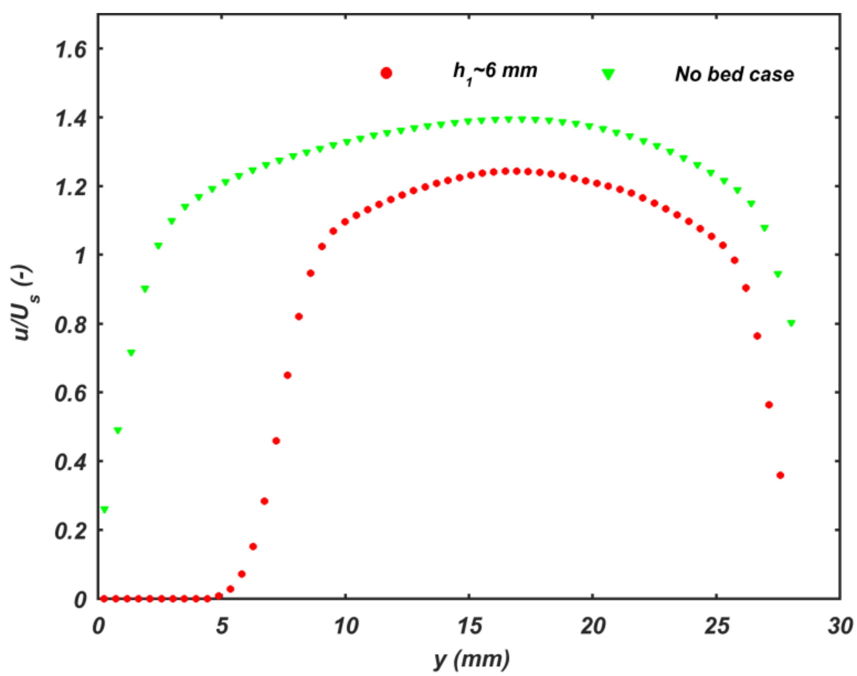

Figure 4-5 Normalized velocity profiles in the lower annulus measured at U_s=0.24 m/s and 6 mm thick solids bed

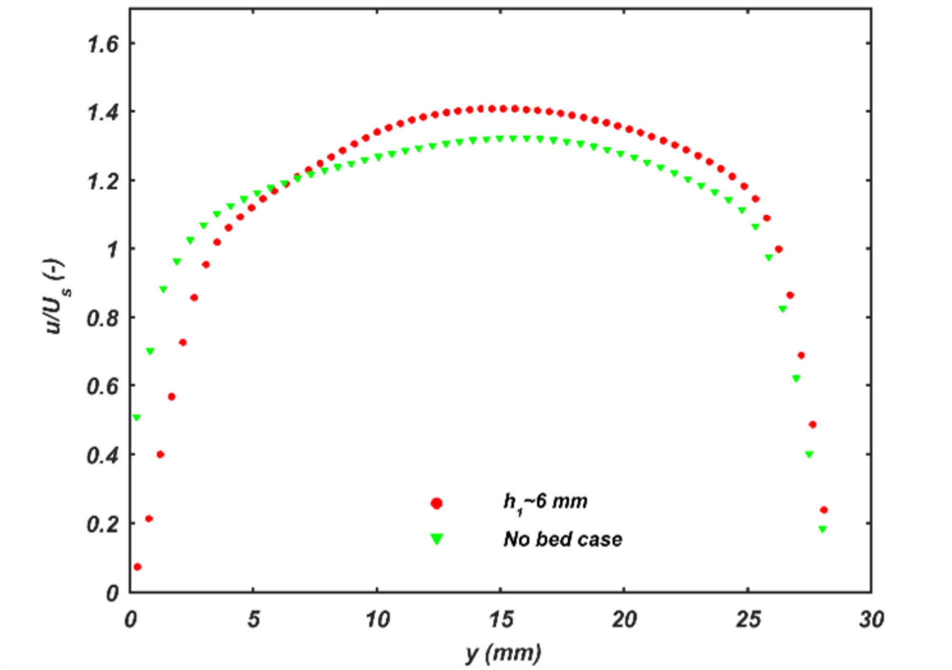

Figure 4-6 Normalized velocity profiles in the upper annulus measured at U_s=0.2 m/s and 6 mm thick solids bed

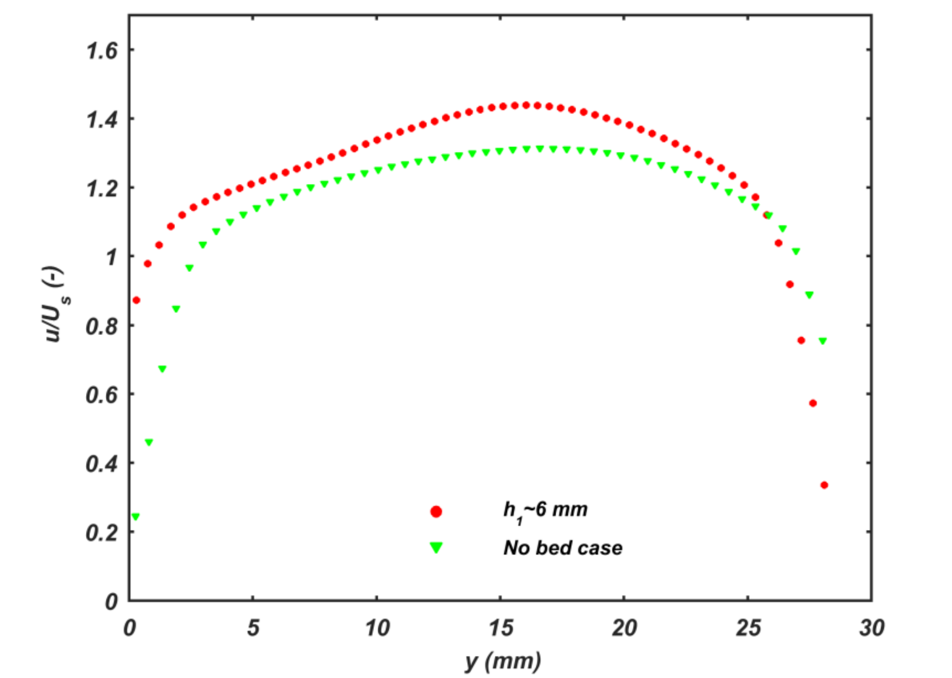

Figure 4-7 Normalized velocity profiles in the upper annulus measured at U_s=0.24 m/s and 6 mm thick solids bed

4.4.1.2. *Impact of Increasing Sand Bed Height on the Annular Velocity Profiles*

Figure 4-8 shows the velocity profiles in the lower annulus measured at 0.2 m/s superficial velocity with the presence of 6 and 16 mm thick sand beds and without the presence of any stationary sand bed. The results show that as the bed height increases, the volumetric flow rate and the peak velocity in the lower annulus decrease. Comparing to the flow with no bed case, 11.5% and 18% reductions in the peak velocity were observed in the lower annulus when the bed thickness was 6 mm and 16 mm, respectively.

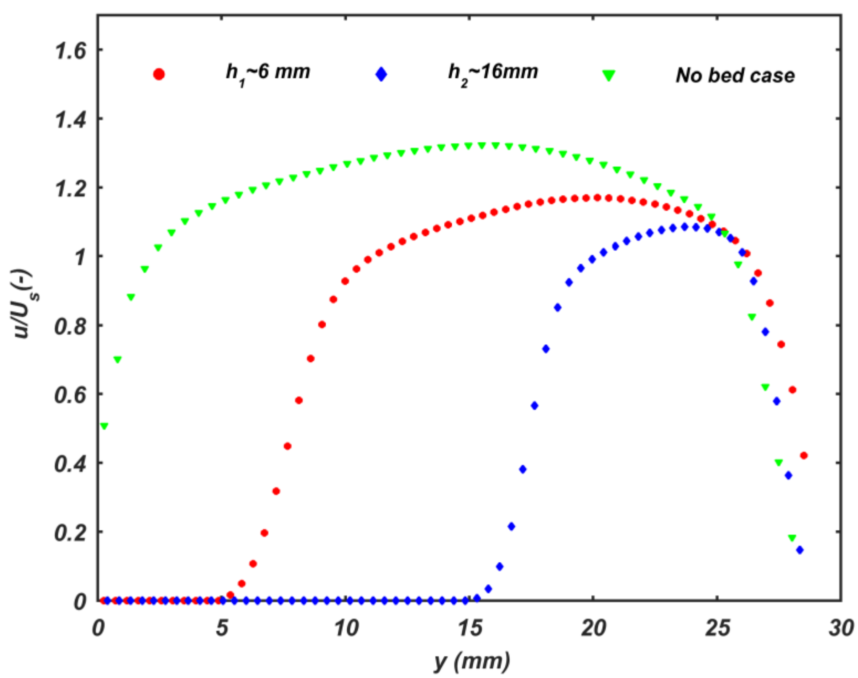

Figure 4-8 Effect of the bed thickness on the normalized velocity profiles in the lower annulus measured at U_s=0.2 m/s

Figure 4-9 shows the velocity profiles in the lower annulus at the critical flow rate of bed erosion (U_s = 0.24 m/s) with first bed heights of 6 mm, 16 mm, and no bed case. Similar to the 0.20 m/s case, the peak velocity in the lower annulus is decreased as the bed height increases. However, the difference in the peak velocity with and without the presence of the bed is reduced at this flow rate. The difference between peak velocities in the lower annulus with and without sand bed was 10.5% when the bed height was 6 mm and 16.5% when the initial bed height was 16 mm. This slight change in percent reduction in peak velocities (as compared to the case of U_s = 0.20 m/s) could be caused either by a reduction in bed height due to bed erosion (at the critical flow rate) or by the movement of sand particles at the bed interface. The increase in the local velocity caused by bedload transport was also reported by Carbonneau and Bergeron (2000). The similar mechanism is responsible for the growth in the local velocity in the lower annulus. Based on the balance of the mean and turbulent kinetic energy budget, the increase in the local velocity caused by bed load transport of particles is accompanied by a reduction in the turbulent kinetic energy. In another word, an increase in the local velocity causes a decrease in the turbulence level. It will be shown later that both the Reynolds stress and the turbulence intensity also decreases at this flow rate.

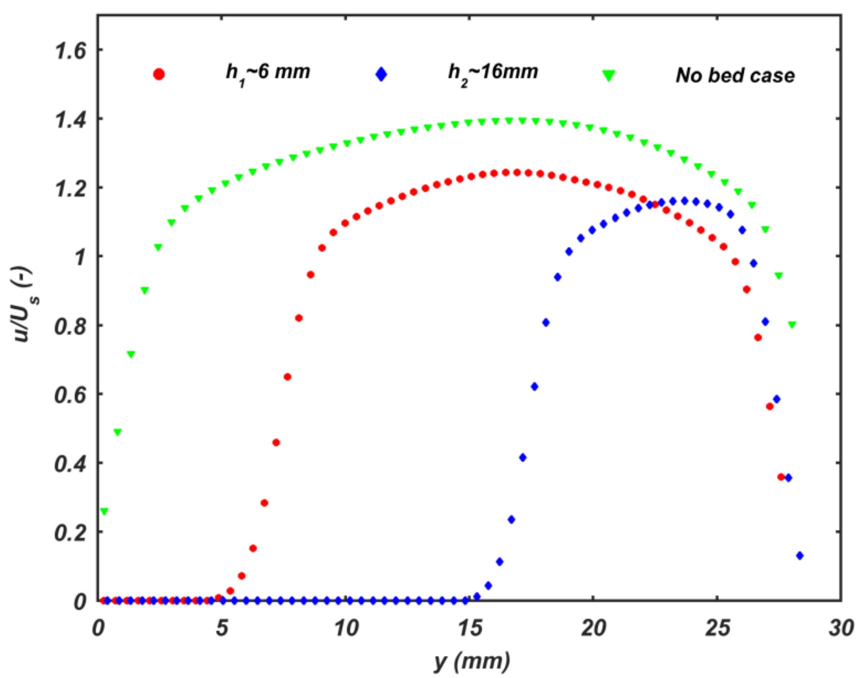

Figure 4-9 Effect of the bed thickness on the normalized velocity profiles in the lower annulus measured at U_s=0.24 m/s

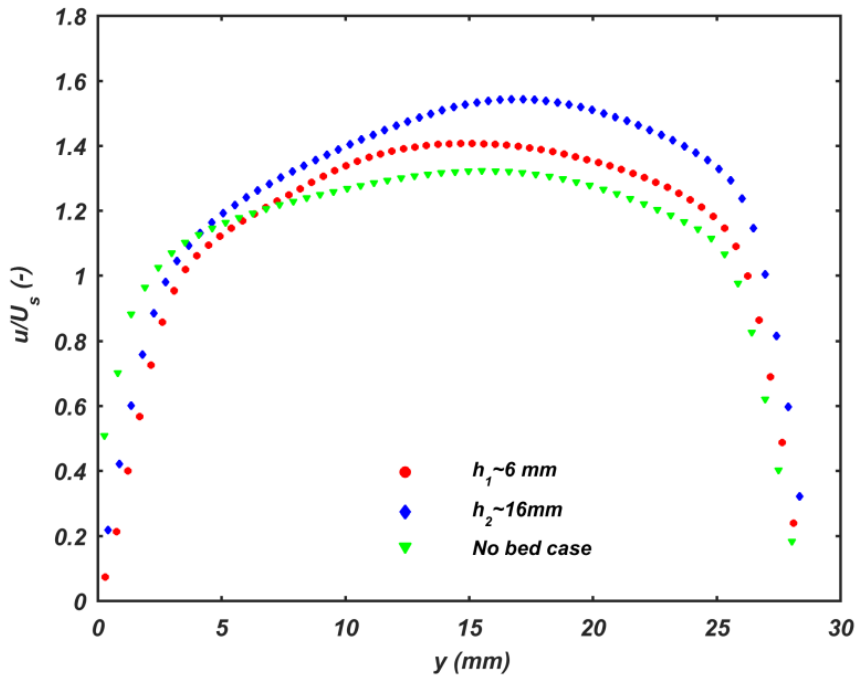

Figure 4-10 Normalized velocity profiles in the upper annulus measured at U_s=0.2 m/s

Figure 4-10 shows the change in velocity profiles in the upper annulus with the increasing bed height. Velocity profiles were compared for the cases of no stationary sand bed, 6 and 16 mm thick sand beds. The superficial velocity of the fluid was 0.20 m/s. The peak velocities in the upper annulus were 6% and 16.7% higher than that of the case with no sand bed when the bed height was 6 mm and 16 mm, respectively.

Figure 4-11 shows the velocity profiles in the upper annulus with no stationary sand bed, 6 and 16 mm thick sand beds at the superficial fluid velocity of 0.24 m/s. In this case, the peak velocities in the upper annulus were 9.6% and 20% higher than that of the case with no sand bed when the bed height was 6 mm and 16 mm, respectively.

The results are shown in Figure 4-10 and Figure 4-11 indicate that as the bed deposit height increases, the more fluid volume is diverted from, the lower annulus to the upper annulus. As a result, a higher peak velocity is observed in the upper annulus as the bed thickness increases.

Figure 4-12 shows a comparison of the velocity profiles in the upper and lower annulus when there is a stationary bed in the lower annulus. These results are given in the case where the superficial velocity was 0.2 m/s and bed thickness was 6 mm. The peak velocity in the upper annulus is 17% higher than that of the one in the lower annulus. Figure 13 shows a comparison of the velocity profiles in the lower and upper annulus for the case where the superficial velocity was 0.2 m/s and the bed thickness was 16 mm. The peak velocity in the upper annulus was 30% higher than that of the one in the lower annulus in this case. The significant increase in the peak velocities in the upper annulus (i.e., 17% increase with 6 mm bed height and 30% increase with 16 mm bed height) is mainly because of the increasing bed height in the lower annulus causes more fluid volume is diverted from lower annulus to upper annulus.

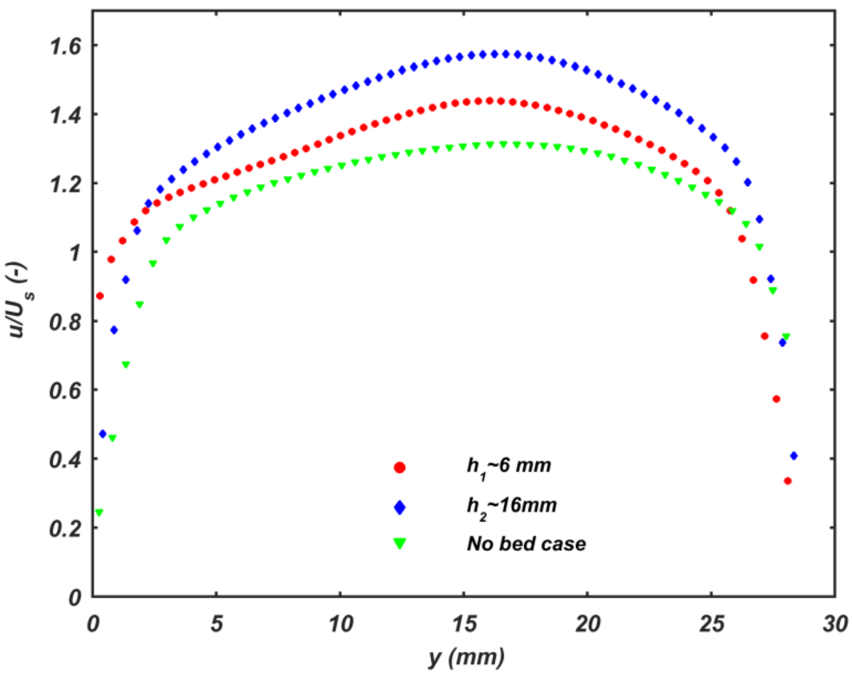

Figure 4-11 Normalized velocity profiles in the upper annulus measured at U_s=0.24 m/s

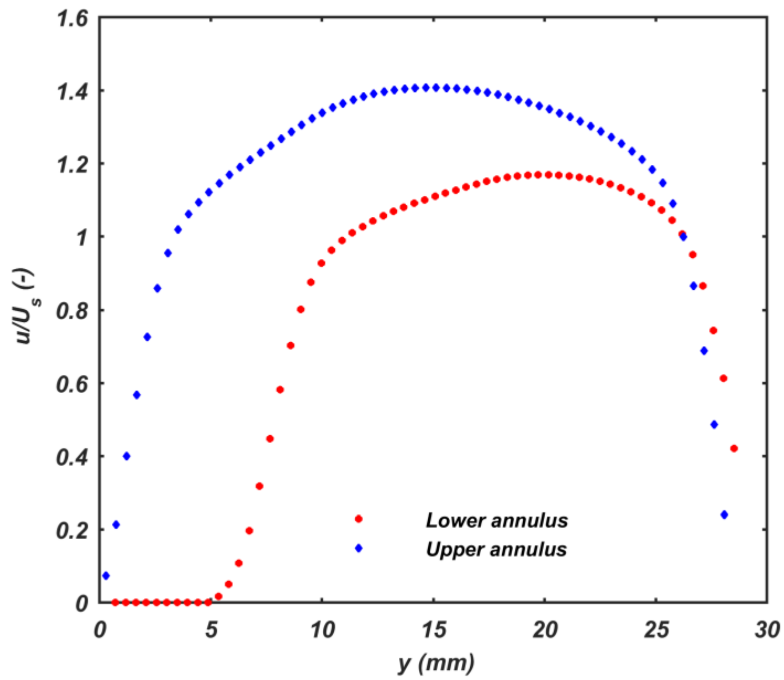

Figure 4-12 Normalized velocity profiles in the upper and lower annulus measured at U_s=0.2 m/s and 6 mm thick solids bed

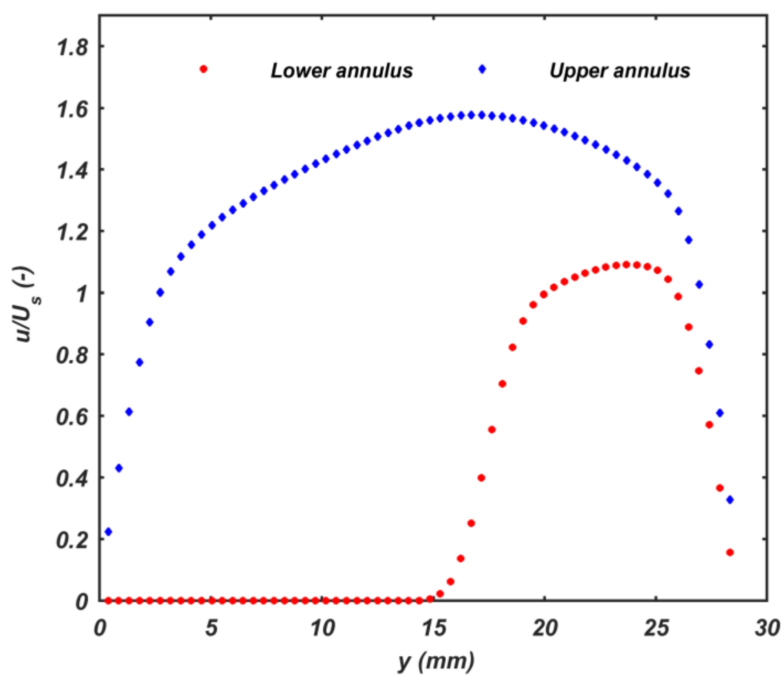

Figure 4-13 Normalized velocity profiles in the upper and lower annulus measured at U_s=0.2 m/s and 16 mm thick solids bed

4.4.1.3. Near Wall Velocity Profile

Results presented so far showed the overall changes of the velocity profile in the whole annulus caused by the presence of the bed deposits in the lower annulus. These initial data were obtained from PIV measurements focusing on the entire annular cross-section. For a more accurate determination of the velocity profiles near the bed/fluid interface, two additional experiments were conducted. Here, the PIV measurements were obtained by focusing only the area at the immediate vicinity of the bed/fluid interface. Effects of the two stationary bed heights (i.e., 8 mm and 14 mm) were tested. The goal of these experiments was to assess the impact of the cuttings bed deposition on the near-bed turbulent flow characteristics (i.e. velocity, Reynolds stress, radial stress, etc.).

Near-wall velocity distribution was determined regarding the dimensionless distance and dimensionless velocity units (i.e., wall units), which are defined by the equations 3 and four respectively.

$$y^+ = \frac{\rho y u_\tau}{\mu} \qquad \textbf{Eq.(4-3)}$$

$$u^+ = \frac{u}{u_\tau} \qquad \textbf{Eq.(4-4)}$$

In these equations y is the vertical distance measured from the bed surface, ρ and μ are fluid density and viscosity respectively. The friction velocity, u_τ, is defined as a function of the shear stress at the bed/fluid interface, τ_b and the fluid density, ρ, (Eq.(4-5)).

$$u_\tau = \sqrt{\frac{\tau_b}{\rho}} \qquad \textbf{Eq.(4-5)}$$

Calculating the shear stress at the bed interface using the measured frictional pressure loss data cannot be done accurately. That is because the measured frictional pressure loss is a result of the shear stress on all the surfaces inside the annuli (i.e., the outer face of the inner pipe, the inner face of the outer pipe and the bed/fluid interface). Instead, we suggest using the velocity (u) versus the vertical distance (y) data plotted on a semi-logarithmic scale. Eq shows the model defining the velocity profile in the logarithmic region. 6 (Kundu et al. 2012).

$$u = \frac{u_\tau}{\kappa} Ln\left(\frac{y}{y_o}\right) = \frac{u_\tau}{\kappa} Ln(y) + \frac{u_\tau}{\kappa} Ln\left(\frac{1}{y_o}\right), \quad \textbf{Eq.(4-6)}$$

In Eq.(4-6)κ is the von Karman constant and is equal to 0.41 for the flow of water. The y_o is called characteristic roughness and determines whether the flow is smooth or rough. The first step in finding the friction velocity is to plot the measured values of velocity (u) versus distance (y) in the semi-logarithmic scale. Using the slope of the resultant line and the Eq.(4-6), one can determine the friction velocity, u_τ.

The characteristic roughness, y_o, depends on the flow regime. The flow regime (i.e. hydraulically smooth, transitional or rough) is determined by the roughness Reynolds number (Eq.(4-7)).

$$Re_{u_\tau} = \frac{\rho \varepsilon u_\tau}{\mu} \quad \textbf{Eq.(4-7)}$$

In the Eq.(4-7), ε is the equivalent roughness height, which is very often assumed to be equal to the mean particle size (Ramadan et al. 2003, Duan 2009). For $Re_{u_\tau} < 5$, the flow is considered to be hydraulically smooth. If $Re_{u_\tau} > 70$, the flow is assumed to be fully rough. Transitional flow regime exists for $5 < Re_{u_\tau} < 70$.

The characteristic roughness, y_o, for a hydraulically smooth condition is given by the Eq.(4-8) (Kundu et al. 2012).

$$y_o = \frac{\mu}{9\rho u_\tau} \quad \textbf{Eq.(4-8)}$$

By introducing y_0 defined by the Eq.(4-8) into the Eq.(4-6), one can obtain the velocity profile for hydraulically smooth condition (Eq.(4-9)).

$$u^+ = 2.44Ln(y^+) + 5.5 \quad \textbf{Eq.(4-9)}$$

The Eq.(4-9) is valid for the flow inside the smooth annuli (Lawn and Elliott 1972, Rodriguez-Corredor 2014, Bizhani et al. 2015). For fully rough flow (i.e. $Re_{u_\tau} > 70$), however, viscous sublayer vanishes and characteristic roughness becomes dependent on the roughness height:

$$y_o = \frac{\varepsilon}{30}$$ **Eq.(4-10)**

For the fully rough flow, the velocity profile in the logarithmic region takes the form given by the Eq.(4-11).

$$u^+ = 2.44Ln\left(\frac{y}{\varepsilon}\right) + 8.5$$ **Eq.(4-11)**

Velocity profile represented by the Eq.(4-9) is valid for the outer layer of the flow, the so-called logarithmic layer, which starts at $y^+ = 30$. The flow region within the dimensionless distance of $y^+ < 5$ corresponds to the viscous sublayer (Kundu et al. 2012) and the velocity profile in this region is described by the Eq.(4-12).

$$u^+ = y^+$$ **Eq.(4-12)**

One of the main challenges in accurately determining the velocity profiles near a rough surface is defining the location of the "virtual wall" (Chan-Braun et al. 2011). The virtual wall is where the velocity is zero. This is especially more challenging in the case of loose sand bed because the bed interface is not flat. Figure 3 presents two pictures taken near the bed/fluid interface. There are two issues, which need to be addressed before introducing the velocity profiles in the wall units. The first problem is that the bed/fluid interface is not flat. Therefore, one cannot average the velocity data in the direction of the flow. The second issue is the configuration of the particles lying on the bed surface. It appears that the bed roughness is not constant along the bed. Therefore, instead of averaging the velocity data along the bed, we only used the local velocity profiles, where we could exactly identify the location of zero velocity.

Figure 4-14 shows the velocity profiles in wall units measured at U_S=0.2 m/s and two different (8 and 14 mm) bed height conditions. Velocity profiles are very similar to the flow near the beds of different heights. For the flow near the 14 mm thick bed, the upper limit of the logarithmic region is smaller than that of the flow near the 8 mm thick bed. That is because in this case, the flow enters the boundary layer of the inner pipe. In the logarithmic region, there is a downward shift in the velocity profiles as compared to velocity profile of a hydraulically smooth flow defined by Eq.(4-9). The downward shift in the velocity in the log-wall region was about 4.5 wall units. Velocity profiles over the bed deposits show characteristics similar to the flow over a rough surface (Chan-Braun et al. 2011).

Figure 4-15 shows the velocity profiles in wall units measured at the critical flow rate of bed erosion (U_s=0.24 m/s) and two different (8 and 14 mm) bed height conditions. The velocity profiles in the logarithmic region also shifted downward in this case. The downward shift of velocity data in the log-wall region was about 5.8 wall units in this case.

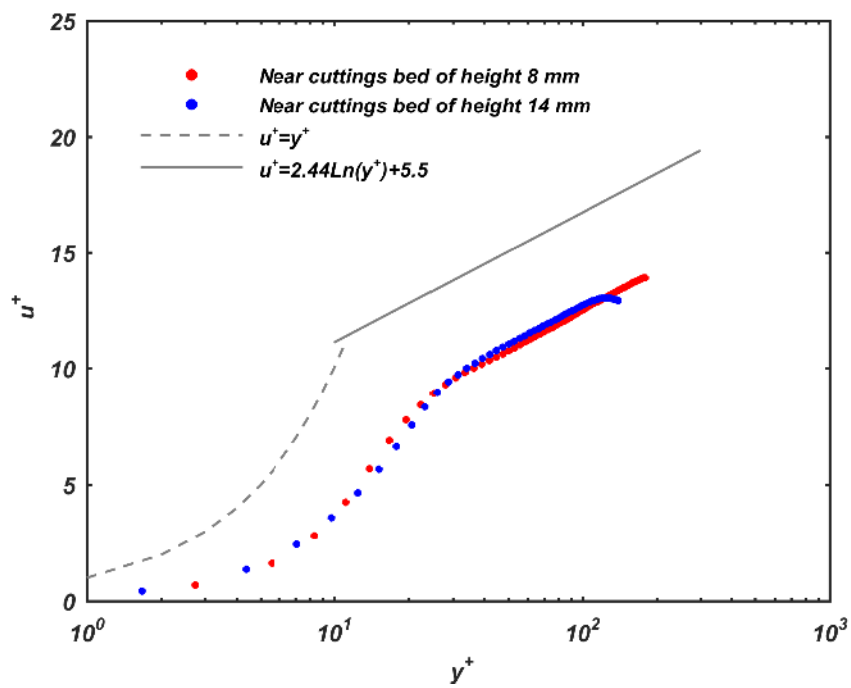

Figure 4-14 Near-wall velocity profiles in the wall units measured at U_s=0.2 m/s

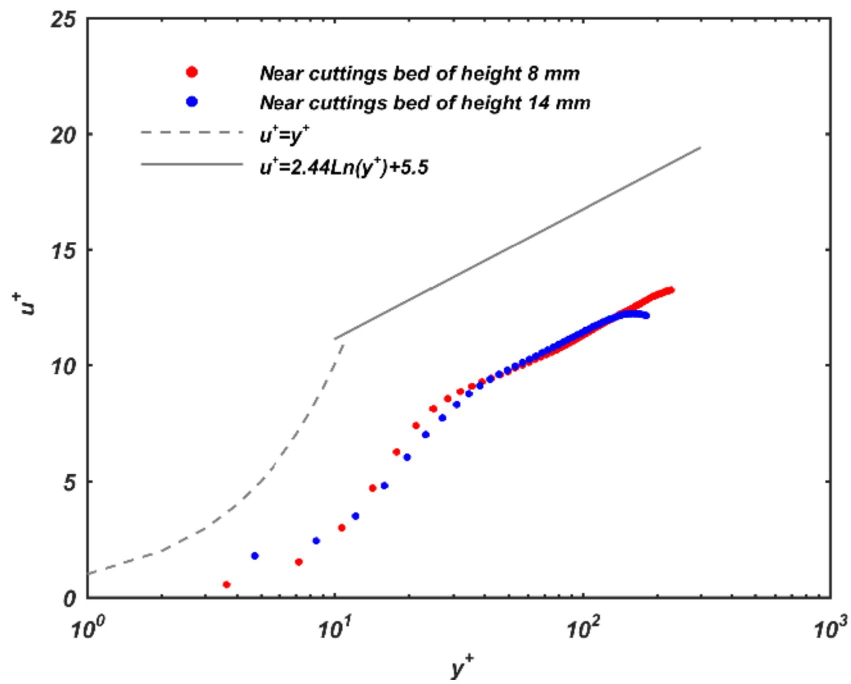

Figure 4-15 Near-wall velocity profiles in the wall units measured at U_s=0.24 m/s

Velocity profiles near the bed interfaces (shown in Figure 4-14 and Figure 4-15) indicate that the bed surface is not hydraulically smooth. To identify whether the flow is in the transitional or fully rough regime, we have matched the model equation given for fully rough flow (Eq.(4-11)) to the actual experimental velocity data measured near the beds. As shown in Figure 4-16, there is a perfect match between the velocity profile described by fully rough flow model (Eq.(4-11)) and the experimental data. Once the flow is confirmed to be fully rough, the Eq.(4-11) can now be used to determine, the equivalent roughness, ε, of the sand bed. For flow at the superficial liquid velocity of 0.2 m/s, the equivalent roughness was estimated to be equal to $2d_{50}$ (Figure 4-16a). For flow at the critical rate (U_s=0.24 m/s), the equivalent roughness was found to be equal to $2.4d_{50}$ (Figure 4-16b). The reason why the roughness height increases at the critical flow rate can be attributed to the bed load transport of particles. Several studies in the past have suggested that the bed load transport causes an extra boundary roughness (Wiberg and Rubin 1989, Best et al. 1997, Carbonneau and Bergeron 2000). The reason for this is the extraction of momentum from the fluid phase by the moving sand particles; as a result of this momentum exchange effective boundary roughness increases. The estimated values of the equivalent roughness, ε, indicate that earlier assumptions made by other researchers that the roughness height is equal to that of particles size in the bed might not be as accurate (Ramadan et al. 2003, Duan 2009). If an assumption is needed to be made about the roughness of the sand bed surface, $2d_{50}$ seems to be a better representative of such roughness value.

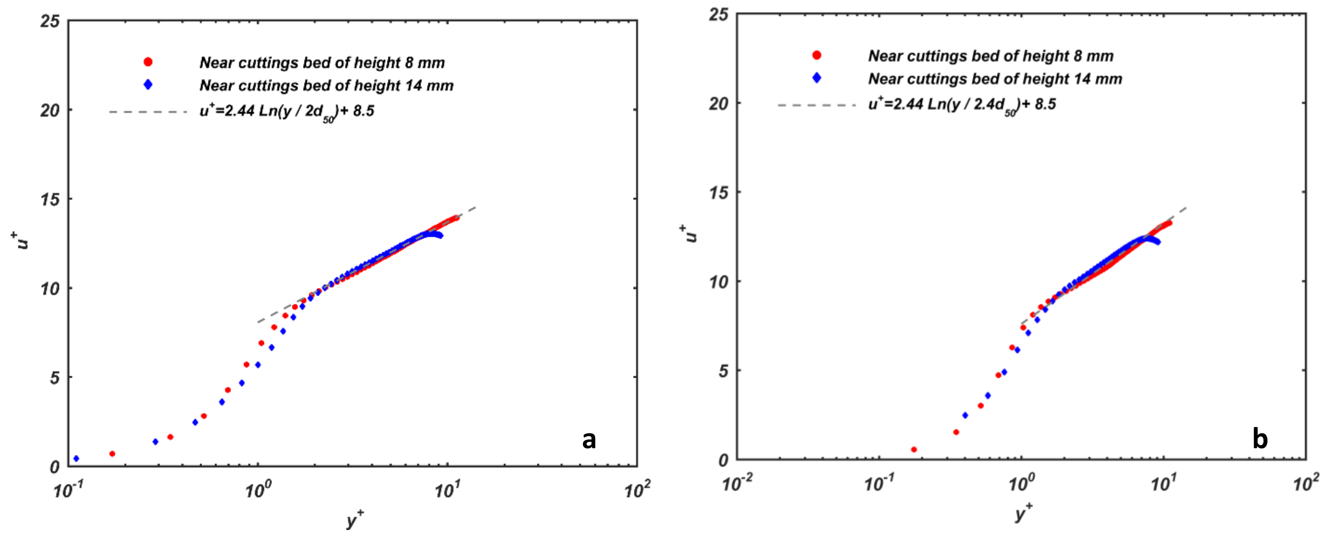

Figure 4-16 Curve fitting of the velocity profiles in the logarithmic region- a) measured at $U_s = 0.2\frac{m}{s}$ b) measured at $U_s = 0.24\frac{m}{s}$

The second challenge in determining the velocity profiles over a stationary bed is that the surface roughness may change the bed. As shown in Figure 4-3, the bed interface is not flat and, therefore, one cannot average the data along the bed. Also shown in Figure 4-3is that the bed roughness may change because of the configuration of the particles at the bed interface. To see if the equivalent surface roughness changes along the bed, velocity profiles are compared over three different cross-sections in the same flow field (i.e. measured over the same bed). The yellow lines in Figure 4-3a represent the three different locations at which the velocity profiles are compared. Figure 4-17 reports the velocity profiles measured at these three cross-sections. It can be seen that the shift in the velocity profiles in the logarithmic wall region varies across the bed. This means that the surface roughness varies along the bed. Therefore, it is not possible to characterize the sand bed with a single roughness height.

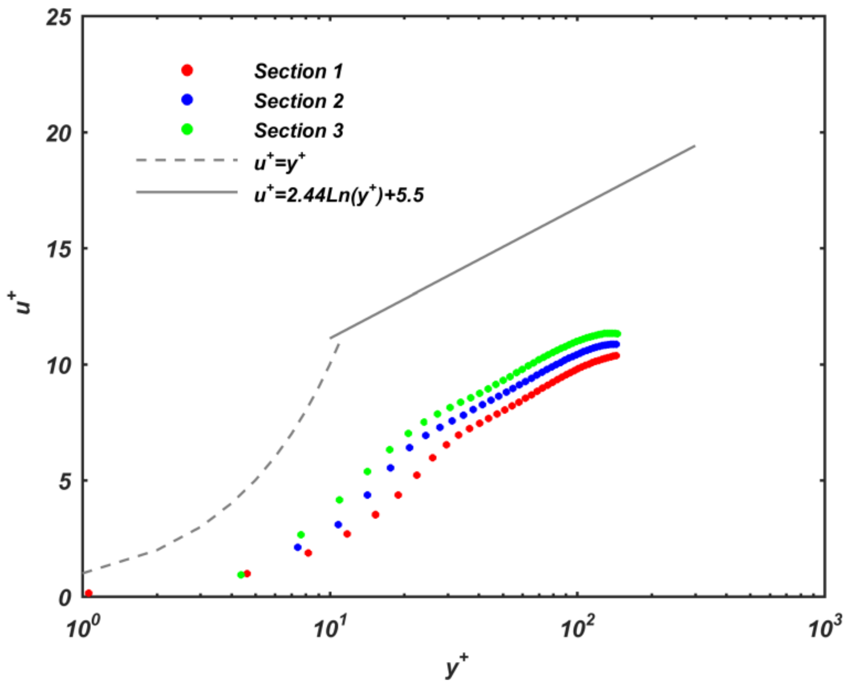

Figure 4-17 Velocity profiles in three sections of the same flow field measured at U_s =0.2 m/s (See Figure 4-3 for further information)

4.4.2. Reynolds shear stress

Reynolds shear stress or turbulent stress arises due to the velocity fluctuations. By definition the Reynolds shear stress is:

$$\tau_{Re} = -\rho\overline{u'v'} \qquad \textbf{Eq.(4-13)}$$

Where u' and v' are the velocity fluctuations in the axial and radial directions respectively. Significance of the Reynolds stress for particle removal from bed deposits can be best understood through the relation between local shear stress and the onset of the particle movement. In sediment transport studies, it is customary to quantify the onset of the bed erosion in terms of the critical bed shear stress (or its dimensionless form called the Shields stress) (Shields 1936, Garcia 2008, Bizhani et al. 2016).

$$\tau^* = \frac{\tau_i}{(\rho_s - \rho) g d_p} \qquad \textbf{Eq.(4-14)}$$

Where τ^* is the Shields stress and is related to the wall or interfacial shear stress (τ_i), ρ_s is the density of the solids, d_p is the particle diameter and g is the acceleration of gravity. The importance of the Shields stress is that it represents the ratio of the fluid drag force acting on the particles to the submerged weight of the particles. Therefore, it's an important parameter in the bed erosion studies. Shields stress is closely related to Reynolds shear stress; total shear stress is a combination of Reynolds stress and the viscous stress at the bed interface. The higher the interfacial shear stress, the higher would be the Shields stress, which would yield to more effective particle removal from bed deposits. The interfacial shear stress is equal to the summation of the Reynolds shear stress and the viscous stress (Eq.(4-15)). However, the viscous stress is only significant near the solid surfaces.

$$\tau_i = -\rho \overline{u'v'} + \mu \frac{\partial u}{\partial y} \qquad \textbf{Eq.(4-15)}$$

4.4.2.1. Impact of the Solids Bed Presence on the Reynolds Stress Profiles

Figure 4-18 shows the variation of the normalized Reynolds stress profiles in the lower annulus. The Reynolds stress profiles were calculated by using the fluctuation velocity data measured at a superficial liquid velocity of 0.2 m/s without and with the presence of (6 mm thick) bed deposits. The maximum value of Reynolds stress near the surface of the 6 mm thick bed is slightly higher than that of the one near the outer pipe wall in the lower annulus when there is no bed deposit. However, the peak value of the Reynolds stress near the inner pipe wall measured with the presence of 6 mm thick solids bed is significantly lower than that of the one measured with no bed.

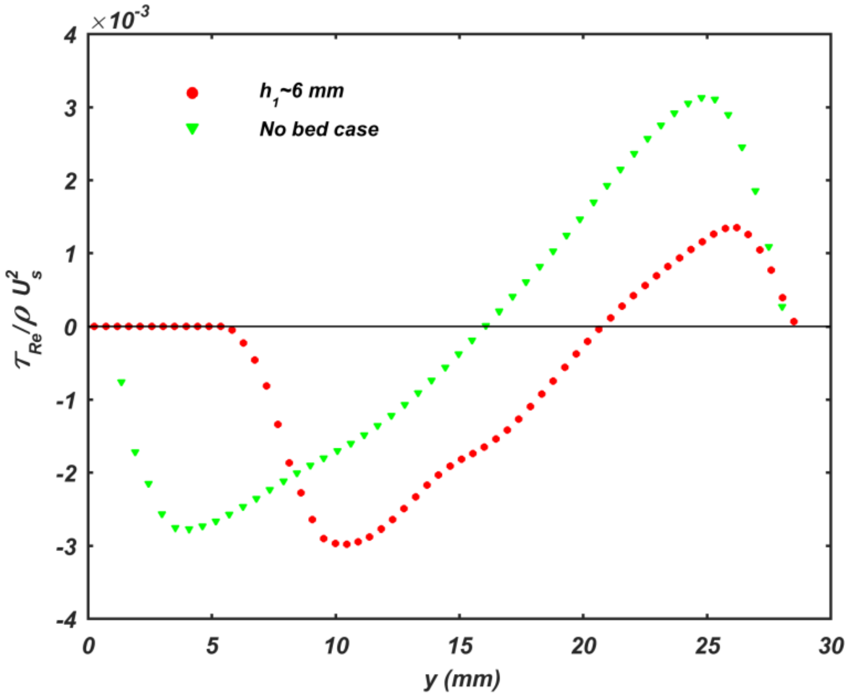

Figure 4-18 Normalized Reynolds shear stress profiles in the lower annulus measured at U_s =0.2 m/s (h≈6 mm)

The fact that Reynolds stress has a higher peak value near the bed rather than near the inner pipe may be attributed to the roughness of the surfaces. It is known that rough surfaces can cause a moderate increase in Reynolds shear stress (Krogstad et al. 1992). According to Carbonneau and Bergeron (2000) presence of sand particles induces additional roughness for the flow. The increase in the roughness causes the flow to dissipate more energy to overcome the additional boundary resistance. Enhancement of the dissipation term in the turbulent kinetic energy budget will results in the improvement of the production term as well. Consequently, the rough surface produces more turbulence. Production of more turbulence is equivalent to the lower mean kinetic energy of the flow or the lower velocity near the bed.

Another observation from the Reynolds stress profiles is the shift in the radial location of the zero shear stress. This is in agreement with the shift in the maximum velocity location towards the inner wall.

Figure 4-19 presents the normalized Reynolds stress profiles measured in the lower annulus at a critical flow rate of bed erosion (U_s= 0.24 m/s) with (6 mm thick) and without the presence of the solids bed. The peak Reynolds stress values near the bed and the inner pipe wall seem to be more balanced in this case comparing to the Reynolds stress values measured at the lower flow rate (U_s=0.2 m/s). Also, compared to the no bed case, there is a decrease in the peak value of the Reynolds stress due to the presence of the solids bed. Here, the effect of the bed presence on the Reynolds stress can be explained by using the results from previous bed load transport studies. At the critical flow rate, particles move at the bed interface in the form of bed load. Bed load transport of the sediment and its impact on carrier fluid turbulence have been studied before, mainly for flow in flumes and channels (Best et al. 1997, Carbonneau and Bergeron 2000, Bigillon et al. 2006, Schmeeckle 2014). The results, however, are not consistent. Some studies showed that the bed load causes an increase in the rate of turbulence production and turbulence Reynolds stresses (Bigillon et al. 2006). Other studies, such as the one conducted by Gore and Crowe (1991) and Best et al. (Best et al. 1997) argued that the attenuation or the enhancement of the turbulence by the sand particles depend much on the ratio of the eddy sizes to that of the particle sizes. Best et al. (Best et al. 1997) also presented criteria based on the Stokes number and the submergence number for the flow in channels to identify whether the bed load causes an amplification or a damping of the turbulence. Carbonneau and Bergeron (2000) showed that the bed load transport could either increase or decrease the rate of turbulence production. Their main argument on the reduction of turbulence by the sediment particles is the extraction of the momentum from the fluid phase by the sediment particles near the bed, which would also result in the reduction of the Reynolds stress.

Another method to identify the impact of the bed load on the turbulence is by the use of the energy budget of the flow concept, which assumes that the mean and the kinetic energy have to balance each other out; meaning that, if one reduces the other will increase. If the mean kinetic energy increases, the rate of turbulence production and dissipation decreases and consequently the Reynolds stress decreases. The increase in the average kinetic energy appears as an increase in the mean velocity. We observed that at the critical flow rate, the mean velocity slightly increased comparing to sub-critical flow rate, which explains the reduction in the Reynolds stress at the critical flow rate as compared to the one measured at the sub-critical flow rate.

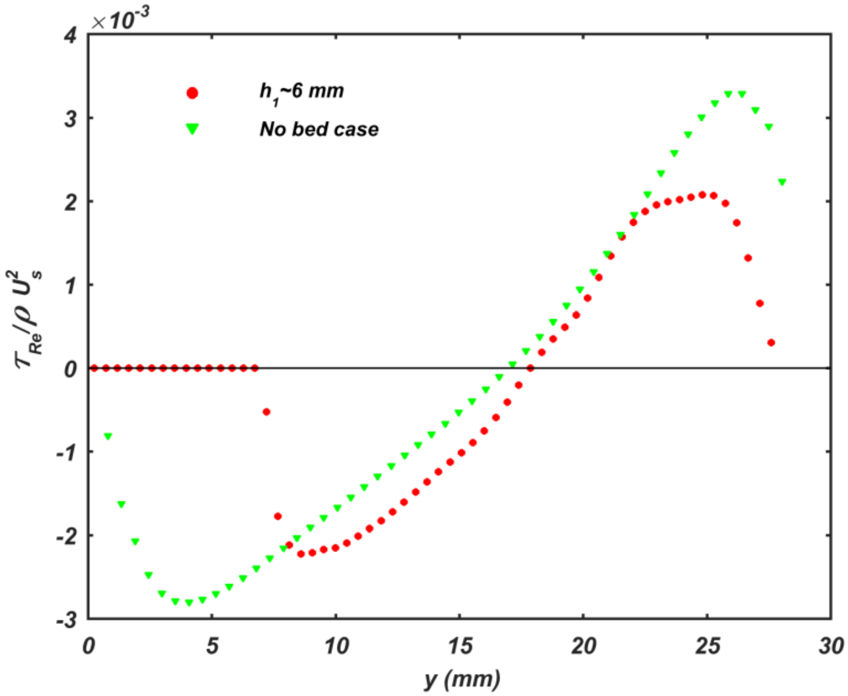

Figure 4-19 Normalized Reynolds shear stress profiles in the lower annulus measured at U_s =0.24 m/s (h≈6 mm)

Figure 4-20 shows the comparison of the normalized Reynolds stress profiles in the upper annulus for the flow over the 6-mm thick bed and no bed cases at the superficial velocity of 0.2 m/s. There is no significant difference in the peak Reynolds stress values in the upper annulus between the flow with and without the presence of the solids bed at the superficial velocity of 0.2 m/s. Figure 4-21 shows a comparison of the normalized Reynolds stress profiles in the upper annulus for the flow over the 6 mm thick bed and no bed case at a superficial velocity of 0.24 m/s. Slightly different peak Reynolds stress values were observed between the flow with and without the solids bed at 0.24 m/s (Figure 4-21).

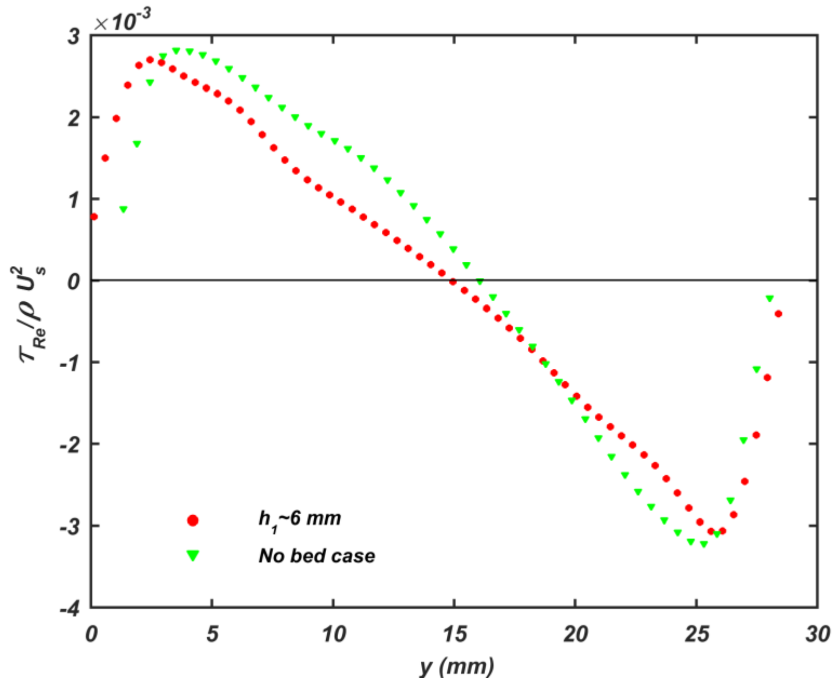

Figure 4-20 Normalized Reynolds shear stress profiles in the upper annulus measured at U_s =0.2 m/s (h≈6 mm)

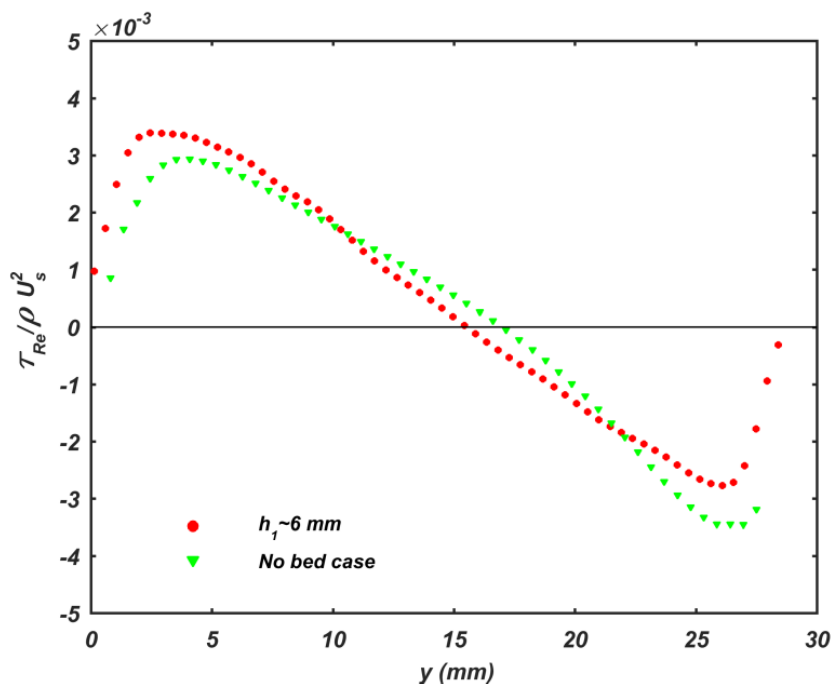

Figure 4-21 Normalized Reynolds shear stress profiles in the upper annulus measured at U_s=0.24 m/s (h≈6 mm)

Figure 4-22 illustrates the comparison of Reynolds stress profiles with the sand bed (6 mm thick) in the lower and upper annulus at a superficial velocity of 0.2 m/s. Reynolds stress in the lower annulus is significantly lower than that of in the upper annulus. This trend is consistent with the observations of the velocity profiles (Figure 4-10). The presence of the bed causes the volumetric flow to be directed away from the lower annulus to the upper annulus and, therefore, causes both the Reynolds stress and the peak velocity to decrease in the lower annulus. The necessary implication of such observations (Figure 4-10 and Figure 4-22) is that the presence of a stationary sand bed causes less drag force on the bed interface (due to the reduction of the local velocity and the shear stress).

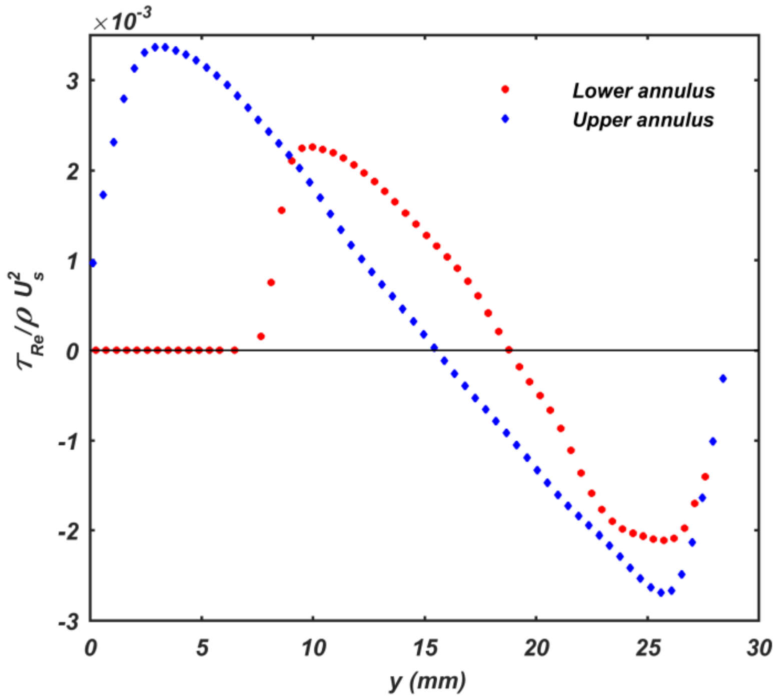

Figure 4-22 Normalized Reynolds shear stress profiles in the upper and lower annulus measured at U_s= 0.2 m/s (h≈6 mm)

4.4.2.2. Impact of the Change in the Sand Bed Height on the Reynolds Stress Profiles

Figure 4-23 shows the comparison of the normalized Reynolds stress profiles in the lower annulus for the cases of flow over 6 and 16 mm thick stationary beds and no stationary bed at a superficial liquid velocity of 0.2 m/s. The peak value of the Reynolds stress near the bed surface is slightly higher for the flow over the sand bed than that of the case with no sand bed. As discussed earlier, the difference in the surface roughness is the most likely reason why the near the bed Reynolds stress increases as compared to the flow without the sand bed case (Krogstad et al. 1992). However, the change in stationary sand bed height from 6 mm to 16 mm did not seem to affect the peak value of Reynolds shear stress near the bed.

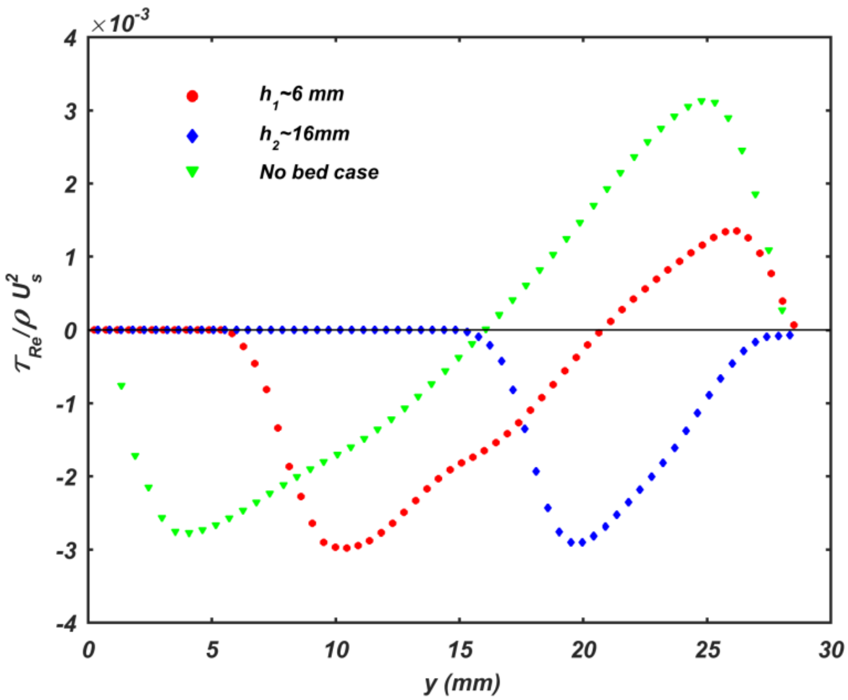

Figure 4-23 Normalized Reynolds shear stress profiles in the lower annulus measured at U_s=0.2 m/s

Another important feature of the Reynolds stress profiles shown in Figure 4-23 is that there is a shift in the radial location of zero shear stress. For the smaller bed height (6 mm), the location of the zero shear stress shifts toward the inner pipe by about 5 mm; a shift close to that of the actual bed height. For the thicker bed (16 mm), however, the location of the zero-shear stress shifts so close to the inner pipe wall that it appears that the Reynolds stress becomes close to zero on the pipe wall. Therefore, the change in the zero-shear stress location is a function of the bed height. The importance of this observation lies in the fact that increasing bed height makes the flow more asymmetric, which means that the Reynolds stress in the lower annulus may eventually become zero if the sand bed becomes sufficiently thick.

Figure 4-24 shows the comparison of the normalized Reynolds stress profiles in the lower annulus for the flow over 6 and 16 mm thick stationary beds and no stationary bed at the critical flow rate (0.24 m/s). There is a reduction in the peak value of the Reynolds stress for the flow over the stationary 6 mm and 16 mm bed comparing to the no bed case. Increasing the cuttings bed height, however, did not affect the Reynolds stress profiles indicating that some other mechanisms must cause the reduction of the Reynolds stress (as compared to the no sand bed case). Since the particles roll and slide along the bed at this flow rate, particles movement can be one of the reasons for this reduction in the Reynolds stress. As discussed earlier, there exist some previous studies in the literature suggesting that the bed load transport can reduce the turbulence (Best et al. 1997, Carbonneau and Bergeron 2000).

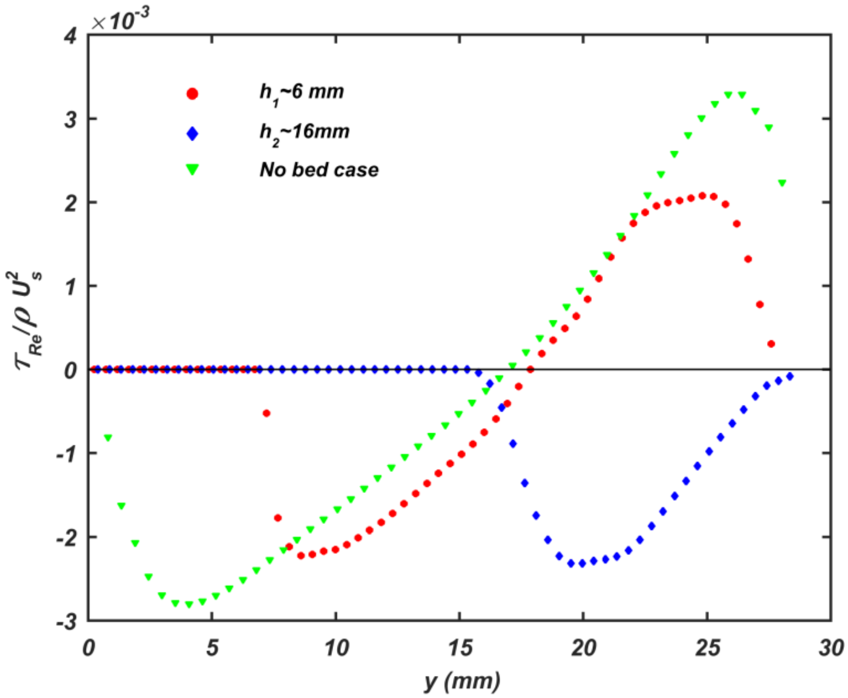

Figure 4-24 Normalized Reynolds shear stress profiles in the lower annulus measured at U_s=0.24 m/s

Figure 4-25 shows the variation of the Reynolds stress profiles in the upper annulus with the increasing bed deposit heights measured at the superficial liquid velocity of 0.2 m/s. When the bed height was 6 mm, the effect of the bed presence on the Reynolds stress was not noticeable. The peak value of the Reynolds stress in the upper annulus was, slightly less than that of the case with no bed presence. When the bed height was 16 mm, however, the Reynolds stress was significantly higher than that of the case with no bed. This might be because the peak velocity was higher in the upper annulus due to the presence of the 16-mm thick bed in the lower annulus, which diverts the more volumetric flow from the lower annulus to the upper annulus.

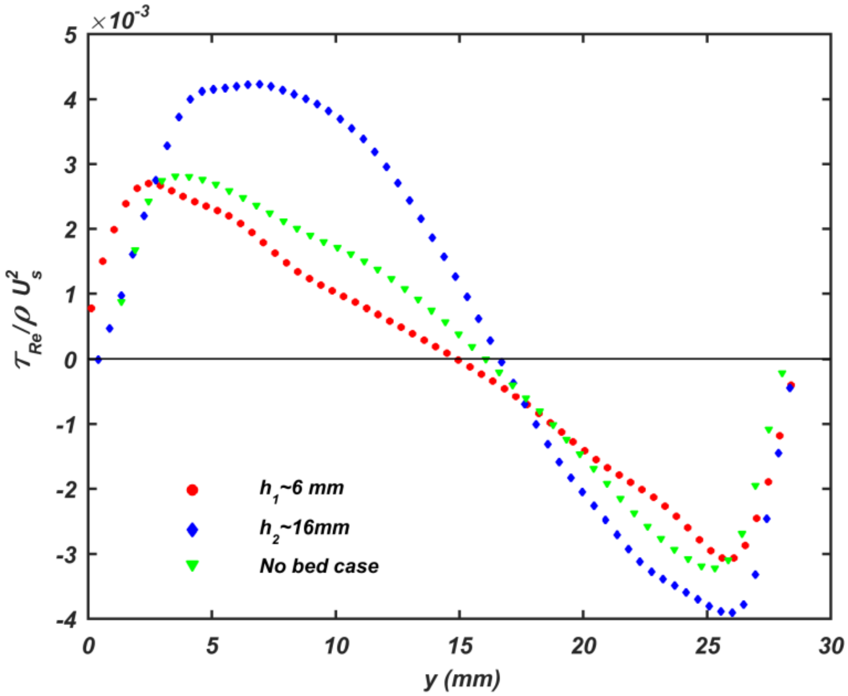

Figure 4-25 Normalized Reynolds shear stress profiles in the upper annulus measured at U_s =0.2 m/s

Figure 4-26 shows the variation of the Reynolds stress profiles in the upper annulus with the increasing bed deposit height measured at the superficial liquid velocity of 0.24 m/s. The Reynolds stress measured at the inner wall of the outer pipe in the upper annulus increases with the increasing bed height. The Reynolds stress profile near the wall of the inner pipe, however, did not exactly follow the same trend as the one observed at the outer wall. Here, the Reynolds stress was still the highest when the bed thickness was 16 mm. However, for the 6-mm thick bed, the Reynolds stress at the inner pipe wall was slightly lower than that of the case for the flow with no bed.

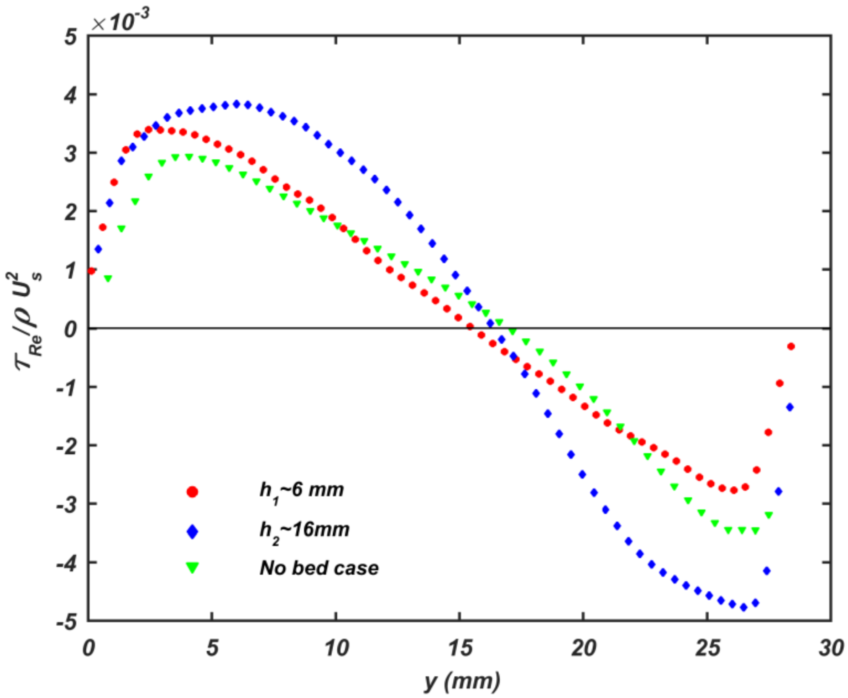

Figure 4-26 Normalized Reynolds shear stress profiles in the upper annulus measured at U_s =0.24 m/s

Overall, it can be said that due to the presence of the cuttings bed in the lower annulus, volumetric flow rate (and the velocity) decreases in the lower annulus. To compensate this decline in the lower annulus, the volumetric flow rate (and the velocity) increases in the upper annulus. The extent to which velocity increases in the upper annulus depends upon the bed height. The increase in the velocity in the upper annulus will result in higher turbulent shear stresses. Since the extent of the increase in velocity was a function of the bed height, the magnitude of the increase in Reynolds stress would also depend on the bed height.

Finally, the Figure 4-27 shows the comparison of the Reynolds stress in the lower and upper annulus with the presence of the 16-mm thick bed at 0.20 m/s velocity. In this particular example, the peak value of Reynolds stress in the upper annulus was 50% higher than the Reynolds stress in the lower annulus. The results indicate a significant decrease in Reynolds stress in the lower annulus due to the presence of the bed comparing to that of the upper annulus.

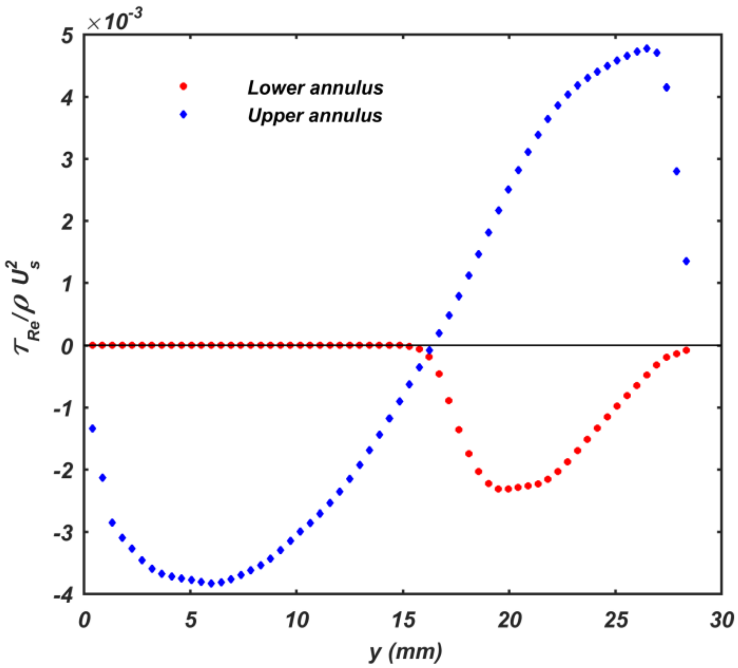

Figure 4-27 Normalized Reynolds shear stress profiles in the upper and lower annulus measured at U_s =0.2 m/s (h≈16 mm)

4.4.2.3. Impact of Bed Height on the Near Bed Reynolds Stress Profiles

In addition to the analyses of velocity profiles very close to the bed surface, results from experiments conducted by focusing on the region very close to the stationary bed surface were also used to analyze the Reynolds stresses very close to the bed surface. The results of these experiments are expected to help in better understanding the impact of the bed height on the turbulent shear stress near a settled sand bed as well as away from the bed.

Figure 4-28 and Figure 4-29 show the effects of 8 and 14 mm thick beds on the Reynolds shear stress profiles measured very close to the bed surface at superficial velocities of 0.2 and 0.24 m/s, respectively. These data reveal much more details about the impact of the bed height on the near bed shear stress than the previous measurements. Close to the bed surface, the Reynolds stresses are the same for both bed heights. Perhaps, this region was located within the viscous sublayer, where the Reynolds stress would not be dominant. The peak values of the Reynolds stresses were also very close to each other for the flow over 8 and 14 mm thick beds, which is also consistent with the results presented earlier. The major difference in the Reynolds stresses starts to be seen after some distance away from the bed surface. For the 8-mm thick bed, Reynolds stress was higher in the core flow than that of the case with 14 mm thick bed. The location of the zero-shear stress was closer to the bed surface when the bed thickness was 14 mm.

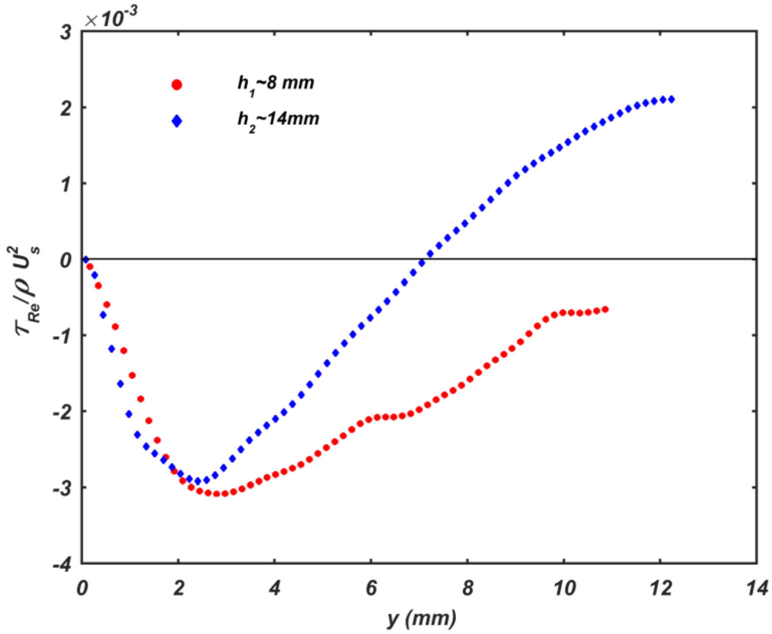

Figure 4-28 Normalized Reynolds stress profiles measured near bed interfaces at U_s =0.2 m/s

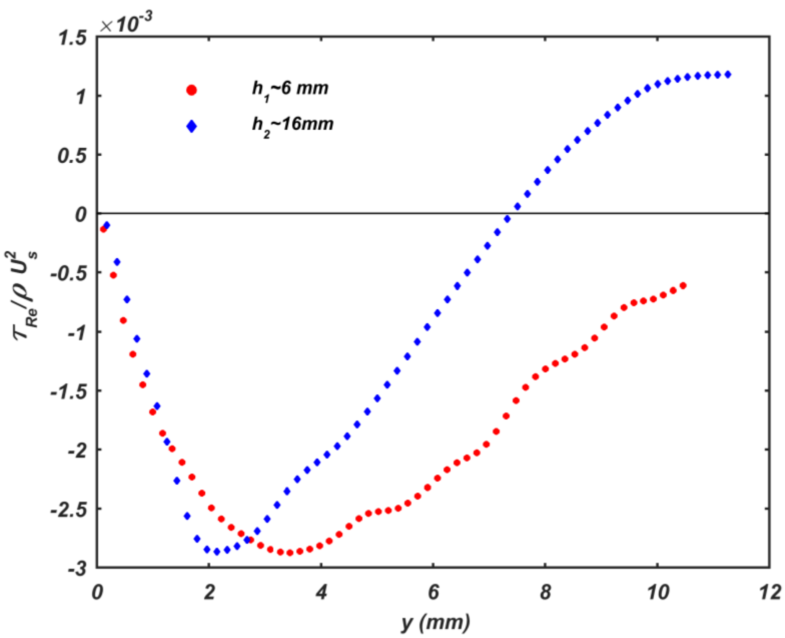

Figure 4-29 Normalized Reynolds stress profiles measured near bed interfaces at U_s =0.24 m/s

4.4.3. Turbulence Intensities

Turbulence intensities or Reynolds normal stresses are the RMS (root mean square) of the velocity fluctuations. Normalized by the superficial liquid velocity, the radial (Eq.(4-16)) turbulence intensity is defined as follows:

$$\frac{v_{rms}}{U_s} = \frac{\sqrt{\overline{v'v'}}}{U_s} \qquad \textbf{Eq.(4-16)}$$

The higher turbulence intensity indicates that a greater level of turbulent energy is available at the interface for the bed erosion. The radial component of turbulence intensity is of particular importance in solid transport and solid suspension. Kelessidis and Bandelis (2004) based on the work of Davies (1987) discussed the eddy fluctuation force, which is essential in keeping particles in suspension in turbulent flow. As shown by Eq.(4-17) (Davies 1987), the eddy fluctuation force is proportional to radial velocity fluctuations. A higher level of radial velocity fluctuation results in a higher eddy fluctuation force. As can be inferred from Eq.(4-16) and Eq.(4-17), the eddy fluctuation force (P_{ed}) is proportional to the radial turbulence intensity.

$$P_{ed} \approx \rho(v')^2 \qquad \textbf{Eq.(4-17)}$$

4.4.3.1. Impact of the Sand Bed Presence on the Radial Turbulence Intensity Profiles

Figure 4-30 presents the normalized radial turbulence intensity (Eq.(4-16)) in the lower annulus for the flow over the 6 mm thick stationary bed and the flow in the annulus without any cuttings bed at the superficial velocity of 0.2 m/s. There is no significant difference between the two radial turbulence intensity profiles as shown in the Figure 4-30. The peak value of radial turbulence intensity, however, is slightly higher for the flow without a solids bed case.

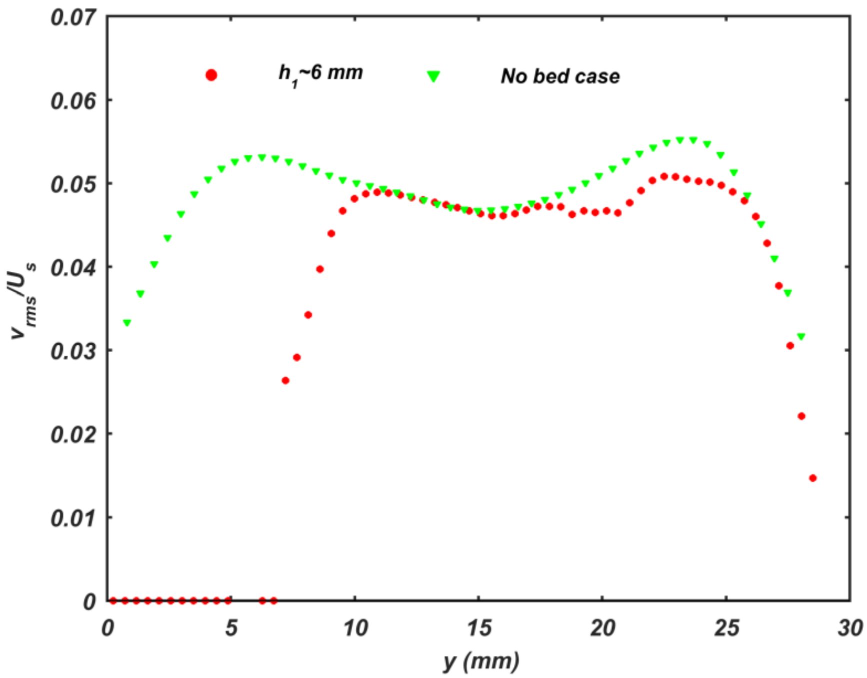

Figure 4-30 Normalized radial turbulence intensity profiles in the lower annulus measured at U_s =0.2 m/s (h≈6 mm)

Figure 4-31 reports the normalized radial turbulence intensity with and without sand bed measured at the critical flow rate (0.24 m/s) of bed erosion. The radial turbulence intensity decreases slightly at this flow rate for the flow over the 6 mm thick solids bed as compared to the flow with no stationary solids bed. These results are also consistent with the observed Reynolds shear stress profiles.

The reduction of radial turbulence intensity as a result of bed load transport has been observed in other studies as well (Bigillon et al. 2006). Nonetheless, once again this behavior is attributed to the reduction of the turbulence by the bed load transport of sand particles (Best et al. 1997, Carbonneau and Bergeron 2000). The implication of this phenomenon for bed erosion is that due to movement of particles, radial turbulence intensity is dampened. Therefore, particles tend to stay near the bed interface and roll and slide along this interface rather than being lifted into the main flow and be carried in suspension.

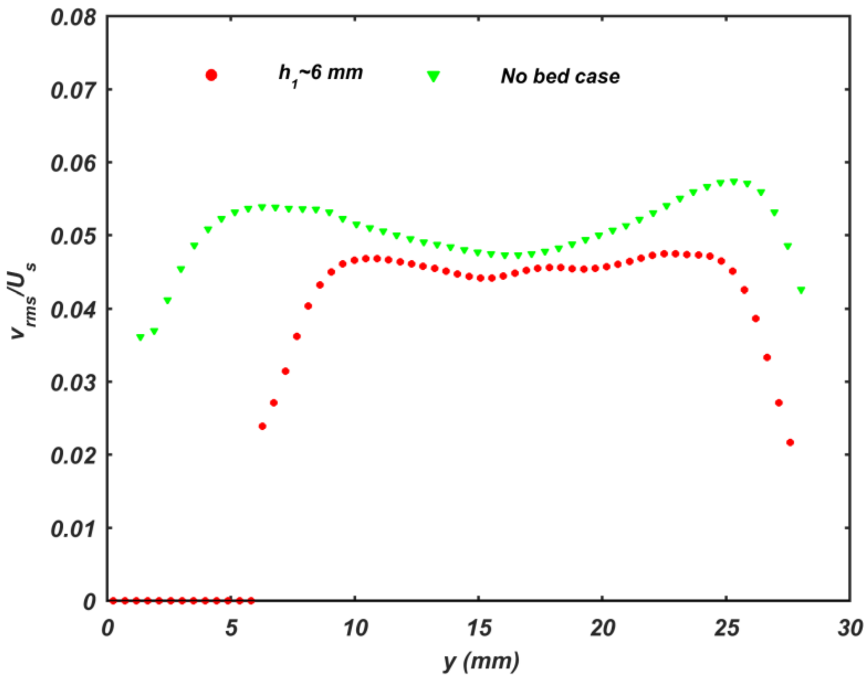

Figure 4-31 Normalized radial turbulence intensity profiles in the lower annulus measured at U_s =0.24 m/s (h≈6 mm)

4.4.3.2. Impact of the Change in Sand Bed Height on the Radial Turbulence Intensity Profiles

Figure 4-32 shows the normalized radial intensity profiles in the lower annulus measured at a superficial liquid velocity of 0.2 m/s with no stationary solids bed, 6 and 16 mm thick solids bed. At this flow rate, there is no significant difference caused by the increasing bed height on the radial intensities. This observation conforms to the Reynolds stress profiles observed at the flow rates less than the critical flow rate. At this sub-critical flow rate, the presence of the solids bed is expected to enhance the production of the turbulence, especially at locations very close to the interface. The main reason for that is the roughness of the bed interface (Krogstad et al. 1992). In fact, that is probably one of the reasons why removing the bigger particles from a bed surface is easier than, the smaller ones (Duan 2009, Bizhani et al. 2016). The smaller size solid particles exhibit less roughness at the interface and, therefore, create less turbulence.

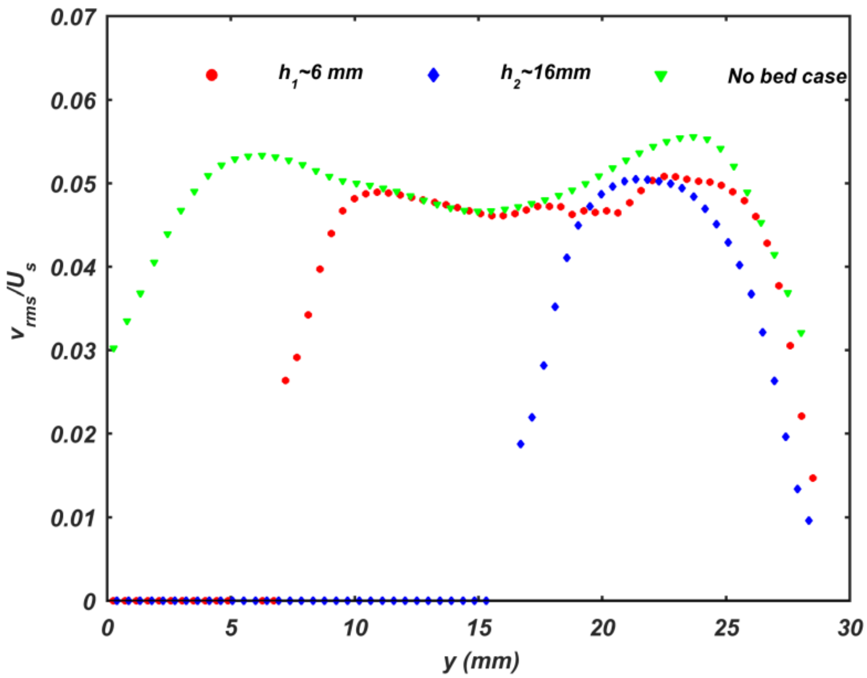

Figure 4-32 Effect of the change in bed height on the normalized radial turbulence intensity profiles in the lower annulus measured at U_s = 0.2 m/s

Figure 4-33 shows the effect of increasing solids bed thickness on the radial turbulence intensity measured at the critical flow rate of the bed erosion. At the critical flow rate, the radial turbulence intensity over the 6 mm thick solids bed decreases as compared to the no stationary bed case. Once the bed is formed, however, increasing the bed height (from 6 mm to 16 mm) does not cause further reduction in the radial turbulence intensity. This behavior is also consistent with the observations of the change in the Reynolds shear stress profiles. The bed load transport, as discussed previously, is thought to be the main reason for the reduction in both the Reynolds shear and the normal stresses at the critical flow rate. These findings agree with results from previous studies of the bed load transport (Best et al. 1997, Carbonneau and Bergeron 2000). The importance of this observation is that due to the reduction in radial fluctuation forces, particles tend to stay near the bed interface rather than being kept in the suspension.

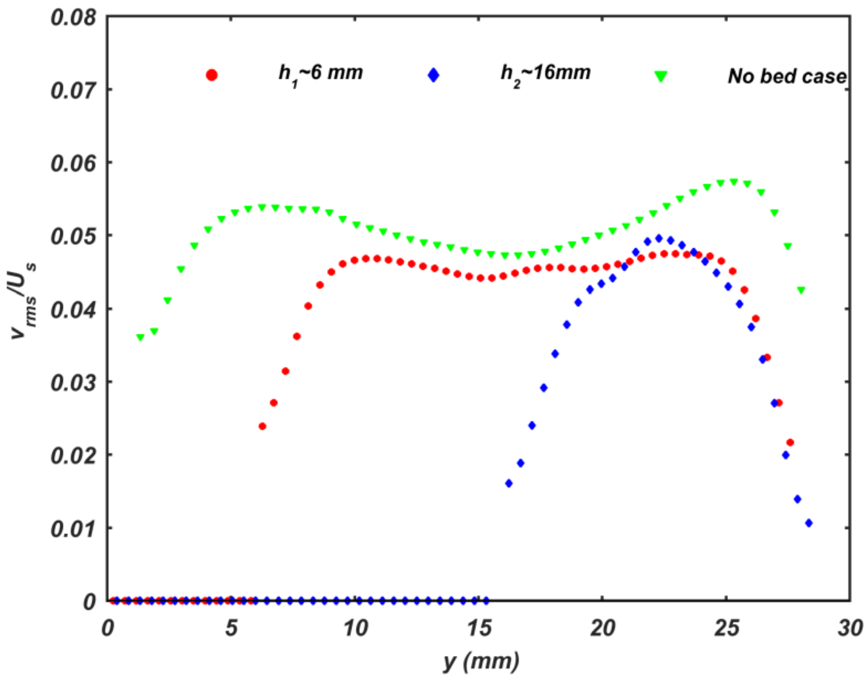

Figure 4-33 Effect of the change in the bed height on the normalized radial turbulence intensity profiles in the lower annulus measured at U_s =0.24 m/s

4.5. Discussion of the Results and Their Practical Implications for the Design of the Industrial Processes Involving Transport of Solids in Pipes and Annuli

The turbulent flow of water over the stationary solids bed of different heights in horizontal concentric annuli was the main subject matter of this study. Results showed that the presence of the stationary solids bed changed the time averaged velocity profiles and reduced the peak fluid velocity in the lower annulus (Figure 4-4 and Figure 4-5). An increase in the solids bed height resulted in further reduction of the velocity in the lower annulus (Figure 4-7 and Figure 4-8). Moreover, a comparison of the velocity profiles in the lower and upper annulus showed that the peak velocities in the upper annulus were 17% and 30% higher than that of the ones in the lower annulus when the bed thickness was 6 and 16 mm, respectively (Figure 4-12 and Figure 4-13). The significant increase in the difference between the peak velocities in the lower and upper annulus (i.e., 17% in 6 mm bed height vs. 30% in 16 mm bed height) also confirmed that the increasing bed height caused further reduction of the velocity in the lower annulus.

Reduction in volumetric flow rate and the peak velocity in the lower annulus would have a significant impact on the bed erosion process. That is mainly because the hydrodynamic forces (i.e., lift and drag forces) strongly depend upon the instantaneous local velocity. In particular, the drag force is proportional to the square of the local axial velocity. Therefore, any reduction in the local velocity at the bed interface would cause a significant decrease in the fluid drag force, which is the primary force responsible for mobilizing and moving the particles. As soon as a stationary sand bed is allowed to form in the lower annulus, conditions for bed erosion deteriorates as the drag force starts to decrease due to the reduction of the local velocity. This can promote deposition of more particles, which means a thicker bed causing further reduction in the local velocity and the corresponding drag force in the lower annulus. This process will continue until an equilibrium bed height is reached for that specific fluid flow rate.

The practical implications of these observations for the design of any industrial process involving transport of solids in pipes and annuli is several folds: i-) As soon as a stationary solids bed forms, volumetric flow rate, and the peak velocity start decreasing in the lower annulus; ii-) This reduction in the peak velocity can further increase the chance of the formation of a thicker bed; iii-) Increasing bed height, causes further reduction in the flow rate and the peak velocity near the bed and as a result; iv-) the situation becomes less favorable for effective transport of solids (i.e., it becomes more favorable for solids to settle down through reduction of the distance a particle can travel before it settles down on the bed surface); v-) For a given constant flow rate, the particle deposition may continue until the bed height reaches a critical value at which annuli's cross section reduces so much that the critical velocity of the bed erosion is attained. This bed height will be the equilibrium bed height, which would remain constant at the given flow rate.

In short, as soon as the first particles start settling down, the situation becomes less favorable for effective transport of the solids, therefore, for any industrial process involving transport of solids in pipes and annuli, it is recommended to prevent the formation of a stationary bed if at all possible.

An accurate estimation of the friction forces acting at the fluid/solid bed interface is essential for developing more realistic mechanistic models of the bed erosion. The magnitude of the friction forces acting at the bed/fluid interface is strongly related to the surface roughness of the bed deposits. Data presented in this study show that characterizing the bed interface with a single roughness height may lead to some errors. That is mainly because the bed interface is not uniform. The condition of the bed interface is not controllable and, therefore, the configuration of particles at the bed interface can lead to different roughness heights along the bed. Nonetheless, if one needs to characterize the bed surface, an equivalent roughness height of 2d50 can be used.

4.6. Conclusions

Results of an experimental study on the turbulent flow of water over two stationary solids beds of different heights in horizontal concentric annuli were presented. Experiments were conducted using industrial sand with mean sieve diameter of (d_{50}) 600 microns. Non-intrusive particle image velocimetry (PIV) technique was used for the measurements.

Results showed that the presence of the stationary solids bed changed the time averaged velocity profiles and reduced the peak fluid velocity in the lower annulus. An increase in the solids bed height resulted in further reduction of the velocity in the lower annulus. The peak velocity decreased by increasing the bed height. At the critical flow rate of the bed erosion, the percentage of the reduction in maximum velocity was lower than that of observed at the sub-critical flow rate. This behavior was attributed to the bed load transport of solids in the annulus. Velocity profiles in the upper part of the annuli showed dependency on the stationary bed height. Velocity values for flow over the solids beds were higher than the case of no bed. The thicker bed caused more increase of the velocity in the upper annulus than the low height bed.

Velocity profiles in wall units showed a downward shift from the universal law for the flow near the solids bed surfaces. Analysis of velocity profiles in the log-wall region revealed that the equivalent roughness varied with the flow rates. For the sub-critical flow rate, an equivalent roughness of $2d_{50}$ characterizes the solids bed surface. At the critical flow rate, the equivalent roughness increased to $2.4d_{50}$. This behavior was attributed to bed load transport of particles at the critical flow rate. Further analysis showed that the bed roughness might also change the bed interface. Therefore, it is not possible to characterize the bed roughness with a single roughness height.

The normalized Reynolds shear stress profiles, when compared with the flow in the same annuli with no sand bed, were different at different flow rates. At a flow rate less than that of critical flow rate, Reynolds stress profiles show slightly higher peak values near the bed interface for the thin and the thick bed than that of the flow without a solids bed. On the other hand, at the critical flow rate, Reynolds stress was reduced for flow over the solids bed as compared to the case with no solids bed. This behavior was explained based on the previous works in sediment transport and was related to bed load transport. Another impact of the cuttings bed on Reynolds stress was the shift in the radial location of zero shear stress towards the inner pipe. Thicker bed caused more shift in the radial location of the zero-shear stress.

Comparison of the Reynolds stress profiles in the lower and upper annulus showed that the Reynolds stress was reduced in the lower annulus as a result of the solids bed presence. Additionally, increasing the solids bed height caused more reduction in Reynolds stress in the lower annulus. Reynolds stress profiles showed higher values in the upper annulus for flow over the cuttings bed. Additionally, the thicker bed caused more Reynolds stress in the upper annulus than the smaller bed.

Near bed measurement of Reynolds stress profiles showed that near the solids bed surface, the Reynolds stress was not influenced by the bed height. However, in the core flow (i.e. away from the bed surface), Reynolds stress remained higher for flow over the smaller bed. Analyses of the bed shear stress revealed that the thicker solids bed caused, the higher wall shear stress.

The radial turbulence intensity was also measured and reported. The radial turbulence intensity is an important property when particles suspension is considered. The results have shown the radial turbulence intensities are affected in the same way as the Reynolds shear stresses. At flow rates less than critical flow rate, the level of radial intensity is almost the same as the no bed case. However, at the critical flow rate, the radial turbulence intensity decreased with the presence of the solids bed.

4.7. Nomenclature

R	Inner Radius of outer pipe (m)
r	Outer Radius of inner pipe (m)

D_H	Hydraulic Diameter (mm) ($D_o - D_{in}$)
D_o	Outer pipe diameter (mm)
D_i	Inner pipe diameter (mm)
y	Distance from outer pipe wall (mm)
L	Pipe length (m)
A	Annular area cross section ($\pi({R_o}^2 - {R_i}^2)$) (m^2)
h	Cuttings bed height (m)
h_1	Small bed height ($\approx 6\ mm$)
h_2	Big bed's height ($\approx 16\ mm$)
Q	Flow Rate (m^3/s)
U_s	Superficial Bulk velocity ($\frac{m}{s}$)
d_{50}	Particles diameter (m)
u	Time average velocity ($\frac{m}{s}$)
$\hat{u}$	Instantaneous axial velocity ($\frac{m}{s}$)
$\hat{v}$	Instantaneous radial velocity ($\frac{m}{s}$)
Δt	Time between two cameras frame (s)
Δs	Displacement of tracer particles (m)
Δx	Axial displacement of tracer particles (m)
Δy	Radial displacement of tracer particles (m)
ρ	Density $\left(\frac{Kg}{m^3}\right)$
μ	Fluid viscosity ($Pa.s$)
τ	Shear Stress (Pa)

τ_{Re}	Reynolds stress $= -\rho\overline{u'v'}$ (Pa)
u'	Axial Fluctuation Velocity ($\frac{m}{s}$)
v'	Radial Fluctuation Velocity ($\frac{m}{s}$)
P_{ed}	Eddy Fluctuation force (N)
V_{RMS}	Root Mean Square of radial fluctuation velocity ($\frac{m}{s}$)
u^+	Dimensionless velocity
y^+	Dimensionless distance
κ	von Karman constant (0.41)
u_τ	Friction velocity ($\frac{m}{s}$)
Re_{u_τ}	Roughness Reynolds number
ε	Equivalent roughness (m)
τ^*	Shields stress
τ_i	Interfacial shear stress (Pa)
ρ_s	Solid's density ($\frac{Kg}{m^3}$)
ν	Kinematic viscosity ($\frac{m^2}{s}$)

4.8. References

Best, J., Bennett, S., Bridge, J. et al. (1997). Turbulence modulation and particle velocities over flat sand beds at low transport rates. Journal of Hydraulic Engineering-Asce **123**(12): 1118-1129, J Hydraul Eng-Asce, DOI: c 10.1061/(Asce)0733-9429(1997)123:12(1118).

Bigillon, F., Couronne, G., Champagne, J. Y. et al. (2006). Investigation of flow hydrodynamics under equilibrium bedload transport conditions using PIV. River Flow 2006, Vols 1 and 2: 859-865, Proc Monogr Eng Wate, DOI: ://WOS:000241916500090.

Bizhani, M., Rodriguez-Corredor, F. E. and Kuru, E. (2015). An Experimental Study of Turbulent Non-Newtonian Fluid Flow in Concentric Annuli using Particle Image Velocimetry Technique. Flow Turbulence and Combustion **94**(3): 527-554, Flow Turbul Combust, DOI: 10.1007/s10494-014-9589-6.

Bizhani, M., Rodriguez Corredor, F. E. and Kuru, E. (2016). Quantitative Evaluation of Critical Conditions Required for Effective Hole Cleaning in Coiled-Tubing Drilling of Horizontal Wells. **SPE** Drilling & Completion **31**(3): 188-199, SPE-174404-PA, DOI: 10.2118/174404-PA.

Carbonneau, P. E. and Bergeron, N. E. (2000). The effect of bedload transport on mean and turbulent flow properties. Geomorphology **35**(3-4): 267-278, Geomorphology, DOI: g10.1016/S0169-555x(00)00046-5.

Chan-Braun, C., Garcia-Villalba, M. and Uhlmann, M. (2011). Force and torque acting on particles in a transitionally rough open-channel flow. Journal of Fluid Mechanics **684**: 441-474, J Fluid Mech, DOI: 10.1017/jfm.2011.311.

Chung, S. Y., Rhee, G. H. and Sung, H. J. (2002). Direct numerical simulation of turbulent concentric annular pipe flow - Part 1: Flow field. International Journal of Heat and Fluid Flow **23**(4): 426-440, Int J Heat Fluid Fl, DOI: 10.1016/S0142-727X(02)00140-6.

Davies, J. T. (1987). Calculation of Critical Velocities to Maintain Solids in Suspension in Horizontal Pipes. Chemical Engineering Science **42**(7): 1667-1670, Chem Eng Sci, DOI: 10.1016/0009-2509(87)80171-9.

Duan, M. Q., Miska, S., Yu, M. J., Takach, N., Ahmed, R., Zettner, C. (2009). Critical Conditions for Effective Sand-Sized-Solids Transport in Horizontal and High-Angle Wells. SPE Drilling & Completion **24**(2): 229-238, **SPE** Drill Completion, DOI: 10.2118/104192-PA.

Escudier, M. P. and Gouldson, I. W. (1995). Concentric Annular-Flow with Centerbody Rotation of a Newtonian and a Shear-Thinning Liquid. International Journal of Heat and Fluid Flow **16**(3): 156-162, Int J Heat Fluid Fl, DOI: 10.1016/0142-727x(95)00012-F.

Garcia, M. H. (2008). Sedimentation Engineering: Processes, Measurements, Modeling, and Practice, American Society of Civil Engineers.

Gaudio, R., Miglio, A. and Dey, S. (2010). Non-universality of von Karman's kappa in fluvial streams. Journal of Hydraulic Research **48**(5): 658-663, J Hydraul Res, DOI: http://dx.doi.org/10.1080/00221686.2010.507338.

Ghaemi, S., Rafati, S.,Bizhani, M., Kuru, E. (2015). Turbulent structure at the midsection of an annular flow. Physics of Fluids **27**(10): 105102, DOI: http://dx.doi.org/10.1063/1.4932109.

Gore, R. A. and Crowe, C. T. (1991). Modulation of Turbulence by a Dispersed Phase. Journal of Fluids Engineering-Transactions of the Asme **113**(2): 304-307, J Fluid Eng-T Asme, DOI: 10.1115/1.2909497.

Japper-Jaafar, A., Escudier, M. P. and Poole, R. J. (2010). Laminar, transitional and turbulent annular flow of drag-reducing polymer solutions. Journal of Non-Newtonian Fluid Mechanics **165**(19-20): 1357-1372, J Non-Newton Fluid, DOI: 10.1016/j.jnnfm.2010.07.001.

Kelessidis, V. C. and Bandelis, G. E. (2004). Flow Patterns and Minimum Suspension Velocity for Efficient Cuttings Transport in Horizontal and Deviated Wells in Coiled-Tubing Drilling. **SPE** Drilling & Completion **19**(4), SPE-81746-PA, DOI: 10.2118/81746-PA.

Krogstad, P. A., Antonia, R. A. and Browne, L. W. B. (1992). Comparison between Rough-Wall and Smooth-Wall Turbulent Boundary-Layers. Journal of Fluid Mechanics **245**: 599-617, J Fluid Mech, DOI: 10.1017/S0022112092000594.

Kundu, P. K., Cohen, I. M. and Dowling, D. R. (2012). Fluid Mechanics, 5th Edition. Amsterdam, Elsevier Science Bv.

Lawn, C. J. and Elliott, C. J. (1972). Fully Developed Turbulent-Flow through Concentric Annuli. Journal of Mechanical Engineering Science **14**(3): 195-204, J Mech Eng Sci, DOI: 10.1243/JMES_JOUR_1972_014_027_02.

Melling, A. (1997). Tracer particles and seeding for particle image velocimetry. Measurement Science & Technology **8**(12): 1406-1416, Meas Sci Technol, DOI: 10.1088/0957-0233/8/12/005.

Miyazaki, K., Chen, G. , Ymamoto, F., Ohta, J., Murai, Y., Horii, K. (1999). PIV measurement of particle motion in spiral gas-solid two-phase flow. Experimental Thermal and Fluid Science **19**(4): 194-203, Exp Therm Fluid Sci, DOI: 10.1016/S0894-1777(99)00020-5.

Nezu, I. and Sanjou, M. (2011). PIV and PTV measurements in hydro-sciences with focus on turbulent open-channel flows. Journal of Hydro-Environment Research **5**(4): 215-230, J Hydro-Environ Res, DOI: 10.1016/j.jher.2011.05.004.

Nouri, J. M., Umur, H. and Whitelaw, J. H. (1993). Flow of Newtonian and Non-Newtonian Fluids in Concentric and Eccentric Annuli. Journal of Fluid Mechanics **253**: 617-641, J Fluid Mech, DOI: 10.1017/S0022112093001922.

Poole, R. J. (2010). Development-Length Requirements for Fully Developed Laminar Flow in Concentric Annuli. Journal of Fluids Engineering-Transactions of the **Asme 132**(6), J Fluid Eng-T Asme, DOI: 10.1115/1.4001694.

Ramadan, A., Skalle, P. and Johansen, S. T. (2003). A mechanistic model to determine the critical flow velocity required to initiate the movement of spherical bed particles in inclined channels. Chemical Engineering Science **58**(10): 2153-2163, DOI: 10.1016/S0009-2509(03)00061-7.

Rehme, K. (1974). Turbulent-Flow in Smooth Concentric Annuli with Small Radius Ratios. Journal of Fluid Mechanics **64**(2): 263-287, J Fluid Mech, DOI: http://dx.doi.org/10.1017/S0022112074002394.

Rodriguez-Corredor, F. E., Bizhani, M. and Kuru, E. (2015). Experimental Investigation of Drag Reducing Fluid Flow in Annular Geometry Using Particle Image Velocimetry Technique. Journal of Fluids Engineering-Transactions of the **Asme 137**(8), J Fluid Eng-T Asme, DOI: 10.1115/1.4030287.

Rodriguez-Corredor, F. E., Bizhani, M., Ashrafuzzaman, M., Kuru, E. (2014). An Experimental Investigation of Turbulent Water Flow in Concentric Annulus Using Particle Image Velocimetry Technique. Journal of Fluids Engineering-Transactions of the **Asme 136**(5), J Fluid Eng-T Asme, DOI: 10.1115/1.4026136.

Schmeeckle, M. W. (2014). Numerical simulation of turbulence and sediment transport of medium sand. Journal of Geophysical Research-Earth Surface **119**(6): 1240-1262, J Geophys Res-Earth, DOI: 10.1002/2013jf002911.

Shields, A. (1936). Anwendung der Ähnlichkeitsmechanik und der Turbulenzforschung auf die Geschiebebewegung. Berlin, Eigenverl. der Preußischen Versuchsanst. für Wasserbau und Schiff.

Sumer, B. M., Chua, L. H. C., Cheng, N.-S. et al. (2003). Influence of Turbulence on Bed Load Sediment Transport. Journal of Hydraulic Engineering **129**(8): 585-596, DOI: 10.1061/(ASCE)0733-9429(2003)129:8(585).

Wiberg, P. L. and Rubin, D. M. (1989). Bed Roughness Produced by Saltating Sediment. Journal of Geophysical Research-Oceans **94**(C4): 5011-5016, J Geophys Res-Oceans, DOI: 10.1029/JC094iC04p05011.

Yan, F. and Rinoshika, A. (2011). Application of high-speed PIV and image processing to measuring particle velocity and concentration in a horizontal pneumatic conveying with dune model. Powder Technology **208**(1): 158-165, Powder Technol, DOI: 10.1016/j.powtec.2010.12.014.

Yan, F. and Rinoshika, A. (2012). Characteristics of particle velocity and concentration in a horizontal self-excited gas-solid two-phase pipe flow of using soft fins. International Journal of Multiphase Flow **41**: 68-76, Int J Multiphas Flow, DOI: 10.1016/j.ijmultiphaseflow.2012.01.004.

Zeinali, H., Toma, P. and Kuru, E. (2012). Effect of Near-Wall Turbulence on Selective Removal of Particles From Sand Beds Deposited in Pipelines. Journal of Energy Resources Technology-Transactions of the Asme **134**(2), J Energ Resour-Asme, DOI: Artn 021003

10.1115/1.4006041.

5.Turbulent Flow of Polymer Solutions over Stationary Cuttings Bed in Horizontal Wells

In this chapter results of PIV experiments for turbulent flow of polymer fluids in the concentric annulus are presented. The experiments were conducted for flow over a stationary sand bed. The velocities at which measurements are performed are either below or equal to the critical flow rate of bed erosion.

5.1. Abstract

Turbulent flow of polymer solutions in the annulus is often encountered in drilling horizontal wells. Additionally, frequently a stationary sand bed, formed from the drilled cuttings, exists in the lower part of the annuli. The presence of this cuttings bed poses several difficulties to the drilling operation's integrity. The only tool for effectively removing the cuttings bed is the drilling fluid. However, it is not well understood how the presence of the cuttings bed affects the flow in the annulus. Knowledge of such modifications is necessary for the effective design of hole cleaning strategies.

In this paper, we investigate the turbulent flow of two polymer solutions over a stationary cuttings bed in a horizontal concentric annulus. The case is identical to hole cleaning operations in Coiled Tubing interventions. State of the art PIV (Particle Image Velocimetry) technique was used for obtaining instantaneous 2-D velocity profiles of the turbulent flow in different sections of the annulus. A large-scale flow loop facility was used as the wellbore simulator. Natural quartz sand with mean sieve diameter of 600 microns was used to simulate drilled cuttings.

Parameters that affect the efficacy of cuttings removal are local fluid velocity and flow turbulence in the lower part of the annulus. Local fluid velocity is believed to control the fluids drag and lift on the cuttings, and hence it represents the driving force for removing the cuttings. Flow turbulence presents an additional source of momentum for cutting removal which has been proven crucial for effective hole cleaning.

Our results show mere presence of stationary cuttings bed causes the flow rate and flow velocity to decrease in the lower part of the annulus. The decrease was found to be independent of polymer concentration. Reduction in flow velocity and flow rate in the lower annulus is only a function of bed height.

Reynolds shear stress is negatively affected in the lower annulus as a result of the cuttings bed. The decrease in the Reynolds stress was more pronounced for the thicker fluid. Comparison of Reynolds shear stress profiles for the two polymer concentrations showed increasing polymer concertation result in a significant decrease of turbulent stress in the lower annulus. However, the profiles of Reynolds stress in the upper annulus showed a slight difference between the two polymer solution.

Finally, axial turbulence intensity profiles are discussed in the paper. Axial turbulence intensity is of utmost importance because it represents the level of velocity fluctuations in the axial direction. Recent studies have shown effective sediment transport requires high peaks in local velocity which translates into high turbulence intensities. Comparison of intensity profiles in the lower and upper annulus showed the presence of the cuttings bed negatively affect the axial intensities. Enhancing the polymer viscosity does not seem to influence the axial intensity as much as it did the Reynolds stress.

5.2. Introduction

Turbulent flow of polymeric fluids is a common phenomenon in oil and gas industry. In drilling long horizontal wells, often drill solids tend to settle down on the lower side of the wellbore and form a stationary cuttings bed. Later in the drilling operation, this solid bed needs to be cleaned to continue the drilling or complete the well. The hole cleaning operation is performed by pumping the drilling fluid down the annulus to sweep the drilling cuttings out of the wellbore. The presence of the stationary sand bed affects the flow. To optimize the hole cleaning efficiency, knowledge of fluid-particles interaction near the bed interface is necessary. The local fluid velocity controls Fluid-particle interaction at the interface of the stationary solid bed and flows turbulence.

In the literature, there are numerous numerical and experimental studies pertinent to turbulent flow in annular conduits (Rehme 1974, Nouri et al. 1993, Escudier and Gouldson 1995, Chung et al. 2002, Japper-Jaafar et al. 2010, Rodriguez-Corredor 2014). These studies mostly investigated the turbulent flow of different types of fluids (i.e. Newtonian and non-Newtonian) without the presence of a stationary solids bed. Rodriguez-Corredor (2014), (2015) and Bizhani et al. (2015) utilized PIV to study the turbulent flow of Newtonian and polymer based drilling fluids in a concentric annulus. The major findings of research in the single phase turbulent flow of Newtonian fluids could be summarized as follows; i) velocity profiles near the pipe walls follow the logarithmic law consistent with the flow of Newtonian fluids in pipes and channels (Japper-Jaafar et al. 2010, Rodriguez-Corredor 2014, Bizhani et al. 2015). Ii) Turbulent activities (i.e. turbulent intensities) near the inner pipe of an annulus are slightly higher than the outer wall (Rehme 1975, Japper-Jaafar et al. 2010, Rodriguez-Corredor 2014, Bizhani et al. 2015). Iii) Maximum velocity and zero shear stress are biased toward the inner wall (Rehme 1975, Rodriguez-Corredor 2014, Bizhani et al. 2015). Another important feature of turbulent flow in the concentric annulus is that radial location of zero shear stress does not coincide with that of maximum velocity(Lawn and Elliott 1972, Chung et al. 2002, Ghaemi 2015).

Previous studies related to turbulent flow in annuluses provide useful information about different aspects of flow in oil wells. However, in a real drilling operation there always exists a stationary solids bed at the bottom of the well. The presence of this sand bed affects the flow. The main focusing point of this study is investigating the turbulent flow of non-Newtonian fluids over a stationary cuttings bed located in a horizontal annulus. As mentioned this scenario arises due to poor hole cleaning in horizontal and extended reach wells.

The presence of a stationary solid bed affects the turbulent flow in two major ways. The first apparent one is due to changing of the flow geometry. In a concentric annulus, the existence of a stationary solid bed makes the flow go through an asymmetric geometry as opposed to the symmetric geometry of the concentric annulus. The second modification of flow comes from the interaction of loose sand particles in the cuttings bed and the fluid flowing through it. The solid particles cause the flow to decelerate or accelerate by either extracting or giving momentum to the fluid. Turbulent flow in annulus without any sediment bed has been the subject matter of many studies in the past (Rehme 1974, Nouri et al. 1993, Escudier and Gouldson 1995, Chung et al. 2002, Japper-Jaafar et al. 2010). On the other hand, there have been few studies where turbulent flow over a stationary cuttings bed located in a horizontal annulus is investigated (Bizhani et al. 2016, Bizhani and Kuru 2017). In an earlier work, the authors investigated the turbulent flow of water over stationary cuttings bed of varying heights in the horizontal annulus (Bizhani and Kuru 2017). The main findings were that presence of a stationary cuttings bed caused the flow velocity to decrease in the lower annulus while turbulent stress was amplified near the cuttings bed interface. It was also found that flow near the bed resembles the flow near rough walls. The roughness height for the bed was considered to be a varying function of shear velocity. There have been some promising studies using optical techniques such as PIV and or PTV (Particle racking Velocimetry) for studying sediment transport related problems (Miyazaki 1999, Yan and Rinoshika 2011, Yan and Rinoshika 2012). These studies have shown the applicability and usefulness of such techniques in shedding light on some of the hard-to-measure flow related quantities in multiphase flows.

In this paper, we investigate the flow of two polymer solutions under turbulent flow condition over a stationary cuttings bed in a concentric horizontal annulus. The cuttings bed is formed with uniform sand particles with mean sieve diameters of 600 microns and density of 2650 kg/m^3. The measurement technique is the state of the art PIV technique. The main goal of this study is to investigate the impact of the presence of the stationary cuttings bed on different aspects of drilling fluid flow in the annulus. The paper also reports data on how increasing polymer concertation may affect the flow.

5.3. Experimental set-up and procedure

The experiments were conducted in a large-scale flow loop facility. A schematic view of the large-scale flow loop facility used in this study is shown in Figure 5-1. In this system, the fluid is circulated through the loop by a centrifugal pump. The pump is equipped with Variable Frequency Drive (VFD) system to control the flow rate. The stainless stress tank and the air driven mixer are used to prepare and store the polymer solutions.

The test section is 9 meters long and is made of high-quality Borosilicate glass pipes. The outer pipe has an inner diameter of 95 mm and a wall thickness of 5 mm. The glass inner pipe has an outer diameter of 38 mm. The inner pipes are 3 meters long each and are centralized. The annulus has a hydraulic diameter of 57 mm and a radius ratio of 0.4 (The annulus hydraulic diameter is equal to $D_H = D_o - D_i$ where D_o and D_i are the outer pipe inner diameter and the inner pipe outer diameter, respectively). The necessary condition for preventing sagging and bending of the inner pipe in the working fluid is that the pipes be near neutral buoyancy condition in the fluid. Inner pipe wall thickness was carefully selected to meet neutral buoyancy condition and, hence, avoid bending of pipes during the experiments (Japper-Jaafar et al. 2010).

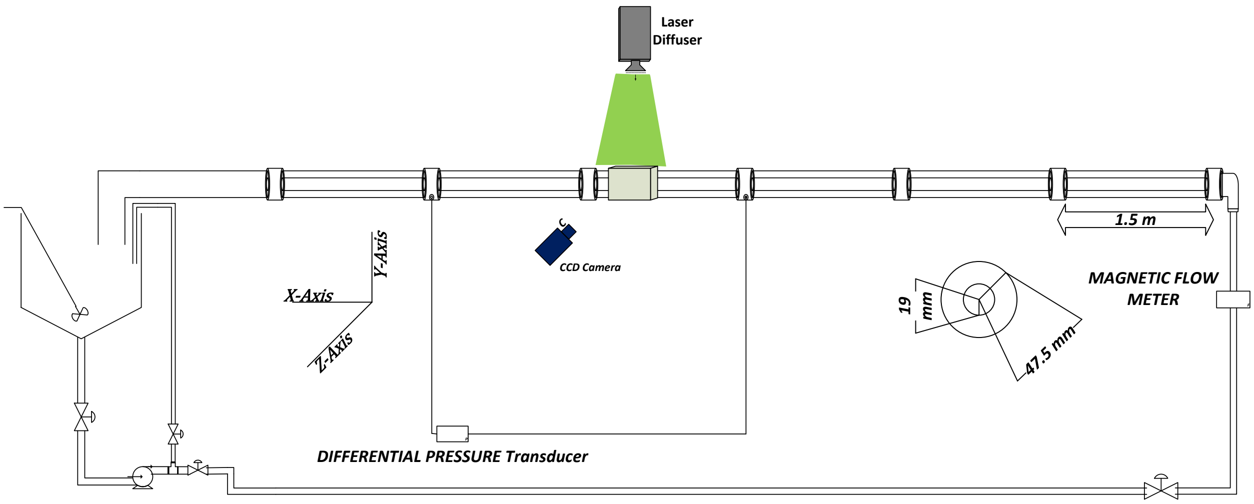

Figure 5-1 The schematic of the flow loop

The flow rate was measured using a magnetic flow meter installed at the inlet of the test section. The flow meter is an OMEGA FMG607-R with an accuracy of $\pm 0.5\%$. A computerized data acquisition system powered by LabView software was connected to all the measurement devices. The software was used to control the pump flow rate as well as logging all the data (i.e. pressure losses, flow rates and fluid temperature in the flow loop).

Forming a stationary cuttings bed was the first stage of the experiments. In this step, water and sand were mixed in the tank while the slurry was circulated through the flow loop at maximum flow rate. The mixture was circulated for 10 to 15 minutes to achieve a steady state condition. The flow was then stopped suddenly. The test section was then isolated using the isolating valves (Figure 5-1). Other parts of the flow loop (i.e. the tank, pump, and transport pipelines) were then carefully washed to remove any solids remained in these parts. During the tests, two filter bags with openings smaller than the particle size (the opening is 100 micron) were installed at the outlet of the annular section to collect any particle which was removed from the test section.

PIV was used to make measurements of the local instantaneous fluid velocity field. Figure 5-2 illustrates the locations of measurement planes in the concentric annulus. To ensure flow fully develops, the test section is at approximately $100D_H$ from the annulus's inlet. The flow is fully develops by this distance in single phase flow (justification is based on the fact that the laminar flow fully develops over a development length of $88D_H$ (Poole 2010), whereas development length for turbulent flow is much shorter (Japper-Jaafar et al. 2010)). To reduce light dispersion and refraction in the test section, a rectangular box was designed and installed around the outer pipe. Additionally, the box was filled with glycerol (99% Wt/Wt pure glycerol) to reduce the light refraction. Glycerol has a refraction index of 1.47, which is similar to the glass pipe, therefore, helps reducing the refraction of the laser light.

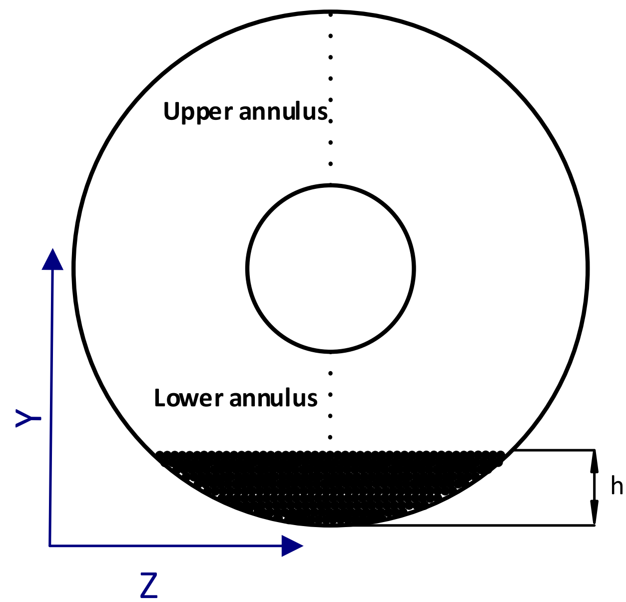

Figure 5-2 Planes of the velocity measurement in the PIV experiments (Bizhani and Kuru 2017)

PIV Setup Description and Post-Processing Procedures

The essences of a planar 2-D PIV are a light source and a recording device. A dual shuttering camera is the typical recording device. A green light double pulse laser was the light source used in this study. Proper orientation of 2-D PIV is shown in Figure 5-1 where the camera view plane is orthogonal to the laser light sheet. PIV works by capturing images of seed particles in the flow. Upon incident of laser light with tracer particles, which are in the flow, the tracer particles reflect the light, which is then detected by the camera. The camera captures two successive images. Processing these pictures with an appropriate algorithm will yield the instantaneous velocity field of the flow.

A Nd: YAG double pulsed laser with a wave length of 532 nm was used in this study. Laser light is converted to a thin light sheet using a cylindrical and a special optical lens. The thickness of the laser light sheet could vary from 0.5 to 3 mm. The thick laser light may incur errors in the measurement as a result of the depth of the field thickness. The light thickness was kept at its minimum as 0.5 mm in this study.

A CCD (charge-coupled device) camera with a resolution of 1376×1040 pixels was used for recording the images. The camera has a double shuttering feature, which enables capturing a pair of pictures in a short and controllable time interval. A 50 mm Nikon AF NIKKOR lens with a 12 mm extension tube was used for recording the images.

Figure 5-3 shows a typical PIV image acquired during the experiments. The sand bed is located at the bottom of the picture. The flow seeded with the special tracers' particles (white dots) flows over the bed. DAVIS 8.3.0 software was used for both the image acquisition and the post-processing of pictures. The software was used for adjusting the appropriate parameters during the experiments (such as the time interval between the two images and the laser power) as well as processing and extracting the data from the pictures. Further details regarding the image processing algorithm are given in the next section.

For tracer particles, hollow glass spheres with a mean diameter of 10 microns were used. The tracer particles are nearly neutral in water ($1.1 \pm 0.05 \frac{g}{cc}$) in order to keep them suspended in the flow. Addition of the trace particles is necessary to enhance the spatial resolution of the PIV images and reduce the bias error towards the sand debris (Melling 1997).

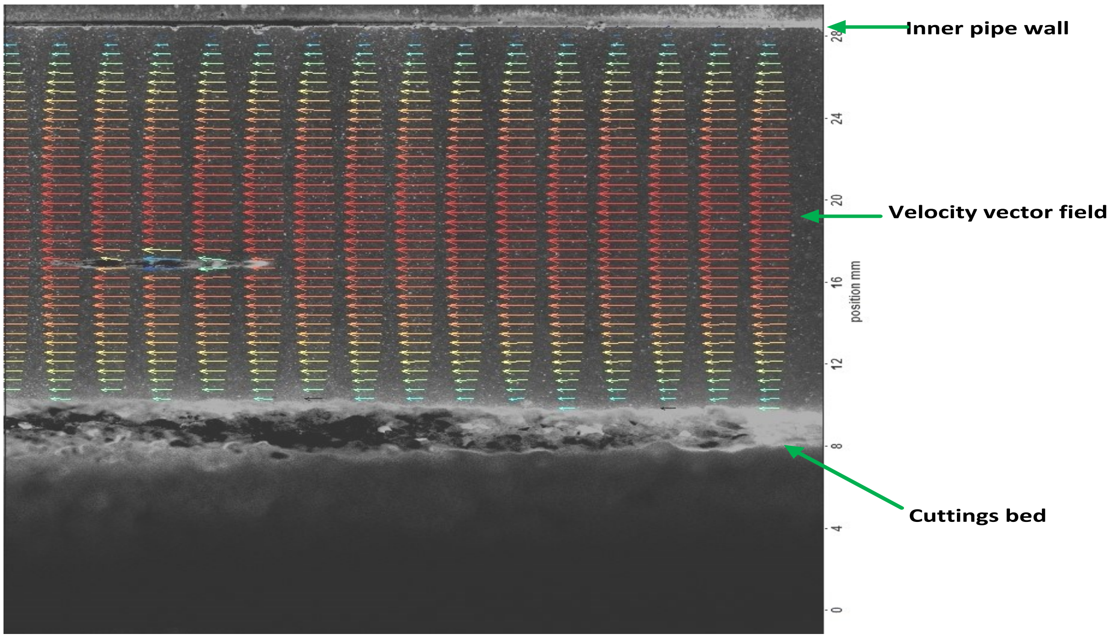

Figure 5-3 The PIV images showing the bed and the tracer particles

5.3.1. PIV Data Post-Processing Procedures

The PIV processing algorithm for velocity calculations follows a cross-correlation based method. After obtaining a pair of images with the tracer particles in the flow, each image is broken down to smaller windows called interrogation windows. The interrogation windows are analyzed in the 2nd image for probable similarities to the same interrogation window in the 1st image (Nezu and Sanjou 2011). To determine the pixel displacement, the cross correlation method was used. This method works by cross correlating the intensity distribution over a small area (the interrogation window) of the flow. The peaks that show the highest correlation are chosen for the most likely destination of the seed particles. After finding the displacement of a seed particle in the two images (Δx and Δy), and having known the time interval (Δt) between the two images, the velocity of the tracer particle or equivalently the fluid velocity vector is calculated as follows:

$$\begin{cases} \hat{u} = \dfrac{\Delta x}{\Delta t} \\ \hat{v} = \dfrac{\Delta y}{\Delta t} \end{cases} \quad \textbf{Eq.(5-1)}$$

The multi-pass cross correlation method with the decreasing of the interrogation window size was used for the particle displacement calculations. An initial interrogation window size of 64×64 pixels followed by the window size of 32×32 pixels was employed in the calculations. The overlap setting was 50%. To enhance the accuracy of the calculated vector fields, the post-processing was also applied on the calculated vectors. The post processing was set to the universal outlier detections.

5.4. Results and Discussions

5.4.1. Fluids characterization

The polymer we used in this study was an anionic water-soluble copolymer of the family of partially-hydrolyzed polyacrylamide (PHPA) polymers. The polymer was in the form of a powder which was easily mixed with tap water. The molecular weight of this polymer is reported to be $10 \times 10^6 \frac{g}{mol}$. Two concentrations of 0.032 and 0.064% (all weight percent) were used for the tests. The mixing and preparation of the solutions were according to the supplier's recommendation.

Rheological characteristics of the fluid samples were determined by using a high-resolution Bohlin C-VOR 150 rheometer. For the range of shear rates encountered in this study, the power law model fits the apparent viscosity data. Figure 5-4 shows the flow behavior curves of the two solutions used here. The K and n values for 0.032 and 0.064% polymer solutions are reported in Eq.(5-2) and Eq.(5-3), respectively.

$$\tau = 0.0046\dot{\gamma}^{0.952} \qquad \textbf{Eq.(5-2)}$$

$$\tau = 0.01226\dot{\gamma}^{0.829} \qquad \textbf{Eq.(5-3)}$$

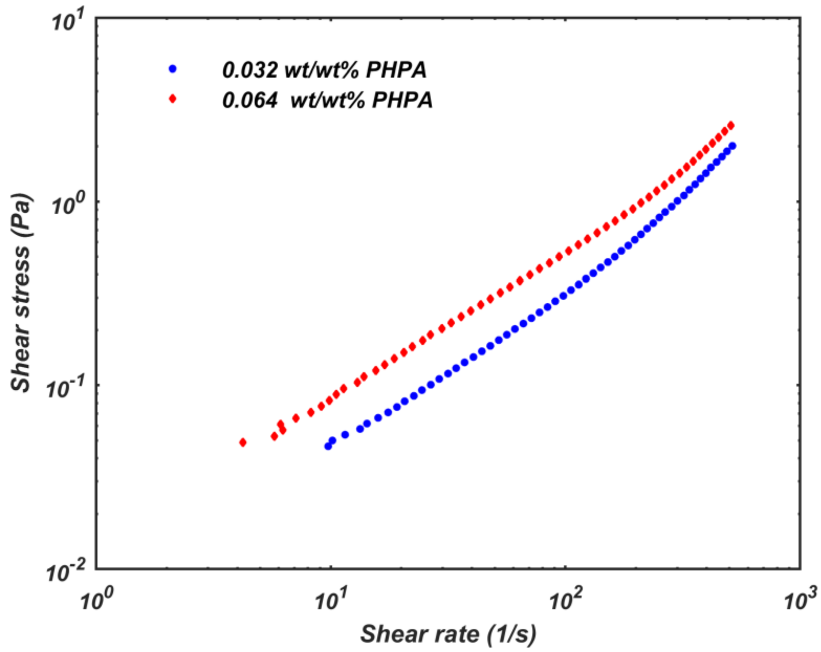

Figure 5-4 Shear stress vs. shear rate data for the two polymer solutions

5.4.2. PIV data

5.4.2.1. Impact of stationary cuttings bed on different aspects of flow

In drilling operations, so often a stationary cuttings bed exists in the horizontal section of the wells. The presence of this cuttings bed causes the flow to adjust its behavior, and hence it affects the performance of the drilling fluid in removing the cuttings properly. It is a common assumption that presence of a stationary bed in lower annulus causes a reduction in fluid velocity and flow rate in the lower annulus. The extents to which the flow velocity and flow rate may reduce have not been studied in the past. Additionally, change in flow velocity and flow rate may cause a shift in the flow regime (turbulent to laminar) in the lower annulus where the cuttings bed exists. The drilling fluid's rheology may also affect the impact of the bed on the flow as well.

From a practical point of view, the parameters that are of importance in hole cleaning are local fluid velocity, shear stress profiles, and turbulence intensity data near the cuttings bed. These parameters are believed to control the interaction of particles and the fluid. Hence, we will discuss these flow properties in detail to assess the impact of the presence of the bed on each of them.

5.4.2.1.1. Mean Velocity Profiles

Figure 5-5 and Figure 5-6 present the time averaged velocity profile data over the stationary cuttings bed for the flow of the 0.032% polymer solution at superficial velocities of 0.48 and 0.56 m/s respectively. The data corresponding to 0.56 m/s is coincided with the critical flow rate at which cuttings start moving on the bed in the form of bedload. Local velocity profiles at both flow rate point to the fact that the mere presence of the cuttings bed causes the flow rate to reduce in the lower annulus. The flow rate is the integral of velocity over the cross-sectional area:

$$Q = \int_A u dA \qquad \textbf{Eq.(5-4)}$$

Where Q is the flow rate, and A is the cross-sectional area. This equation shows the smaller the velocity and cross section, the smaller the flow rate becomes. Therefore, the presence of the cuttings bed causes the flow rate to reduce in the lower annulus by a reduction in both cross-sectional areas and flow velocity. Since the drilling fluid is incompressible, the flow rate in the upper annulus increases to compensate this decrease.

The data of Figure 5-5 & Figure 5-6 shows the presence of a stationary cuttings bed results in redirection of drilling fluid away from the lower annulus. The reduction in the local fluid velocity and flow rate in the lower annulus will negatively affect cutting removal performance of the drilling fluid. A direct consequence of this reduction is that it reduces the carrying capacity of the mud. The presence of a stationary bed results in a more favorable condition for the settling of drill cuttings.

Figure 5-7 reports the local time average velocity profiles for the flow of 0.064% polymer solution over the stationary cuttings bed in both lower and upper annulus at a superficial velocity of 0.48 m/s. These data suggest that reduction of flow rate and velocity in the lower annulus is independent of the solutions concertation. However, an interesting observation here is the parabolic shape of the velocity profiles of the 0.064% polymer solution comparing to 0.032%

solution in the lower annulus. The parabolic shape is a characteristic of the laminar flow. By looking at the velocity profiles' shape, one can say the flow of 0.064% is less turbulent than 0.032%. This is caused by the higher shear viscosity of the 0.064% solution. Although the flow rates and or superficial velocities are similar for both fluids, 0.032% has a smaller viscosity, and hence it is flowing at a higher Reynolds number. The shape of the velocity profile in the lower annulus for 0.064% solution suggests that the flow might be laminar in this part of the annuli because of the reduced velocity and enhanced viscous forces. This can have a negative consequence on hole cleaning as recent studies have shown turbulence is crucial for bed erosion (Diplas et al. 2008, Schmeeckle 2014).

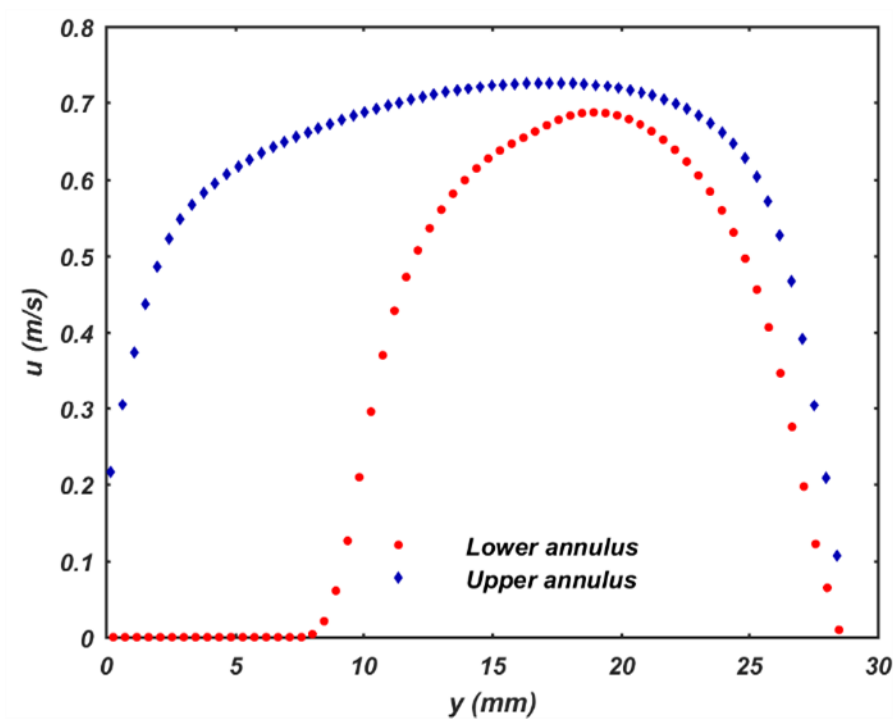

Figure 5-5 Velocity profiles in lower and upper annulus for 0.032% polymer at 0.48 m/s

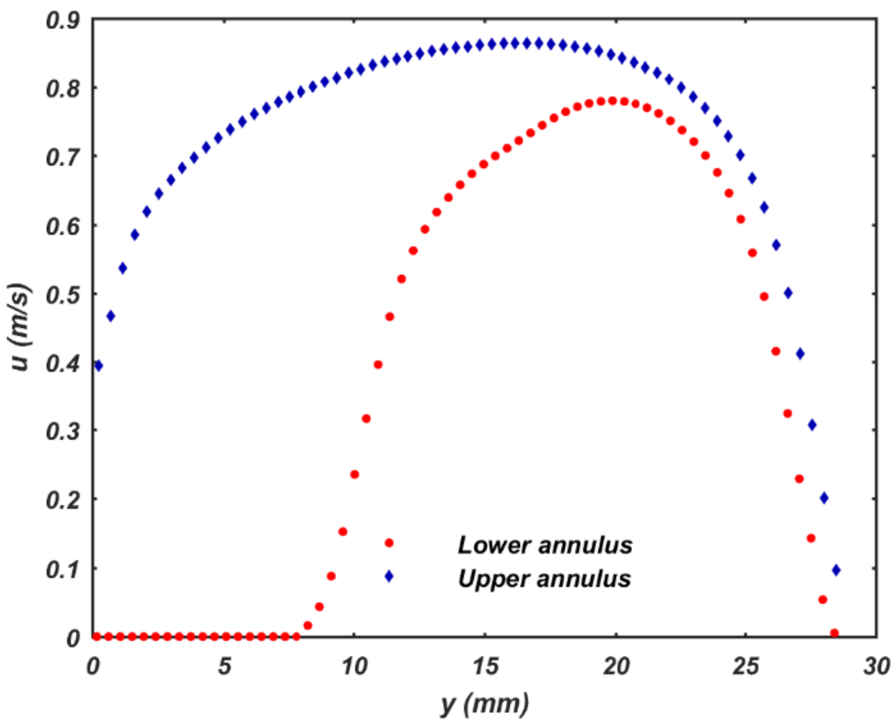

Figure 5-6 Velocity profiles in lower and upper annulus for 0.032% polymer at 0.56 m/s

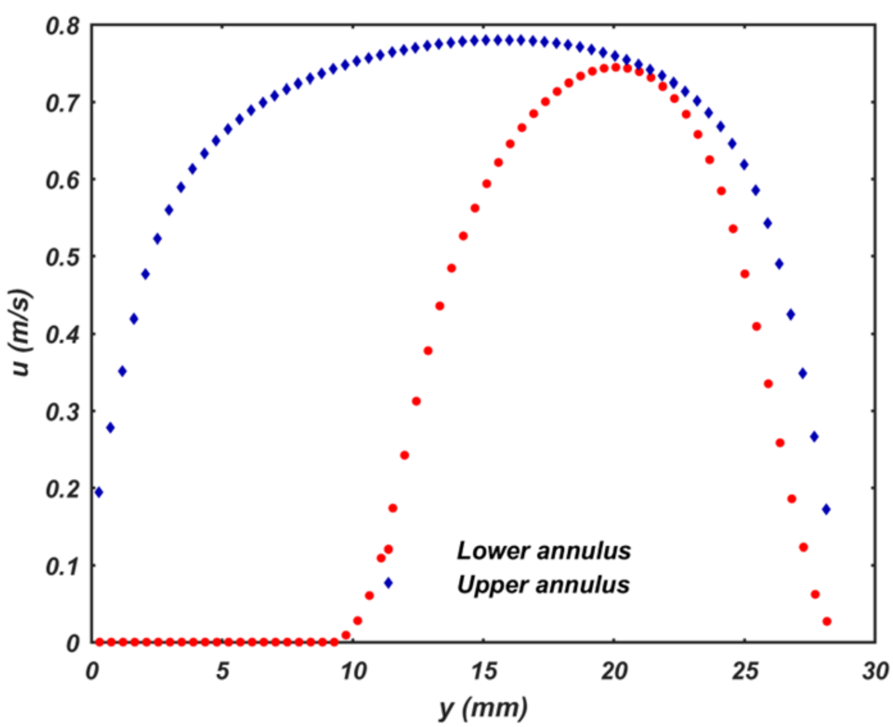

Figure 5-7 Velocity profiles in lower and upper annulus for 0.064% polymer at 0.48 m/s

5.4.2.1.2. *Reynolds shear stress profiles*

Reynolds shear stress or turbulent stress arises due to the velocity fluctuations. The Reynolds shear stress is:

$$\tau_{Re} = -\rho\overline{u'v'} \qquad \textbf{Eq.(5-5)}$$

$Where\ u'$ and v' are the velocity fluctuations in axial an and radial direction respectively.

Figure 5-8 and Figure 5-9 compare the Reynolds shear stress profiles for the flow of 0.032% polymer solution in the lower and upper annulus at two superficial velocities. The data suggest the presence of the cuttings bed causes the Reynolds stress to reduce in the lower annulus significantly. The reduction is more at the lower flow rate. This may have happened because at the lower flow rate the local velocity is low in, the lower annulus and hence the flow is much less turbulent. Another cause can be the movement of the cuttings at the bed interface at higher flow rate. Other studies have shown bedload transport of cuttings may amplify or damp the flow turbulence depending on other parameters (Best et al. 1997, Carbonneau and Bergeron 2000, Bizhani and Kuru 2017). Therefore, the greater reduction in lower flow rate can have different causes.

An interesting feature of Reynolds stress profiles in the upper annulus is that it has higher values near the outer pipe wall. This feature is in contrary to previous findings for the flow of single phase turbulent flow in the annulus (Nouri et al. 1993, Japper-Jaafar et al. 2010). Therefore, in contrast to single phase turbulent flow in the annulus, for turbulent flow over the stationary cutting bed, the level of turbulence is higher near the outer pipe wall.

The reduction in turbulent shear stress in lower annulus suggests hole cleaning will be negatively affected by the presence of the cuttings bed. The presence of the bed causes both flow velocity and turbulent shear stress to reduce near the cuttings bed comparing to that of the upper annulus. The act of allowing the formation of the cuttings bed itself make it harder to erode the bed. Despite that due to limitations imposed by pump or drilling method, the formation of a stationary cuttings bed is almost inevitable (Leising and Walton 2002, Ozbayoglu et al. 2004, Kelessidis and Bandelis 2004a, Li and Luft 2014a, Li and Luft 2014a).

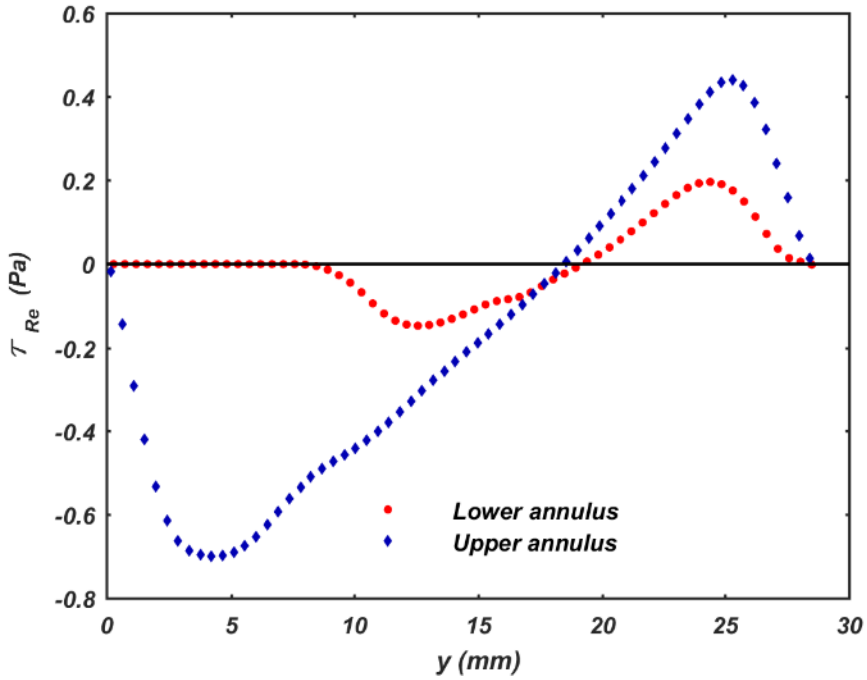

Figure 5-8 Reynolds stress profiles in lower and upper annulus for 0.032% polymer at 0.48 m/s

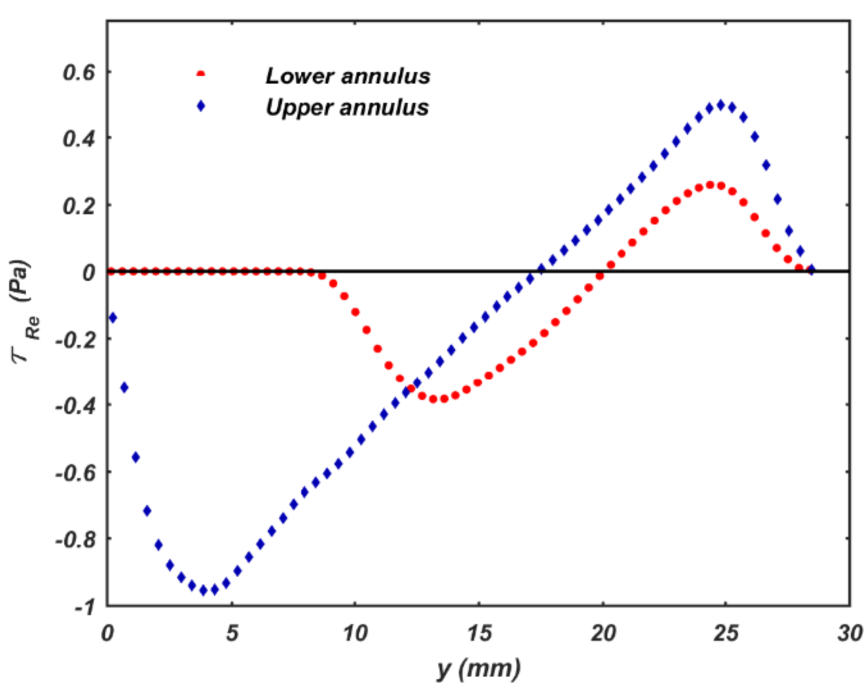

Figure 5-9 Reynolds stress profiles in lower and upper annulus for 0.032% polymer at 0.56 m/s

Figure 5-10 compares the Reynolds shear stress profiles for the flow of 0.064% over the stationary cuttings bed at 0.48 m/s in both lower and upper annulus. The data shows the polymer concentration causes the Reynolds stress to reduce even more than what resulted from the presence of the cuttings bed. Comparing to Reynolds stress in the upper annulus, the lower annulus is almost showing negligible turbulent stress data.

The data of Figure 5-10 is a confirmation of the earlier statement that increasing the polymer concentration (or the viscosity of the solution) drives the flow toward a more laminar state at a fixed flow rate in the lower annulus. Therefore, the parabolic shape of velocity profiles in the lower annulus is accompanied by a severe reduction in the Reynolds stress. This is interesting because this suggests that flow can become essentially laminar in the lower annulus while it is fully turbulent in the upper annulus. This phenomenon is caused by the reduction in local fluid velocity in the lower annulus which causes Reynolds number and inertial forces to decrease.

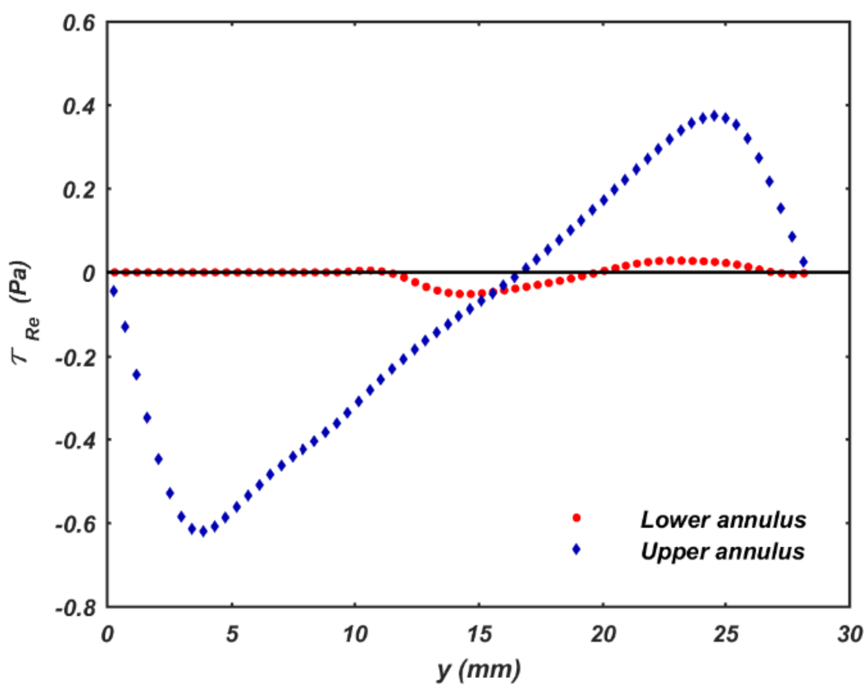

Figure 5-10 Reynolds stress profiles in lower and upper annulus for 0.064% polymer at 0.48 m/s

From a practical point of view, increasing polymer concentration can negatively affect bed erosion not because it reduces the local fluid velocity but because it may result in the transition to flow regime to laminar flow. We know from other studies that turbulence is almost necessary for effective bed erosion (Diplas et al. 2008). Therefore, among other factors that have been discussed in other papers, increasing polymer concentration may result in a local laminar flow in the region near the cuttings bed, and that can hinder effective bed erosion.

5.4.2.1.3. Turbulence intensity profiles

Turbulence intensity or Reynolds normal stress is the RMS (root mean square) of the velocity fluctuations. Turbulence intensity is defined as follows:

$$\tau = 0.0046\dot{\gamma}^{0.952} \qquad \textbf{Eq.(5-6)}$$

Axial turbulence intensity is a measure of velocity fluctuations in the axial direction. A higher turbulence intensity presents a more favorable condition for bed erosion (Diplas et al. 2008).

Figure 5-11 and Figure 5-12 reports the axial turbulence intensity profiles for the flow of 0.032% polymer solution in the lower and upper annulus at two flow rates. Similar to local velocity and turbulent shear stress profiles, the axial intensity decreases in the lower annulus because of the cuttings bed. An interesting feature of the intensity profiles in the upper annulus is that there is a significantly higher turbulence activity near the outer pipe wall (the upper most walls of the annuli). This behavior is different from turbulent flow in an annulus without any cuttings bed. Many of previous studies have shown turbulent activities are higher near the inner wall of the annuli in single phase turbulent flow (Rehme 1974, Japper-Jaafar et al. 2010, Rodriguez-Corredor 2014, Bizhani et al. 2015). Contrary to the previous observations, the presence of a cuttings bed causes a shift in the level of turbulence near the inner wall.

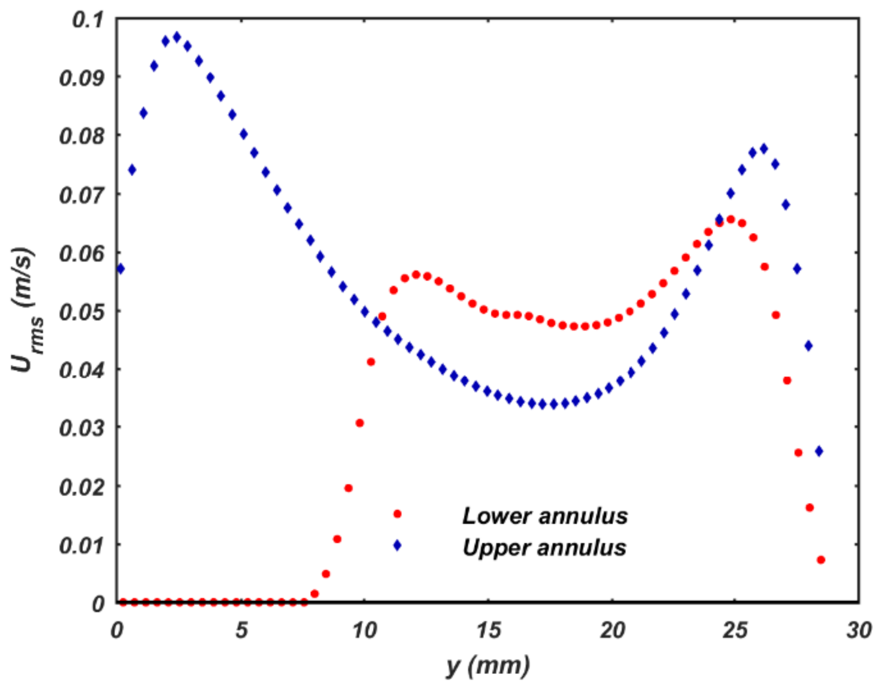

Figure 5-11 U_{rms} profiles in lower and upper annulus for 0.032% polymer at 0.48 m/s

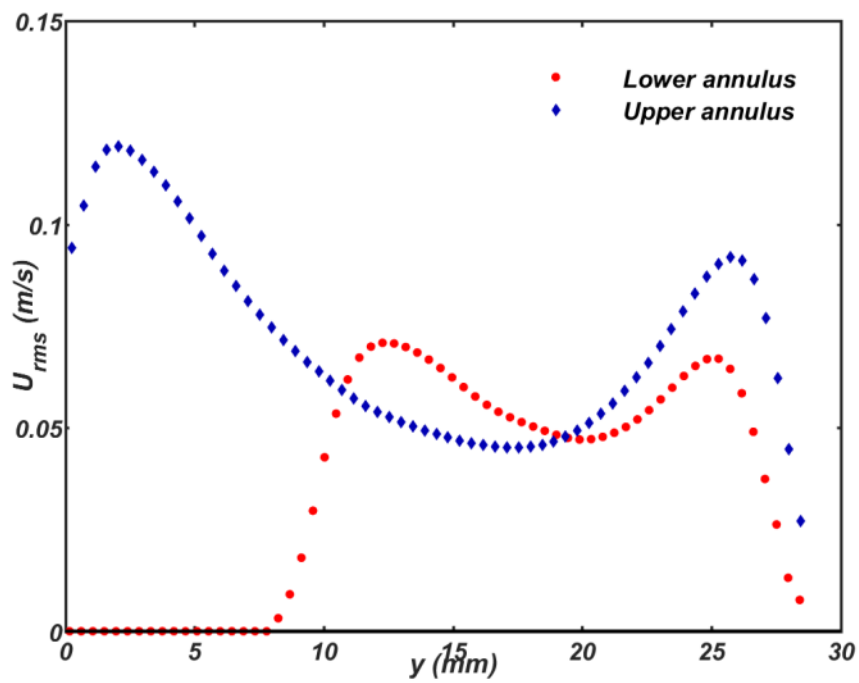

Figure 5-12 U_{rms} profiles in lower and upper annulus for 0.068% polymer at 0.56 m/s

Figure 5-13 reports the axial intensity profiles for the flow of 0.064% polymer solution at a superficial velocity of 0.48 m/s in both lower and upper annulus. Similar to 0.032% solution, a reduction occurs in the lower annulus due to the presence of the cuttings bed. The axial intensity data shows a significantly higher level of turbulence comparing to that of Reynolds shear stress for 0.064% solution. This suggests that the vast reduction in Reynolds shear stress (presented in Figure 5-10) has mainly occurred because of reduction in radial turbulence intensity. Indeed this behavior is associated with the turbulent flow of polymeric fluids (Nouri et al. 1993, Warholic et al. 2001, Ptasinski et al. 2003, Bizhani et al. 2015).

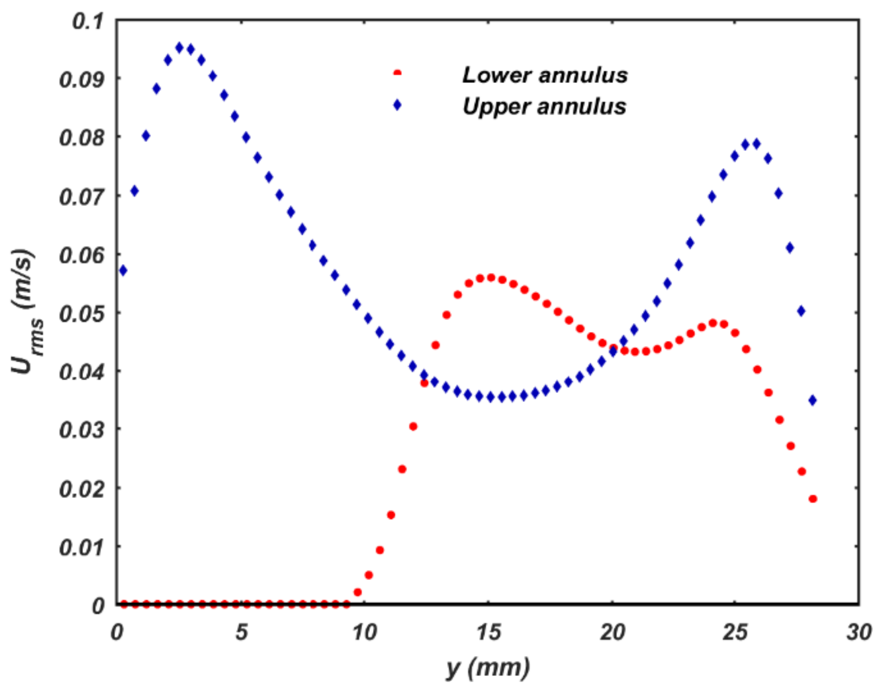

Figure 5-13 U_{rms} profiles in lower and upper annulus for 0.064% polymer at 0.48 m/s

5.4.2.2. Impact of polymer concertation on the flow

Increasing the polymer concentration negatively affects hole cleaning in a sense it causes the minimum flow rate to increase significantly (Bizhani et al. 2016). In this particular study increasing the polymer concentration from 0.032% to 0.064% caused the critical flow rate of bed erosion to increase from 200 lit/min to 256 lit/min. The poor performance of concentrated polymer solution is usually associated with a reduction of flow turbulence (Azar and Sanchez

1997, Li et al. 2005). In this section, we try to compare different aspects of flow in the lower and upper annulus for the flow of the two polymer solutions at the same flow rate to see what exactly happens when polymer concertation is increased.

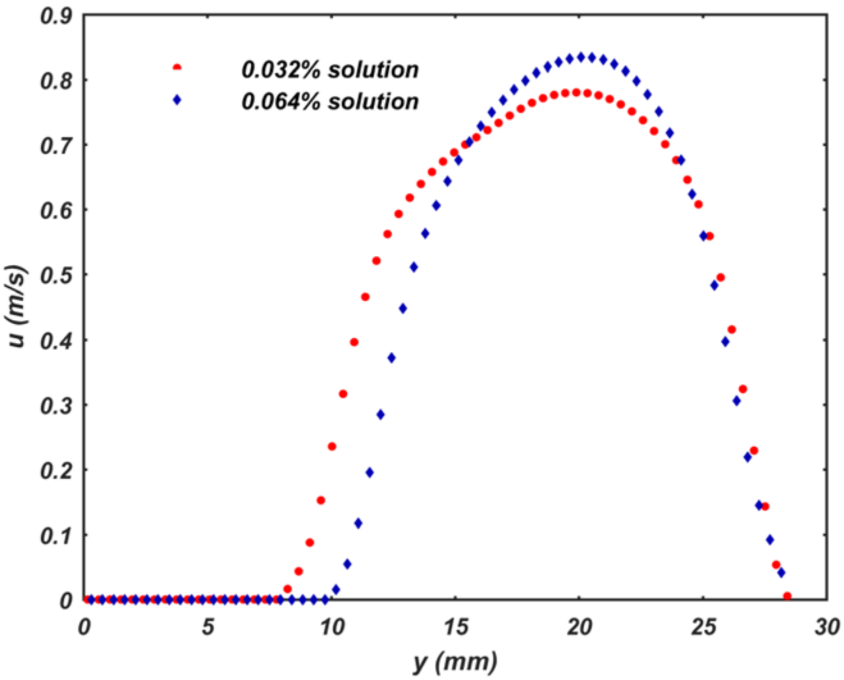

Figure 5-14 Comparison of velocity profiles in lower annulus for flow of 0.032% and 0.064% polymer solution at $U_s = 0.56\frac{m}{s}$

Figure 5-14 and Figure 5-15 compare the velocity profiles in the lower an upper annulus for the flow of the two polymer solutions at the superficial velocity of 0.56m/s respectively. Velocity profiles in the lower annulus show a small difference in term of the shape of the profiles. The profile for the more concentered solution is more parabolic while 0.032% polymer solution shows a flatter profile. This difference in shape is of particular importance because it reveals 0.064% solution exhibits a laminar like profile while 0.032% solution shows a profile like turbulent flows. On the other hand, both polymers are showing similarities in term of velocity magnitude in the lower annulus. This observation implies magnitude of velocity and flow rate in the lower annulus is only affected by the cuttings bed height and not by the fluid type and rheology. While local velocity is not affected by the fluid rheology, the local flow regime is affected by the fluid rheology. For a more viscous fluid, the flow regime would be closer to laminar flow. Therefore, we can conclude that increasing the polymer concentration does not affect the local velocity value in the lower annulus. However, it can influence the shape of the profile because of the flow regime differences.

Comparison of velocity profiles in the upper annulus (Figure 5-15) shows no significant difference between the two fluids. This implies the velocity and flow rate in the upper annulus is only a function of the bed height and not the fluid type. Unlike the lower annulus, both velocity profiles are showing similar shape in the upper annulus.

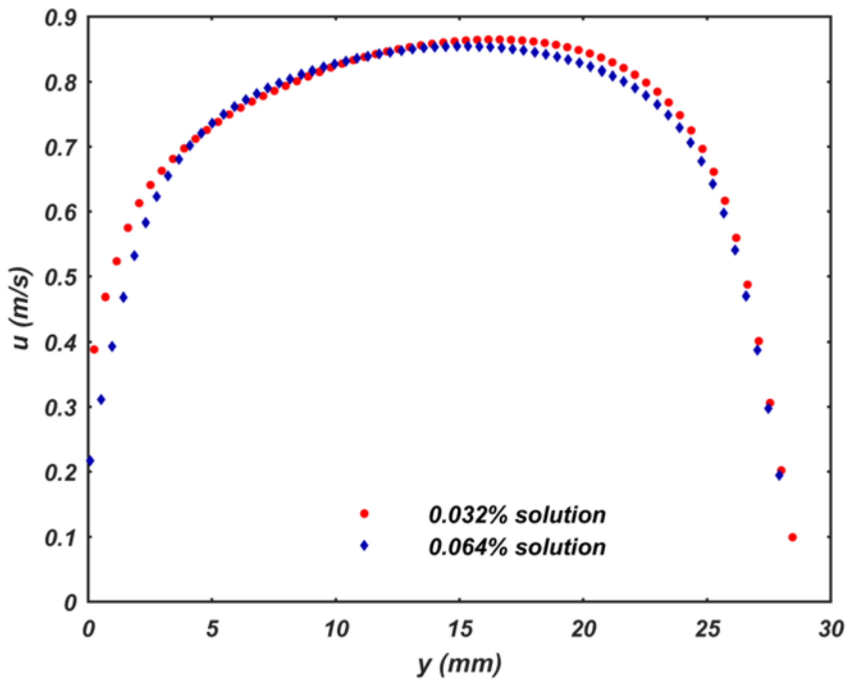

Figure 5-15 Comparison of velocity profiles in upper annulus for flow of 0.032% and 0.064% polymer solution at $U_s = 0.56\frac{m}{s}$

Figure 5-16 and Figure 5-17 compare the Reynolds shear stress profiles for flow of 0.032% and 0.064% polymer solutions in the lower and upper annulus at 0.56 m/s respectively. Reynolds shear stress reduces in the lower annulus as a result of increasing the polymer concentration. The reason for this is because of the increase in the shear viscosity and hence reduction in the flow Reynolds number. Therefore, with the presence of a stationary cuttings bed increasing the polymer concentration causes the Reynolds stress to decrease. The Reynolds shear stress does not have a direct relation with particles removed from the bed. However, reduction in Reynolds stress means less turbulence which may affect cuttings removal in a negative manner (Diplas et al. 2008).

Reynolds stress profiles in the upper annulus show a slight reduction as a result of increasing the concetation. However, the reduction of Reynolds stress in the upper annulus is much less than what happens in the lower annulus. The reduction of Reynolds shear stress is expected because of the increase in the shear viscosity which leads to a decrease in Reynolds number. Reduction in Reynolds number means a smaller Reynolds or turbulent stress.

In term of hole cleaning performance, one cannot judge the performance of each fluid solely based on turbulent stresses; that is because another component of shear stress at the bed interface is the viscous part. What is important in sediment transport is the total fluid shear stress at the bed interface. Hence, the mere reduction in Reynolds shear stress cannot be considered as the main reason for the increase in the critical flow rate associated with the thicker fluid. The total shear stress must be considered.

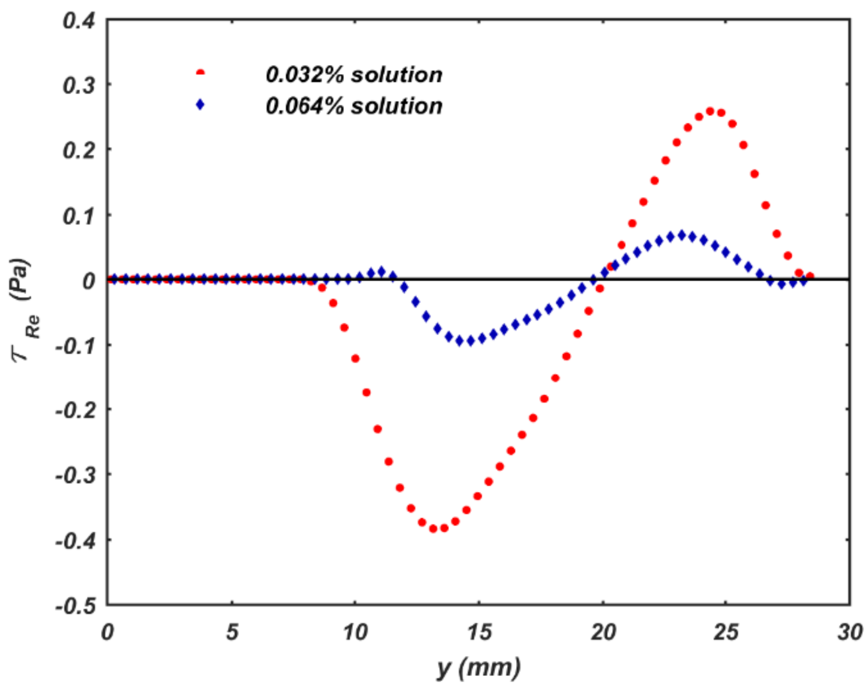

Figure 5-16 Comparison of Reynolds stress profiles in lower annulus for flow of 0.032% and 0.064% polymer solution at $U_s = 0.56\frac{m}{s}$

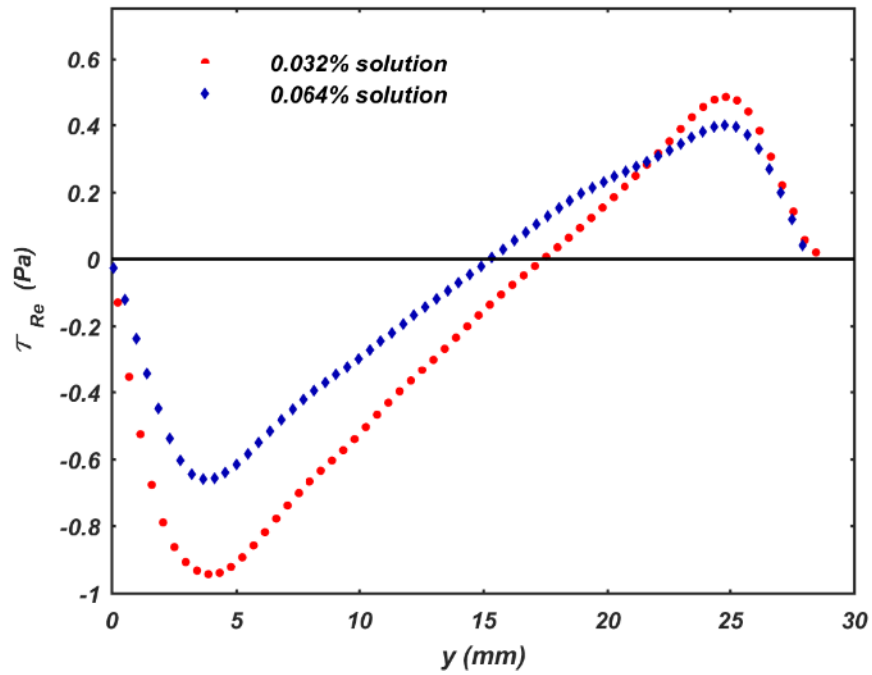

Figure 5-17 Comparison of Reynolds stress profiles in upper annulus for flow of 0.032% and 0.064% polymer solution at $U_s = 0.56\,\frac{m}{s}$

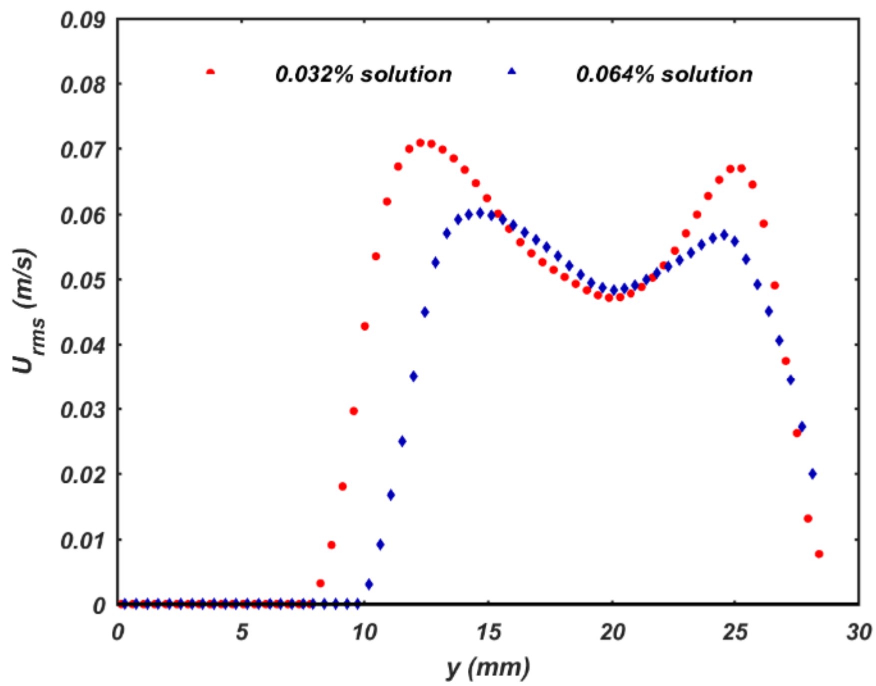

Figure 5-18 Comparison of axial turbulence intensity profiles in lower annulus for flow of 0.032% and 0.064% polymer solution at $U_s = 0.56\,\frac{m}{s}$

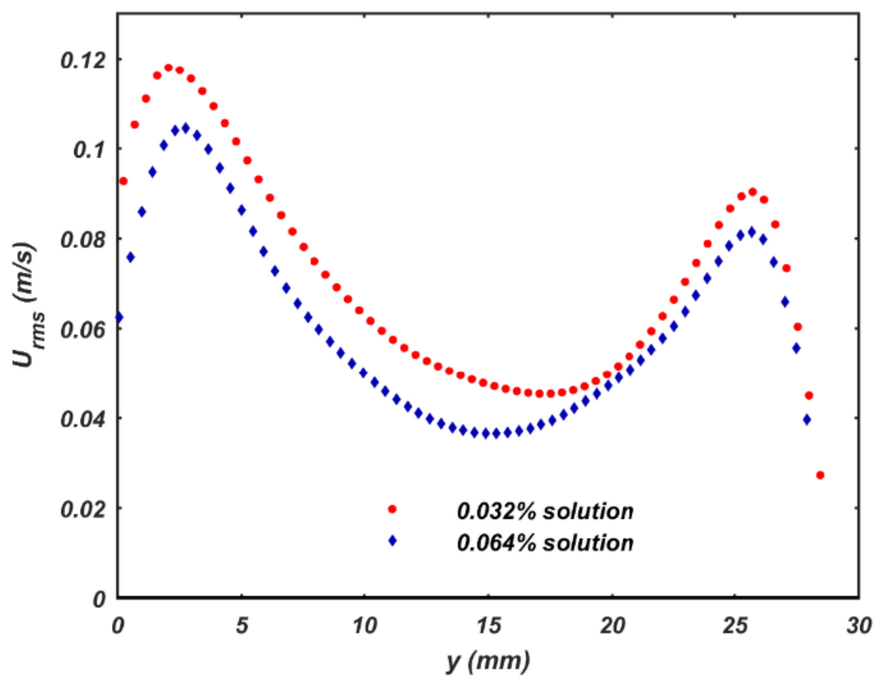

Figure 5-19 Comparison of axial turbulence intensity profiles in upper annulus for flow of 0.032% and 0.064% polymer solution at $U_s = 0.56\,\frac{m}{s}$

Finally, we compare the axial turbulence intensity profiles of the two polymers at a superficial velocity of 0.56 m/s in Figure 5-18 and Figure 5-19. A slight reduction in turbulence intensity is observed in the lower annulus as a result of enhancing polymer concentration. The upper annulus data show similar profiles which mean no significant change. The difference in the level of velocity fluctuations in not significant in the lower annulus and hence poor hole cleaning performance of higher polymer concentration cannot be associated with the reduction of flow turbulence in the lower annulus.

5.5. Discussion on the implications of the results for hole cleaning

Our results indicate the presence of a stationary cuttings bed in the annulus causes the local flow rate and flow velocity to reduce in the lower annulus where the cuttings bed resides. This implies the condition would become more favorable for depositing more cuttings. Due to the reduction of flow velocity and turbulence, carrying capacity of the drilling fluid reduces.

Increasing the polymer concertation does not affect the flow velocity in the lower annulus. However, it affects the turbulence. It causes the flow to be driven to a more laminar state. This in turn can have a negative impact on the cuttings removal.

5.6. Conclusions

Results of an experimental study where the impact of the presence of a stationary sand bed on characteristics of the turbulent flow of polymer solutions in a concentric annulus was examined were presented and discussed. The discussion was focused on important factors and assumptions usually used in the drilling industry for developing effective hole cleaning strategies.

The results revealed the presence of a stationary cuttings bed causes the flow rate and flow velocity to decrease in the lower annulus comparing to that of the upper annulus. The reduction of local velocity was found to be independent of the polymer concentration.

Reynolds shear stress data were also measured and presented for both lower and upper annulus. A reduction in Reynolds stress was observed as a result of the presence of the sand bed in the lower annulus. Furthermore, increasing the polymer concertation caused the Reynolds stress to further decrease in the lower annulus. The data in the upper annulus revealed there Reynolds stress is higher near the wall of the outer pipe; which is in contrary to previous findings for the flow of single phase turbulent flow in the annulus.

Finally, data for axial turbulence intensity were presented and discussed. The axial turbulence intensity showed a decrease in the lower annulus as a result of the presence of the sand bed. Increasing the polymer concentration led to a slight reduction of axial intensity in the lower annulus. Upper annulus data, however, were not affected by increasing the polymer concentration.

5.7. Nomenclature

R	Inner Radius of outer pipe (m)
r	Outer Radius of inner pipe (m)
D_H	Hydraulic Diameter (mm) $(D_o - D_{in})$

D_o	Outer pipe diameter (mm)
D_i	Inner pipe diameter (mm)
y	Distance from outer pipe wall (mm)
L	Pipe length (m)
A	Annular area cross section ($\pi({R_o}^2 - {R_i}^2)$) (m^2)
h	Cuttings bed height (m)
Q	Flow Rate (m^3/s)
U_s	Superficial Bulk velocity ($\frac{m}{s}$)
d_p	Particles diameter (m)
u	Time average velocity ($\frac{m}{s}$)
$\hat{u}$	Instantaneous axial velocity ($\frac{m}{s}$)
$\hat{v}$	Instantaneous radial velocity ($\frac{m}{s}$)
Δt	Time between two cameras frame (s)
Δs	Displacement of tracer particles (m)
Δx	Axial displacement of tracer particles (m)
Δy	Radial displacement of tracer particles (m)
ρ	Density $\left(\frac{Kg}{m^3}\right)$
η	Fluid viscosity ($Pa.s$)
τ	Shear Stress (Pa)
τ_{Re}	Reynolds stress $= -\rho\overline{u'v'}$ (Pa)
u'	Axial Fluctuation Velocity ($\frac{m}{s}$)
v'	Radial Fluctuation Velocity ($\frac{m}{s}$)

κ von Karman constant (0.41)

u_τ Friction velocity ($\frac{m}{s}$)

5.8. References

Azar, J. J. and Sanchez, R. A. (1997). Important Issues in Cuttings Transport for Drilling Directional Wells. Fifth Latin American and Caribbaean Petroleum Engineering Conference and Exibition. held in Rio de Janeiro, Brazil, 30 August -3 Spetember 1997, SPE-39020-MS,DOI: 10.2118/39020-MS.

Best, J., Bennett, S., Bridge, J. et al. (1997). Turbulence modulation and particle velocities over flat sand beds at low transport rates. Journal of Hydraulic Engineering-Asce **123**(12): 1118-1129, J Hydraul Eng-Asce, DOI: c 10.1061/(Asce)0733-9429(1997)123:12(1118).

Bizhani, M., Corredor, F. E. R. and Kuru, E. (2016). Quantitative Evaluation of Critical Conditions Required for Effective Hole Cleaning in Coiled-Tubing Drilling of Horizontal Wells. **SPE** Drilling & Completion **31**(3): 188-199, DOI: http://dx.doi.org/10.2118/174404-PA.

Bizhani, M. and Kuru, E. (2017). Effect of Sand Bed Deposits on the Characteristics of Turbulent Flow of Water in Horizontal Annuli ASME fluid engineering, Paper under review.

Bizhani, M., Kuru, E. and Ghaemi, S. (2016). Effect of Near Wall Turbulence on the Particle Removal from Bed Deposits in Horizontal Wells. Proceedings of the Asme 35th International Conference on Ocean, Offshore and Arctic Engineering , 2016, Vol 8.

Bizhani, M., Rodriguez-Corredor, F. E. and Kuru, E. (2015). An Experimental Study of Turbulent Non-Newtonian Fluid Flow in Concentric Annuli using Particle Image Velocimetry Technique. Flow Turbulence and Combustion **94**(3): 527-554, Flow Turbul Combust, DOI: 10.1007/s10494-014-9589-6.

Carbonneau, P. E. and Bergeron, N. E. (2000). The effect of bedload transport on mean and turbulent flow properties. Geomorphology **35**(3-4): 267-278, Geomorphology, DOI: g10.1016/S0169-555x(00)00046-5.

Chung, S. Y., Rhee, G. H. and Sung, H. J. (2002). Direct numerical simulation of turbulent concentric annular pipe flow - Part 1: Flow field. International Journal of Heat and Fluid Flow **23**(4): 426-440, Int J Heat Fluid Fl, DOI: 10.1016/S0142-727X(02)00140-6.

Diplas, P., Dancey, C. L., Celik, A. O. et al. (2008). The Role of Impulse on the Initiation of Particle Movement Under Turbulent Flow Conditions. Science **322**(5902): 717-720, Science, DOI: 10.1126/science.1158954.

Escudier, M. P. and Gouldson, I. W. (1995). Concentric Annular-Flow with Centerbody Rotation of a Newtonian and a Shear-Thinning Liquid. International Journal of Heat and Fluid Flow **16**(3): 156-162, Int J Heat Fluid Fl, DOI: 10.1016/0142-727x(95)00012-F.

Ghaemi, S., Rafati, S.,Bizhani, M., Kuru, E. (2015). Turbulent structure at the midsection of an annular flow. Physics of Fluids **27**(10): 105102, DOI: http://dx.doi.org/10.1063/1.4932109.

Green, M. D., Thomesen, C. R., Wolfson, L. et al. (1999). An Integrated Solution of Extended-Reach Drilling Problems in the Niakuk Field, Alaska: Part II- Hydraulics, Cuttings Transport and PWD, SPE-56564-MS,DOI: 10.2118/56564-MS.

Japper-Jaafar, A., Escudier, M. P. and Poole, R. J. (2010). Laminar, transitional and turbulent annular flow of drag-reducing polymer solutions. Journal of Non-Newtonian Fluid Mechanics **165**(19-20): 1357-1372, J Non-Newton Fluid, DOI: 10.1016/j.jnnfm.2010.07.001.

Kelessidis, V. C. and Bandelis, G. E. (2004). Flow patterns and minimum suspension velocity for efficient cuttings transport in horizontal and deviated wells in coiled-tubing drilling. SPE Drilling & Completion **19**(4): 213-227, SPE-81746-PA.

Lawn, C. J. and Elliott, C. J. (1972). Fully Developed Turbulent-Flow through Concentric Annuli. Journal of Mechanical Engineering Science **14**(3): 195-204, J Mech Eng Sci, DOI: 10.1243/JMES_JOUR_1972_014_027_02.

Leising, L. J. and Walton, I. C. (2002). Cuttings-Transport Problems and Solutions in Coiled-Tubing Drilling. SPE Drilling & Completion **17**(1): 54-66, SPE-77261-PA, DOI: 10.2118/77261-PA.

Li, J. and Luft, B. (2014a). Overview Solids Transport Study and Application in Oil-Gas Industry-Theoretical Work. Paper presented at International Petroleum Technology

Conference Kuala Lumpur, Malaysia, 10-12 December 2014. Kuala Lumpur, Malaysia, 10-12 December 2014, IPTC-17832-MS,DOI: 10.2523/IPTC-17832-MS.

Li, J. and Luft, B. (2014b). Overview of Solids Transport Studies and Applications in Oil and Gas Industry - Experimental Work. SPE Russian Oil and Gas Exploration & Production Technical Conference and Exhibition. Moscow, Russia, 14-16 October, SPE-171285-MS,DOI: 10.2118/171285-MS.

Li, J., Wilde, G. and Crabtree, A. R. (2005). Do Complex Super-Gel Liquids Perform Better Than Simple Linear Liquids in Hole Cleaning With Coiled Tubing? SPE/ICoTA Coiled Tubing Conference and Exibition The Woodlands, Texas, USA, 12-13 April 2005, SPE-94185-MS,DOI: 10.2118/94185-MS.

Melling, A. (1997). Tracer particles and seeding for particle image velocimetry. Measurement Science & Technology **8**(12): 1406-1416, Meas Sci Technol, DOI: 10.1088/0957-0233/8/12/005.

Miyazaki, K., Chen, G. , Ymamoto, F., Ohta, J., Murai, Y., Horii, K. (1999). PIV measurement of particle motion in spiral gas-solid two-phase flow. Experimental Thermal and Fluid Science **19**(4): 194-203, Exp Therm Fluid Sci, DOI: 10.1016/S0894-1777(99)00020-5.

Nezu, I. and Sanjou, M. (2011). PIV and PTV measurements in hydro-sciences with focus on turbulent open-channel flows. Journal of Hydro-Environment Research **5**(4): 215-230, J Hydro-Environ Res, DOI: 10.1016/j.jher.2011.05.004.

Nouri, J. M., Umur, H. and Whitelaw, J. H. (1993). Flow of Newtonian and Non-Newtonian Fluids in Concentric and Eccentric Annuli. Journal of Fluid Mechanics **253**: 617-641, J Fluid Mech, DOI: 10.1017/S0022112093001922.

Ozbayoglu, M. E., Miska, S. Z., Reed, T. et al. (2004). Analysis of the Effects of Major Drilling Parameters on Cuttings Transport Efficiency for High-Angle Wells in Coiled Tubing Drilling Operations. SPE/ICoTA Coiled Tubing Conference and Exibition. Huston, Texas, USA, 23-24 March 2004, SPE-89334-MS,DOI: 10.2118/89334-MS.

Poole, R. J. (2010). Development-Length Requirements for Fully Developed Laminar Flow in Concentric Annuli. Journal of Fluids Engineering-Transactions of the **Asme 132**(6), J Fluid Eng-T Asme, DOI: 10.1115/1.4001694.

Ptasinski, P. K., Boersma, B. J., Nieuwstadt, F. T. M. et al. (2003). Turbulent channel flow near maximum drag reduction: simulations, experiments and mechanisms. Journal of Fluid Mechanics **490**: 251-291, J Fluid Mech, DOI: 10.1017/S0022112003005305.

Rehme, K. (1974). Turbulent-Flow in Smooth Concentric Annuli with Small Radius Ratios. Journal of Fluid Mechanics **64**(2): 263-287, J Fluid Mech, DOI: http://dx.doi.org/10.1017/S0022112074002394.

Rehme, K. (1975). Turbulence Measurements in Smooth Concentric Annuli with Small Radius Ratios. Journal of Fluid Mechanics **72**(Nov11): 189-206, J Fluid Mech, DOI: Doi 10.1017/S0022112075003023.

Rodriguez-Corredor, F. E., Bizhani, M. and Kuru, E. (2015). Experimental Investigation of Drag Reducing Fluid Flow in Annular Geometry Using Particle Image Velocimetry Technique. Journal of Fluids Engineering-Transactions of the **Asme 137**(8), J Fluid Eng-T Asme, DOI: 10.1115/1.4030287.

Rodriguez-Corredor, F. E., Bizhani, M., Ashrafuzzaman, M., Kuru, E. (2014). An Experimental Investigation of Turbulent Water Flow in Concentric Annulus Using Particle Image Velocimetry Technique. Journal of Fluids Engineering-Transactions of the **Asme 136**(5), J Fluid Eng-T Asme, DOI: 10.1115/1.4026136.

Schmeeckle, M. W. (2014). Numerical simulation of turbulence and sediment transport of medium sand. Journal of Geophysical Research-Earth Surface **119**(6): 1240-1262, J Geophys Res-Earth, DOI: 10.1002/2013jf002911.

Warholic, M. D., Heist, D. K., Katcher, M. et al. (2001). A study with particle-image velocimetry of the influence of drag-reducing polymers on the structure of turbulence. Experiments in Fluids **31**(5): 474-483, Exp Fluids, DOI: DOI 10.1007/s003480100288.

Yan, F. and Rinoshika, A. (2011). Application of high-speed PIV and image processing to measuring particle velocity and concentration in a horizontal pneumatic conveying with dune model. Powder Technology **208**(1): 158-165, Powder Technol, DOI: 10.1016/j.powtec.2010.12.014.

Yan, F. and Rinoshika, A. (2012). Characteristics of particle velocity and concentration in a horizontal self-excited gas-solid two-phase pipe flow of using soft fins. International Journal of Multiphase Flow **41**: 68-76, Int J Multiphas Flow, DOI: 10.1016/j.ijmultiphaseflow.2012.01.004.

6. Quantitative Evaluation of Critical Conditions Required for Effective Hole Cleaning in Coiled Tubing Drilling of Horizontal Wells[6]

This chapter summarizes the results of the macroscopic investigation of hole cleaning performance of different drilling fluids and drill cuttings. The results have been obtained using a high-speed video camera for identification of the onset of bed erosion under different conditions. Additionally, the frictional pressure losses are measured and used for development of two empirical models for prediction of onset of bed erosion.

6.1. Abstract

The problem of solid clean out in horizontal wellbores was studied experimentally. The special case of drilling fluid circulation with no inner pipe rotation was considered. This case is similar to Coiled Tubing (CT) drilling where frequent hole cleanout must be performed. Sand sized cuttings (ranging from 260 microns to 1240 micron) were used. Critical velocity and wall shear stress required for initiating bed erosion were measured. Water and viscous polymer base fluids with three different polymer concentrations were used.

Results have shown that water always initiates cuttings movement at lower flow rates than polymer solutions. Fluids with higher polymer concentration (and higher viscosity) required higher flow rates to start eroding the bed. Critical wall shear stress was also determined from pressure loss measurements. Analyzing the data revealed that water initiates cuttings removal at

[6] A version of this chapter has been presented as: Bizhani, M., Corredor, F.E.R, Kuru, E., 2016, “Hole Cleaning Performance of Water vs. Polymer-Based Fluids under Turbulent Flow Conditions”, Paper presented at SPE heavy oil conference held in Calgary, Alberta, June 2015

Bizhani, M., Corredor, F.E.R, Kuru, E., 2016, “Quantitative Evaluation of Critical Conditions Required for Effective Hole Cleaning in Coiled Tubing Drilling of Horizontal Wells,” SPE Drilling & Completion, SPE-174404-PA, **31**(3), http://dx.doi.org/10.2118/174404-PA

lower pressure loss than more viscous fluids. Higher viscosity fluids always showed higher pressure loss at the initiation of bed erosion.

For the range of cuttings size studied, results show that an intermediate cuttings size was slightly easier to remove. However, the impact of cuttings size was far less than that of fluid rheology. Overall cuttings size was found to have a small impact on hole cleaning.

Dimensionless analysis of relevant parameters to the process of cuttings movement was performed. It was shown that dimensionless wall shear stress (in the forms of Shields' stress and also ratio of shear velocity to settling velocity) at the onset of bed erosion correlated well with particle Reynolds number. Based on this finding two correlations were developed to predict critical wall shear stress. A procedure was developed to calculate critical flow rate as well. Friction factor data for the flow through annulus with a stationary cuttings bed is also reported.

Keywords: Hole cleaning, horizontal wellbore, non-Newtonian fluids, turbulent flow, critical shear stress

6.2. Introduction

When drilling highly inclined and long horizontal wells, drilled solids tend to settle down on the low side of the wellbore and form a stationary bed. Presence of stationary cuttings bed deposits often causes operational difficulties such as bridging, pack-off, hole fill, excessive torque and drag, bit balling, slow drilling rates, hindering the casing or liner to be run into its desired position, and in severe cases, stuck pipe, lost circulation, and even loss of well control. Therefore, occasionally, drilling must stop to clean the stationary bed. Stopping drilling to clean the well is expensive and must be done promptly. Therefore, this process must be optimized for both proper hole cleaning and faster operation. An optimum combination of fluid rheological properties and flow rate must be determined to minimize the cleaning time.

The problem of cuttings transport in highly inclined wellbores has been investigated since the early 1980s. Numerous experimental studies were conducted to study the impact of different parameters on hole cleaning. Comprehensive reviews of the past work could be found in papers written by (Pilehvari et al. 1996, Kelessidis et al. 2002, Nazari et al. 2010, Xiaofeng et al. 2013, Li and Luft 2014a, Li and Luft 2014a). Parameters affecting cuttings transport could be categorized into three groups (Bilgesu et al. 2007): fluid characteristics, cuttings related factors, and operational variables.

Operational variables include the rate of penetration (ROP), flow rate, hole inclination, inner pipe rotation speed, and eccentricity. Higher flow rates are always favorable as they promote turbulence (Azar and Sanchez 1997) and expedite bed erosion rate (Adari et al. 2000). However, the maximum flow rate is often limited by pump hydraulics, bore hole washout and in the case of CT applications by the down hole motor (Leising and Walton 2002, Kelessidis and Bandelis 2004a). To eliminate this limitation, recently Allahvirdizadeh et al. (2015) investigated the technical feasibility of using polymer based drag reducing fluids for cuttings transport while keeping the frictional pressure loss on the low side.

Eccentricity has been reported to have an adverse impact as it drives the fluid away from the narrower gap where cuttings tend to go (Thomas et al. 1982, Azar and Sanchez 1997, Li and Luft 2014a). Inner pipe rotation enhances cuttings transport, but it is absent in coiled tubing intervention (Leising and Walton 2002, Kelessidis and Bandelis 2004a, Li et al. 2008). A higher ROP introduces more cuttings into the annulus and, therefore, more cuttings must be removed. Higher ROP always causes a higher concentration of cuttings in the annulus (Li and Luft 2014a).

Hole inclination angle has a profound influence on cuttings transport (Tomren et al. 1986, Pilehvari et al. 1996, Larsen et al. 1997). For angles of inclination less than 10 degrees, cuttings transport remains similar to the vertical case. For larger inclination angles dramatic reductions occur in the cuttings transport ability. The main reason for this is the decrease in the vertical component of the fluid velocity (Ramadan et al. 2003). The experimental study by Tomren et al. (1986) showed cutting beds could form at low flow rates at angles of inclination as low as 20 degrees. At inclination angles between 35 to 55 degrees, back sliding of cuttings may occur (Li and Luft 2014a). This effect is known as the “avalanche” effect.

Size, shape, and density of drilled cuttings are the important properties of cuttings; however, there is little control over these parameters as they are dictated by the type of bit used and other conditions. Many of the previous studies on cuttings transport considered large cuttings, e.g. greater than 2 mm (Brown et al. 1989, Martins and Santana 1992). In certain situations fine cuttings are produced; for example using PDC bits in CT interventions (Leising and Walton

2002). According to Pilehvari et al. (1996) and based on the results of experiments conducted by Larsen et al. (1997), small cuttings (0.1 in = 2.54 mm) are harder to remove than bigger cuttings.

Fluid properties, which affect cuttings transport, are density and rheological characteristics. Higher mud weights improve cuttings transport but cause a reduction in the rate of penetration (Martins and Santana 1992, Azar and Sanchez 1997). The primary function of fluid density is to provide the hydrostatic pressure needed to prevent the influx of formation fluid into the wellbore. Therefore, it cannot be used for optimizing the cuttings transport process. The upper limit of the mud density is dictated by a formation's fracture pressure.

Rheological characteristics of the fluid have a rather more complicated impact on the cuttings transport. The problem of cuttings transport, while cuttings are in suspension, is different from eroding a deposited cuttings bed. According to Azar and Sanchez (1997), high fluid viscosity reduces the good cleaning ability in deviated wells. The main functionality of the fluid viscosity is to keep the weighting agents suspended and, therefore, justification must be made in selecting the appropriate amount of viscosifier to be used. Saasen and Løklingholm (2002) pointed out that Xanthan gum must be utilized as much as necessary to prevent barite sag. The three layer bed model proposed by Cho et al. (2000) suggested that a decrease in the flow behavior index would increase bed thickness. Leising and Walton (2002) analyzed three cases of high, medium and low viscosity fluids in coiled tubing drilling (CTD) and recommended low viscosity fluids to be used.

Early investigations on cuttings transport mostly focused on the idea of finding a critical velocity which would prevent the formation of a stationary bed (Li and Luft 2014a). However, in most of the cases prevention of bed formation is impossible. Some experimental work can be found related to bed erosion (Brown et al. 1989, Martins and Santana 1992, Martins et al. 1996, Li and Walker 1999, Adari et al. 2000, Lourenco et al. 2006, Valluri et al. 2006, Rodriguez-Corredor et al. 2014). Adari (1999) and Adari et al. (2000) conducted many experiments to determine the hole clean out time for different conditions. Adari's (1999) study showed that a higher rheology factor (i.e. higher n/K ratio) has better erosion capability. Duan et al. (2007) studied critical re-suspension velocity in an eccentric annulus. Results revealed that water always initiated bed erosion at lower flow rates than Polyanionic Cellulose (PAC) polymer solutions. Less turbulence caused by higher viscosity causes a reduction in erosion capacity of high viscosity fluids (Li et al. 2005). Though previous studies showed water or less viscous fluids have the higher capability in eroding a stationary bed, the thicker fluid has higher suspension ability. The challenge is to keep the solids in suspension and re-entrain the ones already deposited in bed. Ozbayoglu et al. (2004) stated increasing viscosity in CT intervention jobs causes an increase in the thickness of the bed. Walker and Li (2000) have concluded that Hydroxyethyl cellulose (HEC) and Xanvis polymer solutions have a higher carrying capacity compared to water. However, they have less capability for eroding a stationary bed.

In this paper, results of an experimental study on hole cleaning in horizontal wellbores are presented (part of the results included in this paper was also presented in an M.Sc. thesis (Bizhani 2013). The aim of the study is to investigate the critical conditions required to initiate erosion of a stationary bed of cuttings. This is similar to a stationary circulation mode of the solid clean out. The impact of fluid rheology and cutting size are investigated. Natural quartz sands with mean sieve diameters of 260, 350, 600 and 1240 micron and density of 2650 $\frac{kg}{m^3}$ are used to simulate drilled cuttings. Water and viscous fluids prepared with 3 different concentrations of an anionic acrylamide copolymer are used.

6.3. Experimental program

The schematic of the flow loop, which has been used to simulate a horizontal wellbore, is shown in Figure 6-1. The test section is 9-meter-long and made of high-quality optical glass. The inner pipe is also made out of Borosilicate glass with the proper wall thickness to minimize vibration. The outer pipe has an inner diameter of 95 mm; the outer diameter of the inner pipe is 38 mm (hydraulic diameter is 57 mm and radius ratio 0.4).

A 500-litre mixing tank was used for preparing and storing polymer solutions during experiments. An air operated mixer with adjustable rotation per minute (RPM) is utilized for the preparation of the polymer solutions.

The fluid is circulated by using a centrifugal pump. The pump is equipped with a VFD (Variable Frequency Drive). The VFD system allows setting the pump RPM and, hence, the flow rate at any desirable value (ranging from 0 up to 450 liters/min). The flow rate was measured using a magnetic flow meter installed at the inlet of the annular section. The accuracy of the flowmeter is $\pm 0.5\%$.

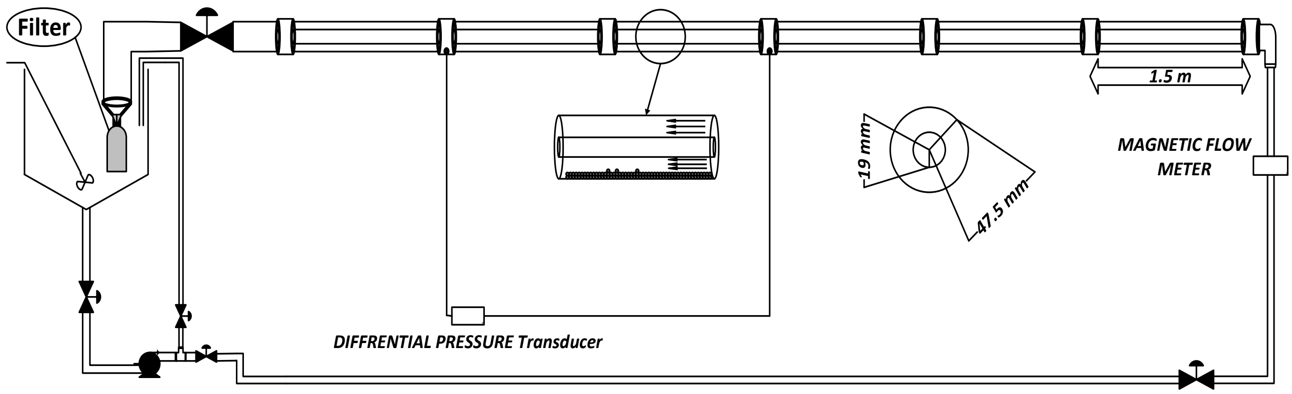

Figure 6-1 Schematic of flow loop

A PX760 type differential pressure transducer with an accuracy of $\pm 0.17\%$ was used to measure the frictional pressure drop. The distance between the two tap lines is 3.08 m. The first tap line is located approximately at $80D_H$ Downstream of the inlet to ensure the flow is fully developed. The second tap line is also far from the outlet end (1.5 m) to avoid any undesired end effects. The measured data includes flow rate and pressure drop. The LabView software was used for data acquisition (National Instrument 2007).

The procedure for conducting experiments is to establish a bed of cuttings first; an example of cuttings bed is shown in Figure 6-2. Once the bed of cuttings is established, the horizontal section of the flow loop is isolated by closing the appropriate valves. The tank, pump and transition pipelines are then washed carefully to remove any cuttings left in these parts. A filter is installed at the outlet of the horizontal section (Figure 6-1). The purpose of installing the filter is to collect the removed cuttings during the experiment.

Figure 6-2 Picture of established cuttings bed ($d_p = 600\ \mu m$)

The movement of the cuttings in the bed was monitored and recorded using a high-resolution camera and a professional quartz light source. The measurements were taken at approximately $100\mathrm{D_H}$ Downstream of the annulus inlet. Experiments start with pumping fluids at low velocity (below the critical velocity of bed erosion). Velocity is increased gradually while monitoring the bed of cuttings for any movement. The procedure is continued until the critical velocity is reached.

6.4. Results and analyses

6.1.1. Rheological characterization of test fluids

For the preparation of polymer solutions used in this study, a water soluble anionic copolymer is used. Reported molecular weight of this polymer is $\mathbf{10 \times 10^6}\ \frac{g}{mol}$. Polymer solutions with 3 concentrations of 0.032, 0.064, and 0.112% (all weight percent) are used. Preparation of polymer solutions is according to supplier's recommendation.

For measuring rheological properties of the polymer solutions, three samples were taken from the annular section of the test facility during each experiment (one at the beginning, one during the experiment and one sample at the end of the test). This step is to make sure that rheology has not changed during the test. Rheological characteristics of the fluid samples were determined by using a high-resolution Bohlin C-VOR 150 rheometer (Bohlin User manuals). Within the range of shear rates experienced in the experiments, the power law model was found to accurately model the shear stress-shear rate relationship of the aqueous polymer solutions. There is a slight variation in fluids rheological parameters (i.e. fluid consistency and behavior index) from one experiment to the other. Table 6-1reports rheological parameters for each of the polymer solutions used in the experiments. An example of curve fitting of rheological data is presented in Figure 6-3.

Table 6-1 Power law constants for the polymer solutions

	$\mathbf{0.032}\frac{\boldsymbol{wt}}{\boldsymbol{wt}}\%$		$\mathbf{0.064}\frac{\boldsymbol{wt}}{\boldsymbol{wt}}\%$		$\mathbf{0.112}\frac{\boldsymbol{wt}}{\boldsymbol{wt}}\%$	
$\boldsymbol{d_p}\ (\boldsymbol{\mu m})$	$\boldsymbol{K}\ (\boldsymbol{Pa.s^n})$	$\boldsymbol{n}$	$\boldsymbol{k}\ (\boldsymbol{Pa.s^n})$	$\boldsymbol{n}$	$\boldsymbol{k}\ (\boldsymbol{Pa.s^n})$	$\boldsymbol{n}$
260	0.0061	0.8923	0.0206	0.7409	-	-
350	0.006	0.8985	0.0175	0.7749	0.0422	0.7069
600	0.0069	0.876	0.0226	0.725	0.0401	0.6986
1240	0.0055	0.9521	0.0166	0.7896	0.0355	0.7253

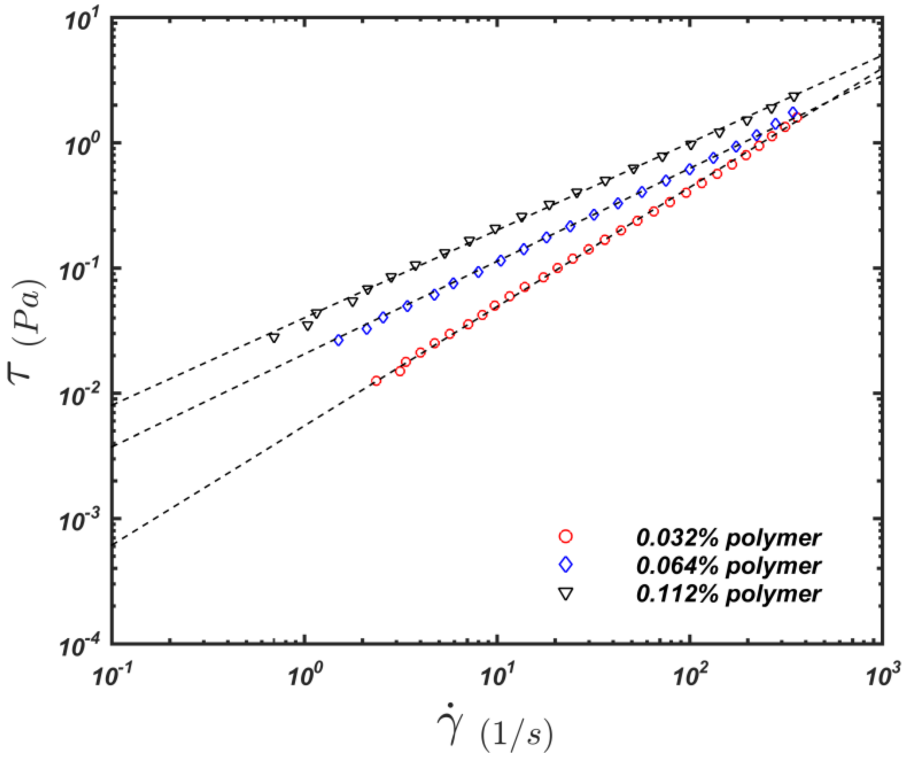

Figure 6-3 Shear stress vs. shear rate relationship for different polymer solutions

6.1.2. Critical conditions of bed erosion

In this section, the data for critical conditions required to initiate cuttings movement are discussed. The critical velocity is defined as the average fluid velocity at which cuttings start to move. This velocity is obtained by monitoring the stationary bed of cuttings and analyzing recorded videos at each flow rate for possible cuttings movement. Average velocity is equal to the flow rate divided by the area open to the flow (for a given bed height and annular geometry, calculation of cross sectional area ($\boldsymbol{A_f}$) available for flow is presented in Appendix A). Critical wall shear stress is obtained by using Eq.(6-2).

$$u = \frac{Q}{A_f}$$ **Eq.(6-1)**

$$\tau_w = \frac{D_H}{4}\left(-\frac{dP}{dL}\right)$$ **Eq.(6-2)**

where Q is the flow rate, D_H is the hydraulic diameter (i.e. $D_H = D_o - D_i$), and $\frac{dP}{dL}$ is the measured frictional pressure loss per unit length.

6.1.2.1. Critical velocity

Table 6-2 shows the critical velocity at the onset of cuttings movement in incipient motion. The data are used to construct Figure 6-4, where performances of different fluids are compared. Results are shown in Table 6-2, and Figure 6-4a indicate that water always initiates cuttings movement at a lower velocity compared to more viscous fluids. As polymer concentration and consequently fluid viscosity increases, progressively higher velocities are needed to start bed erosion. For the smallest size cuttings used (260 microns) the fluid with the highest polymer concentration was not even able to remove the cuttings within the flow rate limit of the pump. These results are in agreement with past studies. Brown et al. (1989), although using much bigger cuttings (6.4 mm), showed that water is more efficient in cleaning a cuttings bed than HEC solutions. Duan et al. (2007) result also suggested that water is favorable for eroding a cuttings bed while polymer solutions are more efficient in preventing the formation of bed. Saasen and Løklingholm (2002) discussed the effect of bed consolidation caused by the interaction of polymer based muds and drilled cuttings and concluded it is best to use Newtonian fluids. Martins and Santana's (1992) experiments revealed that the higher the turbulence, the lower would be the bed thickness. Higher turbulence is achieved when using low viscosity fluids.

Table 6-2 Critical velocities for initiation of cuttings movement ($\frac{m}{s}$)

d_p (μm)	water	0.032% polymer	0.064% polymer	0.112% polymer
260	0.29	0.86	1.04	-
350	0.27	0.85	1.02	1.12
600	0.25	0.65	0.75	1.04
1240	0.33	0.72	0.8	0.96

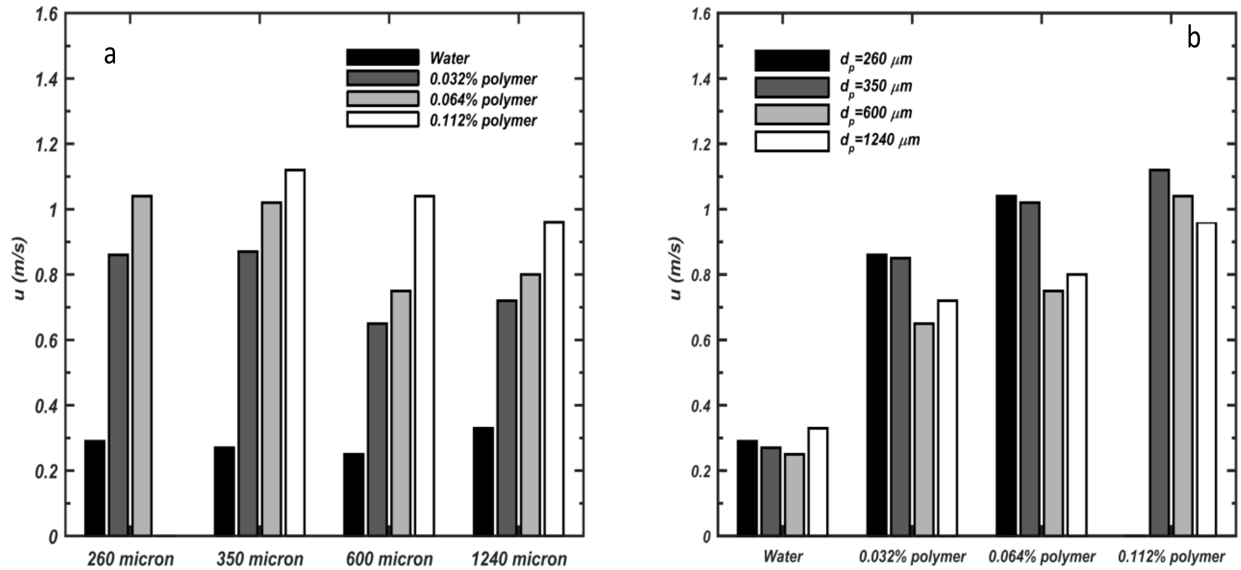

Figure 6-4 Critical velocities (a) impact of fluid viscosity for each size group (b) impact of cuttings size for each fluid

Figure 6-4b depicts the effect of cuttings size on the critical velocity. An intermediate cuttings size (600 microns) appears to be slightly easier to remove than the smaller or larger cuttings. Small cuttings tend to be submerged within the viscous sublayer. In the viscous sublayer fluid velocity is relatively low and therefore hydrodynamic (lift and drag) forces responsible for initiating particle movement are low (Figure 6-5). Inter-particle forces (i.e., Van der Waals force) increase as the particle size decreases (Duan et al. 2007), which also adds to the difficulty of removing small cuttings. Consequently, small size cuttings are harder to remove. One of the effects associated with high viscosity polymeric fluids is the thickening of the viscous sublayer (Wilson and Thomas 1985). This increases the chance of cuttings being submerged in the sublayer when polymer solutions are used. Therefore, higher flow rates are required to initiate movement of small size cuttings with polymer solutions.

Increasing cuttings size from 260 to 600 micron causes a slight reduction in the critical velocity. Further increase in cutting size results in an increase in critical velocity (except for the highest polymer concentration). This increase in critical velocity could be related to the weight increase of the cuttings. As cuttings size increases, net weight increases proportionally to the 3^{rd} power of the cuttings size. As the cuttings size gets bigger, their chance of being hidden in the viscous sublayer decreases and they are exposed to higher local fluid velocities within the core flow, which should help removal of these particles. However, as the particle size increases, its weight also increases (i.e., gravity force increases), which would tend to hold the particle in place. For particles, larger than a certain size the dominant force becomes the gravity (holding force), and beyond that critical particle size, a higher critical velocity is needed to initiate particle movement. Martins and Santana (1992) studied bed erosion with cuttings greater than 2mm. Their results showed smaller cuttings are easier to erode than bigger cuttings (smallest cuttings being of 2mm size). The increasing trend in critical velocity after a certain particle size as observed in our study also suggests that increasing the cuttings size beyond the range studied here (i.e., > 1.2 mm) would increase critical velocity.

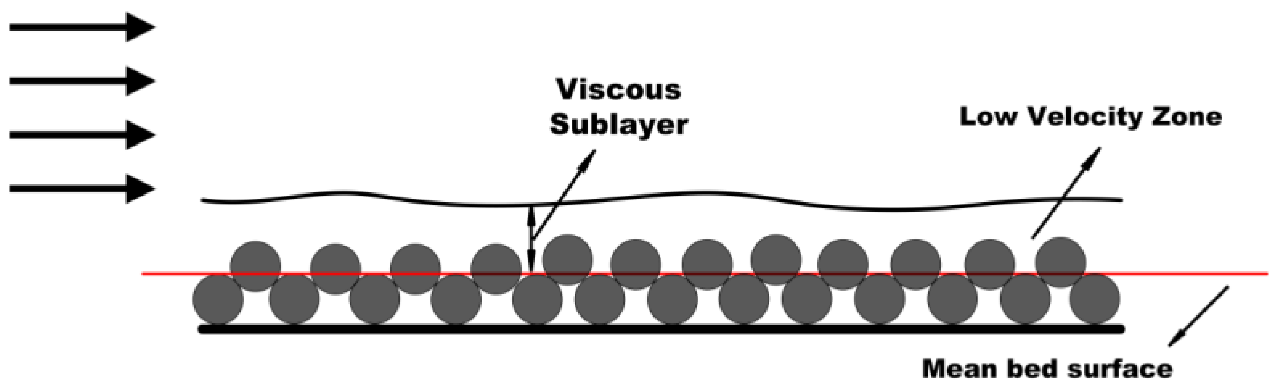

Figure 6-5 Schematic representation of cuttings submerged within viscous sublayer

6.1.2.2. Critical wall shear stress

Table 6-3 summarizes critical wall shear stress (calculated by using Eq.(6-2)) for all of the experiments. The impact of fluid rheological characteristics and cuttings size on critical wall shear stress are depicted in Figure 6-6. In all cases, critical wall shear stress for particle removal is lower for water compared with a polymer-based fluid (Figure 6-6a). An intermediate cuttings size (600 microns) seems to be removed from a lower wall shear stress than bigger or smaller cuttings (Figure 6-6b). However, the impact of cuttings size is far less than that of fluid rheology.

Table 6-3 Critical wall shear stress for initiation of cuttings movement (Pa)

d_p (μm)	water	0.032% polymer	0.064% polymer	0.112% polymer
260	0.45	1.29	2.2	-
350	0.38	1.11	1.69	2.52
600	0.34	0.81	1.38	2.44
1240	0.39	1.06	1.42	2.42

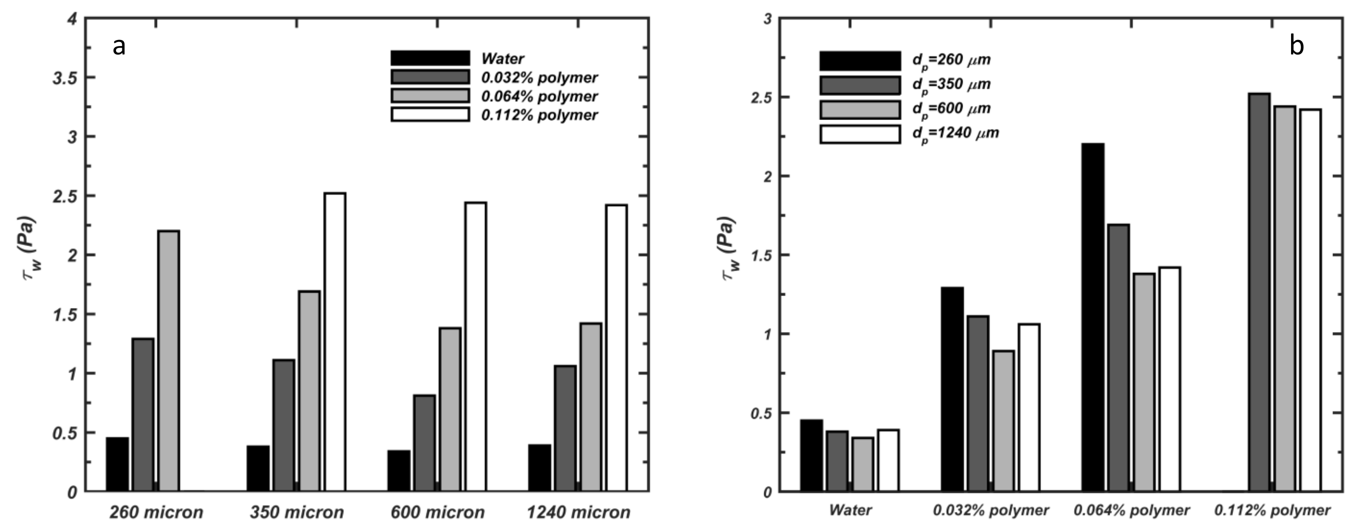

Figure 6-6 Critical shear stress (a) impact of fluid viscosity for each size group (b) impact of cuttings size for each fluid

6.1.2.3. Dimensionless groups

Analyzing critical conditions in dimensional form revealed that viscosity is not favorable when the task is initiating bed erosion. In other words, the higher viscosity was found to hurt critical velocity and pressure loss. However, analyzing data in this manner is limited to the geometry and experimental conditions under which the data were collected. To get more perspective in the process of cuttings removal and scale the data to real field applications, non-dimensional groups are desirable. In this section, critical conditions for the incipient motion are presented in the dimensionless form. Important parameters to consider are cuttings properties (size and density), fluid properties (density and rheological parameters) and local conditions at the bed (i.e. shear stress and a viscosity at the wall) as suggested by Luo et al. (1992). The following definition of particle Reynolds number is chosen to effectively represent cuttings condition at the bed (after Shah et al. 2007).

$$Re_p = \frac{\rho_f \, d_p^n \, V_t^{2-n}}{2^{n-1} \, K} \qquad \textbf{Eq.(6-3)}$$

V_t is cuttings settling velocity in non-Newtonian power law fluids. Shah et al. (2007) presented a generalized approach to calculate the terminal velocity of power law fluids for spherical particles. Their model is adopted in this study to estimate terminal settling velocity of cuttings based on the mean sieve diameter (See Appendix-B for details of the Shah et al. (2007) model used for terminal settling velocity calculations).

The main force initiating particle movement in horizontal wellbores is the fluid drag force. The fluid drag force on a cuttings bed is directly proportional to the shear stress at the bed interface. Therefore, it is important to consider the wall shear stress in the analysis. For critical shear stress, we use the critical Shields' stress or Shields' parameter (Shields 1936) (Eq.(6-4)). Although Luo et al. (1992) identified this parameter as a modified Froud number, this term is rather well known as Shields' parameter in sediment transport studies. It represents the ratio of fluid force on the cutting to its submerged weight.

$$\tau^* = \frac{\tau_w}{\left(\rho_s - \rho_f\right) g d_p} \qquad \textbf{Eq.(6-4)}$$

In Table 6-4, results of the critical Shields' stress are reported. Figure 6-7 summarizes the critical Shields' stress for each fluid. Contrary to dimensional critical wall shear stress, the critical Shields' stress always decreases as cuttings size increases. Increasing fluid viscosity causes an increase in the critical Shields' stress. The conclusion is that for the range of cuttings size tested here, increasing cutting size lowers the critical Shields' stress.

Table 6-4 Shields' stress at the initiation of particle movement

d_p (μm)	water	0.032% polymer	0.064% polymer	0.112% polymer
260	0.106	0.31	0.522	-
350	0.067	0.2	0.298	0.446
600	0.035	0.08	0.142	0.251
1240	0.019	0.05	0.071	0.12

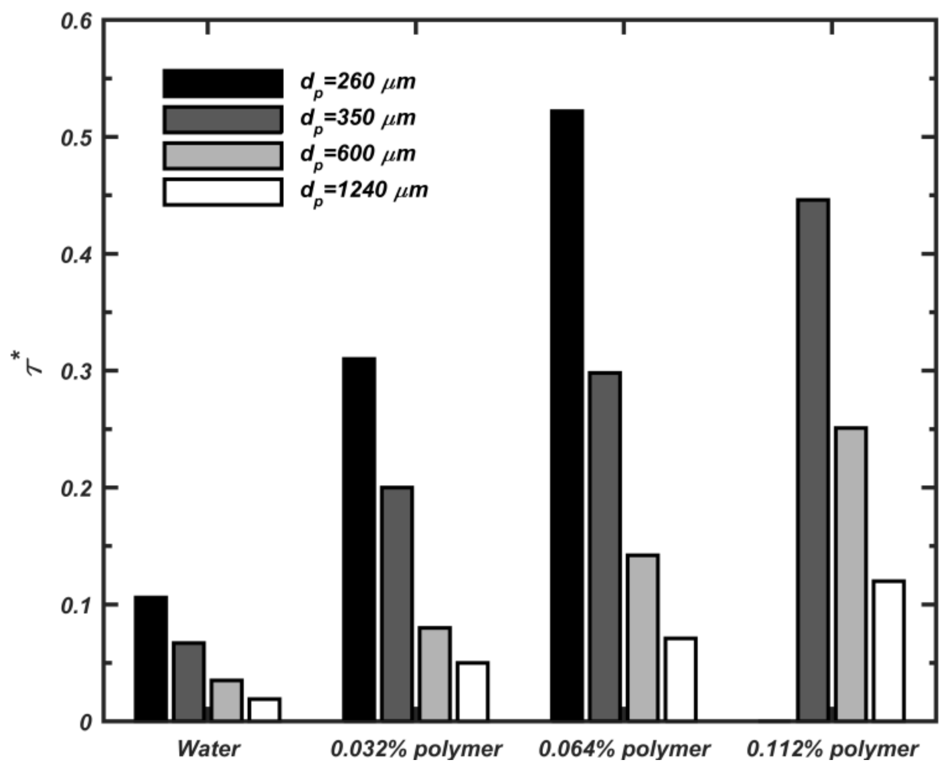

Figure 6-7 Critical Shields' stress for different fluid-cutting pairs

In sediment transport literature, it is common to relate critical Shields' stress to particle Reynolds numbers (Re_p) (Shields 1936, Garcia 2008). In the literature, a number of different definitions for Re_p could be found. After analyzing some of the models given in the literature (Shields 1936, Luo et al. 1992, Shah et al. 2007) we found that defining particle Reynolds number as in Eq.(6-3) best represents fluid and particles state for the specific problem considered here. In Figure 6-8 critical Shields' stress is plotted versus Re_p. Although the Reynolds number covers a rather narrow range (0.1-100), this plot shows that the selected definition of Re_p results in a good correlation of experimental data. Curve fitting of the data yields the relationship between critical Shields' stress and Re_p as shown in Eq.(6-5). Note that results from a similar experimental study conducted by Rodriguez-Corredor et al. (2014) are also included in Figure 6-8.

$$\tau^* = 0.2918\, Re_p^{-0.4589} \qquad \textbf{Eq.(6-5)}$$

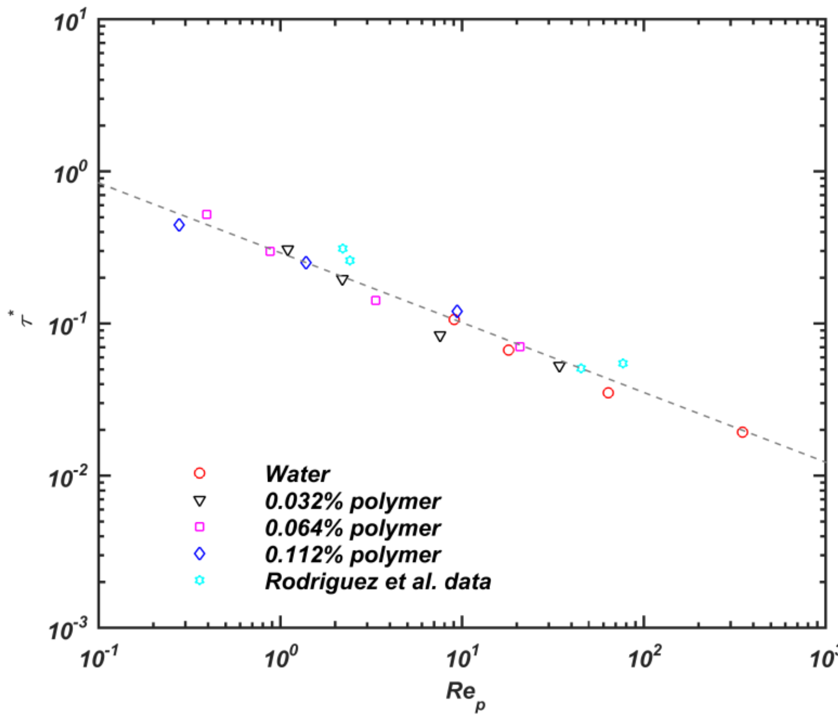

Figure 6-8 Critical Shields' parameter versus particle Reynolds number

Another form of shear stress is the friction velocity. Friction velocity is an important parameter in turbulent flow as it shows the scale of velocity fluctuations in the boundary layer (Eq.(6-6)).

$$u_\tau = \sqrt{\frac{\tau_w}{\rho}} \qquad \textbf{Eq.(6-6)}$$

Another dimensionless group is defined as the ratio of shear velocity to terminal settling velocity (Eq.(6-7)). This ratio represents the strength of turbulence acting to suspend the solid versus the rate at which the cuttings settle in the fluid. This ratio is important when the suspension of solids is desired.

$$\frac{u_\tau}{V_t} = \frac{\sqrt{\frac{\tau_w}{\rho}}}{V_t} \qquad \textbf{Eq.(6-7)}$$

This ratio at the critical condition of cuttings bed erosion was determined and is summarized in Table 6-5 and Figure 6-9. A declining trend of critical dimensionless shear velocity with increasing cuttings size is observed for a given fluid (Figure 6-9). At a given cuttings size, using higher viscosity fluids results in a higher velocity ratio.

Table 6-5 Critical dimensionless shear velocity for different fluids-cuttings pairs

d_p (μm)	Water	0.032% polymer	0.064% polymer	0.112% polymer
260	0.606	2.334	4.647	-
350	0.375	1.45	2.578	4.932
600	0.173	0.613	1.084	2.016
1240	0.07	0.275	0.392	0.676

Figure 6-10 shows the correlation between the critical velocity ratio and particle Reynolds number. Similar to critical Shields' stress, a good correlation is obtained between these two parameters. Using dimensionless shear velocity to define the initiation of particle motion, a slightly better correlation (Eq.(6-8)) of the data is obtained. The R-square for the curve fit is 0.9982, which is regarded as excellent given the fact that it incorporates many variables and is valid for both Newtonian and non-Newtonian fluids.

$$\frac{u_\tau}{V_t} = 2.384\ Re_p^{-0.5952} \qquad \textbf{Eq.(6-8)}$$

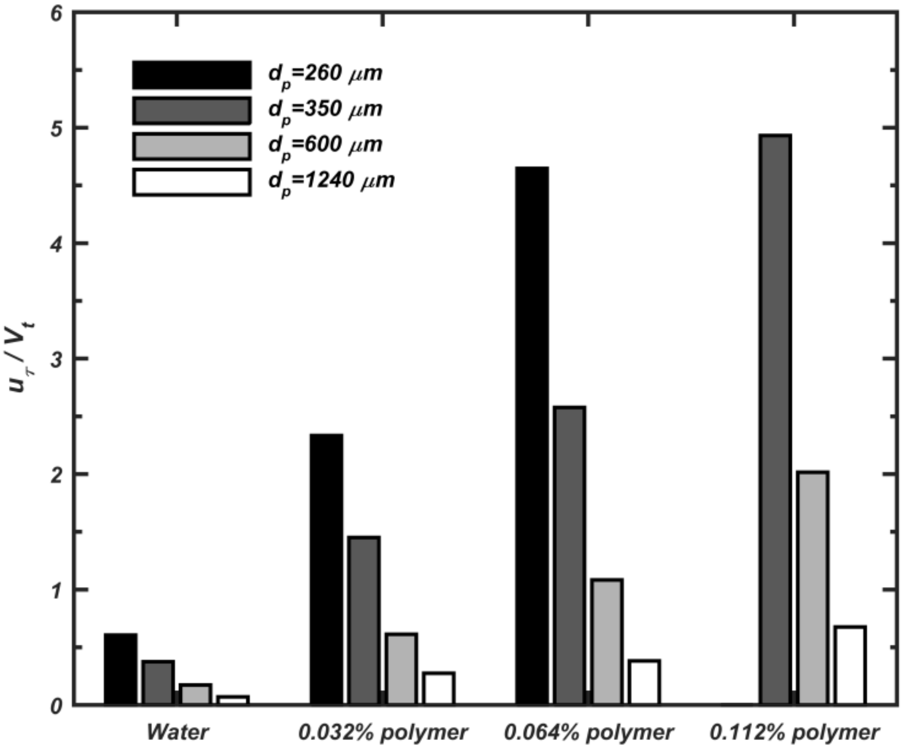

Figure 6-9 Critical dimensionless shear velocity for various fluids-cuttings pairs

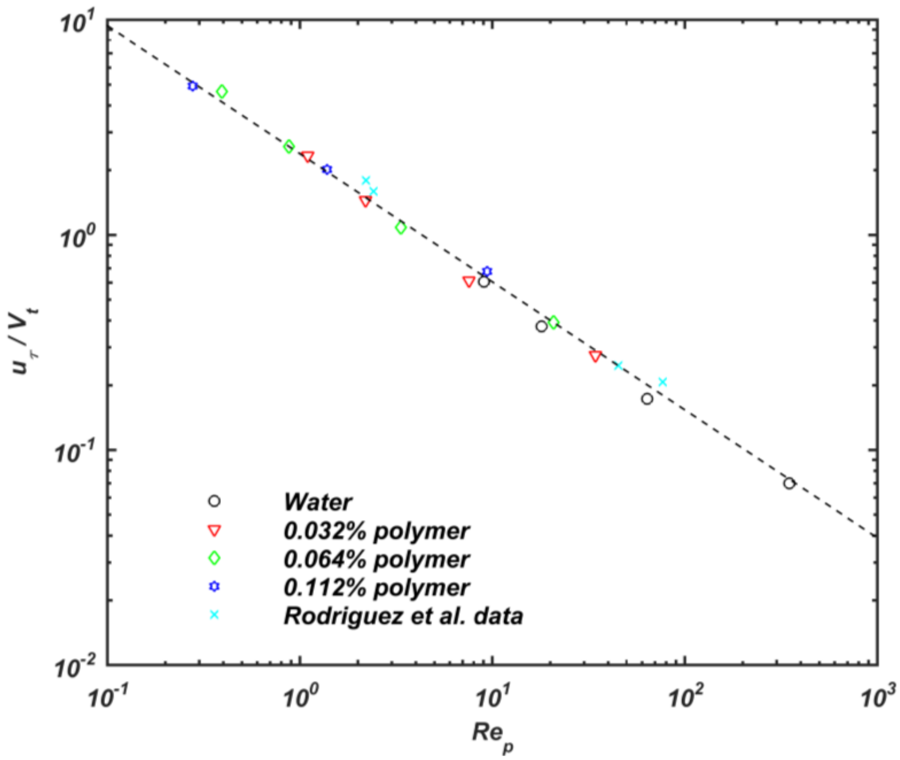

Figure 6-10 Critical dimensionless shear velocity vs. particle Reynolds number

Presenting the data in the form of non-dimensional shear stress versus particle Reynolds number is useful in estimating the critical wall shear stress for a broad range of fluid and cuttings properties. Using the presented definitions of dimensionless groups facilitates scaling of data obtained from different experimental studies. Effects of many parameters are included implicitly. Having a correlation of this type also facilitates sensitivity analysis of the impact of various parameters on hole cleaning performance. Assuming that the correlation given by Eq.(6-5) or Eq.(6-8) holds for the range of Re_p they were developed in, we can predict the impact of different parameters on critical non-dimensional wall shear stress; e.g. impact of fluid consistency and/or flow behavior indices, (K, n) on critical wall shear stress. In Figure 6-11an analysis is conducted to assess the impact of flow behavior index (n) on critical Shields' stress, τ^*. If all the other fluid and particle properties are retained constant, reducing n would result in a reduction of critical shear stress. That means if a choice has to be made between two fluids with same consistency indices but different flow behavior indices, the one with lower n would result in better hole cleaning. This in fact contradicts the argument of Saasen and Løklingholm (2002) where they claimed reducing n would result in a more consolidated bed and hence less effective hole cleaning. On the other hand, Leising and Walton (2002) found low values of n are more favorable in cuttings transport. That is because low values of n cause the velocity profile to be flatter in the core region of the flow. This in turn causes a higher shear rate at the wall and a lower local viscosity at the bed.

The effect of the fluid consistency index, K, on τ^* is shown in Figure 6-12. If the fluid consistency index decreases while all other properties are held constant, critical Shields' stress also decreases. This is in agreement with the experimental results where it was shown that water (least viscous fluid) is more effective in initiating cuttings movement at lower shear stresses. Comparing the orders of magnitude of critical Shields' stress in Figs. 11 and 12 reveals that the fluid consistency index has a more dominant impact on critical Shields' stress than the flow behavior index. These results suggest that to get a better hole cleaning performance, it is better to reduce the fluid consistency index than the flow behavior index.

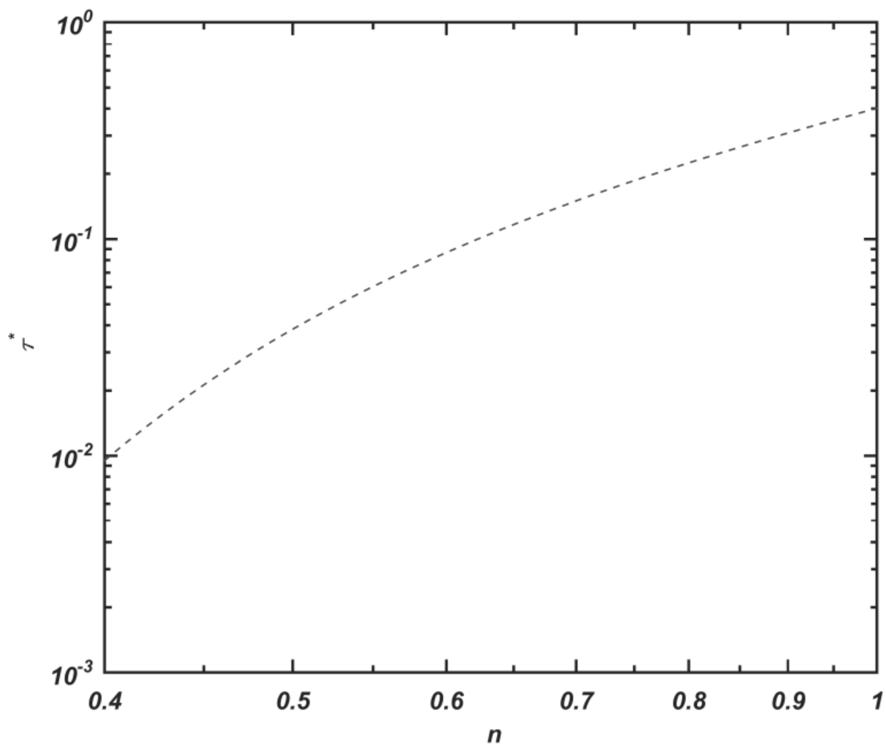

Figure 6-11 Effect of flow behavior index on Shields' stress ($K = 0.0226\ Pa.s^n, d_p = 600\ \mu m$)

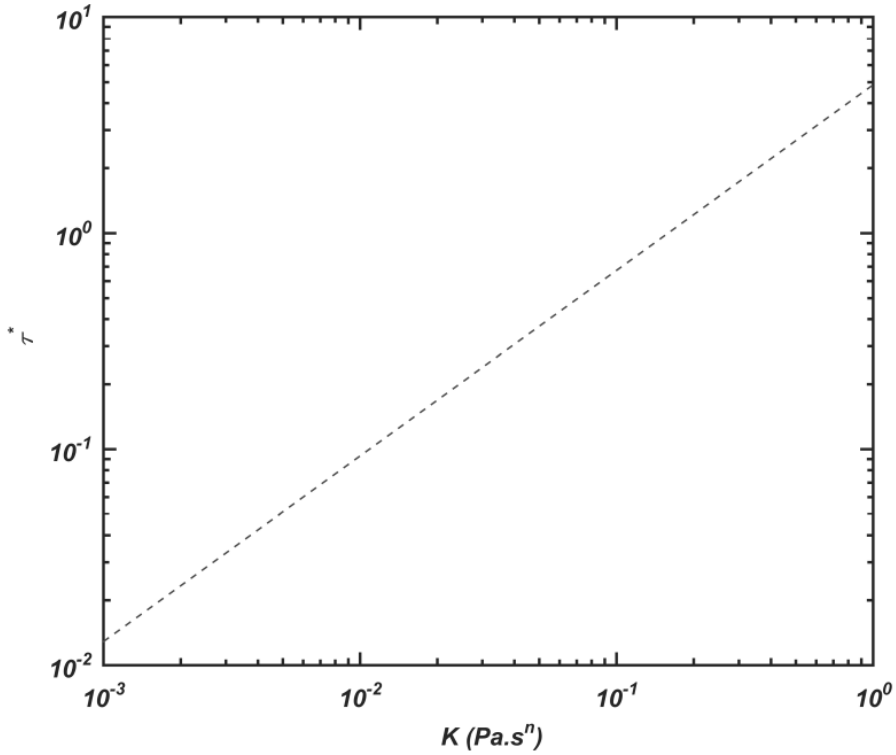

Figure 6-12 Effect of fluid consistency index, K, on Shields' stress ($n = 0.725$, $d_p = 600\ \mu m$).

In summary, it is shown that critical Shields' stress and the ratio of shear velocity to terminal settling velocity correlate well with particle Reynolds number at the point of cuttings bed erosion. For a given fluid and cuttings property, Re_p can be calculated and hence critical wall shear stress can be estimated (Eq.(6-5) and Eq.(6-8)). The critical wall shear stress can be converted to frictional pressure loss using annulus' hydraulic diameter.

6.1.2.4. Calculating critical flow rate

The critical flow rate is the flow rate which results in the critical pressure loss (i.e. initiate erosion of a cuttings bed). From previously developed correlations one can estimate the critical pressure loss. However, to calculate the critical flow rate, we need a relation between pressure loss and flow rate. This link is provided through a friction factor correlation. Sorgun et al. (2011) have proposed using a Blasius type friction factor relation for hydraulic calculations in an annulus with a cuttings bed (Eq.(6-9)).

$$f = \beta N_{Re}^{-\alpha} \qquad \textbf{Eq.(6-9)}$$

In Eq.(6-9) f is friction factor and N_{Re} is flow Reynolds number. The coefficients β and α are functions of bed height. A thicker bed causes a reduction of available flow area and hence an increase in friction factor. Generally, the friction factor is affected by many variables such as pipe eccentricity, fluid properties, presence of cuttings, pipe rotation and so on. A comprehensive model, which can account for all the variables, seems challenging to develop. This is mostly because of the non-linear nature of the impact different variables have on the friction factor. Sorgun et al. (2011) presented two sets of equations for β and α as functions of the bed height in the field. After comparing Sorgun et al. (2011) model predictions with the measured friction factors from this study, we found that there was a significant discrepancy between the measured and calculated friction factors. Additionally, it is hard to measure or estimate thickness of the stationary bed height in the field. After comparing with other available models (Reed and Pilehvari 1993, Duan et al. 2007, Sorgun et al. 2011) it was, clear that the best way to determine coefficients β and α is to obtain some measurements of pressure loss and calibrate the model. Therefore, to obtain meaningful values for β and α some field measurements of pressure loss seem inevitable.

Friction factor correlations (with corresponding coefficients β and α) obtained from pressure loss data measured during the course of our experiments are given in Appendix C. Finally, the procedure to calculate critical flow rate is explained and an example of finding critical flow rate from estimated critical pressure loss is presented in Appendix D.

6.5. Discussion on the limitations of this study

In this study, we have investigated hole cleaning performance of water and polymer based drilling fluids in a horizontal concentric annulus. The inner pipe was not rotating, and hence the experimental conditions were simulating coiled tubing drilling (CTD). One of the limitations of the current study is the position of the inner pipe which was kept fully concentric. The impact of positive eccentricity on hole cleaning has been investigated in the past (Thomas et al. 1982, Nazari et al. 2010, Li and Luft 2014a). All these studies point to the negative contribution of eccentricity to the hole cleaning process. Positive eccentricity causes velocity to reduce in the narrower gap of an annulus, which usually is the lower half where cuttings tend to go. Moreover, eccentricity can substantially reduce the frictional pressure loss (Haciislamoglu 1994) which reduces the shear stress on the cuttings bed. Consequently, the critical flow rate in an eccentric annulus is expected to be higher compared to the concentric case. However, the same statement about critical wall shear stress may not be true. Overall, we can say the results presented in this paper represent the ideal case for hole cleaning. In the event of an eccentric annulus, there should be an increase in the critical flow rate but not necessarily in critical wall shear stress.

The correlations developed for predicting critical shear stresses (Eq.(6-5) and Eq.(6-8)) were based on experimental results, which covered the particle Reynolds numbers (Re_p) range of 0.1-100. In this range, the correlation shows a declining trend of critical parameters with Re_p. This is similar to the classic Shields' diagram used in sediment transport studies (Shields 1936). As shown by Shields' study, it is expected that the critical shear stress reaches a minimum value with increasing particle diameter and beyond a certain particle size critical shear stress starts to increase with increasing particle size. Correlations developed in this study are valid within the range of the Re_p studied here. Using those beyond the range of Re_p, in which they were developed, needs to be confirmed with additional data.

6.6. Conclusions

Results of experimental work on hole cleaning of sand sized cuttings were presented. Experiments were conducted using a flow-loop composed of a horizontal concentric annulus with non-rotating straight (i.e. no buckling) inner pipe. Critical conditions for initiation of cuttings movement were investigated. Cuttings size varied from 260 to 1240 micron. Water and polymer based fluids with three different polymer concentrations were tested as circulating fluid.

The results showed that water always initiated cuttings movement at lower flow rates and pressure loss than polymer solutions. As the polymer concentration and the fluid viscosity increased, it progressively became harder to initiate cuttings movement, implying a negative impact of fluid viscosity on hole cleaning.

For the range of cuttings size tested, intermediate size cuttings were found to be slightly easier to remove than bigger or smaller cuttings. However, the impact of cuttings size on critical conditions was far less than that of fluid's rheological parameters. It is safe to say that cuttings size (within the range used here) has a minimal impact on hole cleaning.

Analyses using non-dimensional groups were also conducted. It was shown that critical wall shear stress in the form of Shields' stress and non-dimensional friction velocity could be correlated with generalized particle Reynolds number. Within the range of particle Reynolds number of 0.1 to100, two correlations (Eqs. 5 and 8) for predicting critical wall shear stress were proposed. The correlation was valid for Newtonian and non-Newtonian fluids. A procedure was also developed to calculate the critical flow rate.

6.7. Nomenclature

A	Constant used in settling velocity calculation
B	Constant used in settling velocity calculation
A_f	Annular cross section available to flow (m^2)
C_d	Drag coefficient
d_p	Cuttings mean sieve diameter (m)
D_o	Annulus, inner diameter of outer pipe (m)
D_i	Annulus, outer diameter of inner pipe (m)
D_h	Hydraulic Diameter in presence of bed (m)
D_H	Annulus hydraulic diameter (m)
f	Fanning friction factor
g	Acceleration of gravity ($\frac{m}{s^2}$)
L	Pipe length (m)
h	Height of stationary bed (m)
K	Fluid consistency index ($Pa.s^n$)
n	Flow behavior index
N_{Re}	Reynolds number
R	Annulus outer pipe radius (m)
r	Annulus inner pipe radius (m)
Re_p	Generalized particle Reynolds number
S_o	Wetted perimeter of wellbore (m)
S_i	Wetted perimeter of drillpipe wall (m)
S_b	Wetted perimeter of a bed (m)
Q	Flow rate ($\frac{m^3}{s}$)
P	Pressure (Pa)
u	Average velocity ($\frac{m}{s}$)

V_t	Settling velocity ($\frac{m}{s}$)
V	Superficial velocity ($\frac{m}{s}$)
$-\frac{dp}{dx}$	Axial pressure gradient ($\frac{Pa}{m}$)
ρ_s	Cuttings density ($\frac{kg}{m^3}$)
ρ_f	Fluid density ($\frac{kg}{m^3}$)
τ	Shear stress (Pa)
τ^*	Shields' stress
τ_w	Wall shear stress (Pa)
$\dot{\gamma}$	Shear rate ($\frac{1}{s}$)
μ_e	Effective viscosity (cp)
α	Constant in friction factor correlation
β	Constant in friction factor correlation

6.8. References

Adari, R. B. (1999). Development of correlations relating bed erosion to flowing time for near horizontal wells. M.Sc. Thesis, University of Tulsa, USA

Adari, R. B., Miska, S. Z., Kuru, E. et al. (2000). Selecting Drilling Fluid Properties and Flow Rates For Effective Hole Cleaning in High-Angle and Horizontal Wells. SPE Annual Technical Conference and Exhibition. Dallas, Texas, 1–4 October 2000., SPE-63050-MS,DOI: 10.2118/63050-MS.

Allahvirdizadeh, P., Kuru, E. and Parlaktuna, M. (2015). A Comparative Study of Cuttings Transport Performance of Water Versus Polymer-Based Fluids in Horizontal Well. Presented at the 20th International Petroleum and Natural Gas Congress and Exhibition of Turkey held in Sheraton Hotel and Convention Center, Ankara , Turkey, May 27-29, 2015.

Azar, J. J. and Sanchez, R. A. (1997). Important Issues in Cuttings Transport for Drilling Directional Wells. Fifth Latin American and Caribbaean Petroleum Engineering Conference and Exibition. held in Rio de Janeiro, Brazil, 30 August -3 Spetember 1997, SPE-39020-MS,DOI: 10.2118/39020-MS.

Bilgesu, H. I., Mishra, N. and Ameri, S. (2007). Understanding the Effect of Drilling Parameters on Hole Cleaning in Horizontal and Deviated Wellbores Using Computational Fluid Dynamics. SPE Eastern Regional Meeting Lexington, Kentucky, USA, 17-19 October 2007, SPE-111208-MS,DOI: 10.2118/111208-MS.

Bizhani, M. (2013). Solids transport with turbulent flow of non-Newtonian fluid in the horizontal annuli. M.Sc. Thesis, University of Alberta, Edmonton, Canada.

Brown, N. P., Bern, P. A. and Weaver, A. (1989). Cleaning Deviated Holes: New Experimental and Theoretical Studies. SPE\IADC Drilling Conference New Orleans, Louisiana, February 28-3 March 1989 SPE-18636-MS,DOI: 10.2118/18636-MS.

Cho, H., Shah, S. N. and Osisanya, S. O. (2000). A Three-Layer Modeling for Cuttings Transport with Coiled Tubing Horizontal Drilling. SPE Annual Technical Conference and Exhibition. Dallas, Texas, 1–4 October 2000., SPE-63269-MS,DOI: 10.2118/63269-MS.

Duan, M., Miska, S. Z., Yu, M. et al. (2007). Critical Conditions for Effective Sand-Sized Solids Transport in Horizontal and High-Angle Wells. SPE Production and Operations Symposium Oklahoma City, Oklahoma, USA, 31 March-3 April 2007., SPE-106707-MS,DOI: 10.2118/106707-MS.

Garcia, M. H. (2008). Sedimentation Engineering: Processes, Measurements, Modeling, and Practice, American Society of Civil Engineers.

Green, M. D., Thomesen, C. R., Wolfson, L. et al. (1999). An Integrated Solution of Extended-Reach Drilling Problems in the Niakuk Field, Alaska: Part II- Hydraulics, Cuttings Transport and PWD, SPE-56564-MS,DOI: 10.2118/56564-MS.

Haciislamoglu, M. (1994). Practical Pressure Loss Predictions in Realistic Annular Geometries. SPE Annual Technical Conference and Exhibition, 25-28 September. New Orleans, Louisiana, SPE-28304-MS,DOI: 10.2118/28304-MS.

Kelessidis, V. C. and Bandelis, G. E. (2004a). Flow Patterns and Minimum Suspension Velocity for Efficient Cuttings Transport in Horizontal and Deviated Wells in Coiled-Tubing Drilling. **SPE** Drilling & Completion **19**(4): 213-227, SPE-81746-PA, DOI: 10.2118/81746-PA.

Kelessidis, V. C., Mpandelis, G., Koutroulis, A. et al. (2002). Significant Parameters Affecting Efficient Cuttings Transport In Horizontal and Deviated Wellbores In Coil Tubing Drilling:

A Critical Review. Paper presented at the 1st International Symposium of the Faculty of Mines (ITU) on Earth Sciences and Engineering, 16-18 May 2002, Maslak, Istanbul, Turkey.

Larsen, T. I., Pilehvari, A. A. and Azar, J. J. (1997). Development of a New Cuttings-Transport Model for High-Angle Wellbores Including Horizontal Wells. **SPE** Drilling & Completion **12**(2): 129-135, SPE-25872-PA, DOI: 10.2118/25872-PA.

Leising, L. J. and Walton, I. C. (2002). Cuttings-Transport Problems and Solutions in Coiled-Tubing Drilling. **SPE** Drilling & Completion **17**(1): 54-66, SPE-77261-PA, DOI: 10.2118/77261-PA.

Li, J. and Luft, B. (2014a). Overview of Solids Transport Studies and Applications in Oil and Gas Industry - Experimental Work. SPE Russian Oil and Gas Exploration & Production Technical Conference and Exhibition. Moscow, Russia, 14-16 October, SPE-171285-MS,DOI: 10.2118/171285-MS.

Li, J. and Luft, B. (2014a). Overview Solids Transport Study and Application in Oil-Gas Industry-Theoretical Work. Paper presented at International Petroleum Technology Conference. Kuala Lumpur, Malaysia, 10-12 December 2014, IPTC-17832-MS,DOI: 10.2523/IPTC-17832-MS.

Li, J., Misselbrook, J. and Seal, J. W. (2008). Sand Cleanout With Coiled Tubing: Choice of Process, Tools, or Fluids? Europec/EAGE Conference and Exhibition. Rome, Italy, 9-12 June 2008, SPE-113267-MS,DOI: 10.2118/113267-MS.

Li, J. and Walker, S. (1999). Sensitivity Analysis of Hole Cleaning Parameters in Directional Wells. SPE/ICoTA Coiled Tubing Roundtable, . Houston, Texas, 25-26 May, SPE-54498-MS,DOI: 10.2118/54498-MS.

Li, J., Wilde, G. and Crabtree, A. R. (2005). Do Complex Super-Gel Liquids Perform Better Than Simple Linear Liquids in Hole Cleaning With Coiled Tubing? SPE/ICoTA Coiled Tubing Conference and Exibition The Woodlands, Texas, USA, 12-13 April 2005, SPE-94185-MS,DOI: 10.2118/94185-MS.

Lourenco, A. M. F., Nakagawa, E. Y., Martins, A. L. et al. (2006). Investigating Solids-Carrying Capacity for an Optimized Hydraulics Program in Aerated Polymer-Based-Fluid Drilling.

IADC/SPE Drilling Conference Miami, Florida, USA, 21-23 February 2006, SPE-99113-MS,DOI: 10.2118/99113-MS.

Luo, Y., Bern, P. A. and Chambers, B. D. (1992). Flow-Rate Predictions for Cleaning Deviated Wells. SPE/IADC Drilling Conference. New Orleans, Louisiana, 18-21 February, SPE-23884-MS., SPE-23884-MS,DOI: 10.2118/23884-MS.

Martins, A. L., Sa, C. H. M., Lourenco, A. M. F. et al. (1996). Optimizing Cuttings Circulation in Horizontal Well Drilling. International Petroleum Conference & Exhibition of Mexico. Villahermosa, Mexico, 5-7 March, 1996., SPE-35341-MS,DOI: 10.2118/35341-MS.

Martins, A. L. and Santana, C. C. (1992). Evaluation of Cuttings Transport in Horizontal and Near Horizontal Wells -A Dimensionless Approach. SPE Latin America Petroleum Engineering Conference. Caracas, Venezuela ,8-11 March, SPE-23643-MS., SPE-23643-MS,DOI: 10.2118/23643-MS.

National Instrument (2007). http://www.ni.com/manuals/ (accessed 18 December 2015).

Nazari, T., Hareland, G. and Azar, J. J. (2010). Review of Cuttings Transport in Directional Well Drilling: Systematic Approach. SPE Western Regional Meeting Anaheim, Califronia, USA, 27-29 may 2010, SPE-132372-MS,DOI: 10.2118/132372-MS.

Ozbayoglu, M. E., Miska, S. Z., Reed, T. et al. (2004). Analysis of the Effects of Major Drilling Parameters on Cuttings Transport Efficiency for High-Angle Wells in Coiled Tubing Drilling Operations. SPE/ICoTA Coiled Tubing Conference and Exibition. Huston, Texas, USA, 23-24 March 2004, SPE-89334-MS,DOI: 10.2118/89334-MS.

Pilehvari, A. A., Azar, J. J. and Shirazi, S. A. (1996). State-Of-The-Art Cuttings Transport in Horizontal Wellbores. International Conference on Horizontal Well Technology. Calgary, Alberta, Canada, 18-20 November, SPE-37079-MS,DOI: 10.2118/37079-MS.

Ramadan, A., Skalle, P. and Johansen, S. T. (2003). A mechanistic model to determine the critical flow velocity required to initiate the movement of spherical bed particles in inclined channels. Chemical Engineering Science **58**(10): 2153-2163, DOI: 10.1016/S0009-2509(03)00061-7.

Reed, T. D. and Pilehvari, A. A. (1993). A New Model for Laminar, Transitional, and Turbulent Flow of Drilling Muds. SPE Production Operations Symposium, 21-23 March, . Oklahoma City, Oklahoma, USA, SPE-25456-MS,DOI: 10.2118/25456-MS.

Rodriguez-Corredor, F. E., Bizhani, M. and Kuru, E. (2014). A Comparative Study of Hole Cleaning Performance-Water Versus Drag Reducing Fluid. ASME 2014 33rd International Conference on Ocean, Offshore and Arctic Engineering, San Francisco, California, USA, June 8–13, 2014, DOI: 10.1115/OMAE2014-24083.

Saasen, A. and Løklingholm, G. (2002). The Effect of Drilling Fluid Rheological Properties on Hole Cleaning. IADC/SPE Drilling Conference. Dallas, Texas, 26-28 February, SPE-74558-MS,DOI: 10.2118/74558-MS.

Shah, S. N., El Fadili, Y. and Chhabra, R. P. (2007). New model for single spherical particle settling velocity in power law (visco-inelastic) fluids. International Journal of Multiphase Flow **33**(1): 51-66, DOI: 10.1016/j.ijmultiphaseflow.2006.06.006.

Shields, A. (1936). Anwendung der Ähnlichkeitsmechanik und der Turbulenzforschung auf die Geschiebebewegung. Berlin, Eigenverl. der Preußischen Versuchsanst. für Wasserbau und Schiff.

Sorgun, M., Aydin, I. and Ozbayoglu, M. E. (2011). Friction factors for hydraulic calculations considering presence of cuttings and pipe rotation in horizontal/highly-inclined wellbores. Journal of Petroleum Science and Engineering **78**(2): 407-414, J Petrol Sci Eng, DOI: DOI 10.1016/j.petrol.2011.06.013.

Thomas, R. P., Azar, J. J. and Becker, T. E. (1982). Drillpipe Eccentricity Effect on Drilled Cuttings Behavior in Vertical Wellbores. Journal of Petroleum Technology **34**(9), SPE-9701-PA, DOI: 10.2118/9701-PA.

Tomren, P. H., Iyoho, A. W. and Azar, J. J. (1986). Experimental Study of Cuttings Transport in Directional Wells. SPE Drilling Engineering **1**(1), SPE-12123-PA, DOI: 10.2118/12123-PA.

Valluri, S. G., Miska, S. Z., Yu, M. et al. (2006). Experimental Study of Effective Hole Cleaning Using "Sweeps" in Horizontal Wellbores. SPE Annual Technical Conference and Exibition. San Antonio, Texas, USA, 24-27 September 2006, SPE-101220-MS,DOI: 10.2118/101220-MS.

Walker, S. and Li, J. (2000). The Effects of Particle Size, Fluid Rheology, and Pipe Eccentricity on Cuttings Transport. SPE/ICoTA Coiled Tubing Roundtable, 5-6 April. Houston, Texas, SPE-60755-MS,DOI: 10.2118/60755-MS.

Wilson, K. C. and Thomas, A. D. (1985). A New Analysis of the Turbulent-Flow of Non-Newtonian Fluids. Canadian Journal of Chemical Engineering **63**(4): 539-546.

Xiaofeng, S., Wang, K., Yan, T. et al. (2013). Review of Hole Cleaning in Complex Structural Wells. The Open Petroleum Engineering Journal **6**: 25-32, DOI: 10.2174/1874834101306010025.

6.9. Appendix A: Hydraulic diameter calculation in the presence of bed deposits

The hydraulic diameter and annular cross section available to fluid in the presence of a sand bed is defined following the work of Duan et al. (2007). For the case of a concentric annulus, assuming a bed of cuttings with the height of h, following relations hold (Figure A- 6-1):

$$S_o = 2R\ arccos\left(\frac{h-R}{R}\right) \quad \textbf{Eq. (A- 6-1)}$$

$$S_i = 2\pi r \quad \textbf{Eq. (A- 6-2)}$$

$$S_b = 2\sqrt{R^2-(R-h)^2} \quad \textbf{Eq. (A- 6-3)}$$

$$A_f = R^2\ arccos\left(\frac{h-R}{R}\right) + (R-h)\sqrt{R^2-(R-h)^2} - \pi r^2 \quad \textbf{Eq. (A- 6-4)}$$

$$D_h = \frac{4A_f}{S_o+S_i+S_b} \quad \textbf{Eq. (A- 6-5)}$$

In the previous equations, A_f is the cross-sectional area available to fluid in the presence of a cuttings bed.

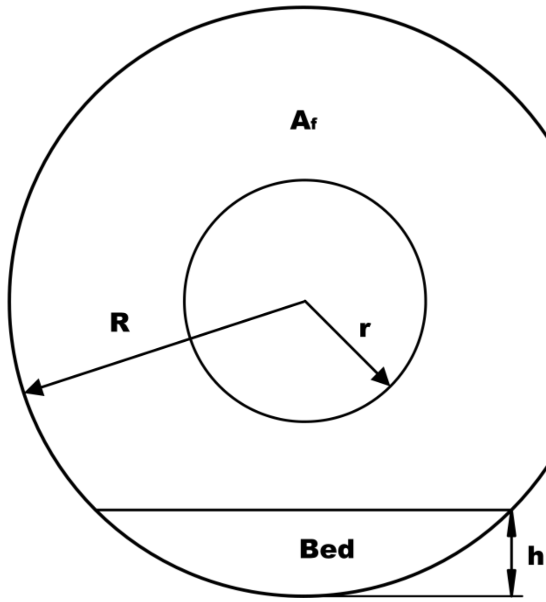

Figure A- 6-1 Schematic of bed and annulus cross section

6.10. Appendix-B: Settling Velocity calculation

The following equations are used in the calculation of the terminal settling velocity (Shah et al. 2007):

$$A = 6.9148n^2 - 24.838n + 22.642 \qquad \textbf{Eq. (B- 6-1)}$$

$$B = -0.5067n^2 + 1.3234n - 0.1744 \qquad \textbf{Eq. (B- 6-2)}$$

$$\sqrt{C_d^{2-n} Re_p^2} = \sqrt{\left[\frac{13.08^{2-n}}{2^{2(n-1)}}\right]\left[\frac{d_p^{2+n}\rho_f^n \left(\rho_s - \rho_f\right)^{2-n}}{K^2}\right]} \qquad \textbf{Eq. (B- 6-3)}$$

$$\sqrt{C_d^{2-n} Re_p^2} = A(Re_p)^B \qquad \textbf{Eq. (B- 6-4)}$$

$$V_t = \left[\frac{2^{n-1}K\, Re_p}{d_p^n \rho_f}\right]^{\frac{1}{2-n}} \qquad \textbf{Eq. (B- 6-5)}$$

6.11. Appendix C: Friction factor correlation

A friction factor correlation is needed to estimate critical flow rate. In this section, friction factor correlations are discussed. Following the work of Sorgun et al. (2011) friction factors are assumed to be of the following form (Eq. C-6-1):

$$f = \beta N_{Re}^{-\alpha} \qquad \textbf{Eq.(C- 6-1)}$$

f is related to pressure loss and superficial velocity as in Eq. C-6-2:

$$\frac{\Delta P}{\Delta L} = \frac{2f\rho V^2}{0.8165(D_o - D_i)} \qquad \textbf{Eq.(C- 6-2)}$$

Velocity is the superficial velocity:

$$V = \frac{Q}{\frac{\pi}{4}(D_o^2 - D_i^2)} \qquad \textbf{Eq.(C- 6-3)}$$

The Reynolds number for the flow of Power law type fluids is given by Eq. C-6-4 (Drilling Mud and Cement Slurry Rheology Manual 1982):

$$N_{Re} = \frac{0.8165\rho V^{2-n}(D_o - D_i)^n}{K(12^{n-1})(\frac{2n+1}{3n})^n} \qquad \textbf{Eq.(C- 6-4)}$$

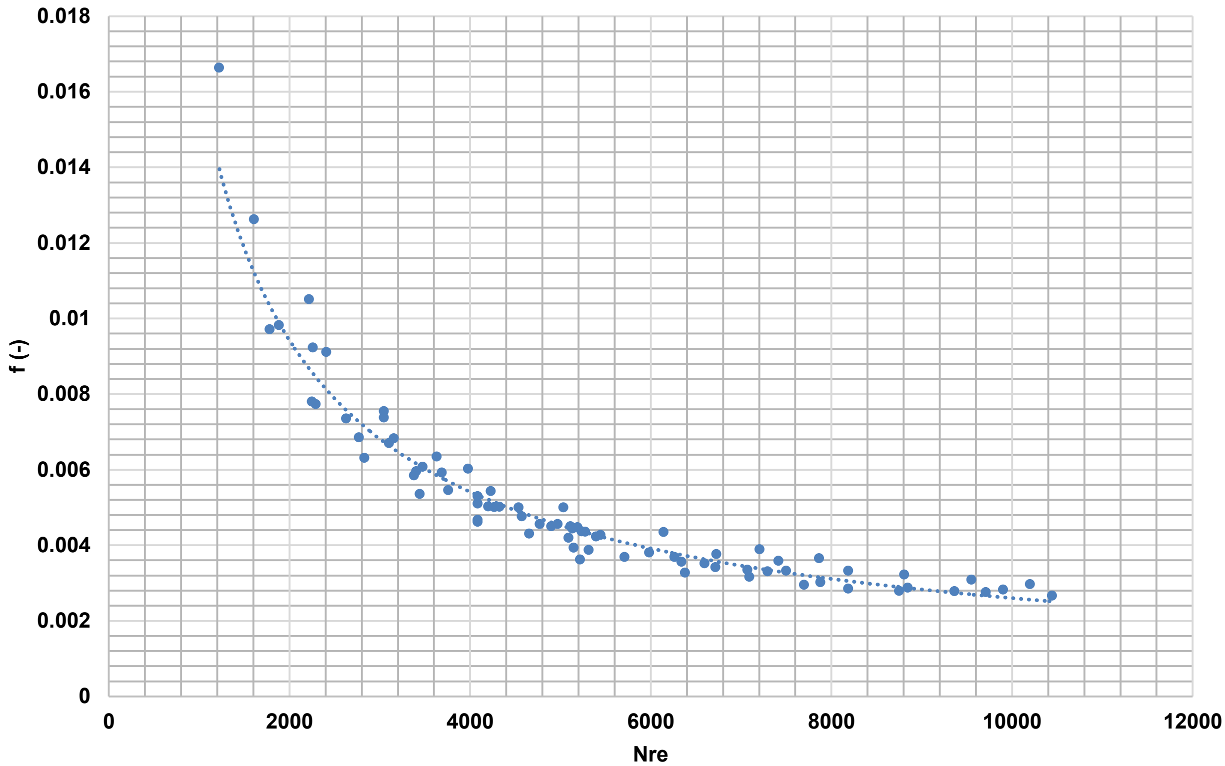

Figure C- 6-1 Friction factor data for polymer solutions

Figure C-6-1 reports friction factor data for polymer solutions

Curve fitting of these data results in a correlation of Eq. C-6-5. Friction factor data for water are reported in Figure C-6-2. The best fit to water friction factor is presented in Eq. C-6-6.

$$f = 4.10376 N_{Re}^{-0.799} \quad \textbf{Eq.(C- 6-5)}$$

$$f = 2608.5 N_{Re}^{-1.317} \quad \textbf{Eq.(C- 6-6)}$$

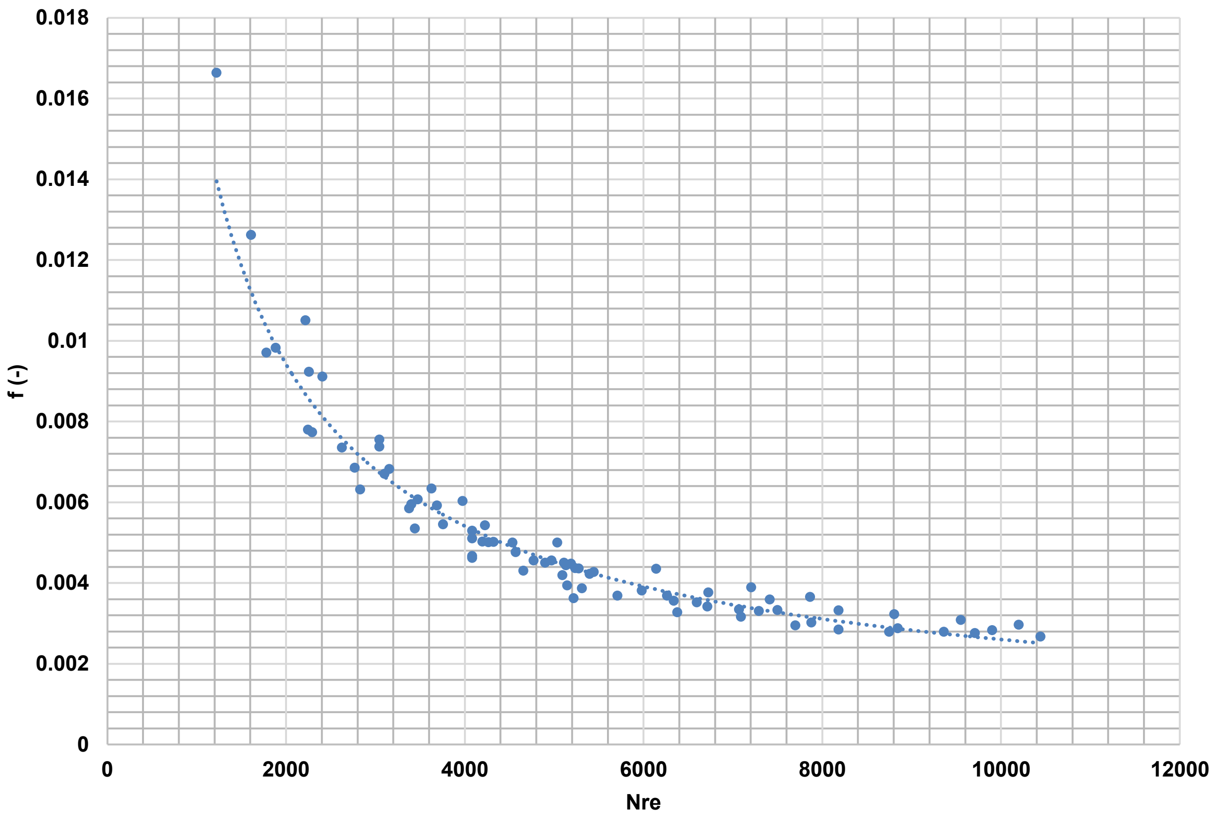

Figure C- 6-2 Friction factor data for water

Note that the friction factor data presented in Figures C-6-1 and C-6-2 are calculated from the pressure drop data that have been collected by the authors during the hole cleaning experiments.

6.12. Appendix D: Calculating critical flow rate

The procedure to calculate critical pressure loss and the critical flow rate for cuttings removal is as follows:

1. Use cuttings and drilling fluid properties to calculate cuttings settling velocity and particle Reynolds number (Eqs. B-6-1 to B-6-5 and Eq.(6-3) respectively)
2. Calculate critical Shields' stress or critical shear velocity required to initiate movement of the cuttings using one of the two correlations available (Eq.(6-5) and Eq.(6-8))

3. Calculate the wall shear stress using the critical Shields' stress or shear velocity (Eq.(6-4) and Eq.(6-7))
4. Use the annulus' hydraulic diameter to calculate critical pressure loss (Eq.(6-2))
5. Use a friction factor correlation to estimate critical flow rate

An example of using this procedure is presented here.

Example: Assume we want to calculate critical flow rate required to initiate erosion of a bed of cuttings composed of 260-micron particles.

Fluid properties: $K = 0.0206\ Pa.s \quad n = 0.7409 \quad \rho = 998\,\frac{kg}{m^3}$

Particles properties: $d_p = 260\ \mu m \ \ \rho = 2650\,\frac{kg}{m^3}$

Annular geometry: $D_o = 0.095\ m \qquad D_i = 0.038\ m \qquad D_H = 0.057\ m$

The first step is to calculate particle Reynolds number and settling velocity:

Particle Reynolds number can be calculated by using Eqs. D-6-1 to D-6-4 as follows:

$$A = 6.9148n^2 - 24.838n + 22.642 = 8.035 \qquad \textbf{Eq.(D- 6-1)}$$

$$B = -0.5067n^2 + 1.3234n - 0.1744 = 0.5280 \qquad \textbf{Eq.(D- 6-2)}$$

$$\sqrt{C_d^{2-n} Re_p^2} = \sqrt{\left[\frac{13.08^{2-n}}{2^{2(n-1)}}\right]\left[\frac{d_p^{2+n} \rho_f^n \left(\rho_s - \rho_f\right)^{2-n}}{K^2}\right]} = 4.9081 \qquad \textbf{Eq.(D- 6-3)}$$

$$Re_p = (\sqrt{C_d^{2-n} Re_p^2}/A)^{1/B} = 0.3931 \qquad \textbf{Eq.(D- 6-4)}$$

By introducing R_{ep} into Eq. D-6-5, particle settling velocity can be found as follows:

$$V_t = \left[\frac{2^{n-1} K\, Re_p}{d_p^n \rho_f}\right]^{\frac{1}{2-n}} = 0.0101\,\frac{m}{s}, \qquad \textbf{Eq.(D- 6-5)}$$

Then we can calculate critical wall shear stress using:

$$\frac{u_\tau}{V_t} = 2.384\ Re_p^{-0.5952} = 4.1558$$ **Eq.(D- 6-6)**

$$\frac{u_\tau}{V_t} = \frac{\sqrt{\frac{\tau_w}{\rho_f}}}{V_t} = 4.1558$$ **Eq.(D- 6-7)**

$$\tau_w = 1.759\ Pa$$ **Eq.(D- 6-8)**

Critical pressure loss could be calculated by using Eq.2:

$$\frac{dP}{dL} = \frac{4}{D_H}(\ \tau_w) = 130.8\frac{Pa}{m}$$ **Eq.(D- 6-9)**

The next step is to estimate the velocity, which results in this pressure loss using a simultaneous solution of the friction factor correlation (e.g. in this case use Eq. C-6-5), the Reynolds number given for the flow of Power Law fluid (Eq. C-6-4), and the Fanning friction pressure loss equation, (Eq. C-6-2). This is done using a solver (e.g. Microsoft Excel) and following equations.

$$f = 4.10376 N_{Re}^{-0.799} = 0.003$$ **Eq.(D- 6-10)**

$$N_{Re} = \frac{0.8165\rho V^{2-n}(D_o - D_i)^n}{K(12^{n-1})(\frac{2n+1}{3n})^n} = 8380$$ **Eq.(D- 6-11)**

$$\frac{\Delta P}{\Delta L} = \frac{2f\rho V^2}{0.8165(D_o - D_i)} = 130.85$$ **Eq.(D- 6-12)**

$$V = 1.008\frac{m}{s}$$ **Eq.(D- 6-13)**

Finally, the required flow rate can be found as:

$$Q = \frac{\pi}{4}(D_o^2 - D_i^2)V = \ 0.00585\frac{m^3}{s}\ (= 351\frac{lit}{min})$$ **Eq.(D- 6-14)**

This compares to the experimentally measured flow rate of 362 lit/min with satisfactory accuracy. Table D-6-1 summarizes the results of a comparison made between predicted and experimentally measured critical pressure loss and critical flow rate values for the 0.064% polymer solution. Critical pressure loss is predicted with good accuracy. However, prediction of flow rate is less accurate. That is because of inaccuracies in the friction factor correlation. Our recommendation is to calculate the critical pressure loss using the developed correlations. To estimate the flow rate a calibration of the friction factor correlation seems necessary for each case. This can perhaps be done by the field engineer using real-time measurements of flow rate and annular frictional pressure loss.

Table D- 6-1 Comparison of predicted and experimentally measured critical pressure loss and critical flow rate for 0.064% polymer solution

	Critical pressure loss		Critical flow rate	
$d_p\ (\mu m)$	$\frac{\Delta P}{\Delta L}_{Experiment}\ (\frac{Pa}{m})$	$\frac{\Delta P}{\Delta L}_{Prediction}\ (\frac{Pa}{m})$	$Q_{Experiment}\ (\frac{Lit}{min})$	$Q_{Prediction}\ (\frac{Lit}{min})$
260	154	130	362	351
350	118	125	355	333
600	97	117	260	312
1240	100	105	279	279

7.Critical Review of Mechanistic and Empirical (Semi- Mechanistic) Models for Particle Removal from Sand Bed Deposits in Horizontal Annuli by Using Water[7]

In this chapter, we presented and discuss the impact of flow turbulence on the removal of sand particles from bed deposits. The data have been collected using PIV technique and in the concentric annulus. The testing fluid was water. Velocity profiles in the vicinity of sand bed deposits are analyzed for assessment of the importance of velocity fluctuations on the effective fluid velocity. Additionally, mean bed shear stress is calculated using different methods. Finally, the concept of critical shear stress and the critical flow rate is discussed.

7.1. Summary

An experimental study was conducted to investigate the turbulent flow of water over cuttings bed using a large-scale horizontal flow-loop. A non-intrusive laser based imaging technique was used to determine instantaneous local velocity near the stationary sand bed-fluid interface in the horizontal annulus. The velocity measured directly at the sand bed/fluid interface was then used for critical evaluation of the accuracy of the assumptions and correlations commonly used for development of mechanistic and semi-mechanistic sediment transport models. In particular, effects of turbulent velocity fluctuations on the magnitude of the hydrodynamic drag and lift forces and the interfacial (bed) shear stress are investigated.

7.1. Introduction

When drilling highly inclined and long horizontal wells, drilled solids tend to settle down on the low side of the wellbore and form a stationary cuttings bed. Presence of a stationary cuttings

[7] A version of this chapter has been published. **Bizhani**, M., Kuru, E., 2017, "Critical Review of Mechanistic and Empirical (Semi- Mechanistic) Models for Particle Removal from Sand Bed Deposits in Horizontal Annuli by Using Water," **SPE** Journal, SPE-187948-PA,

bed often causes operational difficulties such as bridging, pack-off, hole fill, excessive torque, and drag, bit balling, slow drilling rates, hindering the casing or liner to be run into its desired position, and in severe cases, stuck pipe, lost circulation, and even loss of well control (Li and Luft 2014b, Bizhani et al. 2016). Therefore, occasionally, drilling must stop to clean the stationary cuttings bed. Despite significant progress made in drilling fluids, tools, and field practices, along with more than 50 years of university and industry research, field experience indicates that hole cleaning is still a major problem in most highly inclined and horizontal wells.

Hole cleaning is typically performed by pumping drilling fluid down the string and up the annulus to sweep the drilled cuttings out of the wellbore. The drill string may be rotated or pulled out of the well (wiper trip) during this operation to aid the removal of the cuttings (Pilehvari et al. 1996, Nazari et al. 2010, Li and Luft 2014a, Li and Luft 2014b). However, pipe rotation does not exist in Coiled Tubing (CT) drilling (Leising and Walton 2002). Drilling fluid transfers some of its momentum to the cuttings in the bed, and hence the efficiency of the hole cleaning operation much depends upon the interaction of drilling fluid and drill cuttings in the cuttings bed. The complexity of the interaction of fluid-particles coupled with the turbulent flow makes hole cleaning immune to any theoretical treatment.

The problem of cuttings removal in highly inclined wellbores has been the subject of numerous studies since the early 1980s. Most of the previous studies can be categorized into two groups as experimental and theoretical works. In the experimental approach, usually, one or more variables that affect hole cleaning are studied experimentally while all other variables are held constant. Examples of such studies are numerous in the literature (Brown et al. 1989, Ford et al. 1990, Hemphill and Larsen 1996, Larsen et al. 1997, Adari 1999, Adari et al. 2000, Ozbayoglu et al. 2010a, Bizhani 2013, Bizhani et al. 2016). A more elegant way of studying hole cleaning is through mechanistic and semi-mechanistic modeling (Iyoho and Takahashi 1993, Clark and Bickham 1994, Ramadan et al. 2003, Duan et al. 2007, Guo et al. 2010). Li and Luft (2014a), (2014b) have provided two excellent review papers on the past experimental and theoretical hole cleaning studies.

Mechanistic and semi-mechanistic modeling of hole cleaning are appealing over the experimental models in many ways. First and foremost reason is that they incorporate actual physics of the problem into the model (if developed realistically); something that most empirical models lack. Secondly, most of the experimental models are applicable only for a narrow range of operational conditions (e.g. eccentricity or hole size, etc.), while a mechanistic model could be more general. Nonetheless, putting the complex nature of the interaction of turbulent flow and solid particles into equations is not a trivial task.

To develop a realistic mechanistic model, a good understanding of the nature of the interaction between the drilling fluid and drilled cuttings is necessary. Examples of such interaction are abundant both in nature (e.g. flow over river beds) and in the industrial systems (e.g. tailing ponds). Interaction of phases in these systems is bi-directional; the sediment phase can affect the turbulence in the carrier fluid phase and vice versa (Bagchi and Balachandar 2003). Sediment transport in flumes and channels which are pertinent to flow in rivers have been studied extensively in the past (Wiberg and Rubin 1989, Gore and Crowe 1991, Tsuji et al. 1991, Best et al. 1997, Miyazaki 1999, Carbonneau and Bergeron 2000, Sumer et al. 2003). Most of these bed erosion/sediment transport studies, however, involve water flow (as opposed to the flowing of more complex, non-Newtonian drilling fluids involved in hole cleaning operations in drilling oil and gas wells). Results of these studies have shown the complex nature of interactions of the phases in these systems.

Mechanistic and semi-mechanistic hole cleaning models mainly follow two routes for modeling such complex phenomena. The first approach uses a force balance on the cuttings at the bed interface (Clark and Bickham 1994, Ramadan et al. 2003, Duan et al. 2007). In this approach, the onset of the particle movement is predicted based on the net force or the moment that the particle is subjected to. The main forces to consider in this approach are a fluid hydrodynamic force (i.e. drag and lift force), buoyancy, and adhesion (i.e. van der Walls) forces. For accurate prediction of the fluid hydrodynamic force, a realistic prediction of the local fluid velocity is necessary.

One of the main issues with mechanistic hole cleaning models is that they either require local fluid velocity near the cuttings bed as an input or they predict the local fluid velocity as an output. However, in a turbulent flow, the local fluid velocity is not constant at the time and may deviate significantly from its average value. This approach neglects the presence of the fluctuations in the fluid velocity due to turbulent nature of the flow. Another assumption commonly used in most of the mechanistic models is the roughness of the cuttings bed. While different definitions have been utilized for this property (Ramadan et al. 2003, Duan et al. 2007), Bizhani and Kuru (2017) have shown that the bed roughness is approximately equal to twice the cuttings size. Additionally, the recent study of Bizhani and Kuru (2017) revealed that local arrangement of particles in the bed affects local roughness height. Change in the roughness height will cause the local velocity to change accordingly.

In a series of recent bed erosion studies, Bizhani et al. (2016), (2017) investigated the impact of the presence of a stationary sand bed on the characteristics of turbulent flow inside horizontal concentric annuli. They have shown that the mere existence of a stationary sand bed resulted in the reduction of the peak fluid velocity in the lower annulus where the sand bed deposit exists. They also observed that the roughness of the bed surface created more turbulence near the cuttings bed/fluid interface compared to the flow over the smooth face of the drillpipe. The study also showed that the movement of the sand particles in the form of bedload along the bed interface caused reduction of the near wall turbulence.

Semi-mechanistic models are the ones that follow a layer modeling approach. Layer modeling for cuttings transport was introduced into drilling literature by the classical study of Gavignet and Sobey (1989), following the results of an earlier work by Wilson (1976) on slurry transport in pipes. Since the work of Gavignet and Sobey (1989) many different versions of layer modeling of cuttings transport have been published (Iyoho and Takahashi 1993, Nguyen and Rahman 1998, Kamp and Rivero 1999, Cho et al. 2000, Ozbayoglu et al. 2005, Naganawa and Nomura 2006, Espinosa-Paredes et al. 2007, Wang et al. 2009, Guo et al. 2010). Regardless of variations in different models, most of these models involve balancing pressure force and shear stress forces acting on the various surfaces of the annuli (i.e. cuttings bed surface, drillpipe outer surface, casing/wellbore inner surface). Kelessidis and Bandelis (2004a) have provided an excellent review of the most of these layer modeling approaches.

In the layer modeling approach, one momentum equation is used for each layer. Closure equations are often needed to close the system of equations. After solving the set of equations, the concentration profile and average velocity of each phase are obtained. In this approach, the coupling of phases (i.e. cuttings and drilling fluid), is obtained through shear stresses that exist between the phases.

The primary purpose of this paper is to evaluate the accuracy and validity of current available mechanistic and semi-mechanistic models for particle removal from sand bed deposits in horizontal annuli using water using experimental data along with the most recent findings in the field of sediment transport. Our goal is to provide general guidelines for future development of the bed erosion/sediment transport models. The discussions in this paper are backed by the results of the experiments investigating the turbulent flow of water over the cuttings bed using a large-scale horizontal flow loop. A non-intrusive laser based imaging technique (PIV) was used to determine instantaneous local velocity near the stationary cuttings bed-fluid interface. Direct measurements of near wall velocity at the sand bed/fluid interface were then utilized for the evaluations of the accuracy of the assumptions and correlations used for developing bed erosion/sediment transport models using water.

The present work discusses the results of the experiments where particles were removed from sand bed deposits in horizontal annuli by using water as a carrier fluid. Although in real drilling operations water is seldom used for hole cleaning, the result of this study can still be used to improve our understanding of the particle/fluid interaction and relevant mechanisms involved in particle removal from stationary bed deposits in horizontal wells during hole cleaning (bed erosion) operations. In particular, the discussion of the role of flow turbulence (and associated near wall velocity fluctuations) and its importance on particle removal from stationary bed deposits can be extended to more complex (non-Newtonian) fluids typically used in drilling operations. Additionally, the concept of effective fluid velocity and how much it differs from other definitions of velocities often utilized in the literature and the field for modeling purpose have been introduced in the bulk of the paper. This discussion, therefore, shall be relevant to any bed erosion modeling study irrespective of the fluid type used. Finally, this research has been conducted as part of the comprehensive study of understanding the effect of fluid rheological properties and near wall turbulence on the mechanism of particle removal from stationary bed deposits in horizontal annuli. The results and discussions presented here should be considered as an essential first step towards the development of the more complex unified theory of hole cleaning.

The paper is composed of two main sections. The first section is devoted to the discussions of the mechanistic approaches used in the hole cleaning modeling. Experimental results from current study along with the most recent findings in sediment transport field are used to show the inadequacies involved in the mechanistic sediment transport models in horizontal wells. In the second part of the paper, we discussed the semi-mechanistic and empirical approaches used for hole cleaning modeling. Similar to the first section, the shortcomings of the models in this category were shown by using the new experimental data from current study as well as the results from most recent research in the field of sediment transport. The paper identifies the inadequacies and unjustified assumptions currently used for hole cleaning models and provides alternative solutions to these shortcomings. The goal of this article is not to present a simple model to be employed by the industry, but rather to give guidelines for engineers and researchers in their future endeavors for developing more realistic hole cleaning models.

7.2. Experimental set-up and procedure

Cuttings transport experiments were conducted in a large-scale flow loop facility. Figure 7-1 is a schematic view of the flow loop used in this study. Principal components of the flow loop are a 500-liter stainless steel tank, a centrifugal pump and measurement instruments such as magnetic flow meter and differential pressure transducers. There is an air- driven mixer in the tank for preparing the slurry. The centrifugal pump equipped with Variable Frequency Drive (VFD) was used to circulate fluid/solids mixture through the flow loop.

The test section is 9 meters long and is made out of high-quality Borosilicate glass pipes. Outer pipe has an inside diameter of 95mm, and the inner pipe has an outer diameter of 38mm. The annulus has a hydraulic diameter of 57 mm and a radius ratio of 0.4. The necessary condition for minimizing sagging and bending of the inner pipe is near neutral buoyancy condition of an inner pipe in working fluids. Inner pipe wall thickness was carefully selected to meet near neutral buoyancy condition and, hence, avoid bending of pipes during the experiments (Japper-Jaafar et al. 2010, Bizhani et al. 2015).

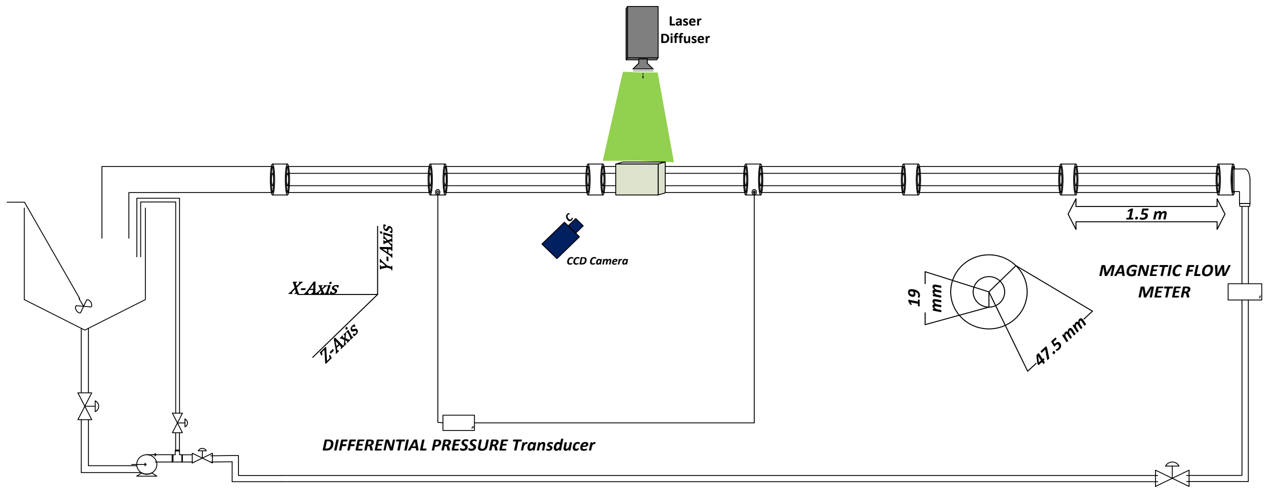

Figure 7-1 Schematic of the flow loop

A magnetic flow meter installed at the inlet of the annulus was used for flow rate measurements. The flow meter is an OMEGA FMG607-R with an accuracy of $\pm 0.5\%$. A computerized data acquisition system powered by LabView software was connected to all the measurement devices. The software was used to control the pump flow rate as well as logging all the data (i.e. pressure losses, flow rates and fluid temperature in the flow loop).

Before conducting an experiment, a stationary cuttings bed was established in the concentric annulus. Water and sand were mixed in the mixing tank. The slurry was then circulated through the flow loop at maximum flow rate. To achieve a steady state condition, the slurry has been distributed for 10 to 15 minutes. The pump was then shut in. Annular section of the flow loop was isolated from the rest of the flow loop using popper valves (Figure 7-1). Cuttings remained in other parts of the flow loop was then washed away carefully. Two filter bags with openings smaller than the particle size (the opening is 100 micron) were installed at the outlet of the annular section to collect any particle which was removed from the test section and prevent them from going back. Cuttings bed height was controlled through some solids put into the flow loop.

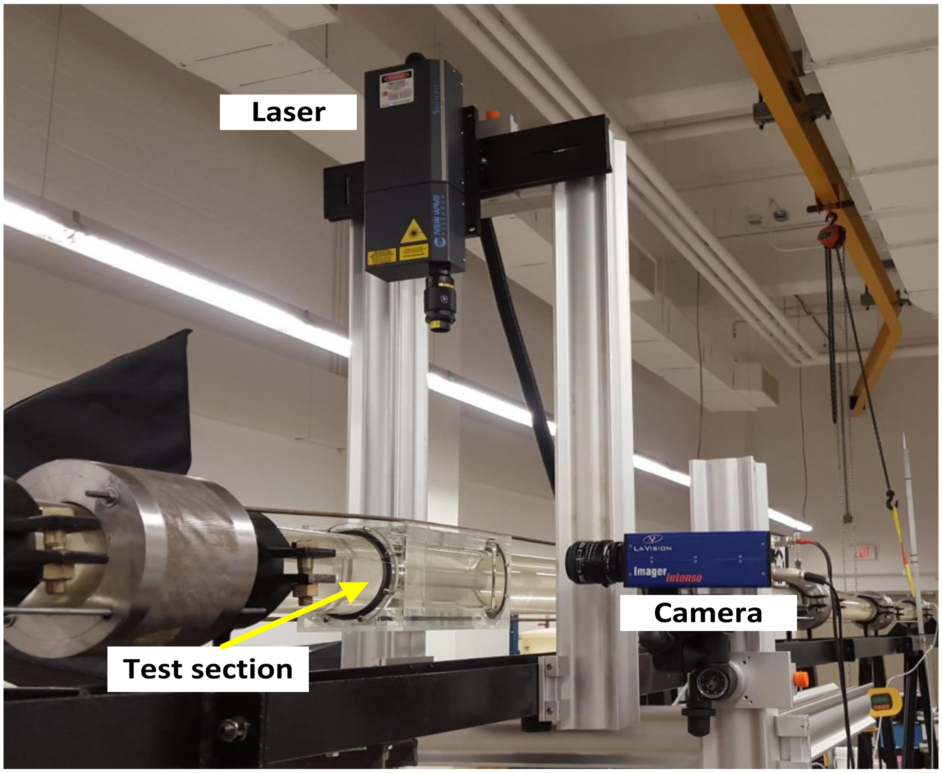

Figure 7-2 —Image of the PIV setup and the test section

For simulating drilled cuttings, natural quartz sand with mean sieve diameter of 600 microns was used. Experiments in this study were carried out at two superficial liquid velocities of 0.2 and $0.24\,\frac{m}{s}$ and two cuttings bed heights of approximately 8 and 14 mm. Superficial velocity is the flow rate divided by the cross section of the annulus (Eq.(1-6)).

$$u_s = \frac{Q}{A} \qquad \textbf{Eq.(7-1)}$$

Q is the flow rate and A is annulus cross sectional area while u_s refers to the superficial velocity. Critical velocity of bed erosion for both bed heights were found to be close to 0.24 m/s. This means cuttings at the bed started rolling and sliding along the bed at this velocity. This critical velocity was recorded previously in another study (Bizhani et al. 2016).

7.3. Velocity Measurement in Turbulent Flow Using PIV Technique

PIV is a nonintrusive laser based imaging technique that can provide high-resolution 2-D instantaneous velocity profiles of the flow field. We have used PIV for measuring the near bed velocity during the flow of water over two stationary cuttings bed. In a recent study (Bizhani and Kuru 2017), the authors measured velocity profiles in the entire annular gap in both upper and lower annulus. However, in this study, the focus was only on the near bed region. The aim of these experiments was to identify the impact of the presence of the stationary cuttings bed on the fluid flow near the cuttings bed. PIV procedures and method of working are explained thoroughly in the next sections.

To ensure measurements were carried out in a fully developed region, measurements were performed at a distance of approximately $100D_H$ from the annuli's inlet (development length for laminar flow is $88D_H$ (Poole 2010), development length for turbulent flow is shorter (Japper-Jaafar et al. 2010)). A rectangular box filled with glycerol is installed around the test section to reduce distortion and perspective errors in PIV images.

7.3.1. PIV Setup Description and Post-Processing Procedures

A planar 2-D PIV set-up consists of a light source and a recording device. A double pulse laser is used as the light source. The recording device is a camera with the double shuttering feature. The flow is seeded with tracer particles. Upon incident with the laser light, the tracer particles reflect the light, which is then detected by the camera. Two successive images are captured by the camera. Processing these pictures with an appropriate algorithm will yield the instantaneous velocity field of the flow. Figure 7-2shows an image of the PIV setup used in this study.

A Nd: YAG double pulsed laser with a wave length of 532 nm was used in this study. Laser light was converted to a planar light sheet by a combination of cylindrical and special optical lenses. The thickness of the laser light sheet could vary from 0.5 to 3 mm. Thick laser light may incur errors in measurement as a result of the depth of field thickness. The light thickness was kept at its minimum value of 0.5 mm in this study.

A CCD (charge-coupled device) camera with a resolution of 1376×1040 pixels was used for recording the images. The camera has a double shuttering feature, which enables capturing a pair of pictures in a short and controllable time interval. A 50 mm Nikon AF NIKKOR lens with a 12 mm extension tube was used for recording the images.

Figure 7-3**a** shows a typical PIV images acquired during the experiments. In this picture, the cuttings bed is located at the bottom while the drilling fluid (water), seeded with tracer particles (bright white dots), is flowing over the top. DAVIS 8.3.0 software was used for both image acquisition and post-processing of images. The software was used for adjusting appropriate parameters during the experiments (such as time interval between two images and laser power) as well as processing and extracting the data from the pictures. For further details regarding image processing algorithm see the next section.

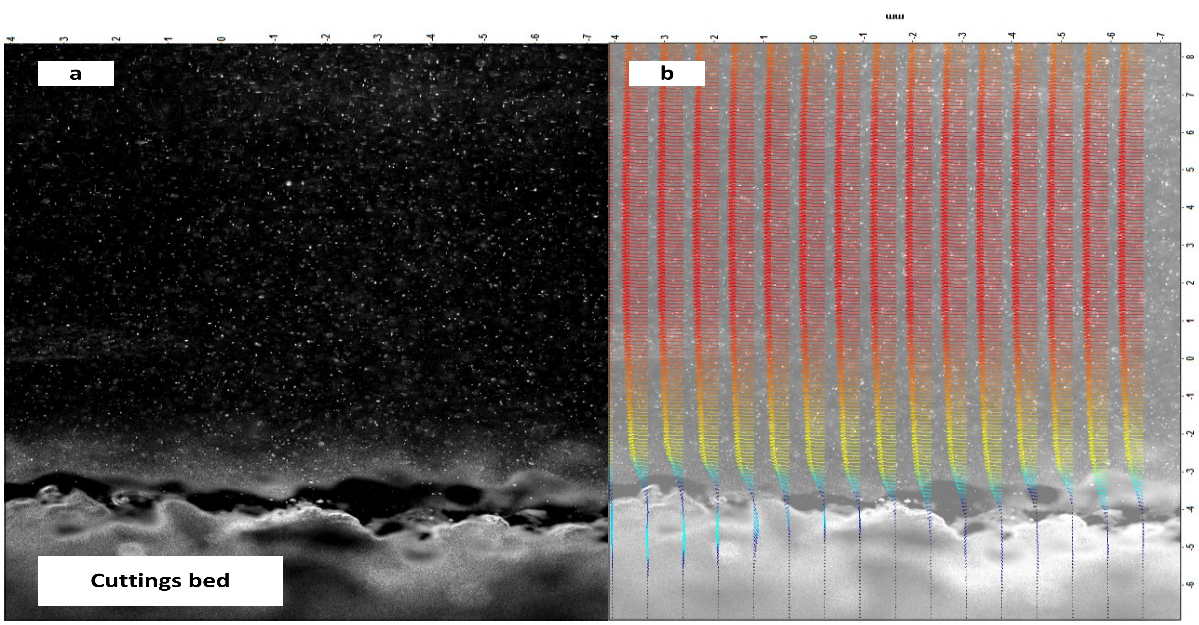

Figure 7-3— a) a typical PIV image acquired during tests, b) resultant velocity vector field

For tracer particles, hollow glass spheres with a mean diameter of 10 microns were used. The tracer particles are nearly neutral in water ($1.1 \pm 0.05 \frac{g}{cc}$) to keep them suspended in the flow. Addition of trace particles is necessary to enhance spatial resolution of PIV images (Melling 1997).

7.3.2. PIV Data Post-Processing Procedures

Processing algorithm for velocity calculations follows a cross-correlation based method. After obtaining a pair of images with tracer particles in the flow, each image is broken down to smaller windows called interrogation windows. Interrogation windows are analyzed in the 2nd image for probable similarities to the same interrogation window in the 1st image (Nezu and Sanjou 2011). To find the pixel displacement, the cross-correlation method was used. The method works by cross correlating the intensity distribution over a small area (interrogation window) of the flow. The peaks that show the highest correlation are chosen for the most probable destination of the seed particles. After finding the displacement of a seed particle in the two images (Δx and Δy) and having known the time interval (Δt) between the two images, velocity of the tracer particle or equivalently fluid velocity vector is calculated as follows:

$$\begin{cases} \hat{u} = \dfrac{\Delta x}{\Delta t} \\ \hat{v} = \dfrac{\Delta y}{\Delta t} \end{cases} \qquad \textbf{Eq.(7-2)}$$

Figure 7-3b shows the final velocity vector field for the flow over the cuttings bed. Multi-pass cross correlation method with decreasing of interrogation window size was used for particle displacement calculations. An initial interrogation window size of 64×64 pixels followed by the window size of 32×32 pixels was employed in the calculations. The overlap setting was 50%. To enhance the accuracy of the calculated vector fields, post-processing was also applied on the calculated vectors. Universal outlier detection setting was used in the post-processing to delete the outlier data points.

7.4. Results and Discussion

7.4.1. Critical Review of Mechanistic Hole Cleaning Models

Mechanistic hole cleaning modeling or more generally mechanistic modeling of sediment transport revolves around the balance of moments on a single particle in the bed. Interaction of solid particles and the fluid flowing over the bed is realized through momentum exchange. The momentum exchange occurs due to differences in velocities of the solid and fluid phases. Exchange of momentum between the solid and fluid phases imposes a hydrodynamic force on the particles. The resultant hydrodynamic force will not necessarily be parallel to the bed surface. This leads to the idea of splitting this force into its components parallel to the bed surface (i.e. drag force) and perpendicular to the bed (i.e. the lift force). Figure 7-4 shows a particle lying on the bed surface, which is exposed to the fluid hydrodynamic forces. The resistive forces, which prevent a particle from moving, are the gravity and frictional forces. In theory, a particle should start moving only if the combined impact of the drag and the lift force surpasses that of the gravity and the friction. The fluid force is not evenly distributed on all the particles. Some particles are in positions where they can be moved more easily; some are hidden and harder to move. The easiest path for the particle in Figure 7-3 to move is to pivot along the line perpendicular to the flow direction. If the bed is assumed fully horizontal, then the impact point for the drag and lift force can be assumed as the center of gravity of the particle. The total moment produced by body forces (gravity) is equal to the weight times the distance from the center of gravity to the pivoting point. Therefore, the necessary condition for the particle to move would be the balance of moments produced by the hydrodynamic force and resistive forces around the pivoting point. The balance of moments around the pivoting point is the framework of all mechanistic hole cleaning models (Ramadan et al. 2003, Duan et al. 2007).

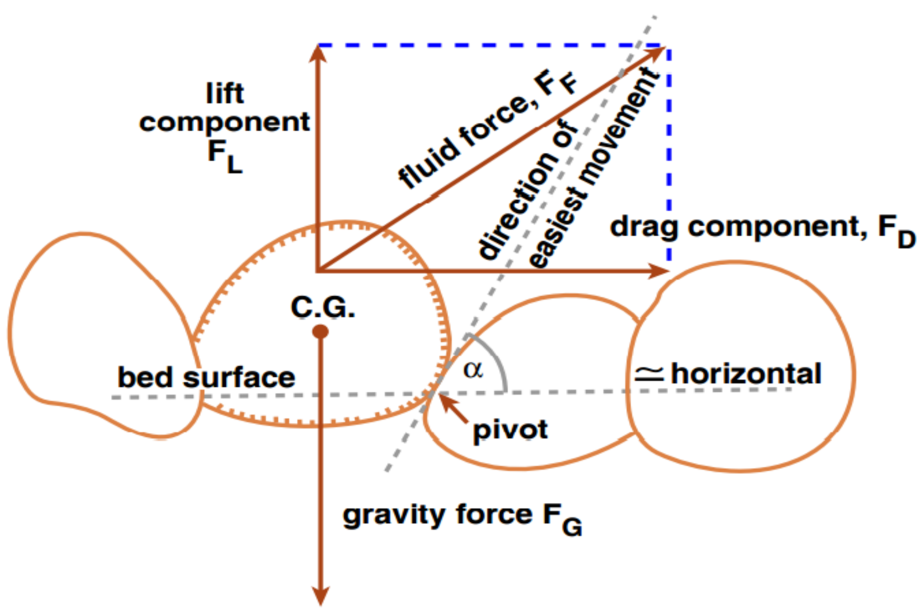

Figure 7-4 —Schematic illustration of different forces acting on a cutting in the bed (Regenerated from MIT Open Course Notes)

Accurate estimation of different forces acting on the particle, however, is not a trivial task. There are several issues which need to be addressed before arriving at an expression that would describe the condition necessary to dislodge the particle. The hydrodynamic forces are directly related to the fluid velocity; hence, the question of what velocity should be used for calculating these forces arises. The second issue to address is the role of the flow turbulence on the dislodgement of the particles. The third issue, which is missing altogether in the drilling literature, is the role of granular materials on the initiation of bed erosion itself. In the following sections, we discuss each issue separately concerning the previous studies and results from our experiments to show the current unjustified assumptions that might have led to the unrealistic results produced by available hole cleaning models.

7.4.2. Effective Fluid Velocity for Cuttings Bed Erosion

The effective fluid velocity concept is very often used in mechanistic hole cleaning models (Ramadan et al. 2003, Duan et al. 2007) to determine the drag (Eq.(7-3)) and the left (Eq.(7-4)) forces, which are assumed to be the main driving forces behind the particle movement. However, from the practical point of view, it is not as clear what velocity value should be used as the "effective velocity" in these mechanistic models for the realistic assessment of the drag and lift forces.

$$\hat{F}_D = \frac{1}{2}\rho_f A_p C_D \hat{u}^2 \qquad \textbf{Eq.(7-3)}$$

$$\hat{F}_L = \frac{1}{2}C_L \rho_f A \hat{u}^2 \qquad \textbf{Eq.(7-4)}$$

Figure 7-5 shows an example of how the velocity profile changes over the bed deposits during the turbulent flow of water in the horizontal annuli. The data shown in Figure 7-4 were measured for the flow of water at 0.2 m/s over the 8 mm thick cuttings bed. The sand particles with formed the bed deposit d_p of 600 microns. An idealistic illustration of the cuttings bed relative to the fluid velocity profile over the bed is also shown in the Figure 7-5. Different configurations of particle deposition might happen at the bed interface. Some larger cuttings stick out into the main flow, which makes them to be removed more easily than the smaller cuttings trapped in the holes between the larger particles.

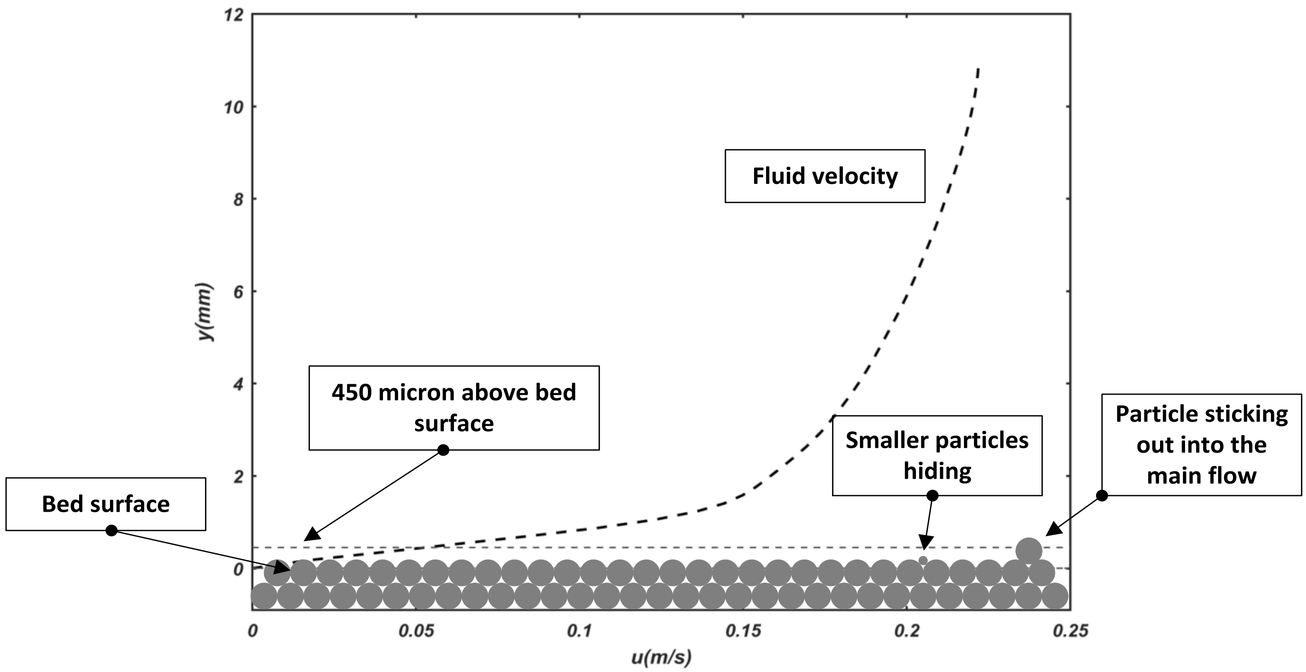

Figure 7-5 —Idealistic illustration of fluid time averaged velocity profile and sand bed interface

Theoretically, the velocity is zero at the horizontal plane defined by the mean bed surface (i.e., no slip effect). A single cutting lying at the top of the cuttings bed is affected only by the local fluid velocity in its immediate vicinity; which is significantly different from the maximum velocity or even from the average velocity of the fluid registered in the annulus (Figure 7-5). The effective fluid velocity for cuttings removal should, therefore, be the fluid velocity measured somewhere above the mean bed surface, but not too far away from the bed-fluid interface. In fact, only the fluid velocity measured around the center of the gravity of the particle should matter as far as cuttings removal is considered.

In the example shown in Figure 7-5, the effective velocity was identified at a distance less than a single particle's diameter (i.e., 600 microns) away from the mean bed surface. As a result, the velocity measured at 450 microns away from the average bed surface was considered to be the effective velocity controlling the drag and lift forces acting on the center of gravity of the single cutting.

In turbulent flow, the effective fluid velocity (i.e. actual velocity controlling the drag and lift forces acting on the cuttings) is the instantaneous velocity, which varies over the time. The instantaneous velocity, $\hat{u}$, can be decomposed into its mean and fluctuating parts (Eq.(7-5)).

$$\hat{u} = u + u' \qquad \textbf{Eq.(7-5)}$$

Where u is the time averaged velocity and u' is the fluctuating part of the instantaneous velocity ($\hat{u}$).

Other definitions of fluid velocities, which are also used in layer modeling approach for cuttings transport, are the superficial liquid velocity and the mean fluid velocity. The superficial velocity, u_s , is related to the pump flow rate and the annular cross-sectional area.

$$u_s = \frac{Q}{\frac{\pi}{4}(D_o^2 - D_i^2)} \qquad \textbf{Eq.(7-6)}$$

Q is the pump flow rate and D_o and D_i are annulus outer and inner diameters respectively. While superficial velocity does not take into account the presence of the stationary cuttings bed, the mean fluid velocity, $\overline{u}$, is affected by the presence of the cuttings bed (i.e. presence of the cuttings bed reduces the annular cross-sectional area available for fluid flow).

$$\overline{u} = \frac{Q}{A_f} \qquad \textbf{Eq.(7-7)}$$

A_f is the cross-sectional area available for fluid flow in the presence of the cuttings bed (calculations pertaining to A_f is presented in the Appendix A).

Comparison of the superficial, the mean, the time average and the instantaneous velocity values measured at constant flow rate (74 Lit/min) and with the presence of 8 mm and 14 mm thick cuttings bed, are presented in Figure 7-6 and Figure 7-7 respectively. The mean fluid velocity has the highest value (0.22 m/s@ 8mm thick bed, and 0.23m/s @ 14 mm thick bed) as it takes into account the reduction in flow area due to the presence of the cuttings bed. The superficial fluid velocity (0.2 m/s, same for both 8 mm and 14 mm thick bed), is also significantly higher than the local velocities.

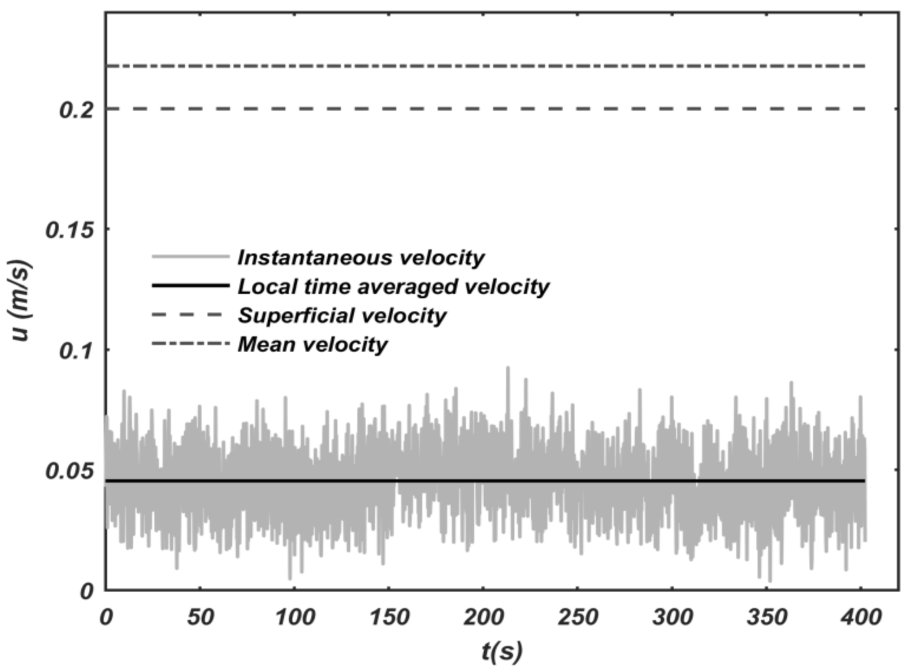

Figure 7-6 —Comparison of the superficial, the mean, the time average and instantaneous velocity values measured at constant flow rate (74 Lit/min) and with the presence of 8 mm thick cuttings bed in the horizontal annulus

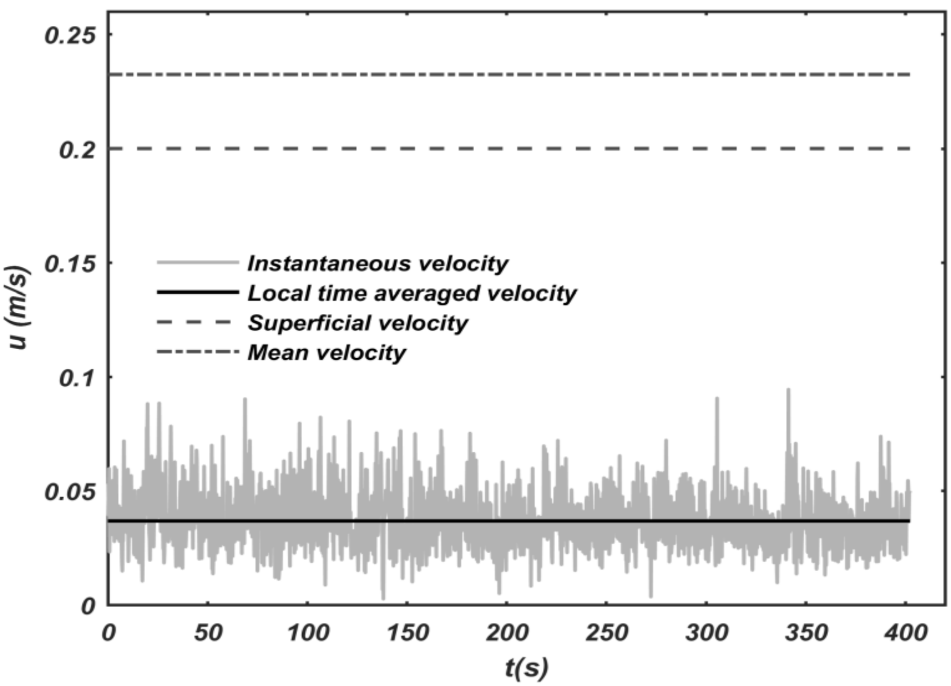

Figure 7-7 —Comparison of the superficial, the mean, the time average and instantaneous velocity values measured at constant flow rate (74 Lit/min) and with the presence of 14 mm thick cuttings bed in the horizontal annulus

The local time average velocity, u, was estimated to be considerably lower than the superficial and the mean fluid velocities (0.045 m/s @ 8mm thick bed, and 0.04 m/s@ 14 mm thick bed). The instantaneous velocity, $\hat{u}$, was varying over the time becoming lower or higher than the time average velocity, but it was all the time significantly lower than the mean and superficial velocity values. Estimating drag or lift forces acting on a single cutting using either the superficial or the mean fluid velocity would, therefore, result in tremendous overestimation of these forces. Neither the mean velocity nor the superficial fluid velocity could be representative of the effective fluid velocity governing the particle removal from the surface of bed deposits. Therefore, when developing mechanistic hole cleaning models these velocities should not be used.

Comparison of local instantaneous and time average velocities near the cuttings bed interface (Figure 7-8 and Figure 7-9) reveals that there is a significant level of velocity fluctuations near the bed interface. Fluctuations in the velocity are caused by the turbulent nature of the flow as well as the uneven and rough surface of the cuttings bed. The ratio of instantaneous velocity to time average velocity vs. time was plotted in Figure 7-8 and Figure 7-9. The results showed that the instantaneous velocity could be up to 2 times higher than its mean value. The effective fluid velocity in hole cleaning is the instantaneous fluid velocity. Considering the time average local velocity as the effective fluid velocity may lead to significant underestimation of actual fluid velocity near the cuttings bed. However, the impact of velocity fluctuations is an artifact of the turbulence and is discussed in more details in the next section.

Accurate estimation of local effective fluid velocity in the turbulent flow can be challenging. The common practice in most mechanistic hole cleaning models is to assume a universal velocity profile that relates local velocity to that of vertical distance from the zero-velocity plane (Ramadan et al. 2003, Duan et al. 2007). However, this approach can be questioned from two perspectives. First of all this method yields time average velocity and hence, it ignores the role of velocity fluctuations. The second issue is associated with the validity of these universal velocity profiles. There has been very little work done related to fluid flow over cuttings bed in annuli's. Hence, these universal velocity profiles need to be validated before use.

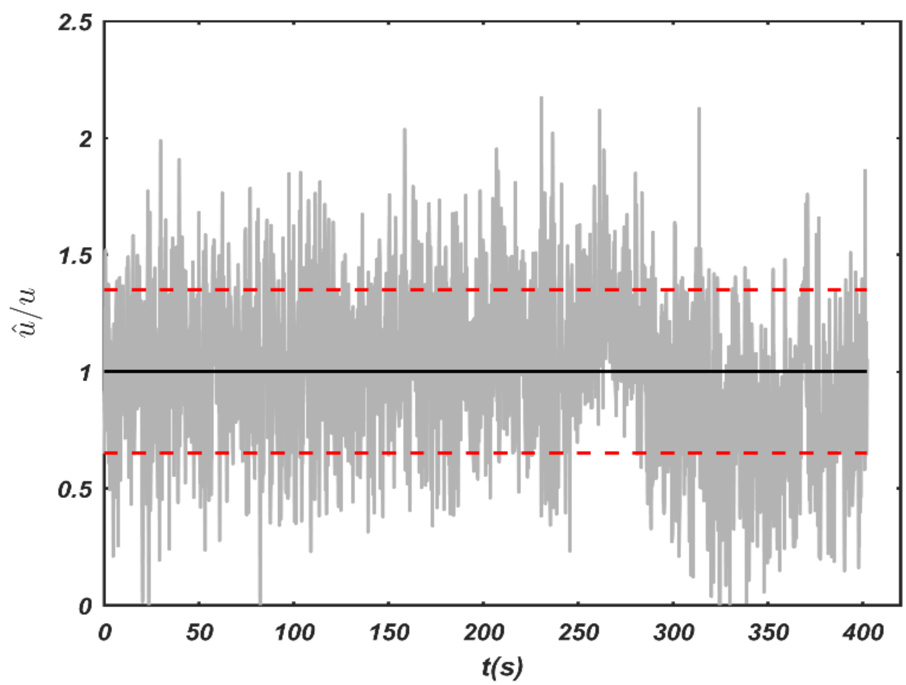

Figure 7-8— Ratio of effective instantaneous velocity to time average velocity near cuttings bed of height 8mm ($U_s = 0.24\frac{m}{s}$)

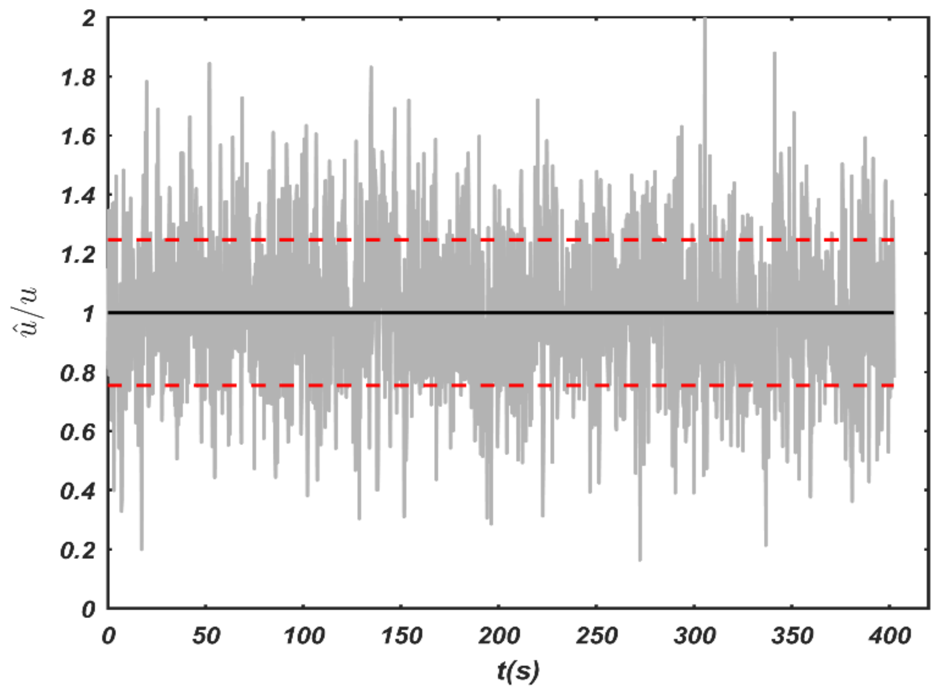

Figure 7-9 —Ratio of effective instantaneous velocity to time average velocity near cuttings bed of height 14mm ($U_s = 0.2\frac{m}{s}$)

7.4.3. Role of Turbulence in Cuttings Bed Erosion

Fluctuations in the effective fluid velocity will result in fluctuations in the effective fluid hydrodynamic force acting on the particles. These fluctuations can create a force high enough to dislodge the particle. Several studies have shown the importance of flow turbulence in sediment transport (Diplas et al. 2008, Heyman et al. 2013, Schmeeckle 2014). However, almost all the cuttings transport models used in drilling industry ignores the role of turbulence in this process. To quantify the extent of the impact of velocity fluctuations on the instantaneous drag force, effective and time average drag forces acting on the cuttings are calculated using the experimentally measured near wall velocity data. The drag force defined by Eq.(7-3). Three is the instantaneous or the effective drag force. The effective drag force can also be written (Eq.(7-8)) as the sum of the steady state (Eq.(7-9)) and unsteady state components (Tsuji et al. 1991, Ramadan et al. 2003).

$$\hat{F}_D = F_D - V_p \frac{\Delta P}{\mathrm{L}} + f_D \qquad \textbf{Eq.(7-8)}$$

$$F_D = \frac{1}{2}\rho_f A_p C_D u^2 \quad \textbf{Eq.(7-9)}$$

In Eq.(7-8) and Eq.(7-9) u is the time average velocity near the center of gravity of the sand particle of interest, C_D is the drag coefficient, $\frac{\Delta P}{\mathrm{L}}$ is the pressure gradient term, A_p and V_p are the projected surface area in the flow and the projected volume respectively. The third term, f_D, in right hand side of the Eq.(7-8) is the unsteady state part of the drag force. F_D is the steady state part of the drag force. According to Ramadan et al. (2003) the unsteady state part of the drag force is negligible comparing to its steady state part.

The drag coefficient depends on the particle Reynolds number. There are numerous correlations available in the literature for estimating the drag coefficient; most of them apply only for single spherical particles. Ramadan et al. (2003) presented a set of equations (Eq.(7-10) and Eq.(7-11)), which can be used for estimating the drag coefficients for particles in the cuttings bed.

$$C_D = \frac{24}{Re_p} + \frac{5}{1 + Re_p^{0.5}} + 0.4 \quad \textbf{Eq.(7-10)}$$

$$Re_p = \frac{\rho_f u d_p}{\mu} \quad \textbf{Eq.(7-11)}$$

The fluid velocity used in the calculation of the particle Reynolds number (Eq.(7-11)) changes by the definition of the drag force (i.e., instantaneous or the time averaged). The drag coefficient presented in Eq.(7-10) is for a single particle. To account for the impact of the presence of other particles in the bed, a correction factor of 0.85 was suggested by Ramadan et al. (2003).

To assess the extent of the magnitude of fluctuation velocities on the drag force, the ratio of drag force calculated based on instantaneous velocity, $\hat{u}$, and time average velocity, u, is calculated. This ratio represents the ratio of the actual drag force to its time averaged value and mathematically defined by the Eq.(7-12).

$$\frac{\hat{F}_D}{F_D} = \frac{C_D(\hat{u})\hat{u}^2}{C_D(u)u^2} \qquad \textbf{Eq.(7-12)}$$

When calculating the instantaneous and the mean drag forces in the Eq.(7-12), the respective velocities (i.e. instantaneous or mean) are used for estimating the particle Reynolds number and the drag coefficient.

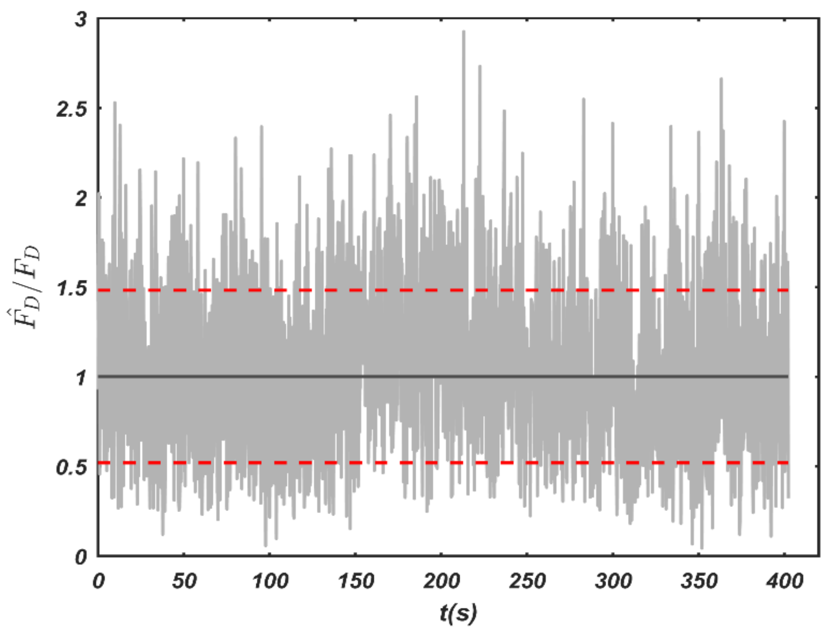

Figure 7-10 —Ratio of instantaneous to average drag force measured near a cuttings bed of height 8mm ($\boldsymbol{U_s = 0.2\,\frac{m}{s}}$)

The drag force ratio (Eq.(7-12)) was calculated using experimental data for flow involving water at two superficial fluid velocities (0.2 and 0.24 m/s) over the two different stationary bed heights (8 and 14 mm). The results are shown in Figure 7-10 and Figure 7-11(the data are presented for two cases only, other cases are similar to the reported cases). A quick look at these figures reveals that the instantaneous drag force could be up to three times higher than that of the average drag force. This means that the assumption made by other researchers (Ramadan et al. 2003, Duan et al. 2007) to ignore the fluctuating part of the drag force is not valid. A particle lying on the cuttings bed may experience a drag force significantly higher than the average drag force. This observation has significant practical implications for the selection of the required minimum flow rate to initiate bed erosion. Theoretical calculations using the average drag force may indicate that hole cleaning will not be initiated under the selected average fluid velocity. However, in reality, the instantaneous drag force (governed by the local instantaneous fluid velocity) can be several times higher, which could create a moment high enough to roll or slide the particle along the bed.

The fluctuations in fluid velocity are creating instantaneous drag force much higher than its average time value. The RMS of fluctuations in the ratio of $\frac{\hat{F}_D}{F_D}$ can be a good indicator of the level of changes in $\widehat{F}_D$. The RMS of fluctuations of the drag force ratio is also plotted in Figure 7-10 and Figure 7-11 (i.e. the dashed lines represent the upper and lower limit of RMS of fluctuations). The upper level of the fluctuations is somewhere between 1.4 to 1.5. That means that the instantaneous drag force deviates from its average value by a factor anywhere between 1.4 to 1.5 (and that is only based on the standard deviation of the data).

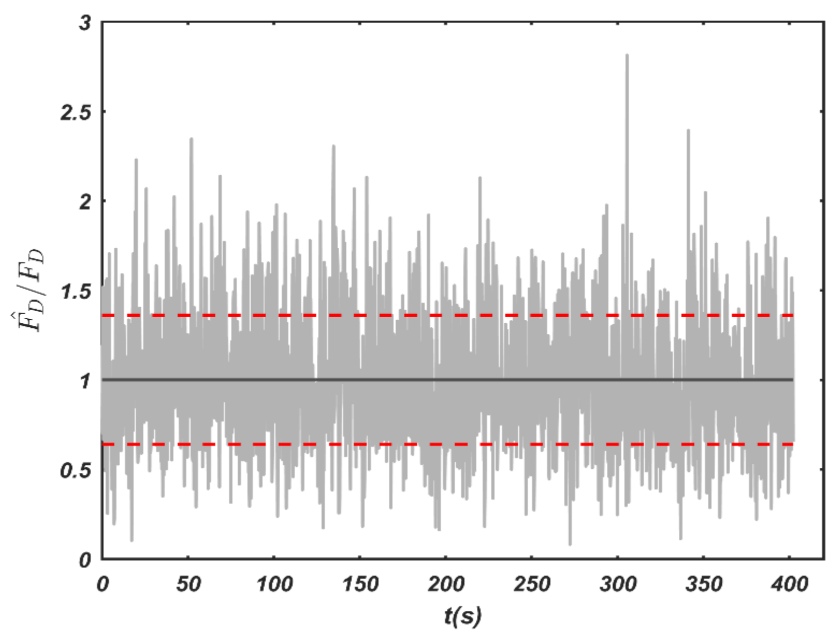

Figure 7-11— Ratio of instantaneous to average drag force measured near a cuttings bed of height 14mm ($U_s = 0.2\frac{m}{s}$).

In many of the previous mechanistic hole cleaning models only the steady part of the drag force has been considered (Clark and Bickham 1994, Ramadan et al. 2003, Duan et al. 2007).

The experimental results from this study show that the drag force can significantly deviate from its mean value. Probably this explains why turbulence is so crucial for effective hole cleaning. In turbulent flow, the local time averaged velocity might be low due to the no slip condition at the bed interface. However, fluctuations in the velocity can increase the drag force momentarily to a level several times higher than its average value. Therefore, turbulent flow can be significantly more efficient in hole cleaning.

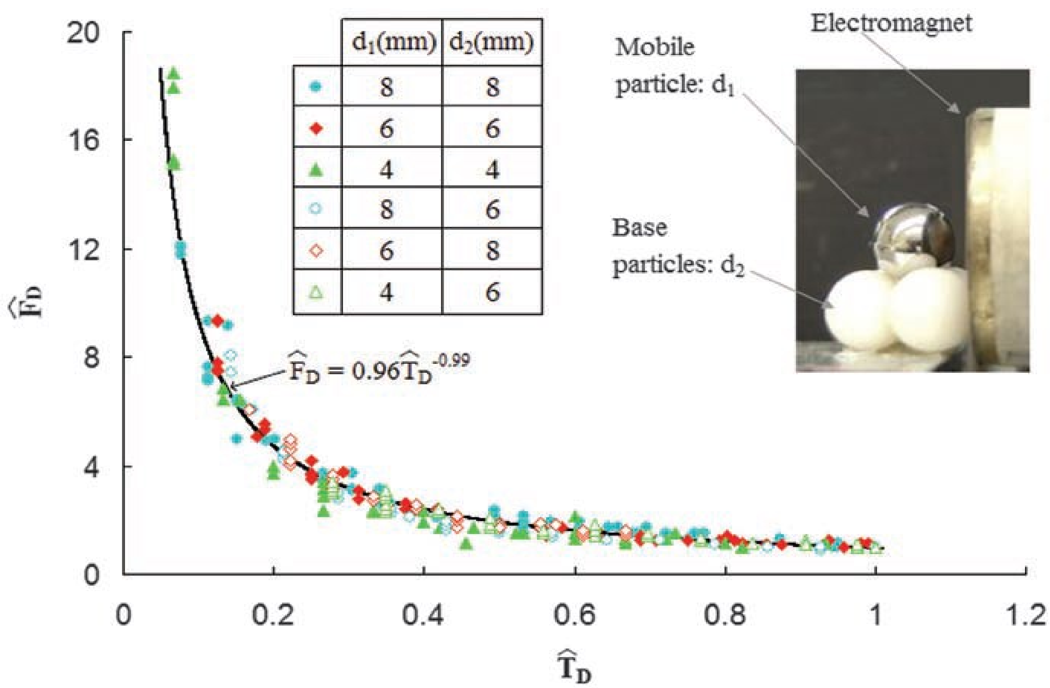

Figure 7-12— Correlation between critical drag force and duration necessary to apply the force (Diplas et al. 2008)

Analyses of local effective fluid velocity and instantaneous drag force data all show the importance and significance of flow turbulence on cuttings removal. In a turbulent flow, the effective fluid velocity and effective drag force can be much higher than their time average values. Hence, it is important to incorporate these velocity fluctuations in any models describing the interaction of the fluid and the particles. As pointed out by Diplas et al. (2008) the current criteria for initiation of movement rely on time average quantities; therefore, failing to capture the impact of velocity fluctuations. In interesting sets of experiments, Diplas et al. (2008) studied the role of flow turbulence on the initiation of motion of particles. They found out that any instance of particles dislodgment was coincided by a peak in the local velocity. However, not all the positive fluctuations in the velocity resulted in particles movement. Their study showed that a peak in the local velocity was necessary but not sufficient for particles dislodgment. In other words, a peak velocity of sufficient magnitude and duration can initiate movement of the particle. The length of the velocity fluctuation is as important as the scale of the peak. The result of their study showed that critical drag force correlates well with the time of applying the force. Figure 7-12indicates the relation between the instantaneous drag forces required to dislodge a particle versus the time of applying the force (Diplas et al. 2008). According to data presented in the Figure 7-12, the critical drag force that results in initiation of the particle movement is a function of the time over which the force was applied. Here $\widehat{F}_D$.is the critical drag force and $\widehat{T}_D$ is the duration or the impulse of the force respectively.

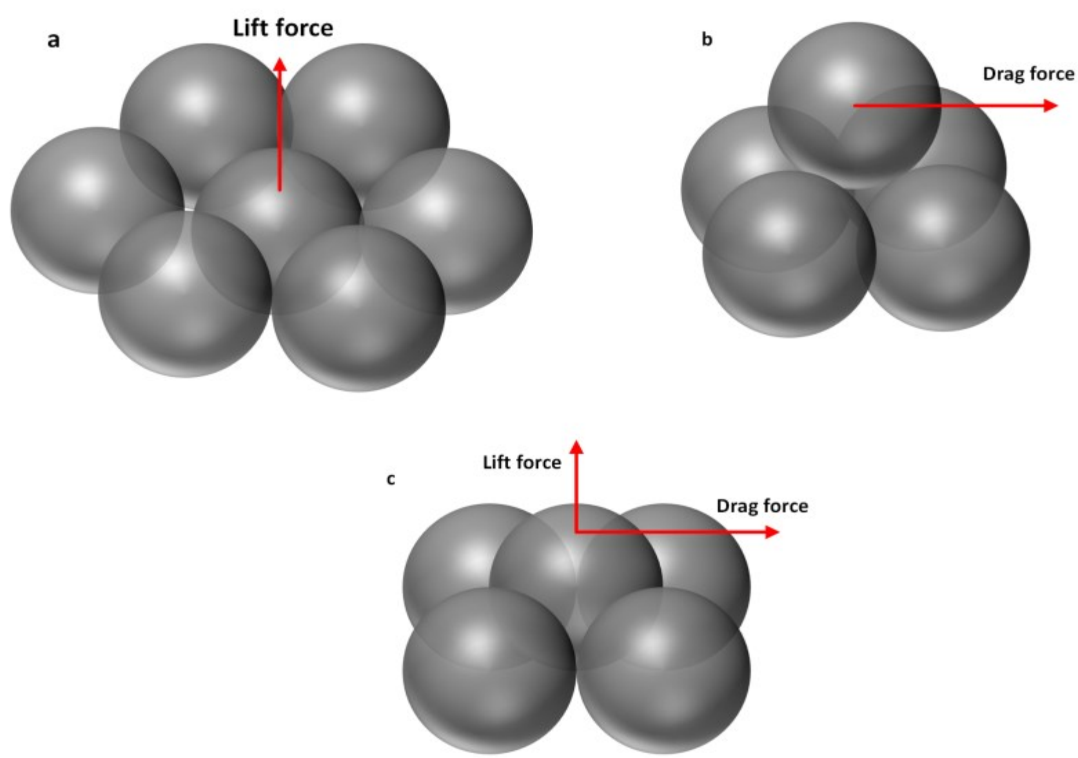

Figure 7-13— Variations in particle's arrangement at the bed interface

The relation between critical drag force and the impulse suggests that if a moment balanced approach is to be used for predicting particles movement, the impulse of the force needs to be considered as well (Diplas et al. 2008). The impulse, which represents the duration over which the force was applied, is as important as the force itself. For very short impulses, the significantly higher drag force is required to move the cuttings. The impulse also changes the mode of movement of the particle. For instance, the very large force applied over a short period will cause the saltation mode.

In addition to the importance of fluid drag force and flow turbulence on cuttings removal, particle size variation as well as the local arrangement of particles significantly affect the resistive and the hydrodynamic forces (Diplas et al. 2008). The hydrodynamic force is composed of an axial force (drag) and a vertical force, namely the lift force. The lift force is not considered as important as that of drag force. However, as mentioned by Diplas et al. (2008) depending on the local arrangement of the particles, the effectiveness of these forces changes. The local arrangement of particles has one of the three possible scenarios shown in Figure 7-13; pure lift (13a), pure drag (13b) and the combination of both forces (13c). In the pure lift regime, only lift force can move the particle vertically before the flow can transport it downstream. In this case, the cutting is completely embedded in the bed. In pure drag regime, the particle is completely exposed to main flow and hence can easily be carried away by the flow. In the most likely scenario, the particle is partially exposed to flow and hence, both drag and lift forces are equally important.

The lift force, similar to drag, varies temporally in the turbulent flow. The lift force is caused by the uneven distribution of the dynamic pressure on the grain surface. Higher fluid velocity at the top of a cutting lying on the cuttings bed interface gives rise to the higher pressure on the lower surface (comparing to the zero velocity at the bottom). This phenomenon results in a net upward force, which is then called the lift force. Similar to the drag force, the lift force can be expressed as follows:

$$F_L = \frac{1}{2} C_L \rho_f A \hat{u}^2 \qquad \textbf{Eq.(7-13)}$$

The lift coefficient is very difficult to derive for complex cases such as particles lying on the cuttings bed. It is only known for simple cases such as the single spherical particle (i.e. Siffman's

(1965) lift force model only applies for a single spherical particle). Nonetheless, for comparison purpose, we present here the expression used by Duan et al. (2007) in their mechanistic model.

$$C_L = 2.47\left(\frac{d_p}{uRe_p}\frac{du}{dy}\right)^{0.5}$$ **Eq.(7-14)**

This expression is valid for $Re_p < 1$, for higher Re_p the following correction to the lift coefficient was suggested.

$$C_L = K_0\eta^{0.9} + K_1\eta^{1.1}$$ **Eq.(7-15)**

$$\eta = \frac{y}{u}\frac{du}{dy}$$ **Eq.(7-16)**

Coefficients K_0 and K_1 are functions of particle Reynolds number and are defined in the Appendix B.

Figure 7-14 and Figure 7-15show the ratio of the effective drag force to the lift force calculated by using the experimental data. Comparison of the data indicates that the drag force is significantly higher than the lift force. On average, the drag force is around 30 to 40 times greater than the lift force. In Figure 7-14 and Figure 7-15 the lower and upper limits of the variation in the ratio of drag to lift force calculated based on the RMS of the fluctuations are also reported (the dashed red lines). Based on the variations, the drag force to the lift force ratio is bounded to a region between 20 to 50. This means that the drag force on its lowest ratio would be around 20 times higher than the lift force. On the upper side, the drag force can be 50 times greater than the lift force. Note that the accuracy of such calculations is limited by the accuracy in predicting the actual lift and the drag coefficients.

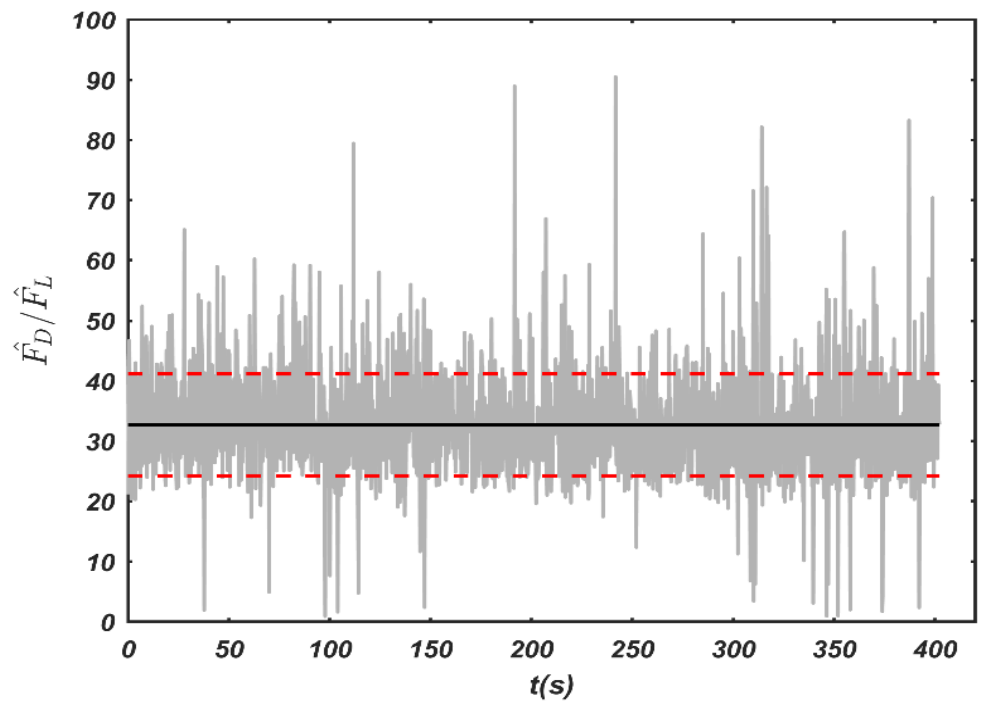

Figure 7-14— Ratio of drag force to lift force measured near a cuttings bed of height 8mm ($U_s = 0.2\frac{m}{s}$)

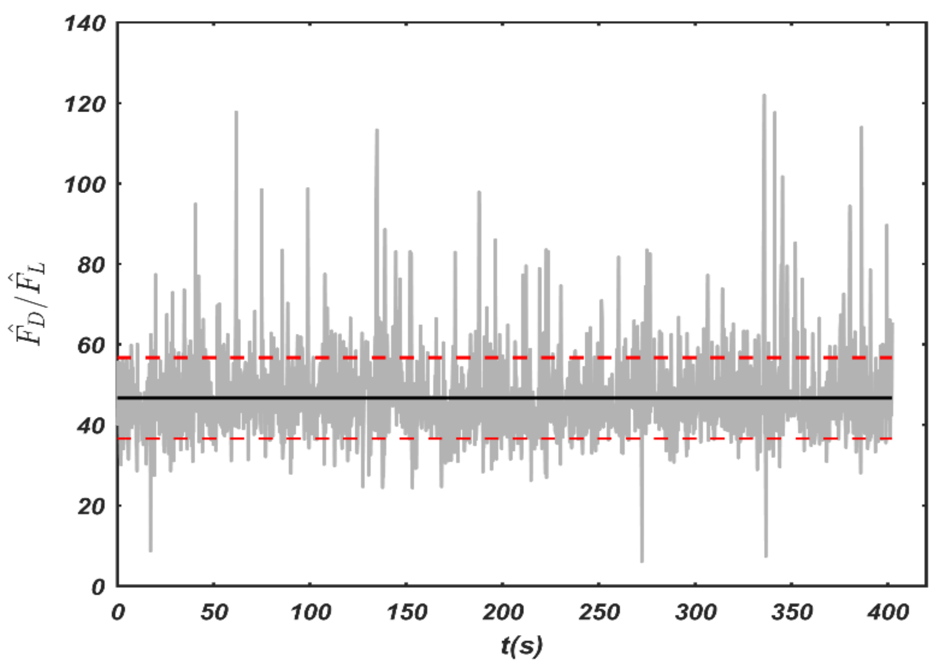

Figure 7-15— Ratio of drag force to lift force measured near a cuttings bed of height 14mm ($U_s = 0.2\frac{m}{s}$)

The combination of the results shown in Figure 7-14 and Figure 7-15together with the discussion about the impact of particles arrangement shows why it is much harder to move a particle that is completely embedded in the cuttings bed. In this case, only the lift force can dislodge the particle. However, the lift force is much smaller than drag force. Temporal variations of the lift force due to turbulence are similar to that of the drag force. Similar to drag force, Diplas et al. (2008) showed that critical lift force correlates with the duration over which the force was applied. This means to capture the full impact of the applied lift force on the particle, in addition to the magnitude of the applied force, the duration of the application of the force should be taken into account as well.

7.4.4. Shortcomings of the Current Mechanistic Hole Cleaning Models

The moment based approach toward sediment transport evolves around moment balanced around a pivoting point for a given particle. In the previous section, we have discussed the difficulties in estimating the true fluid velocity that needs to be used in the calculation of fluid hydrodynamic forces that are responsible for the movement of the cuttings. Further, we have discussed the role of turbulence on the forces experienced by the drilled cuttings in the bed. It was also shown was how the local arrangement of particles in the bed could change the significance of each force. If we assume that fluid-particle interaction could be captured through a moment base model such as the one proposed by Ramadan et al. (2003) or Clark and Bickham (1994), then several consideration must be made before any attempt in developing such models.

The first and foremost consideration must be the accurate estimation of the local effective fluid velocity near the cuttings bed. As we have shown using experimental data, local instantaneous velocity can vary significantly over the time and hence time average velocity cannot be representative of the fluid velocity near the bed; that brings to our attention the importance of turbulence. Turbulence is critical in the movement of the particles (Diplas et al. 2008). Hence, the impact of the flow turbulence must be considered in any mechanistic hole cleaning models. This is particularly challenging because, in addition to the velocity fluctuations, the impulse (i.e. duration of the velocity fluctuations) needs to be considered as well.

Another important factor in modeling sediment transport is the local arrangement of the cuttings. For a particle that is completely embedded in the bed, only lift force can move it. Therefore, the model must include the impact of cuttings arrangement in it.

All the discussions presented so far have assumed a pure hydrodynamic framework for the cuttings removal modeling; that is the interaction of fluid-particle can be captured by the forces that are applied. However, in the next section, we will discuss the importance and relevance of granular material properties on the threshold of particles movement. We will show that in addition to the difficulties mentioned so far, one needs to consider the movement of bed materials in the model as well.

7.4.5. Critical Review of Empirical (Semi-Mechanistic) Hole Cleaning Models

Modeling of sediment transport using mechanistic or the moment based approach have not proven effective and useful in the most field cases because of the limitations that were discussed in the previous sections. Hence, very often a semi-mechanistic and empirical models developed based on the experimental results are used. Traditionally, the Shields' stress is used to represent the onset of particles movement (Shields 1936, Peysson et al. 2009). The Shields' stress is the dimensionless form of the fluid shear stress at the cuttings bed interface and is defined as follows:

$$\tau^* = \frac{\tau_b}{d_p g(\rho_s - \rho_f)} \quad \textbf{Eq.(7-17)}$$

Shields' stress multiplied by d_p^2 represents the ratio of fluids drag force to the particles submerged weight. Onset of particles movement is, usually, quantified by a critical Shields' number (τ_c^*). In the range of $\tau_c^* < \tau^* < 5\tau_c^*$, cuttings movement happens in the form of bedload (Houssais et al. 2015).

Another approach, which has gained popularity in drilling literature during the 1990's and early 2000s, is the layer modeling approach toward cuttings transport (Nguyen and Rahman 1998, Cho et al. 2000, Kelessidis and Mpandelis 2004b). In the layer modeling approach, a balance of forces is used based on the shear stresses on different surfaces in the annuli. Figure 7-16 shows a simple schematic of a two-layer model. The important shear stresses to consider are the interfacial shear stress, τ_b, wall shear stress, τ_w, and shear stress between the bed and the pipe wall, τ_{bw}. The idea is simple; the net force in the axial direction must balance that of the pressure force.

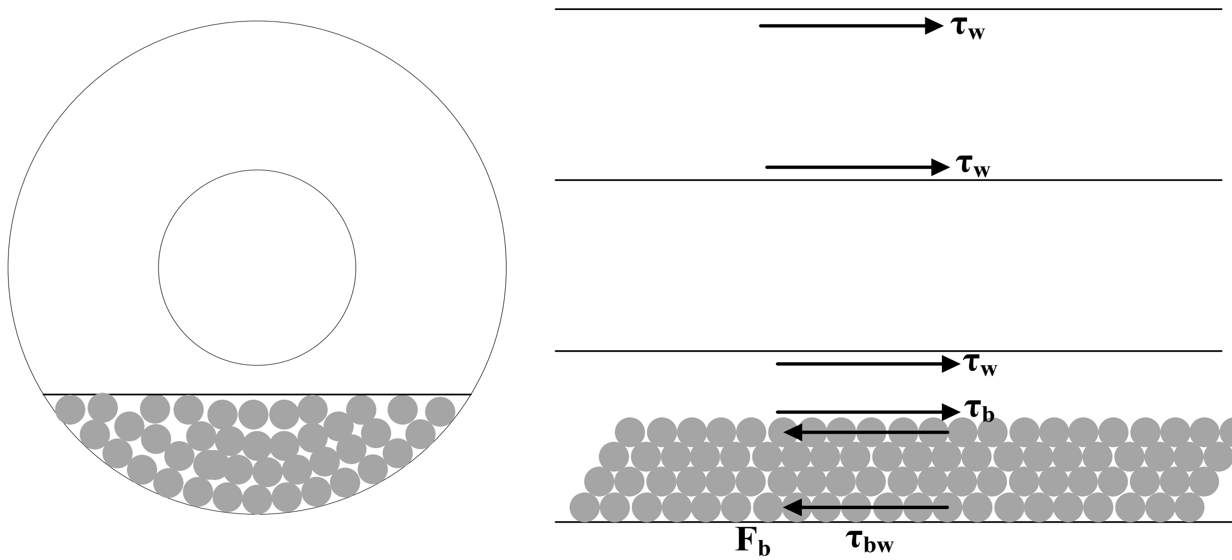

Figure 7-16 — Schematic illustration of shear stresses in a 2 layer model

In the context of layer modeling, one momentum equation is written for each layer. For the simple case of 2 layer modeling, the momentum equations are (Kelessidis and Bandelis 2004a):

$$A_f \frac{dP}{dx} = -\tau_w S_w - \tau_b S_b \quad \textbf{Eq.(7-18)}$$

$$A_b \frac{dP}{dx} = \tau_b S_b - \tau_{bw} S_{bw} - F_b \quad \textbf{Eq.(7-19)}$$

In these equations, S_b is the interfacial bed area, S_{bw} is the bed contact area with the wall, S_w is the wetted perimeter of the pipes and A_b is the bed cross sectional area.

Semi-mechanistic and empirical models of hole cleaning all rely on the accurate estimation of the bed shear stress. In the following sections, we first discuss the difficulties in accurate evaluation of bed shear stress. Following that we analyze the current approach by using the bed shear stress for modeling the hole cleaning. Finally, we discuss the shortcomings and limitations associated with predicting the onset of bed erosion using the bed shear stress.

7.4.6. Variation of the Bed Shear Stress with Time

The fluid shear stress at the bed interface is one of the most important parameters considered in the hole cleaning models. The importance of the bed shear stress can be best understood through its relation to the drag force. The fluid drag force exerted on the cuttings bed can be related to the interfacial shear stress as follows:

$$F_D = c d_p^2 \tau_b \quad \textbf{Eq.(7-20)}$$

In this equation, c is a coefficient that accounts for geometry and packing of the grains as well as the variations in the drag coefficient. If we assume that the coefficient c remained the same for a bed, then one can write:

$$\frac{\hat{F}_D}{F_D} \approx \frac{\hat{\tau}_b}{\tau_b} \quad \textbf{Eq.(7-21)}$$

Where $\hat{\tau}_b$ represents the instantaneous bed shear stress and τ_b the time averaged bed shear stress. Eq. 21 suggests that bed shear stress varies over the time just like the drag force. Therefore, representing the bed shear stress with a single number might not reflect the actual state of the stress at the bed interface. Earlier, we observed that the instantaneous drag force varies significantly over the time. The same statement is also true about the bed shear stress. The instantaneous bed shear stress, at moments, could be much higher than the average bed shear stress.

7.4.7. Assessment of the Mean Bed Shear Stress

Accurate solution of the momentum equations presented in Eqs. 18 and 19 require accurate estimation of the different shear stresses in these equations. The fluid shear stress on the pipe walls can be estimated accurately since it has been studied extensively in the fluid mechanic. Measurement of interfacial shear stress is not as simple as that of the fluid stress on the pipe wall and, hence, there is not much data available on interfacial shear stress. It is a common practice in drilling literature to extend the correlations valid for calculating fluid shear stress on the pipe wall to that of the interfacial shear stress with added roughness (Duan et al. 2007).

In this section, we examine the different approaches to evaluating bed shear stress to assess their accuracy. Accurate solution to momentum equations in any layer modeling of cuttings bed removal requires accurate estimation of the bed shear stress. Therefore, the analyses presented here should serve as a guideline in developing or enhancing more realistic hole cleaning models.

The bed shear stress can be evaluated from experimental data or correlations that relate flow conditions to shear stress. The first and the most accurate method of estimating the bed shear stress is through using the measured velocity profiles. In this approach, a logarithmic velocity profile of the form of Eq.(7-22) is fitted to the experimentally measured velocity profiles. Velocity profile represented by Eq.(7-22) is the universal velocity profile in wall units (Kundu et al. 2012).

$$u = \frac{u_\tau}{\kappa} Ln\left(\frac{y}{y_o}\right) = \frac{u_\tau}{\kappa} Ln(y) + \frac{u_\tau}{\kappa} Ln\left(\frac{1}{y_o}\right) \qquad \textbf{Eq.(7-22)}$$

Where u is the time averaged local velocity, u_τ, is the friction velocity, y is the vertical distance from the bed interface and y_o is the characteristic roughness. If one plots u vs. y in a semi-log scale, the slope of the resultant line would be equal to friction velocity over van Karman constant ($\kappa = 0.41$). The bed shear stress is then calculated using the following relation:

$$\tau_b = \rho u_\tau^2 \qquad \textbf{Eq.(7-23)}$$

It is not always possible to estimate the bed shear stress using the near wall velocity profile if such data are not available. Alternately, the measured frictional pressure loss data can also be used to calculate the bed shear stress.

$$\tau_b = -\frac{D_h}{4}\frac{\Delta P}{\mathrm{L}} \qquad \textbf{Eq.(7-24)}$$

The hydraulic diameter, D_h, used in the Eq.(7-24) is a function of the bed height. The method for calculating D_h for a given bed height is given in the Appendix A. This approach yields an average value of the shear stress inside the annulus. This approach does not differentiate between the shear stress at the bed, τ_b , and the wall shear stress, τ_w. However, it has been proven that this approach can still be useful when accurate estimation of τ_b and τ_w cannot be made separately (Bizhani et al. 2016).

Contrary to the averaging the shear stress method, multi-layer cuttings transport models differentiate the shear stresses on the different surfaces inside the annuli (Kelessidis and Bandelis 2004a, Li and Luft 2014a). In this approach, typically the friction factor correlations are used to estimate the bed shear stress. The bed shear stress is related to the mean fluid velocity (assuming stationary cuttings bed) and the Fanning friction factor (Eq.(7-25)).

$$\tau_b = f_b \frac{\rho \bar{u}^2}{2} \quad \textbf{Eq.(7-25)}$$

$\bar{u}$ is the fluid mean velocity, ρ is the fluid density, and f_b is the Fanning friction factor. To estimate the bed shear stress, the Fanning friction factor needs to be evaluated. In the drilling literature, there are few correlations available for predicting friction factor at the bed. Duan et al. (2007) used the correlations (Eq.(7-26) to Eq.(7-28)) developed by Reed and Pilehvari (1993).

For a laminar flow, the friction factor is given as:

$$f_b = \frac{16}{Re_{gn}} \quad \textbf{Eq.(7-26)}$$

$$Re_{gn} = \frac{D_h \rho_f \bar{u}}{\mu} \quad \textbf{Eq.(7-27)}$$

For a turbulent flow, the friction factor is evaluated using the following relationship:

$$\frac{1}{\sqrt{f_b}} = -4 \log\left(\frac{0.27\varepsilon_{bed}}{D_h} + \frac{1.26}{Re_{gn}\sqrt{f_b}}\right) \quad \textbf{Eq.(7-28)}$$

Definitions of the bed roughness and the hydraulic diameter are given in Appendix A.

Another friction factor correlation proposed by Televantos et al. (1979) has been widely used by other researchers (Kelessidis and Bandelis 2004a, Li and Luft 2014b).

$$\frac{1}{\sqrt{2f_b}} = -0.86\ln\left(\frac{d_p}{3.7D_h} + \frac{2.51}{Re_{gn}\sqrt{2f_b}}\right) \qquad \textbf{Eq.(7-29)}$$

Out of all the correlations and methods used for calculating the bed shear stress, the value obtained by using the near wall velocity profile is the most accurate one. In the following section, we present comparisons of the bed shear stress values calculated by using different friction factor correlations presented above and the experimentally measured bed shear stresses.

Table 7-1 and Table 7-2reports the bed shear stress values calculated by using the experimental data and the methods explained above for flow over the 8 mm and 14 mm bed thickness, respectively. As shown by the data, increasing bed height causes the bed shear stress to increase. This increase is mainly because of the reduction in the flow area, which consequently increases the flow velocity indicating that the bed erosion for a thicker bed will start at the lower volumetric flow rate.

Table 7-1 Bed shear stress - Cuttings bed height is 8mm

	$\boldsymbol{\tau_b\ (Pa)}$			
$\boldsymbol{u_s\ (\frac{m}{s})}$	Based on Velocity profiles	Based on Pressure loss data	Based on Eq.(7-25) and Eq.(7-28)	Based on Eq. 25 and Eq.(7-29)
0.2	0.272	0.255	0.248	0.529
0.24	0.393	0.40	0.351	0.7

The bed shear stress calculated using the frictional pressure loss measurement (Eq. 24) falls within 13% range of the actual bed shear stress. The error in estimation of the bed shear stress, in this case, increases with the increasing bed thickness. Nonetheless, it seems that frictional pressure loss data can be used to calculate the bed shear stress with reasonable accuracy.

The bed shear stress values calculated using the correlation proposed by Duan et al. (2007) is within the 20% range of the actual bed shear stress. Indeed, this prediction is reasonable, if no measurement of either velocity profiles or frictional pressure loss data is available.

Table 7-2 Bed shear stress - Cuttings bed height is 14mm

	τ_b (Pa)			
u_s $(\frac{m}{s})$	Based on Velocity profiles	Based on Pressure loss data	Based on Eq.(7-25) and Eq.(7-28)	Based on Eq.(7-25) and Eq.(7-29)
0.2	0.349	0.305	0.288	0.605
0.24	0.407	0.427	0.411	0.881

The Televantos et al. (1979) correlation overestimates the bed shear stress by more than 100%. Therefore, it is not recommended to use this correlation.

7.4.8. Does the Critical Shear Stress Exist?

There have been numerous attempts in sediment transport and cuttings removal studies in highly inclined wellbores to quantify the onset of solid's bed erosion regarding measurable parameters such as pressure loss and or flow rate. However, these models often have limited success. Newly emerging research on sediments transport studies is shedding light upon the limitations and shortcomings of these approaches.

The traditional approach in estimating onset of particles movement has long been linked to a critical Shields' number. Numerous different correlations in the literature report critical Shields stress (Ouriemi et al. 2007, Peysson et al. 2009, Bizhani et al. 2016). In a recent study, Houssais et al. (2015) looked at the onset of particles movement in a shear flow. The results of their experiment revealed that contrary to consensus, the beginning of particles movement is a continuous process. They found that there is a movement of the bed materials even at small shear stresses. However, this movement is in the form of the bed creeping flow. Therefore, if a stationary bed is sheared at low shear stresses, the particles in the bed creep and rearrange their positions to accommodate for the exerted fluid stress on the cuttings bed. This implies that shearing a cuttings bed at small shear stresses would result in further compaction of the bed. The compaction then makes the bed erosion more difficult.

Houssais et al. (2015) study have shown that particles movement does not stop at a well-defined shear stress. The implication of such observation is that any number reported in the literature as the critical shear stress (or Shields number) becomes subjective to the technique and resolution of the technique used to obtain such number. It would also be affected by the judgment of the researchers who have made the measurements. Another important consequence of the experiments conducted by Houssais et al. (2015) is that the assumption of static friction for the bed does not hold for small shear stresses (or what is called sub-critical shear stress). That is because the bed is continuously rearranging to accommodate the fluid's shear stress on its surface. This assumption is commonly used in the multi-layering approach of cuttings transport in horizontal wells.

Creeping of the bed material as a result of fluid shear stress drives the bed toward a more compacted state, and hence it makes the erosion of the bed more difficult. On the other hand, if the shear stress is high enough to erode the bed in bedload form, the bed materials start to dilate. This in turn makes the erosion easier. Therefore, depending on the shearing history of the cuttings bed, the critical shear stress does vary widely. The consequence of this finding is that the sediment transport is affected by both the fluid hydrodynamic forces as well as the granular flow of the bed material. Capart and Fraccarollo (2011) also found bedload transport of sediments respond to change in flow condition by adjusting granular concentration at the base layer.

Proper modeling of sediment transport requires modeling of both continuum and the granular materials (Ouriemi et al. 2009). The granular material has a viscoplastic behavior (Boyer et al. 2011); that is they exhibit a yield stress before flowing. However, in drilling literature, only the continuum model of the fluid is often used to model the removal of cuttings in the well. There is no mention of the granular materials properties and their flowing characteristics in these models. Boyer et al. (2011) and Houssais et al. (2015) both pointed out to the fact that hydrodynamic forces do not purely govern sediment transport modeling. Therefore, only considering fluid's shear stress on the cuttings bed does not capture the actual physics of this process; granular flow needs to be considered as well.

Modeling of granular material is a complex topic that requires knowledge of granular viscosity and other properties of the granular material. Recent studies (Boyer et al. 2011) suggest that when a granular material is sheared, there is only one suitable dimensionless number and that is the inertial number.

$$I = \frac{d_p}{\dot{\gamma}}\sqrt{\frac{\rho_s}{P^p}}$$ **Eq.(7-30)**

In this equation P^p is the confining pressure while $\dot{\gamma}$ is the shear rate at which the granular material is being sheared at. In fact this dimensionless number represents the ratio of rearrangement time ($d_p\sqrt{\frac{\rho_p}{P^p}}$) to that of strain rate ($\frac{1}{\dot{\gamma}}$). For sufficiently small Stokes number ($St = \frac{\rho_p d_p^2 \dot{\gamma}}{\mu}$), the viscous forces are dominant and hence the system is no longer governed by the inertial number (Eq.(7-30)). In this case the viscous number should be used (Boyer et al. 2011):

$$I = \frac{\mu \dot{\gamma}}{P^p}$$ **Eq.(7-31)**

Using the inertial number or the viscous number, then the behavior of a granular material can be related to these figures. Houssais et al. (2015) found in their study that the onset of granular flow is associated with a critical viscous number. The importance of viscous number or inertial number is that it includes both fluid related factor as well as granular properties. The inclusion of confining pressure is a major factor that has been missing in the entire drilling literature. The confining pressure can have a significant implication on the importance of viscous or inertial forces. Perhaps it is the confining pressure that causes the delay in bed erosion when concentrated polymer solutions are used to erode a cuttings bed.

Overall, the emerging body of research on sediment transport shows the inadequacies in the current hole cleaning models. We have shown that treating the process of cuttings removal from a pure hydrodynamic force framework (i.e. mechanistic modeling) is inadequate in capturing the actual physics of the cuttings removal. Additionally, there are several unjustified assumptions in these models that need to be addressed. On the other hand, the semi-mechanistic approach in modeling cuttings removal also omits some key features of the process and over-simplifies the interaction of cuttings with the fluid.

7.5. Discussion of Limitations of the Current Study and Relevance of the Results for Hole Cleaning Models Developed for Drilling Horizontal Wells

The current paper summarizes the results of an experimental study of the particle removal from sand bed deposits in horizontal annuli by using water. As opposed to more complex non-Newtonian drilling fluids used in drilling operations, water was used in our experiments. Therefore, results presented here do not realistically represent what might have normally been seen as the effect of the fluid rheological properties on the particle removal from cuttings bed deposits.

Results also have limited coverage of the effect of the solids type. The industrial sand was the only type of solids used in the experiments; where as in real drilling operations cuttings of various lithology and size/shape can be encountered.

Although the experiments were conducted using only water, some parts of the results and analyses can be extended to the modeling of hole cleaning in drilling operations regardless of the type of the fluid used. For instance, understanding how the presence of the velocity fluctuations in turbulent flow would influence the drag and lift forces is essential for the realistic modeling of the bed erosion process, irrespective of the type of the fluid. The effect of fluid rheology on the drag and lift forces can be taken into account by adjusting the drag and lift coefficients. The discussion on the influence of fluctuation velocities (due to turbulent flow) on the particle removal applies for all types of fluid rheology.

The role of flow turbulence and velocity fluctuations on the cuttings removal from the bed can be considered independent of the fluid type. The reason being is that the velocity fluctuations are properties of the flow regime and not the fluid type. When there is a turbulent flow, there will always be velocity fluctuations. Therefore, considering the effect of flow turbulence (and velocity fluctuations) in any hole cleaning model, irrespective of the fluid type, is a must. The extent to which turbulence is affecting the particle removal is directly related to the turbulence intensity, which is a function of the local effective (instantaneous) velocity. Therefore, regardless of the type of the fluid used, the knowledge of the effective local velocity is needed to determine the magnitude of the turbulence intensity on the coupling of particles and the fluid. The analysis regarding the effective fluid velocity is independent of the fluid type. The effective fluid velocity is the velocity that is felt by the respective particle. Therefore, differentiating between various definitions of the fluid velocity is necessary for more realistic modeling of the conditions leading to the particle removal.

The current study has been conducted as part of a comprehensive study towards a better understanding of the particle/fluid interaction when removing a particle from bed deposits in horizontal annuli using different fluid types. Therefore, the results and analyses presented here would serve as the baseline for comparison and evaluation of differences arising from using different fluid type.

The objective of this study is to gain a better understanding of the fluid-particle interaction (and removal of sand particles from stationary sand bed deposits in horizontal annuli using water) through microscopic level measurements. This would help better understanding of the physics involved in the other processes (such as cuttings bed erosion in horizontal wells referred here as hole cleaning) where the particle removal from stationary bed deposits is needed by using fluids more complex (such as non-Newtonian, viscoelastic fluids) than water. It could at least be a good starting point.

7.6. Conclusions

In this paper, two main approaches for modeling particle removal from sand bed deposits in horizontal annuli by using water were critically analyzed. Results of an experimental study, where the local fluid velocity at the sand bed-fluid interface was measured, was used to analyze the impact of the flow turbulence on the interaction of sand particles and water. The main theme of the paper was discussing the limitations and unjustified assumptions used in the modeling of particle removal from sand bed deposits in horizontal annuli.

The first part of the paper was devoted to discussing the mechanistic approach of modeling of bed erosion. In this context, difficulties related to the accurate estimation of local effective fluid velocity were presented. Effective velocity is the instantaneous fluid velocity that the cuttings are exposed to. Results of the analysis of different velocities have shown that the effective velocity near the sand bed is much lower than the mean or superficial fluid velocity in the annulus.

Experimental results also showed that the effective velocity varies significantly over time. The significant fluctuations in the near bed velocity highlight the importance of the flow turbulence in the bed erosion. The role of the flow turbulence in particle removal was discussed in detail. In the discussion related to the impact of the flow turbulence, the significance of the impulse and particles arrangement at the bed interface was discussed. Additional analyses of fluctuations velocity have shown that the hydrodynamic forces (drag and lift) vary widely over the time and hence invalidating the common assumption of ignoring the flow turbulence in the current bed erosion/sediment transport models.

The discussion on the mechanistic modeling was further extended to the influence of particles arrangement in the sand bed on the threshold of motion criterion. Comparison of the drag to the lift force showed that the lift force is much smaller than the drag force. This finding along with the discussion of the impact of particles arrangement in the bed explained why it is much harder to remove a particle that is embedded in the bed deposits. Finally, it was concluded that a purely mechanistic approach might not be sufficient in capturing the actual physics of the interaction of fluid-particles.

In the second part of the paper, we have discussed the semi-mechanic and empirical approaches of bed erosion/sediment transport modeling. In this context, rather than local velocity and forces, bed shear stress is considered as the main factor relating the flow condition to sand bed erosion. Experimental results showed that the instantaneous bed shear stress varies with time just like that of the drag force. Nonetheless, the mean bed shear stress was evaluated using different approaches to assess their accuracy. Two experimental methods and two correlations from the literature were used to estimate the bed shear stress. To calculate the actual bed shear stress, velocity data obtained via PIV were used. Results showed the frictional pressure loss data could be used to estimate the bed shear stress with an acceptable accuracy. On the other hand, out of 2 correlations from the literature, only one of them (Duan et al. 2007) was able to predict the bed shear stress with reasonable accuracy.

In the final part of the paper, the validity of the existence of a critical shear stress was discussed. The existence of a critical shear stress (or equivalently critical Shields' stress) has been the main assumption in many of previous bed erosion/sediment transport studies. It is shown that validity of previous measurements is all subjected to the experimental technique that was used. Sand bed erosion does not have a well-defined threshold at which bed erosion ceases or starts. Recent studies have shown that even at the low bed shear stress values, particles in the bed move in the form of a creeping flow. Therefore, the concept of the existence of critical shear stress (as a single number that would indicate whether bed erosion/sediment transport is taking place or not) is questioned.

7.7. Nomenclatures

A	Annular area cross section ($\pi({R_o}^2 - {R_i}^2)$) (m^2)
A_P	Projected area in the flow (m^2)
A_b	Bed cross sectional area (m^2)
C_D	Drag Coefficient
D_h	Hydraulic Diameter (m)
D_o	Outer pipe diameter (m)
D_i	Inner pipe diameter (m)
d_p	Particles diameter (m)
$\hat{F}_D$	Instantaneous Drag force (N)
F_D	Steady part of the drag force (N)
f_D	Unsteady part of the drag force (N)
f_b	Fanning friction factor (-)
F_b	Friction force between bed and pipe wall (N)
h	Cuttings bed height (m)
I	Inertial number (-)
L	Pipe length (m)
U_s	Superficial velocity ($\frac{m}{s}$)
u	Time average velocity ($\frac{m}{s}$)

$\hat{u}$	Instantaneous axial velocity ($\frac{m}{s}$)
u'	Axial Fluctuation Velocity ($\frac{m}{s}$)
u_{rms}	Root Mean Square of axial fluctuation velocity ($\frac{m}{s}$)
$\overline{u}$	Mean fluid velocity ($\frac{m}{s}$)
y	Vertical distance from mean bed surface/or pipe wall (m)
y_o	Characteristic roughness (m)
V_P	Projected volume in the flow (m^2)
Q	Flow Rate (m^3/s)
S_w	Wetted perimeter of the pipes (m)
S_b	Bed interfacial area (m)
S_{wb}	Perimeter of the area of contact between bed and pipe wall (m)
Re_{gn}	Generalized Reynolds number (-)
Re_p	Particle's Reynolds number (-)
Δs	Displacement of tracer particles (m)
Δx	Axial displacement of tracer particles (m)
Δy	Radial displacement of tracer particles (m)
$\frac{\Delta P}{\mathrm{L}}$	Frictional pressure gradient ($\frac{Pa}{m}$)
μ	Fluid viscosity ($Pa.s$)
u_τ	Friction velocity ($\frac{m}{s}$)
τ_{bw}	Shear stress between bed and pipe (Pa)
P^p	Confining pressure (Pa)
St	Stokes number (-)

κ Von Karman constant (0.41)

ε_{bed} Equivalent bed roughness (m)

τ_b Mean bed shear stress (Pa)

$\hat{\tau}_b$ Instantaneous bed shear stress (Pa)

τ^* Shields' stress (-)

ρ_s Solid's density ($\frac{Kg}{m^3}$)

ρ_f Fluid's density ($\frac{Kg}{m^3}$)

$\dot{\gamma}$ Shear rate ($\frac{1}{s}$)

7.8. References

Adari, R. B. (1999). Development of correlations relating bed erosion to flowing time for near horizontal wells. M.Sc. Thesis, University of Tulsa, USA

Adari, R. B., Miska, S., Kuru, E. et al. (2000). Selecting Drilling Fluid Properties and Flow Rates For Effective Hole Cleaning in High-Angle and Horizontal Wells. SPE Annual Technical Conference and Exhibition. Dallas, Texas, 1–4 October 2000., SPE-63050-MS,DOI: 10.2118/63050-MS.

Bagchi, P. and Balachandar, S. (2003). Effect of turbulence on the drag and lift of a particle. Physics of Fluids **15**(11): 3496-3513, DOI: doi:http://dx.doi.org/10.1063/1.1616031.

Best, J., Bennett, S., Bridge, J. et al. (1997). Turbulence modulation and particle velocities over flat sand beds at low transport rates. Journal of Hydraulic Engineering-Asce **123**(12): 1118-1129, J Hydraul Eng-Asce, DOI: c 10.1061/(Asce)0733-9429(1997)123:12(1118).

Bizhani, M. (2013). Solids transport with turbulent flow of non-Newtonian fluid in the horizontal annuli. M.Sc. Thesis, University of Alberta, Edmonton, Canada.

Bizhani, M., Corredor, F. and Kuru, E. (2015). An Experimental Study of Turbulent Non-Newtonian Fluid Flow in Concentric Annuli using Particle Image Velocimetry Technique.

Flow, Turbulence and Combustion **94**(3): 527-554, Flow Turbulence Combust, DOI: 10.1007/s10494-014-9589-6.

Bizhani, M., Corredor, F. E. R. and Kuru, E. (2016). Quantitative Evaluation of Critical Conditions Required for Effective Hole Cleaning in Coiled-Tubing Drilling of Horizontal Wells. **SPE** Drilling & Completion **31**(3): 188-199, DOI: http://dx.doi.org/10.2118/174404-PA.

Bizhani, M. and Kuru, E. (2017). Effect of Sand Bed Deposits on the Characteristics of Turbulent Flow of Water in Horizontal Annuli ASME fluid engineering, Paper under review.

Bizhani, M., Kuru, E. and Ghaemi, S. (2016). Effect of Near Wall Turbulence on the Particle Removal from Bed Deposits in Horizontal Wells. Proceedings of the Asme 35th International Conference on Ocean, Offshore and Arctic Engineering , 2016, Vol 8.

Boyer, F., Guazzelli, E. and Pouliquen, O. (2011). Unifying Suspension and Granular Rheology. Physical Review Letters **107**(18), Phys Rev Lett, DOI: ARTN 188301 10.1103/PhysRevLett.107.188301.

Brown, N. P., Bern, P. A. and Weaver, A. (1989). Cleaning Deviated Holes: New Experimental and Theoretical Studies. SPE\IADC Drilling Conference New Orleans, Louisiana, February 28-3 March 1989 SPE-18636-MS,DOI: 10.2118/18636-MS.

Capart, H. and Fraccarollo, L. (2011). Transport layer structure in intense bed-load. Geophysical Research Letters **38**, Geophys Res Lett, DOI: hArtn L20402 10.1029/2011gl049408.

Carbonneau, P. E. and Bergeron, N. E. (2000). The effect of bedload transport on mean and turbulent flow properties. Geomorphology **35**(3-4): 267-278, Geomorphology, DOI: g10.1016/S0169-555x(00)00046-5.

Cho, H., Shah, S. N. and Osisanya, S. O. (2000). A Three-Layer Modeling for Cuttings Transport with Coiled Tubing Horizontal Drilling. SPE Annual Technical Conference and Exhibition. Dallas, Texas, 1–4 October 2000., SPE-63269-MS,DOI: 10.2118/63269-MS.

Clark, R. K. and Bickham, K. L. (1994). A Mechanistic Model for Cuttings Transport. SPE 69th Annual Tgchniml Conference and Exhlbltion Now ohms, LA, U. S.A., 25-8 .Septemb.ar 1994., SPE-28306-MS,DOI: 10.2118/28306-MS.

Diplas, P., Dancey, C. L., Celik, A. O. et al. (2008). The Role of Impulse on the Initiation of Particle Movement Under Turbulent Flow Conditions. Science **322**(5902): 717-720, Science, DOI: 10.1126/science.1158954.

Duan, M., Miska, S. Z., Yu, M. et al. (2007). Critical Conditions for Effective Sand-Sized Solids Transport in Horizontal and High-Angle Wells. SPE Production and Operations Symposium Oklahoma City, Oklahoma, USA, 31 March-3 April 2007., SPE-106707-MS,DOI: 10.2118/106707-MS.

Espinosa-Paredes, G., Salazar-Mendoza, R. and Cazarez-Candia, O. (2007). Averaging model for cuttings transport in horizontal wellbores. Journal of Petroleum Science and Engineering **55**(3-4): 301-316, J Petrol Sci Eng, DOI: f10.1016/j.petrol.2006.03.027.

Ford, J. T., Peden, J. M., Oyeneyin, M. B. et al. (1990). Experimental Investigation of Drilled Cuttings Transport in Inclined Boreholes. SPE Annual Technical Conference and Exhibition, 23-26 September, New Orleans, Louisiana, hSPE-20421-MS,DOI: 10.2118/20421-MS.

Gavignet, A. A. and Sobey, I. J. (1989). Model Aids Cuttings Transport Prediction. Journal of Petroleum Technology **41**, SPE-15417-PA, DOI: 10.2118/15417-PA.

Gore, R. A. and Crowe, C. T. (1991). Modulation of Turbulence by a Dispersed Phase. Journal of Fluids Engineering-Transactions of the Asme **113**(2): 304-307, J Fluid Eng-T Asme, DOI: 10.1115/1.2909497.

Guo, X.-l., Wang, Z.-m. and Long, Z.-h. (2010). Study on three-layer unsteady model of cuttings transport for extended-reach well. Journal of Petroleum Science and Engineering **73**(1–2): 171-180, DOI: http://dx.doi.org/10.1016/j.petrol.2010.05.020.

Hemphill, T. and Larsen, T. I. (1996). Hole-Cleaning Capabilities of Water- and Oil-Based Drilling Fluids: A Comparative Experimental Study. **SPE** Drilling & Completion **11**(4), SPE-26328-PA, DOI: 10.2118/26328-PA.

Heyman, J., Mettra, F., Ma, H. B. et al. (2013). Statistics of bedload transport over steep slopes: Separation of time scales and collective motion. Geophysical Research Letters **40**(1): 128-133, Geophys Res Lett, DOI: 10.1029/2012gl054280.

Houssais, M., Ortiz, C. P., Durian, D. J. et al. (2015). Onset of sediment transport is a continuous transition driven by fluid shear and granular creep. Nature Communications **6**, Nat Commun, DOI: ARTN 6527 10.1038/ncomms7527.

Iyoho, A. W. and Takahashi, H. (1993). Modeling Unstable Cuttings Transport In Horizontal, Eccentric Wellbores, SPE-27416-MS.

Japper-Jaafar, A., Escudier, M. P. and Poole, R. J. (2010). Laminar, transitional and turbulent annular flow of drag-reducing polymer solutions. Journal of Non-Newtonian Fluid Mechanics **165**(19-20): 1357-1372, J Non-Newton Fluid, DOI: 10.1016/j.jnnfm.2010.07.001.

Kamp, A. M. and Rivero, M. (1999). Layer Modeling for Cuttings Transport in Highly Inclined Wellbores. Latin American and Caribbean Petroleum Engineering Conference, 21-23 April, Caracas, Venezuela, SPE-53942-MS,DOI: 10.2118/53942-MS.

Kelessidis, V. C. and Bandelis, G. E. (2004a). Flow Patterns and Minimum Suspension Velocity for Efficient Cuttings Transport in Horizontal and Deviated Wells in Coiled-Tubing Drilling. **SPE** Drilling & Completion **19**(4): 213-227, SPE-81746-PA, DOI: 10.2118/81746-PA.

Kelessidis, V. C. and E., M. G. (2004b). Hydraulic Parameters Affecting Cuttings Transport for Horizontal Coiled Tubing Drilling. 7th National Congress on Mechanics, Chania, Greece, June, 2004.

Kundu, P. K., Cohen, I. M. and Dowling, D. R. (2012). Fluid Mechanics, 5th Edition. Amsterdam, Elsevier Science Bv.

Larsen, T. I., Pilehvari, A. A. and Azar, J. J. (1997). Development of a New Cuttings-Transport Model for High-Angle Wellbores Including Horizontal Wells. **SPE** Drilling & Completion **12**(2): 129-135, SPE-25872-PA, DOI: 10.2118/25872-PA.

Leising, L. J. and Walton, I. C. (2002). Cuttings-Transport Problems and Solutions in Coiled-Tubing Drilling. **SPE** Drilling & Completion **17**(1): 54-66, SPE-77261-PA, DOI: 10.2118/77261-PA.

Li, J. and Luft, B. (2014a). Overview of Solids Transport Studies and Applications in Oil and Gas Industry - Experimental Work. SPE Russian Oil and Gas Exploration & Production Technical Conference and Exhibition. Moscow, Russia, 14-16 October, SPE-171285-MS,DOI: 10.2118/171285-MS.

Li, J. and Luft, B. (2014b). Overview Solids Transport Study and Application in Oil-Gas Industry-Theoretical Work. International Petroleum Technology Conference. Kuala Lumpur, Malaysia, 10-12 December 2014, IPTC-17832-MS,DOI: 10.2523/IPTC-17832-MS.

Melling, A. (1997). Tracer particles and seeding for particle image velocimetry. Measurement Science & Technology **8**(12): 1406-1416, Meas Sci Technol, DOI: 10.1088/0957-0233/8/12/005.

Miyazaki, K., Chen, G. , Ymamoto, F., Ohta, J., Murai, Y., Horii, K. (1999). PIV measurement of particle motion in spiral gas-solid two-phase flow. Experimental Thermal and Fluid Science **19**(4): 194-203, Exp Therm Fluid Sci, DOI: 10.1016/S0894-1777(99)00020-5.

Naganawa, S. and Nomura, T. (2006). Simulating Transient Behavior of Cuttings Transport over Whole Trajectory of Extended Reach Well. Abu Dhabi International Petroleum Exhibition & Conference, 7-10 November, Abu Dhabi, UAE, SPE-103923-MS,DOI: 10.2118/103923-MS.

Nazari, T., Hareland, G. and Azar, J. J. (2010). Review of Cuttings Transport in Directional Well Drilling: Systematic Approach. SPE Western Regional Meeting Anaheim, Califronia, USA, 27-29 may 2010, SPE-132372-MS,DOI: 10.2118/132372-MS.

Nezu, I. and Sanjou, M. (2011). PIV and PTV measurements in hydro-sciences with focus on turbulent open-channel flows. Journal of Hydro-Environment Research **5**(4): 215-230, J Hydro-Environ Res, DOI: 10.1016/j.jher.2011.05.004.

Nguyen, D. and Rahman, S. S. (1998). A Three-Layer Hydraulic Program for Effective Cuttings Transport and Hole Cleaning in Highly Deviated and Horizontal Wells. SPE-51186-PA, DOI: 10.2118/51186-PA.

Ouriemi, M., Aussillous, P. and Guazzelli, E. (2009). Sediment dynamics. Part 1. Bed-load transport by laminar shearing flows. Journal of Fluid Mechanics **636**: 295-319, J Fluid Mech, DOI: 10.1017/S0022112009007915.

Ouriemi, M., Aussillous, P., Medale, M. et al. (2007). Determination of the critical Shields number for particle erosion in laminar flow. Physics of Fluids **19**(6), Phys Fluids, DOI: Artn 061706 10.1063/1.2747677.

Ozbayoglu, M. E., Miska, S. Z., Reed, T. et al. (2005). Using foam in horizontal well drilling: A cuttings transport modeling approach. Journal of Petroleum Science and Engineering **46**(4): 267-282, DOI: http://dx.doi.org/10.1016/j.petrol.2005.01.006.

Ozbayoglu, M. E., Saasen, A., Sorgun, M. et al. (2010a). Critical Fluid Velocities for Removing Cuttings Bed Inside Horizontal and Deviated Wells. Petroleum Science and Technology **28**(6): 594-602, DOI: 10.1080/10916460903070181.

Peysson, Y., Ouriemi, M., Medale, M. et al. (2009). Threshold for sediment erosion in pipe flow. International Journal of Multiphase Flow **35**(6): 597-600, Int J Multiphas Flow, DOI: 10.1016/j.ijmultiphaseflow.2009.02.007.

Pilehvari, A. A., Azar, J. J. and Shirazi, S. A. (1996). State-Of-The-Art Cuttings Transport in Horizontal Wellbores. International Conference on Horizontal Well Technology. Calgary, Alberta, Canada, 18-20 November, SPE-37079-MS,DOI: 10.2118/37079-MS.

Poole, R. J. (2010). Development-Length Requirements for Fully Developed Laminar Flow in Concentric Annuli. Journal of Fluids Engineering-Transactions of the **Asme 132**(6), J Fluid Eng-T Asme, DOI: 10.1115/1.4001694.

Ramadan, A., Skalle, P. and Johansen, S. T. (2003). A mechanistic model to determine the critical flow velocity required to initiate the movement of spherical bed particles in inclined channels. Chemical Engineering Science **58**(10): 2153-2163, DOI: 10.1016/S0009-2509(03)00061-7.

Reed, T. D. and Pilehvari, A. A. (1993). A New Model for Laminar, Transitional, and Turbulent Flow of Drilling Muds. SPE Production Operations Symposium, 21-23 March, . Oklahoma City, Oklahoma, USA, SPE-25456-MS,DOI: 10.2118/25456-MS.

Saffman, P. G. (1965). Lift on a Small Sphere in a Slow Shear Flow. Journal of Fluid Mechanics **22**: 385-&, J Fluid Mech, DOI: 10.1017/S0022112065000824.

Schmeeckle, M. W. (2014). Numerical simulation of turbulence and sediment transport of medium sand. Journal of Geophysical Research-Earth Surface **119**(6): 1240-1262, J Geophys Res-Earth, DOI: 10.1002/2013jf002911.

Shields, A. (1936). Anwendung der Ähnlichkeitsmechanik und der Turbulenzforschung auf die Geschiebebewegung. Berlin, Eigenverl. der Preußischen Versuchsanst. für Wasserbau und Schiff.

Sumer, B. M., Chua, L. H. C., Cheng, N.-S. et al. (2003). Influence of Turbulence on Bed Load Sediment Transport. Journal of Hydraulic Engineering **129**(8): 585-596, DOI: 10.1061/(ASCE)0733-9429(2003)129:8(585).

Televantos, Y., Shook, C., Carleton, A. et al. (1979). Flow of Slurries of Coarse Particles at High Solids Concentrations. Canadian Journal of Chemical Engineering **57**(3): 255-262, Can J Chem Eng.

Tsuji, Y., Kato, N. and Tanaka, T. (1991). Experiments on the unsteady drag and wake of a sphere at high reynolds numbers. International Journal of Multiphase Flow **17**(3): 343-354, DOI: http://dx.doi.org/10.1016/0301-9322(91)90004-M.

Wang, R.-h., Cheng, R.-c., Wang, H.-g. et al. (2009). Numerical simulation of transient cuttings transport with foam fluid in horizontal wellbore. Journal of Hydrodynamics, Ser. B **21**(4): 437-444, DOI: http://dx.doi.org/10.1016/S1001-6058(08)60169-9.

Wiberg, P. L. and Rubin, D. M. (1989). Bed Roughness Produced by Saltating Sediment. Journal of Geophysical Research-Oceans **94**(C4): 5011-5016, J Geophys Res-Oceans, DOI: 10.1029/JC094iC04p05011.

Wilson, K. C. (1976). A unified Physically-based analysis of solid-liquid pipeline flow. Proceeding of the 4th Int. Conf. on the Hydraulic Transport of SOlids in Pipes, Banff, Alberta, Cabnada, Paper A1.

7.9. Appendix A – Hydraulic Diameter and Bed Roughness Calculation

Hydraulic diameter and annular cross section available to fluid in the presence of sand bed is defined following the work of Duan et al. (2007). For the case of concentric annulus, assuming a bed of cutting with height of h, following relations hold (Figure A- 7-1):

$$S_o = 2R\ arccos\left(\frac{h-R}{R}\right) \quad \textbf{Eq. (A- 7-1)}$$

$$S_i = 2\pi r \quad \textbf{Eq. (A- 7-2)}$$

$$S_b = 2\sqrt{R^2 - (R-h)^2} \quad \textbf{Eq. (A- 7-3)}$$

$$A_f = R^2\ arccos\left(\frac{h-R}{R}\right) + (R-h)\sqrt{R^2-(R-h)^2} - \pi r^2 \quad \textbf{Eq. (A- 7-4)}$$

$$D_h = \frac{4A_f}{S_o + S_i + S_b} \quad \textbf{Eq. (A- 7-5)}$$

In previous equations, A_f is the cross sectional area available to fluid in presence of cuttings bed.

Equivalent bed roughness according to Duan et al. (2007) is:

$$\varepsilon_{bed} = \frac{d_p}{2}(1+\sin(\varphi)) \quad \textbf{Eq. (A- 7-6)}$$

φ is the angle of repose.

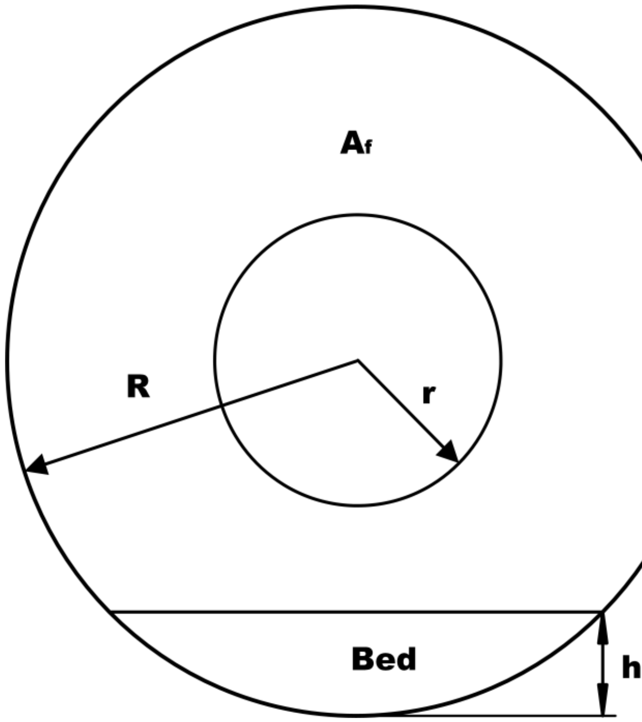

Figure A- 7-1 Schematic of bed and annulus cross section (Bizhani et al. 2016)

7.10. Appendix B-Constants for Calculating Lift Coefficient

$$K_0 = -0.3161R_{ep} + 0.7979 \ (1 \leq R_{ep} \leq 5)$$ **Eq. (B- 7-1)**

$$K_0 = 0.1379R_{ep} - 1.4719 \ (5 < R_{ep} \leq 10)$$ **Eq. (B- 7-2)**

$$K_0 = -1.53 \times 10^{-5}{R_{ep}}^2 + 1.362 \times 10^{-3}R_{ep} - 0.1293 \ (10 < R_{ep} \leq 300)$$ **Eq. (B- 7-3)**

$$K_0 = 9.6 \times 10^{-5}{R_{ep}}^2 - 5.583 \times 10^{-3}R_{ep} - 0.3011 \ (300 < R_{ep} \leq 500)$$ **Eq. (B- 7-4)**

$$K_1 = -0.3739R_{ep} + 3.8318 \ (1 \leq R_{ep} \leq 10)$$ **Eq. (B- 7-5)**

$$K_1 = 8.78 \times 10^{-8} {R_{ep}}^3 - 1.64 \times 10^{-5} {R_{ep}}^2 + 8.12 \times 10^{-3} R_{ep} + 0.1866 (10 < R_{ep} \leq 300)$$ **Eq. (B- 7-6)**

$$K_1 = -1.0925 \times 10^{-5} {R_{ep}}^2 + 5.888 \times 10^{-3} R_{ep} + 0.318 \ \ (300 < R_{ep} \leq 500)$$ **Eq. (B- 7-7)**

8.Particle Removal from Sand Bed Deposits in Horizontal Annuli Using Viscoelastic Fluid[8]

This chapter discusses the impact of fluid viscoelasticity on bed erosion in the concentric annulus. The data were obtained using PIV and two polymer fluids. The analysis in this section focuses on the impact of polymer solutions on flow near the interface of sand bed deposits in horizontal wellbores. A new explanation for the delayed bed erosion by elastic polymer fluids is presented in this chapter.

8.1. Summary

This paper presents results of an experimental study on how the fluid viscoelastic properties would influence the particle removal from the sand bed deposited in horizontal annuli. Water and two different viscoelastic fluids were used for bed erosion experiments. Particle Image Velocimetry (PIV) technique was used to measure the local fluid velocity at the fluid/sand bed interface allowing accurate estimation of the fluid drag forces and the turbulence stresses.

It was found that polymer fluids needed to exert higher level of drag forces (than that of water) on the sand bed to initiate movement of the particles. Results have also shown that, at the critical flow rate of bed erosion, the polymer fluids yielded higher local fluid velocities and turbulent stresses than that of water. Moreover, the local velocity measurements via the PIV technique and the resultant bed shear stress calculations indicated that enhancing polymer concentration under the constant flow rate should also enhance the drag forces acting on the sand bed. However, these improved fluid hydrodynamic forces did not result in any improvement in the bed erosion. Therefore, the mechanism causing the delay in the bed erosion by polymer additives could not be explained by any decrease in the local fluid velocity and the turbulence.

[8] A version of this chapter has been published. Bizhani, M., Kuru, E., 2017, "Particle Removal from Sand Bed Deposits in Horizontal Annuli Using Viscoelastic Fluids,", SPE Journal, SPE-189443-PA

The primary reason for the delayed bed erosion by the polymer fluids was suggested to be linked to their viscoelastic properties. Two possible mechanisms arising from the elastic properties of the polymer fluids that hinder bed erosion were further discussed in the paper. The stress tensor of the viscoelastic fluid flow was analyzed to determine the normal stress differences and the resultant normal fluid force acting on the particles at the fluid/sand bed interface. The normal force induced by the normal stress differences of the viscoelastic fluid was identified as one of the possible causes of the delayed bed erosion by these types of fluids.

8.2. Introduction

Efficient hole cleaning has always been an issue in high angle wellbores. In high angle sections of the well, drilled solids tend to settle down on the low side of the wellbore and form a stationary cuttings bed. Problems such as bridging, pack-off, hole fill, excessive torque and drag, bit balling, slow drilling rates, hindering the casing or liner to be run into its desired position and even stuck pipe can all arise from presence of a stationary cuttings bed in the well (Li and Luft 2014a, Li and Luft 2014b, Bizhani et al. 2016a). As a result, the drilling will have to stop from time to time to conduct hole cleaning operations. This is done by circulating the drilling fluid to sweep the cuttings out of the wellbore. Stopping the drilling to clean the well is expensive and must be done promptly. Therefore, this process must be optimized for both good hole cleaning and faster operation.

The complexity of the cuttings removal process together with the complex rheological behavior of the drilling fluid and turbulent flow makes this problem immune to theoretical treatment. Therefore, only experimental and simplified mechanistic models are available for studying this process. Important parameters affecting hole cleaning (e.g. pump flow rate, pipe rotation) have long been studied in the past. Comprehensive reviews of the previous works could be found in papers written by (Pilehvari et al. 1996, Kelessidis et al. 2002, Nazari et al. 2010, Xiaofeng et al. 2013, Li and Luft 2014a, Li and Luft 2014b). Parameters controlling the transient and 3-D hole cleaning process are categorized into three groups (Bilgesu et al. 2007): fluid related parameters, cuttings related factors, and operational variables. Cuttings related factors are not controllable while operational variables are also dictated by wellbore trajectory, equipment limitations, and drilling method (e.g. pipe rotation may not be available like in coiled tubing intervention (Leising and Walton 2002)). Some of the fluid properties such as density, viscosity, and yield point can be controlled by the operator (Mitchell et al. 2011). The yield point to plastic viscosity ratio (YP/PV) is commonly used as an indicator of hole cleaning efficiency of a drilling fluid. However, YP/PV values are normally measured at by far too high shear rates (Saasen 2014).

The drilling fluid is a complex mixture of different additives. Each additive is added for a particular purpose. For instance, barite is added to increase the mud weight while xanthan gum is added to prevent barite sagging. The combination of different additives in the drilling fluid results in a very complex rheological system. One of the most elusive problems in hole cleaning process is that of the impact of the fluid's rheological properties on the bed erosion. In the drilling literature, most of the studies regarding the effects of drilling fluid rheological properties on the hole cleaning have been limited to the fluid's apparent shear viscosity, plastic viscosity, and yield point (Okrajni and Azar 1986, Becker et al. 1991). Although many fluids used in the drilling applications may have been of viscoelastic nature, the influence of fluid elastic properties on hole cleaning has not been fully investigated. A more comprehensive approach towards the understanding of the combined effects of viscous and elastic properties of the fluids on the hole cleaning efficiency is, therefore, needed.

Field observations, as well as lab studies, have shown that oil based drilling fluids, which have rheological properties similar to that of water based drilling fluids will clean the inclined holes more efficiently than water based fluids. (Saasen 1998, Saasen and Løklingholm 2002, Ytrehus et al. 2015). The difference in the performance of these types of fluids with similar apparent viscosities is linked to their viscoelastic properties.

Walker and Li (2000) reported that polymer based drilling fluids have a higher carrying capacity. However, a delay in the onset of the bed erosion was reported with the use of polymer additives in the drilling fluid (Rabenjafimanantsoa et al. 2005, Duan et al. 2007, Bizhani et al. 2016a). Few attempts have been made to explain the different behavior of the polymer based drilling fluids in bed erosion and carrying cuttings in suspension.

Powell et al. (1991) and Zamora et al. (1993) recommended the use of viscoelastic fluids possessing very high low shear rate viscosity (LSRV) values for better hole cleaning. The power law index (n) of these high LSRV fluids is low, typically approximately 0.2. The low n value leads to flatter velocity profiles in the center of the annulus (resulting a lower maximum velocity and higher viscosity in the core flow) and sharper velocity gradient close to the wall, which results in higher shear rate and, consequently, higher shear stress at the bed interface. Accordingly, the high wall shear stirs the cuttings up from the bed and entrains them in the core; once in the core, they are held there by the elevated LSRV. This structure is believed to be conducive to good hole cleaning in highly deviated wells.

Other researchers claimed that the addition of polymers causes the flow turbulence to decrease and, hence, increases the critical flow rate required for the initiation of particle removal (Azar and Sanchez 1997, Li et al. 2005).

Formation of gel like structures between bed materials and polymer molecules was suggested by Saasen et al. (1998) to contribute to the delayed onset of the bed erosion by polymer fluids. Field observations, however, indicated that in addition to gel strength, elastic properties of drilling fluids played a significant role in hole cleaning (Saasen and Løklingholm 2002). Saasen and Løklingholm (2002) reported that the smaller the elastic strain that was necessary to break the gel, the easier was to clean the hole. Saasen and Løklingholm (2002) also claimed that polymer fluids cause the bed to become more consolidated, and hence, made the bed harder to erode. Additionally, they argued that polymers usually react in the bed and form a cross-linked structure with the bed material, which then makes the bed erosion more difficult.

As summarized above, though some results were controversial, past field experience and the lab data provided evidence regarding the possible effect of viscoelasticity on the hole cleaning. However, actual mechanisms of how the fluid viscoelastic properties affect hole cleaning still need to be identified. To get a better understanding of the behavior of particles in complex viscoelastic fluids and provide further clarification of the effect of elasticity on the hole cleaning more fundamental studies are required.

In this paper, the impact of rheological characteristics (viscoelasticity) of the fluid on the particle removal from bed deposits has been investigated from a microscopic point of view. A non-intrusive laser-based imaging technique called Particle Image Velocimetry (PIV) is used for collecting the data. This method requires transparent wellbore and drilling fluid. The primary goal of this study is to investigate the mechanisms responsible for the increase in critical flow rate of bed erosion as a result of adding polymers to drilling fluids. Parameters that control cuttings removals such as local fluid velocity at the cuttings bed interface and bed shear stress are recorded for different drilling fluids. Turbulence quantities such as Reynolds shear stress and turbulence intensities are measured as well. The cuttings bed was formed using natural quartz sand particles with mean sieve diameters of 600 microns. The rheological characteristics of the polymer fluids thoroughly studied using a high-resolution rheometer.

In the first part of the paper, a comparison is made between water and a dilute polymer solution. The discussion in this section is to mark the differences caused by adding a minute amount of polymers to the flow structures that causes a significant increase in the critical flow rate. In the second part of the paper, results for two polymer solutions are compared. The discussion in this section focuses on differences in local flow conditions caused by increasing polymer concentration at the same pump flow rate. Finally, in the last part of the paper, we try to explain some of the observations using the state of stress tensor in viscoelastic fluids and its implications for hole cleaning in horizontal wells.

8.3. Experimental set-up and test procedures

A large-scale wellbore simulator composed of a 9 meters long annular section (with an outer pipe having a 95mm inner diameter and an inner pipe having 38mm outer diameter) was used in this study. The test section is composed of 6 pipes connected via specially designed joints. The inner pipe is centralized using three thin metal rods. The thickness of the inner pipes is chosen carefully to minimize sagging and vibration of the inner tubes during experiments (Japper-Jaafar et al. 2010, Bizhani et al. 2015). PIV measurements require 100% transparent test section. For that reason, the entire annular section of the wellbore is made of Borosilicate glass pipes.

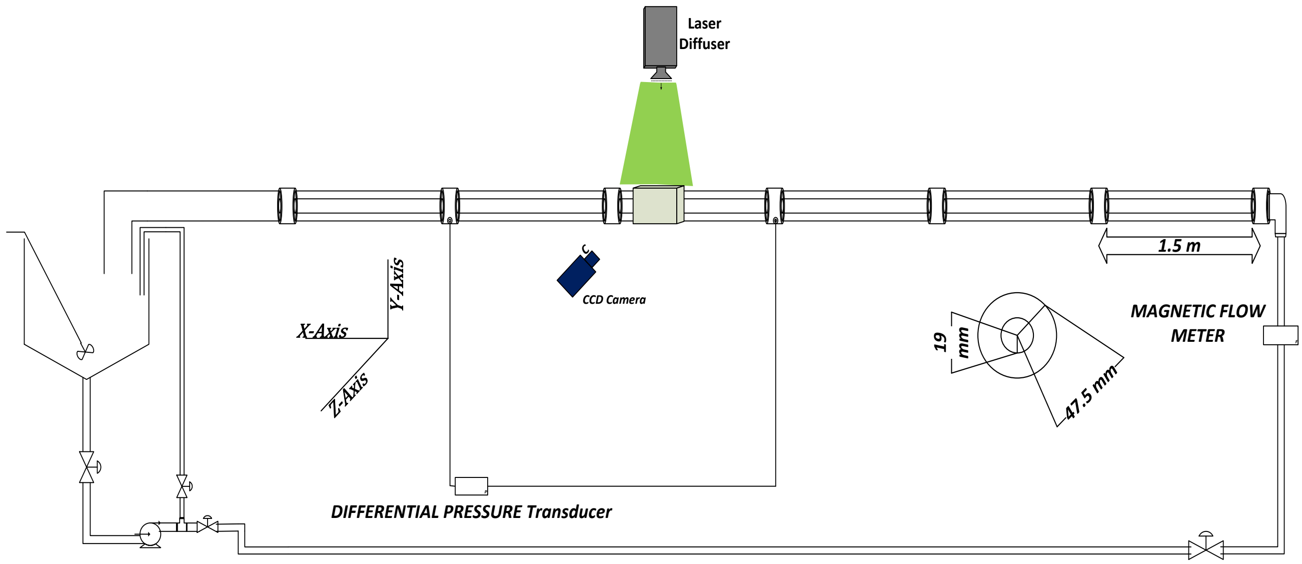

Figure 8-1 Schematic of the flow loop

A schematic view of the flow loop is shown in Figure 8-1 Schematic of the flow loop. An air operated mixer in the 500-liter stainless steel tank was used for mixing the polymers as well as the slurry during the experiments. The centrifugal pump provided the required fluid flow rate, which was controlled through Variable Frequency Drive (VFD) system installed in the flow loop.

The flow rate was measured by using a magnetic flow meter installed at the inlet of the annulus. The flow meter is an OMEGA FMG607-R with an accuracy of ±0.5%. A high accuracy OMEGA DPG409 differential pressure transducer with an accuracy of ±0.08% was used to record the frictional pressure loss in the annulus. The locations of pressure transducer tap lines are at 80Dh and 132Dh from the inlet of the flow loop, which ensure a fully developed flow while avoiding end effects on the measurements. Measurement instruments of the flow loop were all connected to a computerized data acquisition system powered by LabVIEW software. The software was used to control the pump flow rate as well as logging all the data (i.e. pressure loss, flow rate and fluid temperature in the flow loop).

The stationary cuttings bed was established in the concentric annulus by circulating slurry of sand and water (with mass loading of 3.5%) at highest pump flow rate in the flow loop. The slurry was circulated for 10-15 minutes to obtain constant and uniform bed thickness across the entire length of the annulus. After reaching the steady state bed height condition, the pump was shut off. The annular section of the flow loop was then isolated from the other sections using isolation valves (Fig. 1). At this point, the pump, tank, and transport lines of the flow loop were washed carefully to remove any sand remained in these sections. Two filter bags with openings (100 microns) smaller than the sand particle size were installed at the outlet of the annular section to collect any particles which were removed from the test section during the bed erosion test. The sand bed height can be controlled by the initial concentration of cuttings in the tank. However, in this study, the bed thickness was tried to be kept constant. The sand bed thickness was nearly the same (varying by less than 2mm) for comparing bed erosion performance of two fluids. After forming a stationary sand bed in the annulus, bed erosion tests could be conducted.

8.3.1. PIV Setup Description

PIV is a non-intrusive laser base imaging technique that can provide high-resolution 2-D instantaneous velocity profiles of the flow field. A planar 2-D PIV consists of a light source and a recording device. The light source is typically a class four green laser. A camera with the double shuttering feature is the other component of a typical PIV system. PIV fundamentally works by detecting tracer particles in the flow. These tracer particles are small glass beads which follow the fluid’s motion instantaneously. Upon incident of laser light, these tracers reflect the light towards the camera. The camera takes two images of the tracers in quick succession. Processing these pictures with appropriate algorithm yields the instantaneous velocity field of the flow.

The laser used in this study was a Nd: YAG laser. The wavelength of this laser is 532 nm with an energy of 50 mJ per pulse. Laser light is converted to a planar light sheet by a combination of cylindrical and special optical lenses. The thickness of the laser light can vary from 0.5 mm up to 3 mm. The light thickness was kept at its minimum of 0.5 mm in this study.

A CCD (charge-coupled device) camera with a resolution of 1376×1040 pixels was used for recording the images. The double shuttering feature of the camera allows taking two images with adjustable time intervals in between. The time interval can be set as low as 500 ns. A 50 mm Nikon AF NIKKOR lens with a 12-mm extension tube was used for recording the images. The f-stop or the aperture of the lens was set to 8.

The tracer particles utilized in this were hollow glass spheres with a mean diameter of 10 microns. Density of the tracers $1.1 \pm 0.05 \frac{g}{cc}$ which gives near neutrality to them in the working fluids and hence keep them suspended in the flow. Addition of the tracer particle is crucial for enhancing spatial resolution of the PIV images which results in more accurate measurements of the velocity profiles (Melling 1997).

To ensure measurements were carried out in a fully developed region, measurements were performed at a distance of approximately $100D_H$ from the inlet (development length for laminar flow is $88D_H$ (Poole 2010), development length for the turbulent flow is shorter (Japper-Jaafar et al. 2010)). A rectangular box filled with glycerol is installed around the test section to reduce distortion and perspective errors in the PIV images.

Figure 8-2shows a typical PIV image acquired during the experiments. The cuttings bed is visible at the bottom while the drilling fluid, seeded with tracer particles (bright white dots), is flowing over the top. Image acquisition and processing have been performed using DAVIS 8.3.0. The software was used for adjusting appropriate parameters during the experiments (such as time interval between two images and laser power).

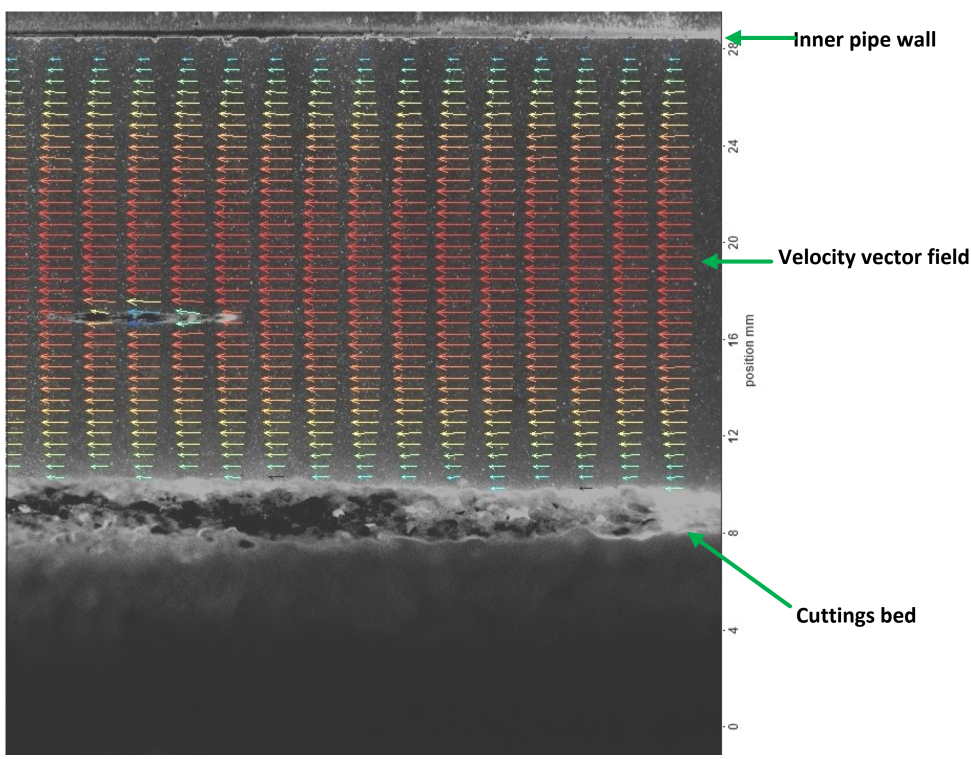

Figure 8-2 Typical PIV image acquired during the tests

8.3.2. PIV Data Post-Processing Procedures PIV

Processing of PIV images follows a cross-correlation based method. Each pair of images is broken down to smaller windows called interrogation windows. Interrogation windows in the - the second image is analyzed for probable similarities to that of the first image (Nezu and Sanjou 2011). The cross-correlation approach was used to find the pixel displacement. Cross-correlation works by cross correlating the local intensity distribution over the interrogation windows. The chosen destiny of each tracer particle is the peak with the highest correlation. After finding the displacement of each tracer particle (Δx and Δy), by using the time interval (Δt) between the images instantaneous velocity can be obtained using following equation:

$$\begin{cases} \hat{u} = \dfrac{\Delta x}{\Delta t} \\ \hat{v} = \dfrac{\Delta y}{\Delta t} \end{cases} \qquad \text{Eq.(8-1)}$$

A total number of 1000 images are taken for calculation of velocity field using PIV. Multi-pass cross-correlation method with decreasing of interrogation window size was used for particle displacement calculations. Interrogation window size of 64×64 pixels followed by the window size of 32×32 pixels was used in the calculations. Adaptive weighting function with an overlap setting 50% was used for vector field calculations. To enhance the accuracy of the calculated vector fields post-processing was also applied on the calculated vectors. In the post-processing, any vectors with peak ratio less than 1.1 were removed. The setting for the post-processing was adjusted to universal outlier detections to remove the outlier vectors. The universal outlier detector function compares a vector to its surrounding vectors. If the vector exhibits significant difference (in terms of the direction and the magnitude), it is detected as an outlier and is removed. The accuracy of the presented data is limited by the accuracy of PIV method which is 0.1 pixel (Nobach and Bodenschatz 2009). Taking into consideration other sources of errors (such as noises in the images), the variations in the measured velocity profiles is less than 3% (the inherent inaccuracy is less than 1% of the measured velocity profiles).

8.4. Results and Discussion

8.4.1. Rheological characterization of the polymer fluids

An anionic water-soluble copolymer of the family of partially-hydrolyzed polyacrylamide (PHPA) polymer was used in this study. The molecular weight the polymer is $10 \times 10^6 \frac{g}{mol}$. Two fluids with 0.032 and 0.064% (all weight percent) polymer concentrations were used.

Rheological characteristics of the fluid samples were determined by using a high-resolution Bohlin C-VOR 150 rheometer[26]. For the range of shear rates encountered in this study, the power law model fits the apparent viscosity data. Figure 5-4 shows the flow behavior curves of the two solutions used here. The K and n values for 0.032 and 0.064% polymer solutions are reported in Eq.(5-2) and Eq.(5-3), respectively.

$$\tau = 0.0046\dot{\gamma}^{0.952} \qquad \textbf{Eq.(8-2)}$$

$$\tau = 0.01226\dot{\gamma}^{0.829} \qquad \textbf{Eq.(8-3)}$$

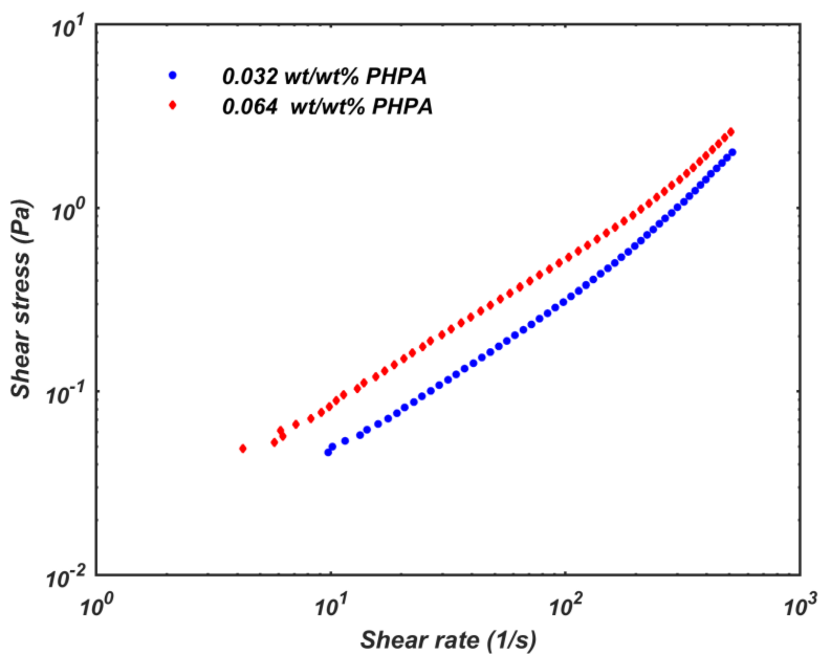

Figure 8-3 Shear stress vs. shear rate data for the two polymer solutions

Oscillatory rheometry (i.e. frequency sweep) measurements were also performed to determine the viscoelastic properties of the polymer solutions. The viscous and elastic moduli of the samples were measured over a range of frequencies. The measurement was conducted at a constant stress of 0.00598 Pa (hence, variable strain amplitude). Figure 8-4 and 8-5 shows the data collected from frequency sweep tests for 0.032 and 0.064% polymer solutions respectively. At low frequencies (high time scales) the loss (viscous) modulus (G'') is dominant over that of storage (elastic) modulus (G') for both samples. The longest relaxation time for the 0.032% solution appears to be 0.17 seconds while that of 0.064% solution is 0.45 seconds.

The relaxation time is a valuable property in identifying the type of the flow. If the time scale of the flow (i.e., reciprocal of shear rate) exceeds the relaxation time of the polymers, the flow is in the viscous dominant region. Otherwise, the flow is in the dominant elastic region where the elastic modulus is higher than the viscous modulus. The crossover shear rates for transition from viscous to the elastic regime were 5.9 and 2.2 1/s for 0.032% and 0.064% polymer fluids, respectively. We later will use these values to discuss the results related to bed erosion experiments.

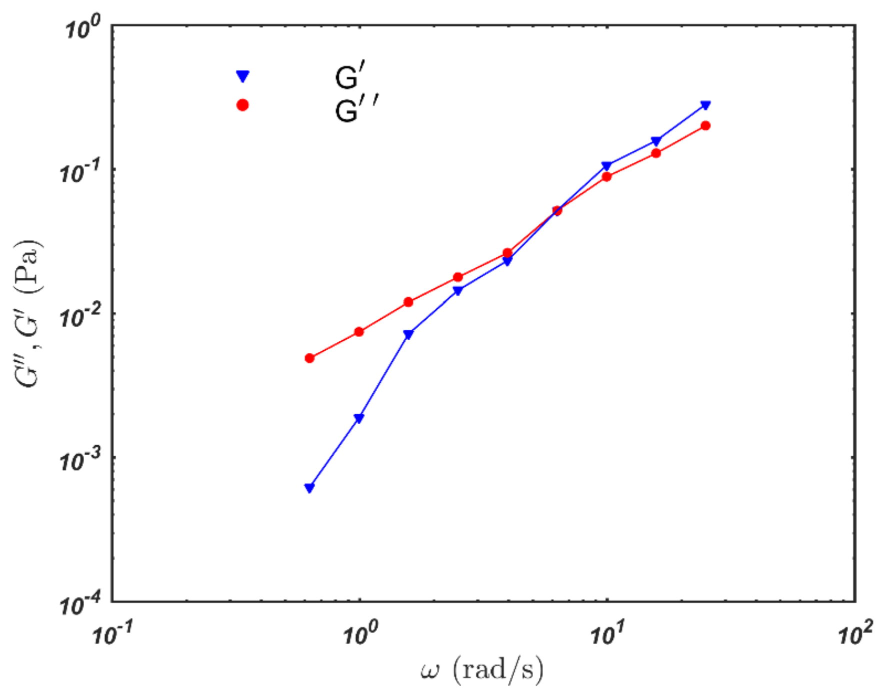

Figure 8-4 Viscous and elastic moduli of the 0.032% polymer solution vs. angular frequency

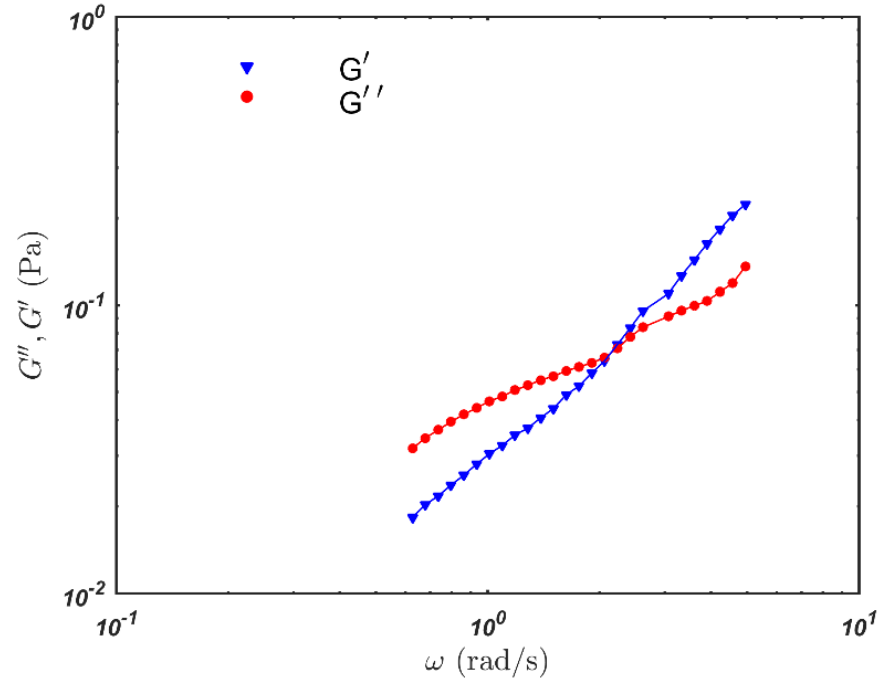

Figure 8-5 Viscous and elastic moduli of the 0.064% polymer solutions vs. angular frequency

A complete description of the viscoelastic fluid rheology requires the knowledge of shear viscosity (or the apparent viscosity) as well as parameters related to fluid elastic properties (such as first and second normal stress differences). A detailed discussion of the state of the stresses acting on the fluid is, therefore, needed. The most general state of the stress for an anisotropic material in simple shear flow can be described by the total stress tensor as shown by Eq.(8-4) (Bird et al. 1987).

$$\boldsymbol{\pi} = p\boldsymbol{\delta} + \boldsymbol{\tau} = \begin{bmatrix} p + \tau_{xx} & \tau_{xy} & 0 \\ \tau_{yx} & p + \tau_{yy} & 0 \\ 0 & 0 & p + \tau_{zz} \end{bmatrix} \qquad \textbf{Eq.(8-4)}$$

In an anisotropic, incompressible material, there are only three independent stress quantities of rheological significance, namely two differences of normal components and one tangential component: $\tau_{xx} - \tau_{yy}$, $\tau_{yy} - \tau_{zz}$, and τ_{yx}. The third difference $\tau_{xx} - \tau_{zz}$ of normal components is the sum of the first two differences, and the other non-zero tangential (shear) component τ_{xy} is a function of the shear viscosity and equal to τ_{yx} (Lodge 1964). The terms N_1 and N_2 are used to define the first and second normal stress differences as defined by equations 5 and 6, respectively.

$$N_1 = \tau_{xx} - \tau_{yy} \quad \textbf{Eq.(8-5)}$$

$$N_2 = \tau_{yy} - \tau_{zz} \quad \textbf{Eq.(8-6)}$$

For an inelastic Newtonian or non-Newtonian fluid, the normal stress differences are zero, that is:

$$\tau_{xx} = \tau_{yy} = \tau_{zz} \quad \textbf{Eq.(8-7)}$$

For viscoelastic fluids, however, the normal stress differences are not zero. Figure 8-6 schematically shows the components of stress tensor in the one-dimensional steady shearing flow of a viscoelastic fluid (Chhabra and Richardson 1999).

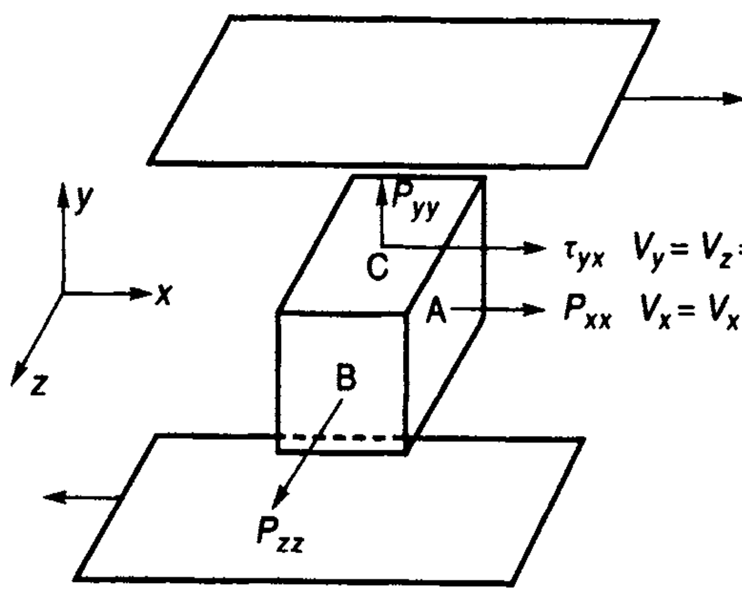

Figure 8-6 Non-zero elements of stress in one-dimensional steady shearing motion of a viscoelastic fluid (Chhabra and Richardson 1999).

In polymer based fluids (or more generally viscoelastic fluids) the normal stress differences are not zero due to the anisotropies developed in the polymer molecules. These stress differences are associated with the strain-induced anisotropy in a fluid, and in the case of polymer-based liquids, the anisotropy arises from the departure of molecules from their equilibrium, symmetrical average shape (Dealy et al. 2013). For a Newtonian fluid, the first and second normal stress difference is zero. Hence, a full description of fluid's rheological behavior can be sufficiently obtained from the Newtonian viscosity. On the other hand, for a viscoelastic polymer based fluid, the first and second normal stress differences are not zero. Therefore, a complete description of the rheology of these fluids requires the knowledge of the apparent viscosity and the two normal stress differences.

The anisotropies induced in the microstructures of the polymers caused by the flow are the main reason for the existence of non-zero normal stress difference. In the absence of flow, the coils like structures have a spherical pervaded volume. In the shear flow, the polymer molecules stretch toward the direction of the flow. This results in a pervaded volume that is ellipsoidal and oriented towards the direction of flow. The restoring forces are different in different directions. This results in the anisotropic normal forces (Deshpande 2010).

The non-zero first and second normal stress difference in polymer solutions has interesting consequences. The most related phenomenon to annular flow is the unequal distribution of pressure in each cross sections of the flow. According to Bird et al. (1987) measurements have shown the pressure is higher on the inner wall of annuli than its outer wall. This phenomenon does not happen in the flow of Newtonian fluids.

Another consequence of non-zero normal stress difference is the expansion of fluid when it goes through a diameter change. In this case, due to normal forces and the incompressibility of the fluid, the fluid expands. According to Bird et al. (1987) a negative N_1 and positive N_2 can loosely be thought of as an additional compressive force in the y direction (i.e. perpendicular to the direction of the flow). For flow between two parallel plates, a Newtonian fluid only requires shear stress to maintain the steady flow. However, for a viscoelastic fluid flow, a normal force must be applied to keep the plates in place because of the normal forces in the fluid (Bird et al. 1987).

For incompressible fluids, the normal stress has no significance if the stresses are the same in all directions (i.e. Newtonian fluids). Only non-zero normal stress difference can cause deformation, i.e. stretching and compression. The shear viscosity (μ), the first (N_1) and the second normal (N_2) stress differences are all functions of the shear rate (Bird et al. 1987, Dealy et al. 2013).

$$\mu = \frac{\tau_{xy}}{\dot{\gamma}} \qquad \textbf{Eq.(8-8)}$$

$$N_1(\dot{\gamma}) = \tau_{xx} - \tau_{yy} = \Psi_1(\dot{\gamma})\,\dot{\gamma}^2 \qquad \textbf{Eq.(8-9)}$$

$$N_2(\dot{\gamma}) = \tau_{yy} - \tau_{zz} = \Psi_2(\dot{\gamma})\,\dot{\gamma}^2 \qquad \textbf{Eq.(8-10)}$$

Ψ_1 and Ψ_2 are the first and second normal stress difference coefficients (Bird et al. 1987). For any viscometric flow, these three viscometric functions completely describe the rheological behavior of a fluid. For a Newtonian (or non-viscoelastic fluids) fluid, N_1 and N_2 are zero, therefore only shear viscosity is required to describe the fluids. For sufficiently low shear rates, viscoelastic fluids show Newtonian behavior (Dealy et al. 2013).

Measurements of the first and the second normal stress differences are not as straightforward as that of the apparent shear viscosity. Using a cone and plate viscometer, only the low shear rate measurements (up to 1 $\frac{1}{s}$) can be conducted because of what is called the edge fracture phenomenon (Baird 2008). However, Lin et al. (2014) suggested that using a bigger cone and reducing the shearing time of the sample can help in curbing the edge fracture phenomenon. In this study, we used a 40-mm cone for measuring the fluids properties. In the viscosity measurement, the shearing time is typically 20 minutes. On the other hand, for normal stress measurements the shearing time was reduced to less than 1 minute to avoid the edge fracture. The second normal stress difference is much harder to measure. It is not possible to measure N_2 using cone-plate viscometer. However, comparing to the first normal stress difference, it is an order of magnitude smaller (Bird et al. 1987). Some studies suggest it is approximately 20% of the first normal stress difference (Dealy and Wissbrun 1999).

Figure 8-7 shows the measured first normal stress difference for the two polymer solutions. The measurements were conducted by using a rheometer with a cone-plate geometry and the reduced shearing time. For shear rates greater than 1 1/s and less than 100 1/s, both polymers exhibit a plateau in the measured first normal stress difference. The plateau in the first the normal stress difference curves for shear rates greater than one was also observed by Tonmukayakul et al. (2013), who suggested the equilibrium of network structure at these frequencies was the main reason for the plateau. Dealy et al. (2013) argued that normal stress difference has a quadratic relation with that of shear rate. Therefore, at higher shear rates, the change in the first normal stress difference with that of the shear rate will no longer be linear or plateau. The transition in the shape of first normal stress difference curves is likely caused by the change in the equilibrium state of the network structures at higher shear rates in the system.

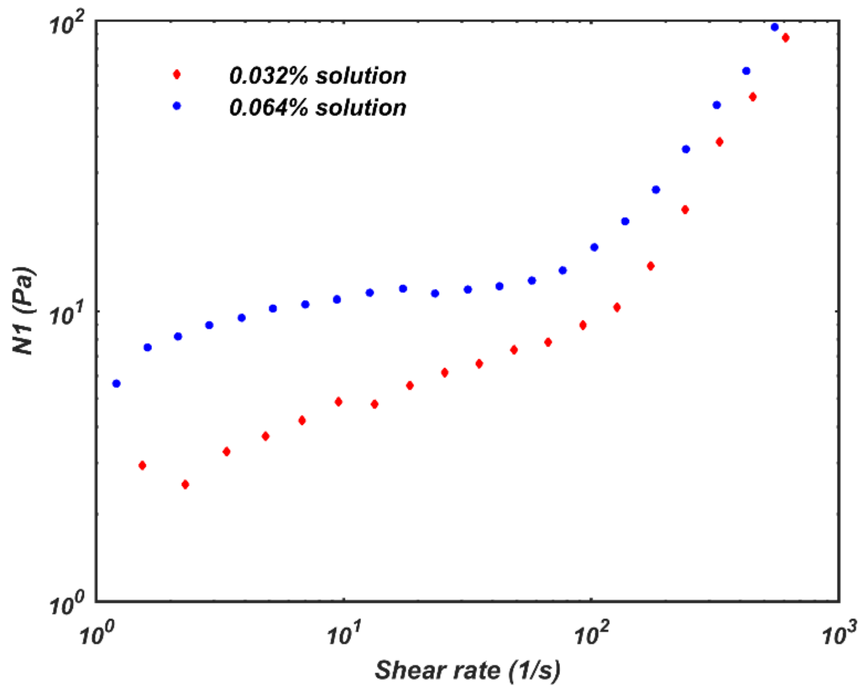

Figure 8-7 The first normal stress difference vs. shear rate for the two polymer solutions.

8.4.2. Bed Erosion Experiments

8.4.2.1. Velocity and Turbulent Stress Profiles near the Bed Interface

Previous studies on hole cleaning have shown that the addition of even a small amount of polymer to water based drilling fluids delays the initiation of bed erosion. From a macroscopic point of view, the negative impact of polymer addition on the hole cleaning was observed in the form of an increase in the critical flow rate required for the onset of bed erosion (Bizhani et al. 2016a). The reason, however, is not well understood. One of the often-used explanations was suggested as the reduction of the near wall turbulence caused by the increase in the shear viscosity due to polymer addition (Azar and Sanchez 1997, Li et al. 2005). However, as it will be explained in the remaining part of this paper, our experimental observations suggest that this may not be the real case.

Macroscopic hole the bed erosion cannot provide detailed insight on how the drilling fluid's rheology influences particle removal from the bed surface. The local fluid velocity and the shear stress at the bed interface are the two most important factors affecting the particle movement. More specifically, the fluid hydrodynamic forces (i.e. the drag and lift) control the removal of the cuttings from the bed deposits. In this study, we have investigated the factors controlling the sand bed erosion by comparing the performances of water and a dilute polymer solution at their critical flow rate (i.e., the minimum flow rate required for the onset of the bed erosion). The polymer solution has a concentration of 0.032% w/w. The rheological properties of the polymer fluid were presented in Figure 5-4 and Eq.(5-2). The recorded critical flow rate for water was 90 liter/min while that of the polymer solution was 200 liters/min. The following section provides the detailed results and discussions on the possible reasons behind such a drastic (more than two folds) increase in the critical flow rate caused using a small amount of polymer.

Figure 8-8 compares the local velocity profiles over the stationary cuttings bed for water and 0.032% polymer solution each at their critical flow rate of bed erosion. The critical flow rate for the polymer solution is more than twice that of water (i.e., the polymer fluid requires much higher velocity than water to initiate bed erosion). The velocity profile in water flow is flatter, which is a characteristic of the turbulent flow. Comparison of velocity profiles near the bed interface (y=0) at the onset of the bed erosion shows that the polymer fluid has higher local velocity values than that of water. This means that the drag force exerted on the sand particles by the polymer fluid is also higher than that exerted by water. The drag force equation is given Eq.(8-11).

$$F_D = \frac{1}{2}\rho A_p C_D u^2 \qquad \textbf{Eq.(8-11)}$$

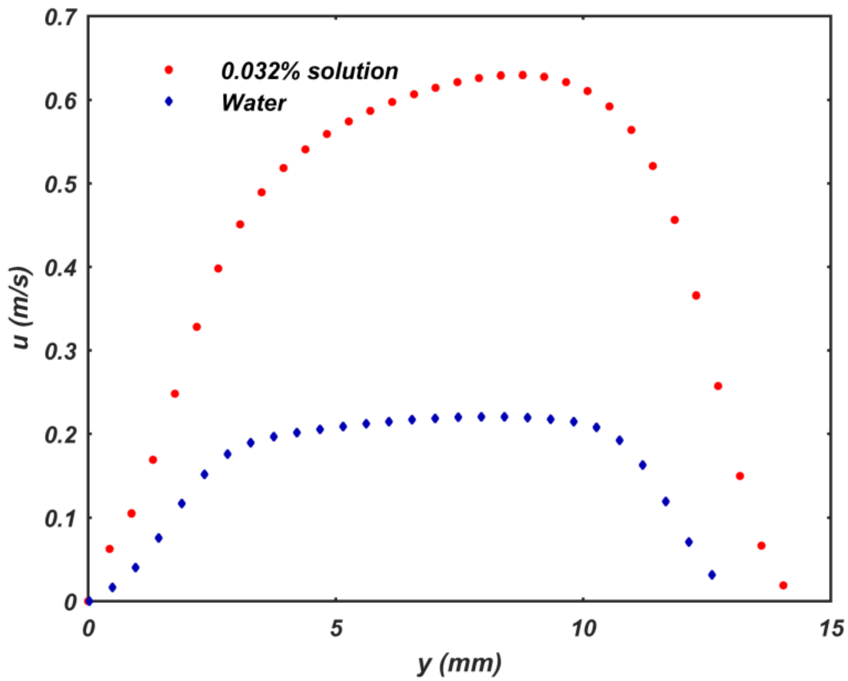

Figure 8-8 Velocity profiles measured over the cuttings beds using water and 0.032% polymer fluid at the critical flow rate of each fluid

In this equation, u is the local velocity, ρ is the fluid density, A_p is the projected area of the cuttings in the flow, and C_D is the drag coefficient. Details of calculations pertinent to drag coefficient for water and polymer fluids are presented in the Appendix A. According to the drag force results (calculated by using Eq.13) shown in Figure 8-8, the polymer fluid exerts higher drag force on the sand particles at its critical flow rate than that of water. This is interesting because one would expect to see similar levels of drag force at the onset of the sand bed erosion for all the fluids. However, as implied by the results shown here, the polymer fluid has to exert a higher drag force than that of water on the cuttings in order to mobilize them. The polymer fluid has to dissipate more energy to mobilize the same sand particle while water can do that at lower rate of energy consumption. This observation suggests that the increase in the critical flow rate due to added polymer cannot be associated with the decrease in local fluid velocity or the associated drag force acting on the sand bed.

Figure 8-9 compares the Reynolds shear stress profiles for water and 0.032% polymer fluid at their critical flow rate. The Reynolds shear stress (or turbulent stress) arises due to velocity fluctuations in the flow and is defined according to Eq.(8-12).

$$\tau_{Re} = -\rho\overline{u'v'} \qquad \textbf{Eq.(8-12)}$$

Similar to velocity profiles, a higher Reynolds stress value is observed at the initiation of particle movement when we used the polymer fluid. Therefore, we cannot justify the suggestion that reduction of turbulence is the main reason for hindering of the critical flow rate by polymer fluids. That is because 0.032% polymer fluid shows higher turbulence stress at the critical flow rate of the bed erosion.

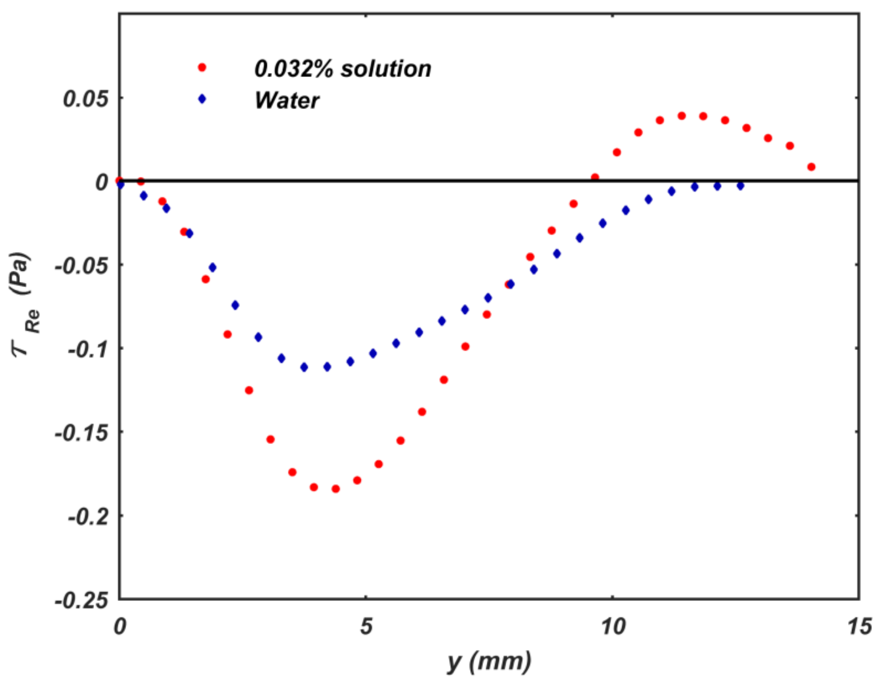

Figure 8-9 Reynolds stress profiles measured over the cuttings bed using water and 0.032% polymer fluid.

The normal Reynolds stress (also called axial turbulence intensity) data of water and polymer fluids are compared in the Figure 8-10. The Eq.(8-13) gives the definition of the normal Reynolds stress.

$$U_{rms} = \sqrt{\overline{u'u'}} \qquad \textbf{Eq.(8-13)}$$

The normal Reynolds stress is critical in sand particle removal because it represents the level of velocity fluctuations. Recent studies have indicated the significance of turbulent velocity fluctuations in particles removal (Diplas et al. 2008, Bizhani and Kuru 2017b). Figure 8-10 indicates that polymer fluid has higher normal Reynolds stress at the onset of sand bed erosion; also confirming earlier remark that reduction of turbulence by polymer addition cannot be the reason for the delay in reaching the critical flow rate.

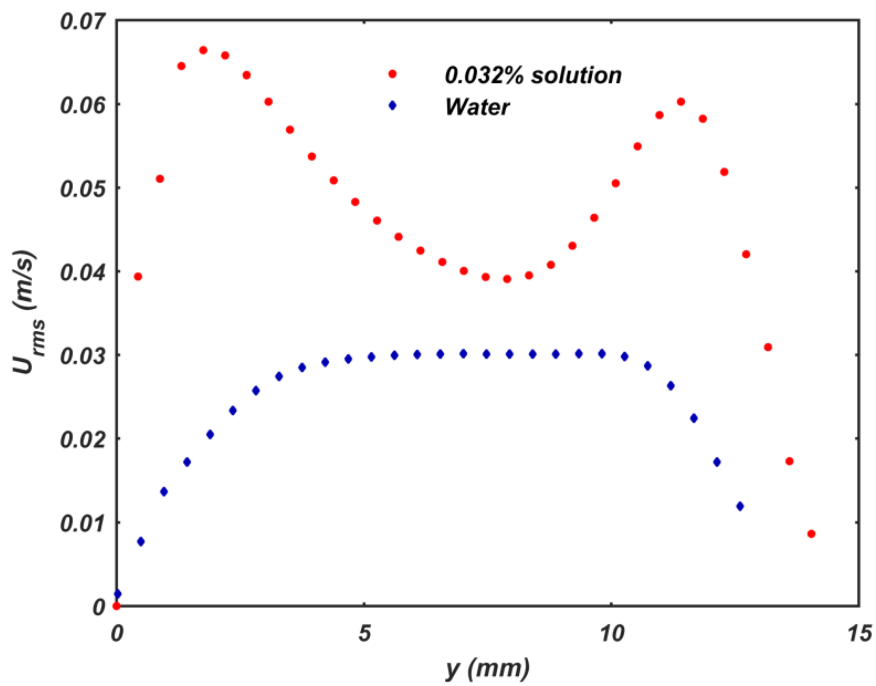

Figure 8-10 Axial turbulence intensity profiles measured over the cuttings beds using water and 0.032% polymer fluid

8.4.2.2. Average Bed Shear Stress

The PIV data have shown that at the minimum flow rate of bed erosion, the polymer fluid has higher local fluid velocity and turbulence activities near the cuttings bed than that of water. This finding is somehow in contradiction with previous understanding of how the use of polymer fluids would influence the flow conditions near the stationary cuttings bed.

In addition to the local fluid velocity and turbulence activities near the cuttings bed, the bed shear stress is traditionally considered as one of the most important factors influencing the cuttings removal. The bed shear stress is a direct measure of the fluid's drag force on the cuttings bed, as a higher bed shear stress is equivalent to greater drag force. The frictional pressure loss is directly proportional to the bed shear stress. Average bed shear stress is related to frictional pressure loss as given by Eq.(8-14).

$$\tau_b = -\frac{D_h}{4}\frac{\Delta P}{\mathrm{L}} \qquad \textbf{Eq.(8-14)}$$

The hydraulic diameter, D_h, used in the Eq.(8-14) is a function of the bed height. In sediment transport studies, to analyze the importance of bed shear stress, very often a non-dimensional form of the shear stress, called Shield's parameter (Shields 1936), is used (Eq.(8-15)).

$$\tau^* = \frac{\tau_b}{g d_p(\rho_s - \rho_f)} \qquad \textbf{Eq.(8-15)}$$

In Eq.(8-15), ρ_f is the fluid density, ρ_s solid density and d_p is the cuttings size. Shields' parameter represents the ratio of fluid drag force to that of cuttings' submerged weight. For the same fluid density and cuttings' properties, a higher bed shear stress results into a higher Shields' stress. Equivalently, a higher drag force is exerted on the cuttings. For the results presented in this paper, the cuttings are all the same and the fluid densities are also similar. Therefore, a higher bed shear stress translates to a higher fluid drag force on the bed.

Table 8-1 compares the average bed shear stress data for water and 0.032% polymer fluid at their minimum flow rate of bed erosion. In another word, the shear stresses reported in Table 1 are the critical shear stresses for bed erosion for each type of fluid. The polymer fluid has a critical shear stress more than twice higher than that of water. The critical Shields' stress is also more than twice higher for the polymer solution. This confirms the earlier conclusion that at the critical flow rate, polymer solution exerts a larger drag force on the sand bed than water.

Table 8-1 Critical bed shear stress values for water and the 0.032% polymer solution

	Water	0.032% Polymer Fluid
Bed shear stress (Pa)	0.427	0.91
Shields' stress	0.044	0.093

Comparison of near wall velocity profiles, Reynolds stresses, and bed shear stress data recorded during particle removal experiments using water and 0.032% polymer fluid did not provide much-needed insight as for the explanation of why the addition of polymer additives delays the onset of the bed erosion. Both PIV data and bed shear stress data are showing that the polymer fluid has to exert a higher drag force on the sand bed to move the sand particles. At the same time, the polymer fluid showed a greater level of turbulence at the onset of sand particle movement. Therefore, the suggestion that addition of polymer additives causes the critical flow rate to increase because of reduction in local fluid velocity or turbulence cannot be fully justified. Results shown here clearly indicate that polymer fluid has to dissipate much more energy to move the same sand particles than water. The reason for this observation is not clear yet and needs further explanation.

8.4.3. Impact of Increasing the Polymer Concentration

Further bed erosion experiments were conducted by using polymer fluids with two different concentrations of 0.032% and 0.064%. The rheological properties of two fluids were presented in Figure 5-4. The effect of the local velocity and turbulence conditions on sand particle removal were investigated by using the constant flow rate of 200 liters/min. This flow rate corresponds to the critical flow rate of bed erosion for 0.032% polymer fluid. The more viscous fluid with 0.064% polymer concentration has a critical flow rate of 256 liters/min. In this case, the objective was to determine the changes in the near wall velocity profile, Reynolds stress and the bed shear stress and their impact on sand particle removal because of increasing polymer concentration of the fluids.

To ensure that both polymer fluids are flowing under the same flow regime, we have determined generalized Reynolds number (Re_g) in each case by using the Eq.(8-16).

$$Re_g = \frac{\rho D_h^n U^{2-n}}{8^{n-1} K} \quad \textbf{Eq.(8-16)}$$

Table 8-2 reports the Reynolds numbers for the flow of both polymer fluids at the rate of 200 liters/min. The critical Reynolds number for a flow of a power law fluid through annulus can be estimated using the following equations:

$$Re_{Lam} < 3470 - 1370n \quad \textbf{Eq.(8-17)}$$

$$Re_{Tur} > 4270 - 1370n \quad \textbf{Eq.(8-18)}$$

The critical Reynolds numbers for transition to turbulent flow was estimated to be 2960 and 3100 for the 0.032 and 0.064% polymer fluids respectively. The laminar flow regime prevails at Reynolds numbers below 2160 and 2300 for 0.032 and 0.064% polymer fluids. The lowest Reynolds number observed during the experiments was 5537, confirming that at the pump flow rate of 200 lit/min, the turbulent flow regime prevailed during the flow of both fluids.

Table 8-2 Generalized Reynolds number for the flow of two polymer fluids at the rate of 200 lit/min

Q($\frac{\mathbf{Liter}}{\boldsymbol{min}}$)	**0.032% polymer**	**0.064% polymer**
200	8574	5537

8.4.3.1. Local Flow Conditions at the Bed

The local fluid velocity at the cuttings bed interface is one of the most influential parameters as long as the interaction of the fluid sand particle is concerned. The local fluid velocity controls the drag and lift force and hence the momentum exchange between the phases. Figure 8-11 shows the comparison of the time average local velocity profiles over the stationary sand bed for the 0.032% and 0.064% polymer fluids at constant flow rate (200 liters/min). Surprisingly, there was no discernible difference in the velocity profiles, especially near the cuttings bed interface. This is despite the fact the 0.032% polymer fluid erodes the bed at this flow rate, and the 0.064% fluid does not. The drag force equation (Eq.(8-11)) predicts that 0.064% polymer fluid exerts a higher drag force on the bed at the same flow rate than the 0.032% polymer fluid (i.e., same local velocity but with higher viscosity results in a higher drag force). A similar comparison between 0.032% polymer fluid and water revealed that the polymer fluid had to exert more drag force on the bed to move the sand particles. This statement can be extended to the more general form that with the increasing polymer concentration, higher drag force would be required to mobilize the sand particles in the stationary bed.

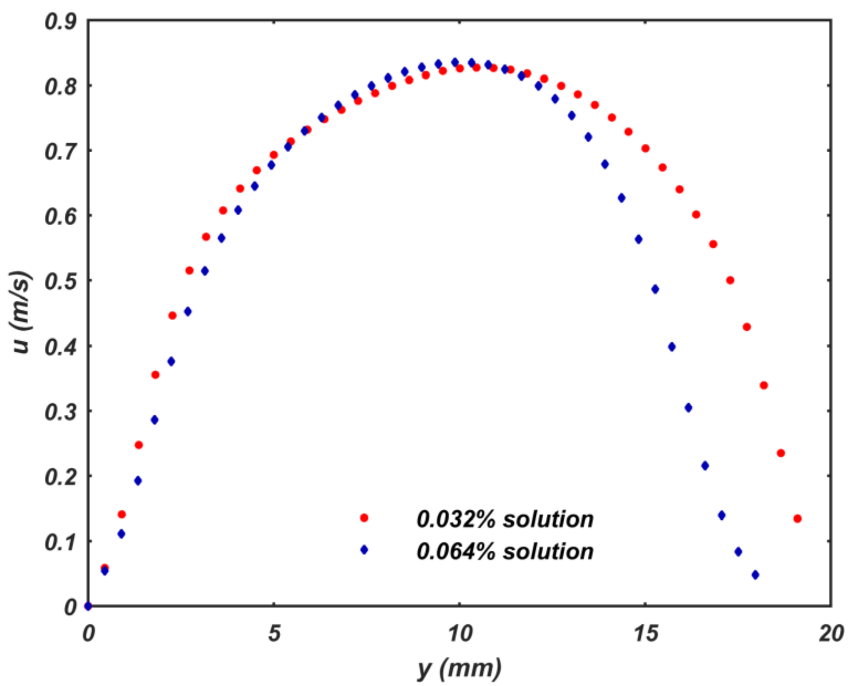

Figure 8-11 Comparison of velocity profiles measured over stationary cuttings bed using two polymer fluids at $U_s = 0.56\frac{m}{s}$

The axial turbulence intensity are compared in Figure 8-12. A significant reduction in Reynolds stress was observed for the more viscous fluid (with 0.064% polymer concentration). The decline in the Reynolds shear stress is expected because increasing polymer concentration causes Reynolds number to decrease because of increasing viscosity. Therefore, the turbulence was reduced by increasing the polymer concentration at the same flow rate.

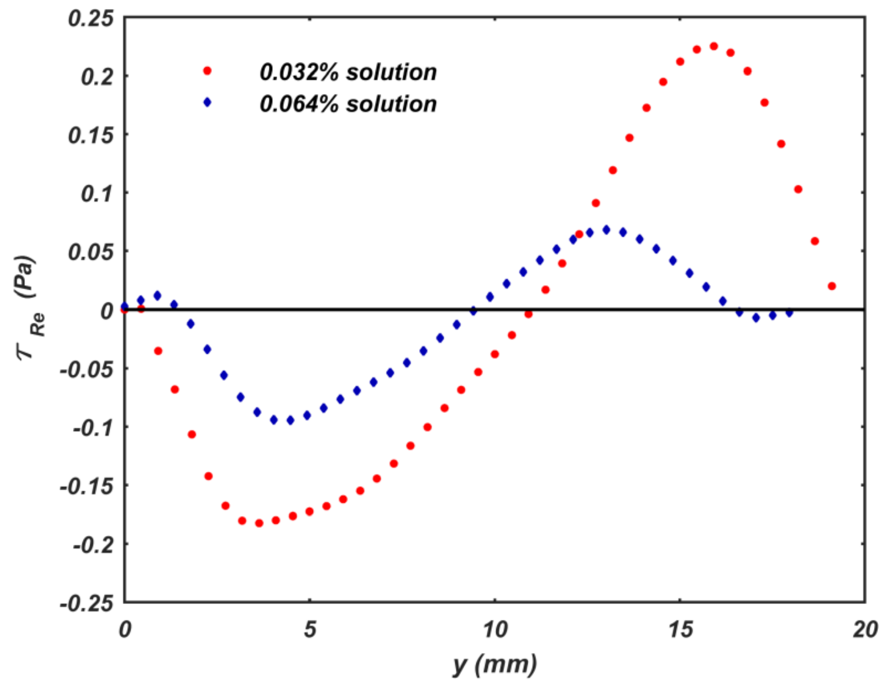

Figure 8-12 Comparison of Reynolds stress profiles over stationary cuttings bed for two polymer solutions at $U_s = 0.56\frac{m}{s}$

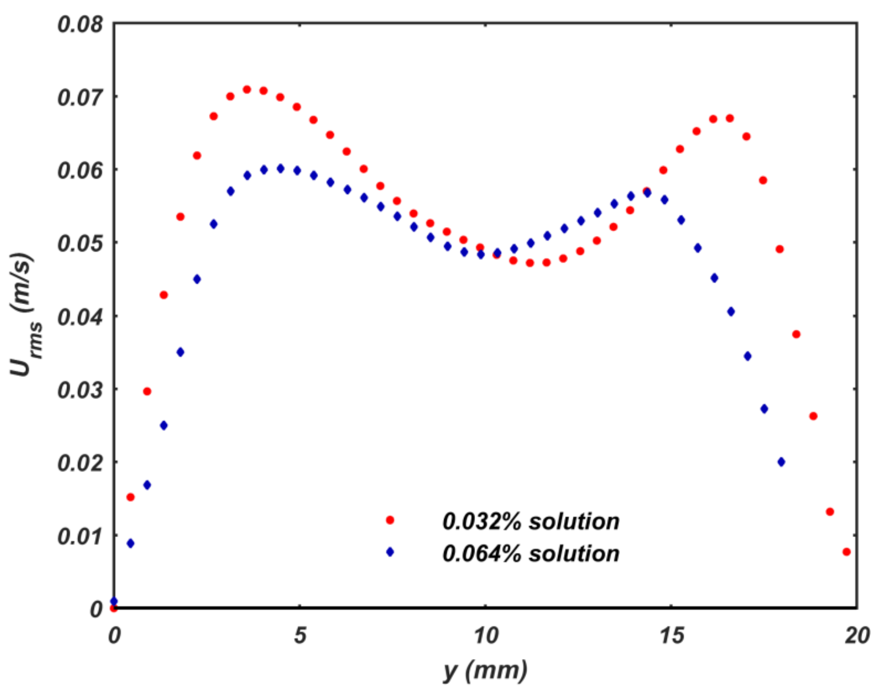

Figure 8-13 Comparison of axial turbulence intensity profiles over stationary cuttings bed for two polymer fluids at $U_s = 0.56\frac{m}{s}$

The Reynolds normal stress data are compared to the two polymer fluids in Figure 8-13. There is a slight reduction in the Reynolds normal stress for 0.064%. The decline in the turbulence intensity can play a role in the delay of bed erosion for the thicker fluid. However, the reduction is not as much to account for the significant increase in the critical flow rate of bed erosion.

8.4.3.2. Average bed shear stress

Table 8-3 reports the bed shear stress values measured for the two polymer fluids. The 0.064% polymer fluid exhibits a higher bed shear stress, and hence, it exerts a larger drag force on the bed than the 0.032% fluid. However, the greater shear stress is not caused by the increasing flow turbulence. That is because a decrease in Reynolds stress for the more viscous fluid was observed. Therefore, the higher bed shear stress (seen as the increase in the frictional pressure loss) is essentially caused by a higher viscosity (i.e. viscous stress). Also indicated by these results was that increasing the bed shear stress alone cannot assure a better hole cleaning.

Table 8-3 Comparison of the bed shear stress values of 0.032% and 0.064% polymer fluids at 0.56 m/s

	0.032% Polymer fluid	**0.064% Polymer fluid**
Bed shear stress (Pa)	0.91	1.4
Shields' Stress	0.093	0.144

8.4.4. Discussion of the near wall velocity distribution, turbulence, and interfacial bed shear stress results

In the previous sections, two primary comparisons were made to find an answer to the question why adding small amounts of polymer or increasing polymer concentration causes a significant increase in the minimum flow rate required for the onset of bed erosion. In the first case, local velocity profiles, turbulent normal and shear stresses for water and 0.032% polymer fluid each at their critical flow rate of bed erosion (90 and 200 lit/min respectively) were compared. The results showed that the polymer fluid had to have a higher local velocity near the bed interface and consequently exert a greater drag force on the bed than that of water at the onset of particle movement. Comparison of the Reynolds shear and normal stresses also showed that polymer fluid had higher turbulence activity near the bed than water at the time the particle starts moving. The polymer solution had a higher critical bed shear stress as well. Therefore, the increase in critical flow rate for bed erosion caused by adding polymers cannot be explained by the reduction in local velocity or the bed shear stress. It cannot be attributed to the decrease in turbulence by polymer additives either because, at the onset of the bed erosion, the polymer fluid had higher turbulence near the bed. Overall, the results from the first part of the analyses showed that the polymer fluid should exert greater drag force than water on the sand particles to initiate bed erosion.

In the second part, the near wall velocity distribution, the Reynolds stresses, and the bed shear stress (which are all considered as important variables controlling the bed erosion rate) were compared using fluids of 2 different polymer concentrations (0.032% and 0.064%) circulated at the same flow rate. The comparison was made at the critical flow rate for bed erosion using 0.032% polymer fluid (200 lit/min). The initial sand bed was formed using water to eliminate any impact of polymers in the formation of bed structures (i.e., gelling and bed compaction). Comparison of velocity profiles showed that increasing polymer concentration did not affect the local velocity values near the bed. This implies that the main force responsible for mobilizing the sand particles (i.e., the drag force) is higher for the more concentrated polymer solution (due to higher overall shear viscosity). A reduction in the Reynolds shear stress was observed because of increasing polymer concentration. Additionally, a higher bed shear stress was registered for the flow of 0.064% polymer fluid. The PIV results together with the calculations of bed shear stresses showed that at the same flow rate, increasing polymer concentration results in a higher fluid drag force on the cuttings bed. However, this increase in the fluid drag force on the cuttings bed did not lead to a better hole cleaning.

To better understand the difference in the level of drag force exerted on the cuttings bed at the onset of bed erosion by each fluid, the measured time-averaged local velocity profiles were used to calculate the drag force profile near the cuttings bed. Figure 8-14 shows the drag force profiles near the bed interface for water, 0.032% and 0.064% polymer solutions at their critical flow rates of bed erosion (90, 200 and 256 liter/min, respectively). Details of calculations pertinent to drag coefficient for each fluid is presented in Appendix A. The data of Figure 8-14 further consolidate the conclusion we made earlier that a polymer based fluid should exert a higher drag force on the same sand bed to be able to erode the sand particles. Increasing the polymer concentration causes the critical drag force for particle removal to increase.

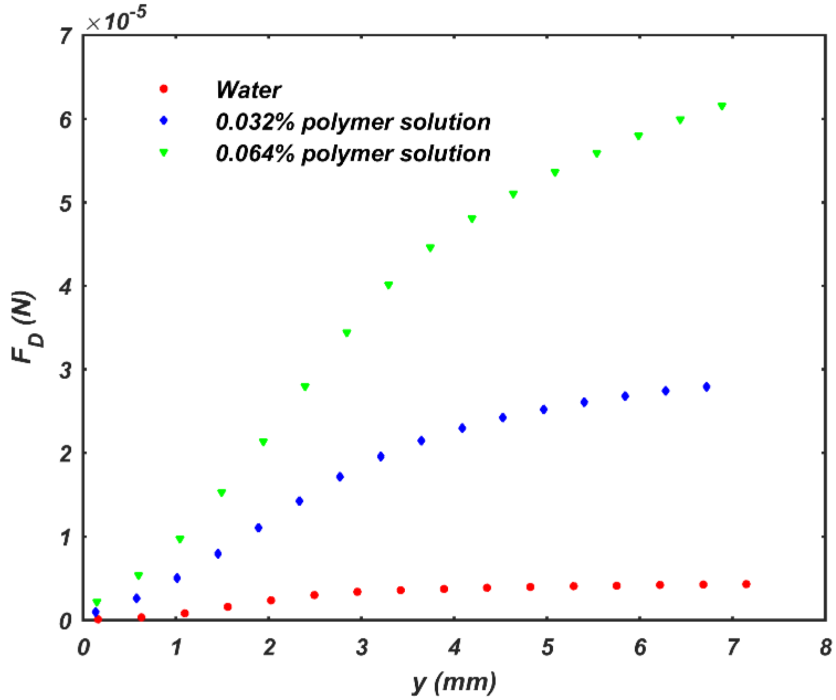

Figure 8-14 Profiles of drag force near the cuttings bed interface for water, 0.032% and 0.064% polymer solutions at 90, 200 and 256 lit/min respectively (each fluid at its critical flow rate of bed erosion)

8.5. Impact of Fluid Viscoelastic Properties on the Bed Erosion

The results presented in the previous sections showed that polymer fluids require higher flow rate to initiate the bed erosion than that of water. It is also shown that the hindered onset of the bed erosion with polymer fluids is not because of the reduction of the fluid hydrodynamic (drag and lift) forces. Actual causes of why polymer fluids require higher flow rates to initiate bed erosion are not known, and viable explanations of these observations are yet to be developed. In the following section, we will make a case, supported by our experimental observations, that viscoelastic properties of the polymer fluid could be the main reason behind the hindered onset of the bed erosion with polymer fluids.

The initiation of particle movement from the surface of the bed deposits can be explained by using a mechanistic model of forces involved in the process. Particles lying at the bed/fluid interface are subjected to multiple forces (Figure 8-15). These forces are of two types;

mobilizing forces and resistive forces. The main mobilizing forces are the fluid dynamic (drag and the lift) force. The forces resisting the particle movement are the gravity (buoyed weight of sand particles), the friction, and in the case of small size particles, Van der Walls force (Ramadan et al. 2003, Duan et al. 2007). The necessary condition for the particle to move is that the total moment produced by the mobilizing forces around the pivoting point to surpass that of resistive forces (Clark and Bickham 1994).

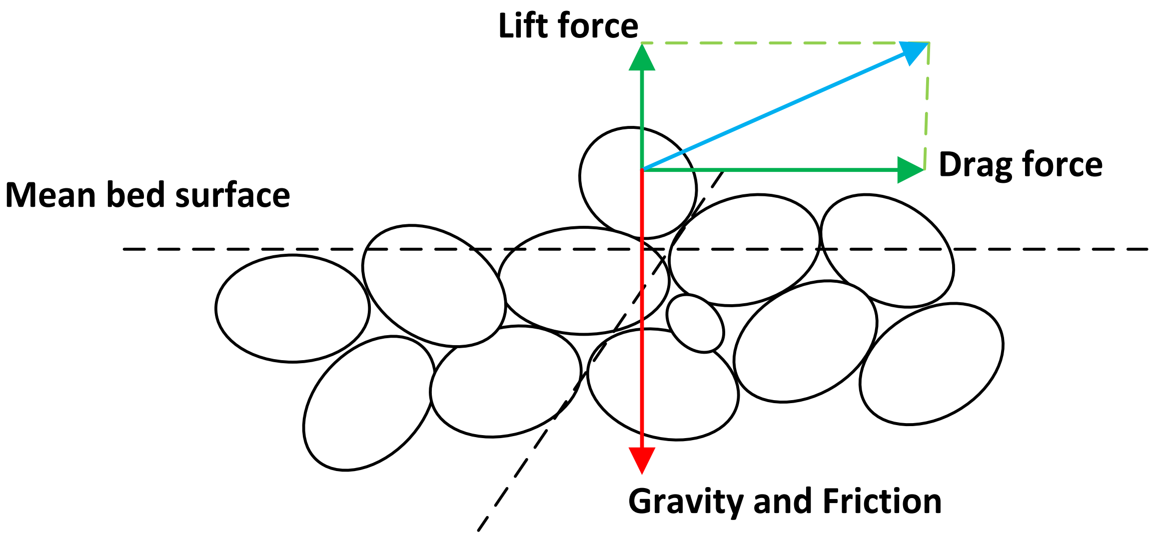

Figure 8-15 Schematic illustration of different forces acting on cutting in the bed

The hydrodynamic (drag and lift) forces vary with the flow conditions and the fluid properties. A higher fluid velocity and viscosity results in higher hydrodynamic force at the bed interface. On the other hand, the resistive forces are mainly functions of physical properties of the solid particles (i.e. density, size, shape), and hence, they are not variable. These are the fundamental assumptions in most of the mechanistic and semi-mechanistic hole cleaning models (Clark and Bickham 1994, Duan et al. 2007). The results presented earlier showed that the polymer fluid exerts a higher drag force on the cuttings than water to mobilize them (i.e. at the onset of the particle movement). Since the threshold of particle movement only depends on the net moment produced around the pivoting point, the implication from our experimental results is that both resistive and mobilizing forces must be functions of the fluid type and flow conditions. Otherwise, the particles would have started moving once they were subjected to the same critical hydrodynamic forces. These conclusions, however, contradict with the assumption that the forces, which resist the movement of the cuttings, remain constant. We know that gravity and frictional forces should remain constant if the solid physical properties and the fluid density are the same. Therefore, based on our experimental observations (i.e. the delay of the onset of the particle removal with the increasing polymer concentration of the fluid) reported in the preceding sections, we concluded that there must be an additional resistive force introduced into the particle removal process from other sources.

The other resistive force, in this case, arises from the viscoelastic nature of the polymer fluids. The non-zero normal stress difference, which is a characteristic of viscoelastic fluids, can be thought of the source of an additional compressive force acting in the direction perpendicular to the flow direction (Bird et al. 1987). This additional force is absent in the case of water flow. The force balance presented in Figure 8-15 and Figure 8-16a only represent the force balance for a non-viscoelastic fluid. The resistive forces, in this case, are constant and only depend on the cuttings physical characteristic (i.e. cuttings size, shape, and density). On the other hand, for the flow of viscoelastic fluids, a new resistive force arising from the non-zero first normal stress difference should be taken into consideration (Figure 8-16b). The additional force is a function of the polymer concentration. The higher polymer concentration results in a higher normal stress difference (Figure 5-4), and consequently greater normal fluid force.

The additional normal fluid force resulting from non-zero normal stress difference has significant consequences, which would potentially influence the efficiency of particle removal process. The first and the most immediate impact of normal fluid force is the consolidation of the sand bed. Thus, higher hydrodynamic forces would be required to roll or slide the same cutting as the polymer concentration (and the elasticity) of the fluid increases. Several field case and laboratory studies also reported that the use of polymer based drilling fluids resulted in a more consolidated bed, and therefore, more challenging hole cleaning situations (Saasen 1998, Saasen and Løklingholm 2002).

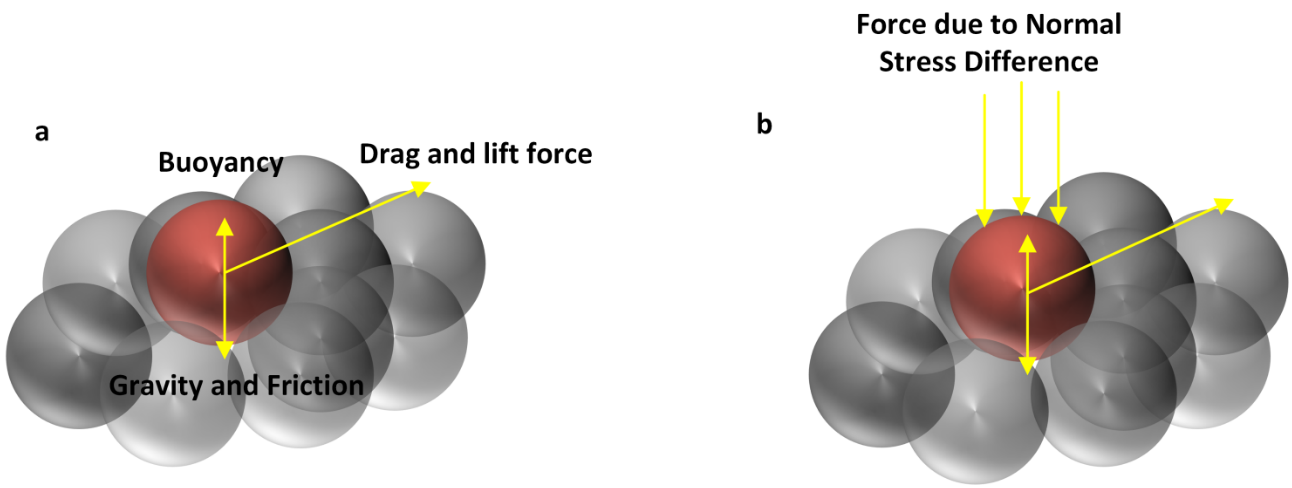

Figure 8-16 Illustration of force balance on a single particle a) typical for non-elastic fluids b) added normal force due to non-zero normal stress difference of elastic fluid.

The second impact of the additional normal fluid force appears when the threshold of the particle motion is of interest. For the particle shown in Fig. 15 to start moving, the total moment produced by the hydrodynamic forces needs to surpass that of resistive forces around the pivoting point. In the case of Newtonian (or more generally inelastic) fluids, the holding forces are the gravity and friction forces. However, when we use viscoelastic fluids, the presence of non-zero normal stress difference can also contribute to the resistive forces and, hence, add to the difficulty of removing the particles from the surface of the bed deposits. Increasing polymer concentration (and the fluid elasticity) would increase the minimum flow rate required for the bed erosion regardless of the particle physical properties. Different bed erosion performances of water and oil based drilling fluids, despite having similar shear viscosities as reported by Bui et al. (2012) and Werner et al. (2017), therefore, can be explained by the fact that these fluids have different viscoelastic properties. The disparity of the non-zero normal stress differences of these fluids would create variance in the normal fluid forces, which could be the main reason for the observed difference in their particle removal performances.

In addition to the normal fluid force phenomenon, the flowing characteristic of viscoelastic fluids also negatively affects bed erosion. According to Gomaa et al. (2015), a viscoelastic material when flowing in the elastic regime behaves considerably differently than flowing in the viscous dominant regime. In the dominant elastic regime, the fluid stretches and deforms, much like a rigid solid, when subjected to a shear stress. This deformation causes a significant reduction in the settling velocity. We can use the same argument to show that this flow behavior of elastic fluids can cause a delay in the bed erosion. Near the bed interface (typically the highest shear rate in the wellbore exist here) the flow is most likely in the dominant elastic regime. This means that if a particle needs to be detached from the sand bed, the layer of polymer fluid above it will stretch and deform rather than flowing. The stretching prevents the particle from penetrating the fluid. The extra resistance by the fluid dissipates the particle momentum, hence, delaying the onset of bed erosion. The elastic properties of the drilling fluid create a shield over the bed that prevents the bed materials from interacting with the flow outside the boundary layer. The flexible polymer coils absorb and store the energy of the particles and release it back to the main flow.

In the current study, shear rates of 180 and 245 1/s have been registered over the beds for flow of 0.032% and 0.064% polymer fluids at their critical flow rate of bed erosion, respectively. These shear rates were calculated using the measured velocity profiles. These values are much higher than the cross-over shear rates from viscous dominant region to the elastic regime (5.9 and 2.1 1/s for 0.032% and 0.064% fluids respectively). Therefore, the flow near the cuttings bed is in the elastic dominant regime which means the shielding effect due to the normal elastic force is present.

Saasen (2014) pointed out to the difference in the mechanism upon which water and oil based drilling fluids build viscosity. Oil based drilling fluids are constructed as a combined emulsion and dispersion. No long chain polymers are creating long range structure effects (as opposed to water based drilling fluids). Hence, this normal fluid force discussion and flowing characteristic of viscoelastic fluids may explain why hole cleaning is easier with OBM (N_1=N_2=0) than with WBM.

In the next section, an attempt is made in quantifying the elastic normal fluid force caused by anisotropy in the diagonal stress tensor.

8.6. Normal Fluid Force Due to Non-Zero Stress Differences of Viscoelastic Fluid Flow

The normal fluid force is due by the gradient of the normal stress in the vertical direction. To better understand the order of magnitude of this force, we will compare it to the submerged weight of the cuttings. The submerged or buoyed weight can be estimated as follows (assuming spherical solid particles):

$$F_g = \frac{1}{6}\pi d_p^3\, g\,(\rho_s - \rho_f) \qquad \textbf{Eq.(8-19)}$$

The rheological behavior of incompressible, isotropic elastic liquids can be described by τ_{yx}, $N_1 = \tau_{xx} - \tau_{yy}$ and $N_2 = \tau_{yy} - \tau_{zz}$, where τ_{ij} denotes the components of the stress tensor, and N_1 and N_2 are the first and the second normal stress difference, respectively. N_1 is positive for polymer fluids in general, whereas N_2 is in general negative and absolutely only a small fraction of N_1 (Bird et al. 1987).

Tropea et al. (2007) presented the theory of the measurement of the 1st normal stress difference using cone and plate viscometer. Assuming that the free surface, overwhich the viscoelastic fluid flow takes place, has a spherical shape, Tropea et al. (2007) have shown that the total force exerted by the flowing viscoelastic fluid on the plate is related to N_1 as given by Eq. 8-20 :

$$F_N = N_1 \frac{\pi}{2} R^2 \qquad \textbf{Eq.(8-20)}$$

Where R is the radius of the plate. Equation 8- 20 presents the theoretical basis for estimating N_1 using a cone and plate rheometer. For a given cone and plate geometry and shear rate condition, the rheometer allows measuring the normal force, F_N, exerted by the viscoelastic fluid, which is then used to estimate N_1 via Eq. 8-20.

In this study, an estimate of the normal fluid force was obtained by using the modified version of the Eq.20, where we assumed only half of the surface area of the spherical particle is exposed to the viscoelastic fluid flow. The resultant form of the normal force equation is given as follows:

$$F_N = N_1 \frac{\pi}{8} \, d_p^2 \qquad \textbf{Eq.(8-21)}$$

Where d_p is the particle diameter, N_1 is the first normal stress as measured by the cone and plate rheometer for the polymer fluids used in this study.

The normal fluid force presented by Eq. 8-21 is the force exerted on the plate by the flow of viscoelastic fluids. It ignores the presence of the second normal stress difference. The free surface of the plate, overwhich the viscoelastic fluid flow takes place, is assumed to have a spherical shape. Therefore, the results should be considered as an approximation of the normal fluid force in such a complex situation as the viscoelastic fluid flow over the sand bed.

Hence, by using the measured values of first normal stresses (Figure 8-7) and the average diameter of the sand particles (i.e. 600 micron) used in our experiments and assuming a projected area in the direction of the force equal to the area of a circle with diameter equal to 600 microns, estimates of the normal (elastic) forces as a function of shear rate were obtained. The bed shear rates were obtained from the measured velocity profiles ($\dot{\gamma}_b = \frac{du}{dy}$). Summary of different forces that are important for bed erosion using various fluids are reported in Table 8-4. Note that the results shown in Table 8-4 were calculated at the critical flow rates of bed erosion, which were experimentally determined for each fluid.

The results shown in Table 8-4 reveals some interesting findings. For the 0.032% polymer fluid, the normal (elastic) force is about 95% of the effective weight of the particles. Similarly, the fluid's normal force for 0.064% polymer fluid is 193% of the effective weight of the particles. In other words, the particles at the surface of the bed deposits experience a normal force about one and two times more than their submerged weight when using viscoelastic polymer fluids (of 0.032% and 0.064% polymer concentrations, respectively) to erode them. Assuming other resistive forces (i.e. friction forces) are negligible compared to the submerged weight (Ramadan et al. 2003), then, the normal fluid (elastic) force emerges as one of the main resistive forces in the bed erosion when using viscoelastic polymers.

Table 8-4 Comparison of the magnitudes of the normal fluid force and other significant forces involved in bed erosion

	$F_g\ (N)$	$F_N(N)$	$F_D(N)$	$\frac{F_N}{F_g} \times 100$	$\frac{F_D}{F_N + F_g}$
Water	1.83×10^{-6}	0	5.72×10^{-7}	0	0.31
0.032% solution	1.83×10^{-6}	1.73×10^{-6}	2.6×10^{-6}	95	0.73
0.064% solution	1.83×10^{-6}	3.53×10^{-6}	5.4×10^{-6}	193	1

The ratio of drag force to the summation of the buoyancy and the normal fluid force is also reported in Table 8-4. Physically, this ratio can be thought of as the proportion of the moment produced by the drag force to that of resistive forces. Therefore, a ratio of one means that the same moments is generated by the dynamic fluid (drag) forces and resistive forces, and the particle is at the threshold of movement. This ratio for water was about 0.31. For 0.032% and 0.064% polymer fluids, the same proportion was 0.73 and 1 respectively. Since the forces reported in Table 8-4 were calculated at the critical flow rate, it was expected that the ratio of drag force to the resistive forces to be close to one. However, for water and 0.032% polymer fluid, the drag force to the sum of the holding forces ratio was less than one. There might be several reasons causing this ratio to be less than one.

Neglecting turbulence and other mobilizing forces (such as lift force) are believed to be the main cause of the observed ratio of the drag force to that of resistive forces being less than one at the onset of bed erosion for water and 0.032% polymer fluid. We used the time-averaged local flow velocity to calculate the drag force. Therefore, the contribution of fluctuation velocities was not included in the reported numbers. It has been shown by Bizhani and Kuru (2017b) that the turbulence can significantly improve the fluid drag forces acting on the particles. Therefore, a ratio of the fluid's drag force to the summation of buoyancy and normal force at the onset of the bed erosion being less than one implies the significance of the flow turbulence in particles dislodgement. The results shown in Table 8-4, in that respect indicate the importance of flow turbulence in calculating the fluid drag force. Additionally, other mobilizing forces such as lift force could also contribute towards the moment produced by the fluid.

The force ratio (i.e., drag force to the summation of the buoyancy and the normal fluid force at the onset of the bed erosion) for 0.032% and 0.064% polymer fluids is 0.73 and 1 respectively. Comparing to water (where the force ratio was 0.31), these results imply that as the polymer concentration increases, the contribution of the instantaneous turbulence fluctuations on the drag force may not be as significant as in the case of water. This is mainly because the local time-averaged fluid velocity (at the onset of the particle movement) near the bed interface increases with the increasing polymer concentration. As the local time-averaged velocity increases, the ratio of fluctuation velocity to that of the average velocity decreases. Consequently, the effective drag force becomes less and less dependent on the variations due to velocity fluctuations. Therefore, although the 0.032% polymer fluid has a higher turbulence intensity than water (Fig. 10), since the local time-averaged velocity of the 0.032% polymer fluid (at the onset of particle movement) is much greater than that of water, the relative contribution of the fluctuation velocities to the effective drag force may not be as high as that of water.

In conclusion, we are now able to suggest a reasonable explanation for the observed increase in the critical flow rate of bed erosion when using polymer fluids. When viscoelastic fluids are used to erode a bed deposit, the developed anisotropies in the fluid structures give rise to a normal fluid force that acts against the bed erosion (i.e. particle removal from the bed deposits). This normal force is a function of the shear rate and is negligible at low shear rates (i.e. viscous force dominated regime). On the other hand, forces that are responsible for particle removal (i.e. drag and lift force) are also small at the low flow velocities. To initiate the bed erosion, the flow rate must be increased above a certain critical flow rate. Increasing the flow rate causes the shear rate near the bed also increase and enhance dynamic fluid forces. At the same time, the normal (elastic) fluid forces also increase with the increasing shear rate. Therefore, the increase in the fluid dynamic forces is countered by an increase in the normal fluid forces. To initiate the erosion process, the flow velocity and, hence, the resultant fluid dynamic forces (i.e. drag and lift) must be increased to a level where the fluid dynamic forces surpass the resistance caused by the sum of the normal fluid force and gravity force. A higher polymer concentration (or stronger viscoelasticity) results in a higher normal fluid force. Hence, it increases the critical flow rate of bed erosion.

8.7. Conclusions

In this paper result of a microscopic study on the impact of the rheology of viscoelastic fluids on the bed erosion was presented and discussed. The primary objective of the study was to investigate mechanisms responsible for the increase in the minimum flow rate of bed erosion caused by polymer fluids as compared to water. The PIV imaging technique in a transparent flow loop was used for data collection. Natural quartz sands with mean sieve diameters of 600 microns were used together with water and two polymer fluids to simulate bed erosion process.

Parameters that control sand particle removal from the stationary bed were studied from both microscopic and macroscopic perspective. The macroscopic parameters affecting bed erosion are the flow rate and the bed shear stress. The microscopic parameters such as local fluid velocity and flow turbulence near the sand bed were measured using the PIV technique. The combination of both macroscopic and microscopic results provided a better understanding of the effect of adding or enhancing polymer concentration on various parameters affecting bed erosion.

Comparison of the local fluid velocity and the flow turbulence at the onset of bed erosion for 0.032%w/w polymer fluid and water revealed that the polymer fluid has a higher local fluid velocity and the turbulence at the bed interface; implying a higher drag force was imposed at the bed interface by the polymer fluid. The existence of the higher drag forces at the critical flow rate of the bed erosion by polymer fluid flow was also confirmed by the bed shear stress calculations. Results from the first part of the study, therefore, have confirmed that the delay in bed erosion does not happen due to the reduction of the flow turbulence or the local fluid velocity by polymer additives.

In the second part of the paper, PIV measurements of the local fluid velocities were conducted by using polymer fluids of two different concentrations at the same flow rate. The results revealed that increasing polymer concentration caused improvement of the fluid drag forces acting on the particles in the bed. This was mainly due to the fact that increasing the polymer concentration enhanced the shear viscosity of the fluids while the local fluid velocities for both polymer fluids did not change. Moreover, the bed shear stress was higher for the fluid with higher polymer concentration. Based on these results, it was therefore, concluded that the delay in the bed erosion due to the flow of polymer fluid (with increased shear viscosity) could not be associated with any decrease in local fluid velocity and/or any reduction of the fluid hydrodynamic forces at the bed interface.

To explain this rather controversial phenomenon, we have looked at the impact of the viscoelastic polymer fluid rheology on the bed erosion. It was shown that for viscoelastic polymer fluids, an additional normal fluid force appears that hinders the removal of the particles from sand bed deposits. This normal fluid force arises due to the non-zero first and second normal stress differences in the shear flow of polymer fluids. This additional force causes the sand bed to become more consolidated while imposing an additional resistive force against the mobilization of the particles. Estimation of the normal fluid force shows that this normal fluid force is considerably higher than the submerged weight of the sand particles.

In addition to the normal fluid force phenomenon, the flowing characteristic of viscoelastic fluids also negatively affects the bed erosion. Near the bed interface (typically the highest shear rate in the wellbore exist here) the flow is most likely in the dominant elastic regime. This means that if a particle needs to be detached from the sand bed, the layer of the polymer fluid above it will stretch and deform rather than flowing. The stretching prevents the particle from penetrating the fluid. The extra resistance by the fluid dissipates the particle momentum, hence, delaying the onset of bed erosion. The elastic properties of the drilling fluid create a shield over the bed that prevents the bed materials from interacting with the flow outside the boundary layer.

8.8. Nomenclatures

A_P	Projected area in the flow (m^2)
C_D	Drag Coefficient
D_h	Hydraulic Diameter (m)
d_p	Particles diameter (m)
F_D	Steady part of the drag force (N)
F_g	Buoyed weight of the particle in the drilling fluid (N)

F_N	Normal fluid force (N)
K	Fluid consistency index ($Pa.s^n$)
n	Flow behavior index
L	Pipe length (m)
N_1	First normal stress difference (Pa)
N_2	Second normal stress difference (Pa)
g	Acceleration of gravity ($\frac{m}{s^2}$)
$\hat{u}$	Instantaneous axial velocity ($\frac{m}{s}$)
U	Average fluid velocity ($\frac{m}{s}$)
$\hat{v}$	Instantaneous radial velocity ($\frac{m}{s}$)
u'	Axial Fluctuation Velocity ($\frac{m}{s}$)
v'	Radial Fluctuation Velocity ($\frac{m}{s}$)
u_{rms}	Root Mean Square of axial fluctuation velocity ($\frac{m}{s}$)
y	Vertical distance from mean bed surface/or pipe wall (mm)
Q	Flow Rate (m^3/s)
Re_g	Generalized Reynolds number (-)
Re_{Lam}	Critical Generalized Reynolds number for laminar flow (-)
Re_{Tur}	Critical Generalized Reynolds number for fully turbulent flow (-)

Δs	Displacement of tracer particles (m)
Δx	Axial displacement of tracer particles (m)
Δy	Radial displacement of tracer particles (m)
ΔP	Pressure drop (Pa)
μ	Fluid viscosity ($Pa.s$)
τ_{xx}	Normal stress in x direction (Pa)
τ_{yy}	Normal stress in y direction (Pa)
τ_{zz}	Normal stress in z direction (Pa)
τ_{xy}	Shear stress (Pa)
τ_{Re}	Reynolds stress (Pa)
τ	Shear stress (Pa)
Ψ_1	First normal stress difference coefficient
Ψ_2	Second normal stress difference coefficient
τ_b	Mean bed shear stress (Pa)
τ^*	Shields' stress (-)
ρ_s	Solid's density ($\frac{Kg}{m^3}$)
ρ	Fluid density ($\frac{Kg}{m^3}$)
$\dot{\gamma}$	Shear rate ($\frac{1}{s}$)

8.9. References

Azar, J. J. and Sanchez, R. A. (1997). Important Issues in Cuttings Transport for Drilling Directional Wells. Fifth Latin American and Caribbaean Petroleum Engineering Conference and Exibition. held in Rio de Janeiro, Brazil, 30 August -3 Spetember 1997, SPE-39020-MS,DOI: 10.2118/39020-MS.

Baird, D. G. (2008). First Normal Stress Difference Measurements for Polymer Melts At High Shear Rates in a Slit-Die Using Hole and Exit Pressure Data. Journal of Non-Newtonian Fluid Mechanics **148**(1–3): 13-23, DOI: http://dx.doi.org/10.1016/j.jnnfm.2007.04.007.

Becker, T. E., Azar, J. J. and Okrajni, S. S. (1991). Correlations of Mud Rheological Properties With Cuttings-Transport Performance in Directional Drilling. **SPE** Drilling Engineering **6**(1), SPE-19535-PA, DOI: 10.2118/19535-PA.

Bilgesu, H. I., Mishra, N. and Ameri, S. (2007). Understanding the Effect of Drilling Parameters on Hole Cleaning in Horizontal and Deviated Wellbores Using Computational Fluid Dynamics. SPE Eastern Regional Meeting Lexington, Kentucky, USA, 17-19 October 2007, SPE-111208-MS,DOI: 10.2118/111208-MS.

Bird, R. B., Armostrong, R. C. and Hassager, O. (1987). Dynamics of Polymeric Liquids, V1. New York, Wiley.

Bizhani, M., Corredor, F. and Kuru, E. (2015). An Experimental Study of Turbulent Non-Newtonian Fluid Flow in Concentric Annuli using Particle Image Velocimetry Technique. Flow, Turbulence and Combustion **94**(3): 527-554, Flow Turbulence Combust, DOI: 10.1007/s10494-014-9589-6.

Bizhani, M., Corredor, F. E. R. and Kuru, E. (2016a). Quantitative Evaluation of Critical Conditions Required for Effective Hole Cleaning in Coiled-Tubing Drilling of Horizontal Wells. **SPE** Drilling & Completion **31**(3): 188-199, DOI: http://dx.doi.org/10.2118/174404-PA.

Bizhani, M. and Kuru, E. (2017b). Critical Review of Mechanistic and Empirical (Semi-Mechanistic) Models for Particle Removal from Sand Bed Deposits in Horizontal Annuli by Using Water. SPE Journal, SPE-187948-PA, DOI: https://doi.org/10.2118/187948-PA.

Bui, B., Saasen, A., Maxey, J. et al. (2012). Viscoelastic Properties of Oil Based Drilling fluids. Annual Transactions of the Nordic Rheology Society **20**: 33-47.

Chhabra, R. P. and Richardson, J. F. (1999). Chapter 1 - Non-Newtonian fluid behaviour. Non-Newtonian Flow in the Process Industries. Oxford, Butterworth-Heinemann**:** 1-36.

Clark, R. K. and Bickham, K. L. (1994). A Mechanistic Model for Cuttings Transport. SPE 69th Annual Tgchniml Conference and Exhlbltion Now ohms, LA, U. S.A., 25-8 .Septemb.ar 1994., SPE-28306-MS,DOI: 10.2118/28306-MS.

Dealy, J. M., Wang, J., Dealy, J. M. et al. (2013). Melt Rheology and Its Applications in the Plastics Industry. Dordrecht ; New York, Springer.

Dealy, J. M. and Wissbrun, K. F. (1999). Role of Rheology in Extrusion. Melt Rheology and Its Role in Plastics Processing: Theory and Applications. Dordrecht, Springer Netherlands**:** 441-490.

Deshpande, A. P. (2010). Rheology of Complex Fluids. New York: xiii, 257 p.

Diplas, P., Dancey, C. L., Celik, A. O. et al. (2008). The Role of Impulse on the Initiation of Particle Movement Under Turbulent Flow Conditions. Science **322**(5902): 717-720, Science, DOI: 10.1126/science.1158954.

Duan, M., Miska, S. Z., Yu, M. et al. (2007). Critical Conditions for Effective Sand-Sized Solids Transport in Horizontal and High-Angle Wells. SPE Production and Operations Symposium Oklahoma City, Oklahoma, USA, 31 March-3 April 2007., SPE-106707-MS,DOI: 10.2118/106707-MS.

Gomaa, A. M., Gupta, D. V. S. V. and Carman, P. S. (2015). Proppant Transport? Viscosity Is Not All It's Cracked Up To Be. SPE Hydraulic Fracturing Technology Conference, 3-5 February, The Woodlands, Texas, USA, SPE-173323-MS,DOI: 10.2118/173323-MS.

Japper-Jaafar, A., Escudier, M. P. and Poole, R. J. (2010). Laminar, transitional and turbulent annular flow of drag-reducing polymer solutions. Journal of Non-Newtonian Fluid

Mechanics **165**(19-20): 1357-1372, J Non-Newton Fluid, DOI: 10.1016/j.jnnfm.2010.07.001.

Kelessidis, V. C., Mpandelis, G., Koutroulis, A. et al. (2002). Significant Parameters Affecting Efficient Cuttings Transport In Horizontal and Deviated Wellbores In Coil Tubing Drilling: A Critical Review. Paper presented at the 1st International Symposium of the Faculty of Mines (ITU) on Earth Sciences and Engineering, 16-18 May 2002, Maslak, Istanbul, Turkey.

Leising, L. J. and Walton, I. C. (2002). Cuttings-Transport Problems and Solutions in Coiled-Tubing Drilling. **SPE** Drilling & Completion **17**(1): 54-66, SPE-77261-PA, DOI: 10.2118/77261-PA.

Li, J. and Luft, B. (2014a). Overview of Solids Transport Studies and Applications in Oil and Gas Industry - Experimental Work. SPE Russian Oil and Gas Exploration & Production Technical Conference and Exhibition. Moscow, Russia, 14-16 October, SPE-171285-MS,DOI: 10.2118/171285-MS.

Li, J. and Luft, B. (2014b). Overview Solids Transport Study and Application in Oil-Gas Industry-Theoretical Work. International Petroleum Technology Conference. Kuala Lumpur, Malaysia, 10-12 December 2014, IPTC-17832-MS,DOI: 10.2523/IPTC-17832-MS.

Li, J., Wilde, G. and Crabtree, A. R. (2005). Do Complex Super-Gel Liquids Perform Better Than Simple Linear Liquids in Hole Cleaning With Coiled Tubing? SPE/ICoTA Coiled Tubing Conference and Exibition The Woodlands, Texas, USA, 12-13 April 2005, SPE-94185-MS,DOI: 10.2118/94185-MS.

Lin, Y., Phan-Thien, N. and Khoo, B. C. (2014). Normal Stress Differences Behavior of Polymeric Particle Suspension in Shear Flow. Journal of Rheology **58**(1): 223-235, DOI: 10.1122/1.4855496.

Lodge, A. S. (1964). Elastic Liquids; an Introductory Vector Treatment of Finite-Strain Polymer Rheology. London, New York;, Academic Press.

Melling, A. (1997). Tracer particles and seeding for particle image velocimetry. Measurement Science & Technology **8**(12): 1406-1416, Meas Sci Technol, DOI: 10.1088/0957-0233/8/12/005.

Nazari, T., Hareland, G. and Azar, J. J. (2010). Review of Cuttings Transport in Directional Well Drilling: Systematic Approach. SPE Western Regional Meeting Anaheim, Califronia, USA, 27-29 may 2010, SPE-132372-MS,DOI: 10.2118/132372-MS.

Nezu, I. and Sanjou, M. (2011). PIV and PTV measurements in hydro-sciences with focus on turbulent open-channel flows. Journal of Hydro-Environment Research **5**(4): 215-230, J Hydro-Environ Res, DOI: 10.1016/j.jher.2011.05.004.

Nobach, H. and Bodenschatz, E. (2009). Limitations of Accuracy in PIV Due To Individual Variations of Particle Image Intensities. Experiments in Fluids **47**(1): 27-38, DOI: 10.1007/s00348-009-0627-4.

Okrajni, S. and Azar, J. J. (1986). The Effects of Mud Rheology on Annular Hole Cleaning in Directional Wells. **SPE** Drilling Engineering **1**(4), SPE-14178-PA, DOI: 10.2118/14178-PA.

Pilehvari, A. A., Azar, J. J. and Shirazi, S. A. (1996). State-Of-The-Art Cuttings Transport in Horizontal Wellbores. International Conference on Horizontal Well Technology. Calgary, Alberta, Canada, 18-20 November, SPE-37079-MS,DOI: 10.2118/37079-MS.

Poole, R. J. (2010). Development-Length Requirements for Fully Developed Laminar Flow in Concentric Annuli. Journal of Fluids Engineering-Transactions of the **Asme 132**(6), J Fluid Eng-T Asme, DOI: 10.1115/1.4001694.

Rabenjafimanantsoa, H. A., Time, R.W. and Saasen, A. (2005). Flow regimes over particle beds experimental studies of particle transport in horizontal pipes. Annual Transactions of the Nordic Rheology Society, 13.

Ramadan, A., Skalle, P. and Johansen, S. T. (2003). A Mechanistic Model to Determine the Critical Flow Velocity Required Initiating the Movement of Spherical Bed Particles in Inclined Channels. Chemical Engineering Science **58**(10): 2153-2163, DOI: 10.1016/S0009-2509(03)00061-7.

Saasen, A. (1998). Hole Cleaning During Deviated Drilling - The Effects of Pump Rate and Rheology. European Petroleum Conference, 20-22 October, The Hague, Netherlands, SPE-50582-MS,DOI: 10.2118/50582-MS.

Saasen, A. (2014). Annular Frictional Pressure Losses During Drilling-Predicting the Effect of Drillstring Rotation. Journal of Energy Resources Technology-Transactions of the **Asme** **136**(3), DOI: Artn 034501 10.1115/1.4026205.

Saasen, A., Eriksen, N. H., Han, L. Q. et al. (1998). Is Annular Friction Loss the Key Parameter? Oil Gas-European Magazine **24**(1): 22-24.

Saasen, A. and Løklingholm, G. (2002). The Effect of Drilling Fluid Rheological Properties on Hole Cleaning. IADC/SPE Drilling Conference. Dallas, Texas, 26-28 February, SPE-74558-MS,DOI: 10.2118/74558-MS.

Shields, A. (1936). Anwendung der Ähnlichkeitsmechanik und der Turbulenzforschung auf die Geschiebebewegung. Berlin, Eigenverl. der Preußischen Versuchsanst. für Wasserbau und Schiff.

Tonmukayakul, N., Morris, J. F. and Prudhomme, R. (2013). Method for estimating proppant transport and suspendability of viscoelastic liquids. Google Patents. United States, US 20110219856 A1.

Tropea, C., Yarin, A. L. and Foss, J. F. (2007). Springer handbook of experimental fluid mechanics. Heidelberg: 1557 p.

Walker, S. and Li, J. (2000). The Effects of Particle Size, Fluid Rheology, and Pipe Eccentricity on Cuttings Transport. SPE/ICoTA Coiled Tubing Roundtable. Houston, TX, 5–6 April 2000., SPE-60755-MS,DOI: 10.2118/60755-MS.

Werner, B., Myrseth, V. and Saasen, A. (2017). Viscoelastic Properties of Drilling Fluids and Their Influence on Cuttings Transport. Journal of Petroleum Science and Engineering **156**: 845-851, DOI: http://dx.doi.org/10.1016/j.petrol.2017.06.063.

Xiaofeng, S., Wang, K., Yan, T. et al. (2013). Review of Hole Cleaning in Complex Structural Wells. The Open Petroleum Engineering Journal **6**: 25-32, DOI: 10.2174/1874834101306010025.

Ytrehus, J. D., Taghipour, A., Sayindla, S. et al. (2015). Full Scale Flow Loop Experiments of Hole Cleaning Performances of Drilling Fluids. Proceedings of the Asme 34th International Conference on Ocean, Offshore and Arctic Engineering, 2015, Vol 10.

8.10. Appendix A: Drag coefficient correlations

Throughout the paper, to calculate the drag coefficient for the polymer solutions, following correlation was used (this correlation was proposed by (Duan et al. 2007)).

$$C_{Du} = \frac{24}{Re_p}(2-n) \quad Re_p < 0.2(2^n) \qquad \textbf{Eq. (A- 8-1)}$$

$$C_{Du} = \frac{37}{(\frac{Re_p}{2^n})^{1.03}} + n\left(1 - \frac{20.9}{\left(\frac{Re_p}{2^n}\right)^{1.11}}\right) \quad 0.2(2^n) < Re_p < 24(2^n) \qquad \textbf{Eq. (A- 8-2)}$$

$$C_{Du} = \frac{37}{(\frac{Re_p}{2^n})^{1.03}} + 0.25 + 0.36n \quad 0.2(2^n) < Re_p < 100(2^n) \qquad \textbf{Eq. (A- 8-3)}$$

$$Re_p = \frac{\rho \hat{u}^{2-n} d_p^n}{K} \qquad \textbf{Eq. (A- 8-4)}$$

Following corrections to results of previous correlations was proposed for calculating drag force on a particle which is in a compact bed.

$$C_D = 0.8 C_{Du}\left[1 + \left(0.5 \times 10^{-4} Re_p + 0.0179\right)\eta\right] \qquad \textbf{Eq. (A- 8-5)}$$

$$\eta = \frac{\partial \hat{u}}{\partial y}\frac{\hat{u}}{y} \qquad \textbf{Eq. (A- 8-6)}$$

For water (i.e. Newtonian fluid) the following correlation was used (Ramadan et al. 2003):

$$C_D = \frac{24}{Re_p} + \frac{5}{1 + Re_p^{0.5}} + 0.4$$ **Eq. (A- 8-7)**

$$Re_p = \frac{\rho u d_p}{\mu}$$ **Eq. (A- 8-8)**

A correction factor of 0.85 was proposed to the result of previous correlation to account for the impact of particles in the bed on the drag force.

9 Assessemnt of of the Equivalent Sand Bed Roughness and the Interfacial Friction Factor in Hole Cleaning with Water in Horizontal Eccentric Annulus[9]

In this chapter results of PIV experiments during solid bed removal using water is presented and discussed. Specifically, the sand bed roughness height and friction factors in the annulus are analyzed in this chapter

9.1 Summary

In this study, we have investigated the turbulent flow of water over the sand bed deposited in a horizontal eccentric annulus. The primary objective was to determine the impact of the presence of a sand bed on the parameters strongly involved in bed erosion process such as local fluid velocity profiles near the interface, equivalent sand bed roughness, average and interfacial friction factors. The particle image velocimetry (PIV) technique was used to measure the velocity distribution at the water/sand bed interface. The bedload transport of particles caused an abrupt increase in the equivalent sand bed roughness. Analyses of the velocity profiles in the wall units confirmed that the sand bed roughness is variable and can be several times greater than the mean particle size. The interfacial (fi) and the average friction factors (fa) were evaluated and compared to flow under the stationary bed and the bedload transport conditions. The interfacial friction factor increased drastically at the onset of the bed erosion. We have also found that depending on the bed height (or the surface area of the bed at the interface), the interfacial friction factor can be significantly different from the average friction factor. The results presented here provide much-needed experimental data for the validation of the mechanistic,

[9] A version of this chapter has been submitted for publication: Bizhani M, Kuru E., Assessemnt of of the Equivalent Sand Bed Roughness and the Interfacial Friction Factor in Hole Cleaning with Water in Horizontal Eccentric Annulus., SPE journal

semi-mechanistic (empirical) and numerical (CFD) models of the bed erosion process. The major conclusion of the study is that the difference between the average and interfacial friction factors should be taken into account for more realistic multi-layer modeling of the hole cleaning.

Keywords: Hole cleaning, Equivalent sand bed roughness, Interfacial friction factor, Sediment transport, Turbulent flow

9.2 Introduction

Removal of a stationary cuttings bed (i.e. hole cleaning) is a routine operation encountered when drilling long horizontal, extended reach and multi-lateral wells. Cleaning stationary sand beds is also part of post-hydraulic fracturing operations (Li and Luft 2014b, Bizhani et al. 2016). Timely removal of the settled solids is essential for trouble free and profitable drilling. The interaction of the drilling fluid and cuttings in the bed is the primary factor controlling the efficiency of the bed erosion and hole cleaning process.

Hole cleaning is typically performed by pumping the drilling fluid down the string and up the annulus to sweep the drilled cuttings out of the wellbore. The turbulent flow is very often needed for effective removal of cuttings. The drilling fluid and the solid particles interact in a four-way coupling. That is both the drilling fluid and the cuttings affect the flow property of each other. Additionally, the particles interact and affect each other. The complexity of the interaction of the phases in addition to difficulties in predicting turbulent flow makes the cuttings bed removal process immune to theoretical treatment.

The drilling literature is filled with experimental studies of hole cleaning (Brown et al. 1989, Ford et al. 1990, Hemphill and Larsen 1996, Adari 1999, Adari et al. 2000, Ozbayoglu et al. 2010a, Bizhani 2013, Bizhani et al. 2016). In addition to the experimental and field studies, numerous mechanistic and semi-mechanistic models have been developed to predict and improve the hole cleaning operations (Iyoho and Takahashi 1993, Clark and Bickham 1994, Ramadan et al. 2003, Duan et al. 2007, Guo et al. 2010). Li and Luft (2014a), (2014b) have provided two excellent review papers on the past experimental and theoretical hole cleaning studies.

Most of the previous studies on hole cleaning and bed erosion have been conducted by using what we call a "macroscopic" approach. In this method, often one or more of the parameters that affect cuttings bed removal varies, and the impact on the entire system is studied. For example, the impact of the pump flow rate on the height of the stationary sand bed may be explored in this manner. This approach, although it provides useful information and guidelines for the design of the hole cleaning operations, does not provide detailed insight into the interaction of fluid and particles in the bed. Investigating the hole cleaning using microscopic approach, however, would provide the information about the local parameters such as local fluid velocity and turbulence characteristics. The microscopic method provides insightful information on the interaction of solid-fluid in the annulus. Knowledge of such local variables is often required in the development of mechanistic models of hole cleaning (Li and Luft 2014a, Li and Luft 2014b).

Characteristics of the turbulent flow inside an annulus that contains a stationary cuttings bed are fundamentally different from the flow in the same annulus without any deposited sand bed. The first change that the presence of a cuttings bed may cause to the flow is either enhancing or decreasing the frictional pressure loss. The frictional pressure drop in the annulus controls the dynamic pressures down the hole and, hence, the equivalent circulating density (ECD) (Mitchell et al. 2011). Sorgun et al. (2011) studied friction factor in the horizontal annulus with the presence of cuttings bed and the inner pipe rotation. The authors have developed a correlation that relates height of the stationary cuttings bed to the frictional pressure loss.

The friction factor derived from the pressure loss measurements is called the average friction factor. The average friction factor relates the pressure loss in the annulus to the Reynolds number, similar to friction factor correlations developed by Reed and Pilehvari (1993). Another form of friction factor that may be of interest in hole cleaning is the interfacial friction factor at the bed/fluid interface. The interfacial friction factor relates the shear stress at the bed interface to the flow Reynolds number. It is often used in the development of multi-layer cuttings removal models (Kelessidis and Bandelis 2004a).

There have been several correlations proposed for prediction of interfacial friction factor (Martins et al. 1996, Kelessidis and Bandelis 2004a, Duan et al. 2007). Duan et al. (2007) proposed modifying the hydraulic diameter and the surface roughness; one can then use the correlations developed for prediction of average friction factor to estimate the interfacial friction factor. They specifically used the relationship designed by Reed and Pilehvari (1993) to evaluate interfacial friction factor. Televantos et al. (1979) also followed the same approach of extending the correlation for flow in an annulus with no cuttings bed to predict interfacial friction factor.

In addition to friction factor, the flow field is also affected by the presence of a loose sand bed. The local fluid velocity at the bed interface is not necessarily the same as that of the flow near the pipe wall. Knowledge of the local fluid velocity is necessary for the development of the mechanistic hole cleaning models (Ramadan et al. 2003). The local fluid flow field controls the momentum exchange between the phases, and hence, it determines whether the bed erosion will take place or not (Li and Luft 2014b).

To develop a realistic mechanistic model, a good understanding of the nature of the interaction between the drilling fluid and drilled cuttings is necessary. Examples of such interaction are abundant both in nature (e.g. flow over river beds) and in the industrial systems (e.g. tailing ponds). Interaction of phases in these systems is bi-directional; the sediment phase can affect the turbulence in the carrier fluid phase and vice versa (Bagchi and Balachandar 2003). Sediment transport in channels, which are pertinent to flow in rivers, have been studied extensively in the past (Wiberg and Rubin 1989, Gore and Crowe 1991, Tsuji et al. 1991, Best et al. 1997, Miyazaki 1999, Carbonneau and Bergeron 2000, Sumer et al. 2003). Examples of such studies are not as common in the drilling literature. Few attempts have been made to implement new measurement techniques such as PIV to study solid transport with particular reference to drilling industry (Rabenjafimanantsoa et al. 2005, Rabenjafimanantsoa 2007, Zeinali et al. 2012, Bizhani et al. 2016, Bizhani and Kuru 2017, Bizhani and Kuru 2017). Rabenjafimanantsoa et al. (2005) used non-intrusive measurement techniques to study flow in pipes in the presence of a secondary phase. The study was mostly focused on the mechanism of dune formation. Zeinali et al. (2012) utilized PIV to study selective removal of sand particles in turbulent flow in pipes.

In a series of recent bed erosion studies, Bizhani et al. (2016), (2017) investigated the impact of the presence of a stationary sand bed on the characteristics of turbulent flow inside the horizontal concentric annulus. They have shown that the mere existence of a stationary sand bed resulted in the reduction of the peak fluid velocity in the lower annulus. They also observed that the roughness of the bed surface created more turbulence near the cuttings bed/fluid interface compared to the flow over the smooth face of the drill pipe. Their study also showed that the movement of the sand particles in the form of bedload along the bed interface caused reduction of the near wall turbulence.

The primary purpose of this paper is to present results of hard-to-measure variables in solid transport and bed erosion in a fully eccentric annulus. The variables include interfacial friction factor and local fluid velocity near the interface of an erodible sand bed. This study looks at the impact of the presence of a sand bed on the different aspects of the flow that seems to be the controlling parameters in bed erosion, and hence, hole cleaning. The results have been obtained by using a large-scale flow loop facility equipped with state-of-the-art PIV tool. The instantaneous fluid velocity at the interface of three beds of different initial height and near the pipe wall of the annulus has been measured. The results presented in this paper can provide the much-needed experimental data for validation of CFD and other computer models.

9.3 Experimental procedures

The experiments in this study have been conducted in a large-scale horizontal flow loop facility. The flow loop, which is schematically shown in Figure 9-1, includes a 500-liters stainless steel tank, a centrifugal pump and measurement instruments such as magnetic flow meter and differential pressure transducers. The centrifugal pump equipped with Variable Frequency Drive (VFD) was used to circulate fluid/solids mixture through the flow loop.

The annular section of the flow loop is 9 meters long. The tubes in this section are made of high-quality Borosilicate glass. The choice of glass pipes was forced due to the use of optical measurement techniques. The outer and inner tubes are 95 mm and 38 mm in internal and external diameter respectively. The radius ratio is 0.4 and eccentricity is one. Eccentricity is defined as the ratio of the distance between the centers of the pipes to the difference of radii's.

$$e = \frac{L}{R - r} \qquad \textbf{Eq.(9-1)}$$

L is the distance between centers of inner and outer tubes; R and r are radii's of the outer pipe and inner pipe respectively. The inner tube is resting against the wall of the outer tube (i.e., e =1); refer to Figure 9-1 for more detail. The inner tube is kept in its position and is not allowed to move during the experiments.

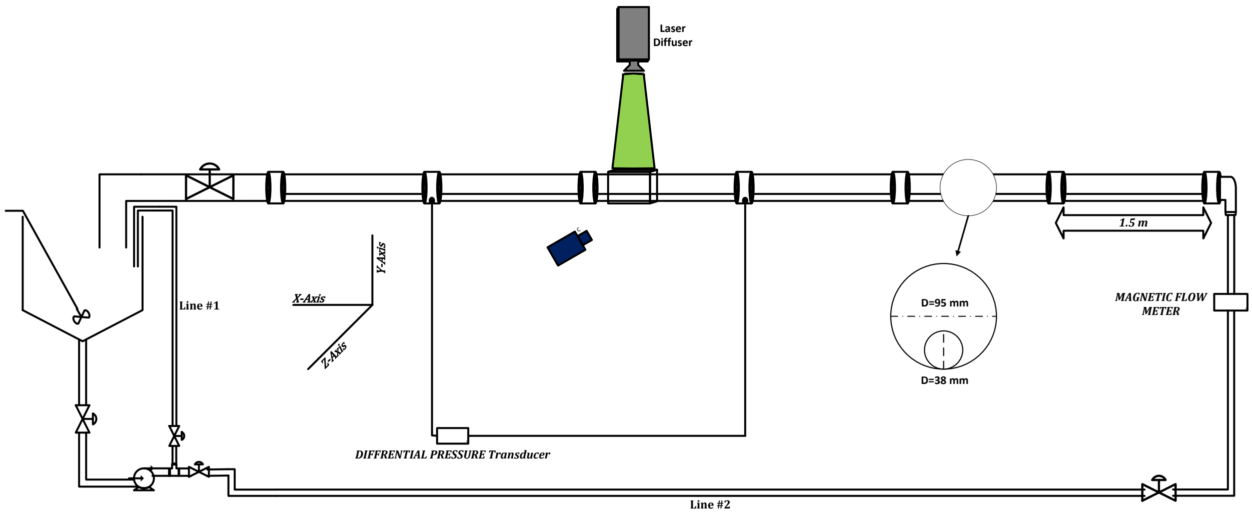

Figure 9-1 Schematic view of the flow loop and configurations of pipes, laser and camera, and the test section

The flow rate was measured using a magnetic flow meter. The flow meter is an OMEGA FMG607-R with an accuracy of $\pm 0.5\%$. Measurement devices are all connected to a computerized data acquisition system powered by LabView software. The software was used to control the pump flow rate as well as logging all the data (i.e. pressure losses, flow rates and fluid temperature in the flow loop).

A high accuracy OMEGA DPG409 differential pressure transducer with an accuracy of $\pm 0.08\%$ was used to record the frictional pressure loss in the annulus. The distance between the two tap lines is 3.08 meter. The first hole is located approximately $\sim 80D_H$ Downstream of the inlet to ensure the flow is fully developed.

The procedure of conducting the experiments is briefly explained here. Experiments started with establishing a stationary sand bed in the annulus. In this step, water and sand were mixed in the tank while the slurry was circulated through the flow loop at the maximum flow rate for 10 to 15 minutes. After reaching steady state condition (i.e. the bed height was uniform across the entire length of the annulus), the pump was shut down. In the next step, the control valves (Figure 9-1) were used to isolate the annular section of the flow loop from the rest of the system. All other parts of the flow loop (except annular section) was then carefully washed to remove any sand particle remained in these sections. Two filter bags with openings smaller than the particle size (the opening is 100 micron) were installed at the outlet of the annular section. The filter bags prevent the sand particles from going back to the annular section during the experiments. Hence, the flow loop was acting like an open-end flow loop in that regard.

The sand bed height was varied through changing the amount of initial sand in the system. To achieve three different bed heights in this study, total mass loading of the solids in the system has varied from as low as 3.5% to up to 14%.

The sand particles that have been used in this study are natural quartz sands with a density of 2650 kg/m^3. Sieve analysis of washed sand samples (Figure 9-2) has shown that sand particles are uniform in size distribution. The d_{50} of the samples were determined to be 600 microns.

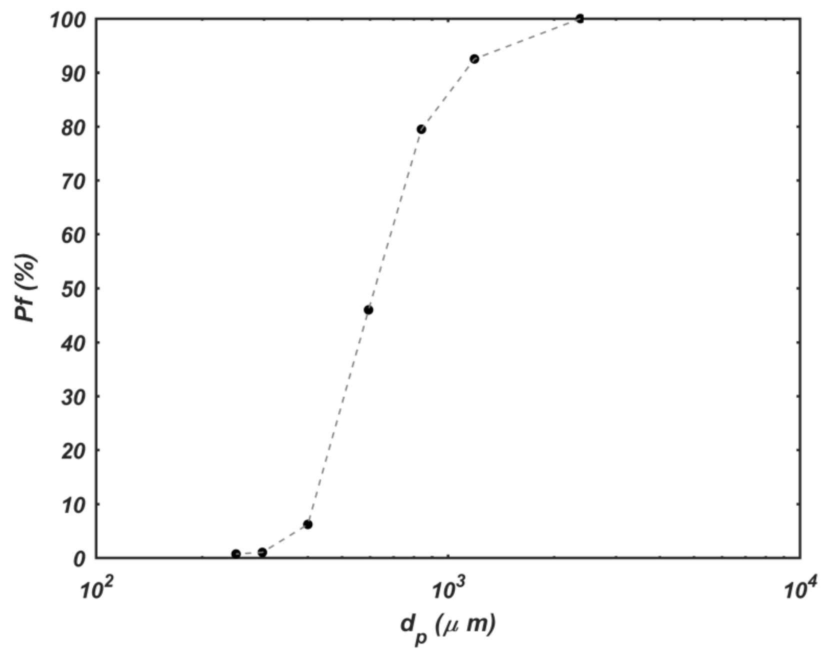

Figure 9-2 Sieve analysis results of washed sample of the sand particles

To ensure the PIV measurements were carried out in a fully developed region of the flow, the measurements were made at approximately $100D_H$ ($D_H = 2(R - r)$) away from the inlet of the annulus. Since the bed is uniform in thickness in the entire annulus, the flow should be fully developed in the measurement window. In single phase flow a development length of $88D_H$ is required for a fully developed laminar flow (Poole 2010), whereas development length for turbulent flow is much shorter (Japper-Jaafar et al. 2010).

Due to the cylindrical shape of glass pipes, image distortion is a major issue in the PIV measurements. A rectangular box was designed and installed around the outer tube to reduce laser light refraction. Additionally, the box is filled with glycerol (99% Wt/Wt pure glycerol) to reduce the light refraction. Glycerol has a refraction index of 1.47, which is similar to the glass pipe, therefore, helps to minimize the refraction of the laser light.

PIV Setup Description and Post-Processing Procedures

A Nd: YAG double pulsed laser with a wavelength of 532 nm and 50 mJ/pulse was used in this study. The laser light is converted to a planar light sheet by a combination of the cylindrical and the special optical lenses. The thickness of the laser light sheet was 0.5.

A CCD (charge-coupled device) camera with a resolution of 1376×1040 pixels was used for recording the PIV images. The camera has a double shuttering feature, which enables capturing a pair of pictures in a short and controllable time interval. A 60 mm Nikon AF NIKKOR lens with a 36-mm extension tube was used for recording the images. The f-stop or the aperture setting of the lens was set to 8. The scaling factor for images has been registered to be 31.76 µm/pixel.

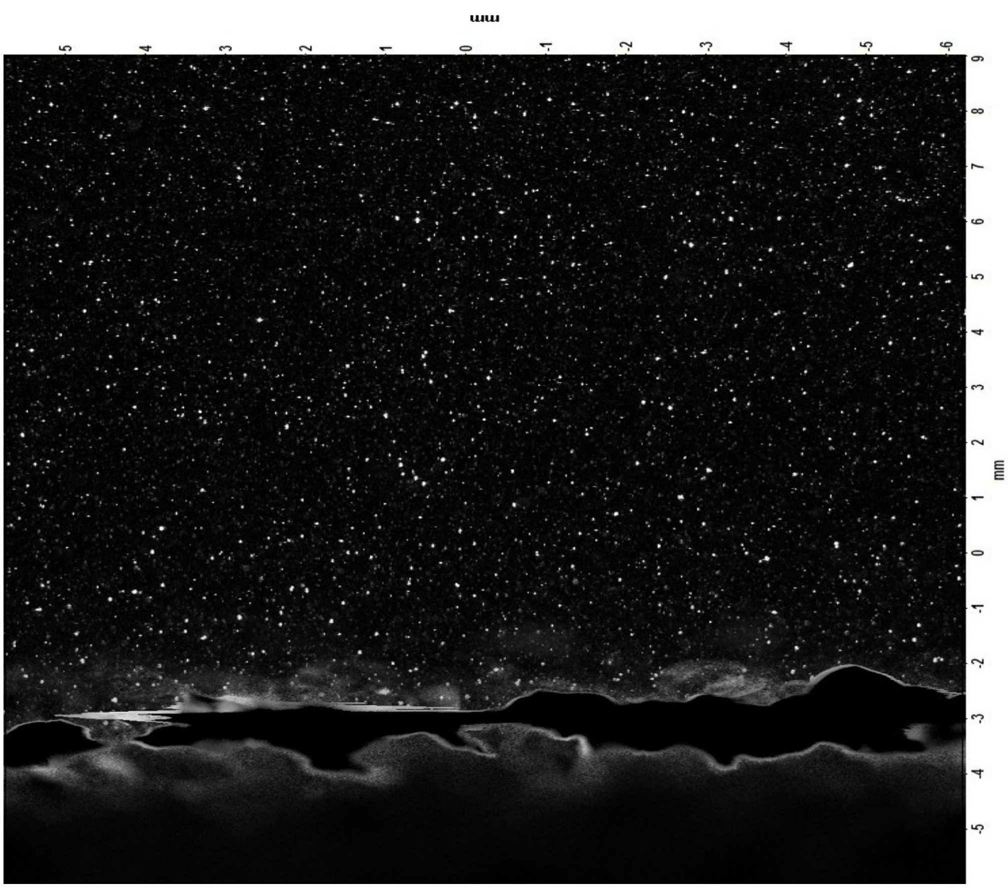

Figure 9-3 A typical PIV of the sand bed and tracers in the fluid

Figure 9-3 shows a typical PIV image acquired during the experiments. In this picture, the sand bed is located at the bottom while the fluid seeded with tracer particles (bright white dots) is flowing over the top. DAVIS 8.3.0 software was used for both the image acquisition and the post-processing of pictures. The software was used for adjusting the appropriate parameters during the experiments (such as the time interval between the two images and the laser power) as well as processing and extracting the data from the pictures. Further details regarding the image processing algorithm are given in the next section.

Hollow glass spheres with a mean diameter of 10 microns were used as tracer particles. The tracer particles are nearly neutral in water ($1.1 \pm 0.05 \frac{g}{cc}$) to keep them suspended in the flow. The addition of the trace particles is necessary to enhance the spatial resolution of the PIV images and reduce the bias error towards the sand debris (Melling 1997).

9.3.1 PIV Data Post-Processing Procedures

The PIV processing algorithm for velocity calculations follows a cross-correlation based method. After obtaining a pair of images with the tracer particles in the flow, each image is broken down to the smaller windows called the interrogation windows. The interrogation windows are analyzed in the 2nd image for probable similarities to the same interrogation window in the 1st picture (Nezu and Sanjou 2011). To determine the pixel displacement, the cross-correlation method was used. The method works by cross correlating the intensity distribution over a small area (the interrogation window) of the flow. The peaks that show the highest correlation are chosen for the most likely destination of the seed particles. After finding the displacement of a seed particle in the two images (Δx and Δy) and having known the time interval (Δt) between the two images, the velocity of the tracer particle or equivalently the fluid velocity vector is calculated as follows:

$$\begin{cases} \hat{u} = \dfrac{\Delta x}{\Delta t} \\ \hat{v} = \dfrac{\Delta y}{\Delta t} \end{cases} \qquad \textbf{Eq.(9-2)}$$

A total number of 3000 pictures have been recorded for each data set. The multi-pass cross-correlation method with the decreasing of the interrogation window size was used for the particle displacement calculations. An initial interrogation window size of 64×64 pixels followed by the window size of 32×32 pixels was utilized in the calculations. The overlap setting was 50%, and the weighting function was set to adaptive. To enhance the accuracy of the calculated vector fields, the post-processing was also applied on the calculated vectors. Universal outlier detection function was used in the post processing.

9.3.2 Measurement details

Experiments were conducted with the fully eccentric inner pipe configuration (i.e. inner pipe was sitting at the bottom of the horizontal flow loop). Measurement of instantaneous velocity was carried out in a plane perpendicular to the bed interface. Figure 9-4 schematically shows the location of the measurement plane. For consistency and to be able to compare the results, measurements without any cuttings bed were also made along the same plane.

Three beds of different height have been tested in this study. Figure 9-4 shows the relative height of each bed and locations of measurement planes. The bed A had a height less than the inner pipe radius r (i.e. $h<r=19$ mm). The bed B had a height bigger than r and less than 2r (i.e. $r < h < 2r$). Finally, the bed C had a height that was greater than 2r (i.e. with bed C, the inner pipe was buried in sand completely).

The experiments in all the cases started at the minimum operating flow rate of the flow loop. This flow rate was 64 liters/min. In each case, the flow rate was increased by increments of about 15 liters/min. PIV and pressure drop measurements were carried out at each flow rate. For each bed, measurements were conducted up to a flow rate where bed erosion in the form of a moving layer of sand at the bed/fluid interface started taking place. At 64 liters/min, beds A and B were completely stationary (i.e. no particles were observed to move). For bed C, however, some movement of bed particles occurred at this flow rate.

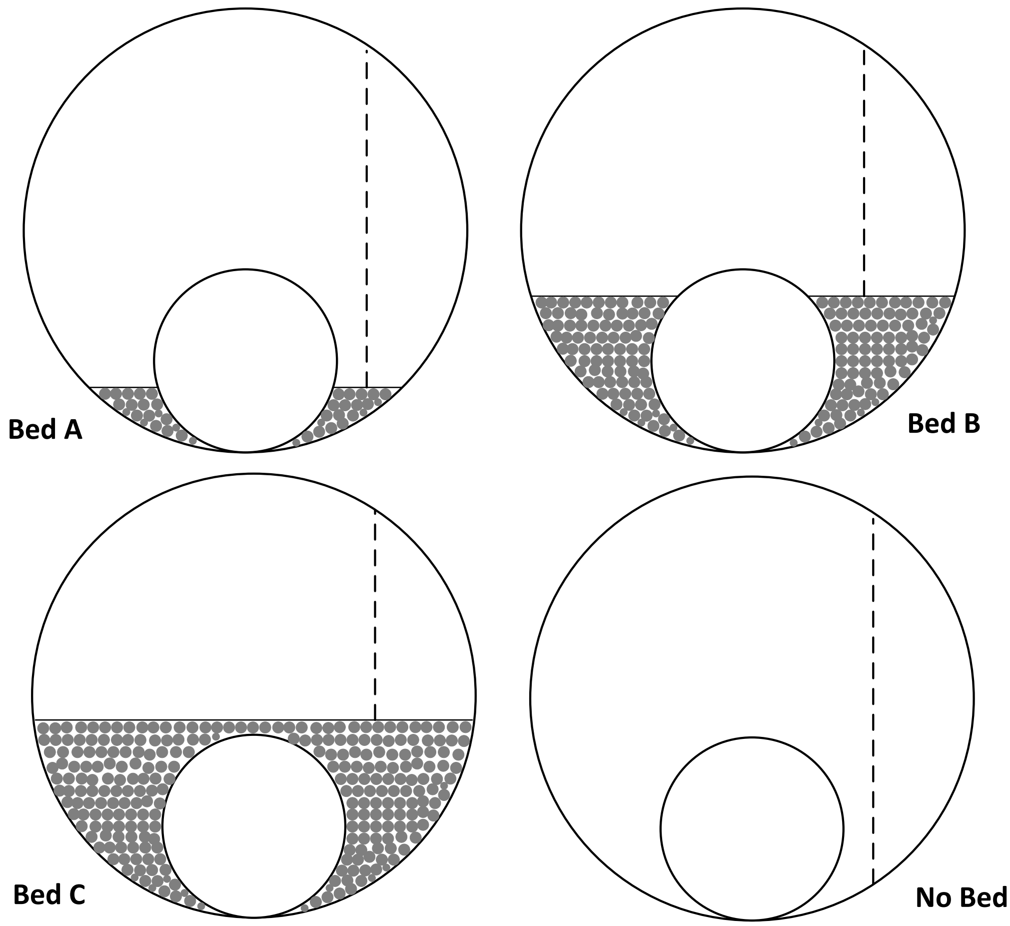

Figure 9-4 Schematic representation of the eccentric annulus with measurement plane and the relative height of the sand bed

For convenience let's define superficial fluid velocity as follows:

$$U_s = \frac{Q}{\pi(R^2 - r^2)} \quad \text{Eq.(9-3)}$$

Where Q is the pump flow rate, and U_s is the superficial fluid velocity. In the present work, all the experiments with different flow geometries (i.e. Bed A, B, and C) were conducted at the same flow rates, and hence, the comparisons were made at the same the superficial velocities.

The actual fluid velocity in the annulus is different from the superficial velocity. The former is affected by the presence of the stationary sand bed because the cross-sectional area of the annulus decreases due to the portion of the annulus occupied by the bed. The bulk fluid velocity or the real fluid velocity in the annulus is:

$$U_b = \frac{Q}{A_f}$$ **Eq.(9-4)**

A_f designates the flow area available to flow. Details about geometrical calculation pertinent to A_f is presented in Appendix A.

The Reynolds number can then be calculated using the bulk fluid velocity.

$$Re = \frac{\rho U_b D_h}{\mu}$$ **Eq.(9-5)**

D_h is the hydraulic diameter. Details of calculation pertinent to D_h is also presented in Appendix A.

Table 9-1 reports the flow rates, superficial velocities, bulk velocities, and Reynolds numbers for experiments conducted with the bed A. At U_s=0.35 m/s; there was a moving layer of particles at the bed interface. This flow rate is referred as the critical flow rate of bed erosion.

Table 9-1 Details of measurements conducted with bed A

$\boldsymbol{Q}\ (\frac{\boldsymbol{lit}}{\mathbf{min}})$	$\boldsymbol{U_s}(\frac{\boldsymbol{m}}{\boldsymbol{s}})$	$\boldsymbol{U_b}(\frac{\boldsymbol{m}}{\boldsymbol{s}})$	$\boldsymbol{Re}$
64	0.18	0.19	11700
79	0.22	0.23	14300
93.6	0.26	0.28	16950
109	0.30	0.32	19700
124	0.35	0.36	22450

Table 9-2 reports the superficial velocities, bulk velocities, and flow Reynolds numbers under which experiments were conducted for the bed B. In this case, the onset of the bed erosion (i.e. critical velocity) was observed at the superficial velocity, U_s, of 0.3 m/s.

Table 9-2 Details of measurements conducted with bed B

$Q\ (\frac{lit}{\min})$	$U_s(\frac{m}{s})$	$U_b(\frac{m}{s})$	Re
64	0.18	0.22	14000
79	0.22	0.27	17400
93.6	0.26	0.32	20600
108.6	0.30	0.37	23900

Table 9-3 reports the operational variables under which experiments for the bed C were conducted. Since this bed was much thicker than the other two beds, bed load transport of particles started at a much lower superficial velocity. At superficial velocity, U_s= 0.18 m/s some occasional movement of bed materials was observed.

Table 9-3 Details of measurements conducted with bed C

$Q\ (\frac{lit}{\min})$	$U_s(\frac{m}{s})$	$U_b(\frac{m}{s})$	Re
64	0.18	0.26	15200
79	0.22	0.32	18850

9.4 Results and discussion

The knowledge of velocity profiles is necessary in mechanistic modeling of particle removal from bed deposits. The mechanistic models either require the local fluid velocity as an input to calculate the hydrodynamic forces (i.e., drag and lift forces) acting on the particles or predict the local fluid velocity that is needed to move the particle. Very often, the researchers make assumptions regarding the universal velocity profiles near the bed interface to estimate the local fluid velocity at the sand bed/water interface (Ramadan et al. 2003, Duan et al. 2007). In the first part of the paper, we are presenting measurements of the local fluid velocities near the interface of the sand beds with different heights. The results invalidate previous assumptions regarding the use of the universal velocity profiles at the sand bed/water interface.

Additionally, with the growth in computing power, the number of papers with CFD modeling of bed erosion process is significantly rising. Therefore, the velocity profiles presented here can be used for validating the accuracy of the results from these models.

9.4.1 Velocity profiles in wall units

The velocity profiles in the vicinity of sand bed interface are of great importance in the development of mechanistic hole cleaning modeling. To present the velocity data in a meaningful manner, we use the wall units. The wall units are defined according to the Eq.(9-6) and Eq.(9-7):

$$y^+ = \frac{\rho y u_\tau}{\mu} \qquad \textbf{Eq.(9-6)}$$

$$u^+ = \frac{u}{u_\tau} \qquad \textbf{Eq.(9-7)}$$

In these equations, y^+ and u^+ are the dimensionless distance and velocity respectively. U_τ is the friction velocity, and y is the vertical distance measured from the point of zero velocity.

Two challenging tasks need to be addressed before we can transform the velocity data into wall units. The first challenge is to calculate the local friction velocity. According to the definition given by Eq.(9-8), the friction velocity is related to wall shear stress (Kundu et al. 2012).

$$u_\tau = \sqrt{\frac{\tau_b}{\rho}} \qquad \textbf{Eq.(9-8)}$$

The bed shear stress (or wall shear stress), τ_b, cannot be deduced from frictional pressure loss data because more than one surface is involved in the flow through the annulus (i.e. outer pipe wall, inner pipe wall and the bed surface). The alternative solution to this is to use the velocity profile data to calculate the friction velocity. In this approach, local velocity is plotted versus y in a semi-log scale. Assuming a logarithmic profile prevails, then following equation must describe the velocity in the logarithmic region (Kundu et al. 2012):

$$u = \frac{u_\tau}{\kappa} Ln\left(\frac{y}{y_o}\right) = \frac{u_\tau}{\kappa} Ln(y) + Constant \quad \textbf{Eq.(9-9)}$$

In Eq.(9-9), κ is the von Karman constant and is equal to 0.41 for the flow of water. y_o is called characteristic roughness and determines whether the flow is smooth or rough. If one plot u versus y, then, the slope of the line in the logarithmic region is equal to $\frac{u_\tau}{\kappa}$. Since we assume von Karman constant is 0.41, then, the friction velocity can be calculated. In all the results presented hereafter, the friction velocity has been determined according to the procedure described.

The second challenge in accurately determining the velocity profiles near a rough surface is defining the location of the "virtual wall" (Chan-Braun et al. 2011, Chan-Braun 2012). In the literature, there exist some definitions of the virtual wall. Chan-Braun (2012) defined the virtual wall as 0.8D (D is the roughness height). However, this approach is for cases where roughness element has a fixed height, and the boundary is fixed. In this study, the bed materials are loose, and they are continuously rearranging. Therefore, we cannot define a point as the virtual wall. Instead, we define the virtual wall where the velocity is zero. The zero velocity is determined from the velocity profiles.

In addition to difficulties associated with the virtual wall definition, the bed surface is not flat. Therefore, one cannot average the velocity data in the direction of the flow. The second issue is the configuration of the particles lying on the bed surface. It appears that the bed roughness is not constant along the bed. Therefore, instead of averaging the velocity data along the bed, we only used the local velocity profiles, where we could exactly identify the location of zero velocity.

For comparison purposes, the law of the wall and the linear profile in the sublayer are included in these figures as well. The linear velocity in the viscous sublayer is (Kundu et al. 2012):

$$u^+ = y^+ \quad \textbf{Eq.(9-10)}$$

The logarithmic law for the flow in the eccentric annulus is (Nouri et al. 1993):

$$u^+ = 2.44Ln(y^+) + 4.9 \quad \textbf{Eq.(9-11)}$$

Figure 9-5 reports the velocity profiles near the bed A's interface measured at 5 different superficial velocities. For the first three superficial velocities (0.18, 0.22 and 0.26 m/s), the velocity profiles show an excellent agreement with Eq.(9-11) in the logarithmic region. In the viscous sublayer, however, there is a small downward shift in the velocity profiles. The specific definition of the virtual wall may have caused the change in the sublayer. The agreement of the velocity profiles with the prediction of Eq.(9-11) implies that flow is essentially hydraulically smooth near the bed interface at these flow velocities. At U_s=0.3 m/s the velocity profiles show a downward shift Δu^+=3.36. The downward shift is a characteristic of the rough flow. At U_s=0.35 m/s, the downward shift, Δu^+, increases to 4.92 implying a higher roughness height.

The reasons why flow becomes hydraulically rough at the higher flow rates while it exhibits a smooth behavior at lower flow rates can be explained by the increase in the boundary roughness Reynolds number and the bedload transport of particles. At the superficial velocity of 0.3 m/s, particles start moving at the bed interface. The downward shift of the velocity profiles at this velocity is then associated with the movement of the particles at the bed interface. At Us=0.35 m/s, there was a layer of moving particles at the bed interface. The higher rate of particles transport at the bed interface causes further increase to the boundary roughness. Therefore, it is concluded that movement of sand particles, even at small rates, creates higher roughness heights at the bed interface.

The reason why the roughness height increases at the critical flow rate can be attributed to the bedload transport of particles. Several studies in the past have suggested that the bedload transport causes an extra boundary roughness (Owen 1964, Smith and McLean 1977, Wiberg and Rubin 1989, Best et al. 1997, Song et al. 1998, Carbonneau and Bergeron 2000). The reason for this is that the extraction of momentum from the fluid phase by the moving sand particles; as a result of this momentum exchange, effective boundary roughness increases. Owen (1964) identified the shedding of the turbulent eddies from saltating particles as the source of the bedload roughness. Further details of the bed equivalent roughness height will be discussed in the next section.

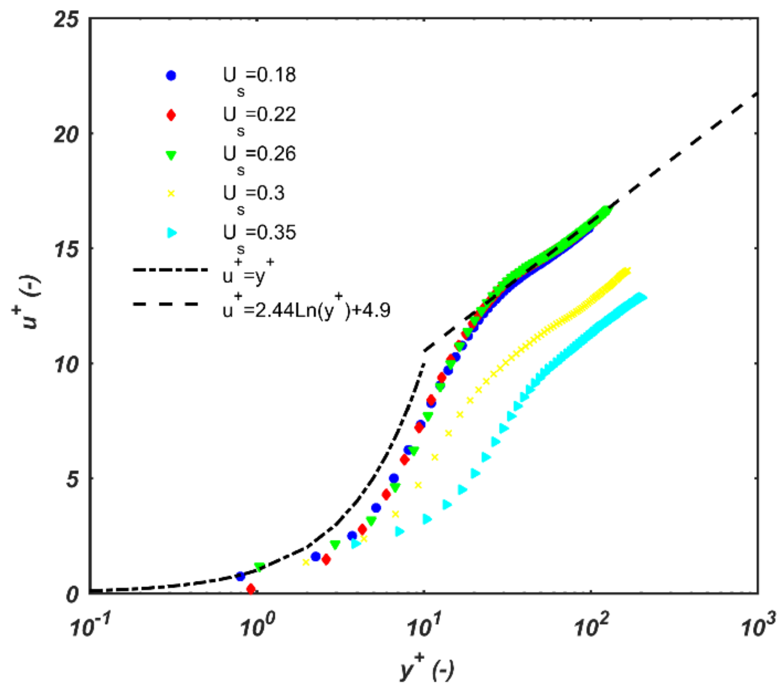

Figure 9-5 Velocity profiles in the wall units measured over bed A

Velocity profiles over the bed B areas are reported in Figure 9-6. Velocity profiles corresponding to U_s=0.18 and 0.22 m/s are laying very close to each other and show a downward shift of 6.8 concerning the logarithmic relation of Eq.(9-11). For the first two superficial velocities, there is no particle movement at the bed interface; hence, the roughness function is constant. At U_s=0.26 m/s and 0.3 m/s, the downward shift of the velocity profile increases to 8.7 and 9.2 respectively. At U_s=0.26 m/s, particles start moving sparsely at the bed interface, and that causes the roughness to increase further. At the highest velocity, U_s=0.30 m/s, the moving layer of particles at the bed interface induces even greater roughness, causing the velocity to shift downward further. From the data presented in Figure 9-5 and Figure 9-6, it appears that as soon as particles start moving in the bed, the roughness function Δu^+ starts increasing. Further increase in the flow velocity, which results in increasing bedload rate, causes further increase in the roughness function. More details on the equivalent roughness height are discussed in the next section.

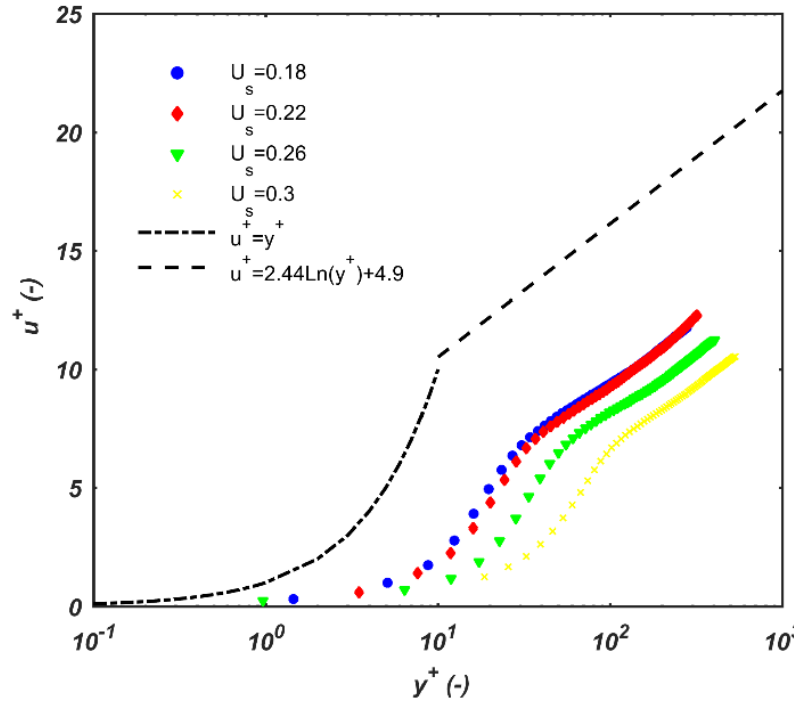

Figure 9-6 Velocity profiles in wall units measured over bed B

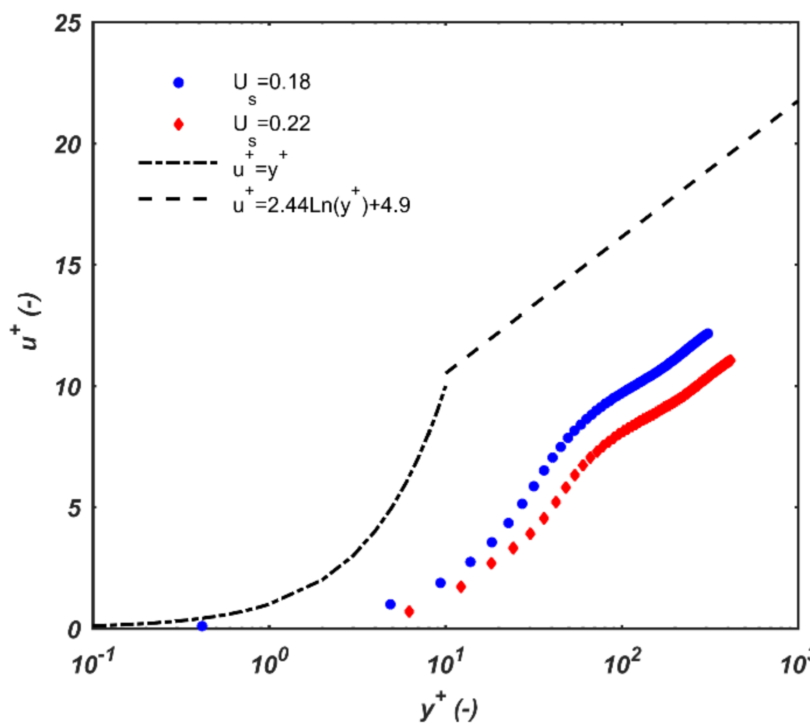

Figure 9-7 Velocity profiles in the wall units measured over bed C

The same argument presented earlier can be used to explain the increased roughness height at the critical flow rate. Movement of the bed materials extracts momentum from the flow; hence, the flow is dissipating more energy to overcome the added boundary roughness. The increased roughness manifests itself in the form of an increase in the flow turbulence, which will be discussed later.

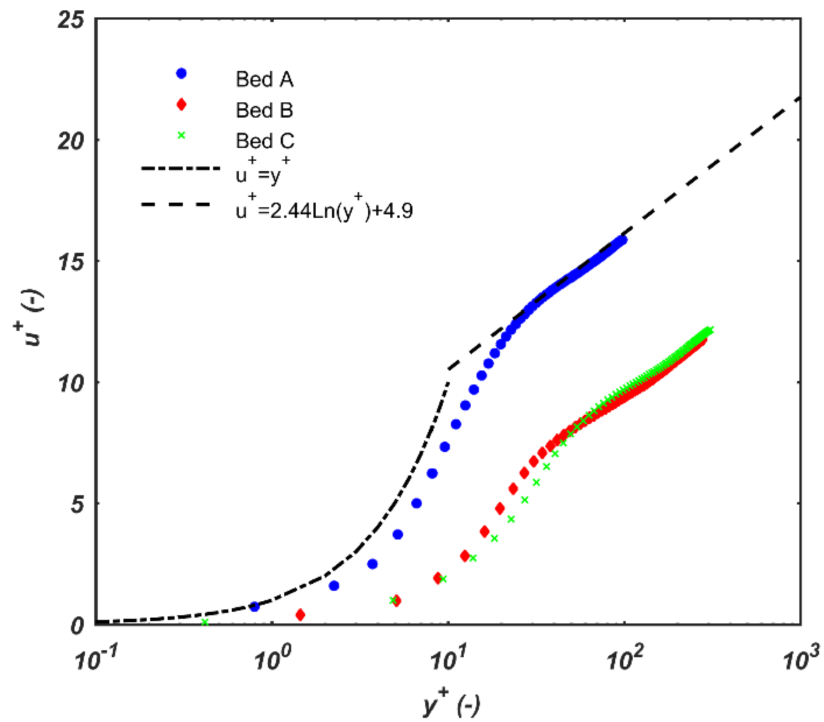

Figure 9-8 Velocity profiles in the wall units measured at U_s=0.18 m/s

Figure 9-7 is the velocity profiles over the bed C. As mentioned earlier for the bed C, bedload transport of particles starts at 0.22 m/s; therefore, the roughness function Δu^+ changes. For U_s=0.18 m/s the downward shift (Δu^+) is 6.6 while at the higher flow velocity of 0.22 m/s, the downward shift (Δu^+) is 8.4. The bedload transport of sand particles is inducing additional boundary roughness, and hence, causing a further change in the velocity profiles in the logarithmic region.

Figure 9-8 compares the velocity profiles at U_s=0.18 m/s for beds A, B, and C. The comparison reveals that increasing the bed height causes the roughness function to change (most likely through a change of the flow regime from smooth to rough near the bed). At U_s=0.18 m/s non of the beds are eroding in the form of bedload. For the bed A, the flow exhibits a smooth like behavior. For the other two beds (B and C), the flow resembles a rough flow. For the beds B and C, the downward shift in velocity is similar, which implies a constant roughness height for fully rough flow when there is no bedload transport of particles. We will investigate the flow regime and equivalent roughness height in the next section.

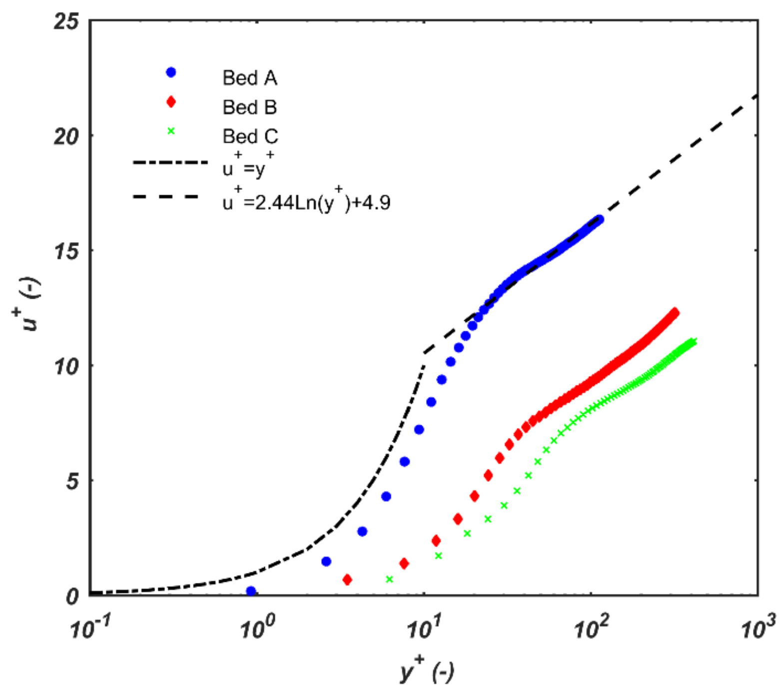

Figure 9-9 velocity profiles in wall units measured at U_s=0.22 m/s

Figure 9-9 compares velocity profiles for the three beds at 0.22 m/s. At this flow rate, only bed C is eroding. Contrary to Figure 9-8 where beds B and C exhibited similar Δu^+, in Figure 9-9 bed C shows higher values of Δu^+; therefore, we can conclude that the bedload transport of particles is responsible for the difference in roughness function Δu^+ of beds B and C.

The main conclusion, which we can take away from the presented data for velocity profiles are 1) the bed roughness can increase significantly by the bedload transport of particles; 2) for a fully rough flow, the bed roughness appears to be constant at velocities less than the critical velocity of the bed erosion.

9.4.2 Equivalent Bed Roughness

In the previous section, we discussed the velocity profiles in wall units. The results showed that, in most cases, the bed exhibit rough wall characteristic. To find out whether the flow is smooth or rough, Eq.(9-11) can be used. In that equation y_o is the characteristic roughness and determines whether the flow is smooth or rough. The characteristic roughness, y_o, depends on the flow regime. The flow regime (i.e. hydraulically smooth, transitional or rough) is determined by the roughness Reynolds number (Eq.(9-12)).

$$Re_{u_\tau} = \frac{\rho \varepsilon u_\tau}{\mu} \qquad \textbf{Eq.(9-12)}$$

In the Eq.(9-12), ε is the equivalent sand grain roughness height, which is very often assumed to be equal to the mean or a constant multiple of particle size in the drilling literature (Ramadan et al. 2003, Duan 2009). The three flow regimes (smooth, transitional and or rough) are determined by roughness Reynolds number. For $Re_{u_\tau} < 5$, the flow is hydraulically smooth. If $Re_{u_\tau} > 70$, the flow is assumed to be fully rough. Transitional flow regime exists for $5 < Re_{u_\tau} < 70$ (Southard 2006):.

For fully rough flow (i.e. $Re_{u_\tau} > 70$), the characteristic roughness becomes dependent on the roughness height:

$$y_o = \frac{\varepsilon}{30} \qquad \textbf{Eq.(9-13)}$$

In this case, the logarithmic velocity profile becomes (Ramadan et al. 2003):

$$u^+ = 2.44Ln\left(\frac{y}{\varepsilon}\right) + 8.5 \qquad \textbf{Eq.(9-14)}$$

For the hydraulically smooth flow, the y_o becomes:

$$y_o = \frac{\mu}{7.5\rho u_\tau}$$ **Eq.(9-15)**

To find the equivalent roughness, a velocity profile of the form of Eq.(9-14) is fitted to the velocity profiles in the logarithmic region. The equivalent roughness is obtained through regression. Figure 9-10 presents a sample case of how the roughness height can be determined using Eq.(9-14) and the velocity data. The roughness height is expressed regarding the mean sieve size of the particle (d_p=600 micron).

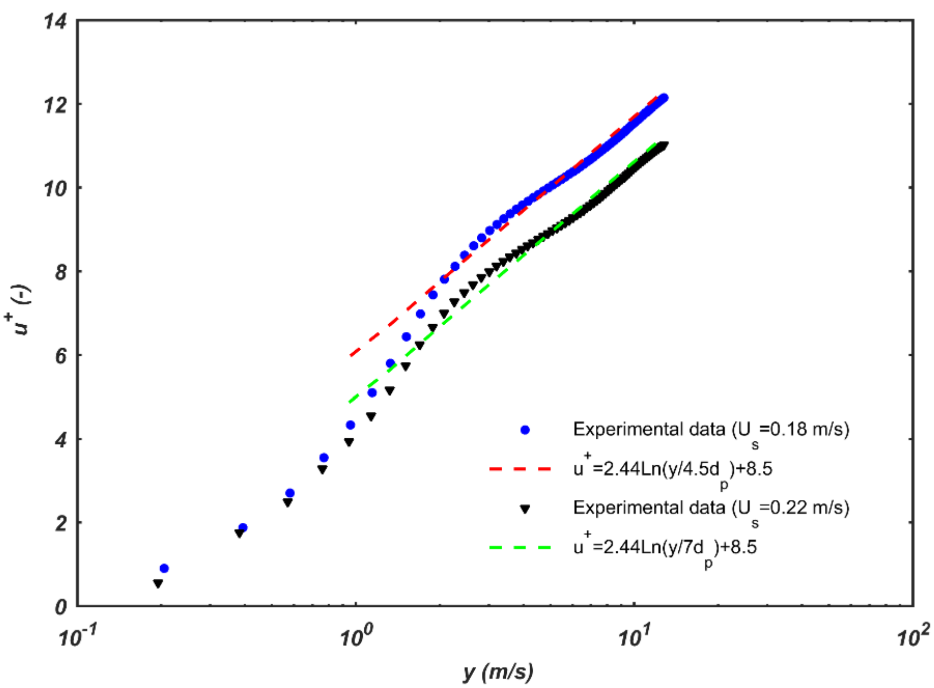

Figure 9-10 Illustration of the procedure on finding equivalent roughness (data for Bed C)

Table 9-4 reports Δu^+, Re_τ, and ε for the flow over the bed A at all the superficial velocities tested. For the flow over the bed A, at superficial velocities of 0.18, 0.22 and 0.26 m/s (all are lower than the critical velocity) the bed exhibits a constant equivalent roughness of approximately $0.6d_p$. The bed A is thin and is in the narrow gap between the two pipes. Hence, at small flow rates, it shows a small characteristic roughness. The roughness Reynolds number indicates that flow at these flow velocities is in the smooth regime (i.e. < 5). Hence, the equivalent roughness does not mean much as the characteristic roughness for the smooth boundaries is defined by Eq.(9-15). At U_s= 0.3 m/s the equivalent roughness increases to 1.5d_p and at U_s=0.35 m/s this number increases to 2d_p. The roughness Reynolds number indicates that the flow is in transitional regime at these superficial velocities ($5 < Re_\tau < 70$). The increase in the equivalent roughness at these flow rates is mostly caused by the bedload transport of particles.

Table 9-4 Equivalent roughness, roughness Reynolds number, and Δu^+ for the flow over the bed A

$U_s(\frac{m}{s})$	Δu^+	Re_τ	$\varepsilon\ (m)$
0.18	0.15	4.5	$0.65d_p$
0.22	0.02	4	$0.54d_p$
0.26	0.045	4.6	$0.6d_p$
0.3	3.36	17.3	$1.5d_p$
0.35	4.92	30	$2d_p$

Table 9-5 reports the equivalent roughness, roughness Reynolds number, and Δu^+ for the flow over the bed B. The data show that the superficial velocities of 0.18 and 0.22 m/s (subcritical velocities where there is no particle movement in the bed) Δu^+ is 6.8 and the roughness Reynolds numbers are 67 and 69. These Reynolds numbers are very close to the fully rough flow regime. The equivalent roughness heights are 5.5 and 5d_p. This means that a constant roughness height characterizes the bed boundary for velocities less than the critical velocity of the bed erosion. At U_s=0.26 m/s the $\boldsymbol{\Delta u^+}$ increases to 8.2 and roughness Reynolds number is 127. The flow is fully rough, and the equivalent roughness increases to 7d_p. At 0.26 m/s some particles move at the bed interface, however, there is not constant layer of moving particles in the bed. At the highest flow velocity of 0.3 m/s, the equivalent roughness is 9.5d_p with a roughness Reynolds number of 220. The bedload transport of particles causes the roughness height to increase by 40% and 90% when the flow regime goes into transition from no bedload to a uniform layer of moving particles as the superficial velocity increases from 0.22 m/s to 0.26 m/s and later to 0.3 m/s, respectively.

Table 9-6 reports Δu^{+} , the roughness Reynolds numbers and the equivalent roughness heights for the flow over the bed C. The roughness Reynolds numbers are 64 (close to fully rough flow) and 134 (a fully rough flow). The equivalent roughness varies from $4.5d_p$ to $7d_p$. The roughness height increased by 56%, which is attributed to the bedload transport.

Table 9-5 Equivalent roughness, roughness Reynolds number, and Δu^{+} for flow over the bed B

$\boldsymbol{U_s(\frac{m}{s})}$	$\boldsymbol{\Delta u^{+}}$	$\boldsymbol{Re_\tau}$	$\boldsymbol{\varepsilon\ (mm)}$
0.18	6.8	67	$5.5d_p$
0.22	6.8	69	$5d_p$
0.26	8.2	127	$7d_p$
0.3	9.7	220	$9.5d_p$

Table 9-6 Equivalent roughness, roughness Reynolds number, and Δu^{+} for flow over bed C

$\boldsymbol{U_s(\frac{m}{s})}$	$\boldsymbol{\Delta u^{+}}$	$\boldsymbol{Re_\tau}$	$\boldsymbol{\varepsilon\ (mm)}$
0.18	6.6	64	$4.5d_p$
0.22	8.4	134	$7d_p$

It is customary and useful to report the equivalent roughness height as a function of the roughness Reynolds number. To put the data in Tables 4 to 6 in a bigger perspective, the equivalent roughness heights are plotted versus roughness Reynolds number as shown in Figure 9-11. There is a good correlation between the boundary roughness and the friction Reynolds number. The relationship in this case is:

$$\varepsilon = 0.2869 d_p Re_\tau^{0.6548} \quad \textbf{Eq.(9-16)}$$

The roughness model that fits the data here cannot be claimed to be universal because roughness type affects the flow (Flack and Schultz 2014). Nonetheless, the correlation can be useful in treating such flows in eccentric annulus contain a stationary sand bed.

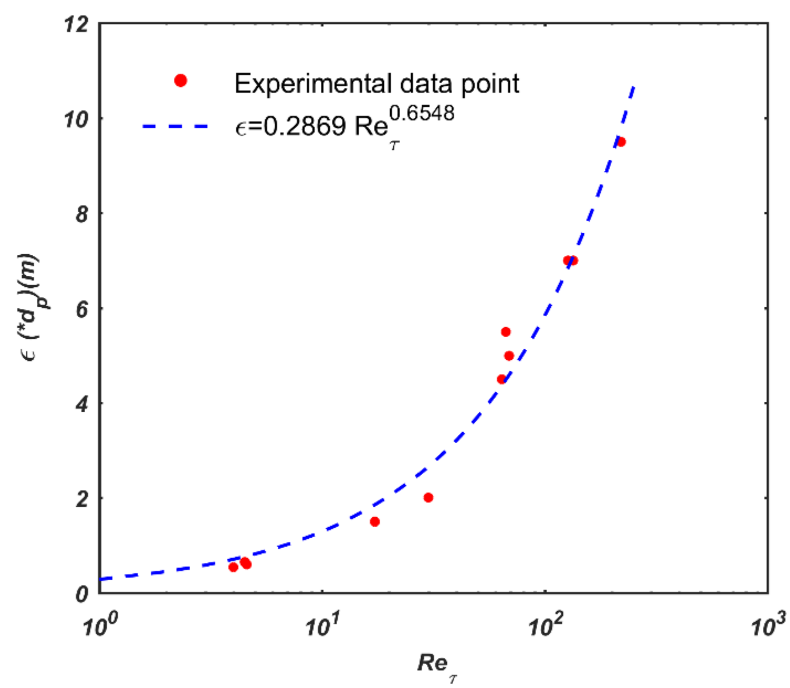

Figure 9-11 Equivalent roughness versus Re_τ for flow along plane 2

9.4.3 Friction factor

The friction factor is one of the most important parameters in evaluating the performance of hole cleaning operation and hydraulic designs. The friction factor is related to wall shear stress as shown by Eq.(9-17) (Kundu et al. 2012):

$$f = \frac{\tau_w}{\frac{1}{2}\rho {U_b}^2} \quad \textbf{Eq.(9-17)}$$

In this equation τ_w is the wall shear stress, ρ is the fluid density, and U_b is the bulk fluid velocity.

The wall shear stress at the bed fluid interface is a rather challenging quantity to evaluate. An average value of wall shear stress in the entire annulus can be estimated using the measured frictional pressure loss data (Escudier and Cullen 1996). Eq.(9-18) is the result of such assumption and simplification.

$$\tau_w = -\frac{D_h}{4}\frac{dP}{dx} \qquad \textbf{Eq.(9-18)}$$

D_h is the hydraulic diameter and is defined in Appendix A. The $\frac{dP}{dx}$ is the recorded frictional pressure loss gradient. The bed shear stress calculated based on the Eq.(9-18) is an average of all shear stresses in the annulus. However, for the flow in the annulus with the presence of a cuttings bed, three distinct wall shear stresses exist. Eq.(9-19) shows the exact force balance in the annulus and, the three wall shear stresses that needs to be considered.

$$-A_f\frac{dp}{dx} = S_{wo}\tau_{wo} + S_{wi}\tau_{wi} + S_b\tau_b \qquad \textbf{Eq.(9-19)}$$

In this equation τ_{wo} is the wall shear stress on the inner wall of the outer pipe, τ_{wi} is the wall shear stress on the outer wall of the inner tube, and the τ_b is the shear stress at the bed interface. Each shear stress in Eq.(9-20) is multiplied by the respective boundary area of each domain (e.g. the bed shear stress by the wetted perimeter of the bed). Note that even the shear force on each pipe wall is not the same.

Comparing Eq.(9-18) and Eq.(9-19) reveal that the shear stress calculated based on the Eq. 18 is an area weighted average of the three different shear stresses encountered in the annulus. From this point on, we call the friction factor and the wall shear stress calculated by using Eq.(9-17) and Eq.(9-18), the average friction factor and the average wall shear stress respectively. The interfacial shear stress will be discussed later.

The average friction factor is important in hydraulic calculations regarding ECD limitations and other hydraulic constraints (Mitchell et al. 2011). Knowledge of the average friction factor is also necessary for the design of hydraulic fracturing operations. It is also imperative for hole cleaning operations, where the formation fracture gradient must not be exceeded. Therefore, it is an important parameter to consider.

In the next two sections, we first discuss the average friction factor for flow in the eccentric annulus, and then the interfacial friction factor will be considered.

9.4.3.1 Average friction factor

The average friction factor calculated according to the prescribed procedure (i.e. using Eqns. 17 and 18) is presented in Figure 9-12. The figure shows friction factor data for flow in the same annulus without any cuttings bed as well. The average friction factor is correlated well with the Reynolds number of the flow. The adopted definition of Reynolds number (Eq.(9-5)) considers the impact of the presence of the cuttings bed in the form of a change in both the bulk fluid velocity and the annulus hydraulic diameter.

Several important conclusions can be drawn based on the presented results. First, the presence of the cuttings bed enhances the average frictional pressure loss in the annulus by about 45%. The change in the bed height does not significantly affect the friction factor if the Reynolds number is defined in such a way that it considers the reduction of flow area (i.e. Re is calculated using the bulk velocity rather than the superficial velocity) and change in the hydraulic diameter.

The friction factor data could be best represented using a Blasius type correlation. The Eq.(9-20) is the results of the curve fit to the data in the annulus without any sand bed. Eq.(9-21) the friction factor correlation for the flow in the annulus with sand beds.

$$f_a = 106Re^{-0.952} \quad \textbf{Eq.(9-20)}$$

$$f_a = 328.1Re^{-1.031} \quad \textbf{Eq.(9-21)}$$

The discussion on the average friction factor has several implications for the hydraulic design of drilling operations. First, the presence of a cuttings bed increases the frictional pressure loss in the annulus and may cause problems due to ECD limitations. Consequently, the flow rate and or fluid properties may need to be adjusted to reduce the annular pressure loss. Regarding the hole cleaning, the increase in the frictional pressure loss can have both positive and adverse impact. The positive impact is that it causes the shear stress on the bed to rise, and hence, improving the chance of removing the cuttings. On the other, hand the increase in frictional pressure loss may force the operator to reduce the flow rate and the fluid density to avoid fracturing the formation. Both of these changes will negatively affect hole cleaning.

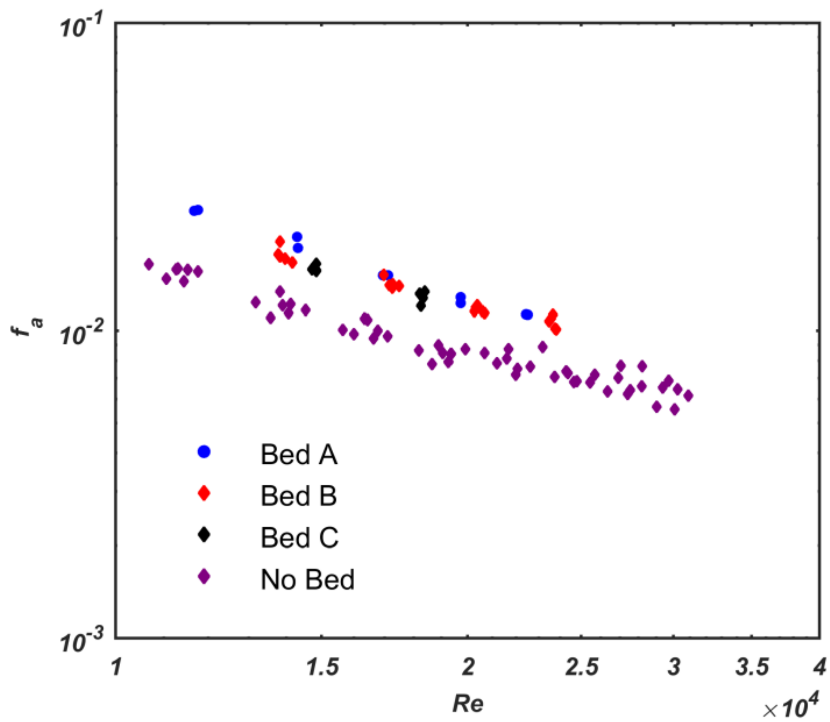

Figure 9-12 Average friction factor data for the flow in the annulus with and without sand bed

In the next section, we will discuss the bed shear stress and interfacial friction factor that is of greater importance in modeling the coupling of solid/liquid phases in multi-layer solid transport models.

9.4.3.2 Interfacial friction factor

The average friction factor presented in the previous section is a measure of the average bed shear stress in the annulus. It is useful when only measurements of frictional pressure losses are available. However, the real bed shear stress, and consequently the interfacial friction factor may be different. The interfacial friction factor can be defined using the bed shear stress data:

$$f_i = \frac{\tau_b}{\frac{1}{2}\rho {U_b}^2} \qquad \textbf{Eq.(9-22)}$$

τ_b is the shear stress at the bed interface. One of the reasons on why average shear stress is used more frequently than the interfacial bed shear stress is because it is more difficult to evaluate the interfacial bed shear stress , τ_b , as compared to the average shear stress. The only possible way to accurately evaluate τ_b is through the separate measurement of this quantity. Nonetheless, that is not a trivial task.

The importance of interfacial friction factor is in the evaluation of fluid drag force acting on the cuttings bed. The bed shear stress multiplied by the bed area is a direct measure of the fluid's drag force on the cuttings bed. Eq.(9-23) is the relation between the drag force and the bed shear stress.

$$F_D = c d_p^2 \tau_b \qquad \textbf{Eq.(9-23)}$$

Where c is a coefficient related to the bed configuration, and d_p is the particle size. According to the Eq.(9-23), a higher shear stress at the bed causes the greater drag force on the particles laying on the bed. Hence, enhancing the chance of removing the cuttings. Another importance of interfacial friction factor is in the layered modeling of cuttings transport (Kelessidis and Bandelis 2004a, Li and Luft 2014b). In these models, often the coupling of the bed layer and suspension layer above is done through momentum exchange represented by the bed shear stress.

Evaluation of the bed shear stress, and consequently interfacial friction factor is much harder than the average friction factor. The bed shear stress (or wall shear stress), τ_b, cannot be deduced from frictional pressure loss data because more than one surface is involved in the flow through the annulus (i.e. outer pipe wall, inner pipe wall and the bed surface). The alternative solution is to use the velocity profile data obtained from PIV measurements and determine the friction velocity u_τ. Once the friction velocity is known, the interfacial bed shear stress τ_b, can be calculated using Eq.(9-8). The whole procedure was explained earlier in the section where we discussed the velocity profiles.

Figure 9-13 shows the measured interfacial bed friction factor, f_i , values for the flow near the bed A. The chart also includes the average friction factor, f_a, data. Comparison of the data reveals that the interfacial friction factor is smaller than the average friction factor. The reduction is especially notable at lower Reynolds numbers. The main reason for the observed difference in friction factors can be attributed to the smaller area of the bed comparing to the pipe walls (S_b vs. $S_{wo}+S_{wi}$). The Bed A is small, and it only accounts for 7.3% of the total wetted area of the annulus ($\frac{S_b}{S_{wo}+S_{wi}+S_b}$). Therefore, much of the frictional pressure loss is due to friction on the pipe walls. The difference in f_i and f_a implies that one cannot use the average friction factor for accurate evaluation of the fluid drag force on the cuttings bed.

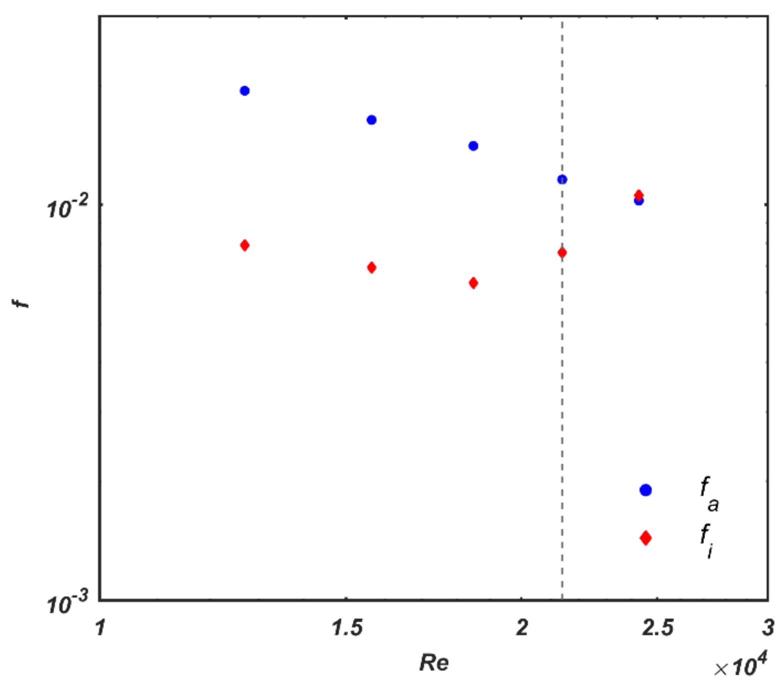

Figure 9-13 Comparison of Interfacial and average friction factor for flow over bed A

Another important feature of f_i that makes it different than f_a is its behavior at higher flow rates. Unlike the average friction factor, the interfacial friction factor shows a sudden increase at higher Reynolds numbers. The interfacial friction factor starts increasing when the flow rate exceeds the critical flow rate of bed erosion where the sand particles start moving along the bed.

Movement of the sand particles, even at small rates, causes the interfacial friction, *fi,* to increase. The reason for this increase may be related to the added boundary roughness due to bedload transport of particles. Earlier studies have shown that the movement of sand particles in the bed causes a sharp increase in the equivalent bed roughness (Owen 1964, Smith and McLean 1977, Wiberg and Rubin 1989, Best et al. 1997, Song et al. 1998, Carbonneau and Bergeron 2000). The added boundary roughness acts as an additional source of energy sink that extracts momentum from the flow. The enhanced energy exchange mechanism manifests itself in the form of an increase in the boundary friction factor.

Figure 9-14 compares the interfacial and average friction factor curves for the flow over the bed B. At the lower Reynolds numbers both friction factors are close to each other. The increase in the bed area comparing to pipe walls (from 7.3% for the bed A to 21% for the bed B) could be the main reason for the enhanced bed shear stress and interfacial friction factor in this case. Comparing to the data of bed A, the results presented in Figure 9-14 imply that interfacial friction factor strongly depends on the height of the stationary sand bed.

The interfacial friction factor, *fi,* starts increasing at the higher Reynolds numbers. The increase in f_i begins at the onset of the bed erosion (even when there is no continuous layer of moving particles at the interface). This behavior does not appear in the average friction factor graphs, and hence, one may not be able to identify the onset of bed the erosion using only the average bed shear stress.

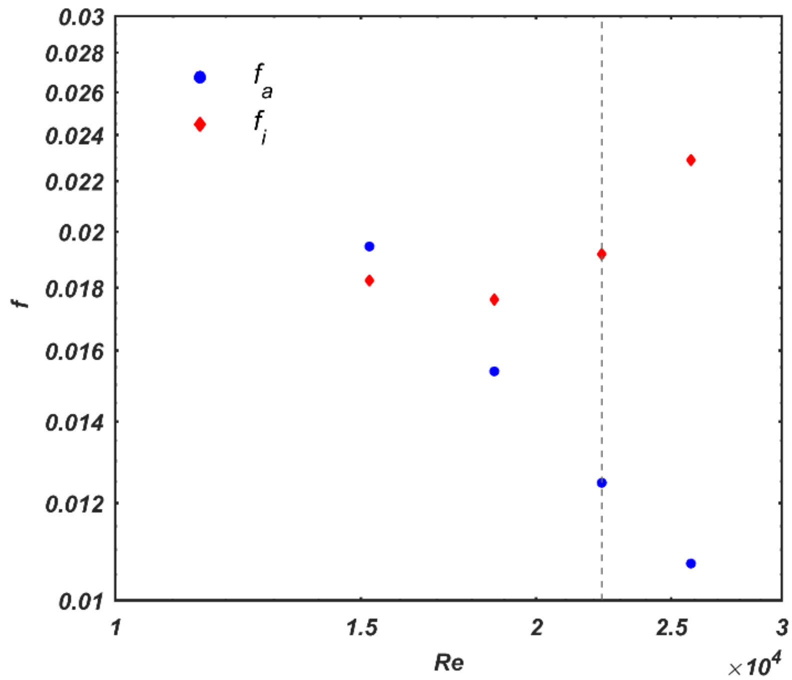

Figure 9-14 Comparison of the interfacial and the average friction factor for the flow over the bed B

The implication of the increase in the interfacial friction factor at higher Reynolds number is that, as soon as the bed erosion starts taking place, it becomes easier to sustain the movement of the particles. One reason for this is the higher rate of momentum exchange at the interface between the fluid and the particles. Additionally, the enhanced interfacial shear stress causes higher drag force on the bed materials, which also helps in removal of the sand particles. Another mechanism, which helps in sustaining the movement of the particles is the bed dilation (Houssais et al. 2015).

Finally, Figure 9-15 compares the interfacial and average friction factors for the flow over the bed C. The interfacial friction factor is higher than the average friction factor in this case. The increase in the bed area (the bed occupies 36% of the total wetted area in this case) is the leading cause of the enhanced interfacial friction factor. The growth of the frictional shear stress due to particles movement is observed in this instance as well.

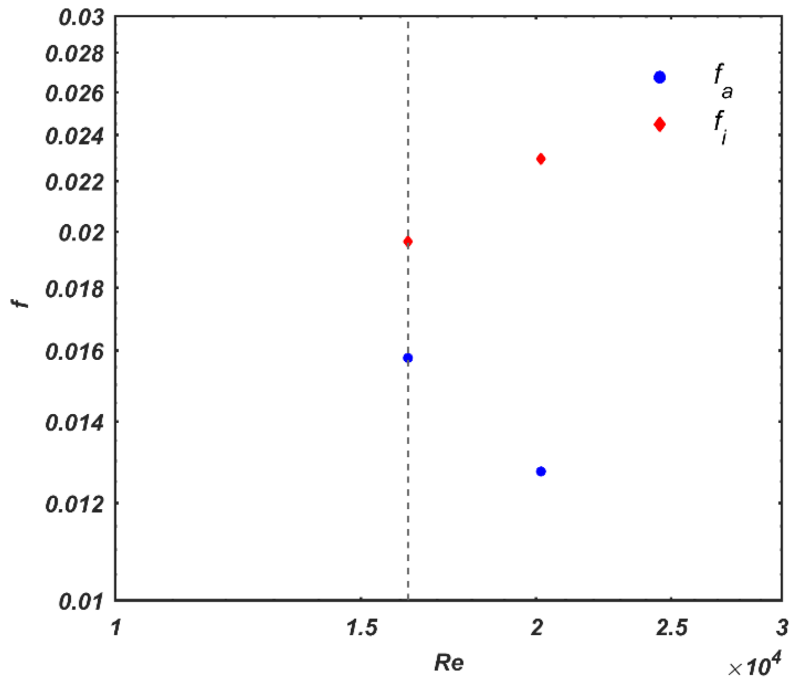

Figure 9-15 Comparison of the interfacial and average friction factor for the flow over the bed C

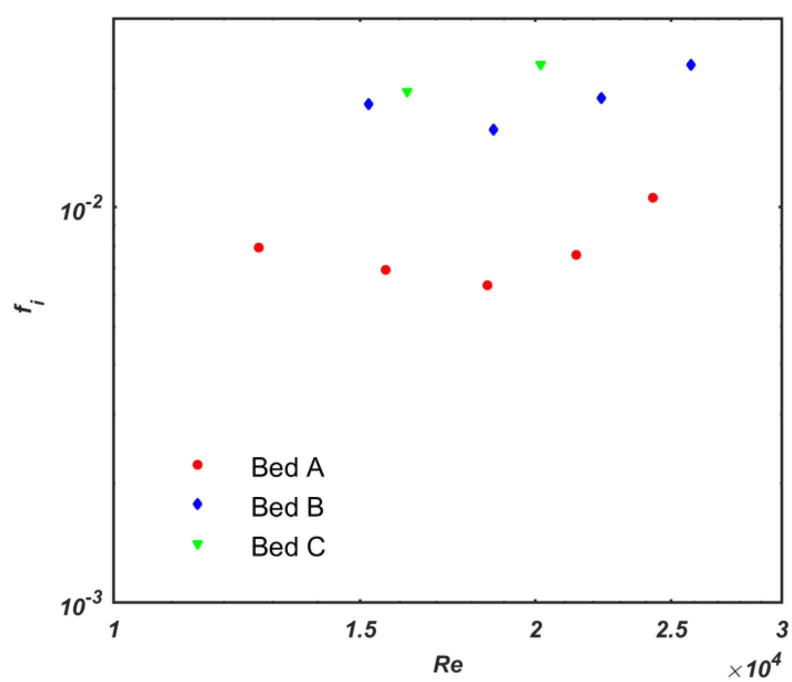

Figure 9-16 Comparison of interfacial friction factor for flow over beds of different heights

Figure 9-16 compares the interfacial friction factor data for beds A, B, and C. Increasing bed height from bed A to B causes a significant increase in the interfacial friction factor; the difference between f_i of the beds B and C is less notable. However, we can conclude that increasing the bed height (equivalently increasing bed surface area) causes the interfacial friction factor to increase. Therefore, the increase in the interfacial friction factor explains the reduction of the critical flow rate for thicker beds.

Two main findings can be made based on the results presented for interfacial friction factors. First, the interfacial friction factor can be significantly distinct from that of the average friction factor. The difference depends on the bed height. Furthermore, at the onset of the bed erosion, the interfacial friction factor shows a sharp increase. This observation is missing altogether in the average friction factor correlations.

The implication of the presented results for hole cleaning and multi-layer modeling of bed erosion is that one must differentiate between the average and interfacial friction factors.

9.5 Implications and importance of the results for hole cleaning modeling

The presented results in this paper have several consequences for the development of mechanistic and semi-mechanistic hole cleaning models.

In the development of mechanistic hole cleaning models, knowledge of local fluid velocity in the vicinity of the sand bed interface is required for accurate estimation of fluid forces on the particles. Figure 9-17 conceptually illustrates the treatment of cuttings in the bed in the mechanistic approach toward solid bed removal modeling. The forces that control dislodgment of the sand particles depends on the local fluid velocity right at the center of gravity of the particle. Therefore, accurate estimation of fluid force requires knowledge of local fluid velocity at the bed interface.

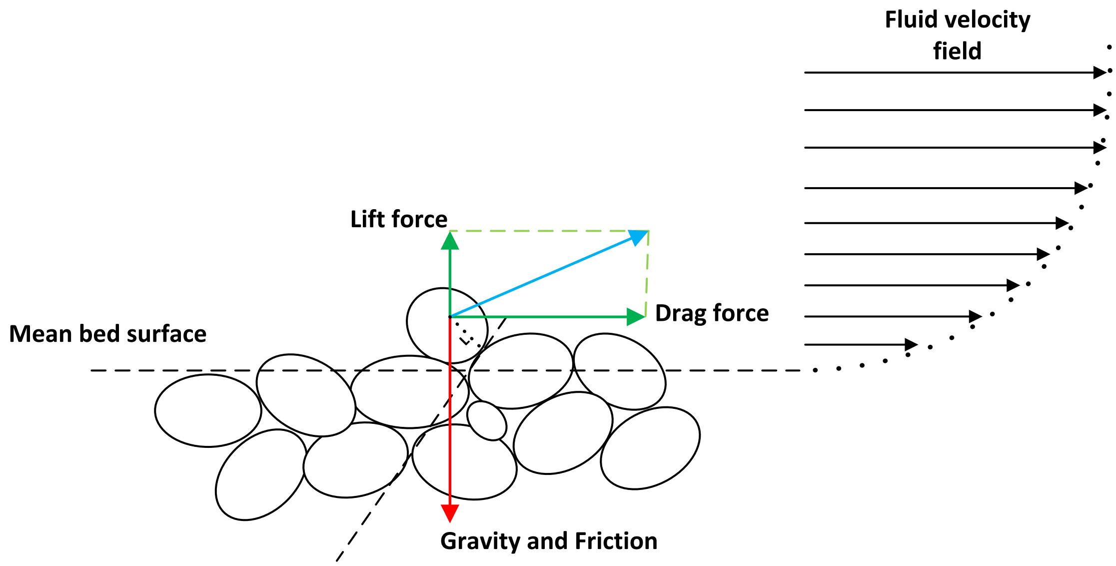

Figure 9-17 Schematic representation of forces acting on a particle in the cuttings bed

The local fluid velocity is often evaluated using the universal velocity profiles (Ramadan et al. 2003, Duan et al. 2007); similar to the ones presented in this paper. As the results indicated in this study, the velocity profiles strongly depend on the flow regime near the bed interface. Often researcher assumes a constant equivalent roughness height characterizes the bed (Ramadan et al. 2003, Duan et al. 2007). However, our data shows the bed roughness is variable and correlates with roughness Reynolds number. Therefore, development of realistic hole cleaning models requires incorporation of the variable surface roughness of the bed interface. Furthermore, the bed erosion induces additional surface roughness which strongly affects the local fluid velocity near the bed interface.

Analysis of interfacial and average friction factor is directly related to semi-mechanistic hole cleaning modeling. In this approach, the coupling of the phases is obtained through friction factor represented by interfacial friction factor. Equation 19 showed that the fluid force on the bed is directly related to the bed shear stress. Therefore, the accurate coupling of the phases in multi-layer hole cleaning models requires Knowle of interfacial friction factor.

In the literature, interfacial friction factor is assumed to be similar to friction factor near a rough wall. However, our data shows this approach is flawed from two perspectives. First, the roughness of the sand bed is variable, and hence, treatment of the bed using a single roughness height is not correct. Additionally, the interfacial friction factor strongly depends on the height (or surface area) of the stationary bed. The thicker the bed is, the higher the interfacial friction factor would bed; the cause for this is the increase in the interfacial surface area. Therefore, it is imperative to differentiate between average friction factor and interfacial friction factor for accurate modeling of the momentum exchange between the phases at the bed interface.

9.6 Conclusions

The local fluid velocity profiles near the sand bed/water interface, the equivalent sand bed roughness, the average (fa) and the interfacial (fi) friction factors were evaluated and compared for flow of water over the stationary and moving bed (in the form of the bedload transport) conditions in an eccentric annulus.

The data were analyzed to validate the two most significant assumptions often made in the development of hole cleaning models. First one is the universality of the velocity profiles near the interface of a sand bed. The second, one is the similarity (or closeness) of the interfacial and average friction factors. The first one is important in the development of mechanistic hole cleaning models. The realistic assessment of a friction factor is, on the other hand, imperative in the development of the more accurate semi-mechanistic models of the solid transport process. Overall, the results are of great significance in understanding the fluid-particle interaction during hole cleaning using the turbulent flow of water in an eccentric annulus.

Analyses of velocity profiles in wall units have indicated that the experiments covered hydraulically smooth, transitionally rough, and fully rough flow regimes. The velocity profiles over the sand beds also showed that the bed roughness is variable. The bedload transport of particles caused a sharp increase in the equivalent roughness of the bed, which could be as high as 9.5 times that of the particle size.

Depending on the bed height (or the surface area of the bed at the interface), the interfacial friction factor can be significantly different from the average friction factor. For the lowest bed height (Bed A), the interfacial friction factor was smaller than that of the average friction factor. On the other hand, for the highest bed height (Bed C), the interfacial friction factor was greater than the average friction factor. The average friction factor in the presence of sand bed was about 45% greater than the flow in the same annulus without any sand bed.

The interfacial friction factor increased significantly at the onset of the bed erosion. This attribute does not appear in the average friction factor correlations. The movement of cuttings and added roughness induced by bedload transport could be the primary causes of the increase in the interfacial friction factor.

The results presented here provide much-needed experimental data for the validation of the mechanistic, semi-mechanistic (empirical) and numerical (CFD) models of the bed erosion process.

The significant difference between the average and interfacial friction factors should be taken into account for more realistic multi-layer modeling of the hole cleaning.

9.7 Nomenclatures

A	Annular area cross section $(\pi(R^2 - r^2))$ (m^2)
A_f	cross-sectional area available to flow (m^2)
d_p	Particles diameter (m)
D_h	Hydraulic Diameter (m)
e	Eccentricity
F_D	Drag force (Pa)
f	Fanning friction factor (-)
f_a	Average friction factor (-)
f_i	Interfacial friction factor (-)
R	Outer pipe radius (m)
r	Inner pipe radius (m)
h	Cuttings bed height (m)
L	Distance between center of pipes/length along the pipe (m)
U_s	Superficial velocity $(\frac{m}{s})$
U_b	Bulk or actual fluid velocity $(\frac{m}{s})$

u	Time average velocity ($\frac{m}{s}$)
$\hat{u}$	Instantaneous axial velocity ($\frac{m}{s}$)
$\hat{v}$	Instantaneous radial velocity ($\frac{m}{s}$)
y	Vertical distance from mean bed surface/or pipe wall (m)
y^+	Distance in wall units
u^+	Velocity in wall units
Q	Flow Rate (m^3/s)
S_{wi}	Wetted perimeter of the inner pipe (m)
S_b	Bed interfacial area (m)
S_{wo}	Wetted perimeter of the outer pipe (m)
Re	Reynolds number (-)
Δs	Displacement of tracer particles (m)
Δx	Axial displacement of tracer particles (m)
Δy	Radial displacement of tracer particles (m)
Δt	Time interval between two PIV images (s)
Δu^+	Roughness function
$\frac{dP}{\mathrm{dx}}$	Frictional pressure gradient ($\frac{Pa}{m}$)
μ	Fluid viscosity ($Pa.s$)
u_τ	Friction velocity ($\frac{m}{s}$)
τ_b	Interfacial/bed shear stress (Pa)
τ_w	Wall shear stress (Pa)
τ_{wo}	Wall shear stress on outer pipe wall (Pa)
τ_{wi}	Wall shear stress on inner pipe wall(Pa)
Re_{u_τ}	Roughness Reynolds number

κ Von Karman constant (0.41)

ε Equivalent roughness height

ρ Fluid's density ($\frac{Kg}{m^3}$)

9.8 References

Adari, R. B. (1999). Development of correlations relating bed erosion to flowing time for near horizontal wells. M.Sc. Thesis, University of Tulsa, USA

Adari, R. B., Miska, S., Kuru, E. et al. (2000). Selecting Drilling Fluid Properties and Flow Rates For Effective Hole Cleaning in High-Angle and Horizontal Wells. SPE Annual Technical Conference and Exhibition. Dallas, Texas, 1–4 October 2000., SPE-63050-MS,DOI: 10.2118/63050-MS.

Bagchi, P. and Balachandar, S. (2003). Effect of turbulence on the drag and lift of a particle. Physics of Fluids **15**(11): 3496-3513, DOI: doi:http://dx.doi.org/10.1063/1.1616031.

Best, J., Bennett, S., Bridge, J. et al. (1997). Turbulence modulation and particle velocities over flat sand beds at low transport rates. Journal of Hydraulic Engineering-Asce **123**(12): 1118-1129, J Hydraul Eng-Asce, DOI: c 10.1061/(Asce)0733-9429(1997)123:12(1118).

Bizhani, M. (2013). Solids transport with turbulent flow of non-Newtonian fluid in the horizontal annuli. M.Sc. Thesis, University of Alberta, Edmonton, Canada.

Bizhani, M., Corredor, F. E. R. and Kuru, E. (2016). Quantitative Evaluation of Critical Conditions Required for Effective Hole Cleaning in Coiled-Tubing Drilling of Horizontal Wells. **SPE** Drilling & Completion **31**(3): 188-199, DOI: http://dx.doi.org/10.2118/174404-PA.

Bizhani, M. and Kuru, E. (2017). Critical Review of Mechanistic and Empirical (Semi-Mechanistic) Models for Particle Removal from Sand Bed Deposits in Horizontal Annuli by Using Water. SPE Journal, SPE-187948-PA, In press.

Bizhani, M. and Kuru, E. (2017). Effect of Sand Bed Deposits on the Characteristics of Turbulent Flow of Water in Horizontal Annuli ASME fluid engineering, Paper under review.

Bizhani, M., Kuru, E. and Ghaemi, S. (2016). Effect of Near Wall Turbulence on the Particle Removal from Bed Deposits in Horizontal Wells. Proceedings of the Asme 35th International Conference on Ocean, Offshore and Arctic Engineering , 2016, Vol 8.

Brown, N. P., Bern, P. A. and Weaver, A. (1989). Cleaning Deviated Holes: New Experimental and Theoretical Studies. SPE\IADC Drilling Conference New Orleans, Louisiana, February 28-3 March 1989 SPE-18636-MS,DOI: 10.2118/18636-MS.

Carbonneau, P. E. and Bergeron, N. E. (2000). The effect of bedload transport on mean and turbulent flow properties. Geomorphology **35**(3-4): 267-278, Geomorphology, DOI: g10.1016/S0169-555x(00)00046-5.

Chan-Braun, C. (2012). Turbulent Open Channel Flow, Sediment Erosion and Sediment Transport, KIT Scientific Publ.

Chan-Braun, C., Garcia-Villalba, M. and Uhlmann, M. (2011). Force and torque acting on particles in a transitionally rough open-channel flow. Journal of Fluid Mechanics **684**: 441-474, J Fluid Mech, DOI: 10.1017/jfm.2011.311.

Clark, R. K. and Bickham, K. L. (1994). A Mechanistic Model for Cuttings Transport. SPE 69th Annual Tgchniml Conference and Exhlbltion Now ohms, LA, U. S.A., 25-8 .Septemb.ar 1994., SPE-28306-MS,DOI: 10.2118/28306-MS.

Duan, M., Miska, S. Z., Yu, M. et al. (2007). Critical Conditions for Effective Sand-Sized Solids Transport in Horizontal and High-Angle Wells. SPE Production and Operations Symposium Oklahoma City, Oklahoma, USA, 31 March-3 April 2007., SPE-106707-MS,DOI: 10.2118/106707-MS.

Duan, M. Q., Miska, S., Yu, M. J., Takach, N., Ahmed, R., Zettner, C. (2009). Critical Conditions for Effective Sand-Sized-Solids Transport in Horizontal and High-Angle Wells. SPE Drilling & Completion **24**(2): 229-238, **SPE** Drill Completion, DOI: 10.2118/104192-PA.

Escudier, M. P. and Cullen, L. M. (1996). Flow of a shear-thinning liquid in a cylindrical container with a rotating end wall. Experimental Thermal and Fluid Science **12**(4): 381-387, Exp Therm Fluid Sci, DOI: Doi 10.1016/0894-1777(95)00137-9.

Flack, K. A. and Schultz, M. P. (2014). Roughness effects on wall-bounded turbulent flows. Physics of Fluids **26**(10): 101305, DOI: 10.1063/1.4896280.

Ford, J. T., Peden, J. M., Oyeneyin, M. B. et al. (1990). Experimental Investigation of Drilled Cuttings Transport in Inclined Boreholes. SPE Annual Technical Conference and Exhibition, 23-26 September, New Orleans, Louisiana, hSPE-20421-MS,DOI: 10.2118/20421-MS.

Gore, R. A. and Crowe, C. T. (1991). Modulation of Turbulence by a Dispersed Phase. Journal of Fluids Engineering-Transactions of the Asme **113**(2): 304-307, J Fluid Eng-T Asme, DOI: 10.1115/1.2909497.

Guo, X.-l., Wang, Z.-m. and Long, Z.-h. (2010). Study on three-layer unsteady model of cuttings transport for extended-reach well. Journal of Petroleum Science and Engineering **73**(1–2): 171-180, DOI: http://dx.doi.org/10.1016/j.petrol.2010.05.020.

Hemphill, T. and Larsen, T. I. (1996). Hole-Cleaning Capabilities of Water- and Oil-Based Drilling Fluids: A Comparative Experimental Study. **SPE** Drilling & Completion **11**(4), SPE-26328-PA, DOI: 10.2118/26328-PA.

Houssais, M., Ortiz, C. P., Durian, D. J. et al. (2015). Onset of sediment transport is a continuous transition driven by fluid shear and granular creep. Nature Communications **6**, Nat Commun, DOI: ARTN 6527 10.1038/ncomms7527.

Iyoho, A. W. and Takahashi, H. (1993). Modeling Unstable Cuttings Transport In Horizontal, Eccentric Wellbores, SPE-27416-MS.

Japper-Jaafar, A., Escudier, M. P. and Poole, R. J. (2010). Laminar, transitional and turbulent annular flow of drag-reducing polymer solutions. Journal of Non-Newtonian Fluid Mechanics **165**(19-20): 1357-1372, J Non-Newton Fluid, DOI: 10.1016/j.jnnfm.2010.07.001.

Kelessidis, V. C. and Bandelis, G. E. (2004a). Flow Patterns and Minimum Suspension Velocity for Efficient Cuttings Transport in Horizontal and Deviated Wells in Coiled-Tubing Drilling. **SPE** Drilling & Completion **19**(4): 213-227, SPE-81746-PA, DOI: 10.2118/81746-PA.

Kundu, P. K., Cohen, I. M. and Dowling, D. R. (2012). Fluid Mechanics, 4th Edition. Amsterdam, Elsevier Science Bv.

Kundu, P. K., Cohen, I. M. and Dowling, D. R. (2012). Fluid Mechanics, 5th Edition. Fluid Mechanics, 5th Edition: 1-891.

Li, J. and Luft, B. (2014a). Overview of Solids Transport Studies and Applications in Oil and Gas Industry - Experimental Work. SPE Russian Oil and Gas Exploration & Production Technical Conference and Exhibition. Moscow, Russia, 14-16 October, SPE-171285-MS,DOI: 10.2118/171285-MS.

Li, J. and Luft, B. (2014b). Overview Solids Transport Study and Application in Oil-Gas Industry-Theoretical Work. International Petroleum Technology Conference. Kuala Lumpur, Malaysia, 10-12 December 2014, IPTC-17832-MS,DOI: 10.2523/IPTC-17832-MS.

Martins, A. L., Sa, C. H. M., Lourenco, A. M. F. et al. (1996). Experimental Determination of Interfacial Friction Factor in Horizontal Drilling With a Bed of Cuttings, SPE-36075-MS,DOI: 10.2118/36075-MS.

Melling, A. (1997). Tracer particles and seeding for particle image velocimetry. Measurement Science & Technology **8**(12): 1406-1416, Meas Sci Technol, DOI: 10.1088/0957-0233/8/12/005.

Mitchell, R. F., Miska, S., Aadnøy, B. S. et al. (2011). Fundamentals of Drilling Engineering, Society of Petroleum Engineers.

Miyazaki, K., Chen, G. , Ymamoto, F., Ohta, J., Murai, Y., Horii, K. (1999). PIV measurement of particle motion in spiral gas-solid two-phase flow. Experimental Thermal and Fluid Science **19**(4): 194-203, Exp Therm Fluid Sci, DOI: 10.1016/S0894-1777(99)00020-5.

Nezu, I. and Sanjou, M. (2011). PIV and PTV measurements in hydro-sciences with focus on turbulent open-channel flows. Journal of Hydro-Environment Research **5**(4): 215-230, J Hydro-Environ Res, DOI: 10.1016/j.jher.2011.05.004.

Nouri, J. M., Umur, H. and Whitelaw, J. H. (1993). Flow of Newtonian and Non-Newtonian Fluids in Concentric and Eccentric Annuli. Journal of Fluid Mechanics **253**: 617-641, J Fluid Mech, DOI: 10.1017/S0022112093001922.

Owen, P. R. (1964). Saltation of uniform grains in air. Journal of Fluid Mechanics **20**(2): 225-242, DOI: 10.1017/S0022112064001173.

Ozbayoglu, M. E., Saasen, A., Sorgun, M. et al. (2010a). Critical Fluid Velocities for Removing Cuttings Bed Inside Horizontal and Deviated Wells. Petroleum Science and Technology **28**(6): 594-602, DOI: 10.1080/10916460903070181.

Poole, R. J. (2010). Development-Length Requirements for Fully Developed Laminar Flow in Concentric Annuli. Journal of Fluids Engineering-Transactions of the **Asme 132**(6), J Fluid Eng-T Asme, DOI: 10.1115/1.4001694.

Rabenjafimanantsoa, H. A. (2007). Particle transport and dynamics in turbulent Newtonian and non-Newtonian fluids. Other Information: Doctoral theses at UIS; ISSN 1890-1387; Numerical Data; Thesis or Dissertation; TH: Thesis (PhD); refs, charts, figs, tabs. Norway: 163 pages.

Rabenjafimanantsoa, H. A., Rune, W. T. and Saasen, A. (2005). Flow regimes over particle beds experimental studies of particle transport in horizontal pipes Annual Transactions of the Nordic Rheology Soceity, 13.

Ramadan, A., Skalle, P. and Johansen, S. T. (2003). A mechanistic model to determine the critical flow velocity required to initiate the movement of spherical bed particles in inclined channels. Chemical Engineering Science **58**(10): 2153-2163, DOI: 10.1016/S0009-2509(03)00061-7.

Reed, T. D. and Pilehvari, A. A. (1993). A New Model for Laminar, Transitional, and Turbulent Flow of Drilling Muds, SPE-25456-MS,DOI: 10.2118/25456-MS.

Smith, J. D. and McLean, S. R. (1977). Spatially averaged flow over a wavy surface. Journal of Geophysical Research **82**(12): 1735-1746, DOI: 10.1029/JC082i012p01735.

Song, T., Chiew, Y. M. and Chin, C. O. (1998). Effect of bed-load movement on flow friction factor. Journal of Hydraulic Engineering-Asce **124**(2): 165-175, J Hydraul Eng-Asce, DOI: Doi 10.1061/(Asce)0733-9429(1998)124:2(165).

Sorgun, M., Aydin, I. and Ozbayoglu, M. E. (2011). Friction factors for hydraulic calculations considering presence of cuttings and pipe rotation in horizontal/highly-inclined wellbores. Journal of Petroleum Science and Engineering **78**(2): 407-414, J Petrol Sci Eng, DOI: DOI 10.1016/j.petrol.2011.06.013.

Sumer, B. M., Chua, L. H. C., Cheng, N.-S. et al. (2003). Influence of Turbulence on Bed Load Sediment Transport. Journal of Hydraulic Engineering **129**(8): 585-596, DOI: 10.1061/(ASCE)0733-9429(2003)129:8(585).

Televantos, Y., Shook, C., Carleton, A. et al. (1979). Flow of Slurries of Coarse Particles at High Solids Concentrations. Canadian Journal of Chemical Engineering **57**(3): 255-262, Can J Chem Eng.

Tsuji, Y., Kato, N. and Tanaka, T. (1991). Experiments on the unsteady drag and wake of a sphere at high reynolds numbers. International Journal of Multiphase Flow **17**(3): 343-354, DOI: http://dx.doi.org/10.1016/0301-9322(91)90004-M.

Wiberg, P. L. and Rubin, D. M. (1989). Bed Roughness Produced by Saltating Sediment. Journal of Geophysical Research-Oceans **94**(C4): 5011-5016, J Geophys Res-Oceans, DOI: 10.1029/JC094iC04p05011.

Zeinali, H., Toma, P. and Kuru, E. (2012). Effect of Near-Wall Turbulence on Selective Removal of Particles From Sand Beds Deposited in Pipelines. Journal of Energy Resources Technology-Transactions of the Asme **134**(2), J Energ Resour-Asme, DOI: Artn 021003 10.1115/1.4006041.

9.9 Appendix A: Derivations of Equations for Hydraulic Diameter and Effective Area Open to Flow in Eccentric Annulus with the Presence of Cuttings Bed

Details of calculation related to hydraulic diameter and cross-sectional area of the annulus in the presence of a sand bed are presented in this appendix (See Figure A- 9-1for details) (Duan 2009).

Case 1: h<2r

$$S_o = 2R\, arccos(\frac{h-R}{R}) \qquad \textbf{Eq. (A- 9-1)}$$

$$S_i = 2r \arccos(\frac{h-r}{r}) \qquad \textbf{Eq. (A- 9-2)}$$

$$S_b = 2\sqrt{R^2 - (R-h)^2} - 2\sqrt{r^2 - (r-h)^2} \qquad \textbf{Eq. (A- 9-3)}$$

$$A_f = R^2\, arccos\left(\frac{h-R}{R}\right) + (R-h)\sqrt{R^2 - (R-h)^2} - r^2 \arccos\left(\frac{h-r}{r}\right) - (r-h)\sqrt{r^2 - (r-h)^2} \qquad \textbf{Eq. (A- 9-4)}$$

Case 2: h>2r

$$S_o = 2R\, arccos(\frac{h-R}{R}) \qquad \textbf{Eq. (A- 9-5)}$$

$$S_i = 0 \qquad \textbf{Eq. (A- 9-6)}$$

$$S_b = 2\sqrt{R^2 - (R-h)^2} \qquad \textbf{Eq. (A- 9-7)}$$

$$A_f = R^2\, arccos\left(\frac{h-R}{R}\right) + (R-h)\sqrt{R^2 - (R-h)^2} \qquad \textbf{Eq. (A- 9-8)}$$

The hydraulic diameter is:

$$D_h = \frac{4A_f}{S_o + S_i + S_b} \qquad \textbf{Eq. (A- 9-9)}$$

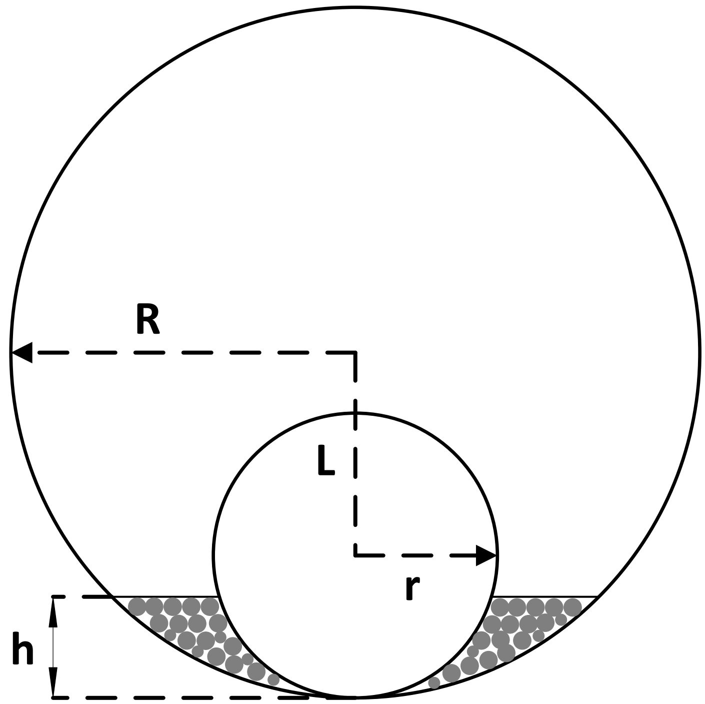

Figure A- 9-1 Illustration of dimensions used in calculations of cross section and hydraulic diameter

10. Characteristics of turbulent flow in fully eccentric horizontal annulus containing sand beds

In this chapter, we present results of PIV measurement for flow turbulent flow of water in the eccentric annulus. The data in this section is a follow-up on the results presented in the previous chapter. The discussions in this chapter include impact of bed height on flow above the bed and the differences in flow in different cross-sections of the annulus.

10.1. Abstract

In this study, we have investigated the turbulent flow of water over the sand beds of 3 different heights in a fully eccentric horizontal annulus. Velocity profiles were measured by using the Particle Image Velocimetry (PIV) technique at two different cross sections of the annulus; one along the symmetry plane vertically dividing the annulus into two equal sections, and the other at R/2 off the center of the annulus (R is the outer pipe radius). The impact of the stationary bed height on the velocity profiles and turbulence stresses are analyzed. Additionally, the difference in the flow down the symmetry plane and off the center of the annulus is also investigated.

It is shown that turbulence stresses over the sand bed vary depending on the height of the stationary sand bed. Comparison of velocity profiles above the bed interfaces revealed that the presence of the sand bed might cause a slight reduction in velocity and velocity gradient near the sand bed. Comparing to flow into the annulus without a cuttings bed, the presence of the sand bed causes a slight enhancement in the production of Reynolds normal and shear stresses. However, for the radial turbulence intensity, it appears that initially, the presence of the bed suppresses radical intensity.

Comparison of turbulence stresses along symmetry and off the center planes of the annulus indicated that height of the stationary sand bed causes the flow to change. For the smallest bed, Reynolds stresses were higher along the center plane of the annulus. On the other hand, for

thicker beds flow showed higher Reynolds shear stress and turbulence intensity over the bed as compared to pipe wall down the center of the annulus. Bedload transport of particles appears to cause an increase in the production of Reynolds normal and shear stresses in all the cases. However, the increase in turbulence comes at the cost of a reduction in mean kinetic energy.

10.2. Introduction

Transport of solid particles by turbulent flow is encountered in many industries. Examples include the pneumatic flow of wastes, flow over river beds, and in oil and gas drilling and production operations. Interaction of solid particles with the fluid is complex and span a broad range of length and time scales. The interaction for concentrated slurries is typically a four-way coupling.

A specific case of solid removal from bed deposits occurs in drilling oil wells. In drilling horizontal wells, which is of interest to this study, drilled solids gravitate to the lower side of the wellbore and gradually accumulate in the form of a stationary sand bed. In later stages of the drilling process, this sand bed needs to be removed to continue drilling or perform completion. The process of removing settled cuttings is known as hole cleaning in the drilling industry (Bizhani et al. 2016). The hole cleaning process is performed by pumping the drilling fluid at highest possible flow rate down the drillstring and up the annulus to sweep the cuttings out of the well. Despite more than 40 years of research conducted by the industry and academia, field experience indicates that hole cleaning is still a major issue causing delays in operation time and a significant increase in drilling cost (Li and Luft 2014a, Li and Luft 2014b).

The complexity of hole cleaning process is several folds. First, the flow is usually turbulent, and hence, theoretical treatment is not possible. Secondly, the coupling of the phases (solid-fluid) and the impact each phase has on the other phase is not well understood. The complexity increases due to the non-uniform size distribution of irregular shaped solid particles generated by the drill bit. Finally, the fluid is usually of non-Newtonian nature. These reasons have forced the researchers to focus on this problem through experimental studies. Nonetheless, experimenting in these types of flows is not a trivial task. Despite the existence of a massive body of research on hole cleaning in drilling literature (Pilehvari et al. 1996, Li and Luft 2014a, Li and Luft 2014b), almost all of these studies investigated the problem in what we can call a macroscopic approach. That is these studies usually alter one parameter (e.g. fluid viscosity, velocity, etc.) and observe its impact on the overall performance of the entire system (e.g. total solids concentration in the system).

Non-intrusive measurement techniques such as particle image velocimetry (PIV) and particle tracking velocimetry (PTV) have enabled new potentials for measuring local fluid-particle interactions in multiphase flows at different time and length scales without disturbing the flow. This type of measurements is different from previous studies in a sense that they provide real-time local information of fluid-particle interaction that can then be used to interpret the influence of various parameters on the process. In a few recent studies PIV and PTV have been used to study multiphase flow in channels and pipes (Miyazaki 1999, Bigillon et al. 2006, Yan and Rinoshika 2011, Rinoshika et al. 2012, Yan and Rinoshika 2012, Zeinali et al. 2012, Zheng et al. 2012). Examples of such studies in annulus are rare (Bizhani et al. 2016, Bizhani and Kuru 2017, Bizhani and Kuru 2017). The literature offers numerous studies related to turbulent flow in both eccentric and concentric annulus (Nouri et al. 1993, Escudier and Gouldson 1995, Japper-Jaafar et al. 2010, Ghaemi 2015). However, the authors are not aware of such study in a fully eccentric annulus with the presence of a sand bed that can be eroded by the flow.

The main goal of our study is to improve the understanding of the factors controlling particle removal from bed deposits. In this capacity, critical information needed to facilitate and improve (mechanistic) modeling approach, are the knowledge of local velocity profiles, and characteristics of the near wall flow turbulence (i.e. turbulence shear stresses, axial and radial turbulence intensities).

The process of sediment transport is a four-way coupling process (that is a movement of solid particles affects the flow and vice versa, particles affect each other too). In this context, the flow turbulence is also affected by the bedload transport of particles or even by the mere presence of the sand bed. Studies in flumes and river beds have shown turbulence can be either amplified or dampened by the secondary phase (Best et al. 1997, Carbonneau and Bergeron 2000). However, there is no consensus on the impact of particles movement on the flow turbulence. Since turbulence has profound implications for sediment transport (Diplas et al. 2008, Heyman et al. 2013, Schmeeckle 2014), it is important to study the impact of sediment transport on the flow turbulence.

In this study, we investigated the turbulent flow of water in a fully eccentric annulus containing sand beds of different heights. The measurements were conducted using PIV technique. The experiments were undertaken to collect near bed instantaneous velocity profiles to study the impact of the particles lying on the surface of the bed on the flow as well as the movement of the particles along the fluid/bed interface on the flow turbulence. Velocity profiles were obtained in two cross sections of the annulus to help better understanding of the flow dynamics in the annulus. Sand particles of mean sieve diameter of 600 microns and uniform size distribution were used to form bed deposits and simulate particle transport.

10.3. Experimental procedure

A schematic view of the large-scale flow loop facility used in this study is shown in Figure 10-1. Principal components of the flow loop are a 500-liter stainless steel tank, a centrifugal pump and measurement instruments such as magnetic flow meter and differential pressure transducers. There is an air-driven mixer in the tank for preparing the slurry. The centrifugal pump equipped with Variable Frequency Drive (VFD) was used to circulate fluid/solids mixture through the flow loop.

The annular section is 9 meters is the length. The pipes in the annular sections are high-quality Borosilicate glass tubes. The outer tube has an inner diameter of 95 mm and a wall thickness of 5 mm. The inner glass pipe has an outer diameter of 38 mm. The radius ratio (i.e. the inner pipe OD/ Outer pipe ID) is 0.4. The eccentricity of the inner pipe is 1 (i.e. fully eccentric pipe). The eccentricity is defined as the ratio of the distance between the centers of the pipes to the difference of radii's.

$$e = \frac{L}{R - r} \quad \textbf{Eq.(10-1)}$$

L is the distance between centers of inner and outer tubes; R and r are the inner radius of the outer pipe and outer radius of the inner pipe, respectively. The inner tube is resting against the wall of the outer tube; refer to Figure 10-1 for more detail. The inner pipes are pinned to the joints and are not moving.

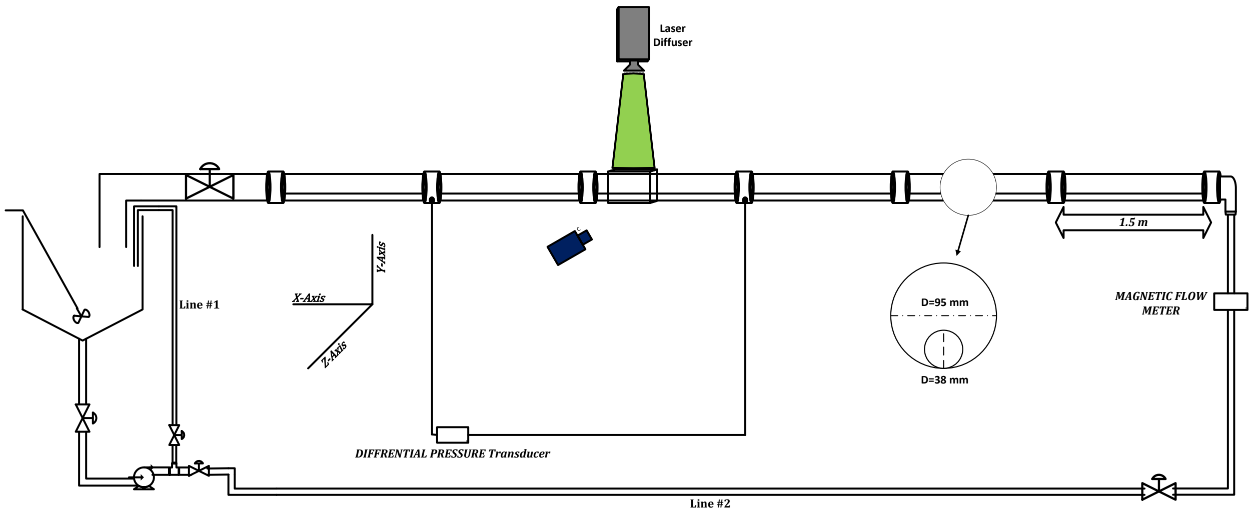

Figure 10-1 Schematic view of the flow loop and configurations of pipes, laser and camera, and the test section

A magnetic flow meter installed at the inlet of the annular section was used for measurement of flow rate. The flow meter is an OMEGA FMG607-R with an accuracy of $\pm 0.5\%$. A computerized data acquisition system powered by LabView software was connected to all the measurement devices. The software was used to control the pump flow rate as well as logging all the data (i.e. pressure losses, flow rates and fluid temperature in the flow loop).

Experiments started by establishing a stationary sand bed in the annulus. In this step, water and sand were mixed in the tank while the slurry was circulated through the flow loop at the maximum flow rate. The slurry was circulated for 10 to 15 minutes to achieve a uniform sand concentration along the flow loop (which would eventually allow us to obtain constant bed height). At this point, the pump was quickly shut down. The closing valves were used to isolate the annular section from the rest of the flow loop (Figure 10-1). Other parts of the flow loop (i.e. the tank, pump, and transport pipelines) were then carefully washed to remove any solids remained in these parts. Two filter bags with openings smaller than the particle size (the opening is 100 micron) were installed at the outlet of the annular section. The purpose of using filter bags is preventing the solids from recirculating in the system and going back to the test section during the experiments. The filter bags would collect any sand particles removed from the test section during the test. Hence, the flow loop was acting like an open-end flow loop in that regard. The sand bed height was varied by changing the amount of initial sand in the system. To achieve three different bed heights in this study, total mass loading of the solids in the system has varied from 3.5% to up to 14%.

The sand particles that have been used in this study are natural quartz sands with a density of 2650 kg/m^3. Sieve analysis of washed sand samples has shown that sand particles are uniform in size distribution. The d_{50} of the samples were determined to be 600 microns.

PIV measurements were carried out at approximately $100D_H$ ($D_H = 2(R - r)$) away from the annulus's inlet. Since the bed is uniform in thickness in the entire annulus, the flow should be fully developed in the measurement window. In single phase flow, a development length of $88D_H$ is required for a fully developed laminar flow (Poole 2010), whereas development length for turbulent flow is much shorter (Japper-Jaafar et al. 2010).

Due to the cylindrical shape of glass pipes, image distortion is a major issue in the PIV measurements. A rectangular box was designed and installed around the outer tube to reduce laser light refraction. Additionally, the box is filled with glycerol (99% Wt/Wt pure glycerol) to reduce the light refraction. Glycerol has a refraction index of 1.47, which is similar to the glass pipe, therefore, helps to minimize the refraction of the laser light.

10.3.1. PIV Setup Description and Post-Processing Procedures

A Nd: YAG double pulsed laser with a wavelength of 532 nm and 50 mJ/pulse was used in this study. The laser light is converted to a planar light sheet by a combination of the cylindrical and the special optical lenses. The thickness of the laser light sheet could vary from 0.5 to 3 mm. The thick laser light may incur errors in the measurement as a result of the depth of the field thickness. The light thickness was kept at its minimum as 0.5 mm in this study.

A CCD (charge-coupled device) camera with a resolution of 1376×1040 pixels was used for recording the PIV images. The camera has a double shuttering feature, which enables capturing a pair of pictures in a short and controllable time interval. A 60 mm Nikon AF NIKKOR lens with a 36-mm extension tube was used for recording the images. The f-stop or the aperture setting of the lens was set to 8. The scaling factor for images has been registered to be 31.76 μm/pixel.

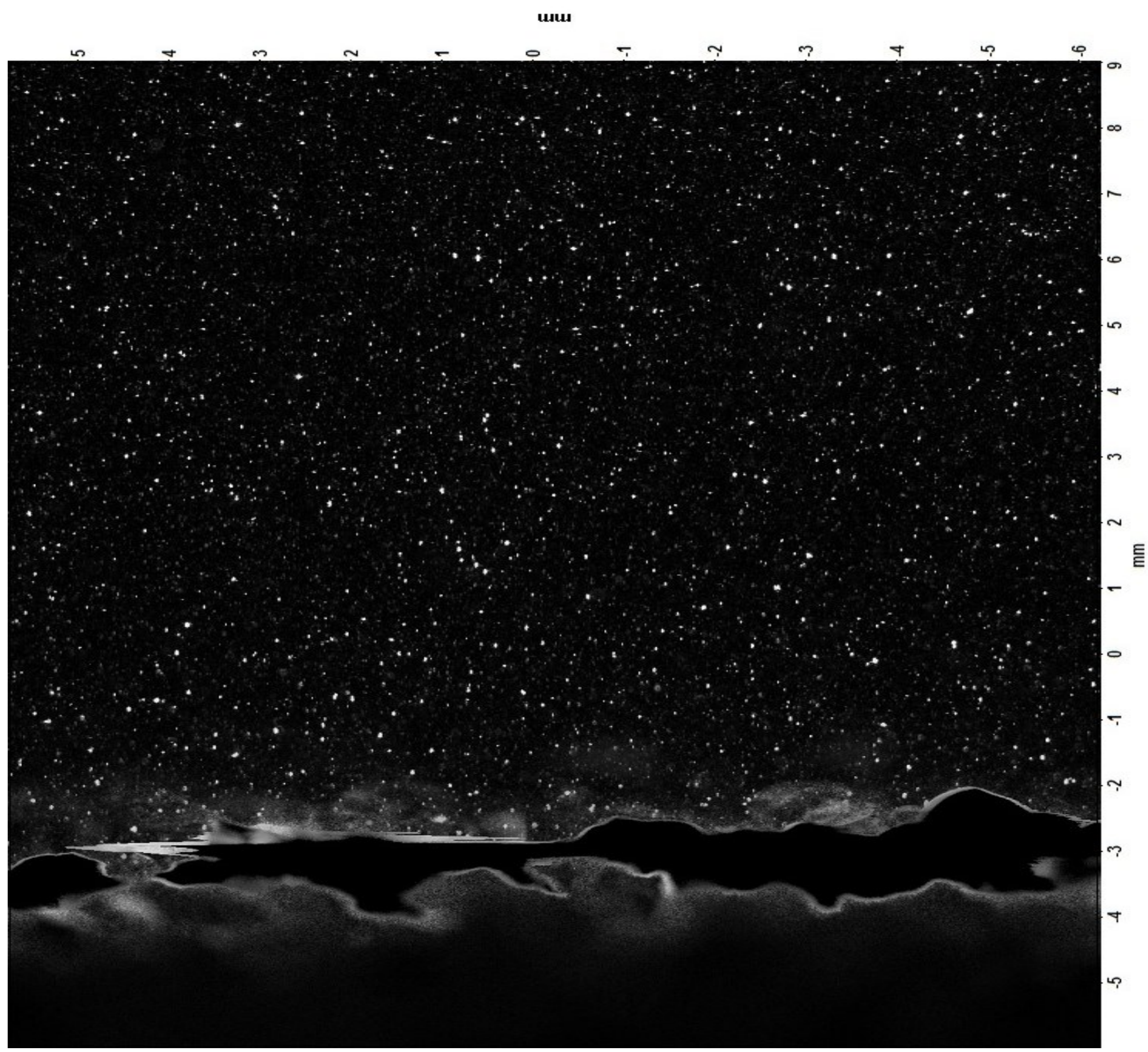

Figure 10-2 A typical PIV of the sand bed and tracers in the fluid

Figure 10-2 shows a typical PIV image acquired during the experiments. In this picture, the sand bed is located at the bottom while the fluid seeded with tracer particles (bright white dots) is flowing over the top. DAVIS 8.3.0 software was used for both the image acquisition and the post-processing of pictures. The software was used for adjusting the appropriate parameters during the experiments (such as the time interval between the two images and the laser power) as well as processing and extracting the data from the pictures. Further details regarding the image processing algorithm are given in the next section.

Hollow glass spheres with a mean diameter of 10 microns were used as tracer particles. The tracer particles are nearly neutral in water ($1.1 \pm 0.05 \frac{g}{cc}$) to keep them suspended in the flow.

The addition of the trace particles is necessary to enhance the spatial resolution of the PIV images and reduce the bias error towards the sand debris (Melling 1997).

10.3.2. PIV Data Post-Processing Procedures

The PIV processing algorithm for velocity calculations follows a cross-correlation based method. After obtaining a pair of images with the tracer particles in the flow, each image is broken down to the smaller windows called the interrogation windows. The interrogation windows are analyzed in the 2nd image for probable similarities to the same interrogation window in the 1st picture (Nezu and Sanjou 2011). To determine the pixel displacement, the cross-correlation method was used. The method works by cross correlating the intensity distribution over a small area (the interrogation window) of the flow. The peaks that show the highest correlation are chosen for the most likely destination of the seed particles. After finding the displacement of a seed particle in the two images (Δx and Δy) and having known the time interval (Δt) between the two images, the velocity of the tracer particle or equivalently the fluid velocity vector is calculated as follows:

$$\begin{cases} \hat{u} = \dfrac{\Delta x}{\Delta t} \\ \hat{v} = \dfrac{\Delta y}{\Delta t} \end{cases} \qquad \textbf{Eq.(10-2)}$$

A total number of 3000 pictures have been recorded for each data set (one data set is one flow rate measured over one plane Figure 10-2). The multi-pass cross-correlation method with the decreasing of the interrogation window size was used for the particle displacement calculations. An initial interrogation window size of 64×64 pixels followed by the window size of 32×32 pixels was utilized in the calculations. The overlap setting was 50%, and the weighting function was set to adaptive. To enhance the accuracy of the calculated vector fields, the post-processing was also applied on the calculated vectors. Universal outlier detection function was used in the post processing.

10.3.3. Measurement details

Measurements of velocity were carried out in two cross sections of the annulus. Figure 10-3 schematically represents the measurement planes. Plane 1 is the symmetry plane of the annulus. Plane 2 is located in the center of the annulus by R/2.

Experiments were conducted at three different sand bed heights (Figure 10-3 shows the relative height of each bed and locations of measurement planes). Bed A had a height smaller than the inner pipe outer radius r (i.e. h<r=19 mm). Bed B had a height bigger than r and smaller than 2r (i.e. r<h<2r). Finally, Bed C had a height greater than 2r (i.e. with bed C, the inner pipe was fully buried in the sand).

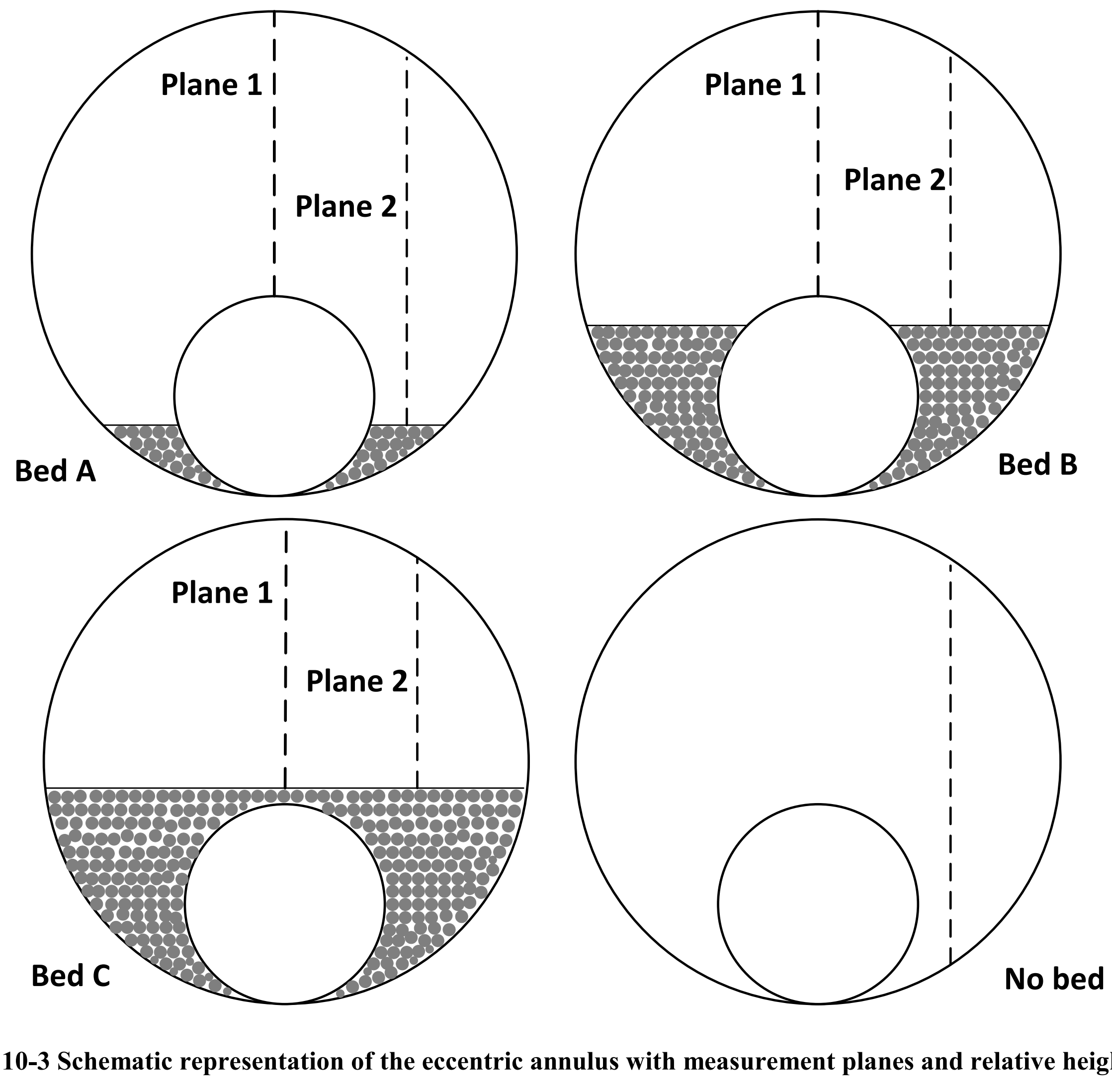

Figure 10-3 Schematic representation of the eccentric annulus with measurement planes and relative heights of the sand beds

For each bed, measurements were conducted up to a flow rate where bed erosion in the form of a moving layer of sand at the bed interface started taking place (please see the attached video file for better understanding of the definition of stationary bed and bedload transport of particles). Each experiment started at the flow rate of 64 lit/min which is the minimum operating flow rate in the flow loop. At this flow rate, beds A and B were completely stationary (i.e. no particles were observed to move). For bed C, however, some movement of bed particles occurred at this flow rate. For each bed height, the flow rate was increased stepwise until bed erosion started taking place in bedload format at a remarkable rate. By noticeable rate, we mean a constant stream of particles was moving at the bed interface.

For convenience, we define the superficial fluid velocity as follows:

$$U_s = \frac{Q}{\pi(R^2 - r^2)} \qquad \textbf{Eq.(10-3)}$$

Where Q is the pump flow rate, and U_s is the superficial fluid velocity. In the present work, PIV measurements were conducted at the same flow rates regardless of the bed height. The use of superficial velocity is convenient for presentations of the results later.

From the fluid mechanic's point of view, however, superficial velocity does not represent the difference in the actual fluid velocities in the annulus. To estimate the actual fluid velocity in the annulus, we must account for the reduction in the flow area by the sand beds. The bulk fluid velocity or the actual (mean) fluid velocity in the annulus is:

$$U_b = \frac{Q}{A_f} \qquad \textbf{Eq.(10-4)}$$

A_f designates the area available for flow. Details of the geometrical calculations pertinent to A_f is presented in the appendix.

The Reynolds number can then be calculated using the bulk fluid velocity.

$$Re = \frac{\rho U_b D_h}{\mu} \quad \textbf{Eq.(10-5)}$$

D_h is the hydraulic diameter. Details of the D_h calculations are presented in the appendix.

Table 10-1 reports the flow rates, superficial velocities, bulk velocities, and Reynolds numbers for experiments conducted with the bed A. In the experiments related to bed A, at U_s=0.3 m/s some particles at the bed interface started moving. However, particles were moving sparsely, and there was no constant stream of bedload layer. At U_s=0.35 m/s, there was a moving layer of particles at the bed interface. The latter (0.35 m/s) was referred as the critical flow rate, consistent with our previous studies (Bizhani et al. 2016).

Table 10-1 Details of measurements conducted with bed A

$\boldsymbol{Q}\ (\frac{\boldsymbol{lit}}{\mathbf{min}})$	$\boldsymbol{U_s}(\frac{\boldsymbol{m}}{\boldsymbol{s}})$	$\boldsymbol{U_b}(\frac{\boldsymbol{m}}{\boldsymbol{s}})$	$\boldsymbol{Re}$
64	0.18	0.19	11700
79	0.22	0.23	14300
93.6	0.26	0.28	16950
109	0.30	0.32	19700
124	0.35	0.36	22450

Table 10-2 reports the superficial velocities, bulk velocities, and Reynolds numbers under which experiments were conducted for the bed B. Moving layer of particles at the bed interface, in this case, was observed at the superficial velocity of U_s=0.3 m/s, slightly lower than that of the case with bed A.

Table 10-2 Details of measurements conducted with bed B

$Q\ (\frac{lit}{min})$	$U_s(\frac{m}{s})$	$U_b(\frac{m}{s})$	Re
64	0.18	0.22	14000
79	0.22	0.27	17400
93.6	0.26	0.32	20600
108.6	0.30	0.37	23900

Table 10-3 reports the operational variables under which experiments for the bed C were conducted. Since this bed was much thicker than the other two beds, bed load transport of particles started at a much lower superficial velocity. At U_s= 0.18 m/s, some occasional movement of bed materials was observed.

Table 10-3 Details of measurements conducted with bed C

$Q\ (\frac{lit}{min})$	$U_s(\frac{m}{s})$	$U_b(\frac{m}{s})$	Re
64	0.18	0.26	15200
79	0.22	0.32	18850

10.4. Results and discussion

The PIV measurements provide accurate and high-resolution data for the flow near the interface of the cuttings bed. In this section, we examine the impact of the presence of the sand beds on different aspects of flow in the annulus. Velocity profiles, Reynolds shear, and normal stress, are compared at various cross-sections of the annulus.

10.4.1. Impact of the presence of stationary bed height on the flow over the sand bed (plane 2)

In this section, the impact of the presence of the sand bed and its initial height on different aspects of flow is considered.

10.4.1.1. Velocity profiles

The local fluid velocity near the interface of the sand bed is an important property in controlling the interaction of the cuttings with the fluid. The instantaneous velocity in turbulent flows is time dependent. It fluctuates and varies over the time. The instantaneous velocity of turbulent flow can be decomposed into its time-averaged and fluctuating parts (Kundu et al. 2012).

$$\hat{u}(t) = \overline{u} + u' \qquad \textbf{Eq.(10-6)}$$

In Eq.(10-6), $\hat{u}$ is the instantaneous velocity and is time dependent. $\overline{u}$, on the other hand, is the time average of the instantaneous velocity, and hence, it is independent of time. u' is the fluctuating part of the velocity and does vary over the time. In this section, we first consider the time-averaged velocity profiles. Afterward, we also investigate the variations in the velocity profiles due to turbulence in the form of instantaneous velocity profiles.

The time-averaged velocity profiles near the interface of the cuttings bed are reported in Figure 10-4. The data have been measured at the superficial fluid velocity of 0.18 m/s. The profiles reveal that increasing the bed height, at the same pump flow rate, causes the local fluid velocity to increase. This is an expected behavior as the available flow area decreases because of the growing bed height. Hence, the average velocity increases in the annulus.

The velocity profiles for flow in the same annulus without any cuttings bed is also reported in Figure 10-4. Overall, flow with no bed shows the smallest velocity in the majority of the region near the wall. However, it is interesting to observe that very close to the y=0, (which corresponds to pipe wall for flow with no bed and sand bed interface for flow near the beds) local velocity is slightly higher near the pipe wall than near the bed interface. In another word, flow in the annulus with no bed shows a sharper change near the wall. The velocity gradient is higher near the pipe wall. The presence of the cuttings bed causes a slight reduction in the velocity gradient near the bed. One possible cause for this is the boundary roughness effect. The bed interface is rough as compared to the pipe wall. Hence, flow is dissipating more energy over the bed interface to overcome the added roughness. Therefore, mean kinetic energy decrease which appears as a reduction in the local fluid velocity.

The critical velocity that controls cuttings-fluid interaction is the velocity near the bed interface. In this case, a slight reduction occurs in the local velocity near the bed interface comparing to the no bed case. Velocity profiles at other Reynolds number have been measured. However, for the sake of brevity and preventing a repetition of the same information, data measured at other flow rates are reported in Appendix B.

The measured velocity profiles show that regardless of the height of the cuttings bed, close to the bed interface all the local time-averaged velocities are similar. Increasing the sand bed height shows its influence on the local velocity away from the bed. The local fluid velocity close to the cuttings bed is expected to control the removal of the particles. The drag force on a particle is directly related to the local fluid velocity near the bed. Therefore, the fact that a thicker bed causes the critical flow rate to decrease does not seem to happen because of an increase in the local fluid velocity near the bed; at least not by an increase in the local time average velocity.

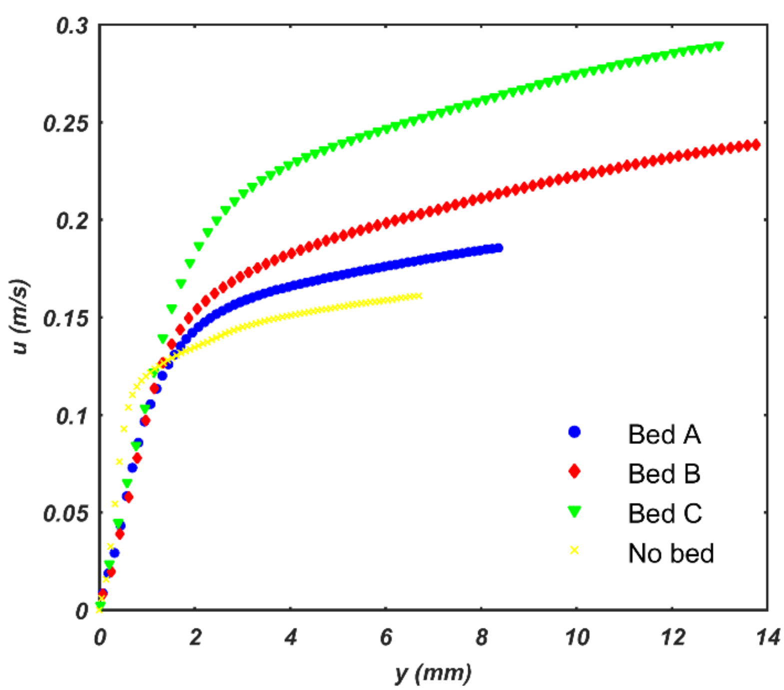

Figure 10-4 Profiles of the time averaged fluid velocity measured at 64 liters/min and over plane 2

The concept of "effective velocity" has been discussed by Bizhani and Kuru (2017). The effective velocity is the instantaneous fluid velocity near the sand bed interface. It is the velocity that the cuttings feel, and hence, it is more relevant in the context of the bed erosion. The instantaneous velocity of the turbulent flow is time dependent. To illustrate the variation in the local instantaneous fluid velocity near the bed, the instantaneous velocity profiles measured over a period of 10 minutes near the bed A and B are reported in Figure 10-5 and Figure 10-6, respectively. The time averaged velocity profiles, as well as the minimum and maximum in the instantaneous velocity near the bed A and B, are also reported in Figure 10-5 and Figure 10-6, respectively.

The data shown in Figure 10-5 and Figure 10-6 illustrate that the instantaneous velocity can significantly deviate from its mean or time-averaged values. The variations are smaller near the bed interface; however, the velocity is low in this region as well. That means even small fluctuations results in significant changes in the fluid drag force acting on the bed.

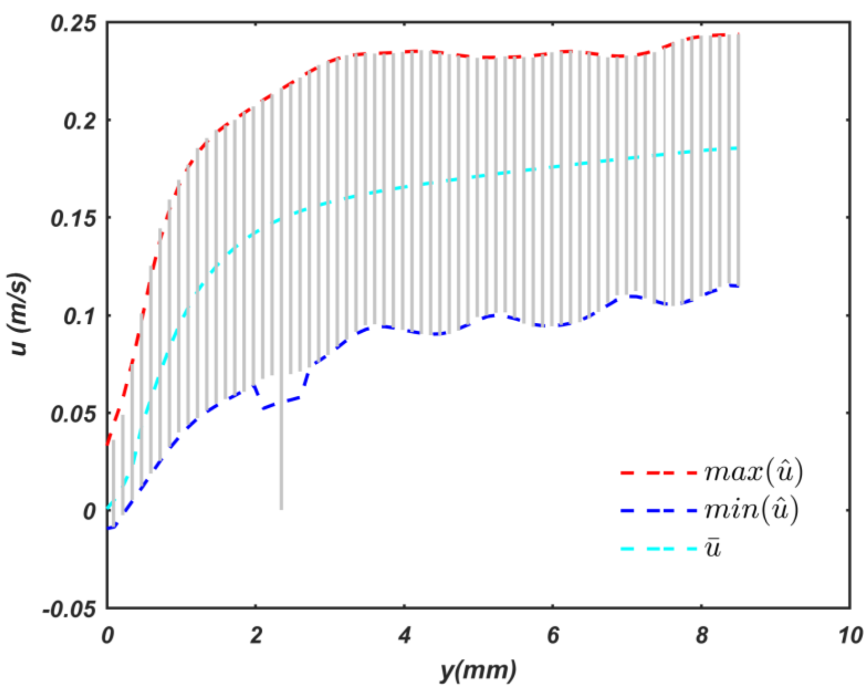

Figure 10-5 Profiles of the instantaneous, $\hat{u}$, and the time average, $\overline{u}$, velocities over the bed A measured at 64 liters/min (note that the gray lines represents the variations in $\hat{u}$ recorded over 10 minutes)

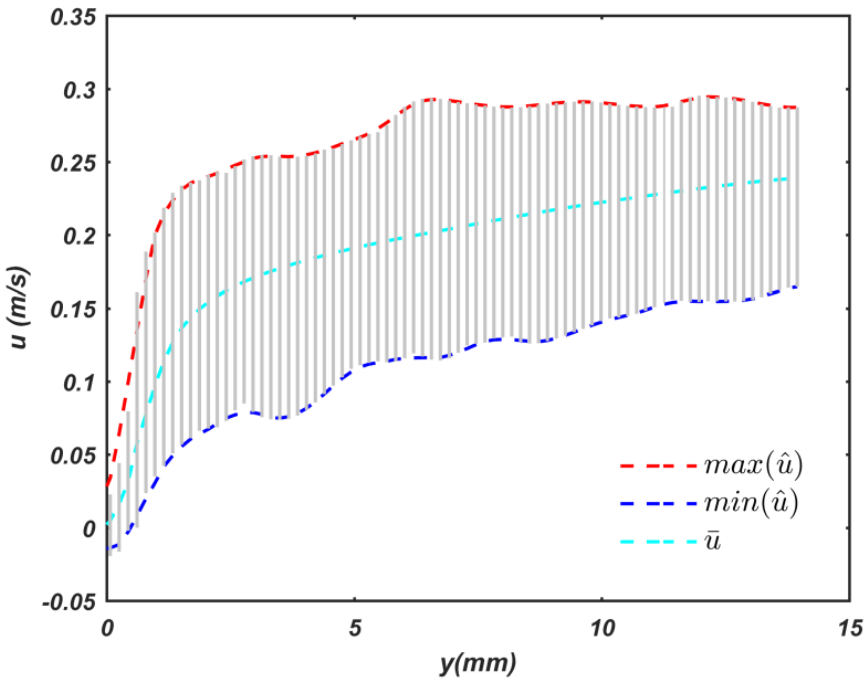

Figure 10-6 Profiles of the instantaneous, $\hat{u}$, and the time average, $\bar{u}, velocities$ over the bed B measured at 64 liters/min (note that the gray lines represents the variations in $\hat{u}$ recorded over 10 minutes)

To better understand the magnitude of the fluctuations in the instantaneous velocity as compared to the time-averaged velocity, Figure 10-7 is reporting the ratio of $\frac{\hat{u}}{\bar{u}}$. This figure shows the maximum and minimum in this ratio measured over 10 minutes near the bed B. The data shown in this figure indicate that the instantaneous velocity can be several times higher than its average value. The ratio becomes bigger as the bed interface is approached. The reason for that is because, near the solid surface the average velocity is low due to the no-slip boundary condition. Therefore, even small fluctuations would be comparable to the local time-averaged velocity.

The variations of velocity profiles near the bed interface (as shown in Figure 10-5 and Figure 10-6) implies that the mean fluid velocity may not thoroughly represent the proper coupling of the phases; an assumption made in the development of several mechanistic bed erosion models (Ramadan et al. 2003, Duan et al. 2007). The importance of flow turbulence on the bed erosion by water has been discussed extensively by Bizhani and Kuru (2017).

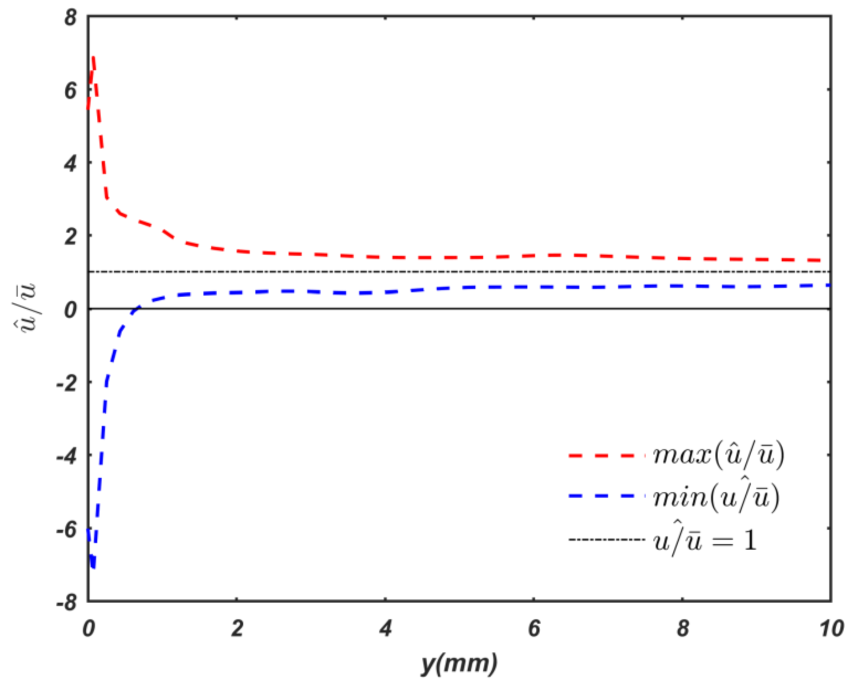

Figure 10-7 Ratio of the instantaneous fluid velocity to the average time velocity measured near the bed B at 64 liters/min

10.4.1.2. Reynolds stress

Turbulence is of extreme importance to sediment transport. In this capacity, the Reynolds normal and shear stresses are measured near the bed interface. The first turbulence entity of interest is the Reynolds shear stress defined as:

$$\tau_{Re} = -\rho\overline{u'v'} \qquad \textbf{Eq.(10-7)}$$

Profiles of the turbulent shear stress measured over three sand beds and with no cuttings bed in the eccentric annulus and along plane 2 are reported in Figure 10-8. The data have been measured at the flow rate of 64 liters/min (note that this is a subcritical flow rate for the bed erosion) for all the cases. The production of turbulent shear stress on the bed A was not significantly different from that of the case without any cuttings bed. However, the measured turbulence shear stress profiles show that the turbulence stress increases with the increasing bed height. The increase is particularly noticeable for the beds B and C.

Part of the reason for the enhanced production of the Reynolds stress with increasing bed height is because the increasing bed height causes the growth in the bulk flow velocity and consequently, flow Reynolds number at the same pump flow rate. The Reynolds number for flow over the beds of different initial height is reported in Table 10-4. As the figures indicate, the Reynolds number increases with the increasing bed height (i.e. 10200 for no bed, and 15,200 for the highest bed height case, Bed C). Therefore, the presence of stationary cuttings enhances production of the turbulence due to the increase in the Reynolds number. Additionally, change in surface roughness may also contribute to the production of the turbulence near the bed interface.

The total shear stress is a summation of its laminar and turbulent parts as shown in Eq.(10-8).

$$\tau = \mu \frac{\partial u}{\partial y} - \rho \overline{u'v'} \quad \textbf{Eq.(10-8)}$$

Improvement in the total shear stress directly results in enhancing the fluid drag force acting on the particles in the bed. The increase in Reynolds shear stress can improve the total (instantaneous) shear stress on the cuttings bed, and hence, improve the solid transport process.

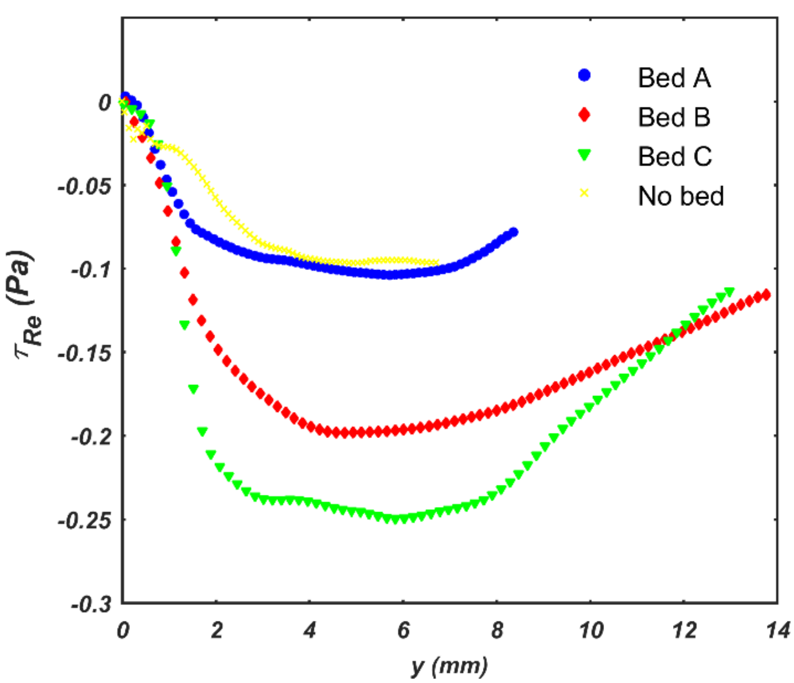

Figure 10-8 Profiles of Reynolds shear stress measured at 64 liters/min

Table 10-4 Flow Reynolds number for experiments at 64 liters/min

$\boldsymbol{Bed\ height}$	$\boldsymbol{Q(\frac{Liters}{min})}$	$\boldsymbol{U_b(\frac{m}{s})}$	$\boldsymbol{Re}$
A	64	0.19	11700
B	64	0.22	14000
C	64	0.26	15200
No bed	64	0.18	10200

10.4.1.3. Axial turbulence intensity

The axial turbulence intensity is a measure of turbulence velocity fluctuations in the direction of the flow. Eq.(10-9) gives the definition of the axial turbulence intensity.

$$U_{rms} = \sqrt{\overline{u'u'}} \qquad \textbf{Eq.(10-9)}$$

The importance of the turbulence and axial turbulence intensity in solid transport and bed erosion have been shown in previous studies (Diplas et al. 2008, Chan-Braun et al. 2011, Bizhani and Kuru 2017). A higher level of fluctuations in fluid velocity is essentially necessary for efficient removal of particles from a stationary sand bed. A higher axial turbulence intensity implies a greater level of velocity fluctuations in this direction. Hence, the greater U_{rms} means increased fluid drag force acting in the axial direction, which would enhance particle removal from bed deposits.

Figure 10-9 compares the measured axial turbulence intensity data over the three beds and no bed case at 64 liters/min. Comparing the axial turbulence intensity, U_{rms}, for the flow over the beds, it appears that increasing the bed height enhances the axial turbulence intensity. The implication of these results is that during sedimentation under constant pump flow rate, the deposition continues until a bed height is reached, where the velocity and the turbulence intensity over the bed increase to a level that the bed erosion starts taking place. This bed height is called the equilibrium bed height.

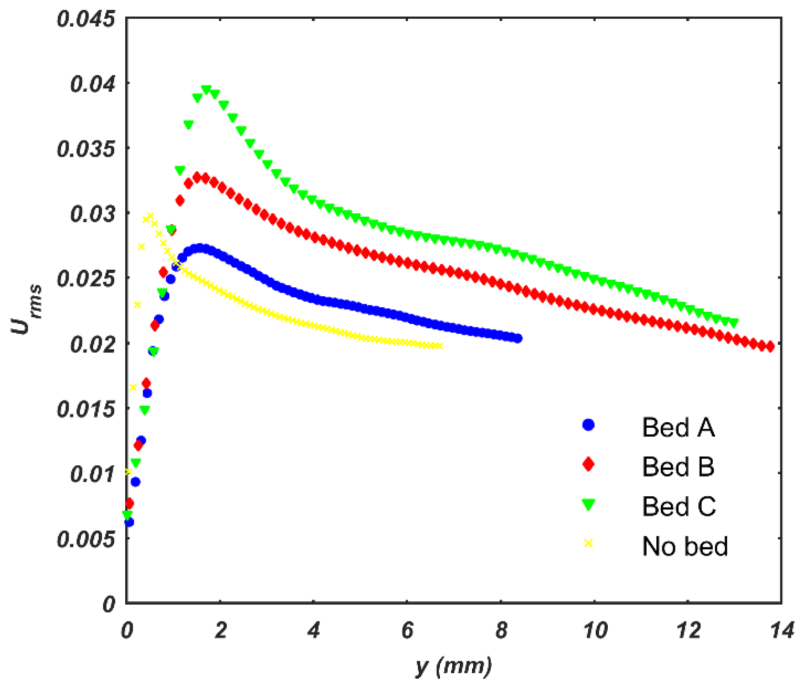

Figure 10-9 Profiles of U_{rms} measured at 64 liters/min

Comparing the measured axial turbulence intensity profiles for the no bed case to that of the flow over the beds, it appears that initially a decrease occurs in turbulence production near the bed with smallest height (i.e. Bed A). However, for beds, B, and C higher turbulence intensity were registered near the bed than that of the pipe wall. The reason for the observed increase in the axial turbulence intensity is the growth in flow Reynolds number due to the reduction of cross-sectional area of the annulus. Another reason could be the change in the surface roughness of the bed interface, a phenomenon which was discussed in the previous chapter.

10.4.1.4. Radial Turbulence intensity

The radial turbulence intensity is another measure of the turbulence strength. The radial intensity, denoted as V_{rms}, is defined according to Eq.(10-10).

$$V_{rms} = \sqrt{\overline{v'v'}} \qquad \textbf{Eq.(10-10)}$$

The radial intensity is not directly related to particle dislodgement from the cuttings bed. However, it is a major factor in suspension of the particles and thereby keeping the particles in the flow. Kelessidis and Bandelis (2004a) based on the work of Davies (1987) discussed eddy fluctuation force, which is essential in keeping particles in suspension in turbulent flow. The eddy fluctuation force (Eq.(10-11)) is proportional to the radial velocity variations. A higher level of radial velocity fluctuation results in a higher eddy fluctuation force, P_{ed}.

$$P_{ed} \approx \rho(v')^2 \qquad \textbf{Eq.(10-11)}$$

Measured radial turbulence intensity profiles for the flow over the beds and no bed case are reported in Figure 10-10. Similar to axial turbulence intensity, an increase in the radial turbulence due to increasing bed height was observed. Comparing to the no bed case, however, it appears that the presence of the cuttings bed initially suppresses the production of radial turbulence intensity. Only bed C shows a higher V_{rms} than the no bed case and that only applies for distances more than 2-mm away from the bed. Close to the bed interface and pipe wall, the accuracy of the data may be compromised due to the reflection of the laser light and small magnitude of velocity fluctuations in the radial direction.

To further confirm the impact of the presence of the sand bed on radial turbulence intensity, we report the measured intensity profiles over beds A and B and no bed case at the flow rate of 94 liters/min in Figure 10-11. The data at this flow rate also shows that compared to the no bed case, the presence of the cuttings bed has caused a reduction in the radial turbulence intensity very close to the pipe wall or bed interface. However, with the increasing bed height, the radial turbulence intensity also increased.

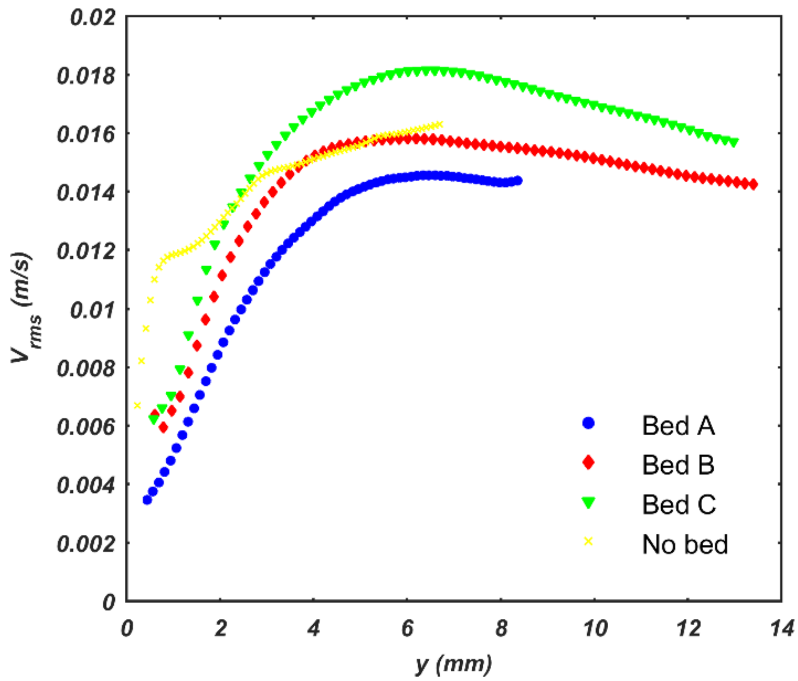

Figure 10-10 Profiles of V_{rms} measured at 64 liters/min

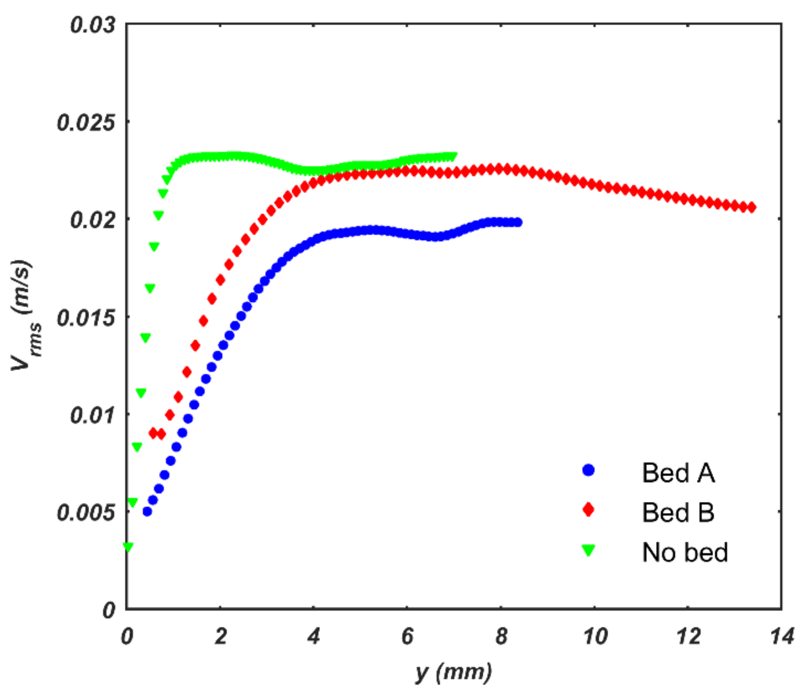

Figure 10-11 Profiles V_{rms} measured at 94 liters/min

10.4.2. Comparison of the flow characteristics on different cross-sections of the eccentric annulus (Plane 1 vs. Plane 2)

10.4.2.1. Characteristics of Turbulent Flow Over the Bed A

In Figure 10-12 and Figure 10-13, we compare the Reynolds stress profiles over the bed A in two cross-sections (i.e. Planes 1 and 2) at U_s=0.18 and 0.35 m/s respectively. The data of Figure 10-12 corresponds to the sub-critical velocity (Us=0.18 m/s) where there is no particle movement in the sand bed. At the superficial flow velocity of 0.18 m/s, considerably higher Reynolds stress exists along the plane 1. This implies that for small bed heights, turbulence is somehow less near the bed interface comparing to the turbulence near the inner pipe wall.

The bedload movement of particles was observed at the superficial velocity of 0.35 m/s (i.e. 0.35 m/s is the critical velocity for the bed erosion). Reynolds shear stresses for the flow over the bed when there is a moving layer of sand in the bed are shown in Figure 10-13. The Reynolds shear stress shows a significant peak near the cuttings bed along the plane 2 (i.e. bed interface). It appears that the movement of sand particles helps in the creation of more turbulence near the bed. Previous studies have also reported the turbulence attenuation and or amplification by moving sand particles (Best et al. 1997, Carbonneau and Bergeron 2000).

A possible explanation for turbulence amplification by moving sand particles has been proposed by Carbonneau and Bergeron (2000). According to Carbonneau and Bergeron (2000), movement of sediment particles at the bed interface may either dampen or enhance production of turbulent kinetic energy; when the production of turbulence is suppressed by moving sand particles, the mean kinetic energy increases. This causes the fluid velocity near the bed also to increase. If turbulence is amplified, that means the production of turbulence is enhanced, and hence, mean kinetic energy decreases. The decrease in mean kinetic energy manifests itself in the form of a decrease in mean flow velocity. In simpler words, there is a balance between mean and turbulent kinetic energy; if one is suppressed the other one would be amplified.

To test the given explanation for the increase in flow turbulence by the bedload transport of particles, the near wall average flow velocity profiles for flow at U_s=0.18 and 0.35 m/s are reported in Figure 10-14 and Figure 10-15 respectively. At the lower superficial velocity, both local velocity profiles show similarity near the sand bed and the pipe wall. However, at the higher velocity, the difference between local velocity profiles near the sand bed and the pipe wall becomes larger. The increase in the difference between mean flow velocities along the planes 1 and 2 supports the argument on the balance of the mean and the turbulent kinetic energy.

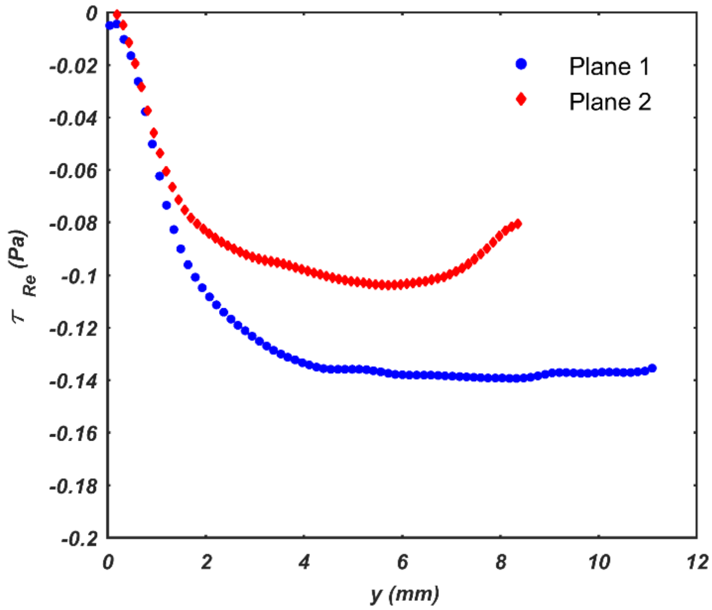

3

Figure 10-12 Reynolds shear stress measured at U_s=0.18 m/s (bed A, planes 1 and 2)

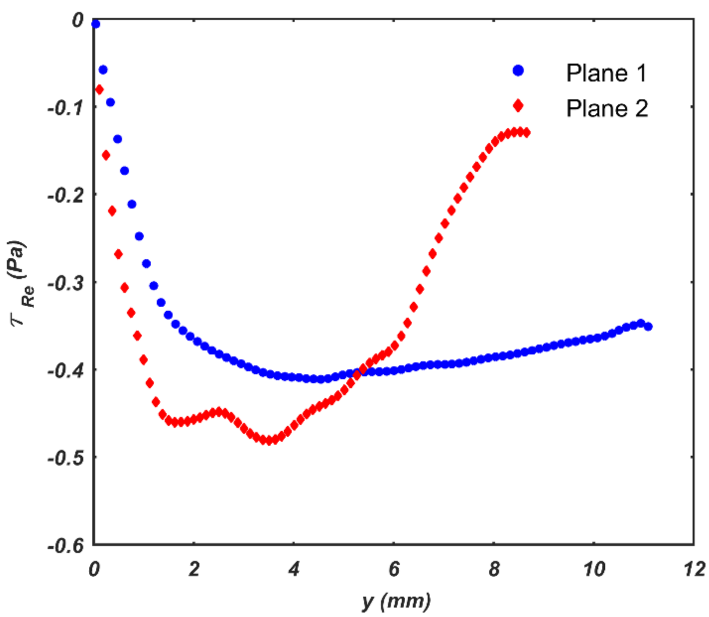

Figure 10-13 Reynolds shear stress measured at U_s=0.35 m/s (bed A, planes 1 and 2)

Another possible cause for the increase in turbulence near the bed interface at higher flow velocities could be the change of flow regime from smooth to rough flow, which was discussed in chapter 9.

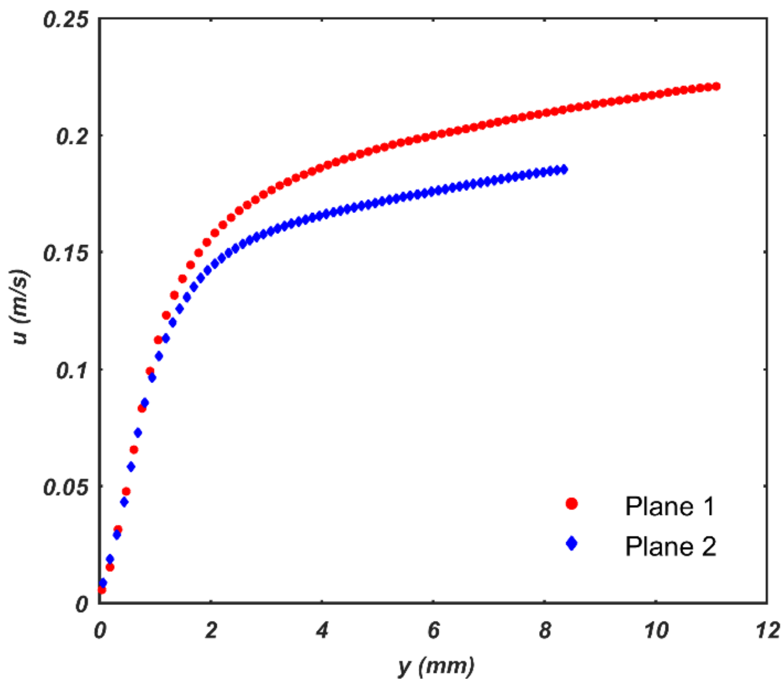

Figure 10-14 Mean flow velocity measured at U_s=0.18 m/s (bed A, planes 1 and 2)

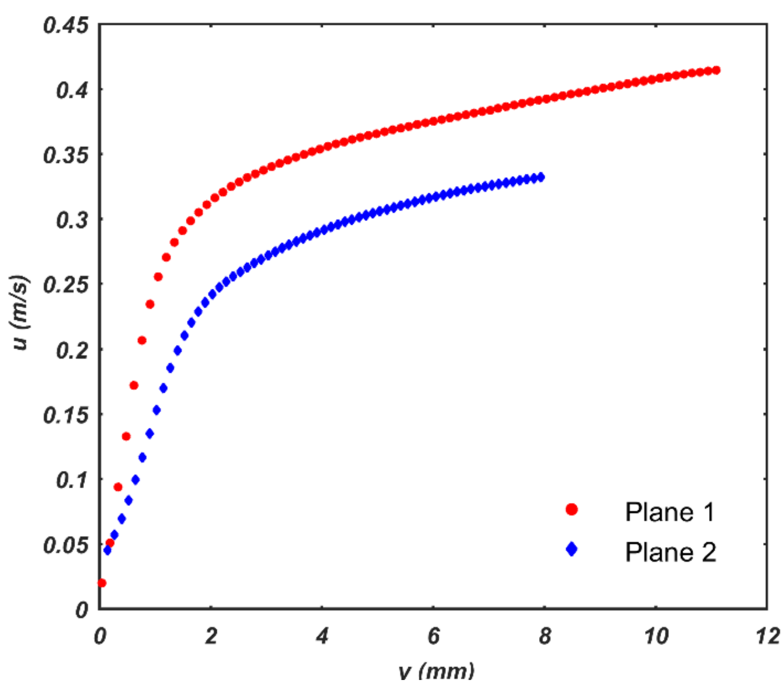

Figure 10-15 Mean flow velocity measured at U_s=0.35 m/s (bed A, planes 1 and 2)

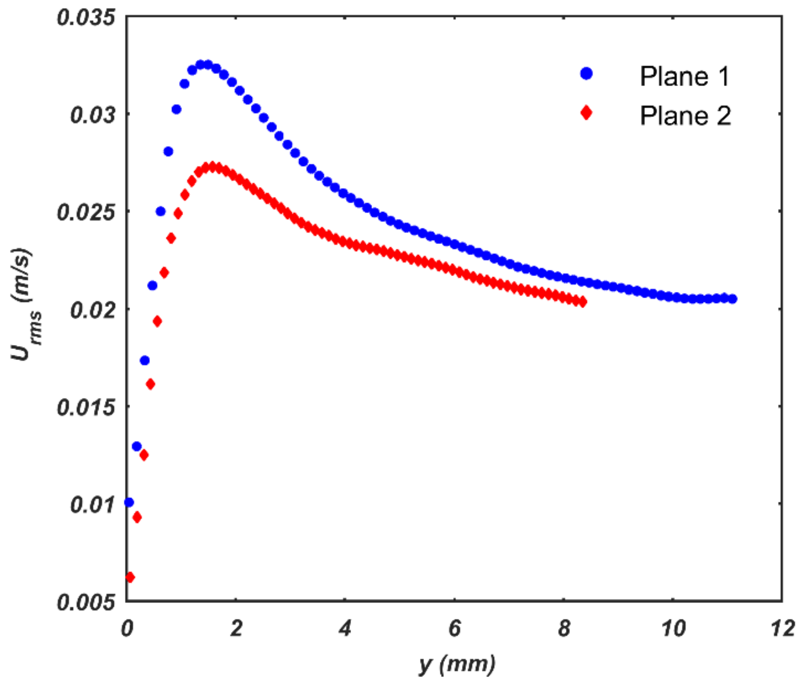

Figure 10-16 Axial turbulence intensity measured at U_s=0.18 m/s (bed A , planes 1 and 2)

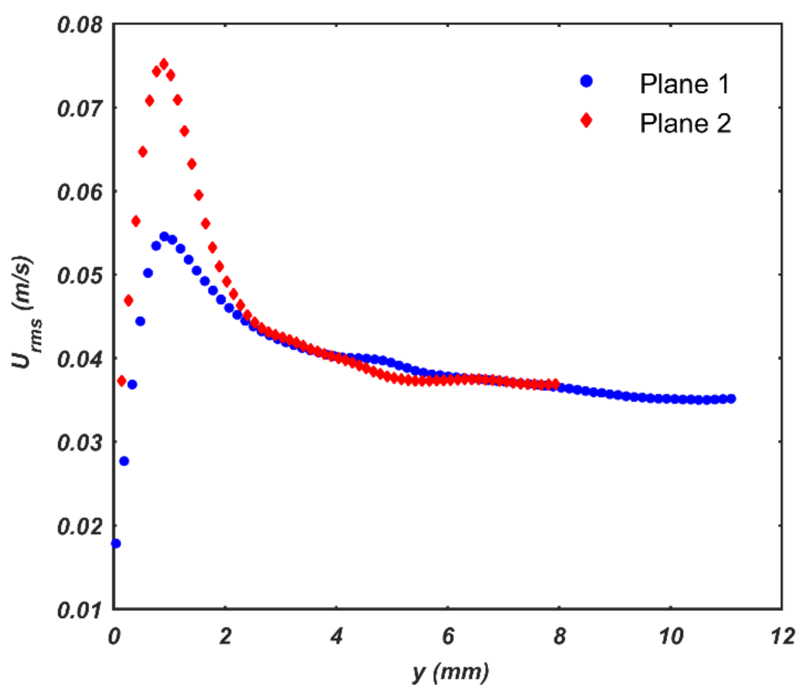

Figure 10-17 Axial turbulence intensity measured at U_s=0.35 m/s (bed A, planes 1 and 2)

Axial turbulence intensity data for flow at U_s=0.18 and 0.35 m/s over the bed A are reported in Figure 10-16 and Figure 10-17, respectively. At the superficial velocity of 0.18 m/s, higher level of turbulence intensity was registered near the pipe wall (plane 1). However, the superficial velocity of 0.35 m/s, the turbulence intensity was greater near the bed interface (plane 2). This behavior is the same as that of the Reynolds shear stress, and similar reasoning can be used to explain the increase in axial turbulence intensity by the bedload transport of particles and transition of flow from smooth to the rough flow regime.

Finally, we report the radial turbulence intensity data in Figure 10-18 and Figure 10-19. The radial turbulence intensity profiles at U_s=0.18 m/s shows a small difference for the flow along the planes 1 and 2. On the other hand, at U_s=0.35 m/s, it appears that radial intensity is enhanced along the plane 2 (i.e. bed interface). The reason can be attributed to the bedload transport of particles and the change in flow regime. Again, here the increase in the turbulent kinetic energy manifests itself in the form of a reduction in the mean kinetic energy.

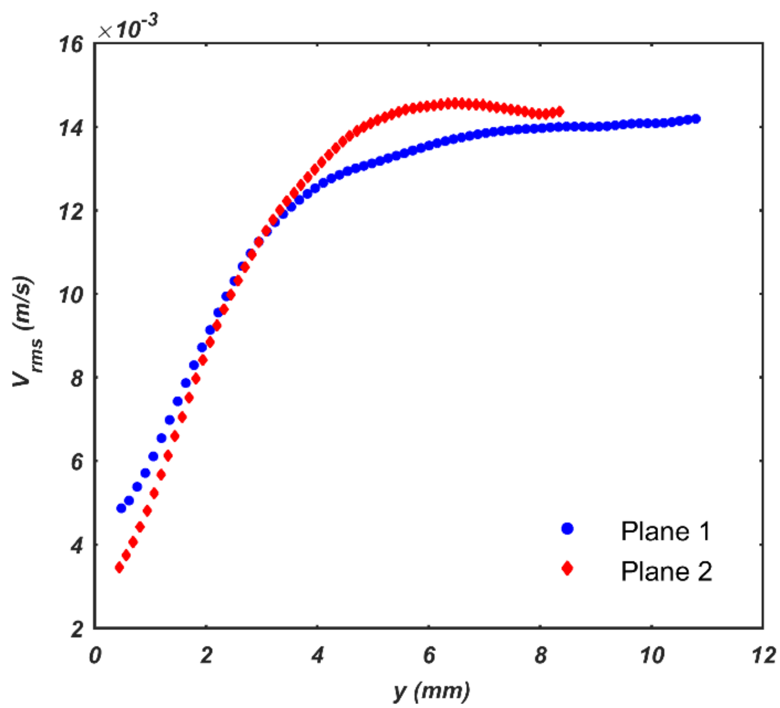

Figure 10-18 Radial turbulence intensity measured at U_s=0.18 m/s (bed A , planes 1 and 2)

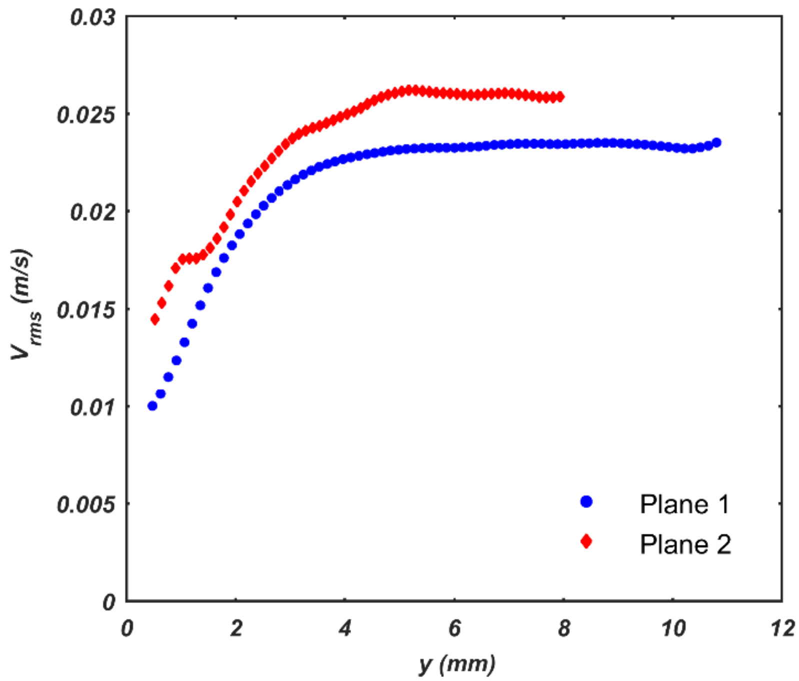

Figure 10-19 Radial turbulence intensity measured at U_s=0.35 m/s (bed A , planes 1 and 2)

10.4.2.2. Characteristics of Turbulent Flow Over the Bed B

In this section, we consider the same quantities as the previous section, only for the bed B. First, we look at Reynolds shear stress data at two different flow velocities of 0.18 and 0.3 m/s. Figure 10-20 compares the measured Reynolds stress data over the planes 1 and 2 at U_s=0.18 m/s. It appears that Reynolds stress is higher over the bed interface (plane 2) comparing to the inner pipe wall (plane 1). This is a changing behavior comparing to the bed A, where the Reynolds stress was higher along the inner pipe wall. Most likely this happens because the bed B is occupying most of the narrow gap between the inner pipe and outer pipe, and hence, the flow velocity increases over the bed. It is well-known from previous studies that rough walls generate more turbulence (Krogstad et al. 1992) because the flow has to overcome the boundary resistance. Hence, the behavior of any boundary regarding the production of turbulent kinetic energy is primarily a function of the roughness Reynolds number. The increase in the Reynolds stress over the sand bed compared to that of pipe wall (as shown in Figure 10-20) could also be caused by the change of the flow regime near the bed interface. The effect of boundary condition (i.e. rough vs. smooth wall) on the turbulence was discussed in chapter 9.

Reynolds stress profiles at 0.3 m/s for the bed B is reported in Figure 10-21. The Reynolds stress is significantly higher along the plane over the bed interface. The Reynolds stress was greater over the bed interface at the lower superficial velocity (0.18 m/s) as well. However, the gap between stress profiles at these two cross sections becomes bigger at the higher superficial velocity. In another word, increasing the flow velocity from 0.18 to 0.3 m/s causes the Reynolds stress to increase more along the bed interface compared to the inner pipe wall. This behavior can be attributed to the bedload transport of particle at the higher flow velocity.

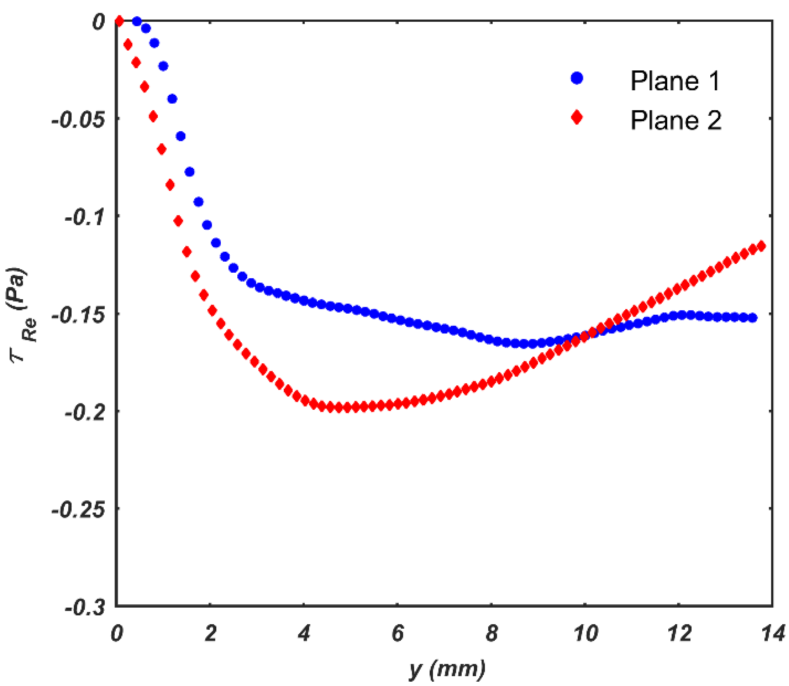

Figure 10-20 Reynolds shear stress profiles measured at U_s=0.18 m/s (bed B, planes 1 and 2)

To see if the balance of mean and turbulent kinetic energy argument used before also applies in this case, we need to look at the average velocity profiles (representative of the mean kinetic energy). Figure 10-22 and Figure 10-23 compare the average flow velocity profiles over the Plane 1 and 2 at superficial flow velocities of 0.18 and 0.3 m/s, respectively. At the lower superficial velocity, near wall velocity profiles on the Plane 1 and 2 are close to each other. However, at the higher superficial velocity, the mean velocity is slightly higher along the plane 1. This confirms that mean kinetic energy has decreased (or did not increase as much as) along the plane 2 comparing to the plane 1 when superficial velocity was increased from 0.18 to 0.3

m/s. The increase in boundary roughness and bedload transport of particles are accountable for the enhancement of turbulence production near the bed.

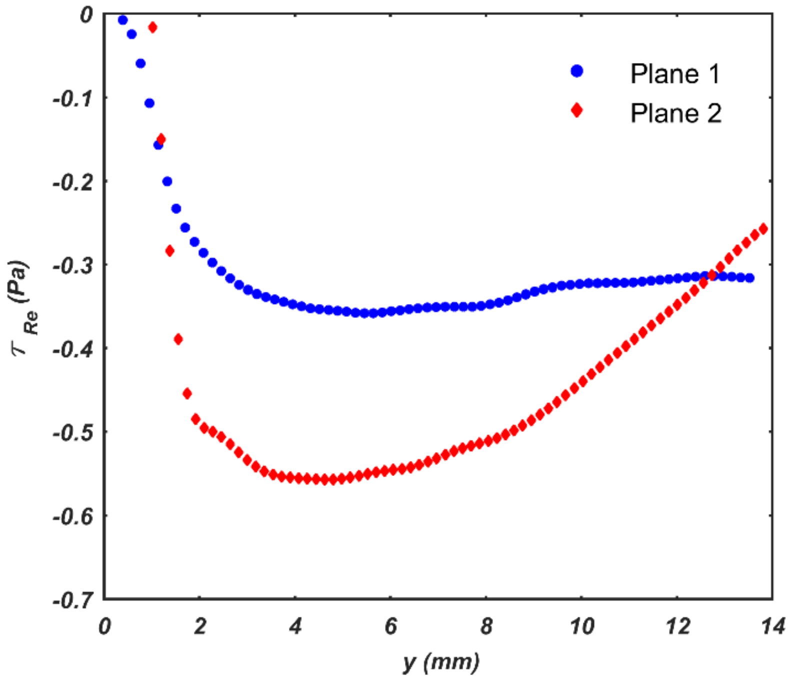

Figure 10-21 Reynolds shear stress profiles measured at U_s=0.3 m/s (bed B , planes 1 and 2)

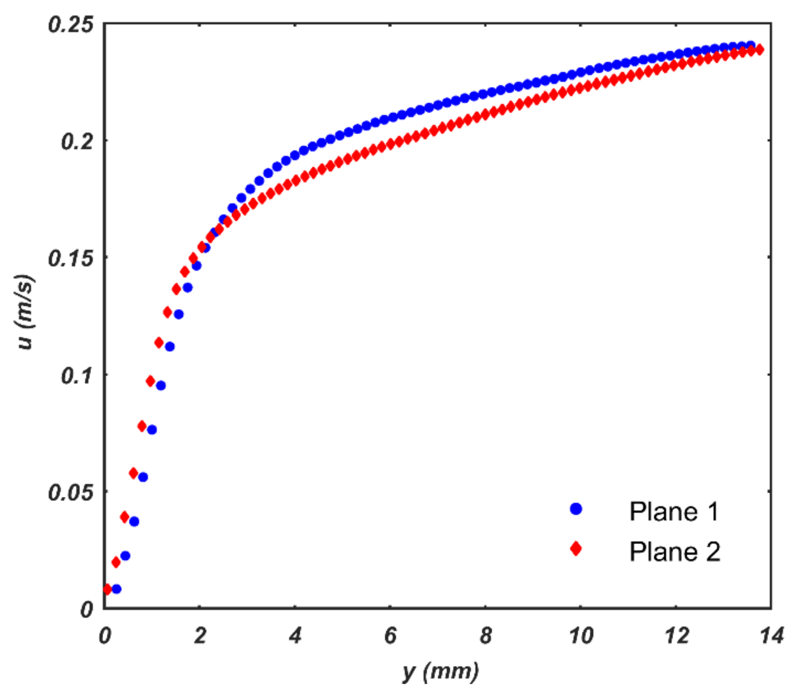

Figure 10-22 Mean velocity profiles measured at U_s=0.18 m/s (bed B , planes 1 and 2)

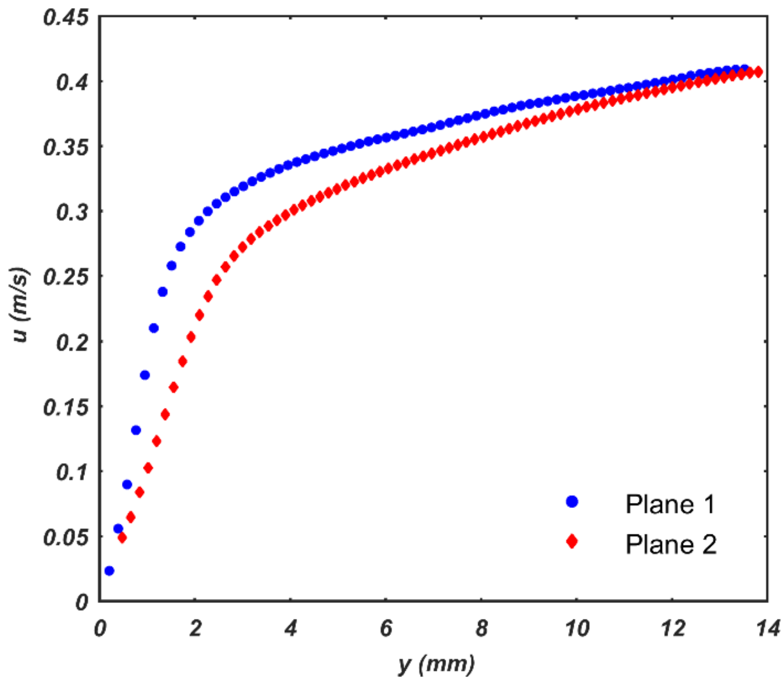

Figure 10-23 Mean velocity profiles measured at U_s=0.3 m/s (bed B , planes 1 and 2)

Profiles of axial turbulence intensities over the bed B are reported in Figure 10-24 and Figure 10-25 for U_s=0.18 and 0.3 m/s. At a superficial velocity of 0.18m/s, both profiles (along with the planes 1 and 2) show very similar values of axial turbulence intensity. This contradicts to the observations from bed A, where the turbulence intensities were higher along the pipe wall (plane 1). This implies that increasing the bed height causes the flow to become more uniform in the annulus. At higher superficial velocity, where the bed erosion takes place, we observe a greater level of axial turbulence intensity near the bed interface comparing to the pipe wall. This increase could be caused by the added roughness height induced by the moving particles. Due to added roughness, the fluid dissipates more energy to overcome the roughness. The consumed energy contributes to the turbulent kinetic energy production and manifests itself in the form of an increase in the flow turbulence.

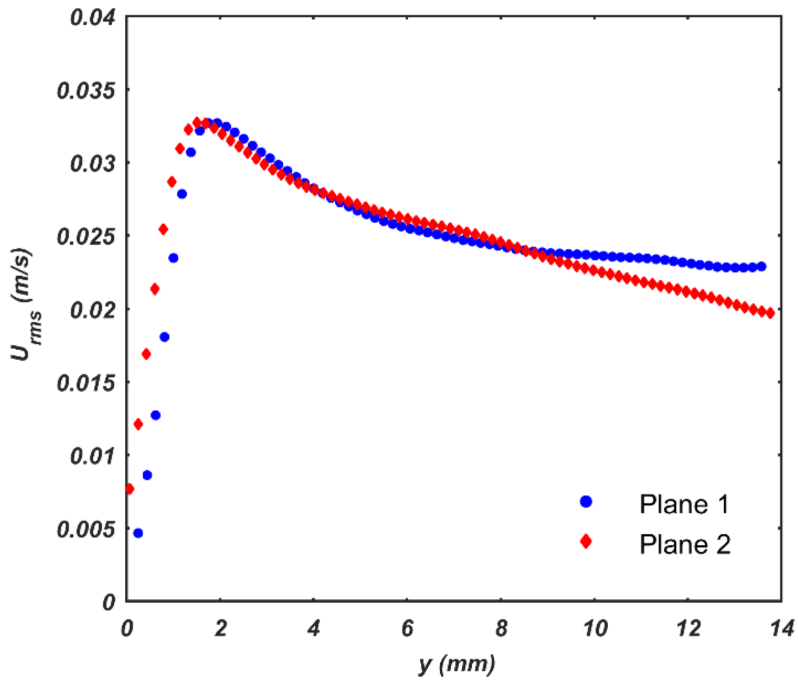

Figure 10-24 Axial turbulence intensity profiles measured at U_s=0.18 m/s (bed B , planes 1 and 2)

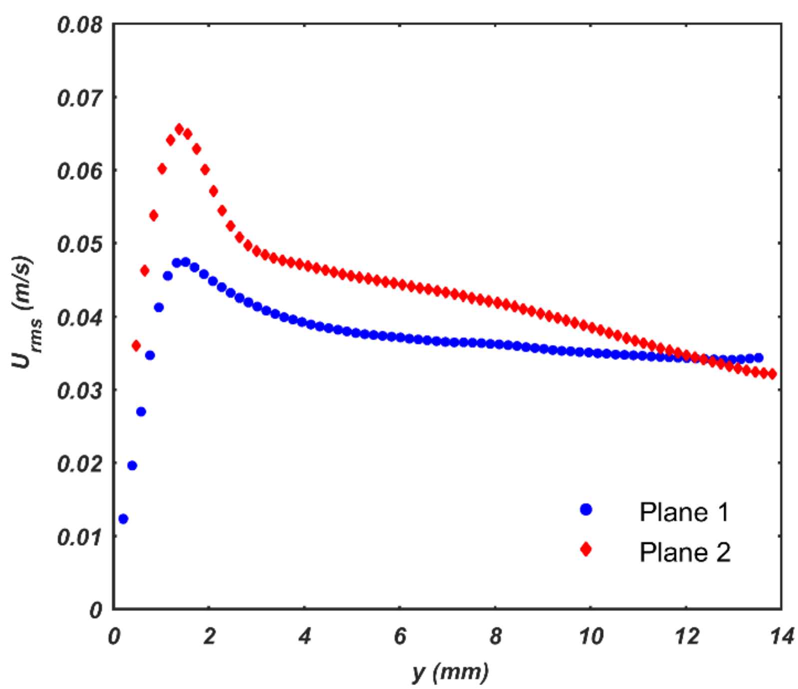

Figure 10-25 Axial turbulence intensity profiles measured at U_s=0.3 m/s (bed B, planes 1 and 2)

Finally, we compare the radial turbulence intensity profiles over the bed B at the two fluid superficial velocities of 0.18 and 0.3 m/s in Figure 10-26 and Figure 10-27, respectively. At a superficial fluid velocity of 0.18 m/s, where the bed is stationary, and no particle moves along the bed, there is slightly higher radial turbulence intensity over the bed comparing to that of the inner pipe wall. This is consistent with the observations about the Reynolds stress and the axial intensity profiles. At the superficial velocity of 0.3 m/s, however, the radial intensity is higher at the bed interface than that of inner pipe wall by a more noticeable margin. This confirms our earlier claim that bedload transport of particles in an eccentric annulus enhances the production of turbulence that comes at the cost of a reduction in the mean kinetic energy.

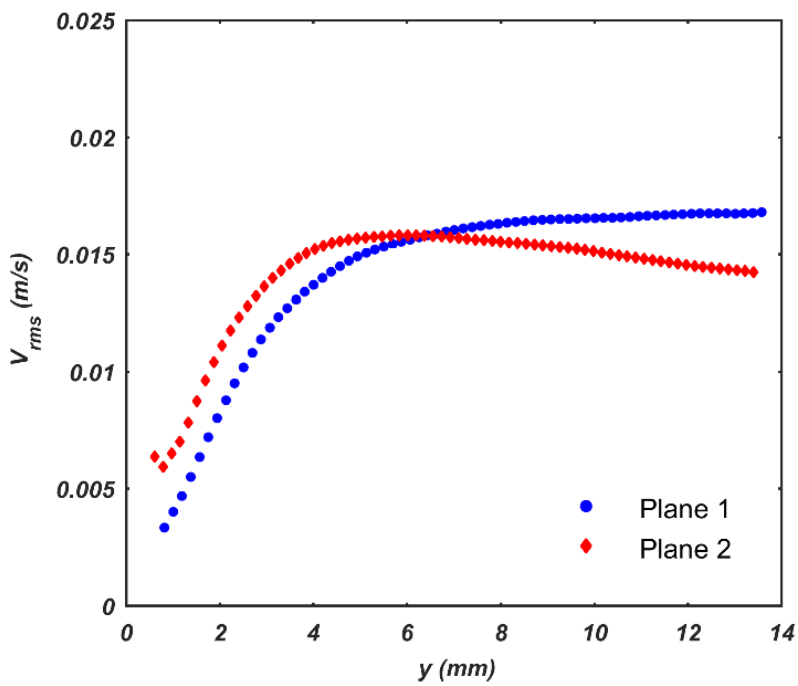

Figure 10-26 Radial turbulence intensity profiles measured at U_s=0.18 m/s (bed B and planes 1 and 2)

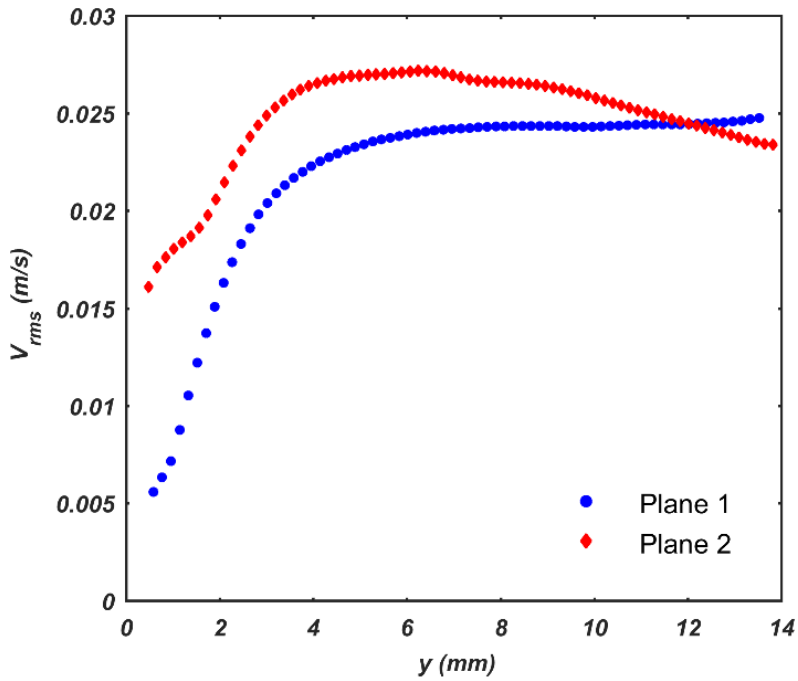

Figure 10-27 Radial turbulence intensity profiles measured at U_s=0.3 m/s (bed B and planes 1 and 2)

10.4.2.3. Characteristics of Turbulent Flow Over the Bed C

The bed C is the thickest bed tested in this study. The bed was thick enough to bury the inner pipe in solids completely. The Reynolds stress profiles measured over this bed are reported in Figure 10-28 and Figure 10-29. The data here point out the fact that there is a higher level of turbulence along the bed interface (plane 2). Unlike the other two beds (A and B) where measurements along the plane 1 were over the inner pipe wall and the measurements along the Plane 2 were over the bed interface, in bed C all measurements in planes 1 and 2 are over the bed interface. Reynolds stress was higher along the plane 2 because the gap between outer pipe wall and the bed interface along this plane was much smaller than the difference between the outer pipe wall of the annulus and the bed interface along plane 1. Therefore, variables such as velocity and Reynolds stress reach their peaks at y values much smaller along the plane 2 than that of 1. On the other hand, the data along the plane 1 reach their peaks at distances further away from the bed. Therefore, near the bed interfaces, plane 2 exhibits higher Reynolds stress and velocity.

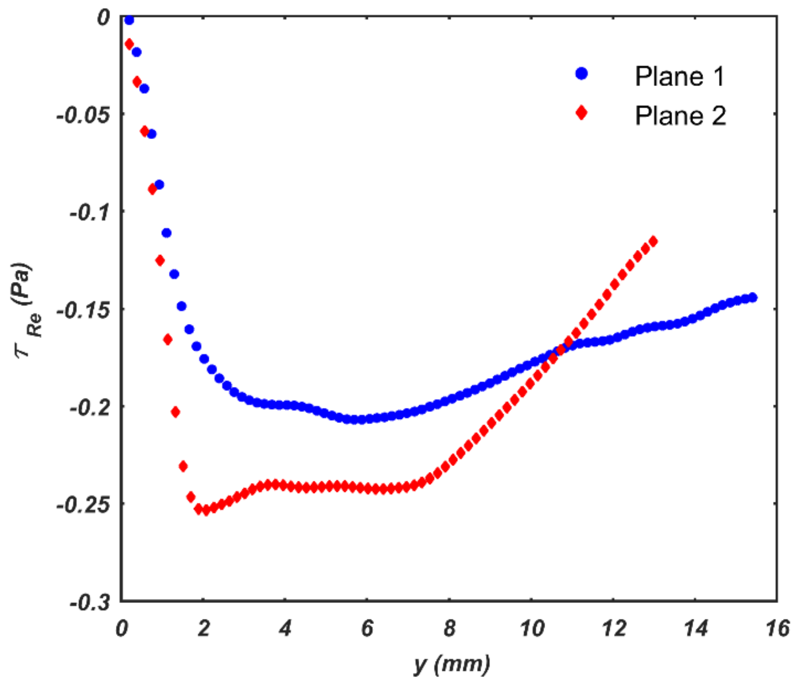

Figure 10-28 Reynolds stress profiles measured at U_s=0.18 m/s (bed C , planes 1 and 2)

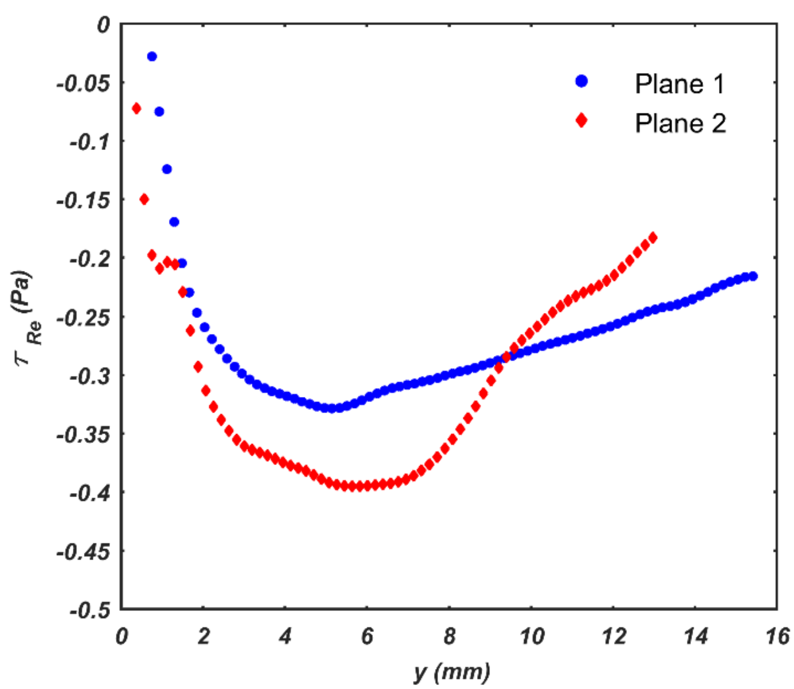

Figure 10-29 Reynolds stress profiles measured at U_s=0.22 m/s (bed C, planes 1 and 2)

Comparison of the local mean velocity profiles over the bed C at superficial velocities of 0.18 m/s and 0.30 m/s in Figure 10-30 and Figure 10-31, respectively, shows that there was a slight reduction in the difference between the local velocities at the higher flow rate. However, since both cases were measured over the bed (i.e., no flow on the pipe wall), we cannot comment on whether there is a reduction or an increase in the turbulence by bedload transport in this case. The local velocity shows slightly higher values along the plane 2. Perhaps, this is mainly because the gap is smaller along the plane 2, and hence, the local velocity reaches its maximum at smaller y values compared to the plane 1.

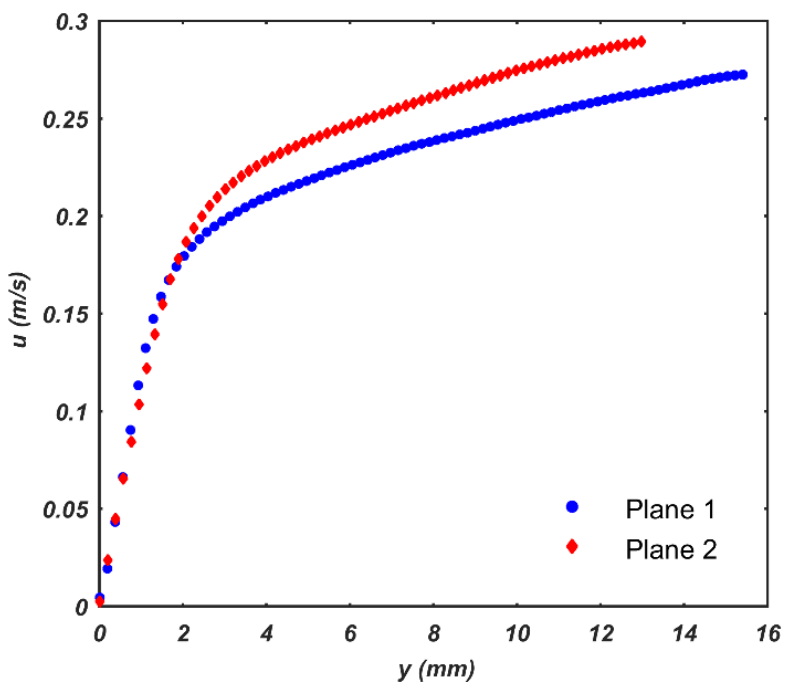

Figure 10-30 Mean velocity profiles measured at U_s=0.18 m/s (bed C , planes 1 and 2)

Figure 10-33 and Figure 10-34 reports the axial turbulence intensity profiles over the bed C at superficial velocities of 0.18 m/s and 0.22 m/s, respectively. The axial turbulence intensity is slightly higher along the plane 2 for both cases. However, the difference is small.

Finally, we report the radial turbulence intensity profiles over the bed C at superficial velocities of 0.18 m/s and 0.22 m/s, in Figure 10-34 and Figure 10-35, respectively. Consistent with the Reynolds shear stress and the axial turbulence intensity profiles, there is a higher level of radial turbulence intensity along the plane 2 for the flow at both superficial velocities.

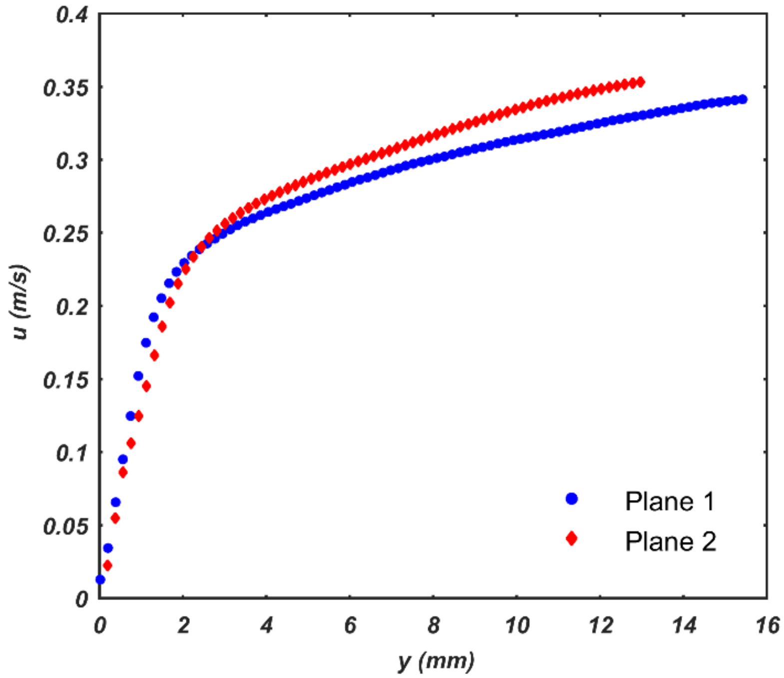

Figure 10-31 Mean velocity profiles measured at U_s=0.22 m/s (bed C , planes 1 and 2)

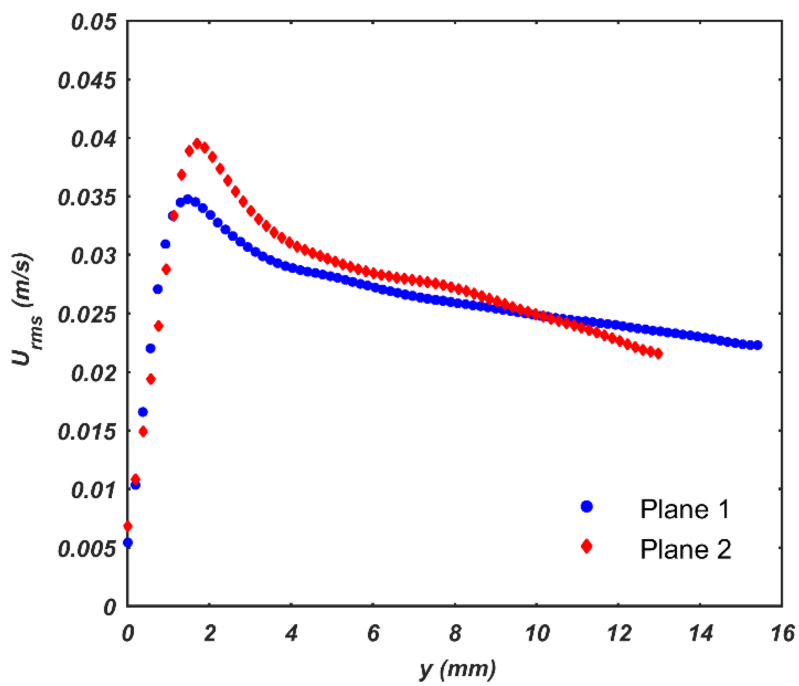

Figure 10-32 Axial turbulence intensity profiles measured at U_s=0.18 m/s (bed C , planes 1 and 2)

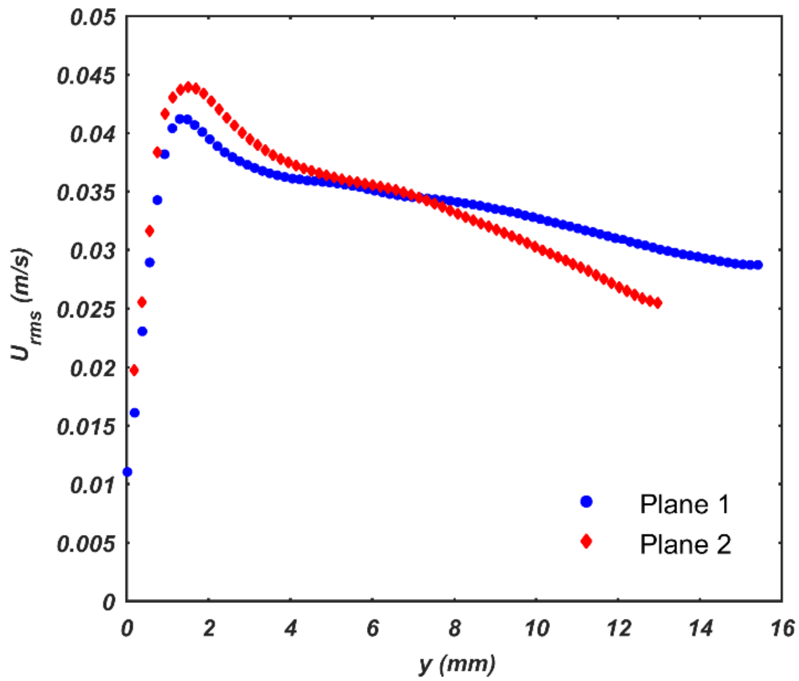

Figure 10-33 Axial turbulence intensity profiles measured at U_s=0.22 m/s (bed C , planes 1 and 2)

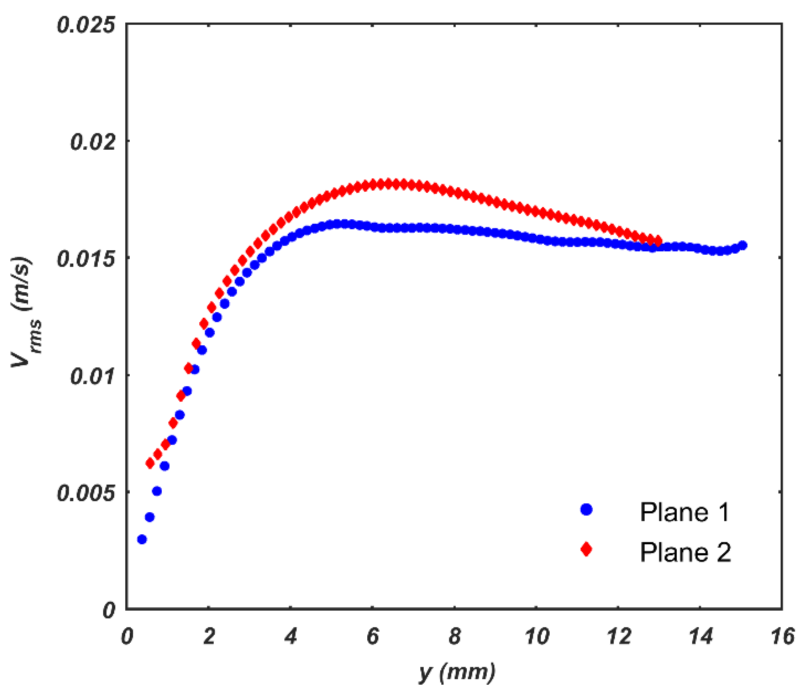

Figure 10-34 Radial turbulence intensity profiles measured at U_s=0.18 m/s (bed C and planes 1 and 2)

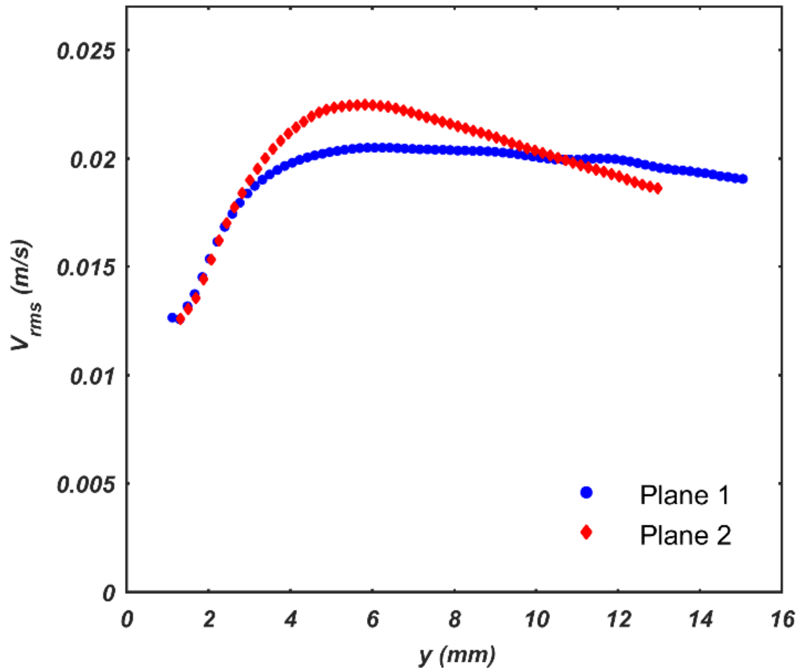

Figure 10-35 Radial turbulence intensity profiles measured at U_s=0.22 m/s (bed C and planes 1 and 2)

10.5. Conclusions

The turbulent flow of water over sand beds of 3 different heights in a fully eccentric horizontal annulus was investigated. The experiments focused on the characteristics of the turbulent flow over the stationary bed and when the bed material starts moving in the form of a moving layer (i.e. bedload transport).

Instantaneous fluid velocity was measured along the two cross-sections of the annulus (Plane 1 and 2) and over the beds of three different heights (Bed A, B, and C). The ratio of the instantaneous local velocity to the mean (time-averaged) velocity indicated that the effective fluid velocity near the bed interface might be several times higher than the time average velocity. Therefore, one should consider the effect of turbulence for more accurate modeling of the bed erosion and sediment transport processes.

Comparing to the no bed case, the presence of the bed height caused Reynolds stress and axial turbulent intensity to increase. However, for the smallest bed height case (Bed A), the axial turbulence intensity was less than the no bed case. The radial intensity profiles over the beds showed a slight decrease as compared to that of the no bed case.

The Reynolds shear stress, the axial and radial turbulence intensities were all found to be increasing with the increasing sand bed height.

We also compare the data collected near the inner pipe wall (i.e. plane 1) and near the bed interface (i.e. plane 2) of the annulus. Reynolds stress data showed a dependency on the height of the sand bed in the annulus. For bed A, flow turbulence was higher along plane 1 for velocities less than the critical flow rate. However, at the critical flow rate turbulence production over the bed was enhances by bedload transport of particles. Hence, Reynolds normal and shear stress were higher along plane 2. For beds B and C, Reynolds stresses were greater along plane two at all the flow rates. Bedload transport of particles was found to enhance production of Reynolds stresses over the bed interface.

10.6. References

Best, J., Bennett, S., Bridge, J. et al. (1997). Turbulence modulation and particle velocities over flat sand beds at low transport rates. Journal of Hydraulic Engineering-Asce **123**(12): 1118-1129, J Hydraul Eng-Asce, DOI: c 10.1061/(Asce)0733-9429(1997)123:12(1118).

Bigillon, F., Couronne, G., Champagne, J. Y. et al. (2006). Investigation of flow hydrodynamics under equilibrium bedload transport conditions using PIV. River Flow 2006, Vols 1 and 2: 859-865, Proc Monogr Eng Wate, DOI: ://WOS:000241916500090.

Bizhani, M. and Kuru, E. (2017). Critical Review of Mechanistic and Empirical (Semi-Mechanistic) Models for Particle Removal from Sand Bed Deposits in Horizontal Annuli by Using Water. SPE Journal **In press**.

Bizhani, M. and Kuru, E. (2017). Critical Review of Mechanistic and Empirical (Semi-Mechanistic) Models for Particle Removal from Sand Bed Deposits in Horizontal Annuli by Using Water. SPE Journal, SPE-187948-PA, In press.

Bizhani, M. and Kuru, E. (2017). Effect of Sand Bed Deposits on the Characteristics of Turbulent Flow of Water in Horizontal Annuli ASME fluid engineering, Paper under review.

Bizhani, M., Kuru, E. and Ghaemi, S. (2016). Effect of Near Wall Turbulence on the Particle Removal from Bed Deposits in Horizontal Wells. Proceedings of the Asme 35th International Conference on Ocean, Offshore and Arctic Engineering , 2016, Vol 8.

Bizhani, M., Rodriguez Corredor, F. E. and Kuru, E. (2016). Quantitative Evaluation of Critical Conditions Required for Effective Hole Cleaning in Coiled-Tubing Drilling of Horizontal Wells. **SPE** Drilling & Completion **31**(3): 188-199, SPE-174404-PA, DOI: 10.2118/174404-PA.

Carbonneau, P. E. and Bergeron, N. E. (2000). The effect of bedload transport on mean and turbulent flow properties. Geomorphology **35**(3-4): 267-278, Geomorphology, DOI: g10.1016/S0169-555x(00)00046-5.

Chan-Braun, C., García-Villalba, M. and Uhlmann, M. (2011). Force and torque acting on particles in a transitionally rough open-channel flow. Journal of Fluid Mechanics **684**: 441-474, DOI: 10.1017/jfm.2011.311.

Davies, J. T. (1987). Calculation of Critical Velocities to Maintain Solids in Suspension in Horizontal Pipes. Chemical Engineering Science **42**(7): 1667-1670, Chem Eng Sci, DOI: 10.1016/0009-2509(87)80171-9.

Diplas, P., Dancey, C. L., Celik, A. O. et al. (2008). The Role of Impulse on the Initiation of Particle Movement Under Turbulent Flow Conditions. Science **322**(5902): 717-720, Science, DOI: 10.1126/science.1158954.

Duan, M., Miska, S. Z., Yu, M. et al. (2007). Critical Conditions for Effective Sand-Sized Solids Transport in Horizontal and High-Angle Wells. SPE Production and Operations Symposium Oklahoma City, Oklahoma, USA, 31 March-3 April 2007., SPE-106707-MS,DOI: 10.2118/106707-MS.

Duan, M. Q., Miska, S., Yu, M. J., Takach, N., Ahmed, R., Zettner, C. (2009). Critical Conditions for Effective Sand-Sized-Solids Transport in Horizontal and High-Angle Wells. SPE Drilling & Completion **24**(2): 229-238, **SPE** Drill Completion, DOI: 10.2118/104192-PA.

Escudier, M. P. and Gouldson, I. W. (1995). Concentric Annular-Flow with Centerbody Rotation of a Newtonian and a Shear-Thinning Liquid. International Journal of Heat and Fluid Flow **16**(3): 156-162, Int J Heat Fluid Fl, DOI: 10.1016/0142-727x(95)00012-F.

Ghaemi, S., Rafati, S.,Bizhani, M., Kuru, E. (2015). Turbulent structure at the midsection of an annular flow. Physics of Fluids **27**(10): 105102, DOI: http://dx.doi.org/10.1063/1.4932109.

Heyman, J., Mettra, F., Ma, H. B. et al. (2013). Statistics of bedload transport over steep slopes: Separation of time scales and collective motion. Geophysical Research Letters **40**(1): 128-133, Geophys Res Lett, DOI: 10.1029/2012gl054280.

Japper-Jaafar, A., Escudier, M. P. and Poole, R. J. (2010). Laminar, transitional and turbulent annular flow of drag-reducing polymer solutions. Journal of Non-Newtonian Fluid Mechanics **165**(19-20): 1357-1372, J Non-Newton Fluid, DOI: 10.1016/j.jnnfm.2010.07.001.

Kelessidis, V. C. and Bandelis, G. E. (2004a). Flow Patterns and Minimum Suspension Velocity for Efficient Cuttings Transport in Horizontal and Deviated Wells in Coiled-Tubing Drilling. **SPE** Drilling & Completion **19**(4): 213-227, SPE-81746-PA, DOI: 10.2118/81746-PA.

Krogstad, P. A., Antonia, R. A. and Browne, L. W. B. (1992). Comparison between Rough-Wall and Smooth-Wall Turbulent Boundary-Layers. Journal of Fluid Mechanics **245**: 599-617, J Fluid Mech, DOI: 10.1017/S0022112092000594.

Kundu, P. K., Cohen, I. M. and Dowling, D. R. (2012). Fluid Mechanics, 5th Edition. Fluid Mechanics, 5th Edition: 1-891.

Li, J. and Luft, B. (2014a). Overview Solids Transport Study and Application in Oil-Gas Industry-Theoretical Work, IPTC-17832-MS,DOI: 10.2523/IPTC-17832-MS.

Li, J. and Luft, B. (2014b). Overview of Solids Transport Studies and Applications in Oil and Gas Industry - Experimental Work, SPE-171285-MS,DOI: 10.2118/171285-MS.

Melling, A. (1997). Tracer particles and seeding for particle image velocimetry. Measurement Science & Technology **8**(12): 1406-1416, Meas Sci Technol, DOI: 10.1088/0957-0233/8/12/005.

Miyazaki, K., Chen, G. , Ymamoto, F., Ohta, J., Murai, Y., Horii, K. (1999). PIV measurement of particle motion in spiral gas-solid two-phase flow. Experimental Thermal and Fluid Science **19**(4): 194-203, Exp Therm Fluid Sci, DOI: 10.1016/S0894-1777(99)00020-5.

Nezu, I. and Sanjou, M. (2011). PIV and PTV measurements in hydro-sciences with focus on turbulent open-channel flows. Journal of Hydro-Environment Research **5**(4): 215-230, J Hydro-Environ Res, DOI: 10.1016/j.jher.2011.05.004.

Nouri, J. M., Umur, H. and Whitelaw, J. H. (1993). Flow of Newtonian and Non-Newtonian Fluids in Concentric and Eccentric Annuli. Journal of Fluid Mechanics **253**: 617-641, J Fluid Mech, DOI: 10.1017/S0022112093001922.

Pilehvari, A. A., Azar, J. J. and Shirazi, S. A. (1996). State-Of-The-Art Cuttings Transport in Horizontal Wellbores. International Conference on Horizontal Well Technology. Calgary, Alberta, Canada, 18-20 November, SPE-37079-MS,DOI: 10.2118/37079-MS.

Poole, R. J. (2010). Development-Length Requirements for Fully Developed Laminar Flow in Concentric Annuli. Journal of Fluids Engineering-Transactions of the **Asme 132**(6), J Fluid Eng-T Asme, DOI: 10.1115/1.4001694.

Ramadan, A., Skalle, P. and Johansen, S. T. (2003). A mechanistic model to determine the critical flow velocity required to initiate the movement of spherical bed particles in inclined channels. Chemical Engineering Science **58**(10): 2153-2163, DOI: 10.1016/S0009-2509(03)00061-7.

Rinoshika, A., Yan, F. and Kikuchi, M. (2012). Experimental study on particle fluctuation velocity of a horizontal pneumatic conveying near the minimum conveying velocity. International Journal of Multiphase Flow **40**: 126-135, DOI: https://doi.org/10.1016/j.ijmultiphaseflow.2011.11.007.

Schmeeckle, M. W. (2014). Numerical simulation of turbulence and sediment transport of medium sand. Journal of Geophysical Research-Earth Surface **119**(6): 1240-1262, J Geophys Res-Earth, DOI: 10.1002/2013jf002911.

Yan, F. and Rinoshika, A. (2011). Application of high-speed PIV and image processing to measuring particle velocity and concentration in a horizontal pneumatic conveying with dune model. Powder Technology **208**(1): 158-165, Powder Technol, DOI: 10.1016/j.powtec.2010.12.014.

Yan, F. and Rinoshika, A. (2012). Characteristics of particle velocity and concentration in a horizontal self-excited gas-solid two-phase pipe flow of using soft fins. International Journal of Multiphase Flow **41**: 68-76, Int J Multiphas Flow, DOI: 10.1016/j.ijmultiphaseflow.2012.01.004.

Zeinali, H., Toma, P. and Kuru, E. (2012). Effect of Near-Wall Turbulence on Selective Removal of Particles From Sand Beds Deposited in Pipelines. Journal of Energy Resources Technology-Transactions of the Asme **134**(2), J Energ Resour-Asme, DOI: Artn 021003 10.1115/1.4006041.

Zheng, Y., Rinoshika, A. and Yan, F. (2012). Multi-scale analysis on particle fluctuation velocity near the minimum pressure drop in a horizontal pneumatic conveying. Chemical Engineering Science **72**: 94-107, DOI: https://doi.org/10.1016/j.ces.2012.01.011.

10.7. Appendix A

Details of calculation related to hydraulic diameter and cross-sectional area of the annulus in the presence of a sand bed are presented in this appendix (See Figure A- 9-1for details) (Duan 2009).

Case 1: h<2r

$$S_o = 2R\, arccos(\frac{h-R}{R}) \qquad \textbf{Eq. (A- 10-1)}$$

$$S_i = 2r \arccos(\frac{h-r}{r}) \qquad \textbf{Eq. (A- 10-2)}$$

$$S_b = 2\sqrt{R^2-(R-h)^2} - 2\sqrt{r^2-(r-h)^2} \qquad \textbf{Eq. (A- 10-3)}$$

$$A_f = R^2\, arccos\left(\frac{h-R}{R}\right) + (R-h)\sqrt{R^2-(R-h)^2} - r^2 \arccos\left(\frac{h-r}{r}\right) - (r-h)\sqrt{r^2-(r-h)^2} \qquad \textbf{Eq. (A- 10-4)}$$

Case 2: h>2r

$$S_o = 2R\, arccos(\frac{h-R}{R}) \qquad \textbf{Eq. (A- 10-5)}$$

$$S_i = 0 \qquad \textbf{Eq. (A- 10-6)}$$

$$S_b = 2\sqrt{R^2 - (R-h)^2}$$ **Eq. (A- 10-7)**

$$A_f = R^2\, arccos\left(\frac{h-R}{R}\right) + (R-h)\sqrt{R^2-(R-h)^2}$$ **Eq. (A- 10-8)**

The hydraulic diameter is:

$$D_h = \frac{4A_f}{S_o + S_i + S_b}$$ **Eq. (A- 10-9)**

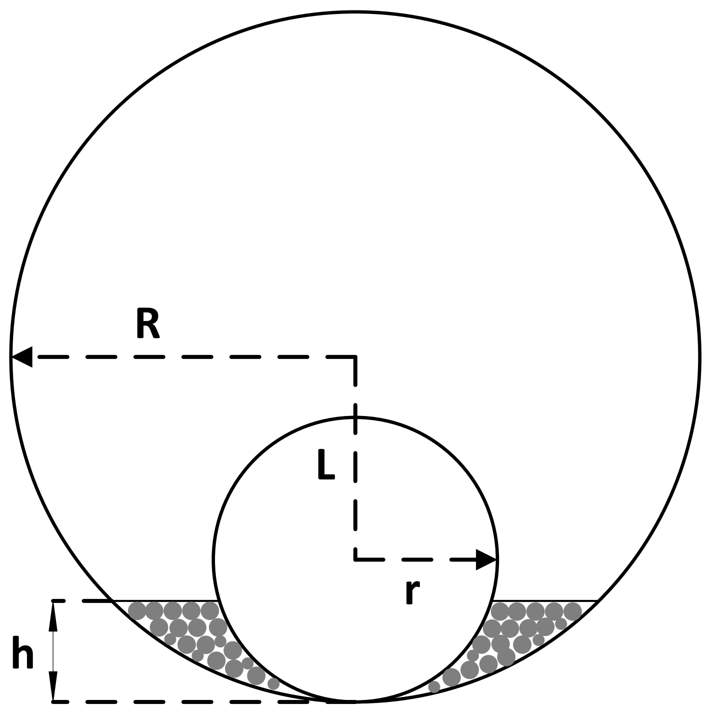

Figure A- 10-1 Illustration of dimensions used in calculations of cross section and hydraulic diameter

10.8. Appendix B

Additional Data for Velocity Profiles, Reynolds Stress, Axial Turbulence Intensity and Radial Turbulence Intensity are presented in this section.

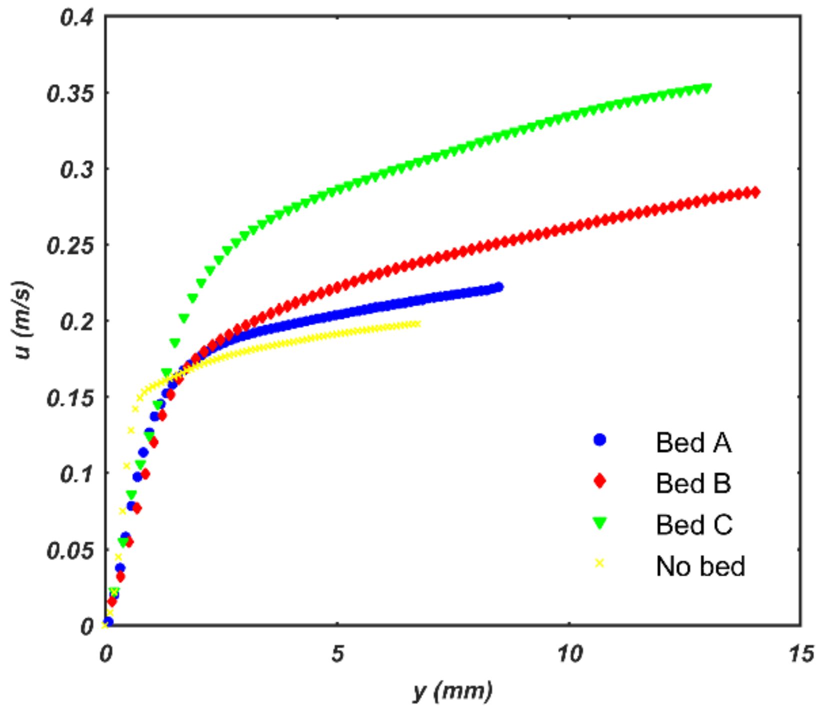

Figure 10-36 Profiles of time averaged fluid velocity measured at 79 liters/min

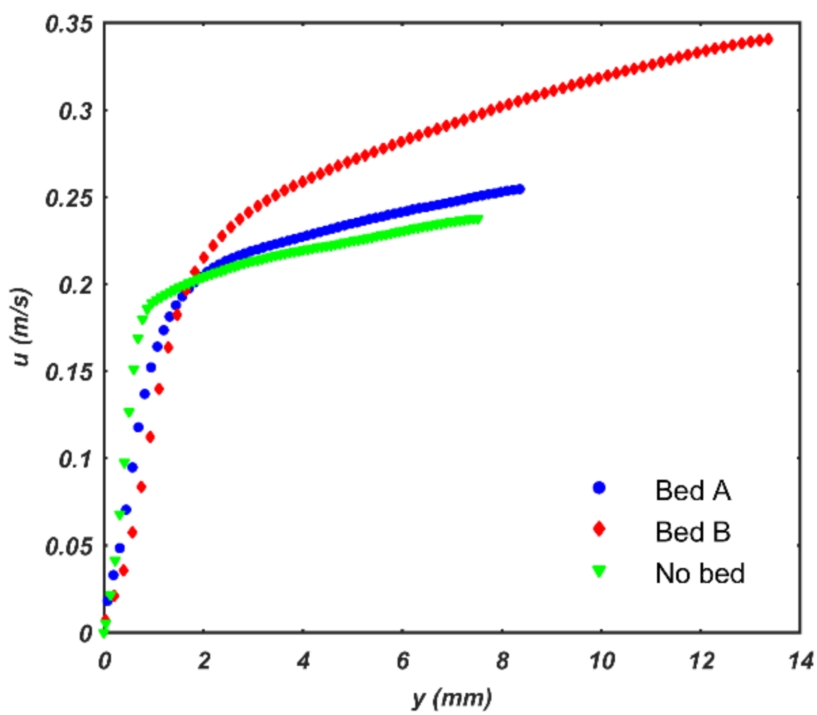

Figure 10-37 Profiles of time averaged fluid velocity measured at 94 liters/min

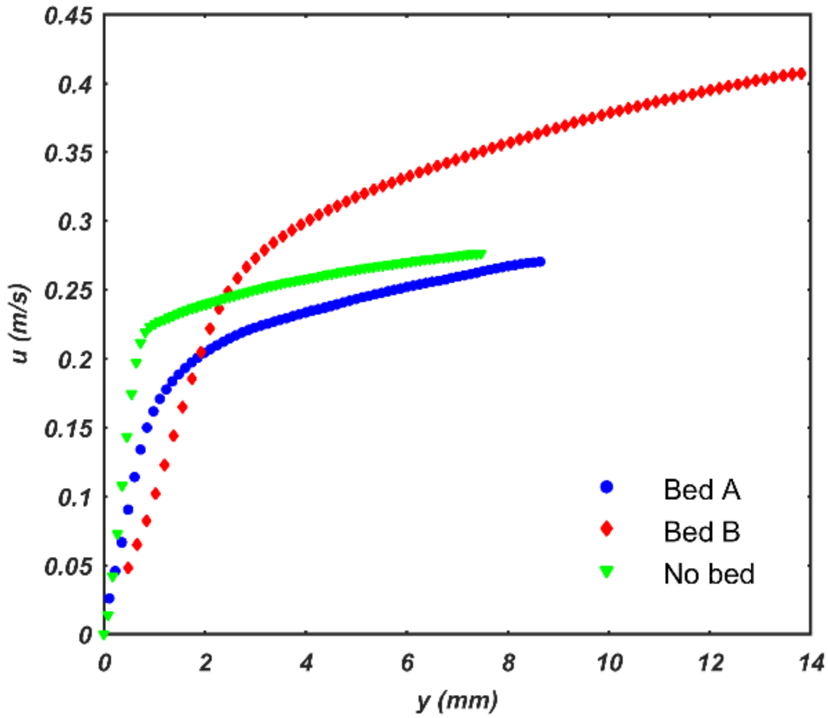

Figure 10-38 Profiles of time averaged fluid velocity measured at 109 liters/min

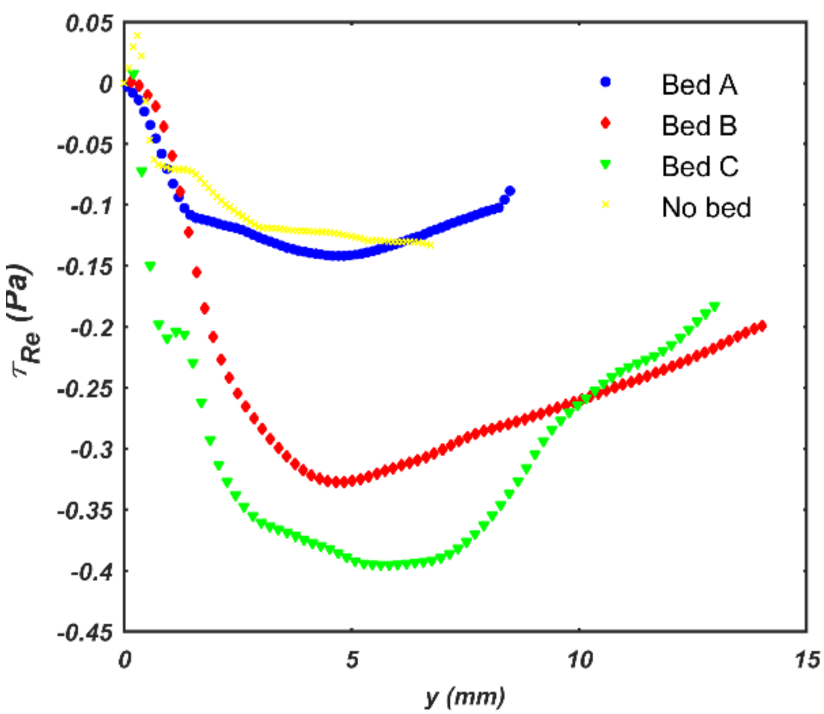

Figure 10-39 Profiles of Reynolds stress measured at 79 liters/min

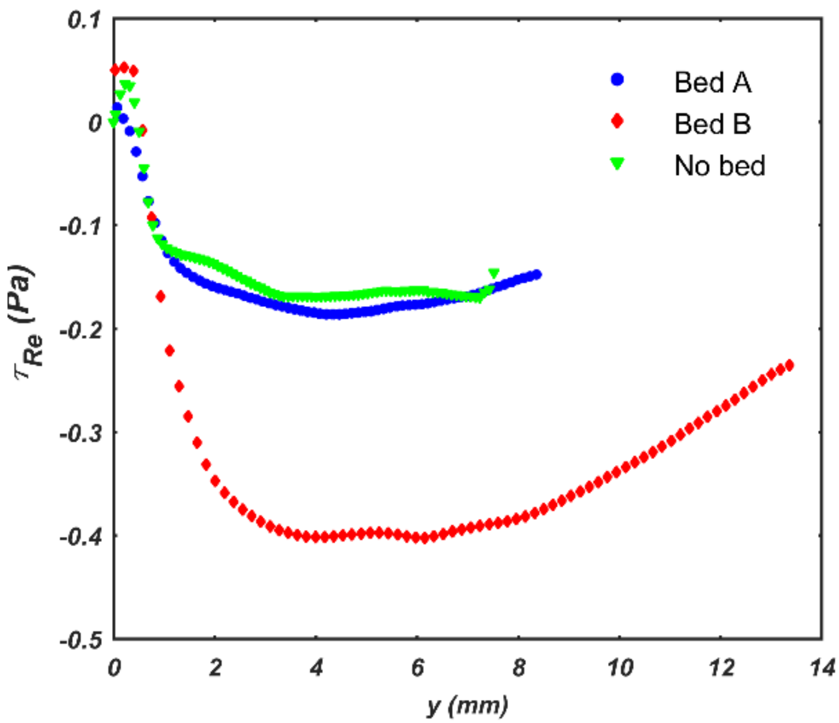

Figure 10-40 Profiles of Reynolds stress measured at 94 liters/min

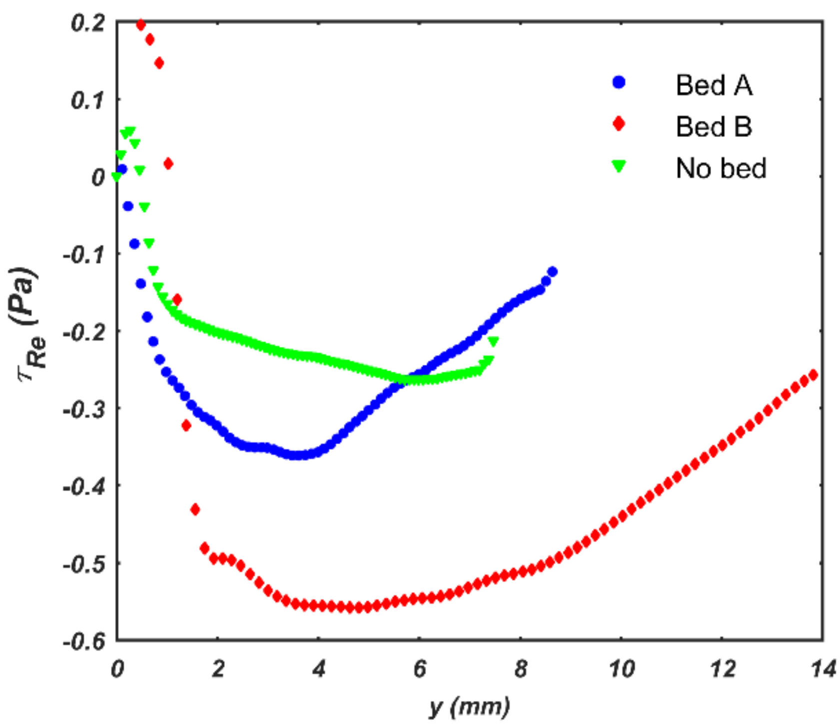

Figure 10-41 Profiles of Reynolds stress measured at 109 liters/min

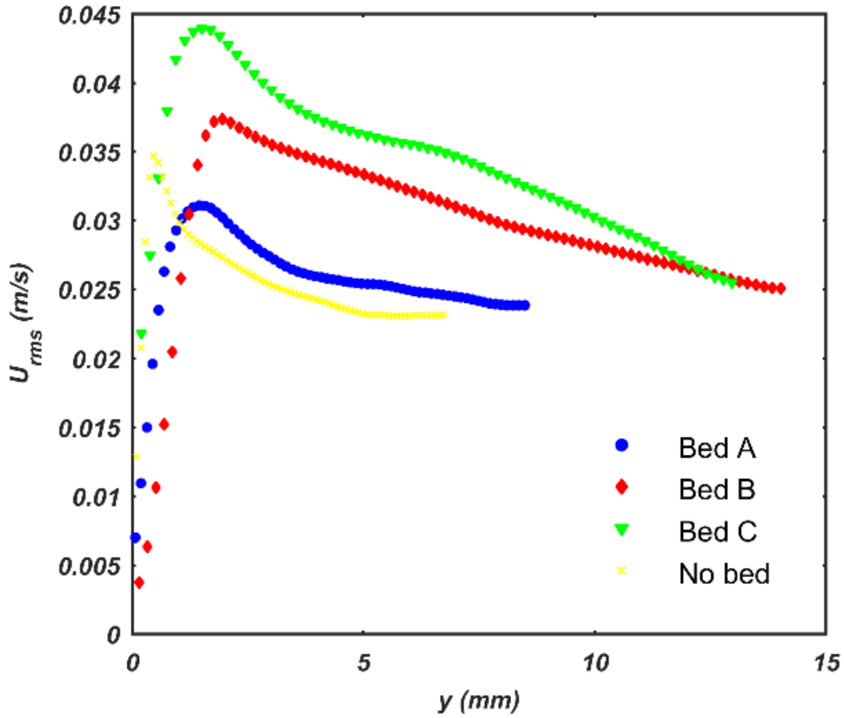

Figure 10-42 Profiles U_{rms} measured at 79 liters/min

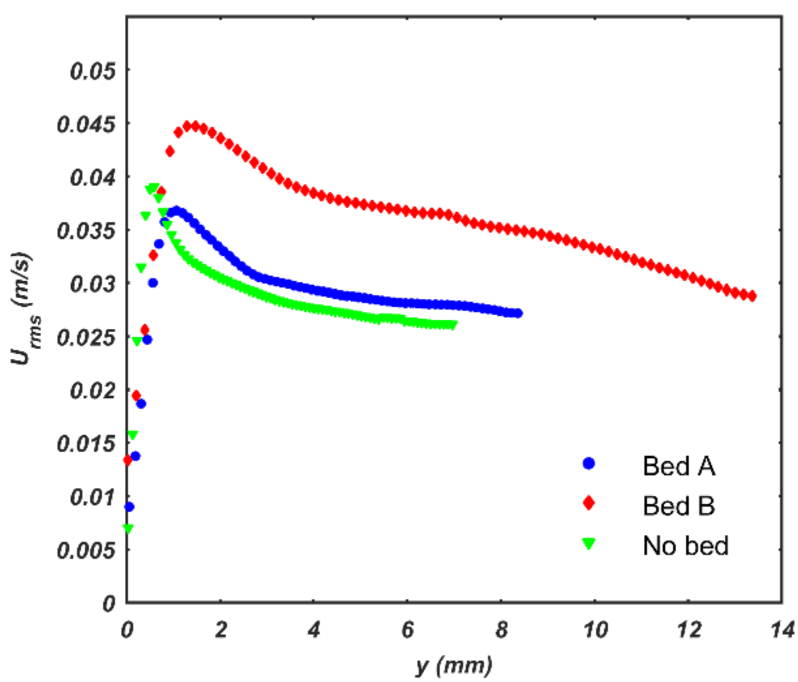

Figure 10-43 Profiles U_{rms} measured at 94 liters/min

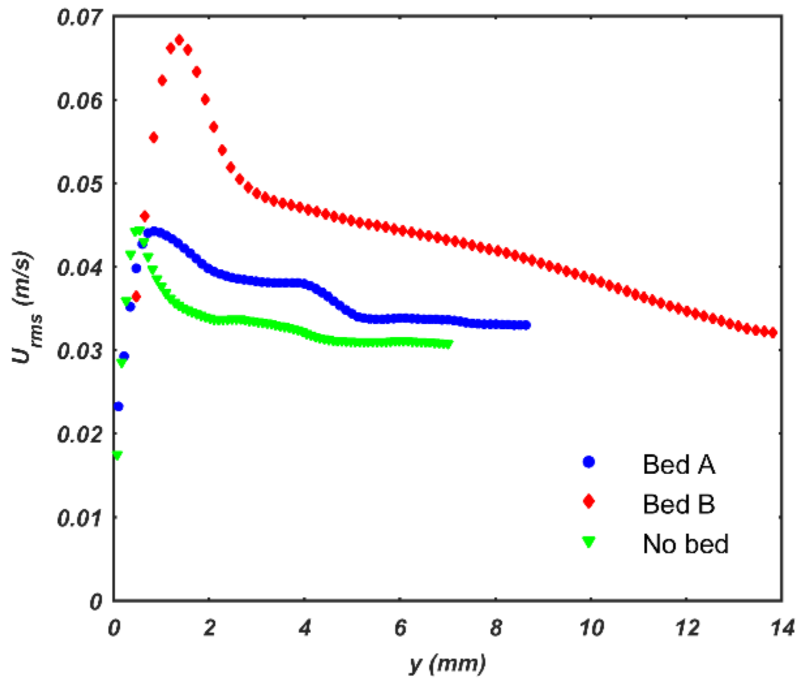

Figure 10-44 Profiles of U_{rms} measured at 109 liters/min

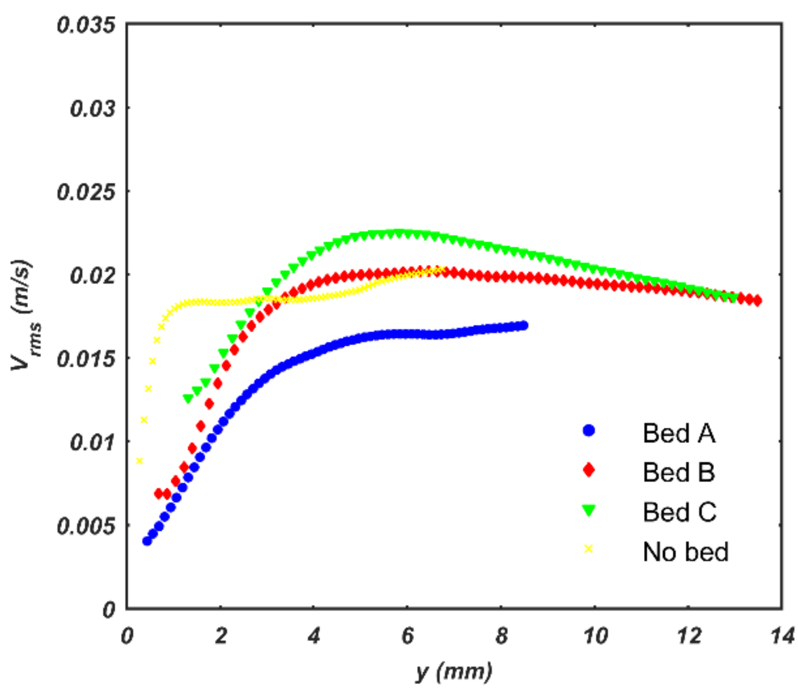

Figure 10-45 Profiles of V_{rms} measured at 79 liters/min

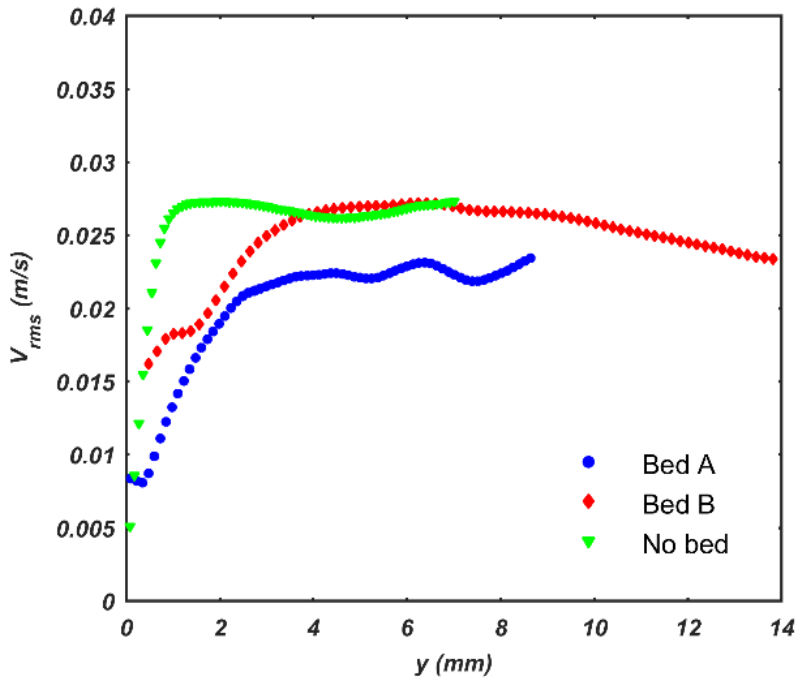

Figure 10-46 Profiles of V_{rms} measured at 109 liters/min

11. Turbulent flow of dilute polymer solutions over loose sand beds in eccentric annulus: an experimental study

In this chapter, we present and discuss the results of PIV experiments conducted for measuring the turbulent flow of polymer fluids over stationary sand beds in the eccentric annulus. The data have been collected for turbulent flow of 0.032% polymer at six different flow Reynolds numbers and three sand bed heights. The data are analyzed to assess the impact of bed surface roughness effect on the flow. Additionally, bedload transport of particles and its influence on the local roughness height is investigated.

11.1. Abstract

In this paper, we present results of experimental work on the turbulent flow of a weakly elastic dilute polymer solution over loose sand beds in an eccentric annulus. This problem is of particular interest to the oil industry. The flow was studied using Particle Image Velocimetry (PIV) technique. Instantaneous velocity profiles have been measured over three sand beds of different initial heights. The data are analyzed to investigate the role of surface roughness and bedload transport of particles on the universal velocity profiles near the sand bed interface. Additionally, measurements of Reynolds normal and shear stresses are reported as well.

Results have indicated the presence of the sand bed does not have any major impact on the velocity profiles in wall unit. Velocity data followed closely the linear law governing the viscous sublayer. In the logarithmic zone, there was an upward shift in the velocity profiles. On the other hand, velocity profiles fell short of the Virk's asymptote. Overall, our results show using polymer causes transition from smooth hydraulic condition to rough flow regime to be delayed by a significant margin.

The impact of the presence of the sand bed and bedload transport of sand bed on Reynolds shear and normal stresses also analyzed. Reynold stress does not show any significant dependency upon the movement of the bed material. Axial turbulence intensity, on the other

hand, showed a small shift in the peak due to movement of particles in the bed. The peak was located on the buffer layer at all the flow velocities tested. Redial turbulence intensity profiles revealed that bedload might enhance production of radial intensity slightly.

11.2. Introduction

Transport of sediment particles via non-Newtonian fluids is encountered in many industries. Examples of such flows include transport of mineral ores, transport of slurries to tailing ponds and in oil and gas sector. A specific case of these classes of flows is faced in the drilling industry. During drilling a long horizontal well, drilled solids tend to gravitate and settle in the form of a stationary sand bed. At later stages of the drilling operation, this stationary sand bed must be removed for successful completion of the well. Removal of the sand bed is typically performed by pumping the drilling fluid down the annulus formed between the borehole and the drill pipe. The flow is turbulent. Additionally, the drilling fluid is a mixture of different additives which almost always exhibit a strong non-Newtonian characteristic.

Turbulent flow of elastic polymer solutions can give rise to a phenomenon that is absent in the flow of Newtonian fluids. The literature offers numerous experimental and numerical works conducted to study the turbulent flow of both Newtonian and non-Newtonian fluids in annular geometry (Rehme 1974, Nouri et al. 1993, Escudier and Gouldson 1995, Chung et al. 2002, Japper-Jaafar et al. 2010, Ghaemi 2015). Certain changes as compared to the flow of Newtonian fluids have been observed during the turbulent flow of complex fluids. The first change to the flow caused by the shear thinning nature of the fluid is the upward shift of velocity profiles in wall units away from the Newtonian fluids curve in the logarithmic region (Pinho and Whitelaw 1990, Nouri et al. 1993, Escudier et al. 1995, Ptasinski et al. 2001, Japper-Jaafar et al. 2010). The upward shift depends on the degree of drag reduction and is bounded to a maximum shift represented by Virk's asymptote (Virk et al. 1970).

Thickening of the buffer layer has been associated with the flow of elastic polymer solutions (Lumley 1969, Wilson and Thomas 1985). Another artifact of polymer additives is the reduction of Reynolds stress (Pinho and Whitelaw 1990, Nouri et al. 1993, Warholic et al. 2001, Ptasinski et al. 2003, Paschkewitz et al. 2005, Japper-Jaafar et al. 2010). The term stress deficit was used by Ptasinski et al. (2003) to describe the generation of shear stress by polymer molecules. In the turbulent flow of such systems, the total shear stress is bigger than the summation of shear stress produced by the solvent and the turbulent stress. Hence, the term stress deficit is used to describe the polymer stress. Additionally, vortex inhibition and suppression of radial velocity fluctuations have also been associated with the turbulent flow of non-Newtonian fluids (Pinho and Whitelaw 1990, Nouri et al. 1993, Warholic et al. 2001, Kawaguchi et al. 2002, Japper-Jaafar et al. 2010).

The studies and the associated phenomenon that we mentioned in the previous paragraph was all conducted using a single phase flow. The presence of a secondary phase that interacts with the primary phase further adds to the complexity of the flow. Turbulent flow over a loose and erodible sand bed can be different from the single-phase flow. These types of flows are typically four-way coupled (Chan-Braun 2012). In another word, the solid phase modifies the flow of the primary phase and vice versa. Additionally, the particles also interact and further complicate the process. Depending on the flow rate, the particles in the bed may move in different modes of movement, and hence, change the rate of momentum exchange in the boundary layer.

One immediate impact of flow over a sand bed as compared to pipe or channel wall is the change in the surface roughness. The roughness of the boundary can significantly affect dynamics of the flow near the bed interface. Depending on whether the flow is hydraulically smooth or rough, velocity profiles and turbulence production changes accordingly. Additionally, movement of sand particles in bedload form further modifies the rate of momentum exchange which can manifest itself in the shape of an additional boundary roughness (Owen 1964, Best et al. 1997, Bigillon et al. 2006). Some researchers even suggest that bedload transport of sediments causes a reduction in von Karman constant (Best et al. 1997, Nikora and Goring 2000, Gaudio et al. 2010).

The literature has few studies to offer for the turbulent flow of Newtonian fluids over sand beds. On the other hand, there is no study on the turbulent flow of drag reducing polymer solutions over erodible sand beds. Part of the reason for the lack of data on the subject is the hardship in conducting experiments in this type of flows. With the advent of non-intrusive measurement techniques such as PIV, it is now possible to study such flows. In few recent studies PIV and Particle Tracking Velocimetry (PTV) have been used to study multiphase flow in channels and pipes (Miyazaki 1999, Bigillon et al. 2006, Yan and Rinoshika 2011, Rinoshika et al. 2012, Yan and Rinoshika 2012, Zeinali et al. 2012, Zheng et al. 2012). These studies show that optical technique can provide useful and valid results for these types of flows.

In this paper, we present results of an experimental work where PIV is utilized to study the turbulent flow of a weakly elastic polymer solution over sand beds of different initial heights in an eccentric annulus. The measurements were conducted at flow rates equal and less than the minimum flow rate required for eroding the bed. The erosion of the sand bed was done in bedload form (i.e. no particles suspension). Profiles of velocity, turbulent normal and shear stress are presented and further discussed. The sand particles that were used are natural quartz sand with a mean sieve size of 600 microns and density of 2650 kg/m^3.

The aim of the current study is to investigate the interaction of fluid-particle system during hole cleaning operations in the drilling industry. However, the results are general and can help in better understanding of the role of fluid's rheology in slurry transport. This paper follows two main agendas. The first is the impact of the presence of a secondary phase on the general aspects of flow in an eccentric annulus. The second important goal is how this can be used for optimization of hole cleaning operations in the drilling industry. The results in this paper are part of a more comprehensive study on the transport of solid particles by fluid in the annulus. The same survey was also conducted using water as the base fluid.

11.3. Experimental procedure

A large-scale flow loop facility was used for the experiments conducted in this study. A 2-D sketch of the flow loop is shown in Figure 11-1. Principal components of the flow loop are a 500-liter stainless steel tank, a centrifugal pump and measurement instruments such as magnetic flow meter and differential pressure transducers. There is an air-driven mixer in the tank for preparing the slurry. The centrifugal pump equipped with Variable Frequency Drive (VFD) was used to circulate fluid/solids mixture through the flow loop.

The test section is 9 meters long and is made of high quality optically clear glass pipes. The outer tube has an inner diameter of 95 mm and a wall thickness of 5 mm. The inner glass pipe has an outer diameter of 38 mm. The radius ratio is 0.4 and eccentricity is 1. Eccentricity is defined as the ratio of the distance between the centers of the pipes to the difference of radii's.

$$e = \frac{L}{R - r} \quad \textbf{Eq.(11-1)}$$

L is the distance between centers of inner and outer tubes; R and r are radii's of the outer pipe and inner pipe respectively. The inner tube is resting against the wall of the outer tube; refer to Figure 11-1 for more detail. The inner tube was kept in place employing a single metal rod in three of the joints.

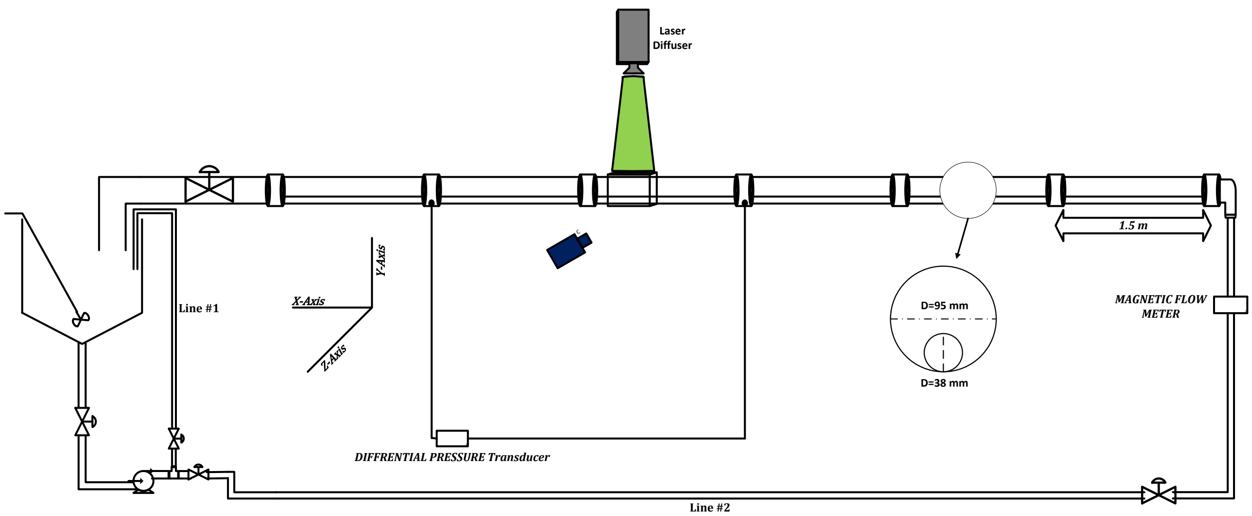

Figure 11-1 Schematic view of the flow loop and configurations of pipes, laser and camera, and the test section

The flow rate was measured using a magnetic flow meter. The flow meter is an OMEGA FMG607-R with an accuracy of $\pm 0.5\%$. Data acquisition was made by a computerized system powered by LabView software. The software was used to control the pump flow rate as well as logging all the data (i.e. pressure losses, flow rates and fluid temperature in the flow loop).

The procedure for conducting the experiments has several steps. Step one was to establish a sand bed of desired initial height in the annulus. In this step, water and sand were mixed in the tank while the slurry was circulated through the flow loop at the maximum flow rate. The circulation was continued for 10 to 15 minutes to achieve a constant bed height in the annular section. The flow was then interrupted by shutting the pump down. The annular part of the flow loop was then isolated from the rest of the flow loop using the control valves (Figure 11-1). Other parts of the flow loop (i.e. the tank, pump, and transport pipelines) were then carefully washed to remove any solids remained in those parts. To prevent sand particles deposited in the annular section from re-circulating in the flow loop during the experiments, two filter bags with openings smaller than the particle size were installed at the outlet of the annular section.

The sand bed height was varied through changing the initial concentration of sand particles in the system. To achieve three different bed heights in this study, total mass loading of the solids in the system was varied from as low as 3.5% to up to 14%. The sand particles that have been used in this study are natural quartz sands with a density of 2650 kg/m^3. Sieve analysis of washed sand samples has shown that sand particles are uniform in size distribution. The d_{50} of the samples were determined to be 600 microns.

The next step is preparing the polymer solution. The fluid was prepared in the tank isolated from the rest of the flow loop. The mixing was done according to the supplier's recommendations. The polymer was mixed in the tank for 20 minutes using the mixer. Afterward, the bypass line of the system was used to circulate the fluid for 15 minutes at a moderate flow rate. This step was performed to make sure the polymer is homogeneously mixed. After mixing the polymer in the tank, the flow was then opened to the annular section. Before any PIV recording, the fluid was circulated in the test section for another 10 minutes for consistency purposes. A sample of fluid was taken a right after starting PIV recording for rheological analysis. The duration of the PIV experiments was kept less than 30 minutes for each solution to prevent polymer degradation by the pump.

At a distance of approximately $100D_H$ ($D_H = 2(R - r)$) away from the annulus's inlet the PIV measurement were carried out. Since the bed is uniform in thickness in the entire annulus, the flow should be fully developed in the measurement window (In single phase flow a development length of $88D_H$ is required for a fully developed laminar flow(Poole 2010), whereas development length for turbulent flow is much shorter (Japper-Jaafar et al. 2010)).

11.3.1. PIV Setup Description and Post-Processing Procedures

The laser that was used in this study was a Nd: YAG double pulsed laser. The green light laser has a wavelength of 532 nm and 50 mJ/pulse energy. The laser light is converted to a planar light sheet by a combination of the cylindrical and the special optical lenses. The thickness of the beams was 0.5mm throughout this study.

A double frame CCD (charge-coupled device) camera with a resolution of 1376×1040 pixels was used for recording the PIV images. A 60 mm Nikon AF NIKKOR lens with a 36 mm extension tube was used. The f-stop or the aperture setting of the lens was set to 8. The scaling factor for images has been registered to be 31.76 μm/pixel.

Figure 11-2 shows a typical PIV image acquired during the experiments. The sand bed is visually visible at the bottom of the picture. The white dots are the tracers in the flow. DAVIS 8.3.0 software was used for both the image acquisition and the post-processing of pictures. The software was used for adjusting the appropriate parameters during the experiments (such as the time interval between the two images and the laser power) as well as processing and extracting the data from the pictures. Further details regarding the image processing algorithm are given in the next section.

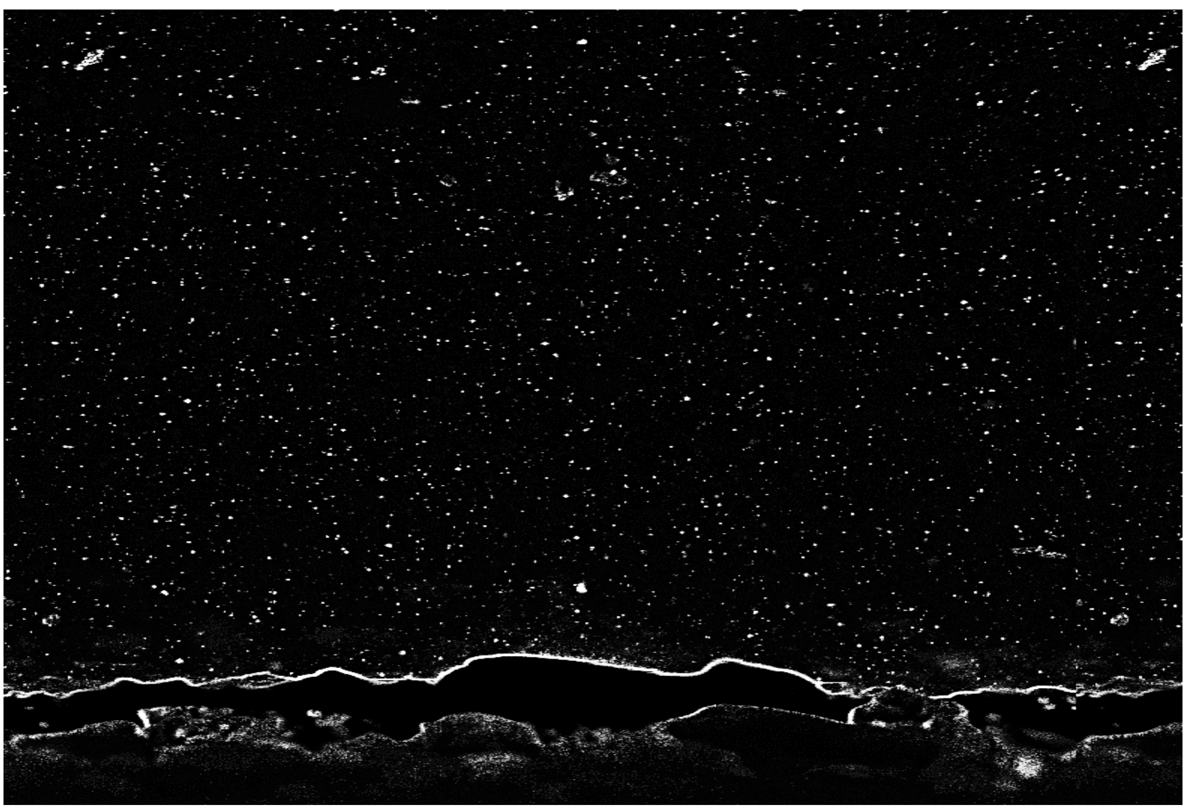

Figure 11-2 A typical PIV of the sand bed and tracers in the fluid

A total number of 1000 pictures have been recorded for each data set. The multi-pass cross-correlation method with the decreasing of the interrogation window size was used for the particle displacement calculations. An initial interrogation window size of 64×64 pixels followed by the window size of 32×32 pixels was utilized in the calculations. The overlap setting was 50%, and the weighting function was set to adaptive. To enhance the accuracy of the calculated vector fields, the post-processing was also applied on the calculated vectors. Universal outlier detection function was used in the post processing.

Hollow glass spheres with a mean diameter of 10 microns were used as tracer particles. The tracer particles are nearly neutral in water ($1.1 \pm 0.05 \frac{g}{cc}$) to keep them suspended in the flow. The addition of the trace particles is necessary to enhance the spatial resolution of the PIV images and reduce the bias error towards the sand debris (Melling 1997).

11.3.2. Measurement details

The PIV measurement was conducted along a plane perpendicular to the interface of the stationary sand beds. The measurement plane is off the center of the annulus. Figure 11-3 schematically shows a cross-sectional view of the annulus in the measurement window as well as the relative height of stationary sand beds.

Experiments were conducted at three different sand bed heights (Figure 11-3 shows the relative height of each bed and locations of measurement planes). Bed A had a height less than the inner pipe radius r (i.e. h<r=19 mm). Bed B had a height bigger than r and less than 2r (i.e. r<h<2r). Finally, Bed C had a height that was greater than 2r (i.e. with bed C, the inner pipe was buried in sand).

Each experiment was started at a flow rate that ensured turbulent flow and yet it was below the critical flow rate required for eroding the bed. In another word, for the first few tested flow rates, the phases were completely stratified. This flow rate was determined to be around 136 liters/min. The flow rate was then increased stepwise, and PIV measurement was conducted at each flow rate. The final flow rate that was tested for each bed height was the so-called critical flow rate of bed erosion (Bizhani et al. 2016). At this flow rate, bed erosion was taking place in the form of a moving layer of the sand particles (bedload).

For convenience in presenting the results, we define superficial fluid velocity as follows:

$$U_s = \frac{Q}{\pi(R^2 - r^2)} \qquad \textbf{Eq.(11-2)}$$

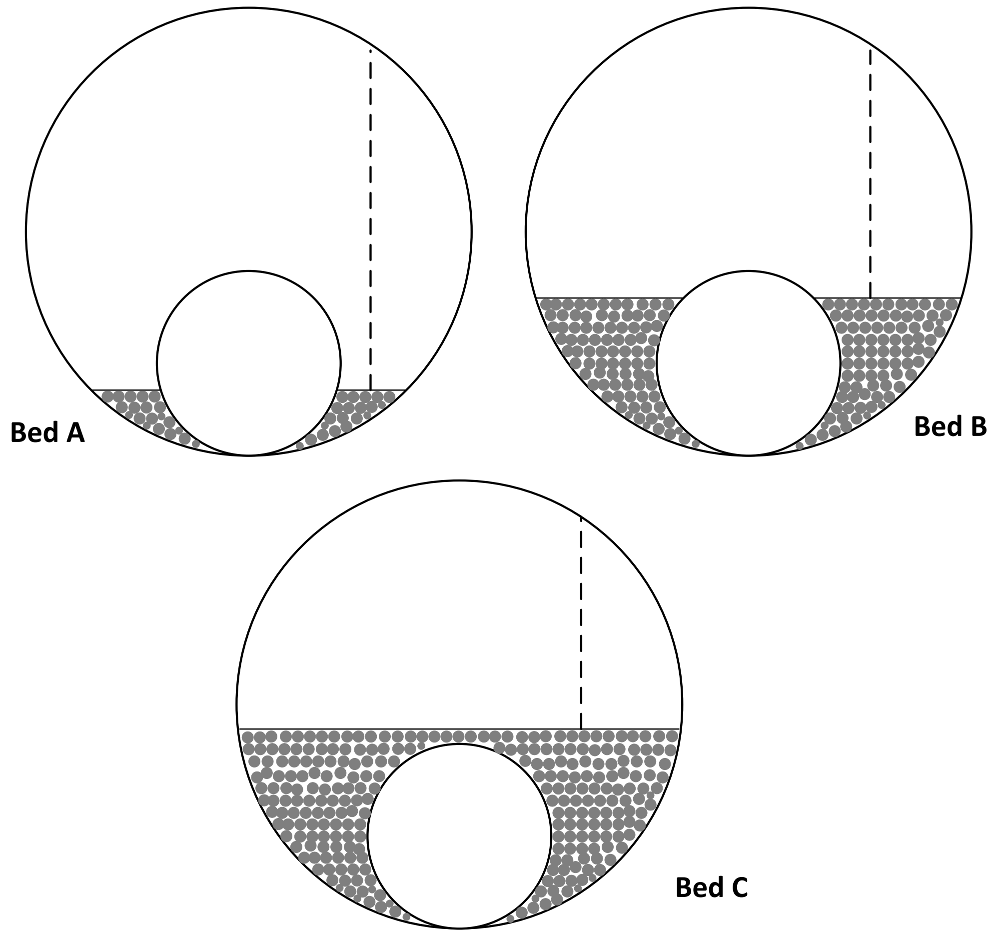

Figure 11-3 Schematic representation of the eccentric annulus with measurement plane and relative height of the sand beds

Where Q is the pump flow rate, and U_s is the superficial fluid velocity. In the present work, all the experiments were conducted at the same flow rates, and hence, the same the superficial velocities.

Superficial velocity does not show the difference in the actual fluid velocities in the annulus. To calculate the actual fluid velocity in the annulus, we must account for the reduction in the flow area by the sand beds. The bulk fluid velocity or the real fluid velocity in the annulus is then:

$$U_b = \frac{Q}{A_f}$$ **Eq.(11-3)**

A_f designates the flow area available to flow. Details about geometrical calculation pertinent to A_f is presented in the appendix.

There is no unique definition for Reynolds number associated with non-Newtonian fluids. One commonly used equation, especially in the drilling industry (Mitchell et al. 2011), is the generalized Reynolds number defined according to Dodge and Metzner (1959) work.

$$Re = \frac{\rho U_b^{2-n} D_h^n}{8^{n-1} K}$$ **Eq.(11-4)**

In Eq.(11-4), D_h is the hydraulic diameter. Details of calculation pertinent to D_h is presented in the appendix.

Table 1 reports the flow rates, superficial velocities, bulk velocities, and Reynolds numbers for experiments conducted with bed A. The critical velocity of bed erosion in bedload form, in this case, was recorded to be 0.66 m/s (superficial velocity).

Table 11-1 Details of measurements conducted with bed A

$Q\ (\frac{lit}{min})$	$U_s(\frac{m}{s})$	$U_b(\frac{m}{s})$	Re
136.3	0.38	0.4	7150
156.1	0.44	0.46	8240
177.2	0.5	0.52	9420
194.4	0.54	0.56	10370
219.2	0.61	0.64	11770
236.5	0.66	0.69	12740

Table 2 reports the superficial velocities, bulk velocities, and flow Reynolds numbers under which experiments were conducted for bed B. The superficial velocity of 0.61 m/s is the critical flow velocity in this case.

Table 11-2 Details of measurements carried out with bed B

$\boldsymbol{Q}\ (\frac{\boldsymbol{lit}}{\mathbf{min}})$	$\boldsymbol{U_s}(\frac{\boldsymbol{m}}{\boldsymbol{s}})$	$\boldsymbol{U_b}(\frac{\boldsymbol{m}}{\boldsymbol{s}})$	$\boldsymbol{Re}$
138	0.38	0.47	8820
157	0.44	0.54	10090
176	0.5	0.6	11380
195.2	0.54	0.67	12680
220	0.61	0.75	14380

Table 3 reports the operational variables under which experiments for bed C were conducted. Since this bed was much thicker than the other two beds, bed load transport of particles started at a superficial velocity of 0.54 m/s.

Table 11-3 Details of measurements conducted with bed C

$\boldsymbol{Q}\ (\frac{\boldsymbol{lit}}{\mathbf{min}})$	$\boldsymbol{U_s}(\frac{\boldsymbol{m}}{\boldsymbol{s}})$	$\boldsymbol{U_b}(\frac{\boldsymbol{m}}{\boldsymbol{s}})$	$\boldsymbol{Re}$
137.5	0.38	0.54	9930
156.7	0.44	0.61	11390
175.5	0.5	0.69	12830
193.5	0.54	0.76	14210

Note that the reported numbers in Tables 1-3 indicate that the minimum Reynolds number is registered for flow over bed A and is 7150. It will be shown later that the flow is turbulent at all the flow rates according to measurements of turbulence intensity and Reynolds stress profiles.

11.4. Results and discussion

11.4.1. Rheology

An anionic water-soluble copolymer of the family of partially-hydrolyzed polyacrylamide (PHPA) polymer was used in this study. The molecular weight of the polymer is reported to be $10 \times 10^6 \frac{g}{mol}$. A concentration of 0.032% by weight has been used in this work. The mixing procedure recommended by the supplier was followed to properly disperse the powder in tap water.

Rheological characteristics of the fluid samples were determined by using a high-resolution Bohlin C-VOR 150 rheometer. For the range of shear rates encountered in this study (1-400 1/s approximately), the power law model was fitted to the apparent viscosity data. Figure 11-4 shows the flow behavior curve of the polymer solution. The K and n values are reported in Eqs. 5.

$$\tau = 0.0046\dot{\gamma}^{0.952} \qquad \textbf{Eq.(11-5)}$$

Oscillatory rheometry (i.e. frequency sweep) was also performed to determine the viscoelastic properties of the polymer fluid. Figure 11-5 reports the data collected from frequency sweep tests. At low frequencies (high time scales) the loss (viscous) modulus (G'') is dominant over that of storage (elastic) modulus (G'). The longest relaxation time appears to be 0.17 seconds. Therefore, the fluid exhibits weak elastic properties.

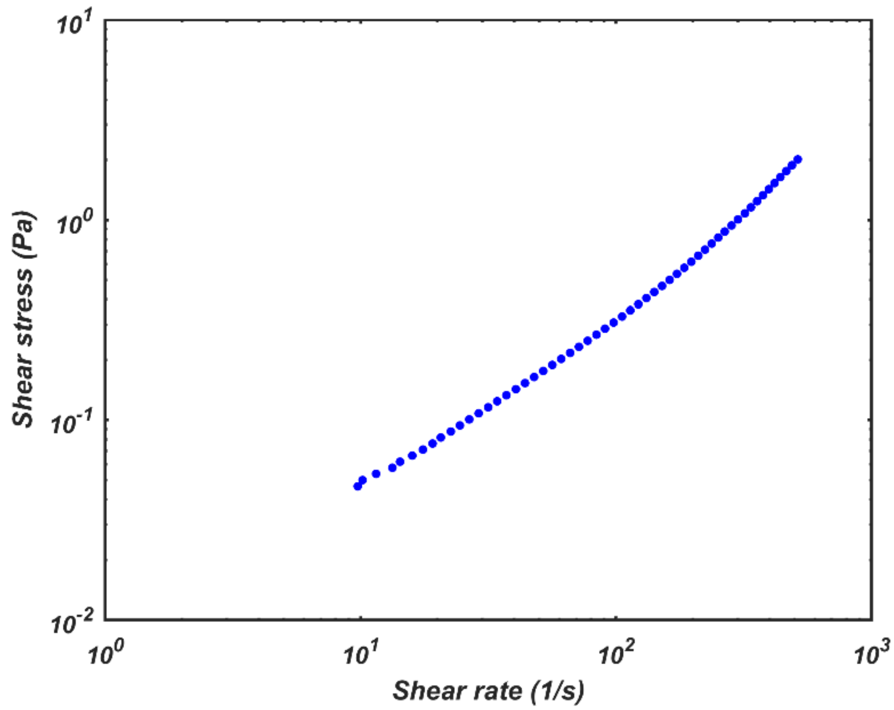

Figure 11-4 Shear stress versus shear rate profile for the polymer solution

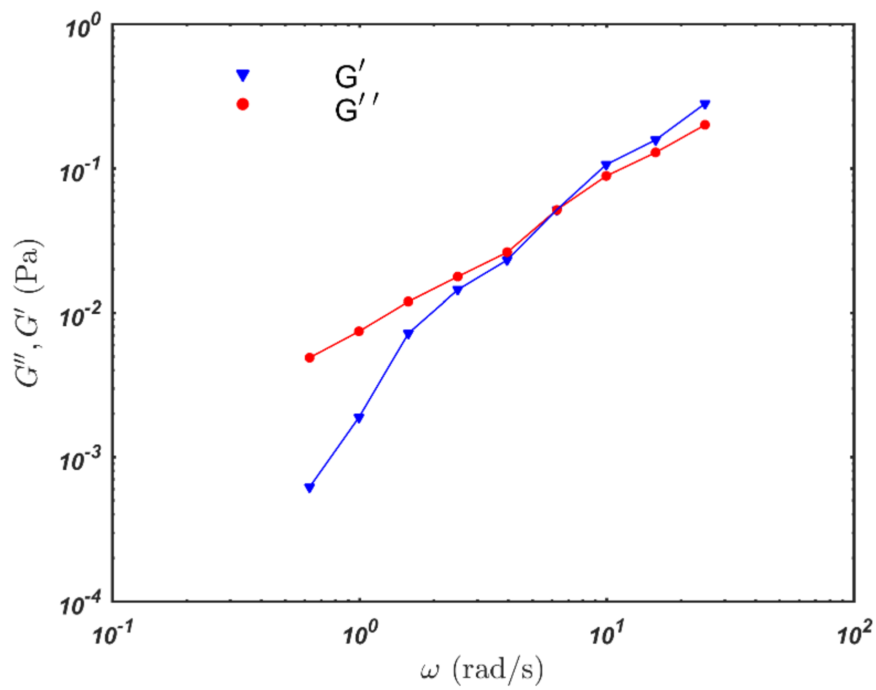

Figure 11-5 Viscous and elastic moduli vs. angular frequency

Measurements of the first and the second normal stress differences are not as straightforward as that of the apparent shear viscosity. Due to edge fracture phenomena, only low shear rate measurements may be possible using cone-plate configuration (Baird 2008). Lin et al. (2014) suggested that using a bigger cone and reducing the shearing time of the sample can help in curbing the edge fracture phenomenon. A 40-mm cone with 4 degrees curvature was utilized in the current study. The shearing time was around 20 minutes for viscosity measurement. On the other hand, for normal stress measurements, the shearing time was reduced to less than 1 minute to avoid the edge fracture. The second normal stress difference is much harder to measure. It is not possible to measure N_2 using cone-plate viscometer. Figure 11-6 shows the measured first normal stress difference for the polymer sample.

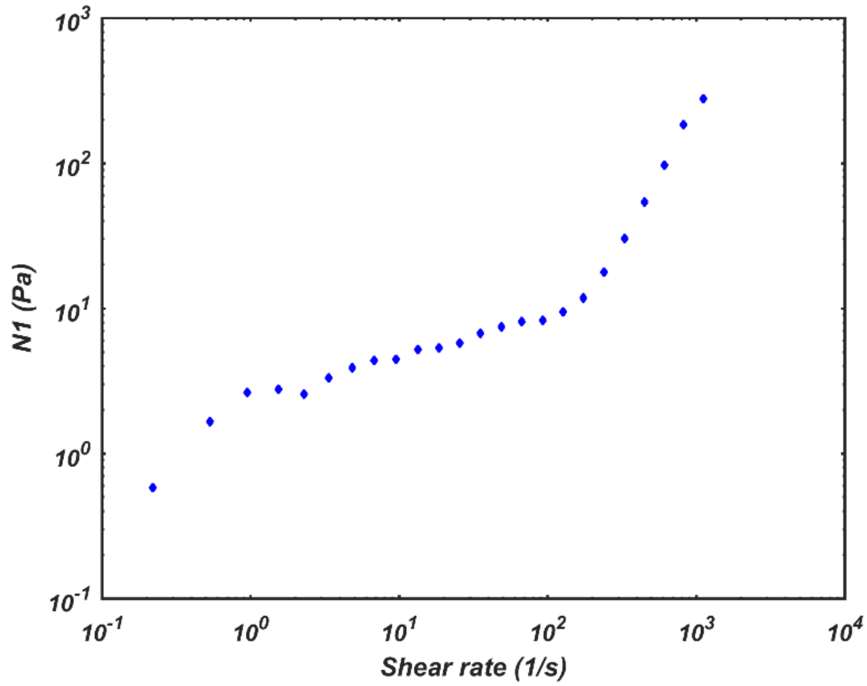

Figure 11-6 The first normal stress difference vs. shear rate.

11.4.2. PIV results

11.4.3. Velocity profiles in wall unit

Velocity profiles near the interface of the sand bed are of interest to this study. We will investigate the velocity profiles in the so-called wall units to assess the impact of the surface roughness and particle movement on the velocity profiles. For the non-Newtonian fluids, the wall units are defined according to the following equations (Pinho and Whitelaw 1990):

$$y^{+} = \frac{\rho y u_{\tau}}{\mu_{w}} \qquad \textbf{Eq.(11-6)}$$

$$u^{+} = \frac{u}{u_{\tau}} \qquad \textbf{Eq.(11-7)}$$

In these equations, y^{+} and u^{+} are the dimensionless distance and velocity respectively. U_{τ} is the friction velocity, and y is the vertical distance measured from the point of zero velocity. μ_{w} is the viscosity at the wall (or the bed interface).

Two challenging tasks need to be addressed before we can transform the velocity data into wall units. The first challenge is to calculate the friction velocity at the bed interface. According to its definition, the friction velocity is related to wall shear stress through Eq.(11-8) (Kundu et al. 2012).

$$u_{\tau} = \sqrt{\frac{\tau_{b}}{\rho}} \qquad \textbf{Eq.(11-8)}$$

The bed shear stress (or wall shear stress), τ_b, cannot be deduced from frictional pressure loss data because more than one surface is involved in the annulus (i.e. outer pipe wall, inner tube wall and the bed surface). The alternative solution that is often used in the flow of Newtonian fluids is to use the slope of the measured velocity profiles in the logarithmic zone and use that to calculate u_{τ}. In this approach, local velocity is plotted versus y in a semi-log scale. Assuming a logarithmic profile prevails, then the following equation describes the velocity in the logarithmic region (Kundu et al. 2012):

$$u = \frac{u_{\tau}}{\kappa} Ln\left(\frac{y}{y_{o}}\right) = \frac{u_{\tau}}{\kappa} Ln(y) + Constant \qquad \textbf{Eq.(11-9)}$$

In Eq.(11-9), κ is the von Karman constant and is equal to 0.41 for the flow of water. y_o is called characteristic roughness and determines whether the surface is hydraulically smooth or rough. If one plot u versus y, then, the slope of the line in the logarithmic region is equal to $\frac{u_\tau}{\kappa}$. Since we assume von Karman constant is 0.41, then, friction velocity can be calculated from the slope. However, this approach cannot be used with flow of shear thinning polymers that result in drag reduction. The reason for this is the reduction in the von Karman constant. The von Karman constant is no longer equal to 0.41.

The third method in evaluating the boundary shear stress, and hence friction velocity, is to use the recorded velocity profiles near the bed interface to calculate the boundary shear rate (velocity gradient). Using the boundary shear rate, then the shear stress can be calculated using the rheological equation. This approach assumes near the bed interface turbulent stress is negligible, and only laminar stress is the dominant part of the shear stress. We will later show that this assumption is valid when analyzing Reynolds stress profiles. In all the analysis presented in this paper, the wall units are evaluated using the friction velocity calculated according to the procedure described.

The second challenge in accurately determining the velocity profiles near a rough surface is defining the location of the "virtual wall" (Chan-Braun et al. 2011, Chan-Braun 2012). Chan-Braun (2012) defined the virtual wall as 0.8D (D is the roughness height). However, this approach is for cases where roughness element has a fixed height, and the boundary is fixed. In this study, the bed materials are loose, and they regularly are rearranging. Therefore, we cannot define a particular point as the virtual wall such as the one defined by (Chan-Braun et al. 2011, Chan-Braun 2012). Instead, we define virtual wall where the velocity is zero. The zero velocity is determined from the velocity profiles.

In addition to difficulties associated with virtual wall definition, the bed surface is not flat (see Figure 11-2). Therefore, one cannot average the velocity data in the direction of the flow. The second issue is the configuration of the particles lying on the bed surface. It appears that the bed roughness is not constant along the bed. Therefore, instead of averaging the velocity data along the bed, we only used the local velocity profiles, where we could exactly identify the location of zero velocity.

For comparison purposes, we will compare the velocity profiles to the well-known profiles in the sublayer and logarithmic region. The linear velocity profile in the sublayer is (Kundu et al. 2012):

$$u^+ = y^+ \qquad \textbf{Eq.(11-10)}$$

The logarithmic law for the flow of Newtonian fluids in a smooth eccentric annulus is (Nouri et al. 1993):

$$u^+ = 2.44Ln(y^+) + 4.9 \qquad \textbf{Eq.(11-11)}$$

Finally, the Virk et al. (1970) asymptote, which marks the maximum that velocity can get in the logarithmic zone, is represented by the following equation:

$$u^+ = 11.7Ln(y^+) - 17 \qquad \textbf{Eq.(11-12)}$$

In Figure 11-7 we report the velocity profiles recorded for flow over bed A at different flow velocities. The results indicate that in the viscous sublayer (y^+<10), the data perfectly matches the linear relations represented by Eq.(11-10). The data in the logarithmic zone show an upward shift to the profile represented by Eq.(11-11). On the other hand, the velocity profiles are located in a window enclosed by the Virk's asymptote and that of Eq.(11-11). This behavior has been reported in many of previous studies on the turbulent flow of drag reducing polymer solutions (Pinho and Whitelaw 1990, Nouri et al. 1993, Escudier et al. 1995, Ptasinski et al. 2001, Japper-Jaafar et al. 2010). The extent to the increase in velocity profiles depends strongly on the degree of drag reduction.

The data in the logarithmic zone extend to a y^+ of about 100. This region is what other researchers sometimes call the elastic sublayer following the work of Lumley (1969).

The behavior of the velocity profiles indicates that the surface roughness does not affect the velocity profiles in the range of velocities tested here. This is in sharp contrast to experiments with water which have shown a strong dependency on the roughness of the surface (Bizhani and

Kuru 2017). Additionally, movement of the sand particles in the form of bedload at higher flow rates (0.6 m/s in this case) does not appear to affect the velocity profiles either. Other studies (Owen 1964, Best et al. 1997, Bigillon et al. 2006) have shown bedload transport of particles causes a sharp increase in the boundary roughness which then causes the velocity profiles to shift downward. However, our results with polymer solutions show that bedload transport of particles does not significantly affect the velocity profiles.

To get a better perspective on the boundary roughness effect on velocity profiles, we can use the so-called boundary roughness Reynolds number. This Reynolds number is defined as follows:

$$Re_\tau = \frac{\rho u_\tau \varepsilon}{\mu_w} \qquad \textbf{Eq.(11-13)}$$

In this equation, ε is the characteristic roughness of the surface. If we assume that characteristic roughness of the bed surface is equal to the particles size (600 microns), then the maximum boundary roughness Reynolds number for velocity profiles reported in Figure 11-7 is six. This means the flow is in the early transitional regime, and hence, the velocity profiles are similar to flow near the smooth surface.

Figure 11-8 reports the measured velocity profiles over bed B at different flow velocities. Similar to bed A, we observe the velocity profiles obey the linear profile of Eq.(11-10) near the sand bed interface. Further away, the velocity profiles show an upward shift comparing to the velocity profiles representative of Newtonian fluids. The velocity profiles are bounded to the window formed between Virk's asymptote and that of Eq.(11-11). The maximum boundary roughness Reynolds number is this case 5.5.

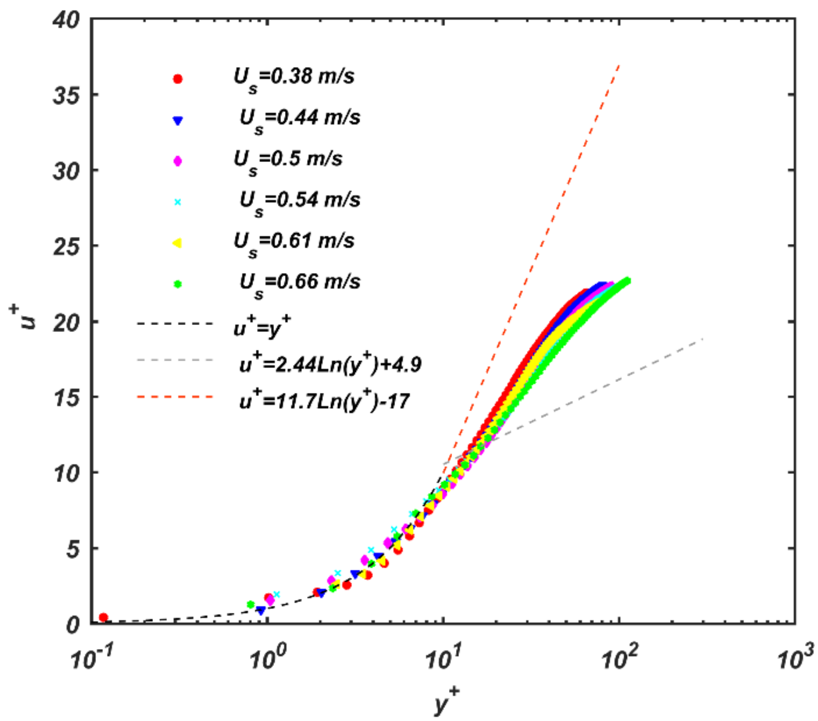

Figure 11-7 Velocity profiles in wall units for flow over bed A

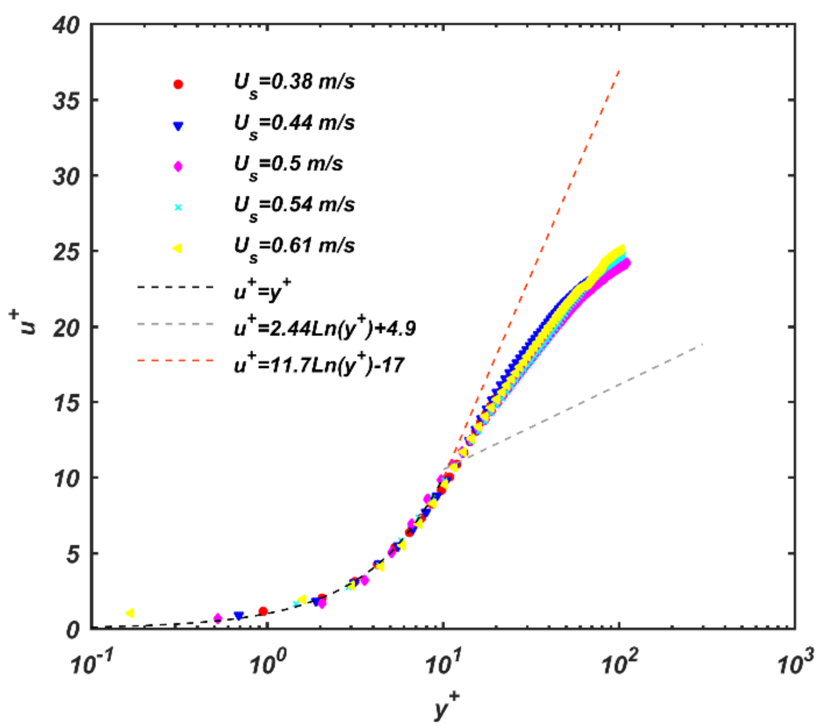

Figure 11-8 Velocity profiles in wall units for flow over bed B

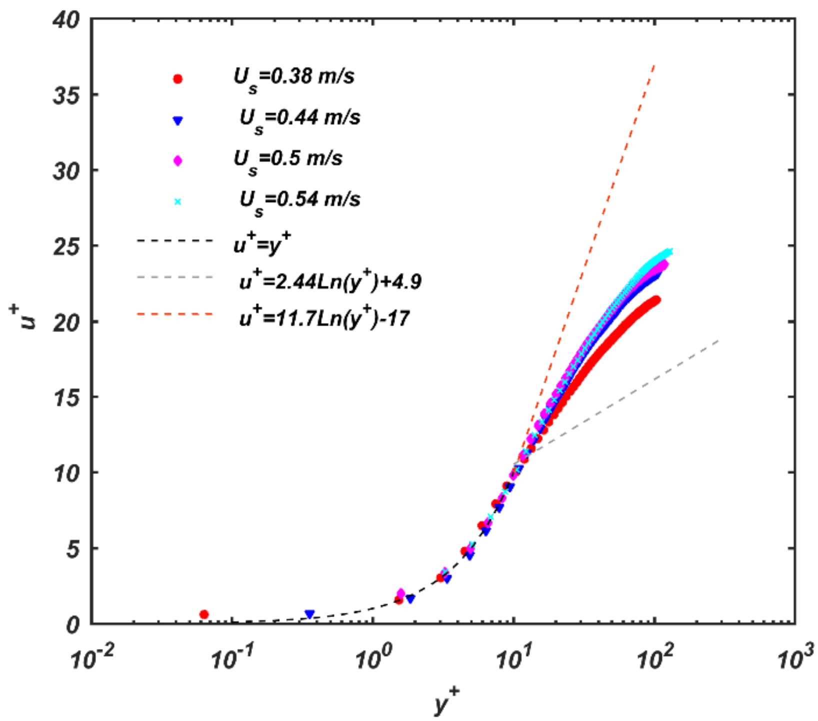

Figure 11-9 Velocity profiles in wall units for flow over bed C

Figure 11-9 compares the measured velocity profiles over bed C. Similar to previous two beds, an excellent match is observed in the sublayer with the Eq.(11-10). Additionally, in the log region, the velocity profiles fall short of Virk's asymptote and above that of Eq.(11-11). The maximum boundary roughness Reynolds number is 6.2.

Finally, we compare all the measured velocity profiles over the three beds in one figure (Figure 11-10). The data reveal that the linear relation of Eq.(11-10) is valid in the entire sublayer for all the cases. Additionally, all the velocity profiles are showing an increase in the logarithmic zone comparing to the velocity profile representative of Newtonian fluid flow. There is no indication of shift of velocity profiles due to particles movement in the bed. In another word, the roughness of the surface does not change due to bedload transport of particles. This behavior is in sharp contrast to that of water where flow was observed to become hydraulically rough at flow velocities as low as 0.3 m/s. Perhaps one of the reasons why water is more efficient in removing the sand particles the fact that the flow becomes rough at much lower flow rates. The rough surface enhances the momentum exchange rate significantly and hence helps in removal of the particles.

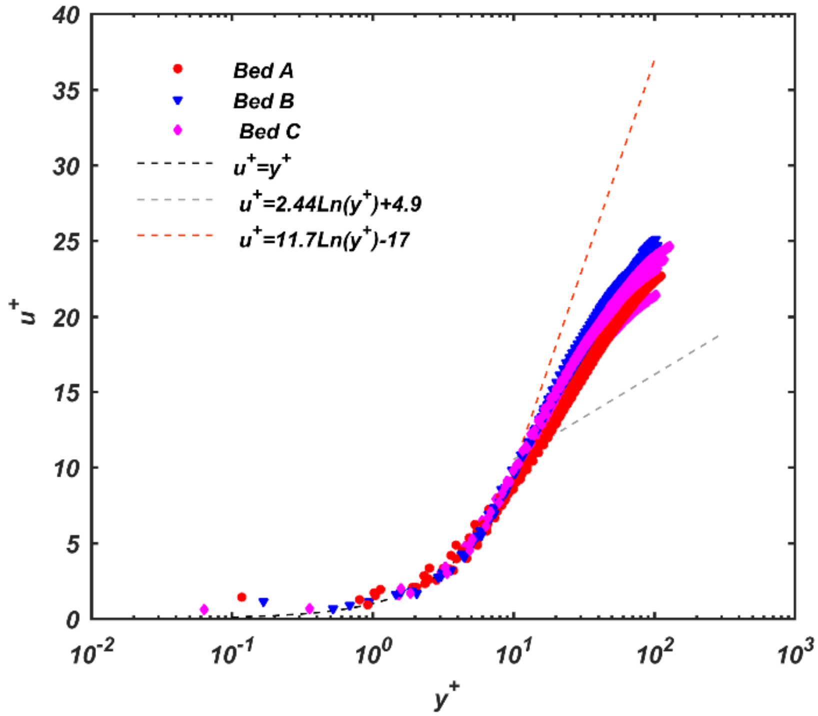

Figure 11-10 Velocity profiles in wall units for flow over all beds

Two important conclusions are drawn based on the results presented in this section. First, it is much harder to obtain a fully rough flow regime near the interface of a sand bed using dilute polymer solutions than when using water. We observed even at flow velocities as high as the critical velocity of bed erosion velocity profiles remained similar to flow near the smooth surface. Nonetheless, our other study has shown at a flow velocity of 0.3 m/s the boundary roughness can be as high as nine times that of mean particle size when using water (refer to the data presented in the previous chapter). This is in sharp contrast to the current experiments were even at velocities as high as 0.66 m/s the boundary mainly smooth. This finding has enormous implications for the design of hole cleaning in drilling operations. Since rough boundaries dissipate more energy, and hence, increase frictional pressure loss, one may use a few polymer additives to avoid this flow regime. The second implication of the current results is for modeling purposes of solid transport using non-Newtonian fluids. Up to the present moment, there has been no independent study where velocity profiles over a sand bed have been directly measured for complex fluids. Therefore, researchers often are forced to assume velocity profiles that are not necessarily representative of the actual flow field for modeling purposes. The presented results can provide the much-needed experimental evidence for validation of CFD and other numerical studies as well.

11.4.4. Reynolds stress

The Reynolds shear stress is an important indicator of turbulent flow. It is defined according to the following equation:

$$\tau_{Re} = \rho\overline{u'v'} \qquad \textbf{Eq.(11-14)}$$

In this equation u' and v' are the velocity fluctuations in the axial and radial direction respectively. The Reynolds shear stress is important from two aspects in this study. First, from the perspective of drag reduction, some studies suggest this property may become zero in fully turbulent flow of drag reducing polymer fluids (Warholic et al. 1999). Additionally, other studies have shown flow near surface of a sand bed can enhance production of turbulence. Bedload transport of particles may enhance or supress production of turbulence (Best et al. 1997, Carbonneau and Bergeron 2000). We will test these hypotheses in this section.

Figure 11-11 reports the measured Reynolds stress profiles over bed A at different flow rates. Although Reynolds shear stress is small at the lower flow rates, it shows a non-zero value at all flow rates. Therefore, the use of elastic polymer solutions does not cause the Reynolds shear stress to disappear. The accuracy of data is less near the y=0 or the bed interface due to light reflection and small magnitude of the Reynolds stresses. However, we can see that for small enough y values, one can neglect the Reynolds stresses, and hence, the procedure we described in estimating bed shear stress for calculation of shear velocity is validated.

The highest Reynolds stress is registered for flow at the highest velocity. At this velocity a moving layer of particles exists at the interface of the cuttings bed. The movement of the particles does not appear to suppress the production of turbulence. On the other hand, we cannot make a comment about whether it enhances the production of Reynolds stresses.

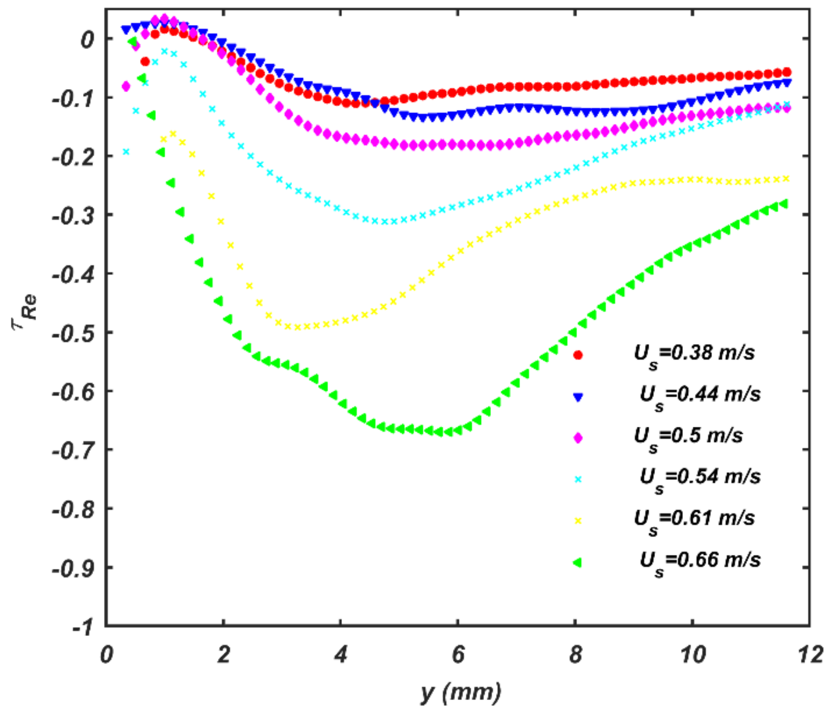

Figure 11-11 Reynolds stress profiles measured for flow over bed A

Figure 11-12 reports the measured Reynolds stress profiles over bed B at different flow rates. The data are similar to bed A, where even at smallest flow rate a non-zero Reynolds stress is registered. The highest Reynolds stress is recorded at the highest flow velocity (0.6 m/s). At this velocity, the bed is eroding. Erosion of the bed in bedload form can cause a reduction in flow turbulence near the bed, shown in other studies (Best et al. 1997, Carbonneau and Bergeron 2000, Bizhani and Kuru 2017). However, these studies are all for Newtonian fluids. Our data indicate that bedload transport of particles has minimal impact on flow characteristic near the bed interface for the tested polymer fluid. The velocity profiles reflected that as well. The profiles of Reynolds stress confirm the same conclusion. The main reason for this is that the flow is barely in the early transitional regime to rough flow. The same particles were used with water and at even velocities as low as 0.18 m/s the flow was in the rough regime. Therefore, the use of polymer solutions, even at small concentrations, delays transition to rough flow by a significant margin. This finding can be used in the design of pipelines for the transport of slurry where the excessive pressure loss needs to be avoided. The use of dilute polymer solutions can help in avoiding the rough and or transitionally rough flow regimes, hence, reducing the frictional pressure loss.

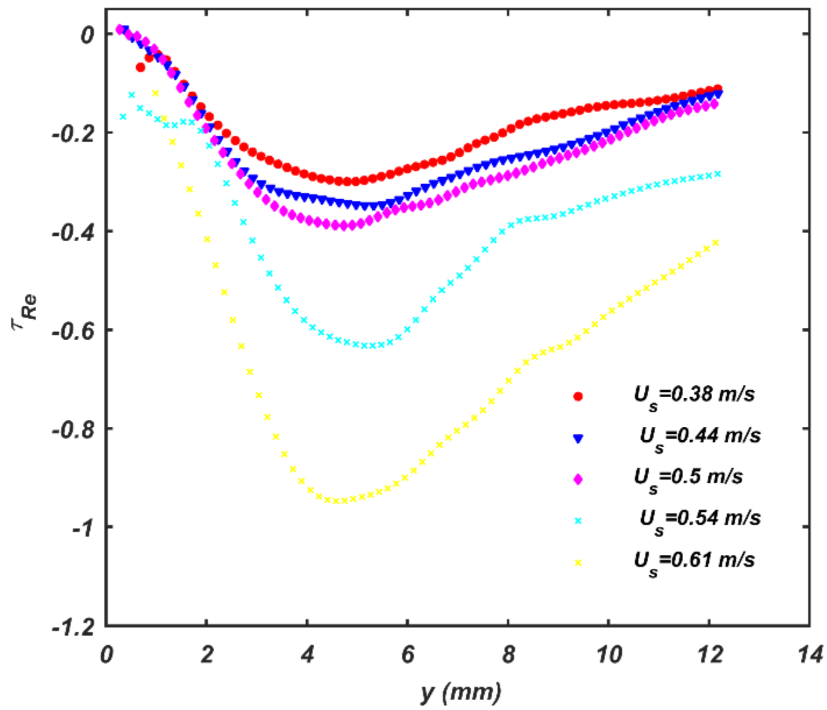

Figure 11-12 Reynolds stress profiles measured for flow over bed B

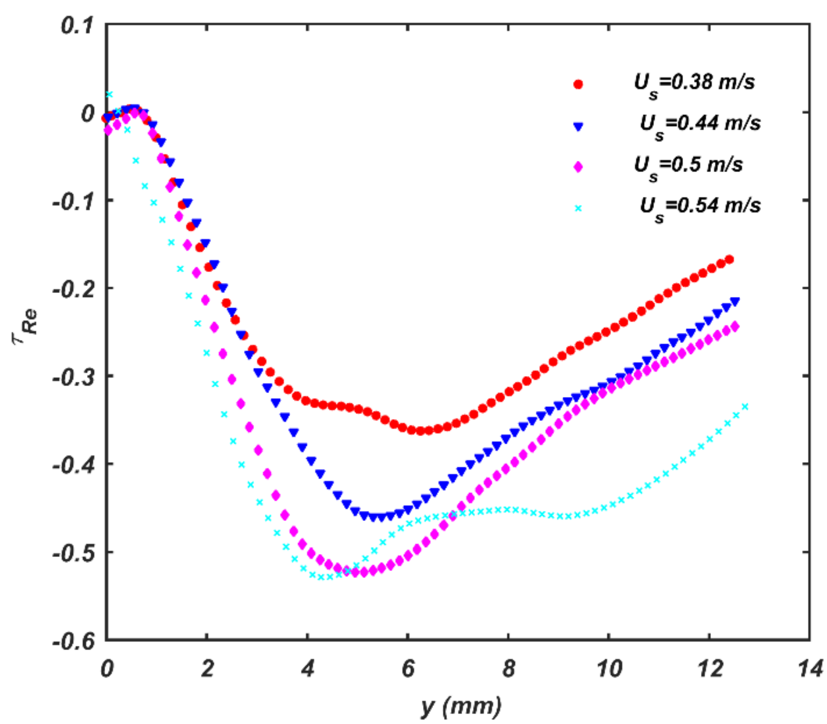

Figure 11-13 Reynolds stress profiles measured for flow over bed C

The stress profiles registered for flow over bed C, at four different flow rates, are reported in Figure 11-13. The data further confirm our earlier conclusions that the flow does not get affected by the bedload transport of particles.

In Figure 11-14 we compare the Reynolds stress profiles over the three beds measured at the same superficial velocity (0.5 m/s). The data show that increasing the height of the stationary sand bed causes the Reynolds stress to increase in the annulus. The main contributor to the increase of Reynolds stress is the growth in the bulk velocity due to the reduction of the annular cross-sectional area. The Reynolds numbers for flow at 0.5 m/s are 9420, 11380, and 12830 for beds A, B, and C respectively. Therefore, the increase in Reynolds shear stress is solely caused by the increase in the flow Reynolds number. The precise meaning of this for drilling operations is that the thicker the stationary bed is, the easier it would be to initiate the erosion of the bed due to higher flow velocity and turbulence in the annulus.

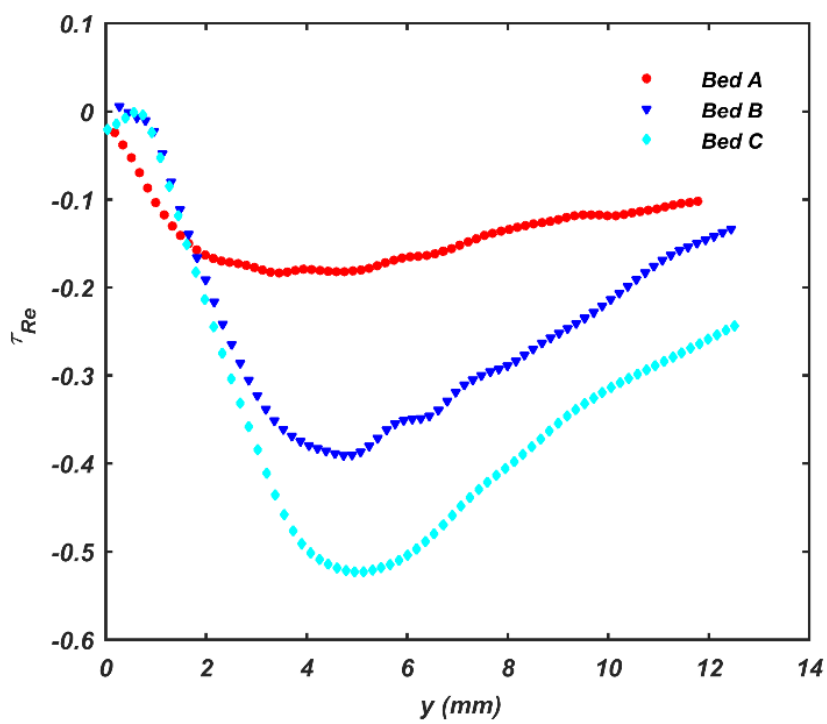

Figure 11-14 Comparison of Reynolds stress profiles at 0.5 m/s for flow over beds of different height

11.4.5. Turbulence intensities

The normal Reynolds stress also denoted as turbulence intensity is another quantity of importance in turbulent flows. The axial and radial turbulence intensities are defined according to the following equations:

$$U_{rms} = \sqrt{\overline{u'u'}} \tag{Eq.(11-15)}$$

$$V_{rms} = \sqrt{\overline{v'v'}} \tag{Eq.(11-16)}$$

Furthermore, we also present the intensity profiles in wall units. The intensities are normalized using the friction velocity.

$$U^{+}_{rms} = \frac{\sqrt{\overline{u'u'}}}{u_\tau} \tag{Eq.(11-17)}$$

$$V^{+}_{rms} = \frac{\sqrt{\overline{v'v'}}}{u_\tau} \tag{Eq.(11-18)}$$

11.4.5.1.1. Axial turbulence intensity

The measure axial turbulence intensity profiles over bed A are reported in Figure 11-15 and Figure 11-16. Figure 11-16 indicates the data without normalization, and Figure 11-16 reports the data in wall units. Profiles in Figure 11-15 reveals that axial intensity is non-zero at all flow velocities. It continuously increases as flow rate increases. Bedload transport of particles and or surface roughness does not appear to have any noticeable impact on the axial intensity. Previous experimental work in drag reduction has shown that use of elastic polymer solutions may result in an amplification of axial velocity fluctuations (Nouri et al. 1993). The increase of axial intensity by drag reducing polymer additives is associated with their elastic properties. The elastic polymer molecules absorb and store energy in the sublayer. The chains then release the elastic energy as they move away from the boundary layer causing an increase in the axial velocity fluctuation (Ptasinski et al. 2003).

Figure 11-15, which is the axial intensity profiles in wall units, show that almost all the cases show a peak in the buffer layer ($y^+<30$). For the first 4 flow rates, the peaks occur close to the y^+ of around 20. Numerical studies have shown that maximum polymer molecule extension takes place at approximately 20 wall units (Ptasinski et al. 2003). The recoil of stretched polymer molecules in the sublayer ultimately give rise to a higher axial intensity in the buffer layer. Given the fact that the bed interface is not smooth and defining the exact location of the wall is challenging in the current work, the peak intensity compares satisfactorily to other studies. At the highest two flow rates, the peak intensity appears to shift further away from the buffer zone slightly. However, the accuracy of measurements due to difficulties in determining the exact location of the wall may be compromised by the moving sand bed layer.

The normalized intensity profiles show all the flow velocity show similar values. The presence of the secondary phase and movement of sand particles does not appear to have any significant impact on the axial intensity profiles.

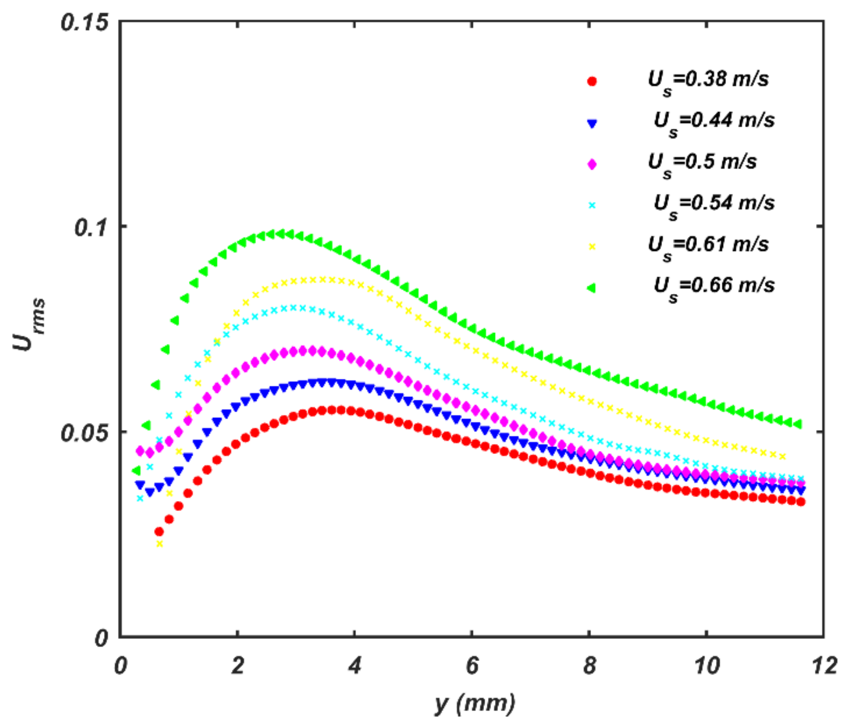

Figure 11-15 Profiles of U_{rms} for flow over bed A

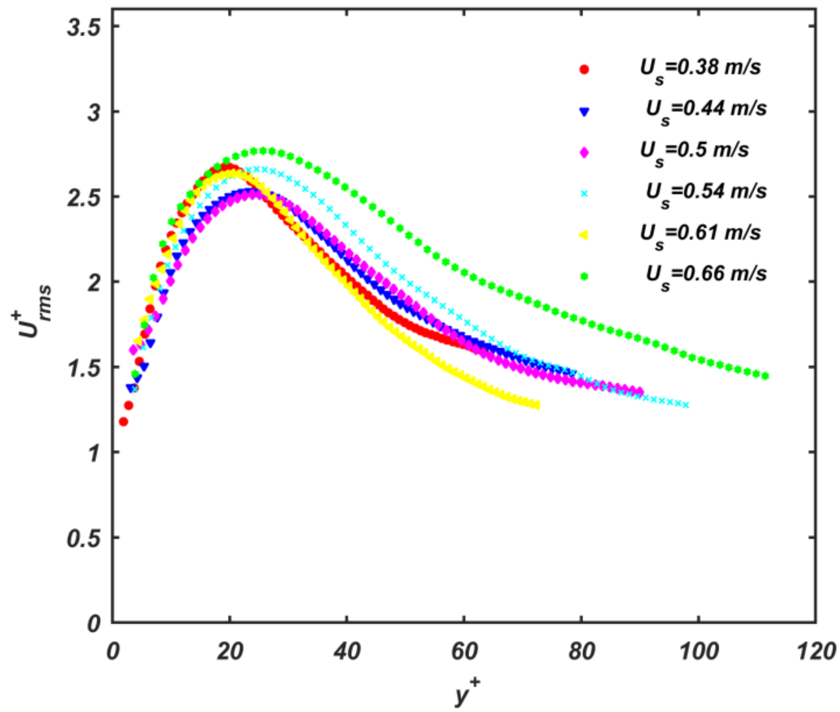

Figure 11-16 Profiles of U^+_{rms} for flow over bed A

We compare the measured axial intensity profiles in dimensional and wall units for flow over bed B in Figure 11-17 and Figure 11-18 respectively. The data are similar to previous two graphs. Increasing the flow velocity progressively causes a higher level of turbulence intensity near the bed.

Profiles of U^+_{rms} show peaks in the buffer zone. The accuracy of the measured peaks depends on the identification of the wall which proved to be challenging in the case of moving sand bed particles. However, a shift to higher y^+ values for the peak intensity is observed for the higher flow rates.

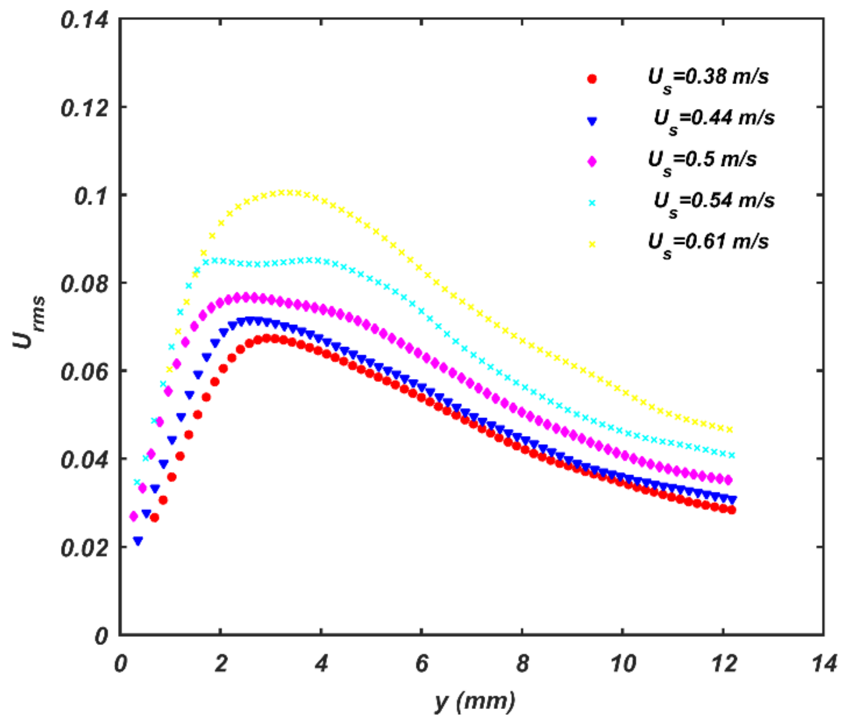

Figure 11-17 Profiles of U_{rms} for flow over bed B

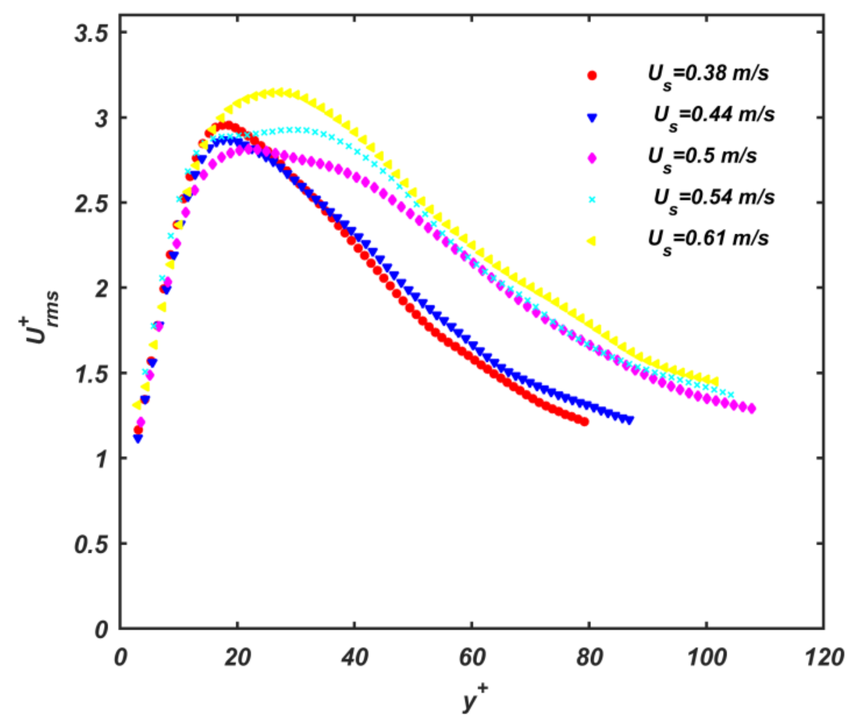

Figure 11-18 Profiles of U_{rms}^{+} for flow over bed B

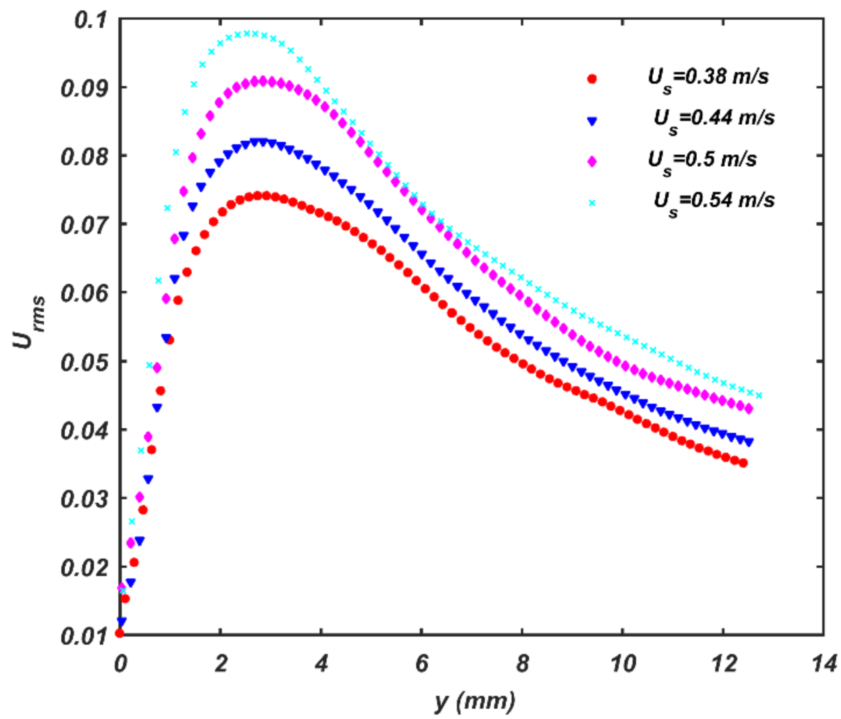

Figure 11-19 Profiles of U_{rms} for flow over bed C

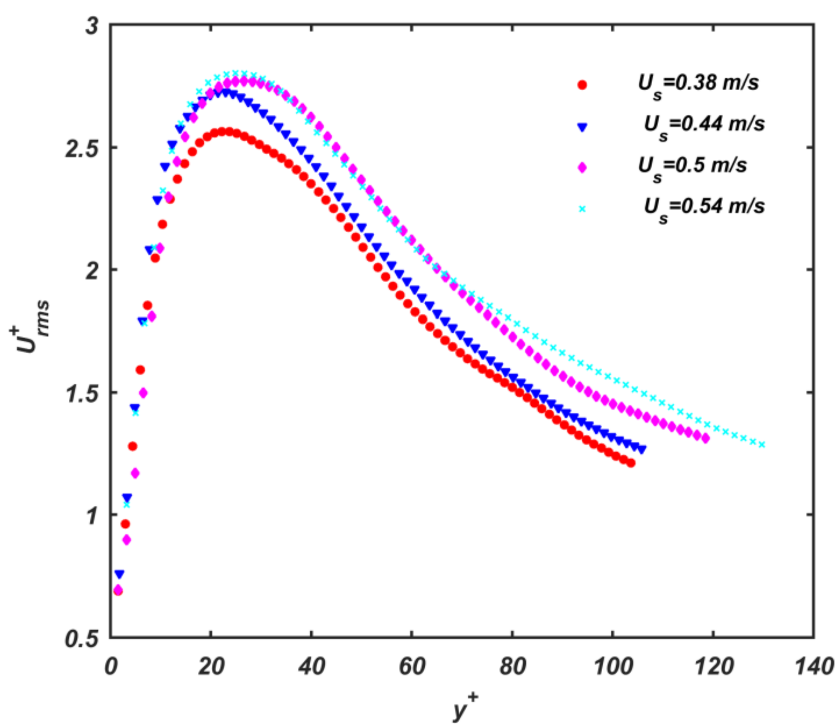

Figure 11-20 Profiles of U^+_{rms} for flow over bed C

Finally, we present the results for U_{rms} and U_{rms}^{+} over bed C in Figure 11-19 and Figure 11-20 respectively. The results are similar to previous two cases, and hence, to prevent repetition of the same points we skip analyzing these data.

Figure 11-21 compares the measured axial turbulence intensity profiles over the three beds at the superficial fluid velocity of 0.5 m/s. The data shows the height of the stationary sand bed progressively causes the intensity to increase over the bed. The main reason for this is the increase in the bulk fluid velocity and flow Reynolds number due to the reduction of annulus cross-sectional area.

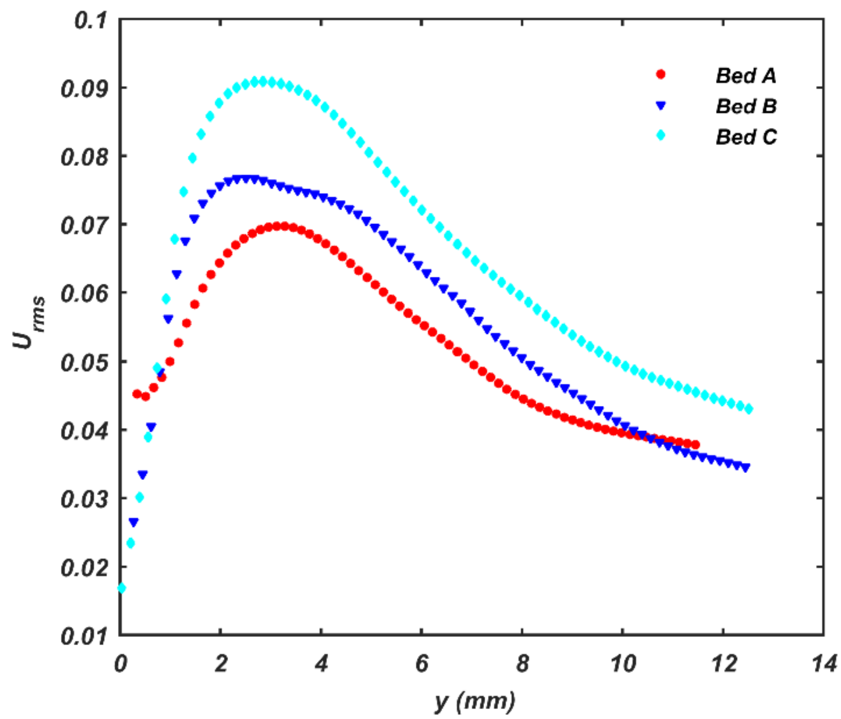

Figure 11-21 Profiles of U_{rms} measured at 0.5 m/s over beds of variable height

11.4.5.1.2. Radial turbulence intensity

The profiles of radial turbulence intensity measured for flow over bed A are depicted in Figure 11-22 and Figure 11-23. Figure 11-22 shows that even at smallest flow rate the radial intensity is not zero. The Reynolds number at this flow rate was 7100. Therefore, the flow is turbulent at all flow rates tested in this study. It was not possible to make accurate measurements of radial intensity profiles very close to the interface of the sand beds. Reflection of the laser light by bed materials, along with the small magnitude of radial intensity near the bed was the main reason for the scatter of data near the bed interface.

Figure 11-23 reports the V_{rms}^{+} profiles. For the first 4 flow rates, all profiles are closely similar. However, the last two flow rates show an increase in the normalized radial intensity. We believe the movement of bed particles at the higher flow rates is the main contributor to this observation. Although movement of particles did not affect previously presented quantities (e.g. velocity), however, it appears that bedload transport of particles amplifies the production of radial turbulence intensity. The increase in V_{rms} can essentially increase production of Reynolds shear stress. The implication of such observation for slurry transport is that particles suspension may become easier in the wake of the enhance radial velocity fluctuations (Davies 1987).

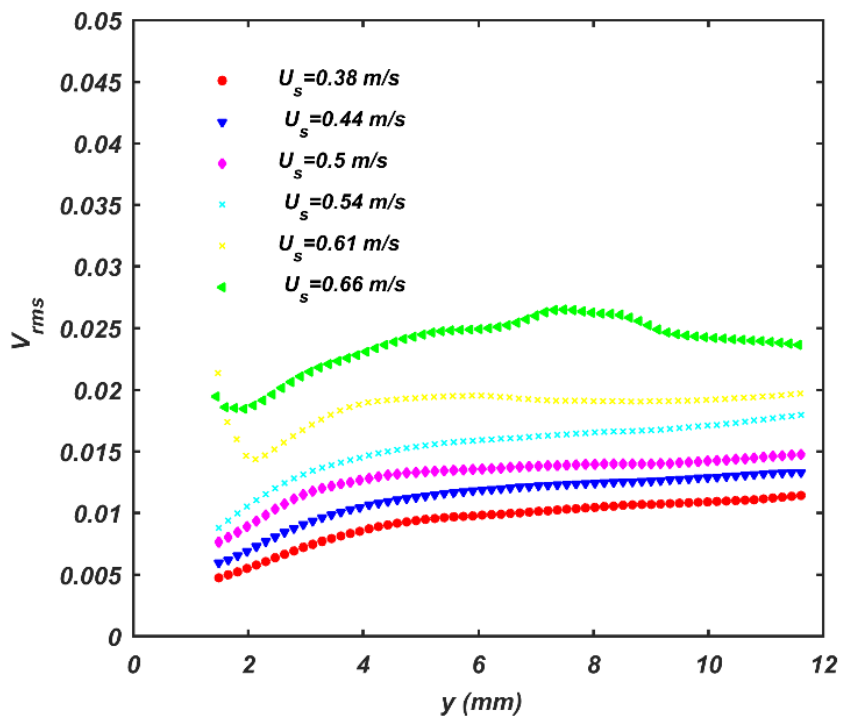

Figure 11-22 Profiles of V_{rms} for flow over bed A

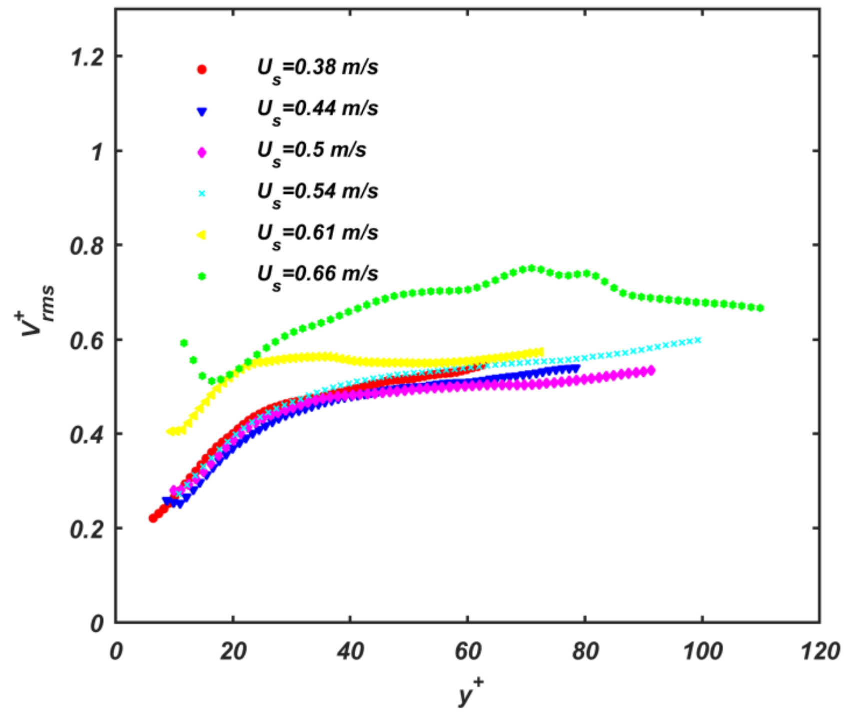

Figure 11-23 Profiles of V^+_{rms} for flow over bed A

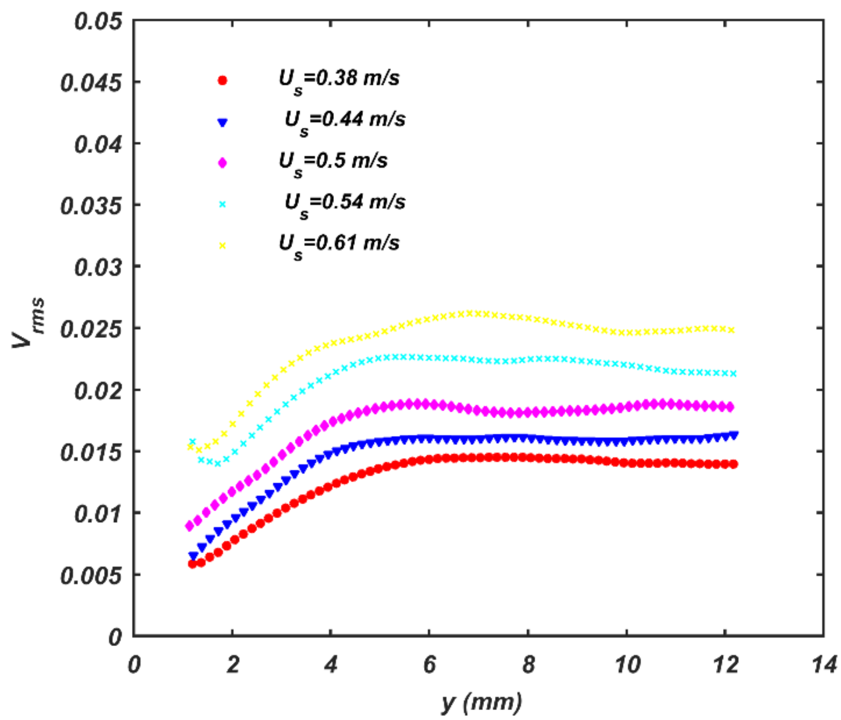

Figure 11-24 Profiles of V_{rms} for flow over bed B

Radial intensity profiles registered for flow over bed B are reported in Figure 11-24 and Figure 11-25. Figure 11-24 is the dimensional intensity profiles. The profiles are similar to the ones reported for flow over bed A.

The $V_{rms}{}^{+}$ profiles show an increase to at highest two flow rates. The cause was associated with the movement of sand particles in the bed.

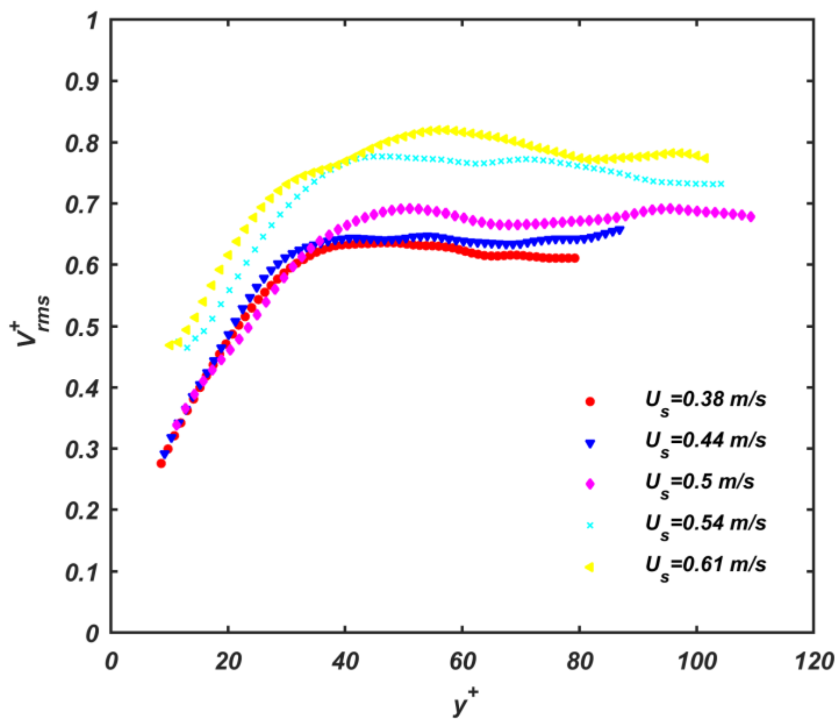

Figure 11-25 Profiles of V^+_{rms} for flow over bed B

Finally, we compare the radial intensity profiles in dimensional and wall units for flow over bed C in Figure 11-26 and Figure 11-27. The general behavior is similar to previous two beds.

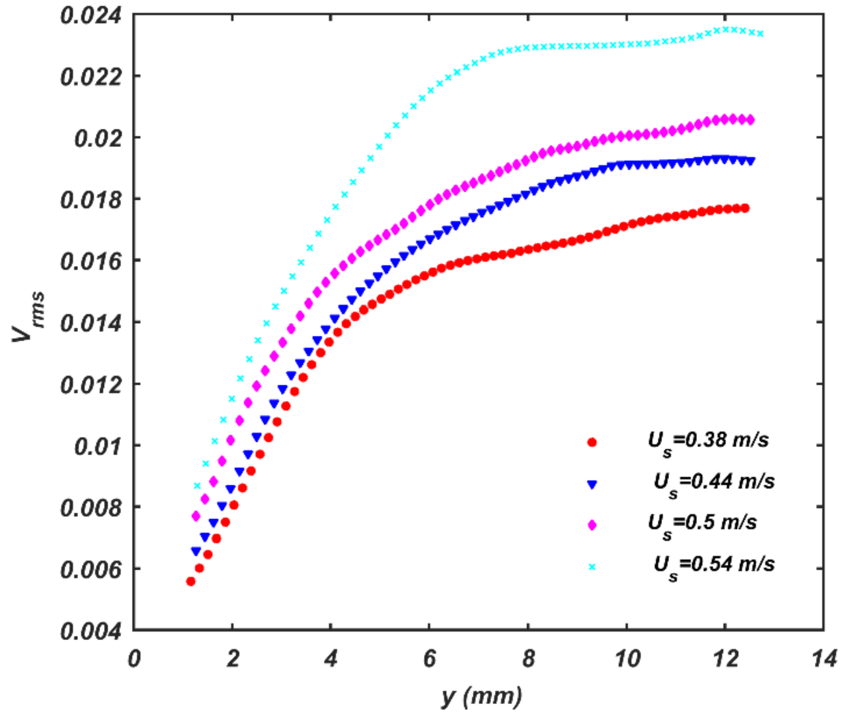

Figure 11-26 Profiles of V_{rms} for flow over bed C

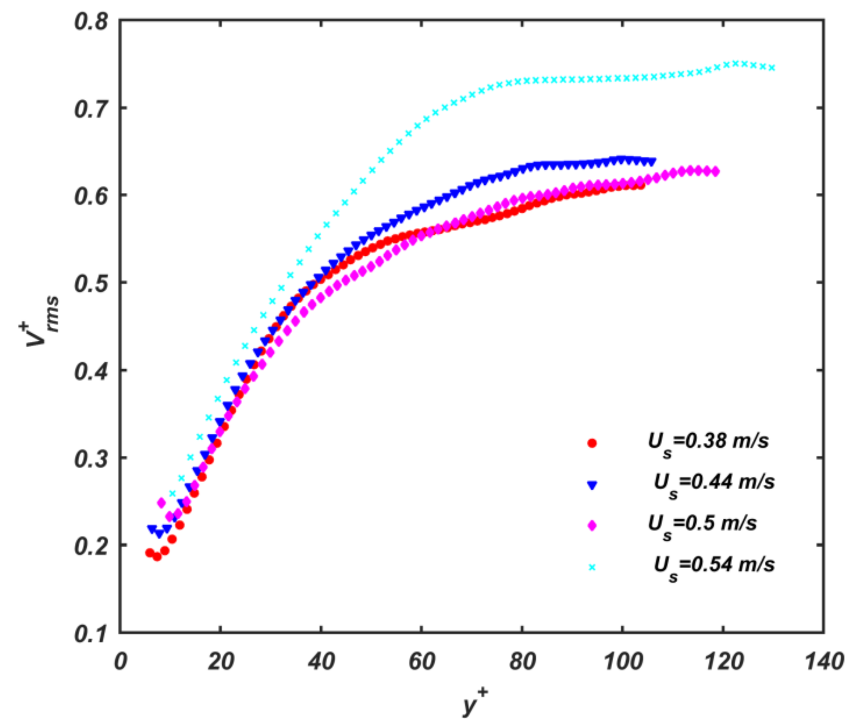

Figure 11-27 Profiles of V_{rms}^{+} for flow over bed C

We compared the radial intensity profiles over three beds of different initial heights in Figure 11-28. The data are presented for the superficial velocity of $0.5\,\frac{m}{s}$. Increasing bed height from bed A to B causes an increase in the radial intensity. The main reason for this is the increase in bulk fluid velocity due to the reduction of flow area by bed B. The difference in profiles for beds B and C are not as significant, especially near the bed interface.

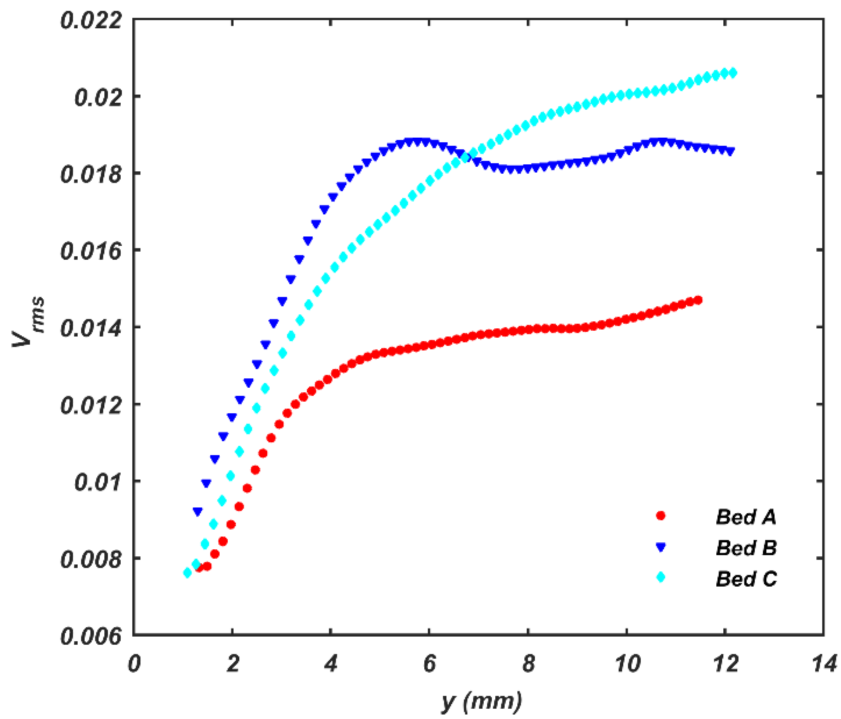

Figure 11-28 Profiles of V_{rms} measured at 0.5 m/s for flow over beds of different height

11.5. Conclusions

This paper reported results of an experimental study where the turbulent flow of a dilute polymer solution was investigated. The experiments were conducted in an eccentric annulus. The measurements were carried out over three sand beds of different initial heights. The measurement technique was the PIV. The sand particles were natural quartz particles with a mean sieve diameter of 600 microns. The experiments have been conducted for flow over a stationary sand bed as well as flow over a moving sand bed in the form of bedload.

The analysis of velocity profiles in the wall unit showed that velocity profiles obey the linear relation of the law of the wall in the viscous sublayer for all the experiments. In the logarithmic region, an upward shift in the velocity occurred compared to the log-law of Newtonian fluids. On the other hand, the velocity profiles in the log-zone fell short of the Virk's asymptote. Movement of the sand particles at the higher flow rates did not affect the velocity profiles. The results indicated the flow is primarily in the hydraulically smooth regime. The results suggest that using of polymer fluids for eroding a sand bed delays the transition to rough hydraulic flow.

Profiles of Reynolds normal and shear stress were also reported and discussed. Reynolds stress showed a non-zero value at all the tested flow rates. It progressively increased with increasing flow rate and the stationary bed height. No noticeable impact on bedload transport of particles was observed in the production of Reynolds stress.

The axial turbulence intensity profiles in wall unit revealed the peak intensity is located in the buffer zone. This observation is in agreement with previously published works on the turbulent flow of drag reducing polymers. Movement of sand particles in the bed appeared to cause a slight shift of the peak intensity to higher y^+ values.

Radial turbulence intensity profiles were also analyzed for the flow of the polymer fluids. The results indicated that radial intensity is non-zero. Profiles of normalized radial intensity in wall units showed that bedload transport of particles might slightly enhance production of velocity fluctuations in the radial direction. The increase of radial intensities was observed at the highest fluid velocity for all the cases.

11.6. Nomenclature

R	Inner Radius of outer pipe (m)
r	Outer Radius of inner tube (m)
D_h	Hydraulic Diameter (mm)
y	Distance from bed interface (mm)
L	Distance between center of pipes (m)
A	Annular area cross-section $(\pi({R_o}^2 - {R_i}^2))$ (m^2)
A_f	Cross-section available to flow (m^2)

h	Cuttings bed height (m)
K	Consistency index $(Pa.S^{1-n})$
n	Flow behavior index
Q	Flow Rate (m^3/s)
U_s	Superficial velocity $(\frac{m}{s})$
U_b	Actual fluid velocity $(\frac{m}{s})$
d_p	Particles diameter (m)
u	Time average velocity $(\frac{m}{s})$
$\hat{u}$	Instantaneous axial velocity $(\frac{m}{s})$
$\hat{v}$	Instantaneous radial velocity $(\frac{m}{s})$
u'	Axial fluctuation velocity $(\frac{m}{s})$
v'	Radial fluctuation velocity $(\frac{m}{s})$
ρ	Density $\left(\frac{Kg}{m^3}\right)$
μ	Apparent viscosity $(Pa.s)$
τ	Shear Stress (Pa)
τ_{Re}	Reynolds stress $= -\rho\overline{u'v'}$ (Pa)
κ	von Karman constant (0.41)
u_τ	Friction velocity $(\frac{m}{s})$

11.7. References

Baird, D. G. (2008). First normal stress difference measurements for polymer melts at high shear rates in a slit-die using hole and exit pressure data. Journal of Non-Newtonian Fluid Mechanics **148**(1–3): 13-23, DOI: http://dx.doi.org/10.1016/j.jnnfm.2007.04.007.

Best, J., Bennett, S., Bridge, J. et al. (1997). Turbulence modulation and particle velocities over flat sand beds at low transport rates. Journal of Hydraulic Engineering-Asce **123**(12): 1118-1129, J Hydraul Eng-Asce, DOI: c 10.1061/(Asce)0733-9429(1997)123:12(1118).

Bigillon, F., Couronne, G., Champagne, J. Y. et al. (2006). Investigation of flow hydrodynamics under equilibrium bedload transport conditions using PIV. River Flow 2006, Vols 1 and 2: 859-865, Proc Monogr Eng Wate, DOI: ://WOS:000241916500090.

Bizhani, M., Corredor, F. E. R. and Kuru, E. (2016). Quantitative Evaluation of Critical Conditions Required for Effective Hole Cleaning in Coiled-Tubing Drilling of Horizontal Wells. **SPE** Drilling & Completion **31**(3): 188-199, DOI: http://dx.doi.org/10.2118/174404-PA.

Bizhani, M. and Kuru, E. (2017). Effect of Sand Bed Deposits on the Characteristics of Turbulent Flow of Water in Horizontal Annuli ASME fluid engineering, Paper under review.

Carbonneau, P. E. and Bergeron, N. E. (2000). The effect of bedload transport on mean and turbulent flow properties. Geomorphology **35**(3-4): 267-278, Geomorphology, DOI: g10.1016/S0169-555x(00)00046-5.

Chan-Braun, C. (2012). Turbulent Open Channel Flow, Sediment Erosion and Sediment Transport, KIT Scientific Publ.

Chan-Braun, C., Garcia-Villalba, M. and Uhlmann, M. (2011). Force and torque acting on particles in a transitionally rough open-channel flow. Journal of Fluid Mechanics **684**: 441-474, J Fluid Mech, DOI: 10.1017/jfm.2011.311.

Chung, S. Y., Rhee, G. H. and Sung, H. J. (2002). Direct numerical simulation of turbulent concentric annular pipe flow - Part 1: Flow field. International Journal of Heat and Fluid Flow **23**(4): 426-440, Int J Heat Fluid Fl, DOI: 10.1016/S0142-727X(02)00140-6.

Davies, J. T. (1987). Calculation of Critical Velocities to Maintain Solids in Suspension in Horizontal Pipes. Chemical Engineering Science **42**(7): 1667-1670, Chem Eng Sci, DOI: 10.1016/0009-2509(87)80171-9.

Dodge, D. W. and Metzner, A. B. (1959). Turbulent Flow of Non-Newtonian Systems. Aiche Journal **5**(2): 189-204, Aiche J, DOI: DOI 10.1002/aic.690050214.

Duan, M. Q., Miska, S., Yu, M. J., Takach, N., Ahmed, R., Zettner, C. (2009). Critical Conditions for Effective Sand-Sized-Solids Transport in Horizontal and High-Angle Wells. SPE Drilling & Completion **24**(2): 229-238, **SPE** Drill Completion, DOI: 10.2118/104192-PA.

Escudier, M. P. and Gouldson, I. W. (1995). Concentric Annular-Flow with Centerbody Rotation of a Newtonian and a Shear-Thinning Liquid. International Journal of Heat and Fluid Flow **16**(3): 156-162, Int J Heat Fluid Fl, DOI: 10.1016/0142-727x(95)00012-F.

Escudier, M. P., Gouldson, I. W. and Jones, D. M. (1995). Flow of Shear-Thinning Fluids in a Concentric Annulus. Experiments in Fluids **18**(4): 225-238, Exp Fluids.

Gaudio, R., Miglio, A. and Dey, S. (2010). Non-universality of von Karman's kappa in fluvial streams. Journal of Hydraulic Research **48**(5): 658-663, J Hydraul Res, DOI: http://dx.doi.org/10.1080/00221686.2010.507338.

Ghaemi, S., Rafati, S.,Bizhani, M., Kuru, E. (2015). Turbulent structure at the midsection of an annular flow. Physics of Fluids **27**(10): 105102, DOI: http://dx.doi.org/10.1063/1.4932109.

Japper-Jaafar, A., Escudier, M. P. and Poole, R. J. (2010). Laminar, transitional and turbulent annular flow of drag-reducing polymer solutions. Journal of Non-Newtonian Fluid Mechanics **165**(19-20): 1357-1372, J Non-Newton Fluid, DOI: 10.1016/j.jnnfm.2010.07.001.

Kawaguchi, Y., Segawa, T., Feng, Z. et al. (2002). Experimental study on drag-reducing channel flow with surfactant additives—spatial structure of turbulence investigated by PIV system. International Journal of Heat and Fluid Flow **23**(5): 700-709, DOI: http://dx.doi.org/10.1016/S0142-727X(02)00166-2.

Kundu, P. K., Cohen, I. M. and Dowling, D. R. (2012). Fluid Mechanics, 4th Edition. Amsterdam, Elsevier Science Bv.

Lin, Y., Phan-Thien, N. and Khoo, B. C. (2014). Normal stress differences behavior of polymeric particle suspension in shear flow. Journal of Rheology **58**(1): 223-235, DOI: 10.1122/1.4855496.

Lumley, J. L. (1969). Drag Reduction by Additives. Annual Review of Fluid Mechanics **1**: 367-&, Annu Rev Fluid Mech, DOI: DOI 10.1146/annurev.fl.01.010169.002055.

Melling, A. (1997). Tracer particles and seeding for particle image velocimetry. Measurement Science & Technology **8**(12): 1406-1416, Meas Sci Technol, DOI: 10.1088/0957-0233/8/12/005.

Mitchell, R. F., Miska, S., Aadnøy, B. S. et al. (2011). Fundamentals of Drilling Engineering, Society of Petroleum Engineers.

Miyazaki, K., Chen, G. , Ymamoto, F., Ohta, J., Murai, Y., Horii, K. (1999). PIV measurement of particle motion in spiral gas-solid two-phase flow. Experimental Thermal and Fluid Science **19**(4): 194-203, Exp Therm Fluid Sci, DOI: 10.1016/S0894-1777(99)00020-5.

Nikora, V. and Goring, D. (2000). Flow Turbulence over Fixed and Weakly Mobile Gravel Beds. Journal of Hydraulic Engineering **126**(9): 679-690, DOI: doi:10.1061/(ASCE)0733-9429(2000)126:9(679).

Nouri, J. M., Umur, H. and Whitelaw, J. H. (1993). Flow of Newtonian and Non-Newtonian Fluids in Concentric and Eccentric Annuli. Journal of Fluid Mechanics **253**: 617-641, J Fluid Mech, DOI: 10.1017/S0022112093001922.

Owen, P. R. (1964). Saltation of uniform grains in air. Journal of Fluid Mechanics **20**(2): 225-242, DOI: 10.1017/S0022112064001173.

Paschkewitz, J. S., Dimitropoulos, C. D., Hou, Y. X. et al. (2005). An experimental and numerical investigation of drag reduction in a turbulent boundary layer using a rigid rodlike polymer. Physics of Fluids **17**(8), Phys Fluids, DOI: Artn 085101 10.1063/1.1993307.

Pinho, F. T. and Whitelaw, J. H. (1990). Flow of Non-Newtonian Fluids in a Pipe. Journal of Non-Newtonian Fluid Mechanics **34**(2): 129-144, J Non-Newton Fluid, DOI: Doi 10.1016/0377-0257(90)80015-R.

Poole, R. J. (2010). Development-Length Requirements for Fully Developed Laminar Flow in Concentric Annuli. Journal of Fluids Engineering-Transactions of the **Asme 132**(6), J Fluid Eng-T Asme, DOI: 10.1115/1.4001694.

Ptasinski, P. K., Boersma, B. J., Nieuwstadt, F. T. M. et al. (2003). Turbulent channel flow near maximum drag reduction: simulations, experiments and mechanisms. Journal of Fluid Mechanics **490**: 251-291, J Fluid Mech, DOI: 10.1017/S0022112003005305.

Ptasinski, P. K., Nieuwstadt, F. T. M., van den Brule, B. H. A. A. et al. (2001). Experiments in turbulent pipe flow with polymer additives at maximum drag reduction. Flow Turbulence and Combustion **66**(2): 159-182, Flow Turbul Combust, DOI: Doi 10.1023/A:1017985826227.

Rehme, K. (1974). Turbulent-Flow in Smooth Concentric Annuli with Small Radius Ratios. Journal of Fluid Mechanics **64**(2): 263-287, J Fluid Mech, DOI: http://dx.doi.org/10.1017/S0022112074002394.

Rinoshika, A., Yan, F. and Kikuchi, M. (2012). Experimental study on particle fluctuation velocity of a horizontal pneumatic conveying near the minimum conveying velocity. International Journal of Multiphase Flow **40**: 126-135, DOI: https://doi.org/10.1016/j.ijmultiphaseflow.2011.11.007.

Virk, P. S., Mickley, H. S. and Smith, K. A. (1970). Ultimate Asymptote and Mean Flow Structure in Toms Phenomenon. Journal of Applied Mechanics **37**(2): 488-+, J Appl Mech.

Warholic, M. D., Heist, D. K., Katcher, M. et al. (2001). A study with particle-image velocimetry of the influence of drag-reducing polymers on the structure of turbulence. Experiments in Fluids **31**(5): 474-483, Exp Fluids, DOI: DOI 10.1007/s003480100288.

Warholic, M. D., Massah, H. and Hanratty, T. J. (1999). Influence of drag-reducing polymers on turbulence: effects of Reynolds number, concentration and mixing. Experiments in Fluids **27**(5): 461-472, Exp Fluids, DOI: DOI 10.1007/s003480050371.

Wilson, K. C. and Thomas, A. D. (1985). A New Analysis of the Turbulent-Flow of Non-Newtonian Fluids. Canadian Journal of Chemical Engineering **63**(4): 539-546.

Yan, F. and Rinoshika, A. (2011). Application of high-speed PIV and image processing to measuring particle velocity and concentration in a horizontal pneumatic conveying with dune model. Powder Technology **208**(1): 158-165, Powder Technol, DOI: 10.1016/j.powtec.2010.12.014.

Yan, F. and Rinoshika, A. (2012). Characteristics of particle velocity and concentration in a horizontal self-excited gas-solid two-phase pipe flow of using soft fins. International Journal of Multiphase Flow **41**: 68-76, Int J Multiphas Flow, DOI: 10.1016/j.ijmultiphaseflow.2012.01.004.

Zeinali, H., Toma, P. and Kuru, E. (2012). Effect of Near-Wall Turbulence on Selective Removal of Particles From Sand Beds Deposited in Pipelines. Journal of Energy Resources Technology-Transactions of the **Asme** **134**(2), J Energ Resour-Asme, DOI: 10.1115/1.4006041.

Zheng, Y., Rinoshika, A. and Yan, F. (2012). Multi-scale analysis on particle fluctuation velocity near the minimum pressure drop in a horizontal pneumatic conveying. Chemical Engineering Science **72**: 94-107, DOI: https://doi.org/10.1016/j.ces.2012.01.011.

11.8. Appendix

Details of calculation related to hydraulic diameter and cross-sectional area of the annulus in the presence of the bed are presented in this appendix (See Fig. A-1 for details) (Duan 2009).

Case 1: h<2r

$$S_o = 2R\ arccos(\frac{h-R}{R}) \qquad \textbf{Eq. (A- 11-1)}$$

$$S_i = 2r\ \arccos(\frac{h-r}{r}) \qquad \textbf{Eq. (A- 11-2)}$$

$$S_b = 2\sqrt{R^2-(R-h)^2} - 2\sqrt{r^2-(r-h)^2} \qquad \textbf{Eq. (A- 11-3)}$$

$$A_f = R^2\ arccos\left(\frac{h-R}{R}\right) + (R-h)\sqrt{R^2-(R-h)^2} - r^2 \arccos\left(\frac{h-r}{r}\right) - (r-h)\sqrt{r^2-(r-h)^2} \qquad \textbf{Eq. (A- 11-4)}$$

Case 2: h>2r

$$S_o = 2R\ arccos(\frac{h-R}{R}) \qquad \textbf{Eq. (A- 11-5)}$$

$$S_i = 0 \qquad \textbf{Eq. (A- 11-6)}$$

$$S_b = 2\sqrt{R^2 - (R-h)^2}$$ **Eq. (A- 11-7)**

$$A_f = R^2\, arccos\left(\frac{h-R}{R}\right) + (R-h)\sqrt{R^2 - (R-h)^2}$$ **Eq. (A- 11-8)**

The hydraulic diameter is:

$$D_h = \frac{4A_f}{S_o + S_i + S_b}$$ **Eq. (A- 11-9)**

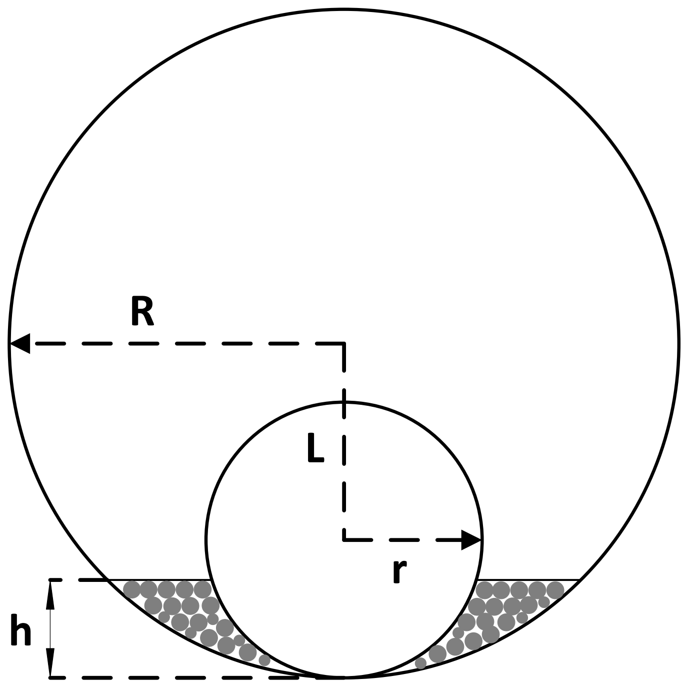

Figure A- 11-1 Illustration of dimensions used in calculations of cross section and hydraulic diameter

12. Modeling turbulent flow of non-Newtonian fluids in concentric annulus using generalized Newtonian models[10]

In this chapter result of a CFD modeling study on the turbulent flow of non-Newtonian fluids in the concentric annulus is discussed. The primary motivation of this work to examine the reliability of the vialabel CFD studies on the topic of solid transport.

12.1. Abstract

Computational Fluid Dynamic (CFD) is used to model the turbulent flow of non-Newtonian polymeric fluids in a concentric annulus. The so-called Generalized Newtonian Fluid (GNF) approach is used. Four turbulence models are tested. Applicability of each model in predicting the turbulent flow of non-Newtonian fluids in the annulus is assessed by comparing results of pressure loss and or velocity profiles with experimental data.

The first tested model is a modified version of Lam-Bremhorst $k-\varepsilon$ turbulence model. The modification was originally developed to model flow of power law fluids in smooth circular pipes. Results of simulation study showed that this model significantly overestimates the pressure losses.

Two $k-\varepsilon$ closure type turbulence models, one developed to model turbulent flow of Herschel-Buckley and the other for power law fluids, are shown to fail in predicting turbulent flow of polymer solutions. One of the models contains a damping function which is analyzed to show its inadequacy in damping the eddy viscosity.

The last tested model is a one-layer turbulence model developed for predicting turbulent flow in annular passages. The model has an adjustable parameter, which is shown to control the slope

[10] A version of this chapter has been presented. • Bizhani, M and E. Kuru, 2015, "Modeling Turbulent Flow of Non-Newtonian Fluids using Generalized Newtonian Models," Proceedings of the ASME 2015 34th International Conference on Ocean, Offshore and Arctic Engineering OMAE2015 May 31-June 5, 2015, St. John's, Newfoundland, Canada

of velocity profiles in the logarithmic region. It is demonstrated that if the model constant is selected carefully, the model accurately predicts pressure loss and velocity profiles.

Keywords: CFD, non-Newtonian, Turbulent, Annuli

12.2. Introduction

During drilling operations drilling fluid is pumped down the drill string and is returned to the surface through the annular space between the borehole and the drill string. Amongst other functionalities of the drilling fluid, transporting the cuttings effectively is of utmost importance. To increase their transport capacity, drilling fluids are commonly formulated using viscosifier such as bentonite, natural or synthetic polymers. Drilling fluids are classified as non-Newtonian fluid with shear thinning characteristics.

In highly inclined and horizontal wellbores, efficient hole cleaning becomes challenging as the cuttings tend to form a bed on the low side of the wellbore. To overcome this problem, drilling fluids are pumped at relatively high flow rates, hence, presenting an interesting application of a turbulent flow of non-Newtonian fluids in annular geometry.

Turbulent flow of non-Newtonian fluids has been the subject of many experimental studies in the past (Virk et al. 1970, Pinho and Whitelaw 1990, Nouri et al. 1993, Escudier et al. 1995, Warholic et al. 1999, Ptasinski et al. 2001, Warholic et al. 2001, Ptasinski et al. 2003, Paschkewitz et al. 2005, Li and Kuru 2009, Japper-Jaafar et al. 2010, Rodriguez-Corredor et al. 2014). Some of the key findings of experimental works are : the shift of velocity profiles away from the Newtonian fluids curve in the logarithmic region (Pinho and Whitelaw 1990, Nouri et al. 1993, Escudier et al. 1995, Ptasinski et al. 2001, Japper-Jaafar et al. 2010, Rodriguez-Corredor et al. 2014), thickening of buffer and sub-layer (Lumley 1969, Wilson and Thomas 1985), Reynolds stress reduction (Pinho and Whitelaw 1990, Nouri et al. 1993, Warholic et al. 2001, Ptasinski et al. 2003, Paschkewitz et al. 2005, Japper-Jaafar et al. 2010, Rodriguez-Corredor et al. 2014), stress deficit (Ptasinski et al. 2001, Ptasinski et al. 2003) and vortex inhibition and suppression of radial velocity fluctuations (Pinho and Whitelaw 1990, Nouri et al. 1993, Warholic et al. 2001, Japper-Jaafar et al. 2010). Also according to Virk's asymptote (Virk et al. 1970) there is a maximum achievable drag reduction for a given flow condition. Experimental study of turbulent non-Newtonian fluids is not a trivial task. It has many complications as it requires constant monitoring of rheology. Also, most non-Newtonian fluids are not transparent which imposes difficulty in using non-intrusive measuring techniques such as Particle Image Velocimetry.

Turbulent flow modeling of Newtonian fluids has been performed in the past by using standard models. Chung et al. (Chung et al. 2002) have conducted a Direct Numerical Simulation (DNS) of turbulent flow in the annulus. Their results were in agreement with experimental data. Large Eddy Simulation (LES) also has been performed for turbulent flow of water in annuli with inner body rotation. Results were also in agreement with previous experimental studies (Chung and Sung 2005). Some other studies modeled turbulent flow with Reynolds Averaged Navier-Stokes (RANS) formulations (Naser 1991, Azouz and Shirazi 1998, Neto et al. 2011)

Modeling turbulent flow of Non-Newtonian fluids, however, has not been as prevalent as its Newtonian counterpart. The reason being is that appropriate RANS models which can account for the unique phenomenon (e.g. drag reduction) associated with turbulent non-Newtonian fluids have not been developed yet. Standard models of Newtonian fluids fail when it comes to the subject of drag reduction (Naser 1991). DNS studies have been performed mostly in the channel and pipe flow to reveal the fundamental characteristics of the turbulent flow of polymer solutions (Sureshkumar et al. 1997, Sibilla and Baron 2002, Ptasinski et al. 2003). Results of DNS models are used to develop models similar to Newtonian fluid models which could readily be used for modeling non-Newtonian fluids flow(Pinho et al. 2008, Iaccarino et al. 2010, Resende et al. 2011). Nevertheless, DNS is limited to low Reynolds numbers flow and is not applicable in practical situations. Currently, there are numerous numbers of emerging papers with closure equations for modeling turbulent drag reduction. Almost all of these recent studies use viscoelastic models of polymer solutions.

Apart from DNS which solves the transport equations in combinations with some viscoelastic laws (e.g. FENE-P); another approach used for modeling turbulent non-Newtonian fluid flow is the so-called Generalized Newtonian Fluid (GNF) approach. In GNF approach, the elastic properties of the fluids are mostly ignored. There are some models, however, which accounts for elastic properties such as extensional viscosity, see for example, (Pinho 2003). These models try to reproduce drag reduction effect by controlling the production of turbulent viscosity by utilizing damping functions (Hassid and Poreh 1978, Azouz and Shirazi 1997, Malin 1997, Ro and Ryou 2012, Podryabinkin and Rudyak 2014) and in some instances by modifying transport equations (Hassid and Poreh 1978). Some of these models are simple zero equation models such as the one proposed by Azouz et al. (Azouz and Shirazi 1997). Others like turbulence model of Hassid et al. (Hassid and Poreh 1978) are of 2 equations family models. Four turbulence models of this type are discussed in the next sections.

In this paper, we examine the GNF approach in modeling the turbulent flow of dilute polymer solutions in the annulus. Results of simulation with four turbulence models are presented in this article. Viscoelastic properties of the polymer solutions are not taken into account by any of these models. First turbulence model is a modified version of Lam-Bremhorst (Lam and Bremhorst 1981) $k-\varepsilon$ turbulence model. The modification was proposed by Malin (1997) and applies to power law fluids. Two high Reynolds number $k-\varepsilon$ turbulence models are also examined (Ro and Ryou 2012, Podryabinkin and Rudyak 2014). The last model is a zero equation turbulence model proposed by (Azouz and Shirazi 1997). Results of simulations are compared with previously published experimental work by the authors (Rodriguez-Corredor et al. 2014). The paper is organized in the following fashion. First we present underlying mathematical equations for each turbulence model. In the next section results of simulation for each model is compared with experimental and theoretical data and conclusions is drawn based on the results. Conclusions of this work are reported at the end.

12.3. Governing Equations

12.3.1. Rheology models

The flow of a shear thinning polymeric solution in the concentric horizontal annulus is considered. The experimental data used for comparison and validation of different models have been previously obtained and published by the authors (Rodriguez-Corredor et al. 2014). The rheology of the polymer solution considered in this study can be described either as a power law model or with a more accurate Bird-Carreau model (Bird 1987). Equations 1 & 2 represent the apparent viscosity of the polymer solution; for more detail, please see [10].

$$\mu = 0.0315\dot{\gamma}^{-0.2479} \qquad \textbf{Eq.(12-1)}$$

$$\frac{\mu - 1.5}{23.2 - 1.5} = (1 + (0.1096\dot{\gamma})^2)^{\frac{0.6541-1}{2}} \quad \textbf{Eq.(12-2)}$$

We have adopted power law model in this study mainly because some of the turbulence models are specifically developed for a fluid of this type. Simulations are performed using the commercial CFD code of FLUENT 15.0. Turbulent flow of non-Newtonian fluid with three solvent Reynolds numbers (see Table 12-1) is modeled. For some of the turbulence models which were found not suitable for modeling the flow of this type of fluids only one or two Reynolds numbers are tested. The solvent Reynolds number is defined as follow:

$$Re_s = \frac{\rho U_B D_H}{\mu_s} \quad \textbf{Eq.(12-3)}$$

μ_s is solvent viscosity (water), D_H annulus hydraulic diameter (57 mm), U_B is the bulk velocity (flow rate divided by cross sectional area) and ρ is the fluid density. For more details on experimental setup and data please refer to (Rodriguez-Corredor et al. 2014).

Table 12-1 Operating conditions under which experimental data were obtained

$U_B\ (\frac{m}{s})$	$Re_s\ (-)$
0.827	47000
1	57000
1.16	66400

12.1.1. Numerical procedure

All the simulations are performed using the commercial CFD code of FLUENT 15.0. Turbulence models are integrated into the solver via C programming and FLUENT UDF functionality. All the cases were run under steady state condition. Coupling between velocity and pressure field was obtained using the SIMPLE algorithm. All the PDE's are discretized in space using QUICK scheme. Gradients are obtained by using Least Square Cell-Based technique. Double precision is used in all the cases. Convergence is decided by monitoring both equations residuals and also monitoring velocity in the middle of the annuli's cross section (i.e. at a radius of 33 mm). The criterion for convergence with residuals level is reported in Table 12-2. Also, maximum velocity (in the middle part of the annular gap) is monitored to ensure no further change occur as solution converges.

Table 12-2 Convergence criterion for residuals

Equation	Residual level
Continuity	10^{-8}
Momentum (x, y and z)	10^{-6}
Turbulence kinetic energy	10^{-5}
Turbulence Dissipation rate	10^{-5}

In this paper we examine 4 turbulence models. Three of these models are from $k-\varepsilon$ closure family and one is based on an algebraic expression of eddy viscosity. For the $k-\varepsilon$ models, one uses low Reynolds number closure. Therefore, to resolve the boundary layer, it is necessary to ensure the first node is placed within a distance of $y^+ < 1$ from the solid walls. This was accomplished in the mesh generation process by employing inflation layers near the pipe walls (seeFigure 12-1).

The other two $k-\varepsilon$ turbulence models are of high Reynolds number type models, which use wall functions. When using wall function, it's important to ensure that the first node is outside the viscous sublayer ($y^+ > 11.2$). According to Ansys FLUENT documentation, it is recommended to avoid any node with $y^+ < 30$. To satisfy this condition a new mesh was generated (Figure 12-2). This new mesh was used to test the high Reynolds number turbulence models with scalable wall function (Which is identical to standard wall function for cases where nearest node to wall has a $y^+ > 11.2$).

12.1.2. Boundary conditions

The domain of interest is an annulus 8-meter-long with a hydraulic diameter of 57 mm and radius ratio of 0.4. The inlet boundary condition is set to velocity inlet with uniform velocity profile (i.e. constant average velocity at the inlet). The outlet is configured to pressure outlet at atmospheric pressure. All the walls are no smooth walls.

12.1.3. Grid independencey analysis

To make sure that numerical solutions are independent of the selected grid, grid independence analysis is performed. The mesh (Figure 12-1) was systematically coarsened, and simulation was performed for each mesh.Table 12-3 reports the number of nodes for each case. For each mesh after convergence, we compare the variation in predicted pressure loss to see if any significant change occurs due to the mesh refinement (results of the analysis are presented for turbulence model of Azouz and Shirazi (1997)).

According to the data presented in Table 12-3 refining the mesh causes no change in the solution (note that we choose the pressure loss to compare as it is an integral quantity and therefore is affected by mesh refinement in the entire domain). This guarantees that the solution is independent of the selected mesh.

Grid independencey analysis for high Reynolds number models is also performed. Results of pressure loss prediction by turbulence model of Podryabinkin and Rudyak (2014) when using two different meshes are reported in Table 12-4. As this result shows no significant change is observed in the predicted pressure loss. Therefore, the solution is regarded as grid independent.

Table 12-3 Grid independency analysis for low Reynolds number turbulence models ($Re_s = 47000$)

N (number of nodes)	$(\frac{dP}{dx})_{simulation}$ $(\frac{Pa}{m})$
861648	152
1096200	152
1134000	152
1234800	152
1589184	152

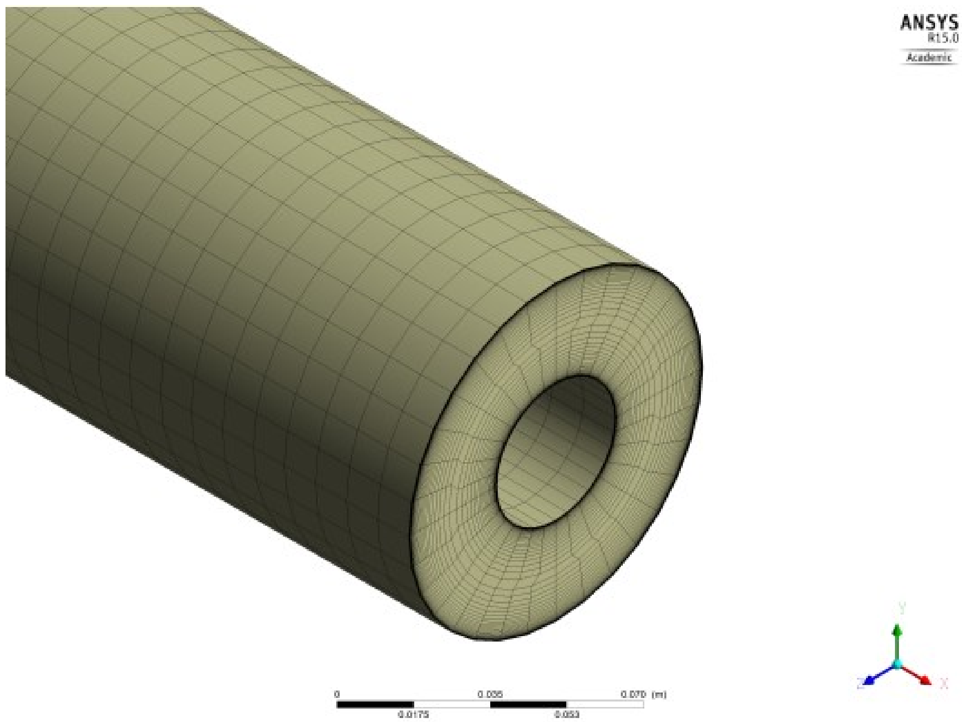

Figure 12-1 Schematic of mesh used for low Reynolds number turbulence models

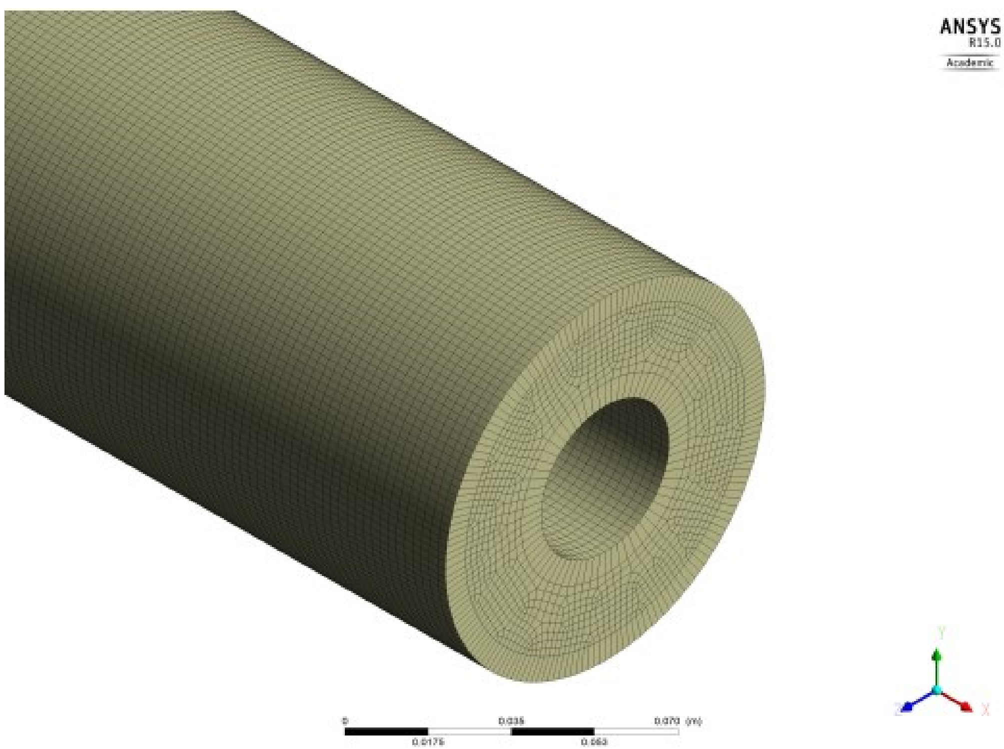

Figure 12-2 Schematic of mesh used for high Reynolds number turbulence models

Table 12-4 Grid independency analysis for high Reynolds number turbulence models ($Re_s = 47000$)

N (number of nodes)	$(\frac{dP}{dx})_{simulation}$ $(\frac{Pa}{m})$
1318356	307
4667298	308

12.2. Governing equations for turbulence model of Malin

Malin (1997) proposed a modification to the low Reynolds number $k - \varepsilon$ turbulence model of Lam-Bremhorst (LB)(Lam and Bremhorst 1981). The modification is applied to the wall damping function of the eddy viscosity. The effect of non-Newtonian behavior is introduced by incorporating flow behavior index in the eddy viscosity damping function. The proposed model was originally developed for flow of power law fluids in smooth circular pipes. The governing equations are as follows (for steady incompressible flow):

$$\frac{\partial \mathrm{u}_k}{\partial \mathrm{x}_k} = 0 \quad \textbf{Eq.(12-4)}$$

$$\frac{\partial}{\partial \mathrm{x}_k}(\rho u_k u_i) = \frac{\partial}{\partial \mathrm{x}_k}\left(\mu(\frac{\partial u_i}{\partial \mathrm{x}_k} + \frac{\partial u_k}{\partial \mathrm{x}_i})\right) - \frac{\partial \mathrm{p}}{\partial \mathrm{x}_i} + \frac{\partial}{\partial x_j}\left(-\rho\overline{u_i' u_j'}\right) \quad \textbf{Eq.(12-5)}$$

μ is the fluid apparent viscosity described by power law model.

In the context of turbulence modeling with eddy viscosity, Reynolds stress is modeled using Boussinesq hypothesis. The relation between Reynolds stresses and eddy viscosity is described as follows.

$$-\rho\overline{u_i' u_j'} = \mu_t\left(\frac{\partial u_i}{\partial x_j} + \frac{\partial u_j}{\partial x_i}\right) - \frac{2}{3}\left(\rho k + \mu_t \frac{\partial u_k}{\partial x_k}\right)\delta_{ij} \quad \textbf{Eq.(12-6)}$$

δ_{ij} is the kronecker delta. μ_t is the eddy viscosity. The eddy viscosity is determined from the following relation (for $k-\varepsilon$ turbulence model):

$$\mu_t = C_\mu \rho f_\mu \frac{k^2}{\varepsilon} \quad \textbf{Eq.(12-7)}$$

Where f_μ is a damping function.

Turbulence kinetic energy and its dissipation rate are calculated from following equations:

$$\frac{\partial}{\partial \mathrm{x}_k}(\rho u_k k) = \frac{\partial}{\partial \mathrm{x}_k}\left(\left(\mu + \frac{\mu_t}{\sigma_k}\right)\frac{\partial \mathrm{k}}{\partial \mathrm{x}_k}\right) + \rho(P_k - \varepsilon) \quad \textbf{Eq.(12-8)}$$

$$\frac{\partial}{\partial \mathrm{x}_k}(\rho u_k \varepsilon) = \frac{\partial}{\partial \mathrm{x}_k}\left(\left(\mu + \frac{\mu_t}{\sigma_\varepsilon}\right)\frac{\partial \varepsilon}{\partial \mathrm{x}_k}\right) + \frac{\rho\varepsilon\left(c_{1_\varepsilon} f_1 P_k - c_{2_\varepsilon} f_2 \varepsilon\right)}{k} \quad \textbf{Eq.(12-9)}$$

P_k is the production of turbulence kinetic energy by mean velocity gradients.

$$P_k = \frac{2\mu_t}{\rho} S^2 \quad \textbf{Eq.(12-10)}$$

S is the strain rate magnitude.

The damping function for eddy viscosity is different from that of LB model (Eq.(12-11).

$$f_\mu = \left[1 - \exp\left(-\frac{0.0165 Re_n}{n^{\frac{1}{4}}}\right)\right]^2 \left(1 + \frac{20.5}{Re_t}\right) \quad \textbf{Eq.(12-11)}$$

$$f_1 = 1 + \left(\frac{0.05}{f_\mu}\right)^3 \quad \textbf{Eq.(12-12)}$$

$$f_2 = 1 + \exp(-Re_t^2) \quad \textbf{Eq.(12-13)}$$

$$Re_n = \sqrt{k}\frac{y_n}{\nu}$$ **Eq.(12-14)**

$$Re_t = \frac{k^2}{\varepsilon\nu}$$ **Eq.(12-15)**

All the constants are the same as reported by the Malin (1997).

12.2.1. Ro and Ryou damping factor

Based on standard high Reynolds number $k - \varepsilon$ turbulence model, Ro and Ryou (2012) proposed a modification for the eddy viscosity damping function. They argued that in the viscous sublayer, velocity profiles are similar for both Newtonian and non-Newtonian fluids; therefore, high Reynolds number model was used. In the buffer layer, velocity profiles for non-Newtonian fluids tends towards Virk's ultimate asymptote (Virk et al. 1970). The extent to which buffer layer reaches is a varying function of drag reduction. Authors proposed that beyond buffer layer (in the region where shear rate is so small that viscosity change is negligible) flow of Newtonian and non-Newtonian fluids become similar.

The proposed model utilizes transport equations similar to the standard $k - \varepsilon$ turbulence model of Newtonian fluids. To create drag reduction effect, a damping function is introduced in the eddy viscosity formulation. The mathematical description of the model is as follows:

$$\mu_t = \rho F_\mu C_\mu \frac{k^2}{\varepsilon}$$ **Eq.(12-16)**

F_μ is the damping function which varies according to drag reduction:

$$F_\mu = (1 - A \times Dr \times B)^2$$ **Eq.(12-17)**

$$Dr = \frac{Dr\%}{Dr\%_{max}}$$ **Eq.(12-18)**

$$Dr\% = \frac{f_N - f_{NN}}{f_N} \times 100$$ **Eq.(12-19)**

$$Dr\%_{max} = \frac{f_N - f_{Virk}}{f_N} \times 100$$ **Eq.(12-20)**

$$A = \frac{1}{(1.16 + 4.36n - 5.53n^2) + (6.48e^{-5} - 2.29e^{-4}n + 1.58e^{-4}n^2)Re_g}$$ **Eq.(12-21)**

$$B = e^{(-0.015n^{-0.25}y^+)}$$ **Eq.(12-22)**

The Reynolds number is defined by using Dodge and Metzner (Dodge and Metzner 1959) generalized Reynolds number correlation:

$$Re_g = \frac{\rho {U_B}^{2-n} {D_H}^n}{k\left(0.75 + \frac{0.25}{n}\right)^n 8^{n-1}}$$ **Eq.(12-23)**

In the previous equations, $Dr\%$ is the degree of drag reduction, $Dr\%_{max}$ is the maximum possible drag reduction obtained according to Virk's asymptote (Virk et al. 1970). f_N &f_{NN} are Newtonian and non-Newtonian friction factor and f_{Virk} is the friction factor obtained using Virk's asymptote. Note that for a flow with zero drag reduction the standard $k - \varepsilon$ model is recovered. This model requires prior knowledge of the flow and drag reduction percentage. Also it must be mentioned that this model was originally developed for pipe flow. For the simulation work presented here, the original equation was modified by using annuli's hydraulic diameter in place of pipe diameter.

12.2.2. Turbulence model of Podryabinkin and Rudyak

Podryabinkin and Rudyak (2014)developed a turbulence model to study fully developed the turbulent flow of Herschel-Buckley fluids in annular passages. The model is a modified version of the standard $k - \varepsilon$ model of Newtonian fluids. Non-Newtonian property of the fluid is introduced to the model through the apparent viscosity term. According to the authors, an effective viscosity may be defined as follow:

$$\mu_e = \dot{\gamma}^{-1}(\tau_0 + k\dot{\gamma}^n) \qquad \textbf{Eq.(12-24)}$$

τ_0 is the fluid yield stress. The model differs from the standard $k-\varepsilon$ in the way shear rate being calculated. For the shear rate we have:

$$\dot{\gamma}^2 = 2S_{ij}S_{ij} + \frac{\rho\varepsilon}{\mu_e} \qquad \textbf{Eq.(12-25)}$$

$$S_{ij} = \frac{1}{2}\left(\frac{\partial \mathrm{u}_i}{\partial \mathrm{x}_j} + \frac{\partial \mathrm{u}_j}{\partial \mathrm{x}_i}\right) \qquad \textbf{Eq.(12-26)}$$

Other governing equations according toPodryabinkin and Rudyak (2014) are:

$$\frac{\partial}{\partial \mathrm{x}_k}(\rho u_k u_i) = \frac{\partial}{\partial \mathrm{x}_k}\left((\mu_e + \mu_t)(\frac{\partial \mathrm{u}_i}{\partial \mathrm{x}_k} + \frac{\partial \mathrm{u}_k}{\partial \mathrm{x}_i})\right) - \frac{\partial \mathrm{p}}{\partial \mathrm{x}_i} - \rho\frac{2}{3}\frac{\partial k}{\partial x_i} \qquad \textbf{Eq.(12-27)}$$

$$\frac{\partial}{\partial \mathrm{x}_k}(\rho u_k k) = \frac{\partial}{\partial \mathrm{x}_k}\left(\left(\mu + \frac{\mu_t}{\sigma_k}\right)\frac{\partial \mathrm{k}}{\partial \mathrm{x}_k}\right) + P_k - \rho\varepsilon \qquad \textbf{Eq.(12-28)}$$

$$\frac{\partial}{\partial \mathrm{x}_k}(\rho u_k \varepsilon) = \frac{\partial}{\partial \mathrm{x}_k}\left(\left(\mu + \frac{\mu_t}{\sigma_\varepsilon}\right)\frac{\partial \varepsilon}{\partial \mathrm{x}_k}\right) + c_{1\varepsilon}\frac{\varepsilon}{k}P_k - c_{2\varepsilon}\rho\frac{\varepsilon^2}{k} \qquad \textbf{Eq.(12-29)}$$

Constants and other relevant equations are the same as for standard $k-\varepsilon$ equation. The only change comparing to standard Newtonian models is the definition of the effective or average viscosity. Eddy viscosity is being calculated with no damping function (similar to Newtonian fluids).

12.2.3. Azouz & Shirazi turbulence model

Azouz and Shirazi (1997) developed a one-layer turbulence model to predict turbulent flow in annular passages. The mixing length approach was used in developing the model where a damping factor was employed to produce drag reduction effect. In this model, eddy viscosity was obtained using two algebraic expressions. Annular space was subdivided into two regions, and one equation for each subdivision was presented. There is no need to solve other transport equations and, hence, the model has the low computational expense. According to the authors, near each wall of the annuli there exists a shear layer. Shear layers extend from solid surface all the way to the plane of zero shear stress. Equations 30 and 31 are to be applied in the inner shear layer and outer shear layer in the calculation of eddy viscosity respectively.

$$\frac{\mu_t}{\mu} = \frac{1}{2}\left\{1 + \left[\frac{\kappa_i \delta_i u_{\tau i}}{3\nu}(1-\zeta_i^2)(1+2\zeta_i^2)\left(1-\left(1-\frac{\delta^*}{\sqrt{\tau^*}}\right)\zeta_i\right)\left(1 - \exp\left(-\frac{y_i^+}{A^+}\right)\right)\right]^2 - \frac{1}{2}\right\}^{\frac{1}{2}}$$ **Eq.(12-30)**

$$\frac{\mu_t}{\mu} = \frac{1}{2}\left\{1 + \left[\frac{\kappa_o \delta_o u_{\tau o}}{3\nu}(1-\zeta_o^2)(1+2\zeta_o^2)\left(1 - \exp\left(-\frac{y_o^+}{A^+}\right)\right)\right]^2 - \frac{1}{2}\right\}^{\frac{1}{2}}$$ **Eq.(12-31)**

In Eqs.30 and 31 κ is the Von Karman constant; for the outer shear layer it is 0.4 but for the inner shear layer it must be determined by equating the two expressions for eddy viscosity at the plane of zero shear stress. δ is the thickness of shear layers (i.e., the distance from the wall to the plane of zero shear stress). $\zeta = 1 - \frac{y}{\delta}$ is the dimensionless distance from the wall. u_τ is the friction velocity, y^+ distance from the wall in wall units, μ and ν are the apparent shear and kinematic viscosity of the fluid described as a power law fluid or a constant in case of Newtonian a fluid. Other parameters are:

$$\delta^* = \frac{\delta_i}{\delta_o}$$ **Eq.(12-32)**

$$\tau^* = \frac{\tau_o}{\tau_i}$$ **Eq.(12-33)**

In each solver's iteration radius of zero shear stress is determined using force balance on each wall of the annuli. According to the following equations radius of zero shear stress is related to wall shear stresses.

$$\tau_i = -\left(\frac{dp}{dx}\right)\left(\frac{{R_0}^2 - {R_1}^2}{2R_1}\right) \quad \textbf{Eq.(12-34)}$$

$$\tau_o = -\left(\frac{dp}{dx}\right)\left(\frac{{R_2}^2 - {R_0}^2}{2R_2}\right) \quad \textbf{Eq.(12-35)}$$

Once the wall shear stresses are calculated the radius of zero shear stress can readily be obtained from Eqs. 34 and 35. Next step is to determine the Van Karman constant for the inner shear layer; this is done by equating the expressions for eddy viscosity at the plane of zero shear stress (Eqs. 30 and 31). After this step, all the necessary information are obtained to perform the next iteration.

The model constant A^+ has a value of 26 for Newtonian fluids flow. For non-Newtonian fluids, this parameter must be determined from friction factor data in pipe flow. Since we do not have any information regarding friction factor in a pipe of same diameter as the annulus, we try to conduct a sensitivity analysis on the effect of this parameter on the simulation results. Different values are tried and based on the results the best value is picked for further analysis.

12.3. Results and Discussion

In the following sections, the near wall velocity profiles in wall unit are obtained using the following equations:

$$u_\tau = \sqrt{\frac{\tau_w}{\rho}} \quad \textbf{Eq.(12-36)}$$

$$u^+ = \frac{u}{u_\tau}$$ **Eq.(12-37)**

$$y^+ = \frac{\rho y u_\tau}{\mu_w}$$ **Eq.(12-38)**

Velocity profiles are compared with the universal law of the wall for viscous sublayer (Eq.(12-39)), the logarithmic relation of Newtonian fluids (Eq.(12-40))and Virk's ultimate asymptote of drag reduction velocity curve (Eq.(12-41)). Experimental data are also included.

$$u^+ = y^+$$ **Eq.(12-39)**

$$u^+ = 2.5\, ln(y^+) + 5.5$$ **Eq.(12-40)**

$$u^+ = 11.7\, ln(y^+) - 17$$ **Eq.(12-41)**

12.3.1. Turbulence modeling using Malin's model

In Table 12-5 results of pressure loss predictions using turbulence model of Malin (Malin 1997) (modified LB model) are compared with experimental data. The power law rheology model is used to describe the fluid. As the results indicate, this model overestimates the pressure loss by almost a factor of 2. This model fails in predicting drag reduction due to the non-Newtonian behavior of the fluid.

Table 12-5 Comparison of pressure drop predictions from Malin's model and experimental data

$\boldsymbol{Re_s}\ (-)$	$(\frac{dP}{dx})_{Exp}\ \left(\frac{Pa}{m}\right)$	$(\frac{dP}{dx})_{Sim}\ \left(\frac{Pa}{m}\right)$	Diff (%)
47000	134	260	94
57000	171	358	110

Near-wall velocity profiles in wall units are reported in Figure 12-3. Within the viscous sublayer ($y^+ < 11$) the model predicts the linear velocity profile consistent with theory and experimental results. In the logarithmic region, however, this model produces results close to Newtonian fluids velocity profile. Final conclusion is that turbulence model of Malin (1997) is not applicable in predicting turbulent flow of non-Newtonian fluids in annulus.

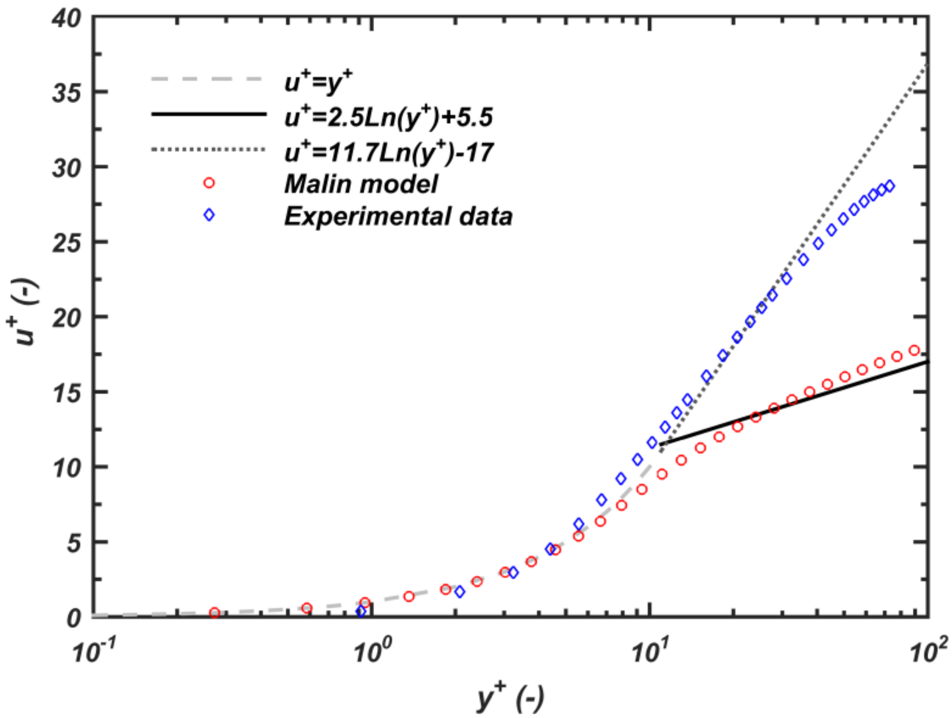

Figure 12-3 Near-wall velocity profiles in wall unit predicted using turbulence model of Malin

12.3.2. Turbulence modeling using Podryabinkin et al. and Ro et al. models

Table 12-6 reports results of pressure loss calculations of turbulence models of Podryabinkin et al. (Podryabinkin and Rudyak 2014) and Ro and Ryou (2012). Results of simulation with standard $k - \varepsilon$ turbulence model and also $k - \omega$ SST model are also included for comparison purposes. Both models overestimate the pressure loss. For the model of Podryabinkin et al. (Podryabinkin and Rudyak 2014) ,alth ough a slight reduction (comparing to Newtonian turbulence models) is observed, one would expect such prediction because the model does not damp the eddy viscosity close to the solid surfaces. Consequently, high production of eddy viscosity leads to overestimation of the Reynolds stresses and the high-pressure loss.

Table 12-6 Comparison of pressure loss predictions of three turbulence models with experimental data

Model	$(\frac{dP}{dx})_{Exp}\left(\frac{Pa}{m}\right)$	$(\frac{dP}{dx})_{Sim}\left(\frac{Pa}{m}\right)$	**Diff (%)**
Podryabinkin et al.	134	307	129
Ro et al.	134	324	142
Standard $k-\varepsilon$	134	342	155
$k-\omega$ SST	134	352	163

The model of.Ro and Ryou (2012), although utilizes a damping function to control the eddy viscosity production, is shown to overestimate the pressure loss. To study the reason, we must analyze the damping function and its components. The damping function proposed by Ro and Ryou (2012) is a function of three parameters (Eq.(12-42)).

$$F_{\mu} = (1 - A \times Dr \times B)^2 \quad \textbf{Eq.(12-42)}$$

The parameter Dr is the percentage of drag reduction which is determined experimentally ($Dr \approx 0.3$). Parameter A primarily depends on the Reynolds number and fluid flow behaviour index. For the flow condition considered here parameter A takes a value of about 0.007. The last parameter of the damping function is B and that is a function of non-dimensional distance from the wall. The parameter B takes its maximum value of 1 close to the solid walls. Figure 12-4 show the damping function F_{μ} calculated from Ro et al. model (Ro and Ryou 2012). The damping function F_{μ}, although is less than unity in the entire cross section but is not high enough to damp the eddy viscosity and produces drag reduction by the right percentage.

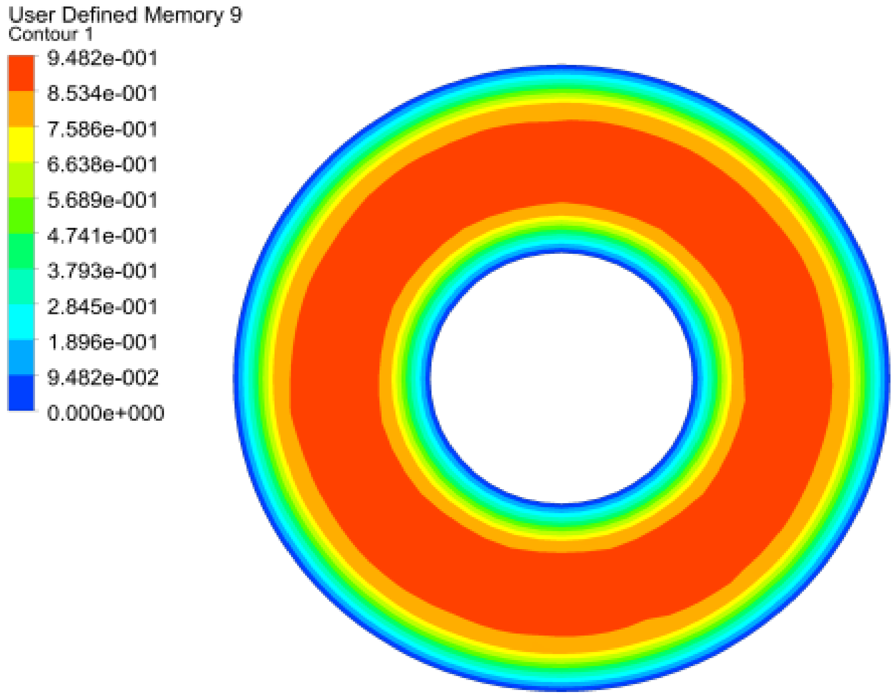

Figure 12-4 Damping function of Ro et al. turbulence model.

One of the possible reasons why Ro and Ryou (2012) model overestimates pressure loss could be attributed to the use of wall functions. Wall functions use empirical correlations to calculate wall shear stress and pressure loss. Use of wall functions is not recommended for low Reynolds number flows or internal flows with small gaps. Also, drag reduction is mainly a wall phenomenon and therefore near wall modeling is greater than other regions of flow.

12.3.3. Turbulence modeling using Azouz and Shirazi model

This turbulence model has a parameter which requires calibration (A^+). A^+ takes a value of 26 for Newtonian fluid flow. To ensure correct implementation of the model, a test case was run for turbulent flow of water. Result of pressure loss prediction for this case is reported in the first row of Table 12-7. The model accurately predicts flow of Newtonian fluids in annulus (velocity profiles also reported later). For the non-Newtonian fluid flow, we tested 5 different values of A^+ (at $Re_s = 47000$). The results are also reported in Table 12-7. Increasing A^+ causes the pressure loss to decrease through controlling the production of eddy viscosity. At $A^+ = 200$ pressure loss is overestimated by 10% while increasing A^+ to 250 caused pressure loss to become some 6% higher than experimental data.

Figure 12-5 shows the near wall velocity profile predicted for turbulent flow of water using the Azouz et al. model [30]. Similar to pressure loss predictions, the model correctly predicts flow behavior of Newtonian fluids in the annulus.

Figure 12-6 shows the near wall velocity profile of turbulent flow of non-Newtonian fluid near the outer wall of the annuli at different values of A^+ . Corresponding pressure losses for these cases are reported in Table 12-7. Increasing A^+ from 40 to 250 continuously shift the velocity profiles in the logarithmic region. At $A^+ = 200$ predicted velocity profiles coincide with those of experiments.

Table 12-7 Impact of parameter A^+ on predicted pressure loss of turbulence model of Azouz et al. (results for $Re_s = 47000$)

A^+	$(\frac{dP}{dx})_{Exp}\left(\frac{Pa}{m}\right)$	$(\frac{dP}{dx})_{Sim}\left(\frac{Pa}{m}\right)$	Diff (%)
Newtonian Case (26)	152	152	0
40	134	246	84
100	134	174	30
150	134	156	17
200	134	147	9.7
250	134	142	6

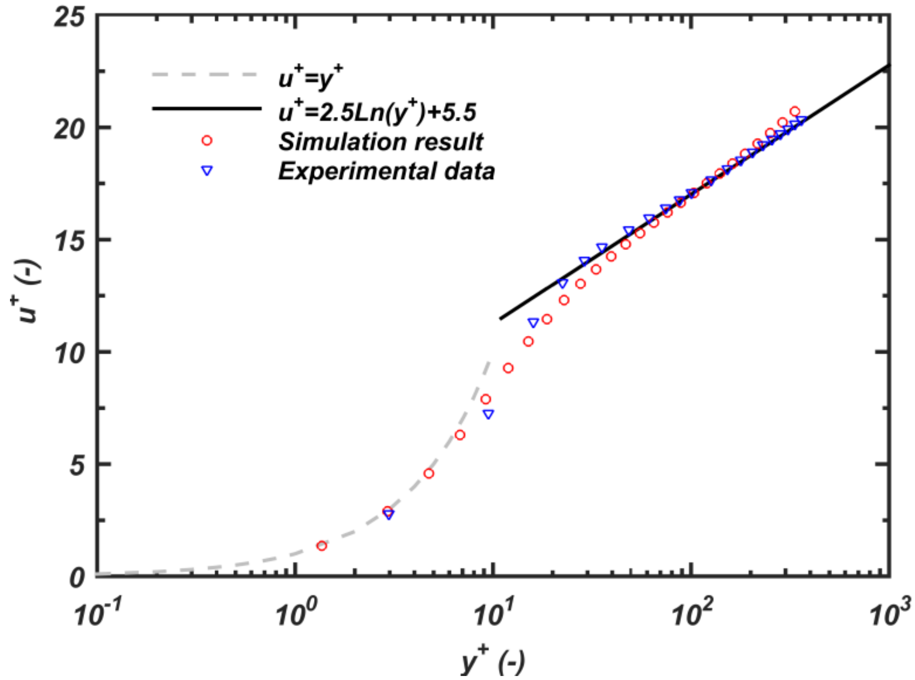

Figure 12-5 Near-wall velocity profile for flow of Newtonian fluids obtained by using Azouz and Shirazi model ($Re_s = 47000$, outer wall of the annuli)

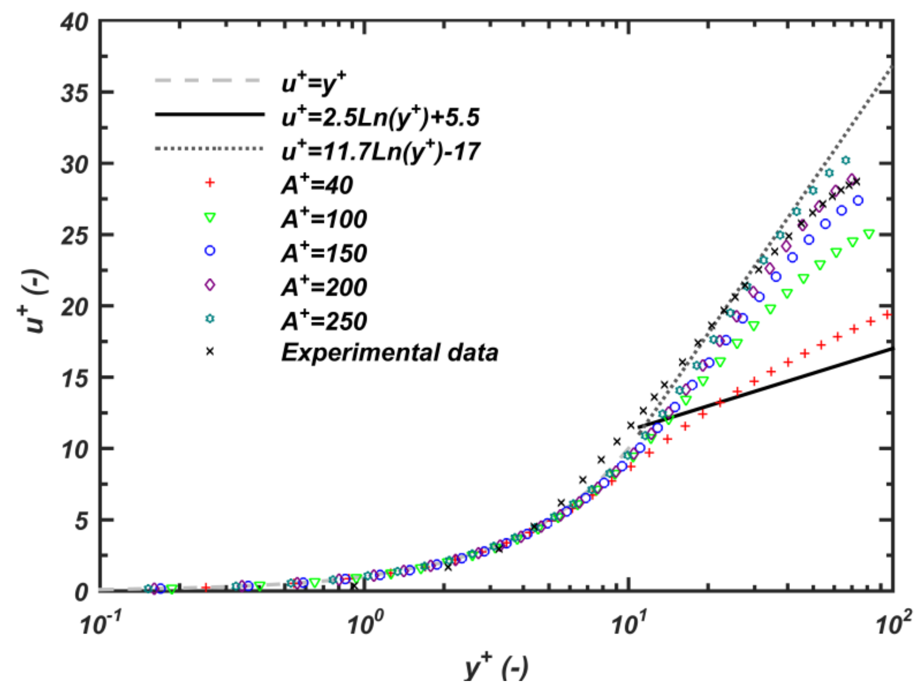

Figure 12-6 Near-wall velocity profile for flow of non-Newtonian fluids obtained by using Azouz and Shirazi model ($Re_s = 47000$, outer wall of the annuli)

In Figure 12-7 the velocity profile calculated at $A^+ = 200$ is compared with experimental data for the whole annular gap in dimensional units. Turbulence model of.Azouz and Shirazi (1997) predicts velocity profiles close to experimental data in the entire annular gap.

Table 12-8 Pressure loss prediction at different Reynolds numbers ($A^+ = 200$)

$Re_s\ (-)$	$(\frac{dP}{dx})_{Expe}\ \left(\frac{Pa}{m}\right)$	$(\frac{dP}{dx})_{Sim}\ \left(\frac{Pa}{m}\right)$	Diff (%)
47000	147	134	9.7
57000	182	171	6
66400	211	206	2.3

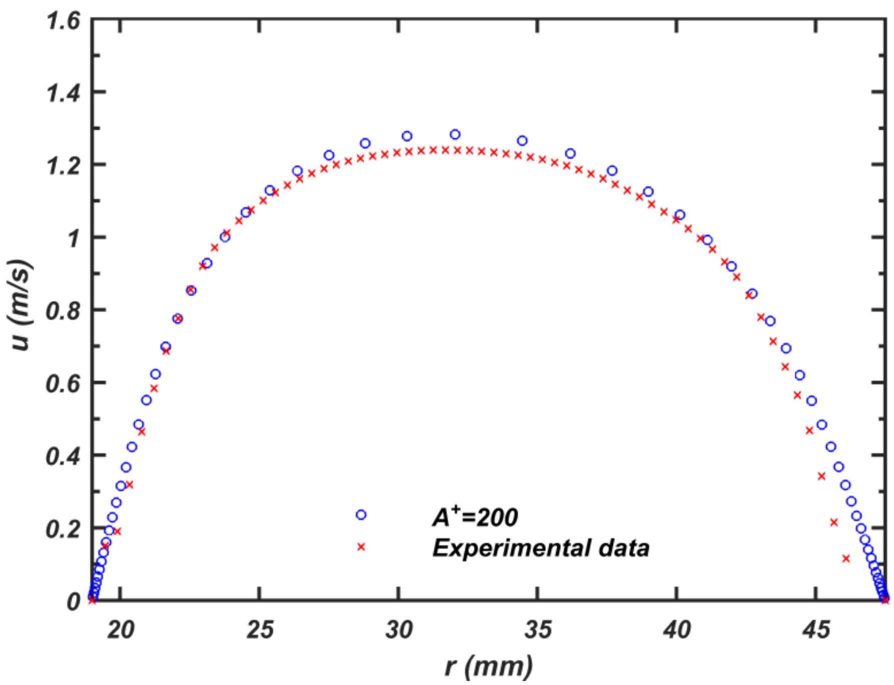

Figure 12-7 Velocity profile in annular gap ($Re_s = 47000$,$A^+ = 200$)

Figure 12-8 is the resultant Reynolds stress profile of calculation at $A^+ = 200$. The model prediction is higher than experimental data. One possible cause of overestimation of Reynolds stress could be attributed to the elastic properties of polymer chains. In fact, it is known that elasticity of polymer chains contributes to total shear stress in flow of such systems. In the current model, this property is neglected and, therefore, for the system to balance the polymer contribution it seems to be reappeared in the Reynolds stresses.

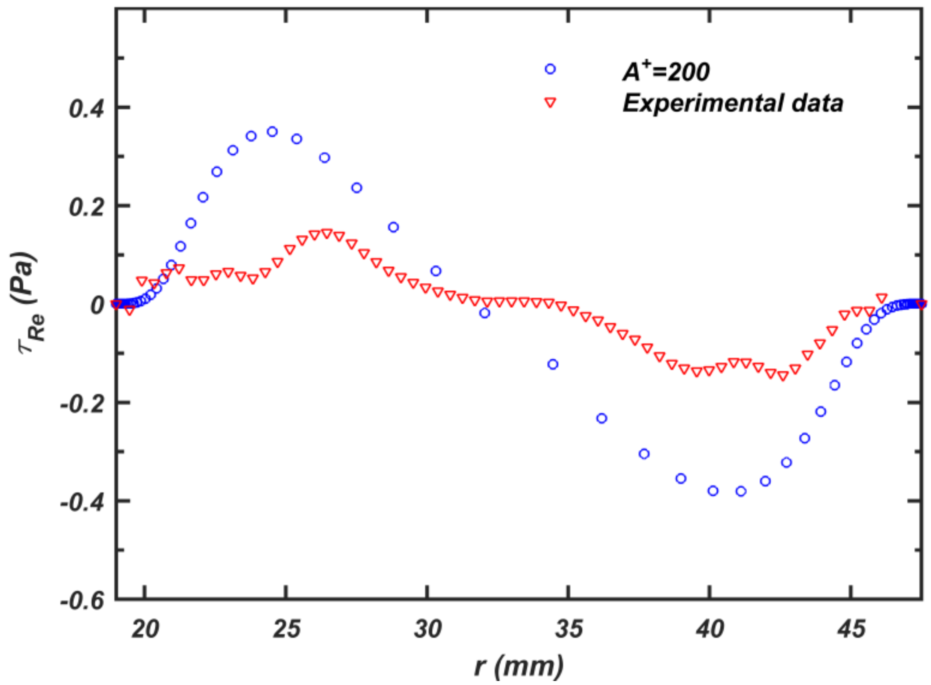

Figure 12-8 Reynolds stress profile ($Re_s = 47000, A^+ = 200$)

12.4. Conclusions

In this paper results of a CFD simulation on modeling turbulent non-Newtonian fluids in concentric annulus are reported. The aim of the paper is to examine the GNF approach in modeling the turbulent flow of polymer solutions. Four turbulence models were tested. Results of modeling were compared with experimentally measured pressure loss and velocity profiles.

Out of the four tested models, three turbulence models which were developed based on $k - \varepsilon$ closure for Newtonian fluids were found to fail in predicting non-Newtonian fluid flow in annulus. Two of these models tried to limit the production of eddy viscosity by employing damping functions which was shown to be insufficient. The third model had a modification to the definition of average viscosity and shear rate. That was also shown to be inadequate.

A zero-equation model developed based on mixing length approach was found to predict the turbulent flow of both Newtonian and non-Newtonian fluids in annulus accurately. This model is unique to annular geometry. The only set back of this model is an adjustable parameter which requires a priori knowledge of friction factor in a pipe with the same diameter as the annuli's hydraulic diameter. On the other hand, since no additional transport equations are involved, the model is relatively cheap regarding computational expense.

Based on the results it can be concluded that generalized Newtonian models cannot accurately capture all relevant flow phenomena of non-Newtonian polymeric fluids. Perhaps turbulence models which incorporate more rheological properties (such as elasticity) be more suitable for modeling flow of such fluids.

12.5. Nomenclature

r	Radius (mm)
R_1	Inner pipe radius (19 mm)
R_2	Outer pipe radius (47.5 mm)
R_0	Radius of zero shear stress (m)
τ_i	Wall shear stress on inner wall (Pa)
τ_o	Wall shear stress on outer wall (Pa)
τ_w	Wall shear stress (Pa)
u_τ	Friction or shear velocity ($\frac{m}{s}$)
ρ	Density ($\frac{kg}{m^3}$)
μ	Apparent viscosity (cp)
$\dot{\gamma}$	Shear rate ($\frac{1}{s}$)
Re_s	Solvent Reynolds stress (-)
U_B	Bulk velocity ($\frac{Flow\ rate}{Cross\ section}$)
u	Mean velocity ($\frac{m}{s}$)
D_H	Hydraulic diameter ($57mm$)
μ_s	Solvent viscosity ($Pa.s$)

μ_t Eddy viscosity ($Pa.s$)

k Turbulent kinetic energy

ε Turbulent dissipation rate

Re_g Generalized Reynolds number

y^+ Dimensionless distance ($\frac{\rho y u_\tau}{\mu_w}$)

μ_w Viscosity at the wall ($Pa.s$)

n Flow behavior index (power law fluids)

k Consistency index ($Pa.s^n$)

u^+ Dimensionless velocity ($\frac{u}{u_\tau}$)

$\frac{dP}{dx}$ Pressure gradient ($\frac{Pa}{m}$)

S Strain rate

12.6. References

Azouz, I. and Shirazi, S. A. (1997). Numerical simulation of drag reducing turbulent flow in annular conduits. Journal of Fluids Engineering-Transactions of the Asme **119**(4): 838-846, J Fluid Eng-T Asme, DOI: Doi 10.1115/1.2819506.

Azouz, I. and Shirazi, S. A. (1998). Evaluation of several turbulence models for turbulent flow in concentric and eccentric annuli. Journal of Energy Resources Technology-Transactions of the Asme **120**(4): 268-275, J Energ Resour-Asme, DOI: Doi 10.1115/1.2795047.

Bird, R. B. (1987). Dynamics of polymeric liquids. New York, Wiley.

Chung, S. Y., Rhee, G. H. and Sung, H. J. (2002). Direct numerical simulation of turbulent concentric annular pipe flow - Part 1: Flow field. International Journal of Heat and Fluid Flow **23**(4): 426-440, Int J Heat Fluid Fl, DOI: Pii S0142-727x(02)00140-6 Doi 10.1016/S0142-727x(02)00140-6.

Chung, S. Y. and Sung, H. J. (2005). Large-eddy simulation of turbulent flow in a concentric annulus with rotation of an inner cylinder. International Journal of Heat and Fluid Flow **26**(2): 191-203, Int J Heat Fluid Fl, DOI: DOI 10.1016/j.ijheatfluidflow.2004.08.006.

Dodge, D. W. and Metzner, A. B. (1959). Turbulent Flow of Non-Newtonian Systems. Aiche Journal **5**(2): 189-204, Aiche J, DOI: DOI 10.1002/aic.690050214.

Escudier, M. P., Gouldson, I. W. and Jones, D. M. (1995). Flow of Shear-Thinning Fluids in a Concentric Annulus. Experiments in Fluids **18**(4): 225-238, Exp Fluids.

Hassid, S. and Poreh, M. (1978). Turbulent Energy-Dissipation Model for Flows with Drag Reduction. Journal of Fluids Engineering-Transactions of the Asme **100**(1): 107-112, J Fluid Eng-T Asme.

Iaccarino, G., Shaqfeh, E. S. G. and Dubief, Y. (2010). Reynolds-averaged modeling of polymer drag reduction in turbulent flows. Journal of Non-Newtonian Fluid Mechanics **165**(7-8): 376-384, J Non-Newton Fluid, DOI: DOI 10.1016/j.jnnfm.2010.01.013.

Japper-Jaafar, A., Escudier, M. P. and Poole, R. J. (2010). Laminar, transitional and turbulent annular flow of drag-reducing polymer solutions. Journal of Non-Newtonian Fluid Mechanics **165**(19-20): 1357-1372, J Non-Newton Fluid, DOI: DOI 10.1016/j.jnnfm.2010.07.001.

Lam, C. K. G. and Bremhorst, K. (1981). A Modified Form of the K-Epsilon Model for Predicting Wall Turbulence. Journal of Fluids Engineering-Transactions of the Asme **103**(3): 456-460, J Fluid Eng-T Asme.

Li, Y. and Kuru, E. (2009). Optimization of Hole Cleaning in Vertical Wells Using Foam. Energy Sources Part a-Recovery Utilization and Environmental Effects **31**(1): 1-16, Energ Source Part A, DOI: Pii 906008054Doi 10.1080/15567030802308601.

Lumley, J. L. (1969). Drag Reduction by Additives. Annual Review of Fluid Mechanics **1**: 367-&, Annu Rev Fluid Mech, DOI: DOI 10.1146/annurev.fl.01.010169.002055.

Malin, M. R. (1997). Turbulent pipe flow of power-law fluids. International Communications in Heat and Mass Transfer **24**(7): 977-988, Int Commun Heat Mass, DOI: Doi 10.1016/S0735-1933(97)00083-3.

Naser, J. A. (1991). Epris Nuclear-Power Division Expert System Activities for the Electric-Power Industry. Expert Systems Applications for the Electric Power Industry, Vols 1 and 2: 15-35.

Neto, J. L. V., Martins, A. L., Neto, A. S. et al. (2011). Cfd Applied to Turbulent Flows in Concentric and Eccentric Annuli with Inner Shaft Rotation. Canadian Journal of Chemical Engineering **89**(4): 636-646, Can J Chem Eng, DOI: Doi 10.1002/Cjce.20522.

Nouri, J. M., Umur, H. and Whitelaw, J. H. (1993). Flow of Newtonian and Non-Newtonian Fluids in Concentric and Eccentric Annuli. Journal of Fluid Mechanics **253**: 617-641, J Fluid Mech, DOI: Doi 10.1017/S0022112093001922.

Paschkewitz, J. S., Dimitropoulos, C. D., Hou, Y. X. et al. (2005). An experimental and numerical investigation of drag reduction in a turbulent boundary layer using a rigid rodlike polymer. Physics of Fluids **17**(8), Phys Fluids, DOI: Artn 085101

Doi 10.1063/1.1993307.

Pinho, F. T. (2003). A GNF framework for turbulent flow models of drag reducing fluids and proposal for a k-epsilon type closure. Journal of Non-Newtonian Fluid Mechanics **114**(2-3): 149-184, J Non-Newton Fluid, DOI: Doi 10.1016/S0377-0257(03)00120-4.

Pinho, F. T., Li, C. F., Younis, B. A. et al. (2008). A low Reynolds number turbulence closure for viscoelastic fluids. Journal of Non-Newtonian Fluid Mechanics **154**(2-3): 89-108, J Non-Newton Fluid, DOI: DOI 10.1016/j.jnnfm.2008.02.008.

Pinho, F. T. and Whitelaw, J. H. (1990). Flow of Non-Newtonian Fluids in a Pipe. Journal of Non-Newtonian Fluid Mechanics **34**(2): 129-144, J Non-Newton Fluid, DOI: Doi 10.1016/0377-0257(90)80015-R.

Podryabinkin, E. V. and Rudyak, V. Y. (2014). Modeling of turbulent annular flows of Hershel-Bulkley fluids with eccentricity and inner cylinder rotation. Journal of Engineering Thermophysics **23**(2): 137-147, J Eng Thermophys-Rus, DOI: 10.1134/S1810232814020064.

Ptasinski, P. K., Boersma, B. J., Nieuwstadt, F. T. M. et al. (2003). Turbulent channel flow near maximum drag reduction: simulations, experiments and mechanisms. Journal of Fluid Mechanics **490**: 251-291, J Fluid Mech, DOI: 10.1017/S0022112003005305.

Ptasinski, P. K., Nieuwstadt, F. T. M., van den Brule, B. H. A. A. et al. (2001). Experiments in turbulent pipe flow with polymer additives at maximum drag reduction. Flow Turbulence and Combustion **66**(2): 159-182, Flow Turbul Combust, DOI: Doi 10.1023/A:1017985826227.

Resende, P. R., Kim, K., Younis, B. A. et al. (2011). A FENE-P k-epsilon turbulence model for low and intermediate regimes of polymer-induced drag reduction. Journal of Non-Newtonian Fluid Mechanics **166**(12-13): 639-660, J Non-Newton Fluid, DOI: DOI 10.1016/j.jnnfm.2011.02.012.

Ro, K. and Ryou, H. (2012). Development of the modified k-E > turbulence model of power-law fluid for engineering applications. Science China-Technological Sciences **55**(1): 276-284, Sci China Technol Sc, DOI: 10.1007/s11431-011-4664-x.

Rodriguez-Corredor, F. E., Bizhani, M., Ashrafuzzaman, M. et al. (2014). An Experimental Investigation of Turbulent Water Flow in Concentric Annulus Using Particle Image Velocimetry Technique. Journal of Fluids Engineering-Transactions of the Asme **136**(5), J Fluid Eng-T Asme, DOI: Artn 051203

Doi 10.1115/1.4026136.

Sibilla, S. and Baron, A. (2002). Polymer stress statistics in the near-wall turbulent flow of a drag-reducing solution. Physics of Fluids **14**(3): 1123-1136, Phys Fluids, DOI: Doi 10.1063/1.1448497.

Sureshkumar, R., Beris, A. N. and Handler, R. A. (1997). Direct numerical simulation of the turbulent channel flow of a polymer solution. Physics of Fluids **9**(3): 743-755, Phys Fluids, DOI: Doi 10.1063/1.869229.

Virk, P. S., Mickley, H. S. and Smith, K. A. (1970). Ultimate Asymptote and Mean Flow Structure in Toms Phenomenon. Journal of Applied Mechanics **37**(2): 488-&, J Appl Mech.

Warholic, M. D., Heist, D. K., Katcher, M. et al. (2001). A study with particle-image velocimetry of the influence of drag-reducing polymers on the structure of turbulence. Experiments in Fluids **31**(5): 474-483, Exp Fluids, DOI: DOI 10.1007/s003480100288.

Warholic, M. D., Massah, H. and Hanratty, T. J. (1999). Influence of drag-reducing polymers on turbulence: effects of Reynolds number, concentration and mixing. Experiments in Fluids **27**(5): 461-472, Exp Fluids, DOI: DOI 10.1007/s003480050371.

Wilson, K. C. and Thomas, A. D. (1985). A New Analysis of the Turbulent-Flow of Non-Newtonian Fluids. Canadian Journal of Chemical Engineering **63**(4): 539-546.

13. Conclusions and recommendations for future work

13.1. Conclusions

In this chapter, we summarize the main conclusions and findings of the presented work. All the concluding remarks have already been extensively discussed in the previous sections. The summary in this chapter is intended to provide a short review of the results and discussions presented in the previous chapters. Some of the terms that are used have been well-defined in previous chapters, and we will not redefine them here.

An executive summary of the most notable findings is given first. The executive summary is a short version of the concluding remarks.

13.1.1. Executive summary

The comprehensive study that has been conducted for studying solid transport in horizontal wells has resulted in finding the following principal conclusions:

- Water always initiated cuttings movement at lower flow rates and pressure loss than polymer solutions. As the polymer concentration and the fluid viscosity increased, it progressively became harder to initiate cuttings movement, implying a negative impact of fluid viscosity on the hole cleaning.
- The use of polymer additives causes the critical drag force required for initiation of bed erosion to increase significantly. Additionally, flow turbulence was confirmed to be higher at the onset of bed erosion using polymer fluids compared to water. Therefore, the typical oil field perception that polymer fluids cause a delay in bed erosion mainly due to the reduction of flow turbulence is not correct.
- Comparison of the bed erosion performance of two polymer fluids at similar flow rates revealed that increasing polymer concentration results in an enhancement of fluid's drag force on the sand bed. However, the increase in the fluid's drag force in the wake of enhanced viscosity did not result in better hole cleaning.

- The non-zero normal stress differences associated with the flow of viscoelastic fluids give rise to a normal elastic force, which acts on the sand bed creating additional resistive force hindering the particle removal from the surface of the bed deposits.
- The combination of the normal force, bed compaction, reduction of flow turbulence and interaction of polymer molecules with bed materials (gelling effect) are the main reasons for the delayed onset of the bed erosion with the use of polymer fluids.
- Velocity fluctuations in the turbulent flow can yield fluid drag forces acting on the cuttings in the bed significantly higher than that of the drag forces calculated by using average velocity.
- The presence of a stationary sand bed in the lower half of a concentric annulus diverts the flow away from the lower annulus creating unfavorable conditions for the removal of particles deposited in the lower annulus.
- Friction factor for the flow over a sand bed is about 45% higher than that of the flow in the same annulus with no sand bed.
- Interfacial friction factor can be substantially different from that of average friction factor calculated by using measured frictional pressure loss.Interfacial friction factor strongly depends on the height of the stationary sand bed in the annulus.
- Interfacial friction factor shows a sharp increase at the onset of the bed erosion.
- Roughness of the sand bed interface strongly depends on the flow condition (i.e. roughness Reynolds number)
- Bedload transport of particles may result in a reduction of flow turbulence near the bed interface for flow in the concentric configuration.
- Bedload transport of particles increases the equivalent roughness of the surface significantly.
- Equivalent roughness of the sand bed can be several times higher than the mean particle size of the bed
- Polymer fluids delay transition to hydraulically rough flow regime by a wide margin compared to water.
- Critical shear stress for particle removal from the sand bed deposited in horizontal annuli correlates well with particles Reynolds number for both Newtonian and non-Newtonian fluids

- Particle size has a minimal impact on the critical flow rate.
- Current turbulence models available in commercial CFD packages fail in modeling turbulent flow of non-Newtonian fluids

13.1.2. Main conclusions

The most important contribution of the current work is the development and execution of using PIV technique for studying hole cleaning. There have been several challenges that needed to be mitigated for successful implementation of PIV. A prototype calibration method required to be built for calibration of the camera. Experiments with non-Newtonian fluids were much more challenging compared to those with water. Polymer degradation and sensitivity of rheological properties to temperature imposed great difficulties in obtaining repeatable results. Nonetheless, a great effort has been put into collecting quality data. Most of the results have either been published or pending publication. This work has created a database for future validation of CFD and numerical modeling of solid transport in oil wells.

The summary and conclusions of each chapter of the thesis are presented separately. The order of presentation is not necessarily the same as the order of thesis chapters. The order of presentations of the conclusions is in accordance with the importance of the findings regarding hole cleaning.

13.1.2.1. Chapter 8

The main contribution of this work is the identification of the role of fluid's rheological characteristic on solid removal in horizontal wells. Using the accurate measurement of fluid velocity profiles and flow turbulence in a large-scale flow loop, we have been able to dismiss and or confirm most of the previous speculations on the role of fluid's rheological properties and viscoelasticity on cuttings bed removal in the annulus. The PIV results have revealed the use of polymer additives causes the critical drag force required for initiation of bed erosion to increase significantly. Additionally, flow turbulence was confirmed to be higher at the onset of bed erosion using polymer fluids compared to water. Therefore, the myth that polymer solutions cause a delay in bed erosion merely due to the reduction of flow turbulence was dismissed. Comparison of the bed erosion performance of two polymer fluids at similar flow rates, using PIV, revealed increasing polymer concentration results in an enhancement of fluid's drag force on the sand bed. However, the increase in the fluid's drag force in the wake of enhanced viscosity did not result in better hole cleaning.

The role of viscoelasticity of the fluids was analyzed using complex phenomenon in the flow of such systems to explain the counter-intuitive hole cleaning performance of these fluids. The non-zero normal stress differences were identified to be the main contributor in hindering the initiation of bed erosion by polymer additives. The role of non-zero normal stress difference has previously been identified in reducing settling velocity of particles in viscoelastic fluids. However, the impact of non-zero normal stress differences for hole cleaning appeared in the form of an additional resistive force for particle removal. The normal fluid force was further discussed, and an equation was developed to estimate this force. Our analysis indicated that this force could be several times bigger than particles' submerged weight. Therefore, one of the unknown impacts of using viscoelastic fluids for hole cleaning has been identified using the measurement of flow velocity and turbulence.

13.1.2.2. Chapter 7

Flow turbulence and its significance in bed erosion and solid transport were studied using water in the concentric configuration of the annulus. The PIV provided high-resolution near bed instantaneous velocity profiles. Comparison of time-averaged and instantaneous velocity data very close to the sand bed interface revealed fluctuations in the velocity has a significant contribution to the local fluid velocity felt by the particles. The term 'effective velocity' was used to describe the actual fluid velocity near the center of the mass of the particles. This velocity governs the fluid's drag and lifts force on the particle. Our analysis showed that the effective velocity could be several times bigger than the time-averaged velocity at times. The significant fluctuations in the near bed velocity highlighted the importance of the flow turbulence in the bed erosion. In the discussion related to the impact of the flow turbulence, the significance of the impulse and particles arrangement at the bed interface was discussed. Additional analyses of fluctuations velocity have shown that the hydrodynamic forces (drag and lift) vary considerably over the time, and hence, invalidating the common assumption of ignoring the flow turbulence in the current bed erosion/sediment transport models.

The influence of particle arrangement in the sand bed on the threshold of particle movement initiation has also been discussed in the chapter discussing the role of flow turbulence in sediment transport. Comparison of the drag to the lift force showed that the lift force is much smaller than the drag force. This finding along with the discussion of the impact of particles arrangement in the bed explained why it is much harder to remove a particle that is embedded in the bed deposit. Finally, it was concluded that a purely mechanistic approach might not be sufficient in capturing the actual physics of the interaction of fluid-particles.

In the same chapter, we also discussed the validity of the critical shear stress approach in modeling sediment transport. The existence of a critical shear stress (or equivalently critical Shields' stress) has been the primary assumption in many of previous bed erosion/sediment transport studies. It is shown that validity of previous measurements is all subjected to the experimental technique and its resolution that was used. Sand bed erosion does not have a well-defined threshold at which bed erosion ceases or starts. Therefore, the concept of the existence of critical shear stress (as a single number that would indicate whether bed erosion/sediment transport is taking place or not) is questioned.

13.1.2.3. Chapter 4

For the turbulent flow of water in the concentric annulus, quantities such as velocity profiles in wall unit, the surface roughness of the bed interface, and impact of the presence of the stationary bed on the flow turbulence have all been investigated thoroughly. Results showed that the presence of the stationary solids bed changed the time averaged velocity profiles and reduced the peak fluid velocity in the lower annulus. An increase in the solids bed height resulted in further reduction of the velocity in the lower annulus. The peak velocity decreased by increasing the bed height. At the critical flow rate of the bed erosion, the percentage of the reduction in maximum velocity was lower than that of observed at the sub-critical flow rate. This behavior was attributed to the bedload transport of solids in the concentric annulus. Velocity profiles in the upper part of the annulus showed dependency on the bed height. Velocity values for flow over the solids beds were higher than the case of no bed. The thicker bed caused more increase of the velocity in the upper annulus than the low height bed.

Velocity profiles near the bed interface in wall units showed a downward shift from the universal law. Analysis of velocity profiles in the log-wall region revealed that the equivalent roughness varied with the flow rates. For the sub-critical flow rate, an equivalent roughness of $2d_p$ characterizes the solids bed surface. At the critical flow rate, the equivalent roughness increased to 2.4d_p. The bedload transport of particles induces the additional boundary roughness. Further analysis revealed that the equivalent bed roughness varies along the axial direction. Therefore, it is not possible to characterize the bed roughness with a single roughness height.

The normalized Reynolds shear stress profiles, when compared with the flow in the same annulus with no sand bed, were different at different flow rates. At a flow rate less than that of the critical flow rate, Reynolds stress profiles show slightly higher peak values near the bed interface for the thin and the thick bed than that of the flow without a solids bed. On the other hand, at the critical flow rate, Reynolds stress was reduced for flow over the solids bed as compared to the case with no sand bed. This behavior was explained based on the previous works in sediment transport and was related to bedload transport of particles. Another impact of the cuttings bed on Reynolds stress was the shift in the radial location of zero shear stress towards the inner pipe. Thicker bed caused more change in the radial position of the zero shear stress.

Comparison of the Reynolds stress profiles in the lower and upper annulus showed that the Reynolds stress was reduced in the lower annulus as a result of the solids bed presence. Additionally, increasing the solids bed height caused more reduction in Reynolds stress in the lower annulus. Reynolds stress profiles showed higher values in the upper annulus for flow over the cuttings bed. The thicker bed caused higher Reynolds stress in the upper annulus than the smaller bed.

Near bed measurement of Reynolds stress profiles showed that the bed height did not influence the Reynolds stress. However, in the core flow (i.e. away from the bed surface), Reynolds stress remained higher for flow over the smaller bed. Analyses of the bed shear stress revealed that the thicker solids bed resulted in a greater wall shear stress.

Comparison of radial turbulence intensity profiles indicated that this quantity is affected in the same manner as the Reynolds shear stresses. At flow rates less than critical flow rate, the level of radial intensity is almost the same as the no bed case. However, at the critical flow rate, the radial turbulence intensity decreased with the presence of the solids bed.

13.1.2.4. Chapter 5

We also presented results and discussed the impact of the presence of a stationary sand bed on flow characteristics of polymer fluids. The primary goal of the experiments was to benchmark the differences in the flow of water and polymer solutions during the solid transport. The results revealed that the presence of a stationary cuttings bed causes the flow rate and flow velocity to decrease in the lower annulus comparing to that of the upper annulus. The reduction of local velocity was found to be independent of the polymer concentration.

Reynolds shear stress data were also measured and presented for both lower and upper annulus. A reduction in Reynolds stress was observed as a result of the presence of the sand bed in the lower annulus. Furthermore, increasing the polymer concentration caused the Reynolds stress to further decrease in the lower annulus. The data in the upper annulus revealed the Reynolds stress is higher near the wall of the outer pipe; which is in contrary to previous findings for the flow of single phase turbulent flow in the annulus.

Finally, data for axial turbulence intensity were presented and discussed. The axial turbulence intensity showed a decrease in the lower annulus as a result of the stationary sand beds. Axial turbulence intensity was slightly reduced due to enhanced polymer concentration. Upper annulus data, however, were not affected by increasing the polymer concentration.

The PIV studies of solid transport and turbulent flow have been conducted in both concentric and eccentric annulus. The concentric configuration represented the best case scenario in term of configuration for solid removal in the well. On the other hand, a fully eccentric annulus is the more realistic setting in an actual drilling operation. In the experiments conducted in the eccentric configuration, turbulent flow over sand beds of varying initial heights was studied. Water and polymer fluid was used as the carrier fluids. PIV measurements were conducted along two planes in the annulus to assess the impact of the presence of the bed on flow in different parts of the well.

13.1.2.5. Chapters 9 and 10

The results of PIV experiments on the turbulent flow of water in the eccentric annulus was presented and discussed in chapters 9 and 10. The tests were conducted at several flow rates; equal to sub-critical and critical flow rates. The experiments revealed that roughness of the sand bed strongly depends on the flow condition in the annulus. Analysis of velocity profiles in wall units indicated that the experiments covered all three flow regimes of hydraulically smooth, transitionally rough, and fully rough flow regimes. Velocity profiles near the inner pipe wall showed a changing pattern. Generally, with the increasing bed height, velocity profiles near the tube wall started deviating from the smooth log law; showing a downward shift which resembles a rough wall behavior. The velocity profiles over the sand beds showed different Δu^+. The bedload transport of particles caused a sharp increase in the equivalent roughness of the bed. Our results indicated that, in the case of bedload transport, the equivalent sand bed roughness could be as high as 9 times that of particles size.

Reynolds stress data showed a dependency on the flow regime of the surface of the interest. In the case of smooth flow regime, which prevailed for the thinnest bed, Reynolds stress was higher along the symmetry plane of the annulus. However, at the critical flow rate of bed erosion, this behavior changed. The increased surface roughness induced by bedload transport of particles was identified as the primary cause of the enhanced Reynolds stress production. For the other two beds, flow regimes were either transitionally rough or fully rough. Hence, a higher Reynolds stress was observed near the bed interface than that of the inner pipe wall. Bedload transport of particles caused an enhancement to the production of Reynolds stress near the bed interface.

Reynolds normal stress profiles were also reported and discussed in chapter 9. Turbulence intensities showed behavior similar to that of Reynolds shear stresses. The intensities were affected by the flow regime over the surface of interest. Bedload transport of particles amplified the production of the turbulence intensities, implying an enhancement of turbulence production near the sand beds caused by rolling particles.

In addition to surface roughness and flow turbulence, variables such as interfacial friction factor and velocity fluctuations were discussed. We reviewed the difference between interfacial and averaged friction factor and showed how different these two quantities might be.

Analysis of friction factors indicated that presence of a stationary sand bed enhances the pressure loss in the annulus. The friction factor in the presence of sand beds was about 45% higher than the flow in the same annulus without any cuttings bed. The impact of increasing bed height was shown to manifest itself as an increase in the Reynolds number. Hence, all friction factors collapsed on the same line.

The measured velocity profiles using PIV was used to evaluate the interfacial friction factor, a quantity that cannot be deduced from frictional pressure loss data. The interfacial friction factor data showed a strong dependence on the height of the sand bed. For smallest bed height, interfacial friction factor was smaller than that of average friction factor. On the other hand, for thickest bed height the interfacial friction factor was higher than the average friction factor. Furthermore, we found that interfacial friction factor starts increasing at the onset of bed erosion. This attribute does not appear in average friction factor curves. The movement of cuttings and added roughness induced by bedload was argued to be the primary cause for the increase in interfacial friction factor.

For the turbulent flow of water in the eccentric annulus, the velocity profiles were presented for both time-averaged and instantaneous profile. The presence of the sand bed causes a slight reduction in the local time-averaged velocity near the bed interface as compared to flow near the pipe wall of the annulus. However, away from the bed interface, velocity was higher for flow over the beds. Analysis of instantaneous velocity profiles showed that strong velocity fluctuations happen near the bed. The ratio of instantaneous velocity to its mean value indicated that effective fluid velocity might be several times greater than its average value. Therefore, one cannot ignore the turbulence when modeling the bed erosion and sediment transport.

Turbulence normal and shear stresses were also reported and discussed. The Reynolds shear stress was shown to increase due to the presence of the sand bed as compared to flow in the annulus with no sand bed. The increase was proportional to the height of the sand bed. The axial turbulence intensity showed a similar trend to that of Reynolds stress. However, for smallest bed, the axial intensity was less than the no bed case. The radial intensity profiles showed a slight decrease over the beds as compared to that of no bed case.

13.1.2.6. Chapter 11

Experiments in eccentric annulus over sand beds of varying height were also conducted using polymer fluid. The analysis of velocity profiles in the wall unit showed that velocity profiles obey the linear relation of the law of the wall in the viscous sublayer for all the experiments. In the logarithmic region, an upward shift in the velocity occurred compared to the log-law of Newtonian fluids. On the other hand, the velocity profiles in the log-zone fell short of the Virk's asymptote. Movement of the sand particles at the higher flow rates did not affect the velocity profiles. The results indicated the flow is primarily in the hydraulically smooth regime. The results suggest that using of polymer fluids for eroding a sand bed delays the transition to hydraulically rough flow.

Turbulence stresses (normal and shear) for the flow of polymer fluid over sand bed deposits in eccentric annulus were presented and discussed in chapter 10. Reynolds stress showed a non-zero value at all the measured flow rates. It progressively increased with increasing flow rate and the stationary bed height. Bedload transport of particles did not have any substantial impact on the turbulence stress profiles.

The axial turbulence intensity profiles in wall unit revealed the peak intensity is located in the buffer zone. This observation is in agreement with previously published works on the turbulent flow of drag reducing polymers. Movement of sand particles in the bed appeared to cause a slight shift of the peak intensity to higher y^+ values.

Radial turbulence intensity profiles were also analyzed for the flow of the polymer fluids. The results indicated that radial turbulence intensity is non-zero. Profiles of normalized radial turbulence intensity in wall units showed that bedload transport of particles might slightly enhance production of velocity fluctuations in the radial direction. The increase of radial turbulence intensities was observed at the highest fluid velocity for all the cases.

13.1.2.7. Chapter 6

So far, all the conclusions and results have been drawn based on the microscopic study of solid transport in the annulus. The PIV was the primary measurement technique in obtaining these results. In another phase of this study, we also investigated hole cleaning from the macroscopic framework. In this part of the research, the bulk variables such as flow rate and pressure loss were measured to study solid transport in the concentric annulus. We investigated the impact of fluid's viscosity and cuttings size on the initiation of sand bed erosion. The threshold of bed erosion was determined using high-resolution videotaping of the bed interface. The results have thoroughly been discussed in chapter six of the thesis.

The results showed that water always initiated cuttings movement at lower flow rates and pressure loss than polymer solutions. As the polymer concentration and the fluid viscosity increased, it progressively became harder to initiate cuttings movement, implying a negative impact of fluid viscosity on the hole cleaning.

For the range of cuttings size tested (260 microns to 1240 microns), intermediate size cuttings were found to be slightly easier to remove than bigger or smaller cuttings. However, the impact of cuttings size on critical conditions was far less than that of fluid's rheological properties. It is safe to say that cuttings size (within the range used here) has a minimal impact on hole cleaning.

Analyses using non-dimensional groups were also conducted. It was shown that critical wall shear stress in the form of Shields' stress and non-dimensional friction velocity could be correlated with generalized particle Reynolds number. Within the range of particle Reynolds number of 0.1 to100, two correlations for predicting critical wall shear stress were proposed. The relationship was valid for Newtonian and non-Newtonian fluids. A procedure was also developed to calculate the critical flow rate.

13.1.2.8. Chapter 12

Apart from the experimental studies of hole cleaning, a CFD modeling of turbulent flow through concentric annulus have also been performed in this research. The objective of the work was to examine the GNF approach in modeling the turbulent flow of polymer solutions. Four turbulence models were tested. Results of modeling were compared with experimentally measured pressure loss and velocity profiles.

Out of the four tested models, three turbulence models which were developed based on $k - \varepsilon$ closure for Newtonian fluids were found to fail in predicting non-Newtonian fluid flow in the annulus. Two of these models tried to limit the production of eddy viscosity by employing damping functions, which were shown to be insufficient. The third model had a modification to the definition of average viscosity and shear rate. That was also shown to be inadequate.

A zero-equation model developed based on mixing length approach was found to be able to reproduce experimentally measured velocity profiles in the annulus. This model is unique to annular geometry. The only set back of this model is an adjustable parameter which requires a priori knowledge of friction factor in a pipe with the same diameter as the annulus's hydraulic diameter. On the other hand, since no additional transport equations are involved, the model is relatively cheap regarding computational expense.

Based on the results it can be concluded that generalized Newtonian models cannot accurately capture all relevant flow phenomena of non-Newtonian polymeric fluids. Perhaps turbulence models which incorporate more rheological properties (such as elasticity) be more suitable for modeling flow of such fluids.

13.2. Recommendation for future works

In the wake of the Knowledge and experience gained over the past six years working in the Advance Drilling Engineering Lab at the University of Alberta, few ideas and recommendations are suggested for future studies. The modifications for implementations of these ideas should not be troublesome.

The first suggested work is studying the role of fluid's viscoelasticity on different aspects of flow in more detail. Similar work on the impact of viscoelasticity on particle settling in quiescent fluids has already been done in the Advanced Drilling Lab. The concept of having two fluids with similar shear viscosity profiles but distinctively different elastic properties can easily be implemented in the bigger flow loop. PIV can be used to study the impact of viscoelasticity on the various aspects of flow (turbulent and laminar). Particles removal experiments, similar to the tests performed in the current study, can be conducted. The results of such experiments can significantly help in better understanding of the extent of the effect of fluid's rheological properties on hole cleaning.

The second recommended work is testing a liquid exhibiting high yield stress. This class of fluids is often labeled as yield power law or Herschel–Bulkley fluids. Several polymers under this type of fluids are suitable for PIV technique (optically transparent). The use of a liquid with a yield stress and PIV can then provide insight on the impact of fluid's yield stress on hole cleaning. PIV measurements can be used in determining interfacial friction factor. This quantity is not directly measurable using a pressure transducer.

Improvements and upgrades to the current flow loop setup and instrumentation can also help in studying other aspects of the hole cleaning and cuttings transport process that is not possible with the current set-up. The current camera is a dual framing camera that can take only up to 5 frames per second. Upgrading to a high-speed camera will enable the analysis of particles' path. The trajectory of the particles can reveal much more information on the fluid force and interaction of particle-fluid. It can also be used in calculating particles settling velocity under dynamic conditions as opposed to quiescent fluid.

Dunes and dynamics of flow around dunes have been studied in the past. However, there has not been an extensive study on the fluid's related factor near the interface of moving dunes in the annulus. The current flow loop set-up can be used to undertake such research. Such study requires the development of algorithm and methods that ensure the suspended particles are masked out of the flow, and hence, it requires knowledge of Particle Tracking Velocimetry (PTV).

Another modification that can be done on the flow loop is to install a solid feeder in the system. The solid feeder can inject particles into the test section at a known rate. With this modification, cuttings transport during the actual drilling operation may be studied as opposed to hole cleaning. The combination of the solid's feeder with a high-speed camera can then be used for studying the evolution of particles' trajectory over the course of the wellbore.

References

Aadnøy, B. S. (2015). Technology Focus. Journal of Petroleum Technology **67**(5): 114.

Acharya, A. R. (1988). Viscoelasticity of Crosslinked Fracturing Fluids and Proppant Transport. SPE Production Engineering **3**(4), SPE-15937-PA, DOI: 10.2118/15937-PA.

Adari, R. B. (1999). Development of correlations relating bed erosion to flowing time for near horizontal wells. M.Sc. Thesis, University of Tulsa, USA

Adari, R. B., Miska, S., Kuru, E. et al. (2000). Selecting Drilling Fluid Properties and Flow Rates For Effective Hole Cleaning in High-Angle and Horizontal Wells. SPE Annual Technical Conference and Exhibition. Dallas, Texas, 1–4 October 2000., SPE-63050-MS,DOI: 10.2118/63050-MS.

Adrian, R. J. (2005). Twenty years of particle image velocimetry. Experiments in Fluids **39**(2): 159-169, DOI: 10.1007/s00348-005-0991-7.

Akhshik, S., Behzad, M. and Rajabi, M. (2015). CFD–DEM approach to investigate the effect of drill pipe rotation on cuttings transport behavior. Journal of Petroleum Science and Engineering **127**(0): 229-244, DOI: http://dx.doi.org/10.1016/j.petrol.2015.01.017.

Ali, M. W. (2002). A Parametric Study of Cutting Transport in Vertical and Horizontal Well Using Computational Fluid Dynamics (CFD). Msc thesis, College of Engineering and Mineral Resources at West Virginia University.

Allahvirdizadeh, P., Kuru, E. and Parlaktuna, M. (2015). A Comparative Study of Cuttings Transport Performance of Water Versus Polymer-Based Fluids in Horizontal Well. Presented at the 20th International Petroleum and Natural Gas Congress and Exhibition of Turkey held in Sheraton Hotel and Convention Center, Ankara , Turkey, May 27-29, 2015.

Anders Brun, Aerts, G. and Jerkø, M. (2015). "How to achieve 50% reduction in offshore drilling costs." Retrieved July 19, 2017.

Andrews, E. D. (1983). Entrainment of gravel from naturally sorted riverbed material. Geological Society of America Bulletin **94**(10): 1225-1231, DOI: 10.1130/0016-7606(1983)94<1225:EOGFNS>2.0.CO;2.

Arnipally, S. K. and Kuru, E. (2017). Effect of Elastic Properties of the Fluids on the Particle Settling Velocity. Proceedings of the ASME 2017 36th International Conference on Ocean, Offshore and Arctic Engineering, OMAE2017-61192, June 25-30, 2017, Trondheim, Norway, Alternative Effect of Elastic Properties of the Fluids on the Particle Settling Velocity.

Asadi, M., Conway, M. W. and Barree, R. D. (2002). Zero Shear Viscosity Determination of Fracturing Fluids: An Essential Parameter In Proppant Transport Characterizations. International Symposium and Exhibition on Formation Damage Control, 20-21 February, Lafayette, Louisiana, SPE-73755-MS,DOI: 10.2118/73755-MS.

Azar, J. J. and Sanchez, R. A. (1997). Important Issues in Cuttings Transport for Drilling Directional Wells. Fifth Latin American and Caribbaean Petroleum Engineering Conference and Exibition. held in Rio de Janeiro, Brazil, 30 August -3 Spetember 1997, SPE-39020-MS,DOI: 10.2118/39020-MS.

Azouz, I. and Shirazi, S. A. (1997). Numerical simulation of drag reducing turbulent flow in annular conduits. Journal of Fluids Engineering-Transactions of the Asme **119**(4): 838-846, J Fluid Eng-T Asme, DOI: Doi 10.1115/1.2819506.

Azouz, I. and Shirazi, S. A. (1998). Evaluation of several turbulence models for turbulent flow in concentric and eccentric annuli. Journal of Energy Resources Technology-Transactions of the Asme **120**(4): 268-275, J Energ Resour-Asme, DOI: Doi 10.1115/1.2795047.

Bagchi, P. and Balachandar, S. (2003). Effect of turbulence on the drag and lift of a particle. Physics of Fluids **15**(11): 3496-3513, DOI: doi:http://dx.doi.org/10.1063/1.1616031.

Baird, D. G. (2008). First normal stress difference measurements for polymer melts at high shear rates in a slit-die using hole and exit pressure data. Journal of Non-Newtonian Fluid Mechanics **148**(1–3): 13-23, DOI: http://dx.doi.org/10.1016/j.jnnfm.2007.04.007.

Becker, T. E. and Azar, J. J. (1985). Mud-Weight And Hole-Geometry Effects On Cuttings Transport While Drilling Directionally, SPE-14711-MS.

Becker, T. E., Azar, J. J. and Okrajni, S. S. (1991). Correlations of Mud Rheological Properties With Cuttings-Transport Performance in Directional Drilling. SPE-19535-PA, DOI: 10.2118/19535-PA.

Beheshti, A. A. and Ataie-Ashtiani, B. (2008). Analysis of threshold and incipient conditions for sediment movement. Coastal Engineering **55**(5): 423-430, DOI: https://doi.org/10.1016/j.coastaleng.2008.01.003.

Best, J., Bennett, S., Bridge, J. et al. (1997). Turbulence modulation and particle velocities over flat sand beds at low transport rates. Journal of Hydraulic Engineering-Asce **123**(12): 1118-1129, J Hydraul Eng-Asce, DOI: c 10.1061/(Asce)0733-9429(1997)123:12(1118).

Bigillon, F., Couronne, G., Champagne, J. Y. et al. (2006). Investigation of flow hydrodynamics under equilibrium bedload transport conditions using PIV. River Flow 2006, Vols 1 and 2: 859-865, Proc Monogr Eng Wate, DOI: ://WOS:000241916500090.

Bilgesu, H. I., Ali, M. W., Aminian, K. et al. (2002). Computational Fluid Dynamics (CFD) as a Tool to Study Cutting Transport in Wellbores, SPE-78716-MS,DOI: 10.2118/78716-MS.

Bilgesu, H. I., Mishra, N. and Ameri, S. (2007). Understanding the Effect of Drilling Parameters on Hole Cleaning in Horizontal and Deviated Wellbores Using Computational Fluid Dynamics, SPE-111208-MS,DOI: 10.2118/111208-MS.

Bird, R. B., Armstrong, R. C. and Hassager, O. (1987). Dynamics of polymeric liquids. New York,, Wiley.

Bird, R. B., Dotson, P. J. and Johnson, N. L. (1980). Kinetic-Theory and Rheology of a Solution of Macromolecules Modeled as Finitely Extensible Bead-Spring Chains. Journal of Rheology **24**(3): 364-365, J Rheol.

Bizhani, M. (2013). Solids transport with turbulent flow of non-Newtonian fluid in the horizontal annuli. M.Sc. Thesis, University of Alberta, Edmonton, Canada.

Bizhani, M. (2013). Solids transport with turbulent flow of non-Newtonian fluid in the horizontal annuli, University of Alberta.

Bizhani, M., Corredor, F. and Kuru, E. (2015). An Experimental Study of Turbulent Non-Newtonian Fluid Flow in Concentric Annuli using Particle Image Velocimetry

Technique. Flow, Turbulence and Combustion **94**(3): 527-554, Flow Turbulence Combust, DOI: 10.1007/s10494-014-9589-6.

Bizhani, M., Corredor, F. E. R. and Kuru, E. (2016). Quantitative Evaluation of Critical Conditions Required for Effective Hole Cleaning in Coiled-Tubing Drilling of Horizontal Wells. **SPE** Drilling & Completion **31**(3): 188-199, DOI: http://dx.doi.org/10.2118/174404-PA.

Bizhani, M. and Kuru, E. (2017). Critical Review of Mechanistic and Empirical (Semi-Mechanistic) Models for Particle Removal from Sand Bed Deposits in Horizontal Annuli by Using Water. SPE Journal, SPE-187948-PA, In press.

Bizhani, M. and Kuru, E. (2017). Effect of Sand Bed Deposits on the Characteristics of Turbulent Flow of Water in Horizontal Annuli ASME fluid engineering, Paper under review.

Bizhani, M., Kuru, E. and Ghaemi, S. (2016). Effect of Near Wall Turbulence on the Particle Removal from Bed Deposits in Horizontal Wells. Proceedings of the Asme 35th International Conference on Ocean, Offshore and Arctic Engineering , 2016, Vol 8.

Bosworth, S., El-Sayed, H. S., Ismail, G. et al. (1998). Key Issues in Multilateral Technology. Oilfiled review

Bourgoyne, A. T., Millheim, K. K., Chenevert, M. E. et al. (1986). Applied Drilling Engineering, Society of Petroleum Engineers.

Boyer, F., Guazzelli, E. and Pouliquen, O. (2011). Unifying Suspension and Granular Rheology. Physical Review Letters **107**(18), Phys Rev Lett, DOI: ARTN 188301 10.1103/PhysRevLett.107.188301.

Brown, N. P., Bern, P. A. and Weaver, A. (1989). Cleaning Deviated Holes: New Experimental and Theoretical Studies. SPE\IADC Drilling Conference New Orleans, Louisiana, February 28-3 March 1989 SPE-18636-MS,DOI: 10.2118/18636-MS.

Buffington, J. M. and Montgomery, D. R. (1998). A systematic analysis of eight decades of incipient motion studies, with special reference to gravel-bedded rivers (vol 33, 1993, 1997). Water Resources Research **34**(1): 157-157, Water Resour Res, DOI: Doi 10.1029/97wr03138.

Bui, B., Saasen, A., Maxey, J. et al. (2012). Viscoelastic properties of oil based drilling fluids. Annual Transactions of the Nordic Rheology Society **20**: 33-47.

Bybee, K. (2011). A Review of Cuttings Transport in Directional-Well Drilling. Journal of Petroleum Technology **63**(02), SPE-0211-0052-JPT, DOI: 10.2118/0211-0052-JPT.

Capart, H. and Fraccarollo, L. (2011). Transport layer structure in intense bed-load. Geophysical Research Letters **38**, Geophys Res Lett, DOI: hArtn L20402 10.1029/2011gl049408.

Carbonneau, P. E. and Bergeron, N. E. (2000). The effect of bedload transport on mean and turbulent flow properties. Geomorphology **35**(3-4): 267-278, Geomorphology, DOI: g10.1016/S0169-555x(00)00046-5.

Carling, P. A. (1983). Threshold of Coarse Sediment Transport in Broad and Narrow Natural Streams. Earth Surface Processes and Landforms **8**(1): 1-18, Earth Surf Proc Land, DOI: DOI 10.1002/esp.3290080102.

Chan-Braun, C. (2012). Turbulent Open Channel Flow, Sediment Erosion and Sediment Transport, KIT Scientific Publ.

Chan-Braun, C., Garcia-Villalba, M. and Uhlmann, M. (2011). Force and torque acting on particles in a transitionally rough open-channel flow. Journal of Fluid Mechanics **684**: 441-474, J Fluid Mech, DOI: 10.1017/jfm.2011.311.

Cheng, E. D. (1969). Incipient motion of large roughness elements in turbulent open channel flow.

Chhabra, R. P. and Richardson, J. F. (1999). Chapter 1 - Non-Newtonian fluid behaviour. Non-Newtonian Flow in the Process Industries. Oxford, Butterworth-Heinemann**:** 1-36.

Cho, H., Shah, S. N. and Osisanya, S. O. (2000). A Three-Layer Modeling for Cuttings Transport with Coiled Tubing Horizontal Drilling. SPE Annual Technical Conference and Exhibition. Dallas, Texas, 1–4 October 2000., SPE-63269-MS,DOI: 10.2118/63269-MS.

Cho, H., Shah, S. N. and Osisanya, S. O. (2001). Effects of Fluid Flow in a Porous Cuttings-Bed on Cuttings Transport Efficiency and Hydraulics, SPE-71374-MS,DOI: 10.2118/71374-MS.

Choi, Y. J., Hulsen, M. A. and Meijer, H. E. H. (2010). An extended finite element method for the simulation of particulate viscoelastic flows. Journal of Non-Newtonian Fluid Mechanics **165**(11): 607-624, DOI: http://dx.doi.org/10.1016/j.jnnfm.2010.02.021.

Chung, S. Y., Rhee, G. H. and Sung, H. J. (2002). Direct numerical simulation of turbulent concentric annular pipe flow - Part 1: Flow field. International Journal of Heat and Fluid Flow **23**(4): 426-440, Int J Heat Fluid Fl, DOI: 10.1016/S0142-727X(02)00140-6.

Chung, S. Y. and Sung, H. J. (2005). Large-eddy simulation of turbulent flow in a concentric annulus with rotation of an inner cylinder. International Journal of Heat and Fluid Flow **26**(2): 191-203, Int J Heat Fluid Fl, DOI: DOI 10.1016/j.ijheatfluidflow.2004.08.006.

Clark, R. K. and Bickham, K. L. (1994). A Mechanistic Model for Cuttings Transport. SPE 69th Annual Tgchniml Conference and Exhlbltion Now ohms, LA, U. S.A., 25-8 .Septemb.ar 1994., SPE-28306-MS,DOI: 10.2118/28306-MS.

Corredor, F. E. R., Bizhani, M. and Kuru, E. (2016). Experimental investigation of cuttings bed erosion in horizontal wells using water and drag reducing fluids. Journal of Petroleum Science and Engineering **147**: 129-142, J Petrol Sci Eng, DOI: 10.1016/j.petrol.2016.05.013.

Dabiri, D. Cross-Correlation Digital Particle Image Velocimetry – A Review. Department of Aeronautics & Astronautics, University of Washington, Seattle, USA

Davies, J. T. (1987). Calculation of Critical Velocities to Maintain Solids in Suspension in Horizontal Pipes. Chemical Engineering Science **42**(7): 1667-1670, Chem Eng Sci, DOI: 10.1016/0009-2509(87)80171-9.

Dealy, J. M. and Larson, R. G. (2006). Structure and Rheology of Molten Polymers: From Structure to Flow Behavior and Back Again, Hanser Publishers.

Dealy, J. M., Wang, J., Dealy, J. M. et al. (2013). Melt rheology and its applications in the plastics industry. Engineering materials and processes,. Dordrecht ; New York: 1 online resource.

Dealy, J. M. and Wissbrun, K. F. (1999). Role of Rheology in Extrusion. Melt Rheology and Its Role in Plastics Processing: Theory and Applications. Dordrecht, Springer Netherlands**:** 441-490.

Deshpande, A. P. (2010). Rheology of complex fluids. New York: xiii, 257 p.

Diplas, P., Dancey, C. L., Celik, A. O. et al. (2008). The Role of Impulse on the Initiation of Particle Movement Under Turbulent Flow Conditions. Science **322**(5902): 717-720, Science, DOI: 10.1126/science.1158954.

Dodge, D. W. and Metzner, A. B. (1959). Turbulent Flow of Non-Newtonian Systems. Aiche Journal **5**(2): 189-204, Aiche J, DOI: DOI 10.1002/aic.690050214.

Doron, P. and Barnea, D. (1993). A 3-Layer Model for Solid-Liquid Flow in Horizontal Pipes. International Journal of Multiphase Flow **19**(6): 1029-1043, Int J Multiphas Flow, DOI: Doi 10.1016/0301-9322(93)90076-7.

Duan, M., Miska, S. Z., Yu, M. et al. (2007). Critical Conditions for Effective Sand-Sized Solids Transport in Horizontal and High-Angle Wells. SPE Production and Operations Symposium Oklahoma City, Oklahoma, USA, 31 March-3 April 2007., SPE-106707-MS,DOI: 10.2118/106707-MS.

Duan, M., Miska, S. Z., Yu, M. et al. (2008). Transport of Small Cuttings in Extended-Reach Drilling. SPE Drilling & Completion, SPE-104192-PA, DOI: 10.2118/104192-PA.

Duan, M. Q., Miska, S., Yu, M. J., Takach, N., Ahmed, R., Zettner, C. (2009). Critical Conditions for Effective Sand-Sized-Solids Transport in Horizontal and High-Angle Wells. SPE Drilling & Completion **24**(2): 229-238, **SPE** Drill Completion, DOI: 10.2118/104192-PA.

Dubief, Y., White, C. M., Terrapon, V. E. et al. (2004). On the coherent drag-reducing and turbulence-enhancing behaviour of polymers in wall flows. Journal of Fluid Mechanics **514**: 271-280, J Fluid Mech, DOI: Doi 10.1017/S0022112004000291.

Eesa, M. and Barigou, M. (2009). CFD investigation of the pipe transport of coarse solids in laminar power law fluids. Chemical Engineering Science **64**(2): 322-333, DOI: http://dx.doi.org/10.1016/j.ces.2008.10.004.

Erge, O., Ozbayoglu, E. M., Miska, S. Z. et al. (2015). Laminar to turbulent transition of yield power law fluids in annuli. Journal of Petroleum Science and Engineering **128**: 128-139, DOI: http://dx.doi.org/10.1016/j.petrol.2015.02.007.

Escudier, M. P. and Cullen, L. M. (1996). Flow of a shear-thinning liquid in a cylindrical container with a rotating end wall. Experimental Thermal and Fluid Science **12**(4): 381-387, Exp Therm Fluid Sci, DOI: Doi 10.1016/0894-1777(95)00137-9.

Escudier, M. P. and Gouldson, I. W. (1995). Concentric Annular-Flow with Centerbody Rotation of a Newtonian and a Shear-Thinning Liquid. International Journal of Heat and Fluid Flow **16**(3): 156-162, Int J Heat Fluid Fl, DOI: 10.1016/0142-727x(95)00012-F.

Escudier, M. P., Gouldson, I. W. and Jones, D. M. (1995). Flow of Shear-Thinning Fluids in a Concentric Annulus. Experiments in Fluids **18**(4): 225-238, Exp Fluids.

Espinosa-Paredes, G., Salazar-Mendoza, R. and Cazarez-Candia, O. (2007). Averaging model for cuttings transport in horizontal wellbores. Journal of Petroleum Science and Engineering **55**(3-4): 301-316, J Petrol Sci Eng, DOI: f10.1016/j.petrol.2006.03.027.

Flack, K. A. and Schultz, M. P. (2014). Roughness effects on wall-bounded turbulent flows. Physics of Fluids **26**(10): 101305, DOI: 10.1063/1.4896280.

Ford, J. T., Peden, J. M., Oyeneyin, M. B. et al. (1990). Experimental Investigation of Drilled Cuttings Transport in Inclined Boreholes. SPE Annual Technical Conference and Exhibition, 23-26 September, New Orleans, Louisiana, hSPE-20421-MS,DOI: 10.2118/20421-MS.

Fredrickson, A. G. and Bird, R. B. (1958). Non-Newtonian Flow in Annuli. Industrial and Engineering Chemistry **50**(3): 347-352, Ind Eng Chem, DOI: Doi 10.1021/Ie50579a035.

GarcÁa, M. H. (2008). Sedimentation Engineering: Processes, Measurements, Modeling, and Practice, American Society of Civil Engineers.

Gaudio, R., Miglio, A. and Dey, S. (2010). Non-universality of von Karman's kappa in fluvial streams. Journal of Hydraulic Research **48**(5): 658-663, J Hydraul Res, DOI: http://dx.doi.org/10.1080/00221686.2010.507338.

Gavignet, A. A. and Sobey, I. J. (1989). Model Aids Cuttings Transport Prediction. Journal of Petroleum Technology **41**, SPE-15417-PA, DOI: 10.2118/15417-PA.

Ghaemi, S., Rafati, S.,Bizhani, M., Kuru, E. (2015). Turbulent structure at the midsection of an annular flow. Physics of Fluids **27**(10): 105102, DOI: http://dx.doi.org/10.1063/1.4932109.

Goel, N., Shah, S. N. and Grady, B. P. (2002). Correlating viscoelastic measurements of fracturing fluid to particles suspension and solids transport. Journal of Petroleum Science and Engineering **35**(1): 59-81, DOI: http://dx.doi.org/10.1016/S0920-4105(02)00164-X.

Gomaa, A. M., Gupta, D. V. S. and Carman, P. (2014). Viscoelastic Behavior and Proppant Transport Properties of a New Associative Polymer-Based Fracturing Fluid. SPE International Symposium and Exhibition on Formation Damage Control, 26-28 February, Lafayette, Louisiana, USA, SPE-168113-MS,DOI: 10.2118/168113-MS.

Gomaa, A. M., Gupta, D. V. S. V. and Carman, P. S. (2015). Proppant Transport? Viscosity Is Not All It's Cracked Up To Be. SPE Hydraulic Fracturing Technology Conference, 3-5 February, The Woodlands, Texas, USA, SPE-173323-MS,DOI: 10.2118/173323-MS.

Gore, R. A. and Crowe, C. T. (1991). Modulation of Turbulence by a Dispersed Phase. Journal of Fluids Engineering-Transactions of the Asme **113**(2): 304-307, J Fluid Eng-T Asme, DOI: 10.1115/1.2909497.

Grass, A. J. (1970). Initial Instability of Fine Bed Sand. Journal of the Hydraulics Division **96**(3): 619-632.

Green, M. D., Thomesen, C. R., Wolfson, L. et al. (1999). An Integrated Solution of Extended-Reach Drilling Problems in the Niakuk Field, Alaska: Part II- Hydraulics, Cuttings Transport and PWD, SPE-56564-MS,DOI: 10.2118/56564-MS.

Gregory B. Dykes, J. (2014). Cuttings Transport Implications for Drill String Design: A Study with Computational Fluid Dynamics. Msc Thesis, Colorado School of Mines.

Guild, G. J., Wallace, I. M. and Wassenborg, M. J. (1995). Hole Cleaning Program for Extended Reach Wells, SPE-29381-MS,DOI: 10.2118/29381-MS.

Guo, X.-l., Wang, Z.-m. and Long, Z.-h. (2010). Study on three-layer unsteady model of cuttings transport for extended-reach well. Journal of Petroleum Science and Engineering **73**(1–2): 171-180, DOI: http://dx.doi.org/10.1016/j.petrol.2010.05.020.

Haciislamoglu, M. (1994). Practical Pressure Loss Predictions in Realistic Annular Geometries. SPE Annual Technical Conference and Exhibition, 25-28 September. New Orleans, Louisiana, SPE-28304-MS,DOI: 10.2118/28304-MS.

Hajidavalloo, E., Sadeghi-Behbahani-Zadeh, M. and Shekari, Y. (2013). Simulation of gas-solid two-phase flow in the annulus of drilling well. Chemical Engineering Research & Design **91**(3): 477-484, Chem Eng Res Des, DOI: DOI 10.1016/j.cherd.2012.11.009.

Harris, P. C., Walters, H. G. and Bryant, J. (2008). Prediction of Proppant Transport from Rheological Data. SPE Annual Technical Conference and Exhibition, 21-24 September, Denver, Colorado, USA, SPE-115298-MS,DOI: 10.2118/115298-MS.

Hassid, S. and Poreh, M. (1978). Turbulent Energy-Dissipation Model for Flows with Drag Reduction. Journal of Fluids Engineering-Transactions of the Asme **100**(1): 107-112, J Fluid Eng-T Asme.

Hemphill, T. (2010). A Comparison of High-Viscosity and High-Density Sweeps as Hole-Cleaning Tools: Separating Fiction From Fact. SPE Annual Technical Conference and Exhibition, 19-22 September, Florence, Italy, SPE-134514-MS,DOI: https://doi.org/10.2118/134514-MS.

Hemphill, T. and Larsen, T. I. (1996). Hole-Cleaning Capabilities of Water- and Oil-Based Drilling Fluids: A Comparative Experimental Study. **SPE** Drilling & Completion **11**(4), SPE-26328-PA, DOI: 10.2118/26328-PA.

Hemphill, T. and Ravi, K. (2010). Modeling of Effect of Drill Pipe Rotation Speed on Wellbore Cleanout, SPE-135703-MS,DOI: 10.2118/135703-MS.

Heyman, J., Mettra, F., Ma, H. B. et al. (2013). Statistics of bedload transport over steep slopes: Separation of time scales and collective motion. Geophysical Research Letters **40**(1): 128-133, Geophys Res Lett, DOI: 10.1029/2012gl054280.

Houssais, M., Ortiz, C. P., Durian, D. J. et al. (2015). Onset of sediment transport is a continuous transition driven by fluid shear and granular creep. Nature Communications **6**, Nat Commun, DOI: ARTN 6527 10.1038/ncomms7527.

Hu, Y. T., Chung, H. and Maxey, J. E. (2015). What is More Important for Proppant Transport, Viscosity or Elasticity? SPE Hydraulic Fracturing Technology Conference, 3-5 February, The Woodlands, Texas, USA, SPE-173339-MS,DOI: 10.2118/173339-MS.

Hussain H. Al-Kayiem, N. M. Z., Muhamad Z. Asyraf and Mahir Elya Elfeel (2010). Simulation of the Cuttings Cleaning During the Drilling Operation. American Journal of Applied Sciences **7**(6): 800-806.

Hussaini, S. M. and Azar, J. J. (1983). Experimental Study of Drilled Cuttings Transport Using Common Drilling Muds. SPE-10674-PA, DOI: 10.2118/10674-PA.

Iaccarino, G., Shaqfeh, E. S. G. and Dubief, Y. (2010). Reynolds-averaged modeling of polymer drag reduction in turbulent flows. Journal of Non-Newtonian Fluid Mechanics **165**(7-8): 376-384, J Non-Newton Fluid, DOI: DOI 10.1016/j.jnnfm.2010.01.013.

Iyoho, A. W. and Takahashi, H. (1993). Modeling Unstable Cuttings Transport In Horizontal, Eccentric Wellbores, SPE-27416-MS.

Japper-Jaafar, A., Escudier, M. P. and Poole, R. J. (2010). Laminar, transitional and turbulent annular flow of drag-reducing polymer solutions. Journal of Non-Newtonian Fluid Mechanics **165**(19-20): 1357-1372, J Non-Newton Fluid, DOI: 10.1016/j.jnnfm.2010.07.001.

Jefri, M. A. and Zahed, A. H. (1989). Elastic and Viscous Effects on Particle Migration in Plane-Poiseuille Flow. Journal of Rheology **33**(5): 691-708, DOI: 10.1122/1.550034.

Jin, S. and Collins, L. R. (2007). Dynamics of dissolved polymer chains in isotropic turbulence. New Journal of Physics **9**, New J Phys, DOI: Artn 360 Doi 10.1088/1367-2630/9/10/360.

Kamp, A. M. and Rivero, M. (1999). Layer Modeling for Cuttings Transport in Highly Inclined Wellbores. Latin American and Caribbean Petroleum Engineering Conference, 21-23 April, Caracas, Venezuela, SPE-53942-MS,DOI: 10.2118/53942-MS.

Kawaguchi, Y., Segawa, T., Feng, Z. et al. (2002). Experimental study on drag-reducing channel flow with surfactant additives—spatial structure of turbulence investigated by PIV system. International Journal of Heat and Fluid Flow **23**(5): 700-709, DOI: http://dx.doi.org/10.1016/S0142-727X(02)00166-2.

Kelessidis, V. C. and Bandelis, G. E. (2004a). Flow Patterns and Minimum Suspension Velocity for Efficient Cuttings Transport in Horizontal and Deviated Wells in Coiled-Tubing Drilling. **SPE** Drilling & Completion **19**(4): 213-227, SPE-81746-PA, DOI: 10.2118/81746-PA.

Kelessidis, V. C., Mpandelis, G., Koutroulis, A. et al. (2002). Significant Parameters Affecting Efficient Cuttings Transport In Horizontal and Deviated Wellbores In Coil Tubing Drilling: A Critical Review. Paper presented at the 1st International Symposium of the Faculty of Mines (ITU) on Earth Sciences and Engineering, 16-18 May 2002, Maslak, Istanbul, Turkey. .

Kelessidis, V. C. and Mpandelis, G. E. (2004b). Hydraulic Parameters Affecting Cuttings Transport for Horizontal Coiled Tubing Drilling. 7th National Congress on Mechanics, Chania, Greece, June, 2004.

Khatibi, M., Time, R. W. and Rabenjafimanantsoa, H. A. (2016). Particles falling through viscoelastic non-Newtonian flows in a horizontal rectangular channel analyzed with PIV and PTV techniques. Journal of Non-Newtonian Fluid Mechanics **235**: 143-153, DOI: http://dx.doi.org/10.1016/j.jnnfm.2016.08.004.

King, I., Trenty, L. and Vit, C. (2000). How the 3D Modeling Could Help Hole-Cleaning Optimization, SPE-63276-MS,DOI: 10.2118/63276-MS.

Krogstad, P. A., Antonia, R. A. and Browne, L. W. B. (1992). Comparison between Rough-Wall and Smooth-Wall Turbulent Boundary-Layers. Journal of Fluid Mechanics **245**: 599-617, J Fluid Mech, DOI: 10.1017/S0022112092000594.

Kundu, P. K., Cohen, I. M. and Dowling, D. R. (2012). Fluid Mechanics, 5th Edition. Fluid Mechanics, 5th Edition: 1-891.

Lam, C. K. G. and Bremhorst, K. (1981). A Modified Form of the K-Epsilon Model for Predicting Wall Turbulence. Journal of Fluids Engineering-Transactions of the Asme **103**(3): 456-460, J Fluid Eng-T Asme.

Larsen, T. I., Pilehvari, A. A. and Azar, J. J. (1997). Development of a New Cuttings-Transport Model for High-Angle Wellbores Including Horizontal Wells. **SPE** Drilling & Completion **12**(2): 129-135, SPE-25872-PA, DOI: 10.2118/25872-PA.

LAVision, F. M., Product Catalogue, 2006.

LaVision. Imager intense, P. c., 2006.

Lawn, C. J. and Elliott, C. J. (1972). Fully Developed Turbulent-Flow through Concentric Annuli. Journal of Mechanical Engineering Science **14**(3): 195-204, J Mech Eng Sci, DOI: 10.1243/JMES_JOUR_1972_014_027_02.

Lee, J., Tehrani, A., Young, S. et al. (2014). Viscoelasticity and Drilling Fluid Performance. (45455): V005T011A015, DOI: 10.1115/OMAE2014-23908.

Leising, L. J. and Walton, I. C. (2002). Cuttings-Transport Problems and Solutions in Coiled-Tubing Drilling. **SPE** Drilling & Completion **17**(1): 54-66, SPE-77261-PA, DOI: 10.2118/77261-PA.

Li, J. and Luft, B. (2014a). Overview of Solids Transport Studies and Applications in Oil and Gas Industry - Experimental Work. SPE Russian Oil and Gas Exploration & Production Technical Conference and Exhibition. Moscow, Russia, 14-16 October, SPE-171285-MS,DOI: 10.2118/171285-MS.

Li, J. and Luft, B. (2014b). Overview Solids Transport Study and Application in Oil-Gas Industry-Theoretical Work. Paper presented at International Petroleum Technology Conference Kuala Lumpur, Malaysia, 10-12 December 2014. Kuala Lumpur, Malaysia, 10-12 December 2014, IPTC-17832-MS,DOI: 10.2523/IPTC-17832-MS.

Li, J., Misselbrook, J. and Sach, M. (2010). Sand Cleanouts With Coiled Tubing: Choice of Process, Tools and Fluids. Journal of Canadian Petroleum Technology, SPE-113267-PA, DOI: 10.2118/113267-PA.

Li, J., Misselbrook, J. and Seal, J. W. (2008). Sand Cleanout With Coiled Tubing: Choice of Process, Tools, or Fluids? Europec/EAGE Conference and Exhibition. Rome, Italy, 9-12 June 2008, SPE-113267-MS,DOI: 10.2118/113267-MS.

Li, J. and Walker, S. (1999). Sensitivity Analysis of Hole Cleaning Parameters in Directional Wells. SPE/ICoTA Coiled Tubing Roundtable, . Houston, Texas, 25-26 May, SPE-54498-MS,DOI: 10.2118/54498-MS.

Li, J., Wilde, G. and Crabtree, A. R. (2005). Do Complex Super-Gel Liquids Perform Better Than Simple Linear Liquids in Hole Cleaning With Coiled Tubing? SPE/ICoTA Coiled Tubing Conference and Exibition The Woodlands, Texas, USA, 12-13 April 2005, SPE-94185-MS,DOI: 10.2118/94185-MS.

Li, Y. and Kuru, E. (2009). Optimization of Hole Cleaning in Vertical Wells Using Foam. Energy Sources Part a-Recovery Utilization and Environmental Effects **31**(1): 1-16, Energ Source Part A, DOI: Pii 906008054 10.1080/15567030802308601.

Lin, Y., Phan-Thien, N. and Khoo, B. C. (2014). Normal stress differences behavior of polymeric particle suspension in shear flow. Journal of Rheology **58**(1): 223-235, DOI: 10.1122/1.4855496.

Lockett, T. J., Richardson, S. M. and Worraker, W. J. (1993). The Importance of Rotation Effects for Efficient Cuttings Removal During Drilling, SPE-25768-MS,DOI: 10.2118/25768-MS.

Lodge, A. S. (1964). Elastic liquids; an introductory vector treatment of finite-strain polymer rheology. London, New York;, Academic Press.

Lourenco, A. M. F., Nakagawa, E. Y., Martins, A. L. et al. (2006). Investigating Solids-Carrying Capacity for an Optimized Hydraulics Program in Aerated Polymer-Based-Fluid Drilling. IADC/SPE Drilling Conference Miami, Florida, USA, 21-23 February 2006, SPE-99113-MS,DOI: 10.2118/99113-MS.

Lumley, J. L. (1969). Drag Reduction by Additives. Annual Review of Fluid Mechanics **1**: 367-&, Annu Rev Fluid Mech, DOI: DOI 10.1146/annurev.fl.01.010169.002055.

Luo, Y., Bern, P. A. and Chambers, B. D. (1992). Flow-Rate Predictions for Cleaning Deviated Wells. SPE/IADC Drilling Conference. New Orleans, Louisiana, 18-21 February, SPE-23884-MS., SPE-23884-MS,DOI: 10.2118/23884-MS.

Malin, M. R. (1997). Turbulent pipe flow of power-law fluids. International Communications in Heat and Mass Transfer **24**(7): 977-988, Int Commun Heat Mass, DOI: Doi 10.1016/S0735-1933(97)00083-3.

Martins, A. L., Campos, W., Liporace, F. S. et al. (1997). On the Erosion Velocity of a Cuttings Bed During the Circulation of Horizontal and Highly Inclined Wells, SPE-39021-MS,DOI: 10.2118/39021-MS.

Martins, A. L., Sa, C. H. M., Lourenco, A. M. F. et al. (1996). Optimizing Cuttings Circulation in Horizontal Well Drilling. International Petroleum Conference & Exhibition of Mexico. Villahermosa, Mexico, 5-7 March, 1996., SPE-35341-MS,DOI: 10.2118/35341-MS.

Martins, A. L., Sa, C. H. M., Lourenco, A. M. F. et al. (1996). Experimental Determination of Interfacial Friction Factor in Horizontal Drilling With a Bed of Cuttings, SPE-36075-MS,DOI: 10.2118/36075-MS.

Martins, A. L. and Santana, C. C. (1992). Evaluation of Cuttings Transport in Horizontal and Near Horizontal Wells -A Dimensionless Approach. SPE Latin America Petroleum Engineering Conference. Caracas, Venezuela ,8-11 March, SPE-23643-MS., SPE-23643-MS,DOI: 10.2118/23643-MS.

Martins, A. L., Santana, M. L., Campos, W. et al. Evaluating the Transport of Solids Generated by Shale Instabilities in ERW Drilling. SPE-59729-PA, DOI: 10.2118/59729-PA.

Martins, A. L., Santana, M. L., Gonçalves, C. J. C. et al. Evaluating the Transport of Solids Generated by Shale Instabilities in ERW Drilling - Part II: Case Studies, SPE-56560-MS,DOI: 10.2118/56560-MS.

Mason, C. (2008). Technology Focus. Journal of Petroleum Technology **60**(5): 74.

Melling, A. (1997). Tracer particles and seeding for particle image velocimetry. Measurement Science & Technology **8**(12): 1406-1416, Meas Sci Technol, DOI: 10.1088/0957-0233/8/12/005.

Min, T., Choi, H. and Yoo, J. Y. (2003). Maximum drag reduction in a turbulent channel flow by polymer additives. Journal of Fluid Mechanics **492**: 91-100, J Fluid Mech, DOI: Doi 10.1017/S0022112003005597.

Min, T., Jung, Y. Y., Choi, H. et al. (2003). Drag reduction by polymer additives in a turbulent channel flow. Journal of Fluid Mechanics **486**: 213-238, J Fluid Mech, DOI: Doi 10.1017/S0022112003004610.

Mishra, N. (2007). Investigation of Hole Cleaning Parameters Using Computational Fluid Dynamics in Horizontal And Deviated Wells. Msc Thesis, Department of Petroleum and Natural Gas Engineering Morgantown, West Virginia.

Mitchell, R. F., Miska, S., Aadnøy, B. S. et al. (2011). Fundamentals of Drilling Engineering, Society of Petroleum Engineers.

Miyazaki, K., Chen, G. , Ymamoto, F., Ohta, J., Murai, Y., Horii, K. (1999). PIV measurement of particle motion in spiral gas-solid two-phase flow. Experimental Thermal and Fluid Science **19**(4): 194-203, Exp Therm Fluid Sci, DOI: 10.1016/S0894-1777(99)00020-5.

Mme, U. and Skalle, P. (2012). CFD Calculations of Cuttings Transport through Drilling Annuli at Various Angles. International Journal of Petroleum Science and Technology **6**(2): 129-141.

Naganawa, S. and Nomura, T. (2006). Simulating Transient Behavior of Cuttings Transport over Whole Trajectory of Extended Reach Well. Abu Dhabi International Petroleum Exhibition & Conference, 7-10 November, Abu Dhabi, UAE, SPE-103923-MS,DOI: 10.2118/103923-MS.

Naser, J. A. (1991). Epris Nuclear-Power Division Expert System Activities for the Electric-Power Industry. Expert Systems Applications for the Electric Power Industry, Vols 1 and 2: 15-35.

Naser, J. A. (1997). Prediction of Newtonian & non-Newtonian Flow Through Concentric Annulus With Centerbody Rotation. Inter Conf on CFD in Mineral & Metal Processing and Power Generation CSIRO 1997.

National Instrument (2007). http://www.ni.com/manuals/ (accessed 18 December 2015).

Nazari, T., Hareland, G. and Azar, J. J. (2010). Review of Cuttings Transport in Directional Well Drilling: Systematic Approach. SPE Western Regional Meeting Anaheim, Califronia, USA, 27-29 may 2010, SPE-132372-MS,DOI: 10.2118/132372-MS.

Negrao, A. (2009). Technology Focus. Journal of Petroleum Technology **65**(5): 66.

Negrao, A. (2014). Technology Focus. Journal of Petroleum Technology **66**(5): 130.

Neto, J. L. V., Martins, A. L., Neto, A. S. et al. (2011). Cfd Applied to Turbulent Flows in Concentric and Eccentric Annuli with Inner Shaft Rotation. Canadian Journal of Chemical Engineering **89**(4): 636-646, Can J Chem Eng, DOI: Doi 10.1002/Cjce.20522.

Nezu, I. and Sanjou, M. (2011). PIV and PTV measurements in hydro-sciences with focus on turbulent open-channel flows. Journal of Hydro-Environment Research **5**(4): 215-230, J Hydro-Environ Res, DOI: 10.1016/j.jher.2011.05.004.

Nguyen, D. and Rahman, S. S. (1998). A Three-Layer Hydraulic Program for Effective Cuttings Transport and Hole Cleaning in Highly Deviated and Horizontal Wells. SPE-51186-PA, DOI: 10.2118/51186-PA.

Nikora, V. and Goring, D. (2000). Flow Turbulence over Fixed and Weakly Mobile Gravel Beds. Journal of Hydraulic Engineering **126**(9): 679-690, DOI: doi:10.1061/(ASCE)0733-9429(2000)126:9(679).

Nouri, J. M., Umur, H. and Whitelaw, J. H. (1993). Flow of Newtonian and Non-Newtonian Fluids in Concentric and Eccentric Annuli. Journal of Fluid Mechanics **253**: 617-641, J Fluid Mech, DOI: Doi 10.1017/S0022112093001922.

Ofei, T. N., Irawan, S. and Pao, W. (2014). CFD Method for Predicting Annular Pressure Losses and Cuttings Concentration in Eccentric Horizontal Wells. Journal of Petroleum Engineering **2014**: 16, DOI: 10.1155/2014/486423.

Okrajni, S. and Azar, J. J. (1986). The Effects of Mud Rheology on Annular Hole Cleaning in Directional Wells. SPE-14178-PA, DOI: 10.2118/14178-PA.

Orszag, S. A. (2006). Analytical theories of turbulence. Journal of Fluid Mechanics **41**(2): 363-386, DOI: 10.1017/S0022112070000642.

Osgouei, R. E., Ozbayoglu, M. E. and K., T. (2013). CFD Simulation of Solids Carrying Capacity of a Newtonian Fluid Through Horizontal Eccentric Annulus. Proceedings of the ASME 2013 Fluids Engineering Division Summer Meeting FEDSM2013 July 7-11, 2013, Incline Village, Nevada, USA, DOI: doi:10.1115/FEDSM2013-16204.

Ouriemi, M., Aussillous, P. and Guazzelli, E. (2009). Sediment dynamics. Part 1. Bed-load transport by laminar shearing flows. Journal of Fluid Mechanics **636**: 295-319, J Fluid Mech, DOI: 10.1017/S0022112009007915.

Ouriemi, M., Aussillous, P., Medale, M. et al. (2007). Determination of the critical Shields number for particle erosion in laminar flow. Physics of Fluids **19**(6), Phys Fluids, DOI: Artn 061706 10.1063/1.2747677.

Owen, P. R. (1964). Saltation of uniform grains in air. Journal of Fluid Mechanics **20**(2): 225-242, DOI: 10.1017/S0022112064001173.

Ozbayoglu, M. E., Miska, S. Z., Reed, T. et al. (2004). Analysis of the Effects of Major Drilling Parameters on Cuttings Transport Efficiency for High-Angle Wells in Coiled Tubing Drilling Operations. SPE/ICoTA Coiled Tubing Conference and Exibition. Huston, Texas, USA, 23-24 March 2004, SPE-89334-MS,DOI: 10.2118/89334-MS.

Ozbayoglu, M. E., Miska, S. Z., Reed, T. et al. (2005). Using foam in horizontal well drilling: A cuttings transport modeling approach. Journal of Petroleum Science and Engineering **46**(4): 267-282, DOI: http://dx.doi.org/10.1016/j.petrol.2005.01.006.

Ozbayoglu, M. E., Saasen, A., Sorgun, M. et al. (2010a). Critical Fluid Velocities for Removing Cuttings Bed Inside Horizontal and Deviated Wells. Petroleum Science and Technology **28**(6): 594-602, DOI: 10.1080/10916460903070181.

Ozbayoglu, M. E., Sorgun, M., Saasen, A. et al. (2010b). Hole Cleaning Performance of Light-Weight Drilling Fluids During Horizontal Underbalanced Drilling. SPE-136689-PA, DOI: 10.2118/136689-PA.

Paschkewitz, J. S., Dimitropoulos, C. D., Hou, Y. X. et al. (2005). An experimental and numerical investigation of drag reduction in a turbulent boundary layer using a rigid rodlike polymer. Physics of Fluids **17**(8), Phys Fluids, DOI: Artn 085101 10.1063/1.1993307.

Payne, M. L., Cocking, D. A. and Hatch, A. J. (1994). Critical Technologies for Success in Extended Reach Drilling, SPE-28293-MS,DOI: 10.2118/28293-MS.

Peden, J. M., Ford, J. T. and Oyeneyin, M. B. (1990). Comprehensive Experimental Investigation of Drilled Cuttings Transport in Inclined Wells Including the Effects of Rotation and Eccentricity, SPE-20925-MS,DOI: 10.2118/20925-MS.

Peysson, Y., Ouriemi, M., Medale, M. et al. (2009). Threshold for sediment erosion in pipe flow. International Journal of Multiphase Flow **35**(6): 597-600, Int J Multiphas Flow, DOI: 10.1016/j.ijmultiphaseflow.2009.02.007.

Peysson, Y., Ouriemi, M., Medale, M. et al. (2009). Threshold for sediment erosion in pipe flow. International Journal of Multiphase Flow **35**(6): 597-600, DOI: https://doi.org/10.1016/j.ijmultiphaseflow.2009.02.007.

Philip, Z., Sharma, M. M. and Chenevert, M. E. (1998). The Role of Taylor Vortices in the Transport of Drill Cuttings, SPE-39504-MS,DOI: 10.2118/39504-MS.

Pilehvari, A. A., Azar, J. J. and Shirazi, S. A. (1996). State-Of-The-Art Cuttings Transport in Horizontal Wellbores. International Conference on Horizontal Well Technology. Calgary, Alberta, Canada, 18-20 November, SPE-37079-MS,DOI: 10.2118/37079-MS.

Pinho, F. T. (2003). A GNF framework for turbulent flow models of drag reducing fluids and proposal for a k-epsilon type closure. Journal of Non-Newtonian Fluid Mechanics **114**(2-3): 149-184, J Non-Newton Fluid, DOI: Doi 10.1016/S0377-0257(03)00120-4.

Pinho, F. T., Li, C. F., Younis, B. A. et al. (2008). A low Reynolds number turbulence closure for viscoelastic fluids. Journal of Non-Newtonian Fluid Mechanics **154**(2-3): 89-108, J Non-Newton Fluid, DOI: DOI 10.1016/j.jnnfm.2008.02.008.

Pinho, F. T. and Whitelaw, J. H. (1990). Flow of Non-Newtonian Fluids in a Pipe. Journal of Non-Newtonian Fluid Mechanics **34**(2): 129-144, J Non-Newton Fluid, DOI: Doi 10.1016/0377-0257(90)80015-R.

Podryabinkin, E. V. and Rudyak, V. Y. (2014). Modeling of turbulent annular flows of Hershel-Bulkley fluids with eccentricity and inner cylinder rotation. Journal of Engineering Thermophysics **23**(2): 137-147, J Eng Thermophys-Rus, DOI: 10.1134/S1810232814020064.

Poole, R. J. (2010). Development-Length Requirements for Fully Developed Laminar Flow in Concentric Annuli. Journal of Fluids Engineering-Transactions of the **Asme** **132**(6), J Fluid Eng-T Asme, DOI: 10.1115/1.4001694.

Powell, J. W., Parks, C. F. and Seheult, J. M. (1991). Xanthan and Welan: The Effects Of Critical Polymer Concentration On Rheology and Fluid Performance. International Arctic

Technology Conference, 29-31 May, Anchorage, Alaska, SPE-22066-MS,DOI: 10.2118/22066-MS.

Ptasinski, P. K., Boersma, B. J., Nieuwstadt, F. T. M. et al. (2003). Turbulent channel flow near maximum drag reduction: simulations, experiments and mechanisms. Journal of Fluid Mechanics **490**: 251-291, J Fluid Mech, DOI: 10.1017/S0022112003005305.

Ptasinski, P. K., Nieuwstadt, F. T. M., van den Brule, B. H. A. A. et al. (2001). Experiments in turbulent pipe flow with polymer additives at maximum drag reduction. Flow Turbulence and Combustion **66**(2): 159-182, Flow Turbul Combust, DOI: Doi 10.1023/A:1017985826227.

Rabenjafimanantsoa A. H., Time, R. W. and Saasen, A. (2007). Simultaneous UVP and PIV measurements related to bed dunes dynamics and turbulence structures in circular pipes. 5th International Symposium on Ultrasonic Doppler Methods for Fluid Mechanics and Fluid Engineering.

Rabenjafimanantsoa, A. H. (2007). Particle transport and dynamics in turbulent Newtonian and non-Newtonian fluids. PhD, University of Stavanger,.

Rabenjafimanantsoa, H. A. (2007). Particle transport and dynamics in turbulent Newtonian and non-Newtonian fluids. Other Information: Doctoral theses at UIS; ISSN 1890-1387; Numerical Data; Thesis or Dissertation; TH: Thesis (PhD); refs, charts, figs, tabs. Norway: 163 pages.

Rabenjafimanantsoa, H. A., Time, R.W. and Saasen, A. (2005). Flow regimes over particle beds experimental studies of particle transport in horizontal pipes. Annual Transactions of the Nordic Rheology Society, 13.

Ramadan, A., Skalle, P. and Johansen, S. T. (2003). A mechanistic model to determine the critical flow velocity required to initiate the movement of spherical bed particles in inclined channels. Chemical Engineering Science **58**(10): 2153-2163, DOI: 10.1016/S0009-2509(03)00061-7.

Ramadan, A., Skalle, P., Johansen, S. T. et al. (2001). Mechanistic model for cuttings removal from solid bed in inclined channels. Journal of Petroleum Science and Engineering **30**(3-4): 129-141, J Petrol Sci Eng, DOI: Doi 10.1016/S0920-4105(01)00108-5.

Ramadan, A., Skalle, P. and Saasen, A. (2005). Application of a three-layer modeling approach for solids transport in horizontal and inclined channels. Chemical Engineering Science **60**(10): 2557-2570, DOI: http://dx.doi.org/10.1016/j.ces.2004.12.011.

Ravi, K. and Hemphill, T. (2006). Pipe Rotation and Hole Cleaning in Eccentric Annulus. IADC/SPE Drilling Conference, 21-23 February, Miami, Florida, USA, SPE-99150-MS,DOI: 10.2118/99150-MS.

Reed, T. D. and Pilehvari, A. A. (1993). A New Model for Laminar, Transitional, and Turbulent Flow of Drilling Muds. SPE Production Operations Symposium, 21-23 March, . Oklahoma City, Oklahoma, USA, SPE-25456-MS,DOI: 10.2118/25456-MS.

Rehme, K. (1974). Turbulent-Flow in Smooth Concentric Annuli with Small Radius Ratios. Journal of Fluid Mechanics **64**(2): 263-287, J Fluid Mech, DOI: http://dx.doi.org/10.1017/S0022112074002394.

Rehme, K. (1975). Turbulence Measurements in Smooth Concentric Annuli with Small Radius Ratios. Journal of Fluid Mechanics **72**(Nov11): 189-206, J Fluid Mech, DOI: Doi 10.1017/S0022112075003023.

Resende, P. R., Kim, K., Younis, B. A. et al. (2011). A FENE-P k-epsilon turbulence model for low and intermediate regimes of polymer-induced drag reduction. Journal of Non-Newtonian Fluid Mechanics **166**(12-13): 639-660, J Non-Newton Fluid, DOI: DOI 10.1016/j.jnnfm.2011.02.012.

Rinoshika, A., Yan, F. and Kikuchi, M. (2012). Experimental study on particle fluctuation velocity of a horizontal pneumatic conveying near the minimum conveying velocity. International Journal of Multiphase Flow **40**: 126-135, DOI: https://doi.org/10.1016/j.ijmultiphaseflow.2011.11.007.

Ro, K. and Ryou, H. (2012). Development of the modified k-E > turbulence model of power-law fluid for engineering applications. Science China-Technological Sciences **55**(1): 276-284, Sci China Technol Sc, DOI: 10.1007/s11431-011-4664-x.

Rodriguez-Corredor, F. E., Bizhani, M., Ashrafuzzaman, M. et al. (2014). An Experimental Investigation of Turbulent Water Flow in Concentric Annulus Using Particle Image

Velocimetry Technique. Journal of Fluids Engineering-Transactions of the Asme **136**(5), J Fluid Eng-T Asme, DOI: Artn 051203 Doi 10.1115/1.4026136.

Rodriguez-Corredor, F. E., Bizhani, M. and Kuru, E. (2014). A Comparative Study of Hole Cleaning Performance-Water Versus Drag Reducing Fluid. ASME 2014 33rd International Conference on Ocean, Offshore and Arctic Engineering, San Francisco, California, USA, June 8–13, 2014, DOI: 10.1115/OMAE2014-24083.

Rodriguez-Corredor, F. E., Bizhani, M. and Kuru, E. (2015). Experimental Investigation of Drag Reducing Fluid Flow in Annular Geometry Using Particle Image Velocimetry Technique. Journal of Fluids Engineering-Transactions of the **Asme 137**(8), J Fluid Eng-T Asme, DOI: 10.1115/1.4030287.

Rodriguez-Corredor, F. E., Bizhani, M., Ashrafuzzaman, M., Kuru, E. (2014). An Experimental Investigation of Turbulent Water Flow in Concentric Annulus Using Particle Image Velocimetry Technique. Journal of Fluids Engineering-Transactions of the **Asme 136**(5), J Fluid Eng-T Asme, DOI: 10.1115/1.4026136.

Rooki, R., Ardejani, F. D., Moradzadeh, A. et al. (2014). Simulation of cuttings transport with foam in deviated wellbores using computational fluid dynamics. Journal of Petroleum Exploration and Production Technology **4**(3): 263-273, J Petrol Explor Prod Technol, DOI: 10.1007/s13202-013-0077-7.

Rubiandini R.S, R. (1999). Equation for Estimating Mud Minimum Rate for Cuttings Transport in an Inclined-Until-Horizontal Well. SPE/IADC Middle East Drilling Technology Conference, 8-10 November, Abu Dhabi, United Arab Emirates, SPE-57541-MS,DOI: 10.2118/57541-MS.

Ruszka, J. (2014). Technology Focus. Journal of Petroleum Technology **66**(11): 110.

Saasen, A. (1998). Hole Cleaning During Deviated Drilling - The Effects of Pump Rate and Rheology. European Petroleum Conference, 20-22 October, The Hague, Netherlands, SPE-50582-MS,DOI: 10.2118/50582-MS.

Saasen, A., Eriksen, N. H., Han, L. Q. et al. (1998). Is annular friction loss the key parameter? Oil Gas-European Magazine **24**(1): 22-24, Oil Gas-Eur Mag.

Saasen, A. and Løklingholm, G. (2002). The Effect of Drilling Fluid Rheological Properties on Hole Cleaning. IADC/SPE Drilling Conference. Dallas, Texas, 26-28 February, SPE-74558-MS,DOI: 10.2118/74558-MS.

Saffman, P. G. (1965). Lift on a Small Sphere in a Slow Shear Flow. Journal of Fluid Mechanics **22**: 385-&, J Fluid Mech, DOI: 10.1017/S0022112065000824.

Sample, K. J. and Bourgoyne, A. T. (1977). An Experimental Evaluation Of Correlations Used For Predicting Cutting Slip Velocity, SPE-6645-MS,DOI: 10.2118/6645-MS.

Sample, K. J. and Bourgoyne, A. T., Jr. (1978). Development Of Improved Laboratory And Field Procedures For Determining The Carrying Capacity Of Drilling Fluids, SPE-7497-MS,DOI: 10.2118/7497-MS.

Sanchez, R. A., Azar, J. J., Bassal, A. A. et al. (1999). Effect of Drillpipe Rotation on Hole Cleaning During Directional-Well Drilling. SPE-56406-PA, DOI: 10.2118/56406-PA.

Sayindla, S., Lund, B., Taghipour, A. et al. (2016). Experimental Investigation of Cuttings Transport With Oil Based Drilling Fluids. (49996): V008T011A035, DOI: 10.1115/OMAE2016-54047.

Schmeeckle, M. W. (2014). Numerical simulation of turbulence and sediment transport of medium sand. Journal of Geophysical Research-Earth Surface **119**(6): 1240-1262, J Geophys Res-Earth, DOI: 10.1002/2013jf002911.

Shah, S. N., El Fadili, Y. and Chhabra, R. P. (2007). New model for single spherical particle settling velocity in power law (visco-inelastic) fluids. International Journal of Multiphase Flow **33**(1): 51-66, DOI: 10.1016/j.ijmultiphaseflow.2006.06.006.

Shields, A. (1936). Anwendung der Ähnlichkeitsmechanik und der Turbulenzforschung auf die Geschiebebewegung. Berlin, Eigenverl. der Preußischen Versuchsanst. für Wasserbau und Schiff.

Sibilla, S. and Baron, A. (2002). Polymer stress statistics in the near-wall turbulent flow of a drag-reducing solution. Physics of Fluids **14**(3): 1123-1136, Phys Fluids, DOI: Doi 10.1063/1.1448497.

Sifferman, T. R. and Becker, T. E. (1992). Hole Cleaning in Full-Scale Inclined Wellbores. SPE-20422-PA, DOI: 10.2118/20422-PA.

Sifferman, T. R., Myers, G. M., Haden, E. L. et al. (1974). Drill Cutting Transport in Full Scale Vertical Annuli. SPE-4514-PA, DOI: 10.2118/4514-PA.

Smith, J. D. and McLean, S. R. (1977). Spatially averaged flow over a wavy surface. Journal of Geophysical Research **82**(12): 1735-1746, DOI: 10.1029/JC082i012p01735.

Solo PIV. Nd:YAG Laser System. Operator's Manual.

Song, T., Chiew, Y. M. and Chin, C. O. (1998). Effect of bed-load movement on flow friction factor. Journal of Hydraulic Engineering-Asce **124**(2): 165-175, J Hydraul Eng-Asce, DOI: Doi 10.1061/(Asce)0733-9429(1998)124:2(165).

Sorgun, M., Aydin, I. and Ozbayoglu, M. E. (2011). Friction factors for hydraulic calculations considering presence of cuttings and pipe rotation in horizontal/highly-inclined wellbores. Journal of Petroleum Science and Engineering **78**(2): 407-414, J Petrol Sci Eng, DOI: DOI 10.1016/j.petrol.2011.06.013.

Southard, J. (2006). Introduction to Fluid Motions, Sediment Transport, and Current-Generated Sedimentary Structures. Massachusetts Institute of Technology: MIT OpenCourseWare, https://ocw.mit.edu. License: Creative Commons BY-NC-SA.

Sumer, B. M., Chua, L. H. C., Cheng, N.-S. et al. (2003). Influence of Turbulence on Bed Load Sediment Transport. Journal of Hydraulic Engineering **129**(8): 585-596, DOI: 10.1061/(ASCE)0733-9429(2003)129:8(585).

Sun, X., Wang, K., Yan, T. et al. (2014). Effect of drillpipe rotation on cuttings transport using computational fluid dynamics (CFD) in complex structure wells. Journal of Petroleum Exploration and Production Technology **4**(3): 255-261, J Petrol Explor Prod Technol, DOI: 10.1007/s13202-014-0118-x.

Sun Xiaofeng, W. K., Yan Tie, Zhang Yang, Shao Shuai, Luan Shizhu (2013). Review of Hole Cleaning in Complex Structural Wells. The Open Petroleum Engineering Journal **6**: 25-32.

Sureshkumar, R., Beris, A. N. and Handler, R. A. (1997). Direct numerical simulation of the turbulent channel flow of a polymer solution. Physics of Fluids **9**(3): 743-755, Phys Fluids, DOI: Doi 10.1063/1.869229.

Tabor, M. and Degennes, P. G. (1986). A Cascade Theory of Drag Reduction. Europhysics Letters **2**(7): 519-522, Europhys Lett, DOI: Doi 10.1209/0295-5075/2/7/005.

Tehrani, M. A. (1996). An experimental study of particle migration in pipe flow of viscoelastic fluids. Journal of Rheology **40**(6): 1057-1077, DOI: 10.1122/1.550773.

Televantos, Y., Shook, C., Carleton, A. et al. (1979). Flow of Slurries of Coarse Particles at High Solids Concentrations. Canadian Journal of Chemical Engineering **57**(3): 255-262, Can J Chem Eng.

Thomas, R. P., Azar, J. J. and Becker, T. E. (1982). Drillpipe Eccentricity Effect on Drilled Cuttings Behavior in Vertical Wellbores. Journal of Petroleum Technology **34**(9), SPE-9701-PA, DOI: 10.2118/9701-PA.

Tomren, P. H., Iyoho, A. W. and Azar, J. J. (1986). Experimental Study of Cuttings Transport in Directional Wells. SPE Drilling Engineering **1**(1), SPE-12123-PA, DOI: 10.2118/12123-PA.

Tonmukayakul, N., Morris, J. F. and Prudhomme, R. (2013). Method for estimating proppant transport and suspendability of viscoelastic liquids. Google Patents. United States, US 20110219856 A1.

Tropea, C., Yarin, A. L. and Foss, J. F. (2007). Springer handbook of experimental fluid mechanics. Heidelberg: xxviii, 1557 p.

Tsuji, Y., Kato, N. and Tanaka, T. (1991). Experiments on the unsteady drag and wake of a sphere at high reynolds numbers. International Journal of Multiphase Flow **17**(3): 343-354, DOI: http://dx.doi.org/10.1016/0301-9322(91)90004-M.

Valluri, S. G., Miska, S. Z., Yu, M. et al. (2006). Experimental Study of Effective Hole Cleaning Using "Sweeps" in Horizontal Wellbores. SPE Annual Technical Conference and Exibition. San Antonio, Texas, USA, 24-27 September 2006, SPE-101220-MS,DOI: 10.2118/101220-MS.

Van den Brule, B. H. A. A. and Gheissary, G. (1993). Effects of fluid elasticity on the static and dynamic settling of a spherical particle. Journal of Non-Newtonian Fluid Mechanics **49**(1): 123-132, DOI: http://dx.doi.org/10.1016/0377-0257(93)85026-7.

Vanoni, V. A. (1975). Sedimentation Engineering: Classic Edition, American Society of Civil Engineers.

Vieira, P., Miska, S., Reed, T. et al. (2002). Minimum Air and Water Flow Rates Required for Effective Cuttings Transport in High Angle and Horizontal Wells, SPE-74463-MS,DOI: 10.2118/74463-MS.

Virk, P. S., Mickley, H. S. and Smith, K. A. (1970). Ultimate Asymptote and Mean Flow Structure in Toms Phenomenon. Journal of Applied Mechanics **37**(2): 488-+, J Appl Mech.

Walker, S. and Li, J. (2000). The Effects of Particle Size, Fluid Rheology, and Pipe Eccentricity on Cuttings Transport. SPE/ICoTA Coiled Tubing Roundtable, 5-6 April. Houston, Texas, SPE-60755-MS,DOI: 10.2118/60755-MS.

Wang Kelin, Y. T., Sun Xiaofeng, Shao Shuai, Luan Shizhu (2013). Review and Analysis of Cuttings Transport in Complex Structural Wells. The Open Fuels & Energy Science Journal **6**: 9-17.

Wang, R.-h., Cheng, R.-c., Wang, H.-g. et al. (2009). Numerical simulation of transient cuttings transport with foam fluid in horizontal wellbore. Journal of Hydrodynamics, Ser. B **21**(4): 437-444, DOI: http://dx.doi.org/10.1016/S1001-6058(08)60169-9.

Warholic, M. D., Heist, D. K., Katcher, M. et al. (2001). A study with particle-image velocimetry of the influence of drag-reducing polymers on the structure of turbulence. Experiments in Fluids **31**(5): 474-483, Exp Fluids, DOI: DOI 10.1007/s003480100288.

Warholic, M. D., Massah, H. and Hanratty, T. J. (1999). Influence of drag-reducing polymers on turbulence: effects of Reynolds number, concentration and mixing. Experiments in Fluids **27**(5): 461-472, Exp Fluids, DOI: DOI 10.1007/s003480050371.

Werner, B., Myrseth, V., Lund, B. et al. (2016). Effects of Oil-Based Drilling-Fluid Rheological Properties on Hole-Cleaning Performance. (49996): V008T011A038, DOI: 10.1115/OMAE2016-54050.

Werner, B., Myrseth, V. and Saasen, A. (2017). Viscoelastic properties of drilling fluids and their influence on cuttings transport. Journal of Petroleum Science and Engineering **156**: 845-851, DOI: http://dx.doi.org/10.1016/j.petrol.2017.06.063.

Wiberg, P. L. and Rubin, D. M. (1989). Bed Roughness Produced by Saltating Sediment. Journal of Geophysical Research-Oceans **94**(C4): 5011-5016, J Geophys Res-Oceans, DOI: 10.1029/JC094iC04p05011.

Wieneke, B. (2005). Stereo-PIV using self-calibration on particle images. Experiments in Fluids **39**(2): 267-280, DOI: 10.1007/s00348-005-0962-z.

Wilson, K. C. (1976). A unified Physically-based analysis of solid-liquid pipeline flow. Proceeding of the 4th Int. Conf. on the Hydraulic Transport of SOlids in Pipes, Banff, Alberta, Cabnada, Paper A1.

Wilson, K. C. and Thomas, A. D. (1985). A New Analysis of the Turbulent-Flow of Non-Newtonian Fluids. Canadian Journal of Chemical Engineering **63**(4): 539-546.

Xiaofeng, S., Wang, K., Yan, T. et al. (2013). Review of Hole Cleaning in Complex Structural Wells. The Open Petroleum Engineering Journal **6**: 25-32, DOI: 10.2174/1874834101306010025.

Yan, F. and Rinoshika, A. (2011). Application of high-speed PIV and image processing to measuring particle velocity and concentration in a horizontal pneumatic conveying with dune model. Powder Technology **208**(1): 158-165, Powder Technol, DOI: 10.1016/j.powtec.2010.12.014.

Yan, F. and Rinoshika, A. (2012). Characteristics of particle velocity and concentration in a horizontal self-excited gas-solid two-phase pipe flow of using soft fins. International Journal of Multiphase Flow **41**: 68-76, Int J Multiphas Flow, DOI: 10.1016/j.ijmultiphaseflow.2012.01.004.

Yateem, K. S., Qahtani, H. B., Saeed, S. S. et al. (2013). Fill Cleanout Operations in Offshore Saudi Arabian Fields: Case Histories toward Improving Economics and Operational Logistics, IPTC-16677-MS,DOI: 10.2523/IPTC-16677-MS.

Yilmaz, D. (2012). Discrete Phase Simulations of Drilled Cuttings Transport Process in Highly Deviated Wells. Msc thesis, Louisiana State University.

Ytrehus, J. D., Carlsen, I. M., Melchiorsen, J. C. et al. (2013). Experimental Study Of Friction And Cutting Transport In Non Circular Borehole Geometry, SPE-166790-MS,DOI: 10.2118/166790-MS.

Ytrehus, J. D., Taghipour, A., Lund, B. et al. (2014). Experimental Study of Cuttings Transport Efficiency of Water Based Drilling Fluids. (45455): V005T011A017, DOI: 10.1115/OMAE2014-23960.

Ytrehus, J. D., Taghipour, A., Sayindla, S. et al. (2015). Full Scale Flow Loop Experiments of Hole Cleaning Performances of Drilling Fluids. Proceedings of the Asme 34th International Conference on Ocean, Offshore and Arctic Engineering, 2015, Vol 10.

Zamora, M., Jefferson, D. T. and Powell, J. W. (1993). Hole-Cleaning Study of Polymer-Based Drilling Fluids. SPE Annual Technical Conference and Exhibition, 3-6 October, Houston, Texas, SPE-26329-MS,DOI: 10.2118/26329-MS.

Zeinali, H., Toma, P. and Kuru, E. (2012). Effect of Near-Wall Turbulence on Selective Removal of Particles From Sand Beds Deposited in Pipelines. Journal of Energy Resources Technology-Transactions of the Asme **134**(2), J Energ Resour-Asme, DOI: Artn 021003 10.1115/1.4006041.

Zhang, F. S. M., M. Yu, E. Ozbayoglu and N. Takach (2014). Pressure Profile in Annulus: Solids Play a Significant Role. Proceedings of the ASME 2014 33rd International Conference on Ocean, Offshore and Arctic Engineering OMAE2014 une 8-13, 2014, San Francisco, California, USA.

Zheng, Y., Rinoshika, A. and Yan, F. (2012). Multi-scale analysis on particle fluctuation velocity near the minimum pressure drop in a horizontal pneumatic conveying. Chemical Engineering Science **72**: 94-107, DOI: https://doi.org/10.1016/j.ces.2012.01.011.

Zou, L., Patel, M. H. and Han, G. (2000). A New Computer Package for Simulating Cuttings Transport and Predicting Hole Cleaning in Deviated and Horizontal Wells, SPE-64646-MS,DOI: 10.2118/64646-MS.